



SAPIENZA

University of Rome

Department of Biology and Biotechnology “Charles Darwin”

**From Epigenetics to Lipid Metabolism: different
approaches to fight cancer**

Giulia Stazi

Ph.D. PROGRAM IN LIFE SCIENCES

XXX cycle

Tutor and Supervisor

Prof. Antonello Mai

Coordinator

Prof. Marco Tripodi

ἀλλὰ χαρτοῖσιν τε χαῖρε καὶ κακοῖσιν ἀσχάλα
μὴ λίην γίγνωσκε δ' οἷος ῥυσμὸς ἀνθρώπους ἔχει.

-Archiloco di Paro-

Director of PhD program

Prof. Marco Tripodi,
Department of Cellular Biotechnology and Hematology,
“Sapienza” University of Rome

Scientific Tutor and main Supervisor

Prof. Antonello Mai, PhD
Full Professor in Medicinal Chemistry
Istituto Pasteur - Fondazione Cenci Bolognetti
Department of Drug Chemistry and Technologies
“Sapienza” University of Rome

Foreign Supervisor

Prof. Stuart Conway, PhD
Department of Chemistry
Chemistry Research Laboratory
University of Oxford

LIST OF PUBLICATIONS:

- Mellini P., Marrocco B, Borovika D, Polletta L, Carnevale I, Saladini S, Stazi G, Zwergel C, Trapencieris P, Ferretti E, Tafani M, Valente S, and Mai A. Pyrazole-based inhibitors of Enhancer of Zeste Homolog 2 induce apoptosis and autophagy in cancer cells. *Phil. Trans. R. Soc. B*. doi: 10.1098/rstb.2017.0150 (ACCEPTED in September 2017, now in Press) *
- Miele E, Valente S, Alfano V, Silvano M, Mellini P, Borovika D, Marrocco B, Po A, Besharat ZM, Catanzaro G, Battaglia G, Abballe L, Zwergel C, Stazi G, Milite C, Castellano S, Tafani M, Trapencieris P, Mai A, Ferretti E. The histone methyltransferase EZH2 as a druggable target in SHH medulloblastoma cancer stem cells. *Oncotarget*. 2017 Aug 2;8(40):68557-68570. doi: 10.18632/oncotarget.19782. PubMed PMID: 28978137.*
- Zwergel C, Czepukojc B, Evain-Bana E, Xu Z, Stazi G, Mori M, Patsilinakos A, Mai A, Botta B, Ragno R, Bagrel D, Kirsch G, Meiser P, Jacob C, Montenarh M, Valente S. Novel coumarin- and quinolinone-based polycycles as cell division cycle 25-A and -C phosphatases inhibitors induce proliferation arrest and apoptosis in cancer cells. *Eur J Med Chem*. 2017 Jul 7;134:316-333. doi: 10.1016/j.ejmech.2017.04.012. PubMed PMID: 28431339.
- Vianello P, Botrugno OA, Cappa A, Dal Zuffo R, Dessanti P, Mai A, Marrocco B, Mattevi A, Meroni G, Minucci S, Stazi G, Thaler F, Trifiró P, Valente S, Villa M, Varasi M, Mercurio C. Discovery of a Novel Inhibitor of Histone Lysine-Specific Demethylase 1A (KDM1A/LSD1) as Orally Active Antitumor Agent. *J Med Chem*. 2016 Feb 25;59(4):1501-17. doi: 10.1021/acs.jmedchem.5b01209. PubMed PMID: 26702542.
- Rodriguez V, Valente S, Rovida S, Rotili D, Stazi G, Lucidi A, Ciossani G, Mattevi A, Botrugno OA, Dessanti P, Mercurio C, Vianello P, Minucci S, Varasi M, Mai A. Pyrrole- and indole-containing tranylcypromine derivatives as novel lysine-specific demethylase 1 inhibitors active on cancer cells. *MEDCHEMCOMM*, 2015, vol. 6; p. 665-670, ISSN: 2040-2503, doi: 10.1039/c4md00507d.

REVIEW PAPERS:

- Stazi G, Zwergel C, Mai A, Valente S. EZH2 inhibitors: a patent review (2014-2016). Expert Opinion on Therapeutic Patents. 2017 Jul; 27 (7): 797-813. doi: 10.1080/13543776.2017.1316976. Review. PubMed PMID: 28394193.*
- Stazi G, Zwergel C, Valente S, Mai A. LSD1 inhibitors: a patent review (2010-2015). Expert Opinion on Therapeutic Patents. 2016 May; 26 (5): 565-80. doi: 10.1517/13543776.2016.1165209. Review. PubMed PMID: 27019002.

*Only these publications are the object of this thesis.

In the aforementioned publications the present PhD student Giulia Stazi cured the main part of synthetic work. Crystallographic investigations, biochemical, cell based and *in vivo* assays have been carried out by the other co-authors.

ABBREVIATIONS LIST

231MFP: human breast cancer cells; aa: amino acids; ABP: affinity based probe; ABPP: affinity based protein profiling; AC: acyl carnitine; ADMA: asymmetric dimethylarginine; AEBP2: Adipocyte Enhancer-Binding Protein 2; AGPS/ADPS: alkylglycerone phosphate synthase/alkyldihydroxyacetone phosphate synthase; AGPSi: AGPS inhibitor; Akt: serine/threonine kinase 1; alkyl-GP: alkyl-glycerol phosphate; AP-1: Activator protein 1 (transcription factor); BBB: blood brain barrier; BET: bromodomain and extra terminal; bFGF: basic-fibroblast growth factor; BRDs: bromodomains; Brij35: Polyoxyethylene(23)lauryl ether; BSA: bovine serum albumin; BTIC: brain tumor initiating cells; C8161: human melanoma cells; CD44: cell-surface glycoprotein involved in cell-cell interactions, cell adhesion and migration; CDCl₃: deuterated chloroform; CDI: 1,1'-carbonyldiimidazole; CE: cross-linking efficiency; CHAPS: 3-[(3-cholamidopropyl)dimethylammonio]-1-propanesulfonate hydrate; CoA: coenzyme A; CREBBP: CREB binding protein; CuAAC: copper-catalysed alkyne azide cycloaddition; *d*₆-DMSO: deuterated dimethyl sulfoxide DAG: diacylglycerol; DAOY: desmoplastic cerebellar medulloblastoma cell line; DAPI: 4',6-diamidin-2-phenylindol; DCE: 1,2-dichloroethane; DCM: dichloromethane; DEX: dexamethasone; DFM: FBS-supplemented medium; DHAP: dihydroxyacetone phosphate; DHAPAT: dihydroxyacetonephosphate acyltransferase (see also GNPAT); DIMAP: 4-dimethylaminopyridine DIPEA: diisopropylethylamine; DMEM: Dulbecco's Modified Eagle Medium; DMF: *N,N*-dimethylformamide; DMSO: dimethylsulfoxide; DNMT1: DNA methyl transferase 1; DOT1L: DOT1 Like Histone Lysine Methyltransferase; DTT: dithiothreitol; EDB: EED-binding domain; EDG: electron donating group; EDTA: ethylenediaminetetraacetic acid; EED: Embryonic Ectoderm Development; EGF: epidermal growth factor; EGFR: epidermal growth factor receptor; EI: electron ionization; EI: electron ionization; EM: electron microscopy; EMT: epithelial-mesenchymal transition; ER: endoplasmic reticulum; ESC: embryonic stem cells; ESI: electrospray ionization; EtOH: ethanol; EWG: electron withdrawing group; EZH1: Enhancer of Zeste Homologue 1; EZH2: Enhancer of Zeste Homologue 2; EZH2i: EZH2 inhibitor; FABP4: fatty acid binding protein 4; FAD: flavin adenine dinucleotide; FASN: fatty acid synthase; FBS: fetal bovine serum; FFAs: free fatty acids; G9a: Euchromatic histone-lysine N-methyltransferase 2 (EHMT2); GATA-4, PLFZ, E2F, c-Myc: transcription factors; GFAP: glial fibrillary acidic protein GL1/2/3: primary glioblastoma cell lines; GNPAT: glyceronephosphate O-acyl transferase (see also DHAPAT); H3K27: histone 3 lysine 27; HATs: histone acetyltransferases; HCT-15: colon cancer cell line; HDACs: histone deacetylases; HEK293: non-cancer human embryonic kidney cell line; Hepes: 4-(2-hydroxyethyl)-1-piperazineethanesulfonic acid; HepG2: human hepatic carcinoma cells; HF: human fibroblasts; HKDMs: histone lysine demethylases; HKMTs: histone lysine methyltransferases; hMSCs: human mesenchymal stem cells; HOTAIR: HOX transcript

antisense RNA; HRAS: Harvey-Rat sarcoma (oncogene); HT-29: colon cancer cell line; IC₅₀: half maximal inhibitory concentration; JARID2: Jumonji and AT-Rich Interaction Domain 2; JMJD3: jumonji domain-containing protein 3- H3K27 demethylases; K562: myelogenous leukemia cell line; KDMs: lysine demethylases; Ki: inhibition constant; KIAA1363: serine hydrolase; KMTs: lysine methyltransferases; LC-MS: liquid chromatography- mass spectrometry; LC-MS: liquid chromatography/mass spectrometry; LDA: lithium diisopropylamide; LNCaP: human prostate cancer cells; LPA: lysophosphatidic acid; LPA: lysophosphatidic acid; LPAe: lysophosphatidic acid-ether; LPC: lysophosphatidylcholine; LPCAT1: lysophosphatidyl choline acyltransferase 1; LPCe: lysophosphatidylcholine-ether; LPE: lysophosphatidylethanolamine; LPGe: lysophosphatidylglycerol-ether; LPI: lysophosphatidylinositol; LPL: lipoprotein lipase; LPS: lysophosphatidylserine; LSD1: Lysine specific demethylase 1; MAG: monoalkylglycerol; MAGL: monoacylglycerol lipase; MAP1LC3A (LC3): microtubule associated protein 1 light chain 3 alpha; MAPK: mitogen-activated protein kinase; MB-SLCs: medulloblastoma stem like cells; MCF7: human breast cancer cells; MCSS and SANT2: EZH2 domain; MDA-MB231: breast adenocarcinoma cell line; MDA-MB231: human breast cancer cells; MEM: cell culture medium; MeOD: deuterated methanol; MITR: myocyte enhancer factor-2-interacting transcriptional repressor; MLL1 complex: myeloid/lymphoid or mixed-lineage leukaemia 1 complex (histone-lysine N-methyltransferase); MMA: monomethyl arginine; MMP-2/9: matrix metalloproteinase-2/9; MS: mass spectrometry; mTOR: mechanistic (mammalian) target of rapamycin (serine/threonine protein kinase); MTS: 3-(4,5-dimethylthiazol-2-yl)-5-(3-carboxymethoxyphenyl)-2-(4-sulfophenyl)-2*H*-tetrazolium; MUM2C: human melanoma cells; NAE: N-acylethanolamine; NB4: acute promyelocytic leukaemia cell line; ncRNA: non-coding RNA; NMP: *N*-methyl-2-pyrrolidone; NP40: Nonoxinol 40 (detergent); NSC: neural stem cells; NSCs: neural stem cells; PA: phosphatidic acid; PA: phosphatidic acid; PAe: phosphatidic acid-ether; PAFe: platelet-activating factor-ether; PAL: photo-affinity labelling; PAMPA: parallel artificial membrane permeability assay; PARP: poly(ADP-ribose)polymerase; PBS: phosphate buffer saline; PC: phosphatidylcholine; PC3: human prostate cancer cells; PC3: prostate cancer cell line; PCe: phosphatidylcholine-ether; PcG: polycomb group; PCLs: Polycomb-like proteins; PCNA: proliferating cell nuclear antigen; PCR: polymerase chain reaction; PEG: polyethylene glycol; Pep: phosphatidylethanolamine-plasmalogen; PG: phosphatidylglycerol PGe: phosphatidylglycerol-ether; PhoRC: Phorepressive complex; PI: phosphatidyl inositol; Pie: phosphatidyl inositol-ether; PK: pharmacokinetic; PMSF: phenylmethylsulfonyl fluoride; PPAR γ 2: Peroxisomal proliferator-activated receptor-gamma; PPI: protein-protein interaction; PRC: polycomb repressive complex; PR-DUB: Polycomb Repressive Deubiquitinase; PRMT1: Protein Arginine Methyltransferase 1; PRMTs: arginine methyltransferases; PS: phosphatidylserine; PSe: phosphatidylserine-ether; PTMs : post-translational modifications; PVDF: polyvinylidene difluoride; qPCR: quantitative polymerase chain reaction; RbAp46/48: Retinoblastoma

Associated protein 47 or 48; RPMI: cell culture medium; RT-PCR: real time polymerase chain reaction; SAH: S-adenosyl homocysteine; SAM: S-adenosyl-L-methionine; SAR: structure activity relationship; SDMA: symmetric dimethylarginine; SDS-PAGE: sodium dodecyl sulfate polyacrylamide gel electrophoresis; SET: Su(var)3-9, Enhancer-of-zeste and Trithorax (methyltransferases catalytic domain; ET7/9: protein lysine methyltransferase; shRNA: small hairpin RNA; SHSY5Y: neuroblastoma cell line; siRNA: small interference RNA; SK-N-BE: neuroblastoma cell line; SKOV3: ovarian cancer cells; SLCs: stem like cells; SM: stem cell-medium; S_N: nucleophilic substitution; Snail: C2H2-type zinc finger protein (transcription factor); SPAAC: strain-promoted alkyne azide cycloaddition; SRM: single reaction monitoring; SUZ12: Suppressor of Zeste 12; TAG: triacylglycerol; TAMRA: 5-carboxytetramethylrhodamine; TBS: Tert-Butyldimethylsilyl chloride; TBTA: tris[(1-benzyl-1H-1,2,3-triazol-4-yl)methyl]amine; TBTU: O-(benzotriazole-1-yl)-N,N,N',N'-tetramethyluronium tetrafluoroborate; TcBDF3: *Tripanosoma Cruzi* bromodomain factor 3; TCEP: tris(2-carboxyethyl)phosphine; TEA: triethylamine; THF: tetrahydrofuran; TLC: thin-layer chromatography; Tris-HCl: 2-Amino-2-(hydroxymethyl)propane-1,3-diol hydrochloride; TSC2: Tuberous Sclerosis Complex 2 (tumor suppressor); Tween-20: detergent; Twist: transcription factor; U-87: glioblastoma cell line; U937: histiocytic lymphoma cell line; UTX: Ubiquitously transcribed tetratricopeptide repeat X chromosome- H3K27 demethylases; Vefs: SUZ12 domain; WDR9(2): WD repeat 9 (2).

INDEX

INDEX	XIII
PART 1: Epigenetics.....	1
1 Introduction (1)	1
1.1 Epigenetics.....	1
1.2 Writers, readers and erasers: the complex interplay of epigenetic players and the epigenetic code.....	2
1.3 The role of covalent histone modifications and chromatin remodeling.....	2
1.4 Histone methylation.....	3
1.5 The PRC2 complex.....	4
1.5.1 PRC2 catalytic core (EZH1 and EZH2), and the importance of the complex.....	6
1.5.2 EZH2 SET domain structure.....	6
1.5.3 PRC2 crystal structure.....	7
1.5.4 PRC2 interactome and target genes	8
1.5.5 Relevance of EZH2 in cancer.....	9
1.5.6 EZH2 mutations (gain or loss of function).....	10
1.5.7 EZH2 in cancer and non-cancer cell stemness.....	11
1.5.8 PRC2 as a druggable target.....	12
1.5.9 Not only EZH2: the rising of dual EZH1/EZH2 inhibitors and the polypharmacology.....	17
1.6 Histone acetylation.....	21
1.7 Bromodomains	22
1.7.1 Bromodomains structure	22
1.7.2 The BET family and BRD4.....	23
1.7.3 BRDs as druggable targets	24
2 Design, synthesis and biological evaluation of novel pyrrole-based EZH2 inhibitors, displaying antiproliferative activity, cell cycle arrest, and H3K27me3 reduction in cancer cells, including glioblastoma primary cells.....	27
2.1 Research project.....	27
2.2 Results and discussion.....	30

2.2.1	Chemistry	30
2.2.2	Biochemical EZH2 enzymatic inhibition assay and structure activity relationship (SAR) 34	
2.2.3	Target selectivity validation	38
2.2.4	In cell evaluation (1).....	40
2.2.5	In cell evaluation (2).....	50
2.3	General conclusions and future perspectives.....	54
2.4	Experimental Section.....	57
2.4.1	Chemistry	57
2.4.2	Biochemistry.....	108
2.4.3	In cell evaluation (1).....	108
2.4.4	In cell evaluation (2).....	109
3	Development of Pyrazole-based Inhibitors of EZH2 able to Induce Apoptosis and Autophagy in Cancer Cells, reduce cell stemness in SHH medulloblastoma cancer stem cells, and impair of tumour growth <i>in vivo</i> *.....	113
3.1	Research project	113
3.2	Results and Discussion	114
3.2.1	Chemistry	114
3.2.2	Biochemical EZH2 enzymatic inhibition assay and structure activity relationship (SAR)	115
3.2.3	Compound 34o activity validation: biochemical screening in presence of different substrates, SAM-competition experiments and screening against a panel of methyltransferases (EZH1, DOT1L, DNMT1, G9a, MLL1 complex, PRMT1, SET7/9)...	116
3.2.4	Effects of 34o in a panel of cancer cells	117
3.2.5	Intracellular inhibition of H3K27 methylation	119
3.2.6	Autophagy induction of 34o in myelogenous leukemia K562 and neuroblastoma SK-N-BE cell lines	120
3.2.7	Effects of 34o on apoptosis induction in neuroblastoma SK-N-BE cell lines	122
3.2.8	Effects of 34o in SHH medulloblastoma cancer stem cells	123
3.2.9	Effects of 34o in an <i>in vivo</i> mouse model of medulloblastoma	127
3.3	Conclusions	129

3.4	Experimental Section	131
3.4.1	Chemistry	131
3.4.2	Biochemistry	145
3.4.3	In cell evaluation	145
3.4.4	Mice experiments	148
4	Design, synthesis and characterization of novel Astemizole analogues as potential PRC2 disruptors.....	151
4.1	Research project.....	151
4.2	Results and discussion.....	153
4.2.1	Chemistry	153
4.3	Conclusions and future perspectives	157
4.4	Experimental Section	158
4.4.1	Chemistry	158
5	Development Of Photoaffinity Probes For BET Bromodomains	179
5.1	Activity-based protein profiling (ABPP)	179
5.1.1	Photoaffinity labelling and photoreactive groups	180
5.1.2	Two step ABP and ligation chemistry.....	181
5.2	Rationale	183
5.2.1	Synthesis of the third generation probe.....	184
5.2.2	BRD(4)1 affinity of compound 50	189
5.2.3	Photo crosslinking experiments with compound 50.....	190
5.3	Conclusions and prospectives	194
5.4	Experimental section.....	196
5.4.1	Chemistry	196
5.4.2	Biochemical methods	209
	PART 2: Ether Lipids Methabolism	212
6	Introduction (2)	214
6.1	Lipid metabolism and cancer	214
6.2	Ether lipids and cancer	215

6.2.1	Ether lipids biosynthesis.....	216
6.2.2	AGPS crystal structure	216
6.2.3	AGPS and Cancer.....	218
6.3	Discovery and development of the first in class AGPS inhibitor	221
7	Development of Alkyl Glycerone Phosphate Synthase Inhibitors: Structure-Activity Relationship and Effects on Ether Lipids and Epithelial-Mesenchymal Transition in Cancer Cells.....	226
7.1	Research project	226
7.2	Results and discussion.....	227
7.2.1	Chemistry	227
7.2.2	ThermoFAD based screening of compounds 77a-q	230
7.2.3	Radioactivity assay of compounds 76, 77a-f, 77h-p.....	232
7.2.4	Three-dimensional structure of AGPS in complex with 77i	233
7.2.5	Effect of AGPS inhibitor 77i on ether lipids levels and on migration rate in 231MFP breast cancer cells.....	234
7.2.6	Compound 77i , but not its analogue 77p, increases E-cadherin and reduces Snail and Mmp2 expression in PC3 and MDA-MB231 cancer cells	234
7.3	Conclusions and future perspectives	238
7.4	Experimental section	240
7.4.1	Chemistry	240
7.4.2	Biochemical and crystallographic methods. Protein Production and Crystallization.	261
7.4.3	Cell based methods.....	261
	References.	264

PART 1: Epigenetics

1 Introduction (1)

1.1 Epigenetics.

The first scientific definition of epigenetics can be attributed to Conrad Waddington. In 1942, he defined epigenetics as “*the branch of biology which studies the casual interactions between genes and their products, which bring the phenotype into being*”.¹ We can better define epigenetics as the study of meiotically/mitotically heritable and potentially stable changes in gene expression that are not caused by alteration of the DNA sequence.² Thus, we can look at epigenetics as the bridge between the genotype and the phenotype, the factor that, according to the Waddington’s epigenetic landscape, drives what potentially can take several different ways, into a defined path. In these regards, epigenetics can explain how in a complex multicellular organism, even though all the cells have the same genome, they can stably differentiate and generate populations of cell with different identities.

To date, there are at least five different events known to contribute to the epigenetic regulation of gene expression. These events include: DNA methylation, histone tails post-translational modifications (PTMs), interchange between histone variants, non-coding RNAs, and nucleosome/chromatin remodeling.^{3,4}

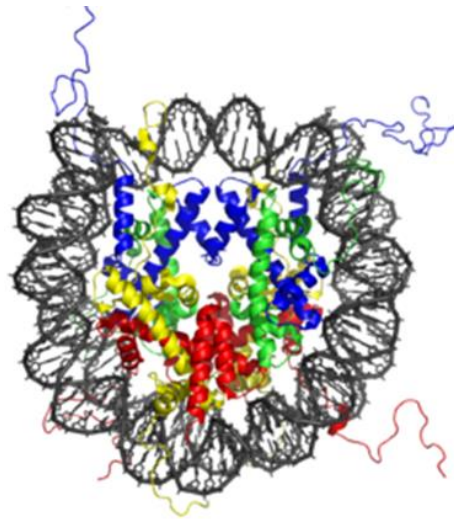


Figure 1.1. The crystal structure of the nucleosome core particle consisting of H2A , H2B , H3 and H4 core histones, and DNA. The view in this picture is from the top through the superhelical axis.

The nucleosome is defined as the fundamental unit of chromatin in eukaryotes. The nucleosome is composed by an octamer containing two copies of each of the four core histones (H2A, H2B, H3, and H4), around which are wrapped 147 DNA base pairs in 1.75 superhelical turns (Figure 1.1).⁵ The close interaction between DNA and histones in the nucleosome clearly explains how the latter can have a strong influence on DNA functions. Nucleosomes are highly dynamic. They can change their position sliding on the DNA,^{6,7} they can partially disassemble,⁸ and their

components can be replaced by histone variants.⁹ One could think that the nucleosome, and histones, have a mere physical role, hiding certain DNA regions from transcription factors, or influencing polymerase progression. However, this is not the sole effect related to the nucleosome-DNA interaction. In fact, the histone tails, protruding from the octamer, are object of numerous PTMs.¹⁰

Aberrant epigenetic mechanisms can drive to genetic mutations, and mutations in the epigenetic regulators cause alterations in the epigenome, leading to inappropriate genes, or signalling pathways activation or inhibition, resulting in a disease state.^{11,12} Interestingly, differently from genetic mutations, epigenetic aberrations are potentially reversible, and can be reverted to their normal state. These evidences encouraged the rise of epigenetic regulators as druggable targets in several disorders.

1.2 Writers, readers and erasers: the complex interplay of epigenetic players and the epigenetic code.

As previously mentioned, DNA methylation, histone tails post-translational modifications (PTMs), interchange between histone variants, non-coding RNAs, and nucleosome/chromatin remodeling, all contribute to define the epigenome of a single cell. Interestingly, none of the epigenetic marks is irreversible, and each of them can communicate a certain information, thus influencing the establishment of other marks, generating what is commonly known as epigenetic crosstalk. Practically, this is realized by the activity of the epigenetic players, that can be divided in writers, readers and erasers. We can define as writers all those enzymes able to impose an epigenetic mark on the chromatin. The erasers are those who remove the mark imposed by the writers, thus being responsible of the reversibility of the epigenetic modifications. The readers, finally, are those proteins or domains able to read the epigenetic code contained on the chromatin and convert it into an information. The interplay between writers, readers and erasers is quite complex, and all the epigenetic modifications are strictly related. An epigenetic mark can thus inhibit or induce the imposition of a second mark, or it can be read and activate secondary processes.

Even though much has been explored to date, there is still a lot to disclose in order to give an exhaustive picture of the epigenetic landscape.

1.3 The role of covalent histone modifications and chromatin remodeling.

Specific enzymes have been identified for acetylation,¹³ methylation,¹⁴ phosphorylation,¹⁵ ubiquitination,¹⁶ sumoylation,¹⁷ ADP-ribosylation,¹⁸ deamination,¹⁹ and proline isomerization.²⁰ Histone tails PTMs contribute to define a closed (heterochromatin) or opened state of the chromatin (euchromatin),^{21,22} and they generate a code able to recruit specific binding proteins which would, in turn, have an effect on chromatin structure and functions (Figure 1.2).^{23,24}

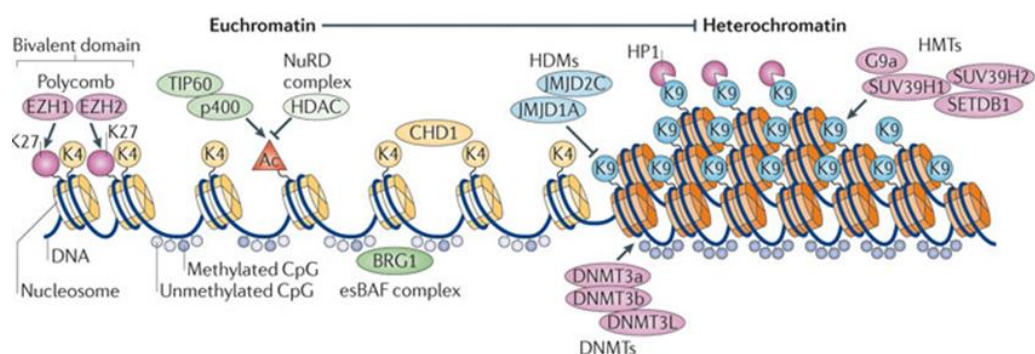


Figure 1.2. Euchromatin (transcriptional activation), and heterochromatin (transcriptional repression) and epigenetic control.

Additionally, chromatin remodelers contribute to positioning and restructuring nucleosomes.^{6,25-31} Interestingly, chromatin remodelers respond to cell stresses, and can be activated on demand to restore chromatin landscape.³¹⁻³³ The distribution of chromatin remodelers is finely regulated *in vivo*, and they have both distinct and redundant functionality.^{27,31,34} Recently, Lai *et al.* reviewed nucleosome dynamics and their effects on gene expression and DNA replication.³⁵ In this review, they underline how the study of nucleosome dynamics should be regarded as the study of genome regulation. The DNA accessibility of various proteins and their complexes is regulated by the interplay between nucleosome occupancy and positioning, affecting thus gene expression programs. A number of different regulatory factors operate in an independent or concerted manner to ensure that a certain organization and composition of nucleosome is maintained at specific genomic loci. The authors suggest that such dynamic and complex organization may be useful to enable the genome to adapt and respond to external stimuli, as well as to recover from chromatin-disruptive activities (such as replication and transcription).³⁵

1.4 Histone methylation.

One of the main PTMs occurring on histones is the methylation at the ϵ -amino group of lysine residues, or at the terminal guanidine group of arginines. The first evidence of protein lysine methylation was on a flagellin from *Salmonella typhimurium*,³⁶ while histone methylation was discovered only some years later.³⁷ Initially, protein methylation was believed to be irreversible. However, in 2004 after the discovery of the first demethylase (LSD1),³⁸ this process was regarded as reversible and dynamic, involved in the regulation of a variety of events.³⁹ Considering that methylation does not change the charge of lysine or arginine residue, it seems that its effect on chromatin structure is indirect. However, each methyl mark should be regarded as a signal that can be recognized by specific reader domains and lead to downstream effects. Histone methyltransferases, able to catalyse the methylation of specific aminoacids transferring activated methyl groups from the SAM co-substrate to the target residue, can be divided in two major types: lysine-specific (KMTs) and arginine-specific methyltransferases (PRMTs). The

lysine specific methyltransferases are the largest class, including 51 members.⁴ With the sole exception of DOT1L, all the KMTs are SET domain containing proteins. The SET domain itself contains the catalytic core. DOT1L contains a different catalytic domain, and for structure and sequence similarity is closer to PRMTs than KMTs.⁴ Nevertheless, all the KMTs have a similar catalytic mechanism, promoting the transfer of a methyl group from *S*-adenosyl-L-methionine (SAM) to the ϵ -amino group of lysine.⁴⁰ Much of what we know about lysine methylation derives from the study of chromatin and histone methylation, so that the enzymes catalyzing these reactions were first named histone lysine methyltransferases (HKMTs) and histone lysine demethylases (HKDMs), respectively.^{41,42} Subsequently, together with the growing body of evidence reporting that these enzymes have non-histone substrates, they were renamed as lysine methyltransferases (KMTs) and demethylases (KDMs). Lysine methylation can occur at three different levels (mono-, di-, and tri-methylation), having different outcomes depending on the differently recruited binding proteins (readers) able to recognize this mark. In contrast to acetylation, regarded exclusively as a gene activating PTM, histone lysine methylation can be associated both with gene activation or silencing, depending on the degree and location of the methylated residue. For example, di- and tri-methylation of H3K9, H3K27, and H4K20 are generally associated with gene silencing, whereas H3K4, H3K36, or H3K79 methylation is a mark of gene expression.^{41,43,44}

Protein arginine methyltransferases can be divided in three classes:

- Type I PRMTs (PRMT1, PRMT2, PRMT3, PRMT4, PRMT6, and PRMT8), are able to produce monomethyl arginine (MMA) and asymmetric dimethylarginine (ADMA) (dimethylation of one of the terminal guanidino nitrogens);
- Type II PRMTs (PRMT5 and PRMT9), able to produce MMA and symmetric dimethylarginine (SDMA) (monomethylation of both terminal guanidino nitrogens);
- Type III PRMT or PRMT7, is the only known PRMT able to produce only MMA.⁴⁵

As lysine methylation, also arginine histone methylation can favour or prevent the interaction of nuclear factors with other nearby histone marks.^{46,47} Arginine methylation can influence histone function either impairing the ability of arginine to form hydrogen bonds,⁴⁸ or recruiting specific reader-domain containing proteins.⁴⁹ Generally, histone SDMA is associated with transcriptional repression, while histone ADMA is related to gene expression.⁵⁰ Commonly methylated arginine residues include: H2AR3, H4R3, H3R8, and H3R2.⁵¹

In our research, we focused our attention on the lysine methyltransferase EZH2 and on the PRC2 complex.

1.5 The PRC2 complex.

First identified in the fruit fly *Drosophila melanogaster* as key repressive regulators of developmental genes (e.g. homeobox *HOX* genes),⁵² the polycomb group (PcG) proteins were later

proved to be highly evolutionary conserved, from unicellular organisms to humans.⁵³ PcG proteins, assembled in multiprotein polycomb repressive complexes (PRCs), control gene silencing mainly, but not only, through histone post-translational modifications (PTMs). Two main polycomb group complexes are described in mammals: polycomb repressive complex 1 (PRC1) and 2 (PRC2). Additionally, have been identified also the Phorepressive complex (PhoRC) and the Polycomb Repressive Deubiquitinase (PR-DUB).⁵⁴⁻⁵⁶ The PRCs possess histone modifying activities. PRC1 monoubiquitinates lysine 119 of histone 2A (H2A), and can compact chromatin by binding to nucleosomes, while PRC2 catalyzes up to tri-methylation of lysine 27 of the histone 3 (H3K27), a repressive chromatin mark.⁵⁶⁻⁵⁸ Interestingly, PRC1 has been shown to recognize and bind H3K27me3, and PRC2 is able to recognize H3K27me3 as well as H2AK119ub1.⁵⁹⁻⁶² In this way PRC1 and PRC2, being recruited at specific genomic loci, can cooperate in silencing gene expression.⁶³

The minimal PRC2 core complex, endowed with a catalytic activity, include the following subunits: Enhancer of Zeste Homologue 1 (EZH1) or Enhancer of Zeste Homologue 2 (EZH2), Suppressor of Zeste 12 (SUZ12), and Embryonic Ectoderm Development (EED). Additional protein subunits such as Retinoblastoma Associated protein 47 or 48 (RbAp46/48, also named RBBP4/7), Adipocyte Enhancer-Binding Protein 2 (AEBP2), Polycomb-like proteins (PCLs), and Jumonji and AT-Rich Interaction Domain 2 (JARID2) have been reported to play a role in the PRC2, modulating its activity in different contexts.⁶⁴ Many of these non-core subunits contain DNA or histone binding domains and can favor the recruitment of PRC2 to certain regions, and here promote H3K27 methylation.^{63,65-67} Since its discovery, there has been an intense research activity in trying to elucidate the PRC2 structure, in order to better explain its functions. Even though structural and biochemical data on individual subunits started to be available around 2007, the first structural study on the PRC2 complex was published only in 2012, when Ciferri *et al.* reported the first low resolution electron microscopy (EM) structure of the PRC2 complex bound to AEBP2.⁶⁸ Here, we will give an overview of the structure and functions of the diverse subunits, as well as of the PRC2. An updated review about PRC2 structure and functions has been recently published by Moritz and Trievel.⁶⁷

Not much is known about SUZ12. SUZ12 may be involved in chromatin silencing in association with the ncRNA HOTAIR, has suggested by the studies of Rinn *et al.*⁶⁹ The C-terminus of SUZ12 contains a Zinc-finger motif, that seems to be involved in ncRNA binding.

Much more is known about EED structure and functions. EED folds into a WD-repeat structure, containing seven copies of the WD-repeat motif forming the seven-bladed propeller structure. WD-domains act as scaffolding elements, thus they can bind many proteins and have different functions. The primary sequence of EED shares only 18 % identity with other WD-repeat proteins, nevertheless, structural comparisons show a good level of conservation of the WD-repeat domain.⁷⁰ In 2007, Han *et al.* first identified a minimal 30-residue (aa 39-68) motif of

EZH2 essential for EED binding, named as EED-binding-domain (EDB). In the same work, they also reported the crystal structure of mouse EED bound with an EDB peptide. The crystal structure showed that the EDB binds to the bottom of the WD-repeat domain. Interestingly, in this work, they demonstrated that the key residues for EZH-EED binding are conserved not only in EZH2 and EZH1, but also in the *Drosophila* homolog. Additionally, they have demonstrated how mutations in critical interaction residues, both in EED or EZH2, totally abolish the interaction.⁷⁰ Following studies by Margueron *et al.* further proved and defined the essential role of EED.⁷¹ They found that EED binds preferentially to histone methylated residues associated with gene silencing, and after crystal structure resolution, they were also able to explain the molecular basis of this selective recognition. Through kinetic studies, they also showed that EED binding to H3K27me3, but not to H3K27me1 or H3K27me2, stimulated PRC2 catalytic activity, thus proving the function of EED as a promoter of the propagation of repressive histone marks.⁷¹

1.5.1 PRC2 catalytic core (EZH1 and EZH2), and the importance of the complex.

The lysine methyltransferases EZH1 or EZH2 constitute the catalytic subunit of the PRC2 complex. They contain the conserved catalytic SET domain found in many other KMTs, and they both use *S*-adenosyl-L-methionine (SAM) as a co-substrate. Even though EZH1 and EZH2 possess a high sequence similarity, with 76 % overall identity and 96 % sequence identity in their catalytic SET domains, they exhibit different catalytic efficiencies, distinct chromatin binding properties, and expression patterns. EZH1 is expressed both in dividing and non-proliferative differentiated/adult cells, while EZH2 is only active in dividing cells.⁶⁴ Besides that, EZH1-containing PRC2 (PRC2-EZH1) displays lower methyltransferase activity than PRC2-EZH2.⁷² Several pieces of evidence suggest that PRC2-EZH2 should establish cellular H3K27me1/2/3 levels, while PRC2-EZH1 is involved in restoring H3K27me1/2/3 that could have been lost upon histone exchange or through demethylase activity.⁷² By themselves, EZH1 and EZH2 are not able to catalyze H3K27 methylation, but they require the co-presence of at least two other protein subunits in the complex: EED and SUZ12.⁷³⁻⁷⁵ EZH2 has been proved to have also PRC2-independent functions, being involved in the methylation of a number of non-histone substrates, such as the transcription factors GATA4 and PLZF.^{76,77} The non PRC2 activity of EZH2 could drive to transcriptional activation, rather than repression.⁷⁸ As all the other epigenetic marks, also H3K27 methylation is reversible due to the activity of the histone demethylases UTX and JMJD3.⁷⁹⁻⁸³

1.5.2 EZH2 SET domain structure

The crystal structure of the EZH2 SET-containing catalytic domain was resolved independently by two different groups in 2013.^{84,85} The crystal structure shows that the catalytic domain is typically folded as a SET domain methyltransferase in absence of binding partners. It contains two zinc binding domains at the N-terminal, each of them binding three zinc ions. The C-terminal

region is composed by the SET domain, with an inserted SET (iSET) motif and a C-terminal SET (cSET) motif following the SET domain. Remarkably, the isolated EZH2 SET-domain, differently from the isolated SET domains of many other methyltransferases, adopts a conformation that does not allow the binding of the co-substrate SAM and of the substrate (auto-inhibited), being thus unable to methylate its H3K27 substrate in the absence of protein interaction partners, EED and SUZ12. The authors proposed that the isolated SET domain acquires an auto-inhibited conformation, and the interactions with N-terminal regions of full length EZH2 and/or other PRC2 subunits induce conformational changes defining an active cofactor binding site.⁸⁵

1.5.3 PRC2 crystal structure

In 2015, Jiao and Liu reported the first crystal structure of an active PRC2 complex (170 kDa) from the yeast *Chaetomium thermophilum* (CtPRC2).⁸⁶ In this work, they show the structure of the PRC2 complex both in a basal and stimulated state. Interestingly, comparing the two structures, they noticed the presence of a mobile EZH2 motif being allosterically modulated and regulating active site accessibility.⁸⁶ Justin *et al.*, in 2016, solved the crystal structure of the stimulated state of a human PRC2 complex (HsPRC2), containing EZH2 and EED polypeptides with the Vefs fragment of the SUZ12 subunit, together with a SAH cofactor, and the two peptides JARID2-K116me3 peptide (a high affinity activator), and H3K27M peptide (based on the oncogenic histone H3 mutation, binding and inhibiting the SET domain) (Figure 1.3A).^{87,88} The reported complex is arranged to form a trilobated tri-dimensional structure, where the first two lobes have regulatory functions, and the third is involved in catalysis. The so-called N lobe is composed by EED and the N-terminal region of EZH2. The middle lobe includes SUZ12 Vefs and the MCSS and SANT2 domains of EZH2. Finally, the catalytic lobe comprises the pre-SET and SET domains of EZH2, and the N-terminus of the Vefs domain. A superimposition of the CtPRC2 and HsPRC2 revealed a surprising evolutionary conservation of the core complex, even though there are evident differences between the two crystal structures (Figure 1.3B). Additionally, the key interactions for the allosteric activation of the SET domain have been highlighted comparing the structures of the isolated SET domain and the HsPRC2 (Figure 1.3C). The most important difference resides in the cSET motif organisation. In fact, in the isolated SET domain, this motif is mostly disordered. Partially occupying the substrate binding pocket, it contributes to the auto-inhibited state. Conversely, in HsPRC2 the cSET motif is flipped out of the substrate cleft, thus being available for catalysis. More detailed information about the HsPRC2 crystal structure, as well as a deep investigation on the oncogenic inhibition of H3K27M, and on enhancement of the catalytic efficiency induced by binding of repressive marks, such as H3K27me3, to the EED subunit are also given in these papers.^{87,88}

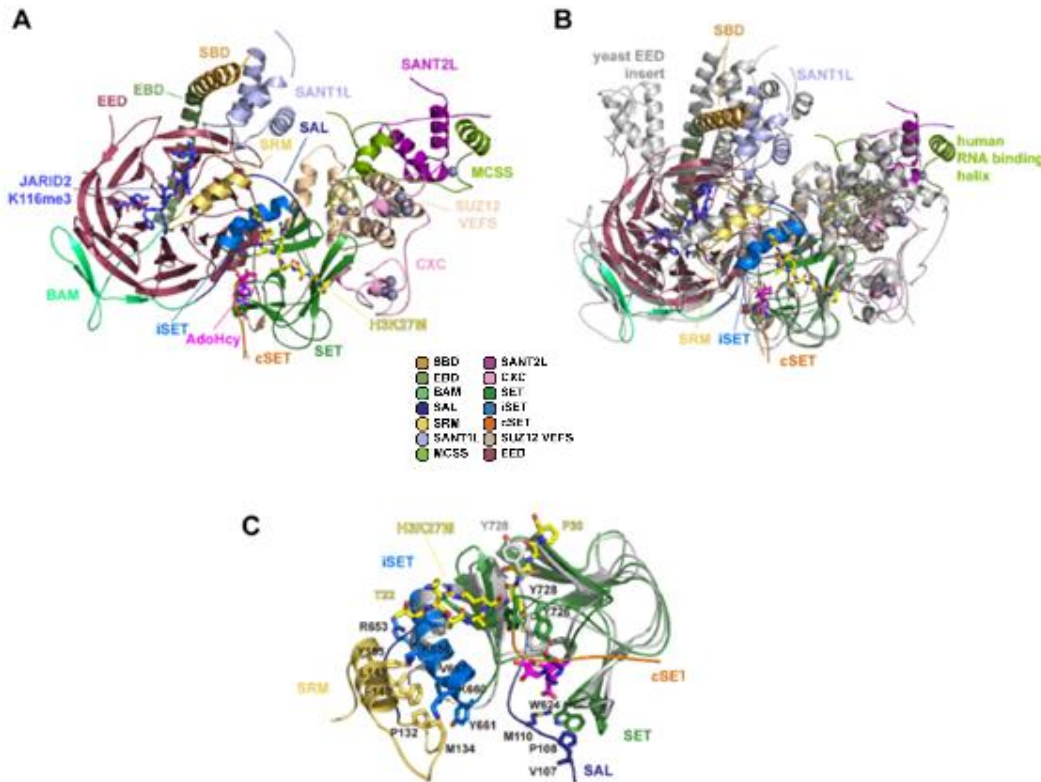


Figure 1.3. Structure and regulation of the HsPRC2 core complex. **A.** HsPRC2 in complex with JARID2K116me3 and H3K27M peptides and SAH (PDB: 5HYN). Proteins, domains, and motifs color code is included. Peptides and SAH are rendered as sticks, and Zn ions are depicted as spheres. **B.** Superimposition of the stimulated CtPRC2 complex (gray) and the stimulated human PRC2 complex (PDB codes 5KJH and 5HYN). **C.** Structural alignment of the isolated SET domain of EZH2 (gray) and the SAL, SRM, iSET, cSET, and SET domains of EZH2 in the HsPRC2 stimulated complex (PDB codes 4MI0 and 5HYN).⁶⁷

1.5.4 PRC2 interactome and target genes

The Polycomb complex is involved in the regulation of several different functions in addition to the *HOX* gene silencing, including X-chromosome inactivation, germline development, cell fate decision, cell cycle regulation, senescence, stem cell pluripotency and cancer metastasis.^{64,89} In humans, the self-renewal ability of embryonic and tissue-specific stem cells is maintained by the PRC2 activity, and its dynamic regulation is critical for proper development and differentiation.⁹⁰ EZH2 has been reported to be downstream of the cell cycle-regulatory retinoblastoma-E2F pathway, being thus implied in the expression of proliferative genes and for E2F-driven proliferation.⁹¹ The PRC2 complex is also involved in silencing of the *Ink4a/Arf* tumor suppressor locus, and EZH2 has been reported to be involved in silencing of *E-cadherin*, *FOXC1* and DNA-damage repair pathways, thus promoting oncogenesis (Figure 4).⁹²⁻⁹⁵ Several molecular mechanisms can modulate PRC2 activity with a tissue specific trend. First of all, the transcription of the different PRC2 subunits can be positively or negatively regulated by different proteins (e.g.

E2F, c-Myc)⁹⁶⁻⁹⁸ and transcription factors (e.g. pRb, p16).⁹¹ Furthermore, EZH2 is post-transcriptionally regulated by microRNAs (miR101, miR29, miR2014)⁹⁹ and can be a substrate of different kinases.¹⁰⁰ Finally, the PRC2 complex can be specifically recruited by certain factors as Twist1 or n-Myc (Figure 1.4).^{101,102}

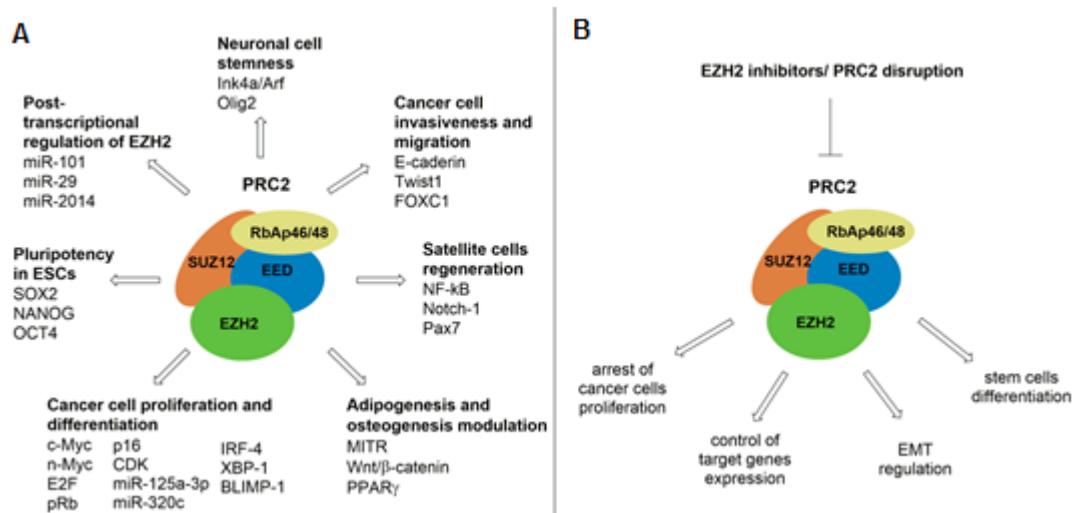


Figure 1.4. A. An overview on PRC2 interactome; **B.** Effects of EZH2 inhibition or PRC2 disruption. ¹⁰³

1.5.5 Relevance of EZH2 in cancer

The wide biological role of EZH2 and, specially, its deep involvement in the regulation of cell cycle progression, as well as its pivotal role in several cellular pathways well explains why its dysfunction is associated with several solid or hematological cancers. Several literature example show its dysregulation in cancers, as well as its involvement in stem cell maintenance and tumor development. ^{78,104,105} EZH2 overexpression has been related to an increase in H3K27me3, involved in the repression of tumor suppressor genes, ^{106,107} as well as to the establishment of specific methylation patterns driving a global epigenetic reprogramming. ¹⁰⁸ EZH2 overexpression in cancer was reported for the first time in prostate ¹⁰⁹ and breast ¹¹⁰ cancers. Its overexpression in prostate cancer was associated with aggressiveness and metastasis,¹⁰⁹ similarly in endometrial, melanoma and bladder cancer it correlated with invasiveness and poor outcome.^{91,109,111-113} Moreover, EZH2 ectopic expression in primary cells was correlated to proliferative advantage.⁹¹ However, it was found that the sole EZH2 overexpression is not sufficient to cause leukemia, but can prevent hematopoietic stem cells exhaustion. ¹¹⁴ Additionally, EZH2 *knock-in* leads to the development of myeloproliferative disorders in mice.¹¹⁵ Tanaka *et al.* found that EZH2 *knock-out* in the MLL-AF9 AML mouse model slowed leukemia progression *in vivo*, and compromised leukemia cell proliferation *in vitro*. ¹¹⁶ Conversely, a recent work by Vo *et al.* showed that, in a mouse model of Myc-driven group 3 medulloblastoma, EZH2 inactivation accelerated tumor initiation and progression. In particular they found that EZH2 normally represses Gfi1 proto-oncogene expression, but in case of EZH2 inactivation Gfi 1 is

overexpressed and collaborates with Myc, inducing tumor development.¹¹⁷ Even though EZH2 is involved in regulating the epithelial-mesenchymal transition (EMT), its role in this process is still debated. On the one hand, in laryngeal squamous cells carcinoma (LSCC), EZH2 is described to promote EMT through down-regulation of E-cadherin (Ca²⁺-dependent cell adhesion molecule E, Figure 1.4), and up-regulation of H3K27me3 *in vitro* and *in vivo*,¹¹⁸ on the other hand it was recently reported to maintain an epithelial phenotype in ovarian cancer cells.¹¹⁹ These evidences could also suggest a different role of EZH2 depending on the cell/cancer type. Recently, EZH2 was described as key regulator of multiple myeloma development through the regulation of different factors, including the oncogenes IRF-4, XBP-1, PRDM1/BLIMP-1 (also known as immune response regulators),¹²⁰⁻¹²³ and c-Myc, and the tumor suppressor microRNAs miR-125a-3p and miR-320c (Figure 1.4).¹²⁴

As previously mentioned, EZH2 has PRC2 independent functions, but also non-canonical functions, whose mechanism is not yet fully understood. However, also these unconventional activities seem to play a role in cancers. For example, in natural killer/T-cell lymphoma EZH2 acts as transcriptional activator. Its activity is methylation-independent, based on binding and activation of the CCND1 promoter.¹²⁵ Some examples of non-histone targets methylation in cancers are given by androgen receptor in prostate cancer,¹²⁶ and STAT3 in glioblastoma.¹²⁷

1.5.6 EZH2 mutations (gain or loss of function)

Activating or inactivating somatic EZH2 mutations and deletions have been found in 22 % of germinal-center diffuse large B-cell lymphomas, 7 % of follicular lymphomas, and 12–23 % of patients having myelodysplastic and myeloproliferative disorders. These mutations have been found within the SET domain, and include Y641F, Y641N, Y641S, Y641H, Y641C¹²⁸, A677G,¹²⁹ and A687V.¹³⁰ The Y641 mutations were originally reported to inactivate the catalytic activity of the PRC2 complex *in vitro*, which was in contrast with the hyper-methylated state reported in EZH2-mutated cancers. Further studies demonstrated that wild-type (WT) EZH2 preferentially mono-methylates H3K27, whereas the Y641 mutants display increased efficiency for H3K27 di- and tri-methylation. In fact, all the reported Y641 mutations are heterozygous, thus the mutant allele is always associated with a WT allele. Hence, Y641 mutant can cooperate with WT EZH2 to increase H3K27 methylation, reproducing a condition similar to EZH2 overexpression.¹³¹ In T-cell acute lymphoblastic leukemia, myeloproliferative disorders, and myeloid malignancies, have been recorded a number of missense, nonsense and frameshift *EZH2* heterozygous or homozygous mutations.¹³²⁻¹³⁴ These mutations have been associated with loss of methyltransferase activity, leading in particular cases to an enhancement of NOTCH1 or RUNX1 oncogenic signaling. These evidences suggest that also loss of EZH2 can contribute to tumor development. Even though there are a number of data about EZH2 mutations in hematological cancers, not much have been investigated about such mutations in solid cancers. In conclusion,

considering that both gain and loss of function EZH2 mutations have been reported in cancers, we could conclude that EZH2 behaves in turn as an oncogene or as an onco-suppressor, based on the context. However, in each situation a balanced EZH2 activity is required to keep homeostasis.

113

1.5.7 EZH2 in cancer and non-cancer cell stemness

The role of EZH2 in maintaining the self-renewal potential in adult and embryonic stem cells (ESC) has been pointed out by numerous studies. Already in 2006, it has been reported that PRC2 was able to maintain pluripotency in ESCs by targeting and repressing a special set of developmental genes (including OCT4, SOX2, NANOG, Figure 1.4), whose expression would promote differentiation.^{90,135} Both the PRCs are involved in a temporal and spatial control of epigenetic modifications in stem cells, repressing undesirable differentiation programs, while stepwise and selectively establishing a specific terminal differentiation program.¹³⁶ A recent study by Shan *et al.* provided new insights in the role played by EZH2/PRC2 in cell fate decision in ESC.¹³⁷ Interestingly, they have shown that PRC2 is differently required for maintaining pluripotency in ESC, being essential for the primed state ESC, but dispensable in naïve state cells. A direct correlation between ESC and poorly differentiated cancer cells has been established by a shared gene expression signature of PRC2 target genes.¹³⁸ Accordingly, EZH2 was found to be essential for the cancer stem cell formation and also for the expansion of an aggressive cancer stem cell population that promotes cancer progression.⁹⁴ In the light of the aforementioned findings, it is evident that EZH2 is primarily regarded as a target in cancer. However, EZH2 activity is also affecting hematopoietic stem cell proliferation and differentiation, thymopoiesis and lymphopoiesis.¹³⁹ Several studies also assessed EZH2 as regulator of T-cell differentiation and plasticity, as well as of the development of autoimmune diseases, and graft-versus-host disease (GVHD). These evidences suggest that modulation of histone methylation may have significant implications in the development of novel therapeutic strategies against GVHD or other T cell-mediated inflammatory disorders. These aspects have been recently well reviewed by Karantanos *et al.*¹³⁹

The capability of EZH2 to maintain the multipotent identity has been proved also in non-cancer adult stem cells, including muscle cell precursors (myoblasts)¹⁴⁰ and neural stem cells (NSCs).¹⁴¹ EZH2 overexpression in NSCs results in increasing oligodendrocytes and decreasing astrocytes differentiation.¹⁴¹ More recently, EZH2 has been reported to be essential for astroglial differentiation in adult mice by inhibition of *Ink4a (p16)/Arf (p19)* and *Olig2* (Figure 1.4).^{142,143} In contrast, EZH2 *knock-out* during mice cerebral development resulted in reduction of H3K27me3 level in cortical progenitor cells, and led to differentiation directly (into neurons), as well as indirectly (in the cerebral cortex).¹⁴³ Aberrant EZH2 expression has been found also in muscular disorders. For instance, in Duchenne muscular dystrophy increased amount of TNF- α

from myotubes inhibited the regenerative potential of satellite cells via epigenetic silencing of the Notch-1 signaling, by NF- κ B-stimulated recruitment of EZH2 and DNMT3b on *Notch1* gene promoter.¹⁴⁴ It has been shown that *Pax7* activation and satellite cells proliferation is promoted by pharmacological inhibition or genetic knockdown of either *p38a* kinase or EZH2, with subsequent muscles regeneration in dystrophic or normal mice.¹⁴⁵ Proliferation of β -cells in pancreatic islets plays a pivotal role in self-renewal and in adaptive islet expansion. In this context, EZH2 has been described to repress *Ink4a/Arf* in β -cells.¹⁴⁶ EZH2 induced *Ink4a* repression in young adult mice was sufficient to increase replication and regeneration of β -cells.¹⁴⁷ Additionally, EZH2 was found involved in osteogenesis and adipogenesis. Human mesenchymal stem cells (hMSCs) can be activated for osteogenesis, after EZH2 inactivation by cyclin-dependent kinase 1-mediated phosphorylation.¹⁴⁸ Dissociation of EZH2 from the promoter region of myocyte enhancer factor-2-interacting transcriptional repressor (*MITR*) gene resulted in its upregulation and association with PPAR γ 2, impairing its activity and preventing adipogenesis, while enhancing osteogenic differentiation from hMSCs.¹⁴⁹ In contrast, EZH2 was able to induce adipogenesis by disrupting the Wnt/ β -catenin signaling through direct binding to the promoters of *Wnt* genes to repress their expression.¹⁵⁰

1.5.8 PRC2 as a druggable target

In the light of these findings, EZH2 has been considered an attractive target for cancer therapy. In time, numerous research groups have developed catalytic SAM-competitive inhibitors of EZH2. After crystal structure resolution, it was also possible to better understand the structural elements required for EZH2 inhibition. However, for different reasons (selectivity, inhibition of PRC2 scaffolding activity, resistance development) researchers started to look also for PRC2 disruptors, thus protein-protein interaction inhibitors able to impair the PRC2-dependent activity of EZH2.

1.5.8.1 EZH2 inhibitors

An overview of the most widely reported EZH2 inhibitors is given in Figure 1.5. Recently, a broader view of patented EZH2 inhibitors have been given in two different reviews.^{103,151}

The carbocyclic adenosine analog 3-deazaneplanocin (DZNep, **1**, Figure 1.5), a derivative of the natural antibiotic neplanocin-A, has been one of the first small molecules to be tested as EZH2 inhibitor.¹⁵² By mechanism, DZNep is an *S*-adenosyl-L-homocysteine hydrolase inhibitor, blocking the methionine cycle and SAM regeneration, thus affecting all SAM-dependent processes. DZNep is thus an indirect and unselective inhibitor.¹⁵³ Despite that, it is currently under preclinical investigation for its relevant antitumor activity in various cancer types, associated with PRC2 inhibition and removal of H3K27me3 marks.¹⁵⁴ The poor PK and toxicological profile of DZNep¹⁵⁵ encouraged the development of novel, potent and selective inhibitors of EZH2. High-throughput biochemical screenings led to the development of SAM-

competitive catalytic EZH2 inhibitors, many of them containing a dimethylpyridone moiety. In 2012 Epizyme, Inc., USA reported EPZ005687 (**2**, Figure 1.5) as a potent, selective and SAM-competitive small-molecule inhibitor of EZH2 with a K_i of 24 nM.¹⁵⁶ Treatment with **2** in EZH2-WT, and Y641- or A677-mutant lymphoma cells, as well as in other cancer cell lines, including breast and prostate cancers, resulted in dose-dependent ablation of H3K27 methylation. Simultaneously, Glaxo Smith Kline (GSK), USA, via a high-throughput biochemical screening, followed by an extensive medicinal chemistry optimization, disclosed GSK126 (**3**, Figure 1.5), able to potently (K_i^{app} of 0.5–3 nM) and selectively inhibit WT and mutant EZH2. GSK126 markedly inhibits the growth of EZH2 mutant diffuse large B-cell lymphoma in xenograft mice,¹²⁹ and is currently being under evaluation in phase I clinical trials against various types of lymphoma.^{157,158} GSK343 (**4**, Figure 1.5) is another potent EZH2 inhibitor which, differently from GSK126, contains an indazole nucleus instead of an indole.¹⁵⁹ EI1 (**5**, Figure 1.5), a SAM-competitive inhibitor, is effective against WT and mutant EZH2, and displays > 10,000-fold selectivity for EZH2 over other methyltransferases, and 90-fold selectivity over EZH1. In cell-based studies, EI1 was reported to reduce H3K27 methylation levels and activate PRC2 target genes. Moreover, it was able to decrease proliferation and to induce cell cycle arrest and apoptosis in Y641 mutant large B-cell lymphoma.¹⁶⁰ Reported as the first orally bioavailable inhibitor in mice, UNC1999 (**6**, Figure 1.5) was a dual and highly selective inhibitor of WT and Y641 mutant EZH2, as well as of EZH1. Also **6** is a SAM-competitive inhibitor, able to reduce H3K27 methylation levels in cells and to induce apoptosis in Y641N mutant large B-cell lymphoma.¹⁶¹ Later, tazemetostat (EPZ6438, **7**, Figure 1.5) was developed by means of a follow up optimization of the Epyzime scaffold (EPZ005687, **2** Figure 1.5). It has greater potency and better PK profile than EPZ005687, including good oral bioavailability.¹⁶² Compound **7** recently entered the clinical arena and is currently studied for B-cell lymphoma, relapsed or refractory non-Hodgkin lymphoma¹⁶³, advanced solid tumors (Phase 1), diffuse large B-cell lymphoma (Phase 2), and follicular lymphoma (Phase 2).¹⁵⁷ A 2,2,6,6-tetramethylpiperidine-containing compound (**8**, Figure 1.5) was reported by Constellation Pharmaceuticals as a EZH2 inhibitor effective in KARPAS-422 lymphoma cells.¹⁶⁴ Nevertheless, because of its poor PK properties, **8** was not suitable for further *in vivo* evaluation. The indole-based compound CPI-360, first reported in 2015, showed a good activity profile in the biochemical assays as well as in a KARPAS-422 mouse xenograft model.¹⁶⁵ More recently, an optimization study on this compound led to the identification of **9** (CPI-1205, Figure 1.5), an highly potent (biochemical IC_{50} = 0.002 μ M, cellular EC_{50} = 0.032 μ M) and selective EZH2 inhibitor. Vaswani *et al.* also disclosed the co-crystal structure of **9** bound to the human PRC2 complex. This compound showed once again a potent antitumor activity in a KARPAS-422 mouse xenograft model. Compound **9** is currently in Phase I clinical trials for B-cell lymphoma treatment (Table 1).¹⁶⁶

compound could give selective EZH2 *versus* EZH1 inhibitors, or keep the simultaneous EZH1/2 inhibition.¹⁶⁸ Remarkably, even if the pyridone moiety was confirmed as important, it was demonstrated to be not sufficient for inhibitor binding.

Up to date, few EZH2 inhibitors are undergoing clinical trial studies as reported by Morera *et al.*¹⁵⁷ In Table 1 we give an updated summary.

1.5.8.2 PRC2 disruptors

EZH2 *knock-down* studies with siRNA and shRNA have been showing that EZH2 is crucial in many tumor types. However, small-molecules EZH2 inhibitors proved to be effective in a smaller range of cancers. One explanation that has been given for this phenomenon, is that with *knock-down* both catalytic and scaffolding activity of EZH2/PRC2 are affected, while classical EZH2 inhibitors target only the first.⁵⁰ On the other hand, considering that EZH2 has both PRC2 dependent and independent functions, we could think about selectively targeting the first. Thus, both issues suggest the need of targeting the PRC2 in an alternative way. Considering that it is a multiprotein complex, whose catalytic activity requires the assembly of a minimal core, targeting protein-protein interactions has been considered an interesting strategy to be applied. The first PRC2 disruptors to be described have been stabilized α -helix of EZH2 peptides (also called SAH-EZH2).^{169,170} SAH-EZH2 have been designed to be an EZH2-EED disruptors, and they have been shown to be effective in this way. SAH-EZH2 disrupted the EZH2-EED complex in a dose dependent way, reduced H3K27 methylation and EZH2 protein levels in cancer cell lines (MLL-AF9 leukemia).¹⁶⁹ High-throughput screenings led to the identification of the first small molecules EZH2-EED disruptors: astemizole (**10**, Figure 1.6), an old anti-histamine drug¹⁷¹ and wedelolactone (**11**, Figure 1.6), a natural compound.¹⁷² Between December 2016 and of March 2017, a series of publications proved the growing interest, and the huge effort done in developing EED-targeting agents as an alternative strategy to inhibit the PRC2 functions.¹⁷³⁻¹⁷⁸ In December 2016, Novartis reported the discovery of five structurally distinct EED binders (**12-16**, Figure 1.6), identified with a high-throughput screen using the PRC2 enzymatic assay as the primary screening assay.¹⁷³ Compounds **12-16** displayed low μ M activities against PRC2, with similar values in presence of EZH1 or EZH2, and they were quite selective in inhibition respect to other HMTs ($IC_{50} > 100 \mu$ M). These compounds were able to inhibit the H3K27me3-stimulated, and the basal PRC2 activity *in vitro*. The co-crystal structure of compounds **12-16** in complex with EED have been resolved, demonstrating a similar “induced fit” in the H3K27me3 pocket of EED. Significant conformational changes of particular residues have been studied in detail. Seems that the induced conformational changes lead to the formation of a deeper pocket as compared to the original aromatic cage found when H3K27me3 peptide is bound.¹⁷³ This work has been a new starting point for different medicinal chemistry projects aiming the development of novel PRC2

disruptors. Indeed, this work was followed by three other publications describing the subsequent development of some of the newly reported scaffolds.

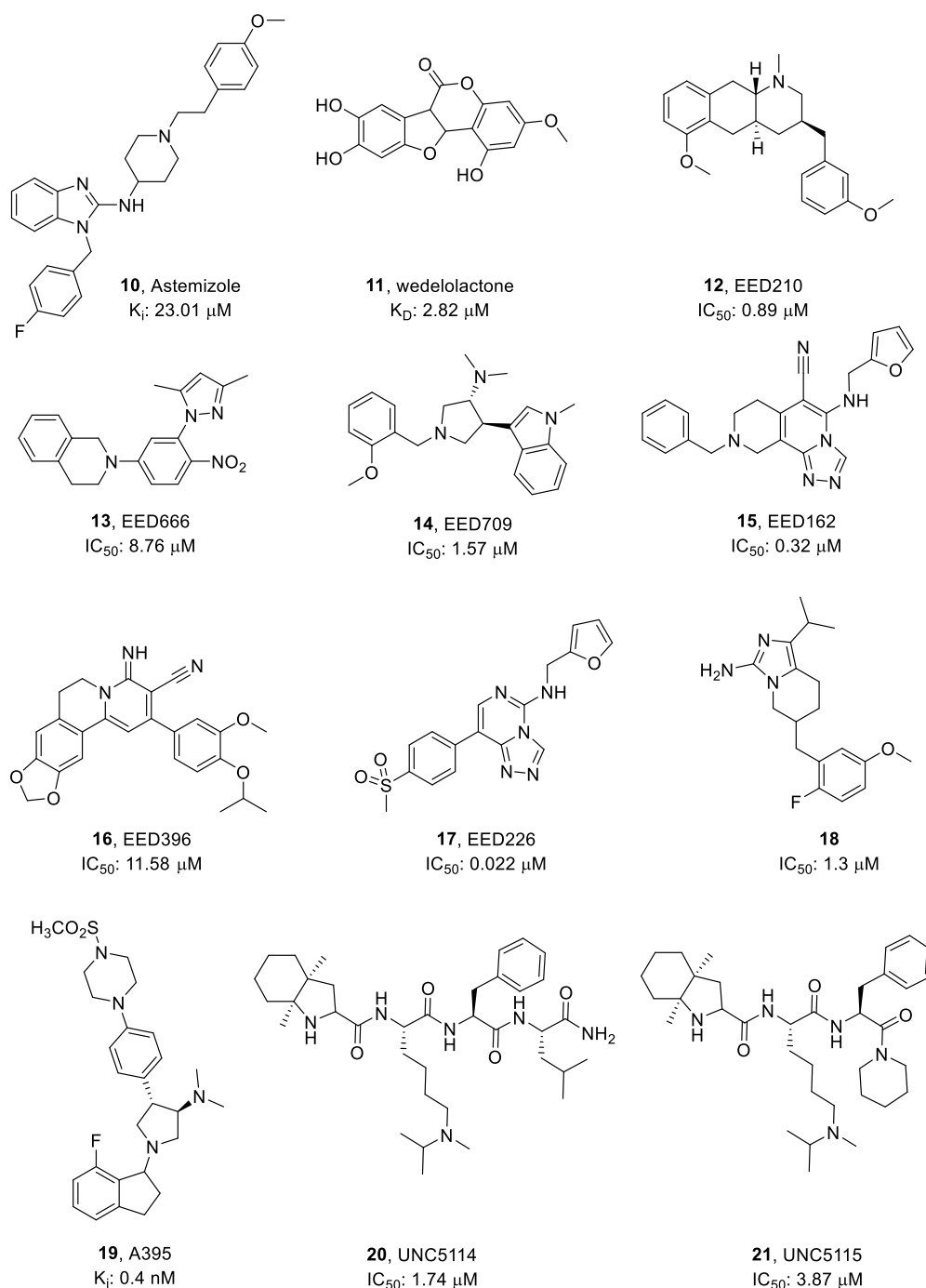


Figure 1.6. PRC2 disruptors and EED binders, an overview.

An optimization study of compound **15**, through X-ray crystallography guided fragmentation and regrowth, yielded compound **17** (EED226, Figure 1.6).¹⁷⁵ Compound **17** is a potent and selective PRC2-EZH2/PRC2-EZH1 inhibitor, notably reducing global H3K27me3 in cells, able to kill selectively cells with a heterozygous Y641N mutation. This compound showed optimal PK properties, encouraging and enabling extensive preclinical studies, demonstrating an optimal tolerability in various species, also inducing regression of tumor xenografts *in vivo*.¹⁷⁵ The

binding mode and mechanism of action of **17** were further investigated. The novel EED ligand binds to the H3K27me3 pocket of EED, thus confirming an allosteric mechanism different from those of the well-known SAM-competitors. It has been shown to modulate gene transcription in a similar way to the SAM-competitive EZH2 inhibitor. Notably, this compound is still effective in cell lines with acquired resistance to SAM-competitive EZH2 inhibitors, and shows a synergistic effect to inhibit cancer cell growth when combined with EZH2 inhibitors.¹⁷⁷ Applying the same deconstruction and regrowth strategy, the Novartis scientists also developed compound **18** from the HTS hit **12** (Figure 1.6). The optimization proceeded step by step, and the activity was validated in cell-based assays, showing a similar outcome than what observed after EZH2 inhibitor treatment. These data encouraged to improve also PKs. Even though some modification induced a loss in efficiency, this study furnished a number of interesting data on EED binders and their biological effect. Additionally, the obtained molecules can be still optimized and can serve as tool compounds to study the biology of EED-mediated inhibition of PRC2 activity.¹⁷⁴ In the same period, also AbbVie Inc. reported the identification of a novel potent and selective EED binder, compound **19** (A-395, Figure 1.6). It binds EED in the H3K27me3 binding pocket and inhibits H3K27 methylation *in vitro* via inhibition of PRC2 activation. It proved to be selective against a number of MTs and a panel of other methyl-lysine binding proteins. Compound **19** showed in cell activity, strongly reducing the H3K27 methylation, and inducing growth inhibition in cancer cell lines, and proved to be effective also in cell lines with acquired resistance to SAM-competitive EZH2 inhibitors. Finally, the novel AbbVie compound was efficacious in a diffuse large B-cell lymphoma (DLBCL) xenografted mouse model (using cell lines containing an activating heterozygous EZH2 A677G mutation).¹⁷⁶ Lastly, Barnash *et al.*, optimized a low affinity methylated Jarid2 peptide to give the first peptidomimetic EED ligands (**20** and **21**, UNC5114 and UNC5115, Figure 1.6), using a coupled combinatorial and structure-based design approach. The binding mode and the exact mechanism of PRC2 inhibition are not yet fully understood. It is sure, however, that the novel peptidomimetic binder is an allosteric inhibitor, targeting the methyl-lysine reader function.¹⁷⁸

Surprisingly, Novartis is already recruiting participants for a Phase I/II clinical trial (NCT02900651), with the aim to evaluate the EED inhibitor MAK683 (structure not disclosed) in patients with advanced malignancies, such as diffuse large B cell lymphoma, nasopharyngeal carcinoma and other advanced solid tumors (Table 1). These evidences suggest the PPI disruption as a valuable and alternative strategy for PRC2 targeting.

1.5.9 Not only EZH2: the rising of dual EZH1/EZH2 inhibitors and the polypharmacology

Respect to EZH2, the role and functions of EZH1 are not as broadly understood. However, in the last years there has been a growing interest in shading light on that. In 2015, Xu *et al.* reported

for the first time specific enzymatic dual inhibition of EZH2 and EZH1 as a promising therapeutic strategy for MLL-rearranged leukemia.¹⁷⁹ They show that the dual inhibitor UNC1999 (**6**, Figure 1.5) efficiently arrests cell proliferation of this type of leukemia *ex vivo* and *in vivo*, while the selective EZH2 inhibitor GSK126 (**3**, Figure 1.5) was not as effective. The importance of this study resides also in the fact that it raises the question around the possibility and the need of simultaneously targeting EZH1 and EZH2, and calls for deeper investigation about the still misty EZH1, its functions and its relation with EZH2.

Concerning EZH2 inhibition, an emerging issue is the drug resistance.^{78,180} Already in 2015, models of acquired resistance to the EZH2 inhibitor EI1 (**5**, Figure 1.5)¹⁶⁰ starting from EZH2-mutated lymphoma cells have been developed by Gibaja *et al.*. They have found two novel secondary mutations (Y111L and Y661D), being associated with resistance to EZH2 inhibitors.¹⁸⁰ Baude *et al.* have previously reported that loss-of function mutations altering the PRC2 subunits in malignant peripheral nerve sheath tumors (MPNSTs) can amplify Ras-driven transcription. Moreover, resistance to EZH2 inhibition was correlated to the co-presence of SWI-SNF mutations and alterations in the Ras-pathway.^{181,182} These findings have great implications for the clinical translation of EZH2 inhibitors and call for the development of novel tools to target the resistant EZH2 mutants. This question has been partially addressed by the novel EED binders, but still intriguing would be the investigation of a possible combination therapy between EZH2 inhibitors and other known or novel epi-drugs or standard drugs (polypharmacology).^{183,184} In the literature there are already some examples of combination therapy. Some examples are the combination of EPZ-6438 (**7** Figure 1.5, tazemetostat) with conventional NHL-directed chemotherapy in preclinical models of EZH2-mutant NHL,¹⁸⁵ or with prednisolone, a glucocorticoid receptor agonist (GRag), again in EZH2-mutant and in germinal-center NHL, or GSK126 (**3**, Figure 1.5) and etoposide association in prostate cancer.¹⁸⁶ Recently, the association of EZH2 inhibitors and IFN γ for cancer treatment was also the object of a patent (WO 2014077784), where the authors showed that EZH2 inhibition restores IFNGR1 expression and sensitizes MYC-dependent prostate cancer cells (DU145, PC3) to IFN γ treatment. Additionally, the combination of epigenetic drugs is also a valuable strategy, as suggested by several scientific evidences proving epigenetic crosstalk.¹⁸⁷ A recent study on glioblastoma brain tumor initiating cells (BTIC), showed first that the EZH2 inhibitor UNC1999 (**6**, Figure 1.5), displaying a cytotoxic activity in the low micromolar range in different BTIC, had also synergistic effects with dexamethasone. The combination of UNC1999 and dexamethasone efficiently suppressed tumour growth *in vivo*. Additionally, the authors also show that the combination of EZH2 and HDAC inhibitors had synergistic effects *in vitro* on the same cell lines, increasing apoptosis and inducing DNA damage.¹⁸⁸

Table 1. An overview on clinical trials on EZH2 inhibitors or PRC2 disruptors. Status (S): R= recruiting participants, A= Active, NR= not recruiting, T= terminated, NYR= not yet recruiting

Study	Phase	Trial number, start date	Disease(s)	Drug	Sponsor	S
An Open-Label, Multicenter, Phase 1/2 Study of E7438 (EZH2 Histone Methyl Transferase [HMT] Inhibitor) as a Single Agent in Subjects With Advanced Solid Tumors or With B-cell Lymphomas	I +II	NCT01897571 06/2013	B-cell lymphomas and advanced solid tumors	7	Epizyme, Inc.	R
A Study to Investigate the Safety, Pharmacokinetics, Pharmacodynamics and Clinical Activity of GSK2816126 in Subjects with Relapsed/Refractory Diffuse Large B Cell Lymphoma, Transformed Follicular Lymphoma, Other Non-Hodgkin's Lymphomas, Solid Tumors and Multiple Myeloma	I	NCT02082977 04/2014	Various types of lymphoma	3	Glaxo Smith Kline	T
A Study Evaluating CPI-1205 in Patients With B-Cell Lymphomas	I	NCT02395601 03/2015	B-Cell lymphoma	9	Constellation Pharmaceuticals	R
A Phase 1 Study of the EZH2 Inhibitor Tazemetostat in Pediatric Subjects With Relapsed or Refractory INI1-Negative Tumors or Synovial Sarcoma	I	NCT02601937 12/2015	Rhabdoid tumors, synovial sarcoma	7	Epizyme, Inc.	R
A Phase II, Multicenter Study of the EZH2 Inhibitor Tazemetostat in Adult Subjects With INI1-Negative Tumors or Relapsed/Refractory Synovial Sarcoma	II	NCT02601950 12/2015	Rhabdoid tumors, synovial sarcoma	7	Epizyme, Inc.	R
Study of the EZH2 Inhibitor Tazemetostat in Malignant Mesothelioma	II	NCT02860286 07/2016	Mesothelioma	7	Epizyme, Inc.	A, NR

Tazemetostat Rollover Study (TRuST): An Open-Label Rollover Study	II	NCT02875548 08/2016	Various types of lymphoma, malignant rhabdoid tumors, synovial sarcoma, epithelioid sarcoma, advanced solid tumors	7	Epizyme, Inc.	R
Safety and Efficacy of MAK683 in Adult Patients With Advanced Malignancies.	I+II	NCT02900651 10/2016	Diffuse Large B-cell lymphoma	MAK683	Novartis	R
Open-Label, Multi-Center, Two-Part, Ph1 Study to Characterize the PKs of an Intravenous Micro-Dose of [14C]-Tazemetostat (EPZ 6438) and the ADME of an Oral [14C]-Labeled Dose of Tazemetostat in Subjects With B-Cell Lymphomas or Adv Solid Tumors	I	NCT03010982 01/2017	Diffuse Large B Cell Lymphoma Primary Mediastinal Lymphoma Mantle-Cell Lymphoma Follicular Lymphoma Marginal Zone Lymphoma	7 and [14C]7	Epizyme, Inc.	R
Open-Label, Multicenter, Two-Part, Phase I Study to Characterize Effects of a Moderate CYP3A Inhibitor on PK of Tazemetostat, the Effects of Tazemetostat on PK of CYP2C8 and CYP2C19 Substrates, and the Effect of Increased Gastric pH on PK of Tazemetostat in B-cell Lymphoma Subjects	I	NCT03028103 03/2017	Diffuse Large B Cell Lymphoma Primary Mediastinal Lymphoma Mantle Cell Lymphoma	7	Epizyme, Inc.	R
Pediatric MATCH: Tazemetostat in Treating Patients With Relapsed or Refractory Advanced Solid Tumors, Non-Hodgkin Lymphoma, or Histiocytic Disorders With EZH2, SMARCB1, or SMARCA4 Gene Mutations	II	NCT03213665 07/2017	Tumors Harboring Alterations in EZH2 or Members of the SWI/SNF Complex	7	National Cancer Institute	R
Tazemetostat in Treating Patients With Metastatic or Unresectable Solid Tumors or B-Cell Lymphomas With Liver Dysfunction	I	NCT03217253, 03/2018	Metastatic or Unresectable Solid Tumors or B-Cell Lymphomas With Liver Dysfunction	7	National Cancer Institute	NYR

1.6 Histone acetylation

First discovered on histones in 1964,¹⁸⁹ protein lysine acetylation regards the lysine ϵ -amino group, and its overall occurrence is the result of the balanced activity of lysine acetyltransferases (HATs), and histone deacetylases (HDACs).^{190,191} HATs and HDACs mainly target lysines on N-terminal histones regions. Lysine acetylation is associated with a neutralization of the positive charge on ϵ -amino groups, thus impairing the DNA-histone interactions and leading to transcriptional activation (Figure 1.7). Histone acetylation, indeed, disrupt the ordered chromatin structure, and enhances access of transcription factors, transcriptional regulatory complexes, and RNA polymerases to promoter regions of DNA. Conversely, histone deacetylation (positively charged histones) is associated with transcriptional repression (Figure 1.7).^{192,193}

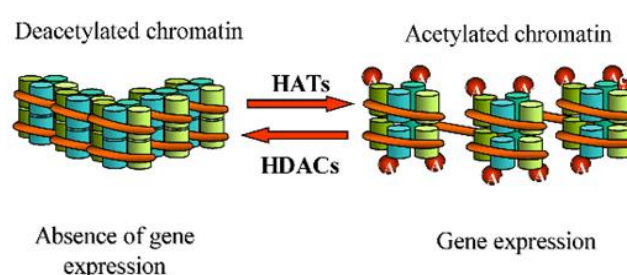


Figure 1.7. Histone acetylation neutralizes the positive charge on histone tails, directly affecting the chromatin status. In deacetylated chromatin, histone tails are positively charged and strongly associated with the negatively charged DNA backbone, leading to transcriptional silencing (heterochromatin); conversely, acetylated chromatin is more accessible and transcriptionally active (euchromatin).

HATs, using acetyl-CoA as acetyl group donor, are divided in four families, including the p300/CBP family, MYST family (TIP60, YBF2, MOZ, and MOF), GNAT family (PCAF and GCN5), and Rtt109 family.¹⁹² They have been studied for their role in gene transcription and regulation, and each of these enzymes have more than one lysine substrates, even though some specificity has been reported in some cases. Additionally, some HATs can acetylate also non-histone substrates, as for example p300/CBP is acetylating p53.¹⁹⁴ Concerning histone deacetylases, they have been divided in four classes. The class I, II and IV, the so called classical HDACs, are zinc dependent enzymes, while the class III or non-classical HDACs are NAD-dependent enzymes of the Sir family, also known as Sirtuins. Even though they are structurally different and use different mechanisms, both HDACs and Sirtuins can silence gene expression through deacetylation on specific promoters or chromosomal domains, and they can regulate other cellular processes by targeting non-histone proteins.^{192,195}

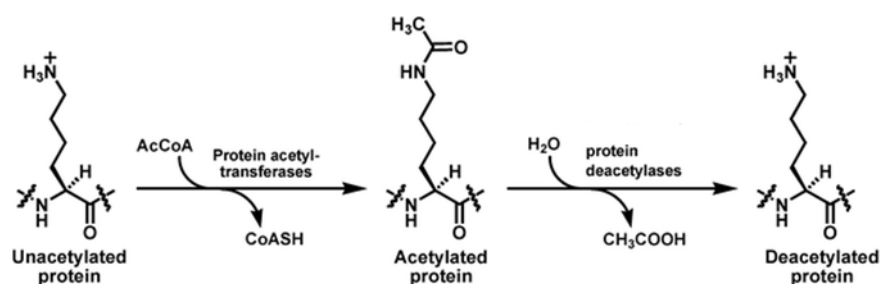


Figure 1.8. Acetylation/deacetylation reactions on lysine ϵ -amino groups.

1.7 Bromodomains

Bromodomains (BRDs) are the main acetyl-lysine readers. They are evolutionary conserved protein-protein interaction domains or modules. The first bromodomain-containing protein have been identified in *Drosophila melanogaster*, encoded in the *brahma* gene (from which the bromodomain name is derived).¹⁹⁶ More recently, also YEATS domains have been shown to bind acetylated lysines, in addition to the crotonylated ones.¹⁹⁷ In humans there are 61 known bromodomains, identified by a genome wide analysis, and they have been found in 46 different proteins. Based on sequence homology and structure similarity, the BRDs have been divided in 8 families (Figure 1.9).¹⁹⁸ BRD-containing proteins recognize acetylated histones and contribute to the regulation of gene expression in multiple ways. As nicely summarized by Fujisawa *et al.*, BRD-containing proteins can:

- act as scaffolds that facilitate the assembly of larger protein complexes;
- serve as transcription factors, or regulate transcription factors;
- have diverse catalytic functions (methyltransferases, acetyltransferases, helicases, chromatin remodelers), thus being directly involved in chromatin remodeling.¹⁹⁹

BRDs are expressed in various tissues, but their expression can vary, thus suggesting that it can be influenced by the context, thus reinforcing the idea of BRDs as key players in gene expression modulation.²⁰⁰ As BRDs play an important role in human cellular homeostasis, their dysregulated activity has been associated with several disorders, including neurological, inflammatory and cancerous diseases.²⁰¹⁻²⁰³

1.7.1 Bromodomains structure

BRDs are small (about 110 aa) and well conserved domains, whose structure was characterized more than 15 years ago.²⁰⁴⁻²⁰⁶ Each bromodomain module is typically composed by four α -helices (α_Z , α_A , α_B , α_C), linked by the ZA and the BC loops. The four α -helices form a small acetylated lysine binding pocket, typically containing hydrophobic amino acids, and an asparagine residue, present in most of the BRDs. This asparagine residue is essential for Kac binding. Indeed, the Kac forms a hydrogen bond with this asparagine residue. Additional hydrogen bonds are established with conserved water molecules in the binding pockets. All

BRDs, except PB1(5), contain four conserved water molecules in this pocket, and some of them contain also two additional water molecules in the ZA channel. The acetyl lysine binding mode has been proved to be conserved by several crystal structures of BRDs in complex with acetylated peptides. The charged surface surrounding the Kac binding pocket of the BRD module mediates the interactions with the rest of the acetylated peptide.¹⁹⁹ An exhaustive and updated review about bromodomains and their roles in health and disease is given by Fujisawa *et al.*¹⁹⁹

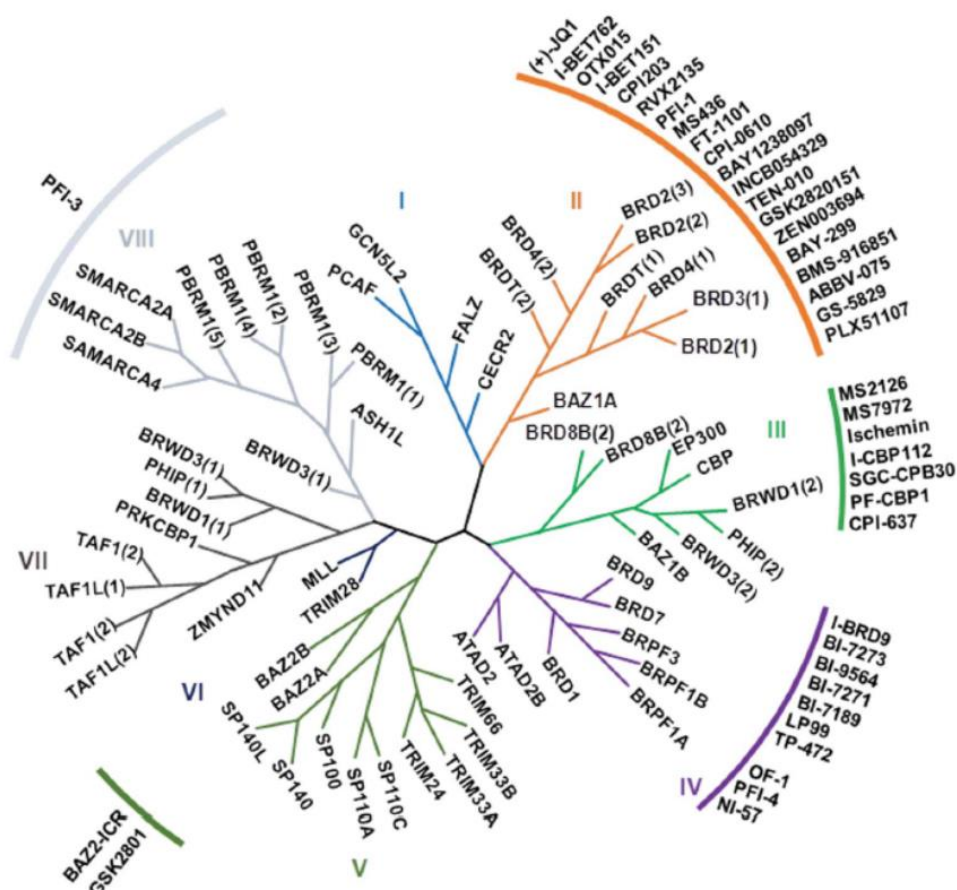


Figure 1.9. Structure-based phylogeny of the human bromodomains and their inhibitors. In humans there are 61 bromodomains found in 46 bromodomain-containing proteins. Roman numerals indicate the eight major structural classes. The phylogenetic tree is derived from data obtained Filipakoupoulos *et al.*,¹⁹⁸ as reported by Perez-Salvia and Esteller.²⁰⁷

1.7.2 The BET family and BRD4

One of the most studied and better known BRDs families is the bromodomain and extra terminal (BET) family. This family includes the ubiquitously expressed BRD2, BRD3 and BRD4, and the testis specific BRDT. The BETs share common structural organization, with a N-terminal composed by two bromodomains in tandem (BD1 and BD2), and an extra-terminal (ET) domain at the C-terminus.²⁰⁷ The BETs are involved in cell cycle regulation. BRD2 functions as a scaffold protein, able to recruit at chromatin level transcriptional cell cycle-regulatory genes as E2F1 and E2F2, and regulates the expression of other genes through interaction with the

SWI/SNIF complex. BRD4, instead, regulates genes involved in the M to early G1 phase transition.²⁰⁸⁻²¹¹ BRD4 is also an important and global regulator of gene transcription. Both BRD2 and BRD4 can recruit the positive transcription elongation factor complex (P-TEFb), and activate genes involved in cell proliferation.²¹² BRD4 has been also reported to be involved in the release of the active P-TEFb from its inactive complex with HEXIM1 protein and 7S snRNA. BET proteins are also involved in the regulation of cancer related genes such as c-MYC, thus being broadly involved in cancer development and progression. It has been found that BRD4 regulates NF- κ B dependent genes, preventing the degradation of RelA, that promotes NF- κ B activity.²¹⁰ In ER breast cancer, BRD3 and BRD4 contribute to tamoxifen resistance, being involved in the activation of ESR1 transcription through interaction with WHSC1.²⁰⁹

1.7.3 BRDs as druggable targets

BRD-containing proteins, have been found overexpressed in several diseases, including cancer and inflammatory diseases. These evidences, together with the key regulatory role of BRDs on cell cycle and cell proliferation, made bromodomains an attractive therapeutic target.²¹³ Even though, the BRDs binding domain is well known, and it makes it easier to target with small molecules, not all the BRDs are equally druggable. A computational analysis of all the 61 BRDs pointed out family I and II as easier to target.²¹⁴

The first BET inhibitors to be reported have been the benzodiazepine (+)-JQ1 (**21**, Figure 1.10)²¹⁵ and I-BET762 (**22**, Figure 1.10).²¹⁶ The discovery of these inhibitors contributed to assess the implication of BETs in several diseases, including first of all cancer, but also^{215,217-219} autoimmune disease,²²⁰ inflammation,²¹⁶ and viral infections including latent HIV-1 reactivation.

221

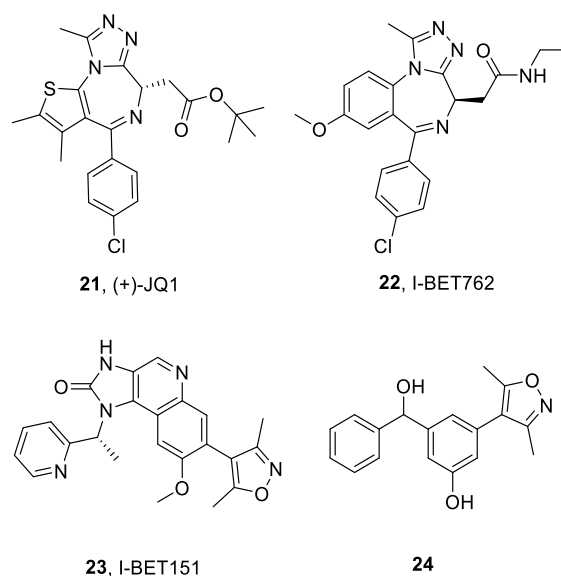


Figure 1.10. Some examples of BET inhibitors.

The growing number of evidences showing BET implication in such pathological states, fostered the research on development of small molecules BET inhibitors.²²² Among the novel developed compounds, many have been useful chemical tool to better explore phenotypes and understand the molecular role of BET inhibition. Additionally, some BET inhibitors, including I-BET762, entered the clinical arena for cancer indications, giving promising results.²⁰⁷

All the BET ligands so far developed contain a specific Kac mimic moiety. Romero *et al.* classified the BET inhibitors based on this moiety, thus dividing them in triazole, dimethylisoxazole, and pyridone-like containing molecules. Only a few compounds are not fitting these groups.²²² In the last years, have been published a number of reviews resembling the progress in development on BRDs inhibitors (Figure 1.10).^{207,222,223}

2 Design, synthesis and biological evaluation of novel pyrrole-based EZH2 inhibitors, displaying antiproliferative activity, cell cycle arrest, and H3K27me3 reduction in cancer cells, including glioblastoma primary cells

2.1 Research project

As part of our ongoing research on development of histone/protein methyltransferases inhibitors, we planned to work also on the development of EZH2 inhibitors. At the beginning of our work, only EZH2 inhibitors bearing a bicyclic heterocyclic (indazole, indole) central core were reported. We developed two projects in parallel: the design and development of pyrrole-based EZH2 inhibitors, and a second one on pyrazole-based EZH2 inhibitors. In this chapter, I will discuss about the design and development of pyrrole-based EZH2 inhibitors. This research project started with a molecular pruning of the known EZH2 inhibitor GSK126 (**3**, Figure 2.1). More in detail, we wanted to identify the required structural elements for inhibition activity, to this aim a molecular simplification approach was the most appropriate one. In a first attempt, we decided to keep fix the 4,6-dimethyl-3-methylamino-2-pyridinone moiety, crucial, even if not sufficient alone for the target binding.^{167,168} Importantly, the design of our molecular core was based on:

- replacement of the indole central core with a pyrrole;
- shifting of the 4,6-dimethyl-3-methylamino-2-pyridinone group from the C(4) indole to the C(3) pyrrole position, keeping an amide linker (Figure 2.1).

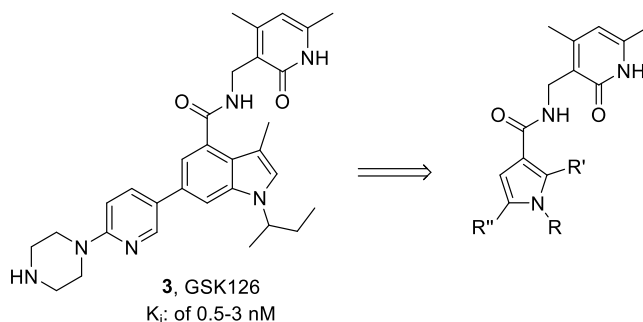


Figure 2.1. Design of novel pyrrole based EZH2 inhibitors.

We next started to explore how to best substitute the pyrrole ring, so to identify the minimal structure requisites for the target binding, and, in the meantime, increase the inhibition potency. First of all, we developed a small series of compounds aimed to investigate about the possible and most favored substitutions at the positions N(1), C(2) and C(5) of the pyrrole ring (Figure 2.2). Thus, we first kept fix a phenyl substituent at the N(1) of the pyrrole, and started to place one by one alkyl substituent groups in position C(2) and C(5) (Figure 2.2, chart 1). All the newly obtained derivatives have been tested in a biochemical assay using the PRC2 multicomponent protein in order to evaluate their inhibition activity. The obtained data suggested that the best

combination was the 2,5-dimethyl substitution (**25c**). Thus, keeping fix these substituents, we studied the effects of N(1) substitution (Figure 2.2, chart 2). Interestingly, compounds **25e-f**, bearing a free NH or only a small methyl group as substituent, displayed poor inhibition activity, but increasing the dimension of the substituent at the N(1), we observed a progressive increase in inhibition potency. Overall, in this first small series, **25c** was the most potent EZH2 inhibitor, and it became our lead for further optimization. We next evaluated the effects of an electrophilic substituent at the N(1) (Figure 2.2, chart 3), but none of the proposed modifications improved the activity, so that **25c** remained our lead compound. We investigated also about the replacement of the phenyl ring with nitrogen-containing heterocycles (Figure 2.2, chart 4).

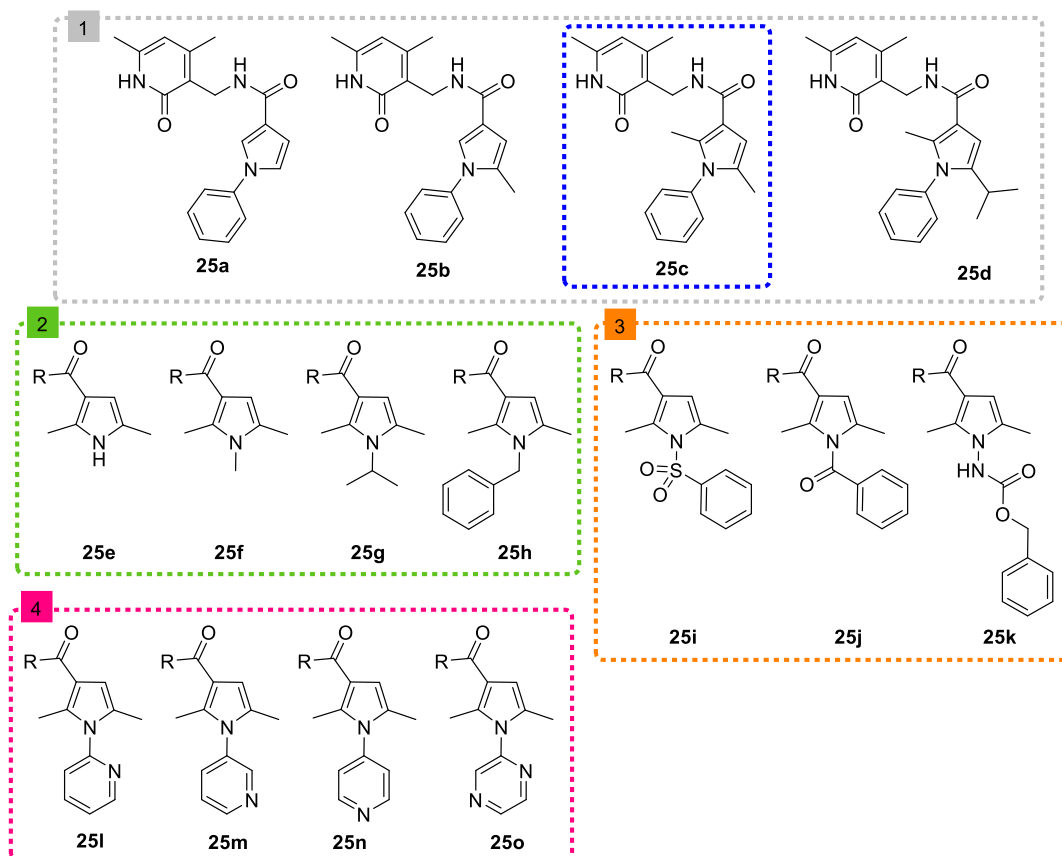


Figure 2.2. Development of novel pyrrole-based EZH2 inhibitors: molecular build up. Chart 1 and 2. Exploring various substitution at C(2), C(5), and N(1) position. Chart 3. Inserting electrophilic substituent at the N(1). Chart 4. Replacement of N1 phenyl ring with nitrogen containing heterocycles.

Even if, once again, none of these compounds showed a better activity than the lead **25c**, we could exploit interesting information for further molecular development. In particular, the enzymatic inhibition data suggested that exploring any substitution in the *meta* and *para* positions of the phenyl ring could be interesting. Prompted by these results, we designed and synthesized a large series of isomers, substituted in *meta* or *para* position with different electron withdrawing (EWG) or electron donating (EDG) groups (Figure 2.3, chart 5). Interestingly, in all

cases the *meta* substituted isomer was more potent than the *para* isomer. Indeed, we went on exploring a broader panel of *meta* substitutions (Figure 2.3, Chart 6).

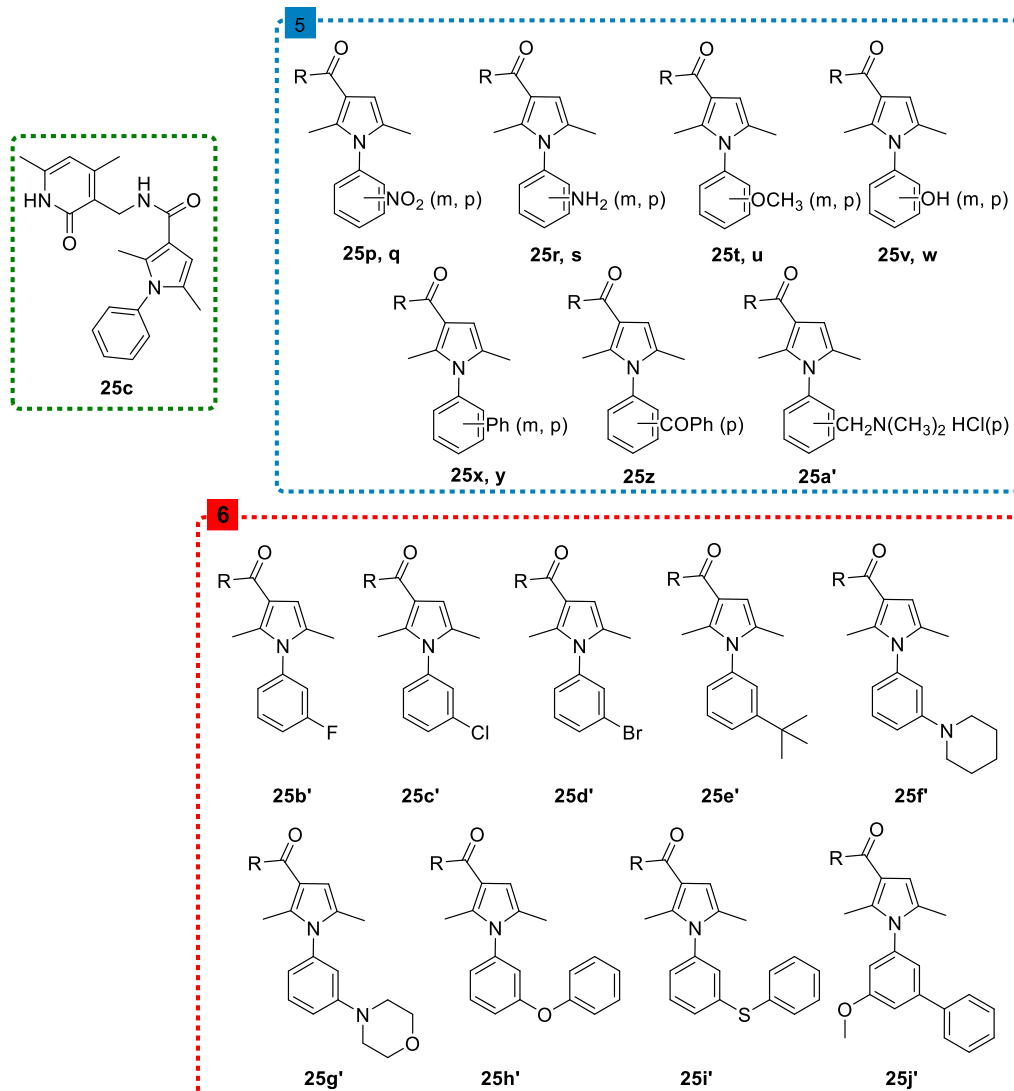


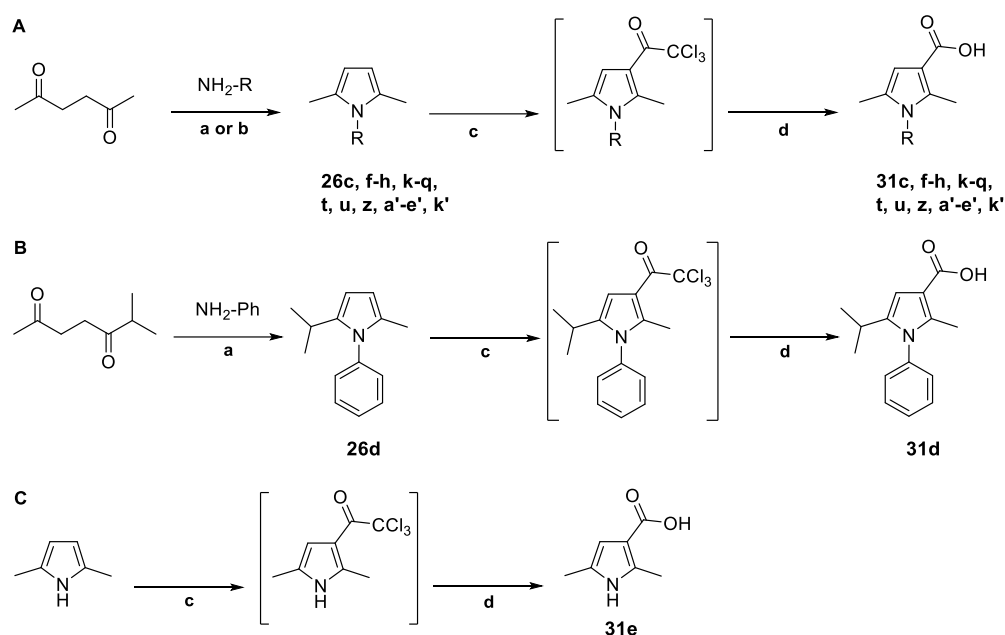
Figure 2.3. Further exploring the substitution on the phenyl ring. Chart 5. Study on various electron withdrawing (EWG) or electron donating (EDG) groups in *meta* or *para* position of the phenyl ring. Chart 6. Further exploring the *meta* substitution.

After a biochemical screening on all the synthesized compounds to evaluate their EZH2 inhibition activity, and selectivity, the most potent inhibitors have been screened in four cancer cell lines (U937, NB4, SHSY5Y, and MDA-MB231). In particular, we investigated on their effects on cell cycle progression, cell viability/apoptosis and H3K27 methylation levels. Compounds **25f'-g'** have been tested in primary glioblastoma cell lines, to evaluate their effects on cell proliferation and H3K27 methylation.

2.2 Results and discussion

2.2.1 Chemistry

The synthesis of the derivatives **25a-z** and **25a'-j'** started with the generation of differently substituted pyrroles through a Paal-Knorr reaction (Scheme 1). More in detail, for pyrroles **26c, f-h, t, u, z, a'-e', k'**, 2,5-hexanedione was reacted with the proper amine/aniline/hydrazine in presence of acetic acid (Scheme 1 A). In case of deactivated anilines (pyrroles **26k-q**), cobalt(II)chloride was used as catalyst (Scheme 1 A). For the synthesis of the pyrrole **26d**, 6-methyl-2,5-heptanedione, instead of 2,5-hexanedione, underwent Paal-Knorr reaction in presence of aniline and acetic acid (Scheme 1 B).

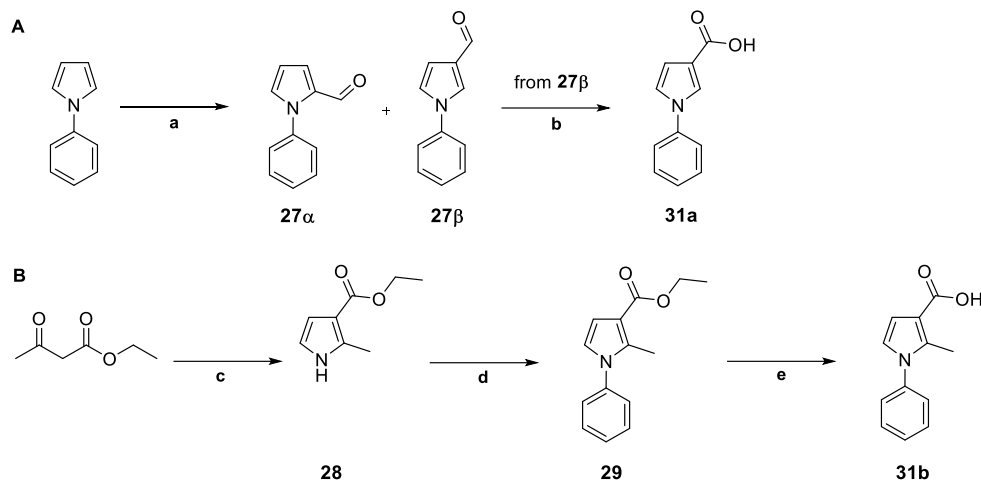


Scheme 1. Reagents and conditions: **a**) glacial CH_3COOH , sealed tube, 100 °C, 1.5 h (35-80 %); **b**) glacial CH_3COOH , $\text{CoCl}_2 \times 6 \text{H}_2\text{O}$, sealed tube, 100 °C, 1h (65-78 %); **c**) trichloroacetyl chloride, dry DCE, sealed tube, 0 °C to 70 °C, 1 h; **d**) I. 2 N KOH (aq), EtOH, r.t. to 60 °C; II. 2 N HCl (aq) (54-73 %).

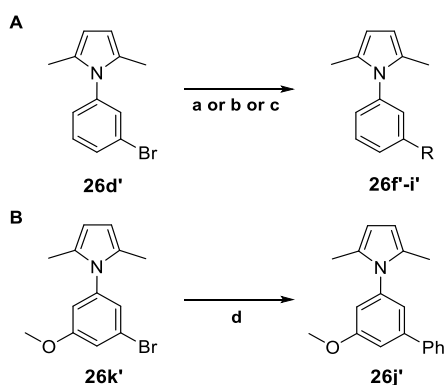
The pyrroles **26c-h, k-q, t, u, z, a'-j'**, and the commercially available 2,5-dimethyl-1H-pyrrole were then involved in a Friedel-Craft acylation in presence of trichloroacetyl chloride to give the corresponding trichloroacetyl derivatives. These intermediates were not isolated, but directly converted in the corresponding carboxylic acids **31c-h, k-q, t, u, z, a'-j'** (Scheme 1).

In order to obtain compound **31a** (Scheme 2 A), 1-phenyl-1H-pyrrole was formylated in presence of oxalyl chloride and *N,N*-dimethylformamide to give a mixture of the α and β formyl derivatives **27 α** , **β** with an overall 80 % yield, being the β formyl derivative 40 % with respect to the other isomer. The aldehyde intermediate **27 β** , was then oxidized in presence of silver nitrate in basic media (Scheme 2 A). The synthesis of the intermediate **31b** proceeded as reported in Scheme 2 B. A reaction between ethyl acetoacetate and 2-chloroacetaldehyde in presence of 17 N aqueous ammonia yielded ethyl 2-methyl-1H-pyrrole-3-carboxylate (**28**). Compound **28** was

involved in an Ullman-like reaction with iodobenzene, giving **29** in 94 % yield. The ethyl ester was hydrolyzed in basic conditions to give the acid **31b**.



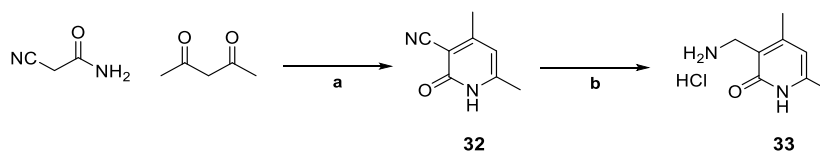
Scheme 2. Reagents and conditions: **a**) I. dry DMF, oxalyl chloride, dry DCE, 0 °C, 15 min; II. 1-phenyl-1H-pyrrole, 2 h ($\alpha + \beta$ 80 %, β 32 %); **b**) I. AgNO₃, 6 N NaOH, MeOH, reflux, 6 h; II. 2 N HCl (aq) (62 %); **c**) 2-chloroacetaldehyde, 17 N NH₃ (aq) (32 %); **d**) iodobenzene, K₃PO₄, N,N'-dimethylethylenediamine, CuI, sealed tube, N₂, 130 °C, 5 h (94 %); **e**) 2 N KOH (aq), EtOH, 70 °C, 18 h (95 %).



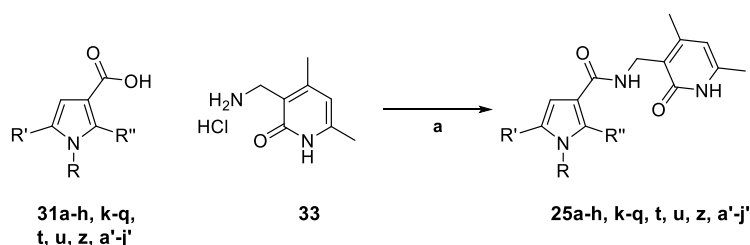
Scheme 3. Reagents and conditions: **a**) piperidine (for **26f'**) or morpholine (for **26g'**), Pd(OAc)₂, PH(tBu)BF₄, KOtBu, dry toluene, sealed tube, N₂, 80 °C, 4 h (76-80 %); **b**) Phenol, Cs₂CO₃, CuI, N,N'-dimethylglycine hydrochloride, dry dioxane, sealed tube, N₂, 90 °C, 48 h (63 %) (for **26h'**); **c**) Tiophenol, Pd₂(dba)₃, xantphos, K₂CO₃, dry *o*-xylene, N₂, reflux, 20 h (97 %) (for **26i'**); **d**) phenylboronic acid, 2 M Na₂CO₃ (aq), Pd(Ph₃P)₄, toluene/ethanol, sealed tube, 100 °C, 8 h (75 %).

The pyrroles intermediates **26f'-i'** were obtained starting from the 1-(3-bromophenyl)-2,5-dimethyl-1H-pyrrole (**26d'**, Scheme 3 A). More in detail, a palladium-catalysed C-N bond formation gave the piperidin (**26f'**) and morpholine (**26g'**) substituted derivatives in good yields.²²⁴ The reaction between **26d'** and phenol in Ullman-like conditions yielded the 3-phenoxy substituted compound **26h'**.²²⁵ Reacting the tiophenol in the same conditions did not yield the expected product. Nonetheless, the 3-phenyltio analogue **26i'** was obtained in 97 % yield through

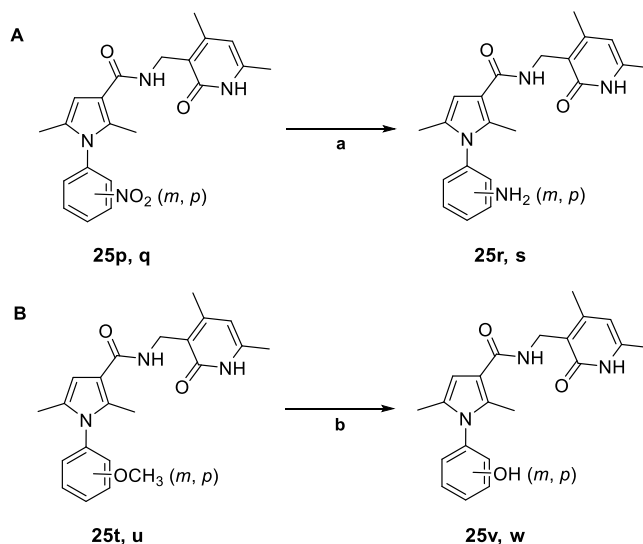
a $\text{Pd}_2(\text{dba})_3/\text{Xantphos}$ catalyzed Buchwald-Hartwig cross-coupling reaction.²²⁶ The *meta* bis-substituted compound **26j'** was obtained reacting the 1-(3-bromo-5-methoxyphenyl)-2,5-dimethyl-1H-pyrrole (**26k'**) with phenylboronic acid in the Suzuki-coupling conditions (Scheme 3 B). The synthesis of the amine **33** was carried following the reported literature procedure.¹⁵⁹ We started with a condensation of 2-cianoacetamide and 2,4-pentanedione to give the intermediate **32** that was hydrogenated by using 10 % palladium on carbon and platinum(IV)oxide as catalysts and then salified by hydrochloric acid (Scheme 4).



Scheme 4. Reagents and conditions: **a**) piperidine, EtOH, 70 °C, 3 h (43 %); **b**) I. H_2 (70 psi), 10 % Pd/C, PtO_2 , CH_3COOH , 40 °C; II. 2 N HCl (aq), EtOH.



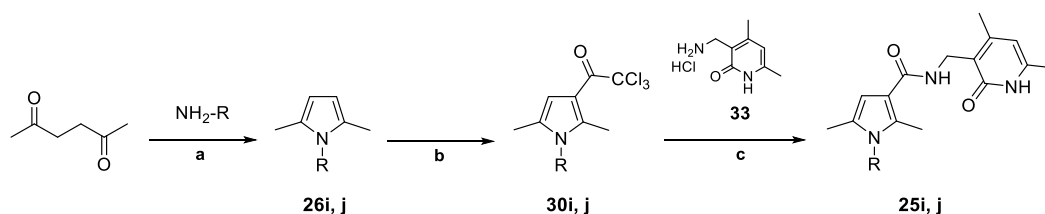
Scheme 5. Reagents and conditions: **a**) triethylamine, O-(benzotriazole-1-yl)-*N,N,N',N'*-tetramethyluronium tetrafluoroborate (TBTU), dry DMF, N_2 , r. t., 4 h (52-75 %).



Scheme 6. Reagents and conditions: **a**) $\text{SnCl}_2 \times 2 \text{H}_2\text{O}$, 37 % HCl (cat.), MeOH, 0 °C to r. t., 30 h (44-52 %); **b**) 1M BBr_3 in DCM, dry DCM, N_2 , -78 °C to r. t., 4 h (54-90 %).

The coupling between the acids **31a-h, k-q, t, u, z, a'-j'**, activated with O-(benzotriazole-1-yl)-*N,N,N',N'*-tetramethyluronium tetrafluoroborate (TBTU) in presence of triethylamine, and the amine **33** yielded the final compounds **25a-h, k-q, t, u, z, a'-j'** (Scheme 5). The final anilines

25r, s were obtained by reduction of the corresponding nitro-derivatives **25p, q** in presence of tin(II)chloride (Scheme 6 A). Whereas, the O-demethylation of compounds **25t, u** in presence of boron tribromide gave the final compounds **25v, w** (Scheme 6 B). The synthesis of the final compounds **25i, j** proceeded similarly to what already observed for the other derivatives. However, in these cases, the trichloroacetyl intermediates **30i, j** were isolated and directly involved in a coupling with the amine **33** (Scheme 7).



Scheme 7. Reagents and conditions: **a**) glacial CH_3COOH , $\text{CoCl}_2 \times 6 \text{H}_2\text{O}$, sealed tube, 100°C , 1 h (21-38 %); **b**) trichloroacetyl chloride, dry DCE, sealed tube, 0°C to 70°C , 1 h (30-41 %); **c**) triethylamine, dry CH_3CN , 20 h (56-63 %).

2.2.2 Biochemical EZH2 enzymatic inhibition assay and structure activity relationship (SAR)

All the new synthesized compounds have been first screened in an *in vitro* enzymatic assay to evaluate their ability to inhibit EZH2 catalytic activity. More in detail, compounds **25a-z**, **a'-j'** have been tested against a human five component PRC2 complex, containing EZH2, EED, SUZ12, RbAp48, and AEBP2. The assay was performed using Core Histone as substrate and ^3H -SAM as co-substrate. SAH and GSK126 (**3**, Figure 2.1) were used as reference compounds (SAH IC_{50} 34.7 μM , **3** IC_{50} 0.009 μM). Compounds **25a-z**, **a'-j'** have been initially screened at two fixed doses (100 μM and 50 μM). Selected compounds have been further tested in a dose range (10 points) to determine their IC_{50} .

The biochemical screening revealed a surprisingly structure activity relationship (SAR) that guided us through all the structure optimization steps. As already mentioned, our study started as a molecular simplification of the scaffold of **3**. The first set of molecules we designed, aimed to define the minimal required substituents at the positions N(1), C(2) and C(5) of the pyrrole core. We first investigated about the effects of the substitution at the positions C(2) and C(5) of the pyrrole. Interestingly, the insertion of methyl groups substituents in these positions progressively improved the inhibition potency (**25a-c**, Figure 2.4). However, the replacement of one of the two methyl groups with a branched isopropyl was not well tolerated (**25d**, Figure 2.4).

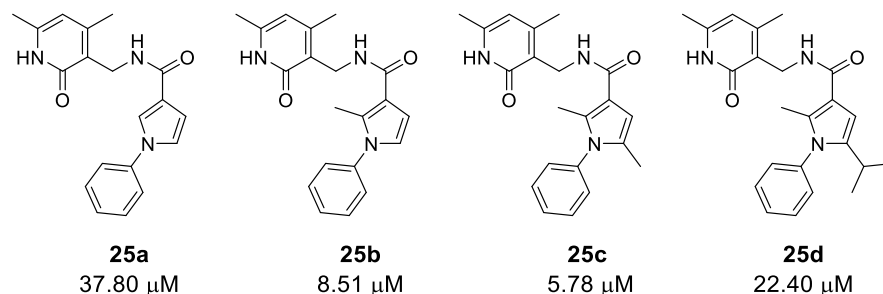


Figure 2.4. IC_{50} data for compounds **25a-d**: 2,5-dimethyl substitution on the pyrrole core is the most favored. The removal of one or both methyl groups, or the replacement of one of them with a branched alkyl group caused a drop in inhibition activity.

Thus, we decided to keep fix the 2,5-dimethyl substitution on the pyrrole core and explore the effects of different substituents at the N(1) (**25c**, **25e-h**, Figure 2.5). A free NH (**25e**) or a small alkyl group substituent (**25f**) were not tolerated, causing nearly a complete lost in activity. The insertion of an isopropyl (**25g**), still aliphatic, but bulkier was tolerated, whereas a N-benzyl substitution (**25h**) further increased the potency of inhibition. Nonetheless, the most potent compound was still **25c**, where the aromatic ring was directly bound to the pyrrole N(1) (Figure 2.5). Prompted by these results, we continued the exploration of this scaffold evaluating the effects of an electrophilic substituent at the N(1) (**25i-k**, Figure 2.6).

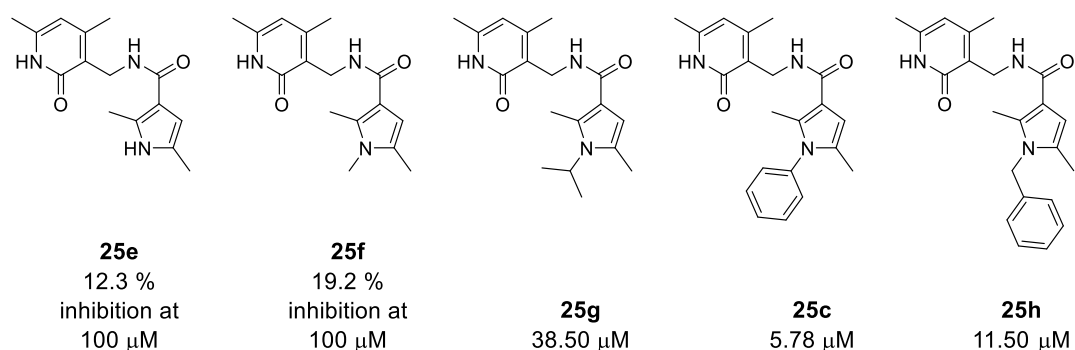


Figure 2.5. IC_{50} data for compounds **25e-f**: keeping fix the 2,5-dimethyl substitution, a free NH or a methyl group at the position N(1) of the pyrrole determined a nearly complete loss in activity. A more branched alkyl group (isopropyl) was better tolerated, as well as a benzyl substituent, even though the highest potency of inhibition was still observed with an aromatic group directly bounded to the pyrrole N(1).

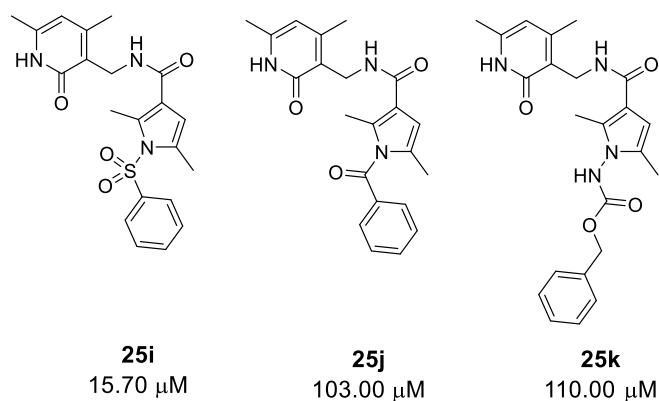


Figure 2.6. IC_{50} data for compounds **25i-k**: an electrophilic substituent at the N(1) did not increase the inhibition potency when compared **25c**.

No one of the substituent that we evaluated was able to increase the inhibition potency when compared to **25c**, that remained our lead. It is worth to notice that only the phenylsulfonyl-substituted compound (**25i**) displayed an activity in the 10^1 μ M range (IC_{50} 15.70 μ M), being thus 10 folds more potent than **25j**, **k** (Figure 2.6).

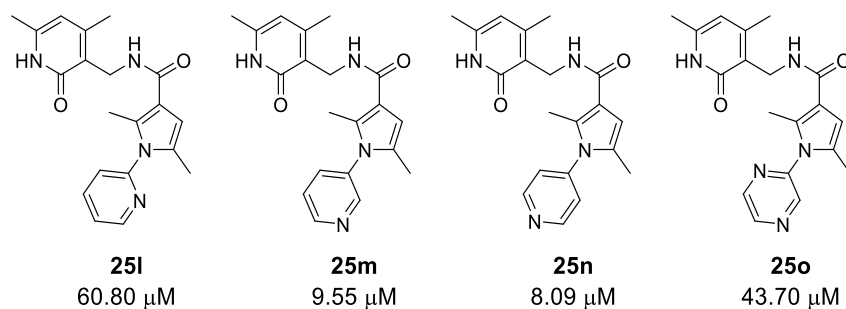


Figure 2.7. IC_{50} data for compounds **25l-o**: the *meta* or *para* position of the phenyl ring of MC3707 are the most interesting to explore for further substitution.

Next, in a small series of derivatives the phenyl ring was replaced with nitrogen-containing heterocycles, a regioisomeric study providing interesting data for the design of new compounds (**25l-o**, Figure 2.7). In particular, only compounds **25m** and **25n**, respectively a pyridine-3-yl and a pyridine-4-yl substituted derivatives, showed an inhibition potency similar to the lead compound (IC_{50} of 9.55 μ M and 8.09 μ M respectively, Figure 2.7). The pyridine-2-yl substitution (**25l**, IC_{50} 60.80 μ M) seemed particularly disfavored, suggesting that there could be a larger chemical space to target and additional contact points around the C(3) and C(4) positions of the phenyl ring (Figure 2.7).

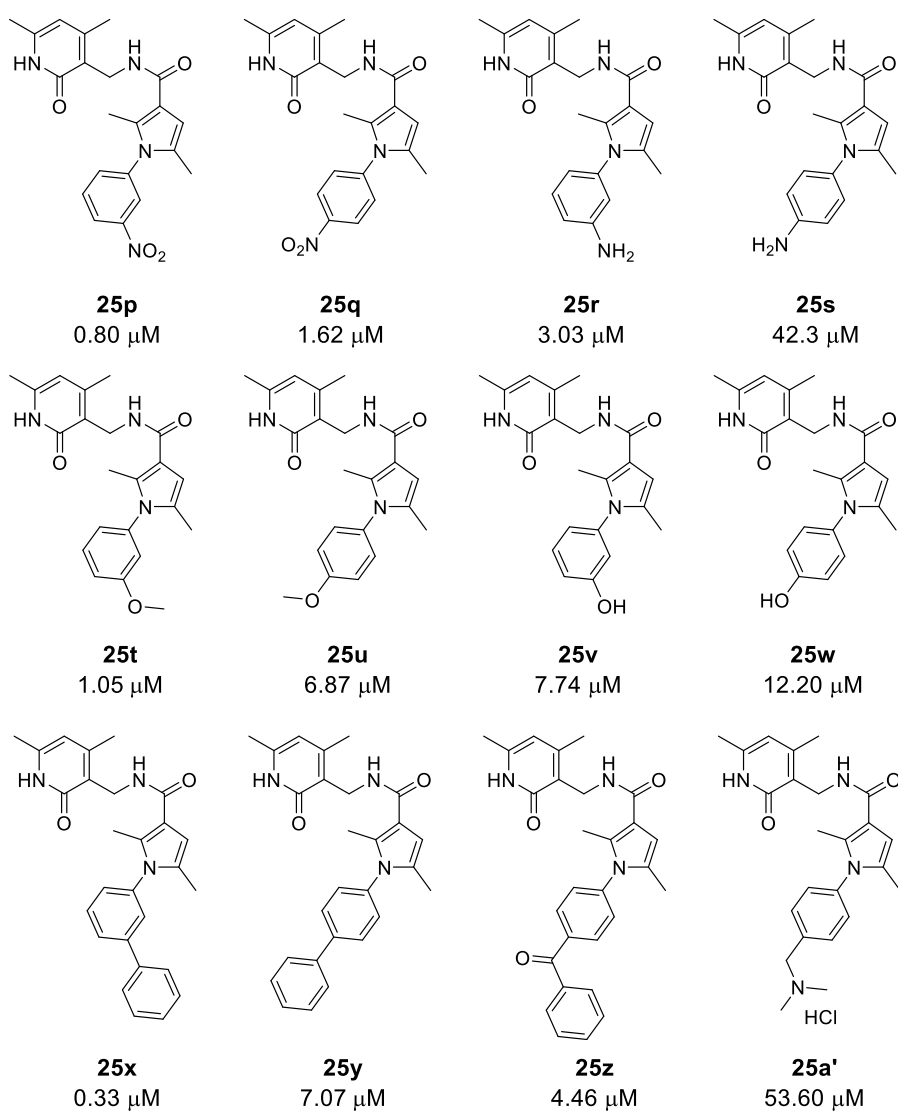


Figure 2.8. IC_{50} data for compounds **25p-z**, **25a'**: exploring the *meta* or *para* substitution on the phenyl ring of **25c**. The *meta* substituted derivatives were always more potent than the *para* isomers regardless the EW or ED nature of the substituent.

In light of these data, we thought that any additional functionalization, aimed to improve the binding potency and thus the inhibition activity, should occur preferably in the *meta* or *para* position of the phenyl ring of our lead **25c**. Therefore, we next synthesized and screened a large

series of isomers, substituted in *meta* or *para* position with different electron withdrawing (EWG) or electron donating (EDG) groups. The IC₅₀ values are summarized in Figure 2.8. Looking at the IC₅₀ data for compounds **25p-z**, **25a'** (Figure 2.8), it is immediate to notice that, in all cases, regardless the electron withdrawing or electron donating nature of the substituents, the *meta* isomer (**25p**, **r**, **t**, **v**, **x**) was always a more potent inhibitor than the *para* one (**25q**, **s**, **u**, **w**, **y**), differently from what observed with the pyridine-containing compounds, where the activity of the two isomers **25m** and **25n** was almost the same. Comparing the difference in IC₅₀ between the *meta* and *para* isomers, seems that the gap is higher for more polar substituent (**25r**, **s** and **25v**, **w**). We could speculate that the more polar groups are less tolerated in the *para* position, whereas more hydrophobic groups are better tolerated. Pleasingly, almost all the new compounds displayed an equal or higher inhibition potency when compared to the lead **25c**. Among them, **25x**, the *meta*-phenyl substituted, was the most potent inhibitor with an IC₅₀ of 0.33 μ M. Finally, a new series of *meta*-substituted derivatives was synthesized and tested, showing all of them IC₅₀ values in the low μ M range (**25b'-j'**, Figure 2.9).

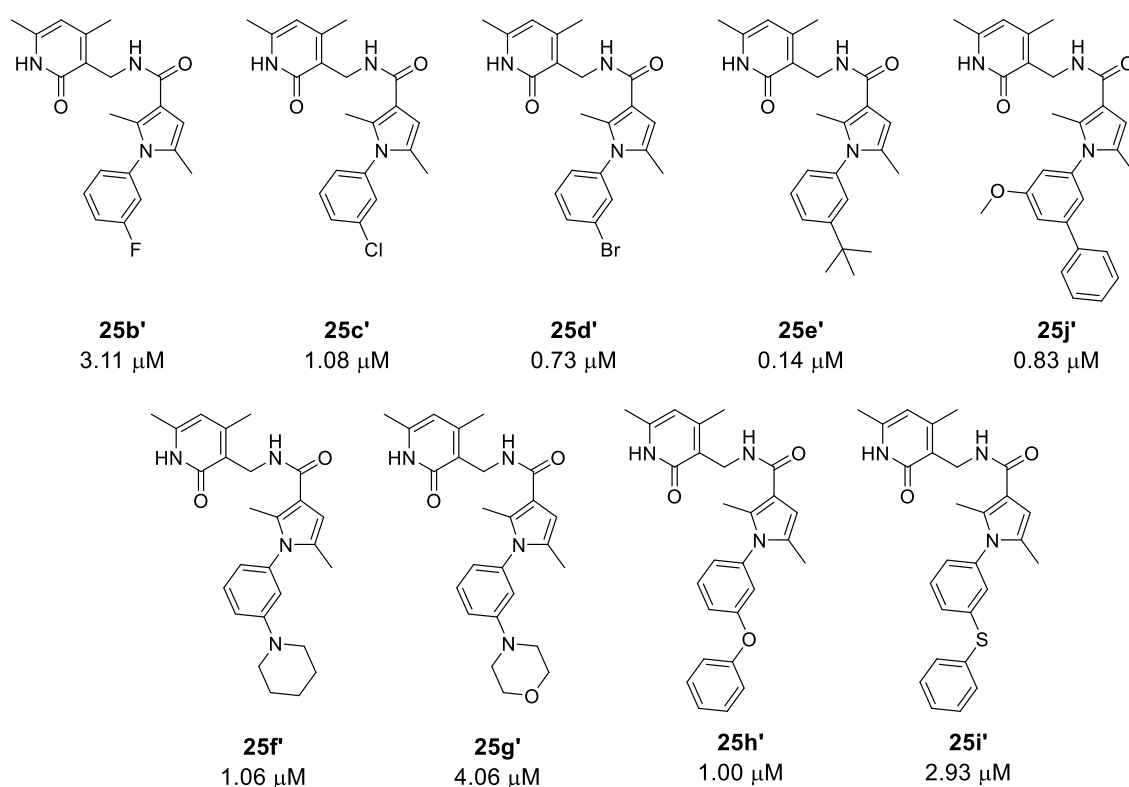


Figure 2.9. IC₅₀ data for compounds **25b'-j'**.

The data reported for the halo-substituted compounds (**25b'-d'**) show how the bulkier and less electronegative the substituent, the higher the inhibition potency. We could speculate that the increase in the dimension and/or the reduction in electronegativity of the halogen could play a role in ameliorating the binding to the target enzyme, thus giving an increased inhibition potency. Compound **25e'**, with a *meta*-*t*-butyl substitution, was the most potent of the whole series

displaying an IC_{50} of 0.14 μ M. The replacement of the phenyl ring with piperidine (**25f'**) or morpholine (**25g'**), or the insertion of a flexible O (**25h'**) or S (**25i'**) bridge between the two phenyl rings of **25x**, was tolerated, but still did not improve the inhibition potency (Figure 2.9). The double *meta* substitution of compound **25j'** was tolerated as well, but gave only an inhibition potency intermediate between those of the mono-substituted analogues (IC_{50} 0.83 μ M).

2.2.3 Target selectivity validation

Biochemical screening of 25c, 25t, 25x, 25y, 25 d' and 25e' against a panel of DNA, histone, and protein methyltransferases (EZH1, DOT1L, DNMT1, G9a, MLL1 complex, PRMT1, SET7/9)

In order to validate the target selectivity of our compounds for EZH2 against other methyltransferases, we tested derivatives **25c**, **t**, **x**, **y**, **d'**, and **e'** against a panel of DNA, histone, and protein methyltransferases. Tables 2 and 3 summarize the results as IC_{50} or percentage of inhibition at 200 μ M and 100 μ M.

Table 2. Percentage of inhibition at 200 μ M (top), and 100 μ M (bottom) of **25c**, **t**, **x**, **y**, **d'**, and **e'** against a panel of methyltransferases. Each data is the mean of at least two independent results. SD is included between \pm 10 %.

Cpd	% of inhibition at	DOT1L	DNMT1	G9a	MLL1 complex	PRMT1	SET7/9
25c	200 μ M	0.1 %	0.3 %	0 %	19.5 %	7.1 %	14.2 %
	100 μ M	1.9 %	0 %	0%	4.9 %	17.8 %	14.8 %
25t	200 μ M	6.7 %	12.8 %	3.2 %	31.8 %	3.6 %	14.9 %
	100 μ M	1.5 %	13.5 %	3.7 %	4.5 %	13.9 %	9.9 %
25x	200 μ M	0 %	0 %	0 %	41.0 %	10.4 %	41.0 %
	100 μ M	0 %	0 %	1.3 %	24.6 %	9.1 %	31.5 %
25y	200 μ M	0 %	17.2 %	0 %	44.5 %	6.9 %	30.4 %
	100 μ M	2.5 %	14.4 %	0 %	51.9 %	8.2 %	34.6 %
25d'	200 μ M	0 %	0 %	7.7 %	22.7 %	25.3 %	50.0 %
	100 μ M	2.8 %	6.2 %	10.1 %	13.0 %	14.4 %	18.5 %
25e'	200 μ M	0.2 %	4.6 %	19.9 %	22.8 %	6.3 %	17.0 %
	100 μ M	0 %	7.1 %	0 %	2.2 %	13.4 %	9.4 %
SAH	-	0.9 μ M	0.09 μ M	0.66 μ M	0.37 μ M	0.33 μ M	56.2 μ M

Table 3. IC₅₀ or % of inhibition at 200 μ M of **25c**, **t**, **x**, **y**, **d'**, and **e'** against EZH1. Each data is the mean of at least two independent results. SD is included between \pm 10 %.

Cpd	SAH	25c	25t	25x	25y	25d'	25e'
EZH1	12.7 μ M	42.8 μ M	3.52 μ M	0.90 μ M	0 %	7.47 μ M	0.92 μ M

Pleasingly, all the derivatives displayed no or very slight inhibition activity against the methyltransferases DOT1L, DNMT1, G9a, MLL1 complex, PRMT1, SET7/9. The only exception was **25y**, showing about 52 % of inhibition at 100 μ M against MLL1 complex. However, doubling the dose of **25y** did not determine an increase in inhibition activity. On the other hand, we found really interesting what observed testing these compounds against EZH1. Our lead compound **25c** had a 42.8 μ M IC₅₀, with 7.4 fold selectivity for EZH2. Intriguingly, while the *para*-substituted compound **25y** was completely inactive, its *meta* isomer **25x**, as well as all the *meta*-substituted derivatives **25t**, **e'**, **d'**, displayed low μ M IC₅₀ values (Table 3), suggesting that playing with the *meta-para* substitution we can get selectivity over the two PRC2 methyltransferases.

2.2.4 In cell evaluation (1)

Preliminary data on cell proliferation, cell cycle and H3K27 methylation in U937, NB4, SHSY5Y, and MDA-MB231 cancer cells (Prof. Lucia Altucci, Department of Biochemistry, Biophysics and General Pathology, Second University of Naples)

To validate the inhibition activity in a more complex context, selected compounds (**25c**, **h**, **m**, **n**, **p-r**, **t**, **x**, **y**, **b'-e'**, **h'**, **j'**, Figure 2.10) have been tested in a panel of cancer cell lines.

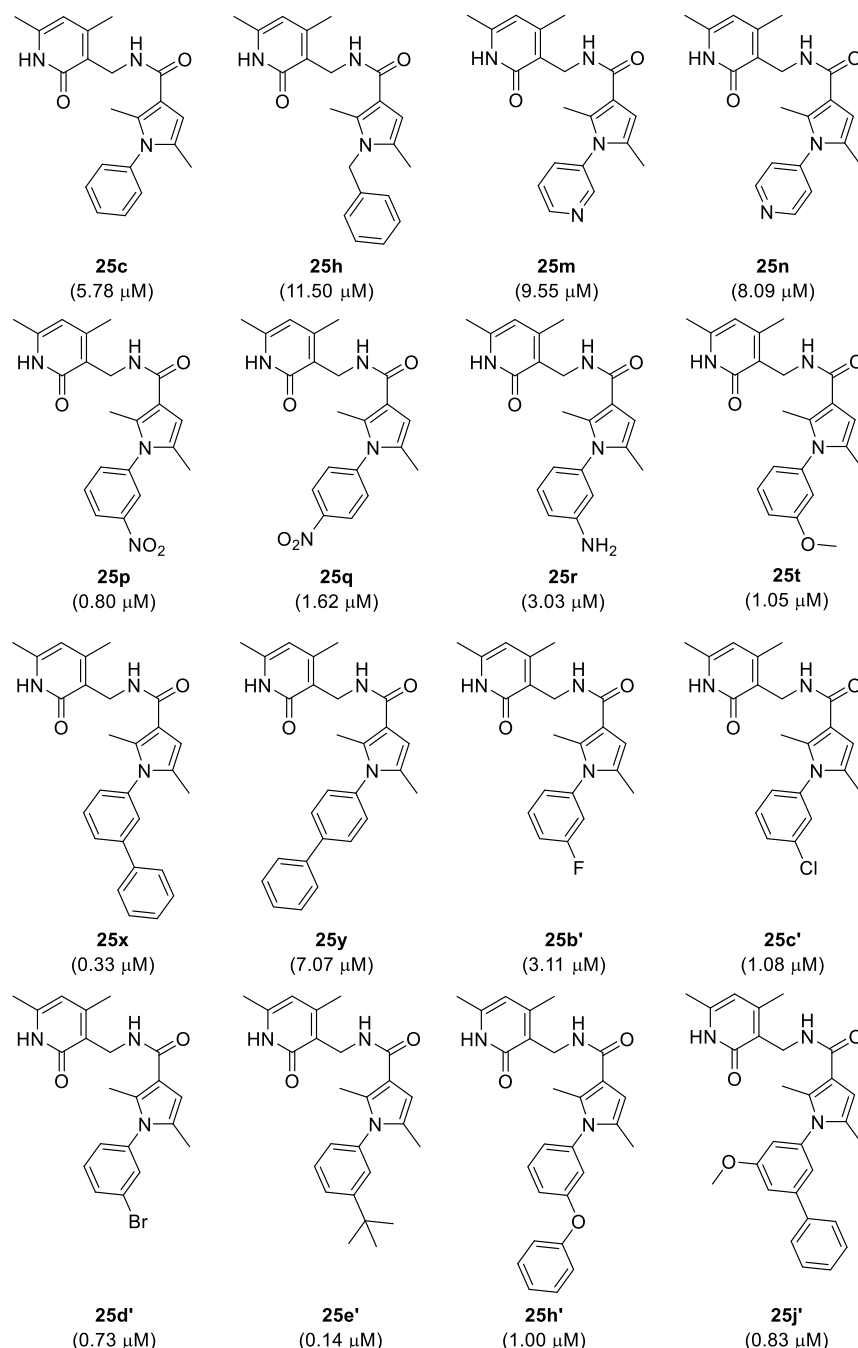


Figure 2.10. Compounds selected for *in cell* validation. Enzymatic IC₅₀ are reported in brackets.

As preliminary cell-based screening, we tested the 16 selected compounds at a fixed dose (50 μ M) after 72 hours incubation in histiocytic lymphoma U937, acute promyelocytic leukemia

NB4, neuroblastoma SHSY5Y, and breast adenocarcinoma MDA-MB231 cancer cell lines. In particular, we looked at their effect on cell proliferation, cell cycle progression and H3K27 methylation levels. **3** (Figure 2.1, GSK126) has been used as positive control. These preliminary assays aimed to validate the activity of our compounds and to choose the best cell line, and the most active compounds for further investigation (longer time treatment and lower dose range).

2.2.4.1 U937 histiocytic lymphoma

In U937 cells, we looked first at the effect of compounds **25c**, **h**, **m**, **n**, **p-r**, **t**, **x**, **y**, **b'-e'**, **h'**, and **j'** on cell cycle progression at a fixed dose after 72 h of treatment (Figure 2.11).

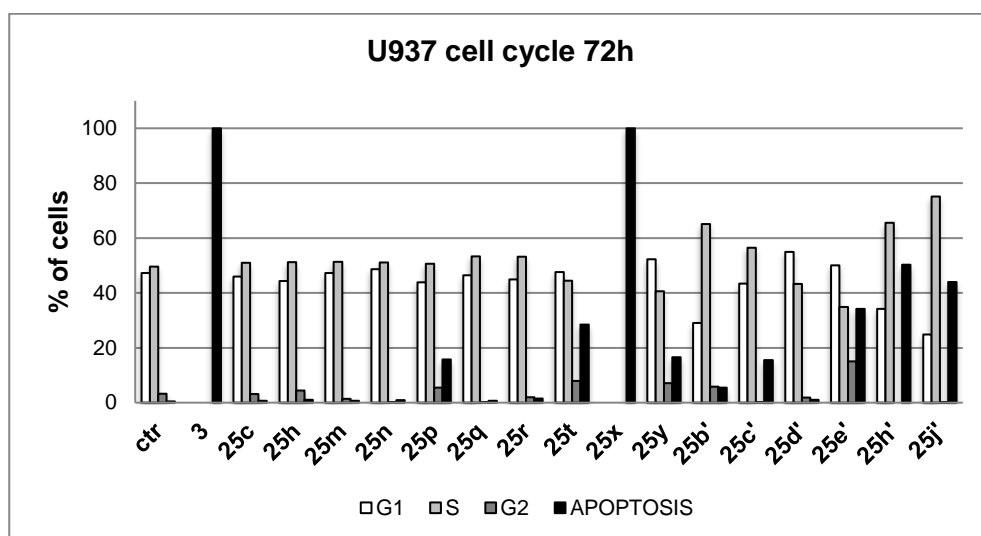


Figure 2.11. Cell cycle progression in U937 cells after treatment with **25c**, **h**, **m**, **n**, **p-r**, **t**, **x**, **y**, **b'-e'**, **h'**, and **j'** at a fixed dose (50 μ M) after 72 h.

All the compounds, including the control **3** (GSK126), have been tested at the final concentration of 50 μ M. The reported data show that the majority of the tested compounds has no strong effect on cell cycle progression. Nonetheless, **25x** displayed a strong apoptotic effect, with 100 % apoptosis. **25p**, **t**, **y**, **c'**, **e'**, **h'**, and **j'** showed mild pro-apoptotic effects. **25d'** and **e'** also increased the number of G1 cells.

We then analyzed the effects of our compounds on U937 cell proliferation. All the novel EZH2i were tested at the fixed dose of 50 μ M. The graphs reported below (Figure 2.12, 2.13) show that many of them were able to reduce the cell proliferation rate, when compared to the control, but only a few of them displayed a significant effect. **25x** was confirmed as the strongest pro-apoptotic, giving 100 % of apoptosis after 72 h of treatment. Also, **25h'** had a cytotoxic effect, but less strong even if prolonged in time. Conversely, the cytotoxic or cytostatic effects of **25y** and **25e'**, respectively, were limited in time during 48 h. **25j'**, instead, showed a longer lasting cytostatic effect (Figure 2.13).

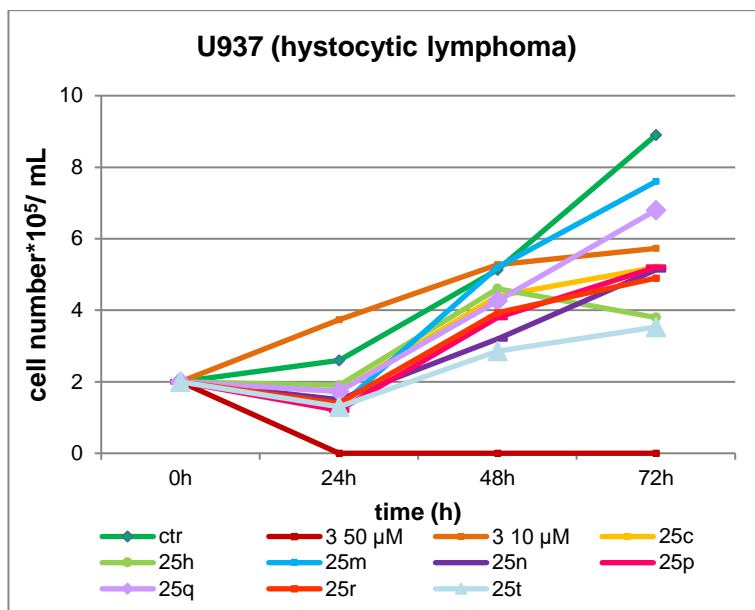


Figure 2.12. Effects of compounds **25c**, **h**, **m**, **n**, **p-r**, **t** (50 μ M) on U937 cell proliferation (trypan blue cell count) after 24, 48 and 72 h treatment.

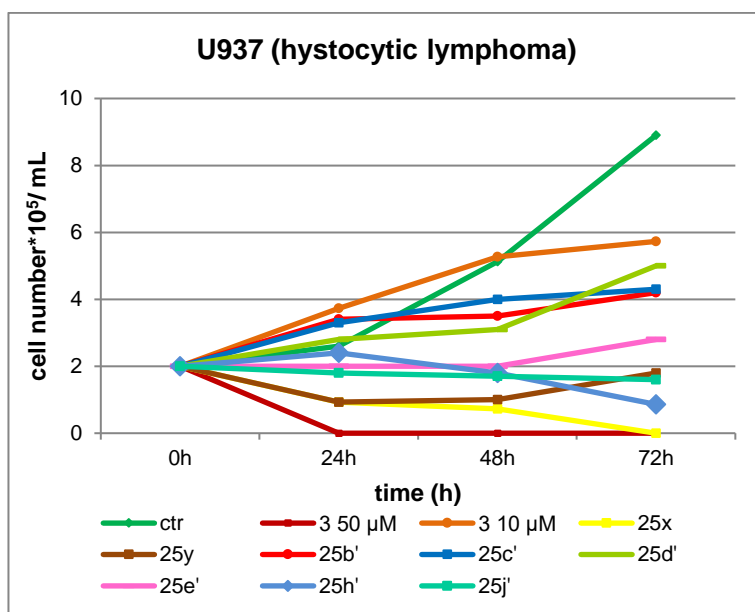


Figure 2.13. Effects of compounds **25x**, **y**, **b'-e'**, **h'**, **j'** (50 μ M) on U937 cell proliferation (trypan blue cell count) after 24, 48 and 72 h treatment.

We next looked at the effects of selected compounds (**25b'-e'**, **25h'**, **25j'**) (50 μ M) on H3K27me3 levels. As shown in Figure 2.14, **25b'** (lane 6) and **25d'** (lane 7) reduced H3K27me3 levels. No relevant effects were observed after treatment with the other tested compounds. Considering the kinetic of the methylation/demethylation equilibrium in cell, we can assess that 72 h is still a short time to appreciate any effect. Additional experiments with longer treatment time are running.

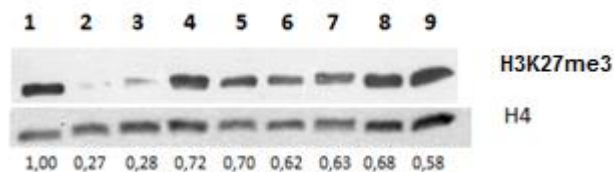


Figure 2.14. Western blot: H3K27me3 levels in U937 cells after 72 h treatment (fixed dose 50 μ M). 1 μ g histone extract. Lane 1= ctr; lane 2= **3** 20 μ M; lane 3= **3** 10 μ M; lane 4= **25e'**; lane 5= **25c'**; lane 6= **25b'**; lane 7= **25d'**; lane 8= **25j'**; lane 9= **25h'**.

2.2.4.2 NB4 acute promyelocytic leukaemia

The same assays have been repeated with compounds **25c**, **h**, **m**, **n**, **p-r**, **t**, **x**, **y**, **b'-e'**, **h'**, and **j'** in the human acute promyelocytic leukaemia cell line NB4. All the compounds, including the control **3** (GSK126), have been tested at the final concentration of 50 μ M.

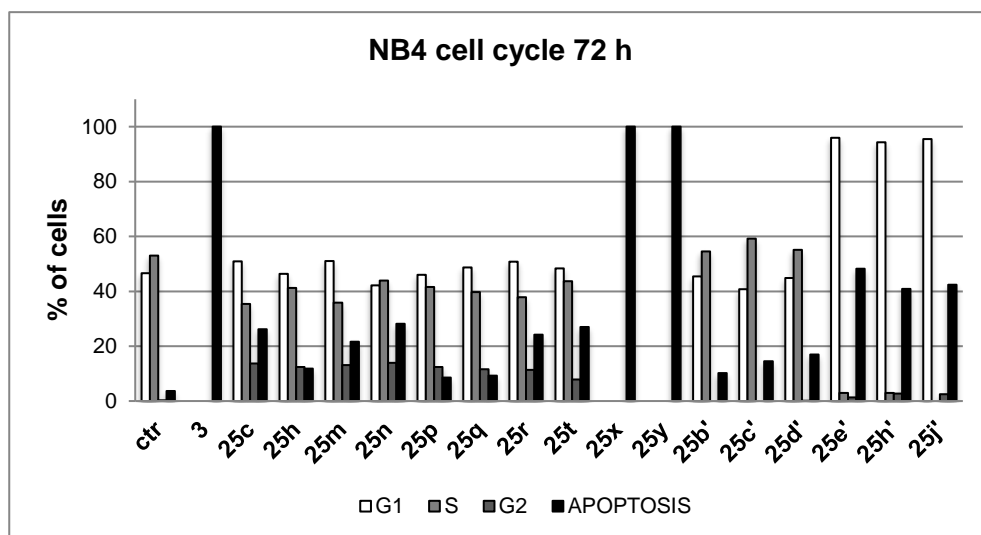


Figure 2.15. Cell cycle progression in NB4 cells after treatment with **25c**, **h**, **m**, **n**, **p-r**, **t**, **x**, **y**, **b'-e'**, **h'**, and **j'** at a fixed dose after 72 h.

The majority of the tested compounds had no strong effects on cell cycle progression, even though many of them induced up to 30 % of apoptosis. Nonetheless, we observed once again a strong cytotoxicity after treatment with compound **25x**, giving 100 % of apoptosis (Figure 2.15). In this cell line, also compound **25y** displayed a strong cytotoxic effect (100 % apoptosis). In order to better appreciate their activity and exclude any unspecific cytotoxic effect, these two compounds should be tested at lower doses. **25e'**, **25h'**, and **25j'** had strong effects on cell cycle progression, markedly increasing the percentage of G1 cells (Figure 2.15). Cell proliferation data (Figure 2.16, 2.17) show how all the tested compounds were able to reduce cell proliferation rate over 72 h, when compared to the vehicle treated control. We can distinguish between two classes of derivatives: those that showed a real cytotoxic effect (**25x**, **y**, **h'**, **e'**, **j'**) and those that only reduced the proliferation rate (**25c**, **h**, **m**, **n**, **p-r**, **t**, **b'-g'**).

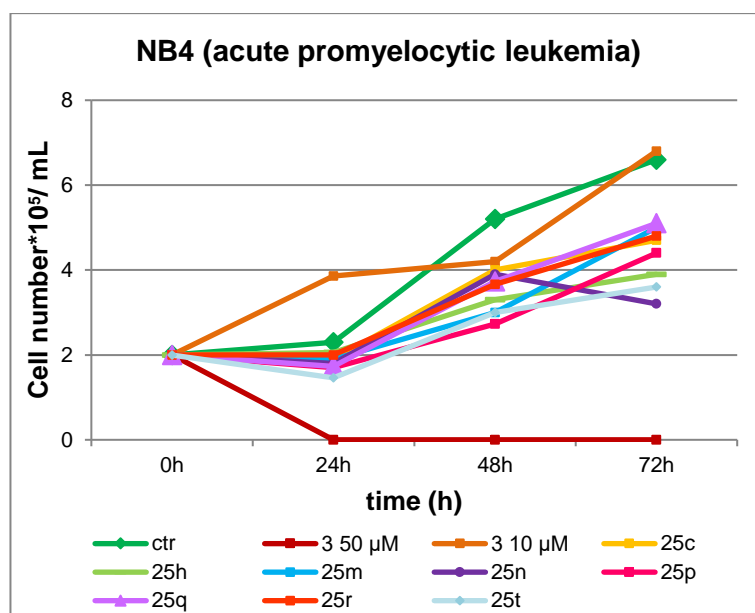


Figure 2.16. Effects of compounds **25c**, **h**, **m-r**, and **t** (50 μ M) on NB4 cell proliferation (trypan blue cell count) after 24, 48 and 72 h treatment.

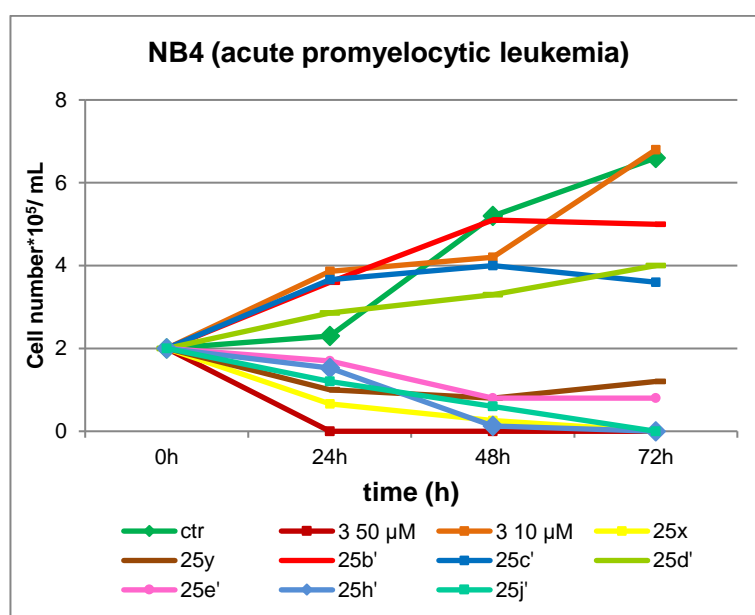


Figure 2.17. Effects of compounds **25x**, **y**, **b'-e'**, **h'**, and **j'** (50 μ M) on NB4 cell proliferation (trypan blue cell count) after 24, 48 and 72 h treatment.

A western blot analysis on histone extracts of NB4 cells treated with compounds **25b'-e'**, **25h'**, **25j'** (50 μ M) after 72 h was performed to evaluate if there were any effects on EZH2-dependent histone methylation (Figure 2.18). The collected data suggest that the tested compounds, even if able to reduce H3K273me levels did not have strong effects (Figure 2.18). However, the effect of compounds **25b'** (lane 6, Figure 2.18) and **25d'** (lane 7, Figure 2.18) at 50 μ M was comparable to the effect of **3** at 20 μ M (Figure 2.18). Longer time treatment experiments are running also on this cell line, in order to better appreciate any effect on histone methylation.



Figure 2.18. Western blot: H3K27me3 levels in NB4 cells after 72 h treatment (fixed dose 50 μ M). 1 μ g histone extract. Lane 1= ctr; lane 2= **3** 20 μ M; lane 3= **3** 10 μ M; lane 4= **25e'**; lane 5= **25c'**; lane 6= **25b'**; lane 7= **25d'**; lane 8= **25j'**; lane 9= **25h'**.

2.2.4.3 SHSY5Y neuroblastoma

When tested in the human neuroblastoma SHSY5Y cell line, compounds **25c**, **h**, **m**, **n**, **p-r**, **t**, and **y** showed only a reduction of cell proliferation rate, without any strong cytotoxicity (Figure 2.19). Once again, compound **25x** was the sole compound showing a stronger effect, blocking cell proliferation (Figure 2.19).

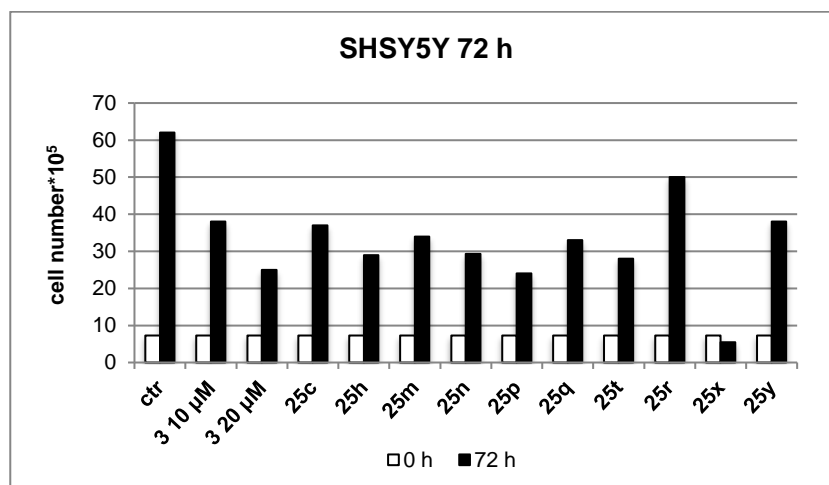


Figure 2.19. Effects of compounds **25c**, **h**, **m**, **n**, **p-r**, **t**, **x** and **y** (50 μ M) on SHSY5Y cell proliferation (trypan blue cell count) after 72 h treatment.

Interestingly, many of the tested compounds reduced H3K27me3 levels in this cell line after 72 h treatment, suggesting that this cell line could be more sensitive to these derivatives (Figure 2.20).

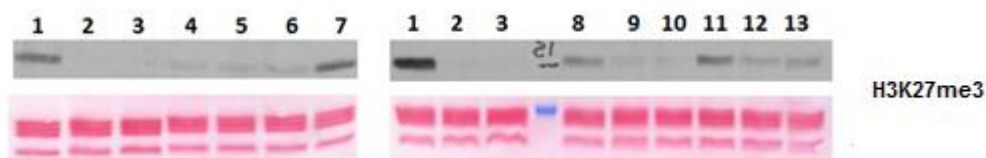


Figure 2.20. Western blot: H3K27me3 levels in SHSY5Y cells after 72 h treatment (fixed dose 50 μ M). 10 μ g histone extract. Lane 1= ctr; lane 2= **3** 20 μ M; lane 3= **3** 10 μ M; lane 4= **25c**, lane 5= **25n**, lane 6= **25m**, lane 7= **25y**; lane 8= **25h**, lane 9= **25t**, lane 10= **25p**, lane 11= **25q**, lane 12= **25r**, lane 13= **25x**

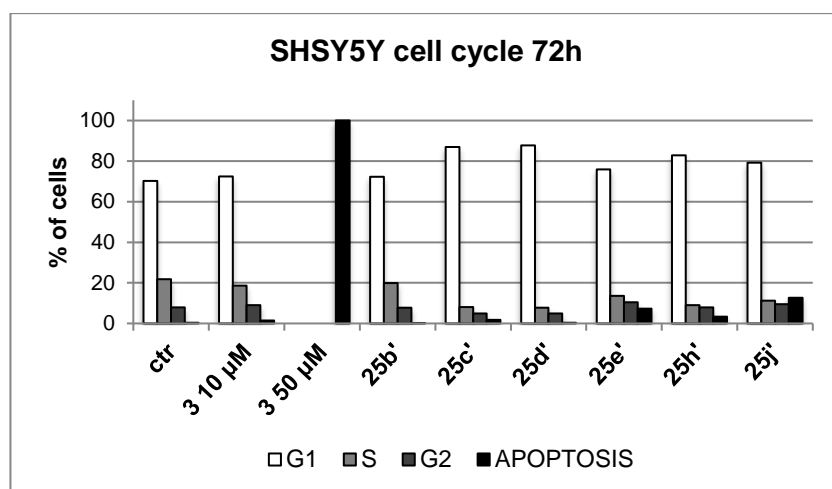


Figure 2.21. Cell cycle progression in SHSY5Y cells after treatment with **25c'-e', h', and j'** at a fixed dose after 72 h.

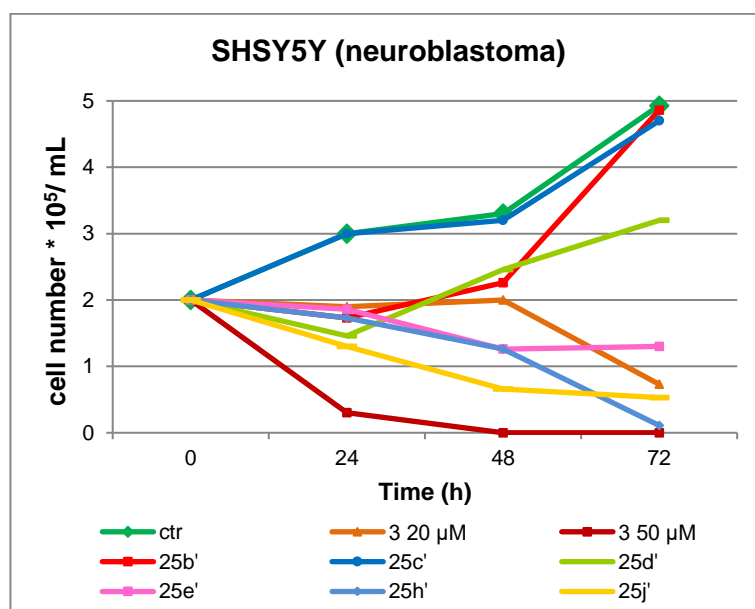


Figure 2.22. Effects of compounds **25c'-e', h', and j'** (50 μM) on SHSY5Y cell proliferation (trypan blue cell count) after 24, 48 and 72 h treatment.

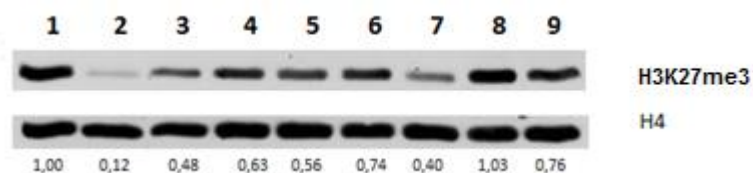


Figure 2.23. Western blot: H3K27me3 levels in SHSY5Y cells after 72 h treatment (fixed dose 50 μM). 1 μg histone extract. Lane 1= ctr; lane 2= **3 20 μM**; lane 3= **3 10 μM**; lane 4= **25e'**; lane 5= **25c'**; lane 6= **25b'**; lane 7= **25d'**; lane 8= **25j'**; lane 9= **25h'**.

In the same neuroblastoma cell line, we looked at the effects of **25c'-e', h', and j'**. Interestingly, almost all of them increased the number of cells in G1 phase, but none of them was able to strongly induce apoptosis (Figure 2.21). **25e', 25h'** and **25j'** displayed the strongest

antiproliferative effects among the tested compounds (Figure 2.22). Western blot analysis showed a reduction of H3K27me3 after treatment with **25c'-e'**. Also **25b'** slightly reduced H3K27me3 (Figure 2.23).

2.2.4.4 MDA-MB231 breast adenocarcinoma

Once tested in the human breast adenocarcinoma cell line MDA-MB231, **25c, h, m, n, p-r, t, x, y**, significantly reduced cell proliferation rate (Figure 2.24). In a western blot analysis on MDA-MB231 histone extracts, compounds **25h, m, t**, and **25y** have been proved to reduce H3K27me3 after 72 h treatment (Figure 2.25).

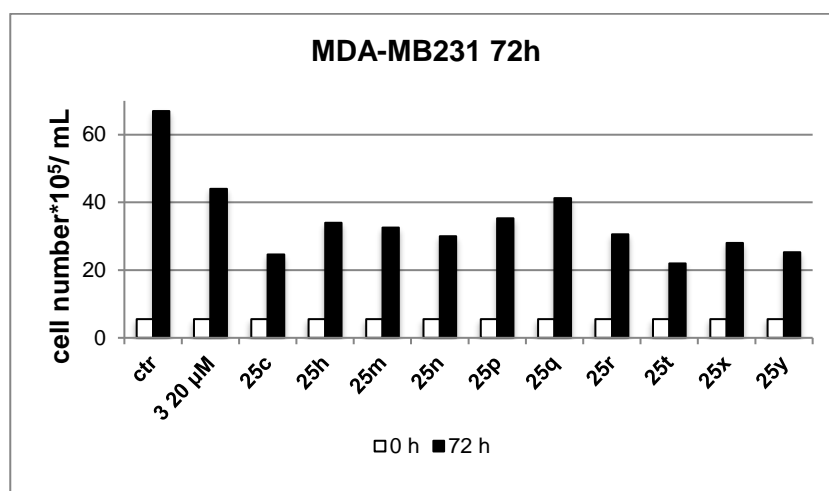


Figure 2.24. Effects of compounds **25c, h, m, n, p-r, t, x, y** (50 μM) on MDA-MB231 cell proliferation (trypan blue cell count) after 72 h treatment.

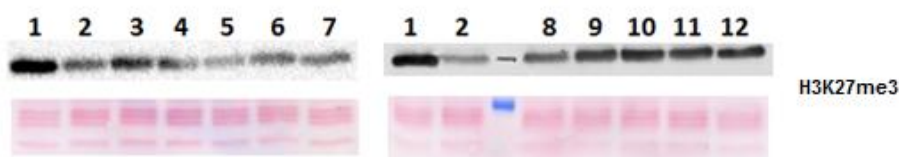


Figure 2.25. Western blot: H3K27me3 levels in MDA-MB231 cells after 72 h treatment (fixed dose 50 μM). 5 μg histone extract. Lane 1= ctr, lane 2= 3 20 μM, lane 3= **25c**, lane 4= **25n**, lane 5= **25m**, lane 6= **25y**, lane 7= **25h**, lane 8= **25t**, lane 9= **25p**, lane 10= **25q**, lane 11= **25r**, lane 12= **25x**.

Cell cycle analysis was performed after 72 hours treatment with compounds **25b'-e', h', j'** (50 μM). The results reported in Figure 2.26, show a marked effect after administration of **25e', h'** or **j'**, with a strong increase in pre-G1 cells number. These data were further confirmed by the results obtained in a time-course cell viability assay (Figure 2.27). **25e', h'**, and **j'** were the strongest anti-proliferative, exerting similar effects after 72 h treatment. **25c'**, instead, seems to have a cytostatic effect. Additionally, western blot analysis after 72 hours treatment (Figure 2.28) showed that compounds **25b'** (lane 7), **25d'** (lane 5), **25h'** (lane 6), and **25j'** (lane 4) are able to reduce H3K27 methylation levels. Compound **25b'** displayed the strongest effect.

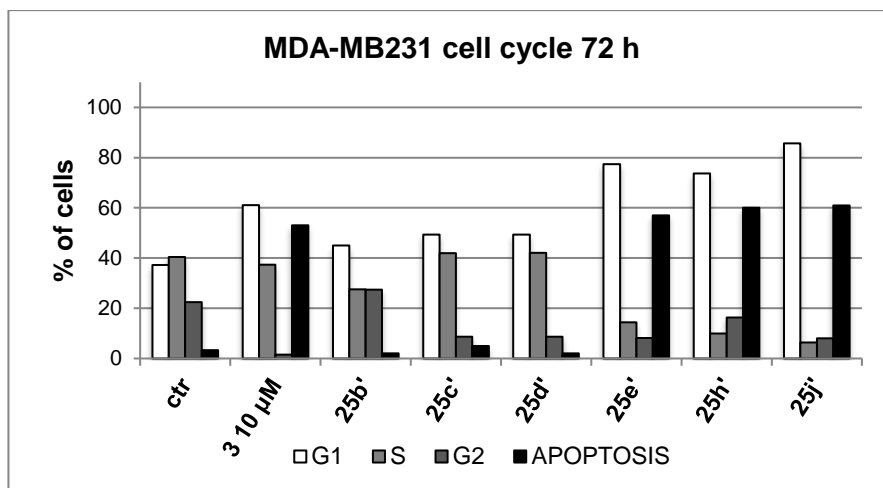


Figure 2.26. Cell cycle analysis in MDA-MB231 cells after treatment with **25b'-e', h', j'** at a fixed dose after 72 h.

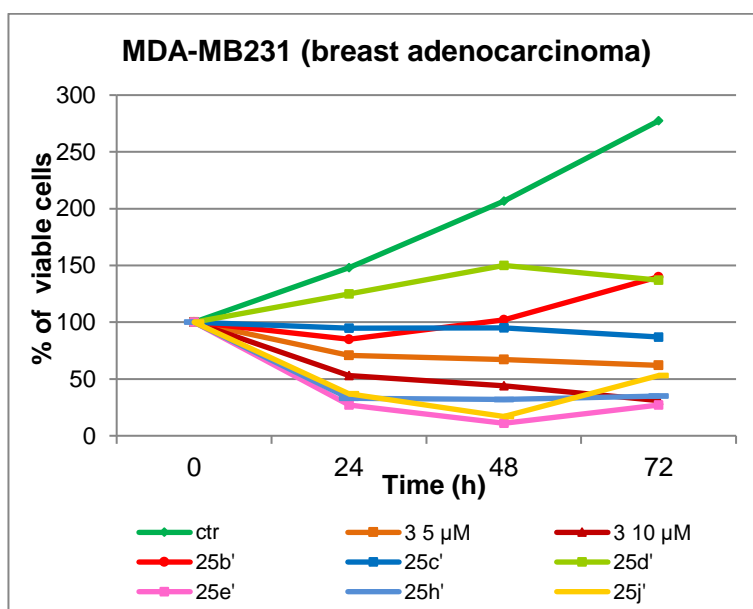


Figure 2.27. Effects of compounds **25b'-e', h', j'** (50 μM) on MDA-MB231 cell viability after 24, 48 and 72 h treatment.

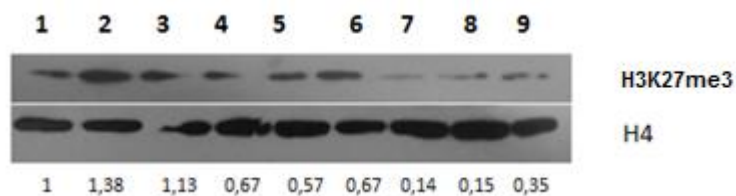


Figure 2.28. Western blot: H3K27me3 levels in MDA-MB231 cells after 24 (a), 48 (b), and 72 h (c) treatment (fixed dose 50 μM). 1 μg histone extract. Lane 1= ctr; lane 2= **25c'**, lane 3= **25e'**, lane 4= **25j'**, lane 5= **25d'**, lane 6= **25h'**, lane 7= **25b'**, lane 8=3 10 μM, lane 9=3 5 μM.

2.2.4.5 In cell evaluation (1): conclusions and future perspectives

As preliminary cell-based assays, the activity of compounds **25c, h, m, n, p-r, t, x, y, b'-e', h', and j'** has been evaluated in different human cancer cell lines at fixed dose (50 μ M) after 72 hours treatment. The preliminary results here presented are not exhaustive, but furnished us interesting information for further investigation. Interestingly, many of the tested compounds were able to reduce cell proliferation rate in all the tested cancer cell lines. In some cases, we recorded strong pro-apoptotic and cytotoxic effects, as for compound **25x**, that gave 100 % apoptosis in different cell lines. Considering the strong toxicity displayed by **25x** and **25y** it could be worth to explore their effects at lower (non-cytotoxic) doses, so to evaluate if it is possible to exclude any unspecific effect. Interestingly, **25h'** and **25j'** had relevant effects on cell cycle progression in different cell lines, increasing the G1 cell number without strong cytotoxicity. In general, in most of the cases effects on H3K27 methylation levels were mild. In U937 cells H3K27 methylation levels were reduced only after **25b'** or **25c'** treatment. In NB4 leukemia cell line, we could not observe relevant effects on H3K27 methylation. Interestingly, the neuroblastoma SHSY5Y cell line was more sensitive to our compounds: H3K27me3 levels were reduced with **25c, m, n, p, r, t, b'-e'**. Also, in breast cancer MDA-MB231 cells we observed H3K27 demethylation after treatment with several of our compounds (**25h, m, t, y, b', d', h', j'**). Overall **25b'** was the compound able to induce H3K27 methylation reduction in all the tested cell lines, even though it was not a strong antiproliferative. We could speculate that this is due to better pharmacokinetic (PK) features of this compound. Considering the kinetic of the methylation/demethylation equilibrium in cell, we can assess that 72 h is still a short time to appreciate the effect of EZH2is. Additional experiments with longer treatment time are ongoing. In the next future, we will also explore the effects of these compounds in a lower dose-range. Dose-dependent cell proliferation studies on different cell lines will be performed. The most responsive cell line will be then selected for further investigation. More in detail, we are planning to study the effect of our compounds on H3K27 methylation in a dose range (and after longer time treatment). The effect on EZH2 target genes expression will be evaluated in the selected cell line. Additionally, we will investigate on the cell death mechanism and/or pro-differentiating effect, by dose and time dependent study on specific markers.

2.2.5 In cell evaluation (2)

Compounds 25f' and 25g' in glioblastoma primary cell cultures, preliminary data (Prof. Susanna Scarpa, Department of Experimental Medicine, Sapienza University, Rome)

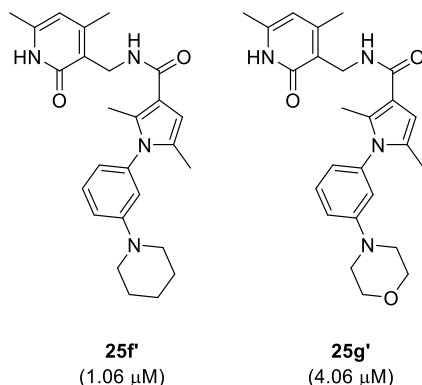


Figure 2.29. Compounds **25f'**-**g'**. Enzymatic IC₅₀ are reported in brackets.

In the group of Prof. Scarpa, three primary cell cultures (GL1, GL2, GL3) were established from surgical tissues of three different patients with glioblastoma following a validated protocol.^{227,228} In order to check the homogeneity of the neoplastic phenotype, each culture was characterized by immunofluorescence staining of two glioblastoma markers, GFAP and nestin.²²⁹ 100 % of cells from GL1, GL2 and GL3 resulted positive for both markers (Figure 2.30).

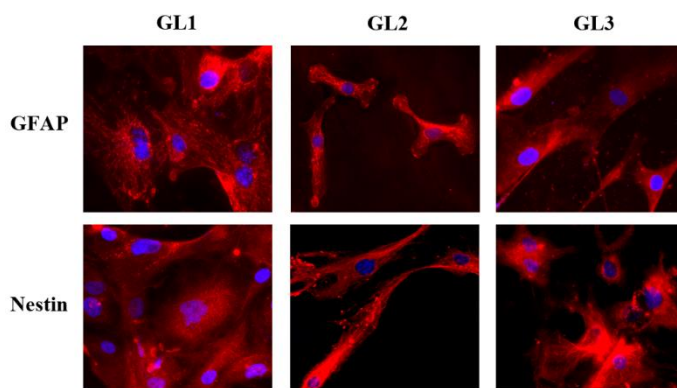


Figure 2.30. Immunofluorescence staining for GFAP and for nestin. RED: anti-GFAP or anti-NESTIN, BLUE: DAPI staining for DNA

In the literature, there is a number of evidences suggesting a potential role of EZH2 in glioblastoma,^{188,230-232} including a recent paper by Grinshtein *et al.*, where the SAM-competitive EZH2 inhibitor **20** (UNC1991, Figure 1.5) has been proved cytotoxic *in vitro* on a diverse collection of brain tumour initiating cell lines at micromolar concentrations. Additionally, the authors showed that **20** synergized with dexamethasone (DEX) and this combination suppressed tumour growth also *in vivo*.¹⁸⁸ In light of these findings, we decided to test two of our

compounds (**25f'**, **g'**, Figure 2.29) in the glioblastoma cell lines established in the Prof. Scarpa group.

First, we evaluated the effects of the two EZH2 inhibitors **25f'** and **25g'** on cell viability and replication in the glioblastoma cell lines U-87, GL1, GL2 and GL3 and in a primary culture of human dermal fibroblasts, HF (used as a control of somatic not transformed cells). All the tested cell lines were treated for 24, 48, or 72 h with 10 μ M, 25 μ M, or 50 μ M **25f'** or **25g'**. After 24 h of treatment no effects were evident (data not shown). After 48 h of incubation we started to observe a decrease in cell viability in all four glioblastoma cell cultures. The decrease in glioblastoma cells viability reached significant values after 72 h of treatment with both molecules already at 10 μ M of concentration (Figure 2.31 a, c, d, e).

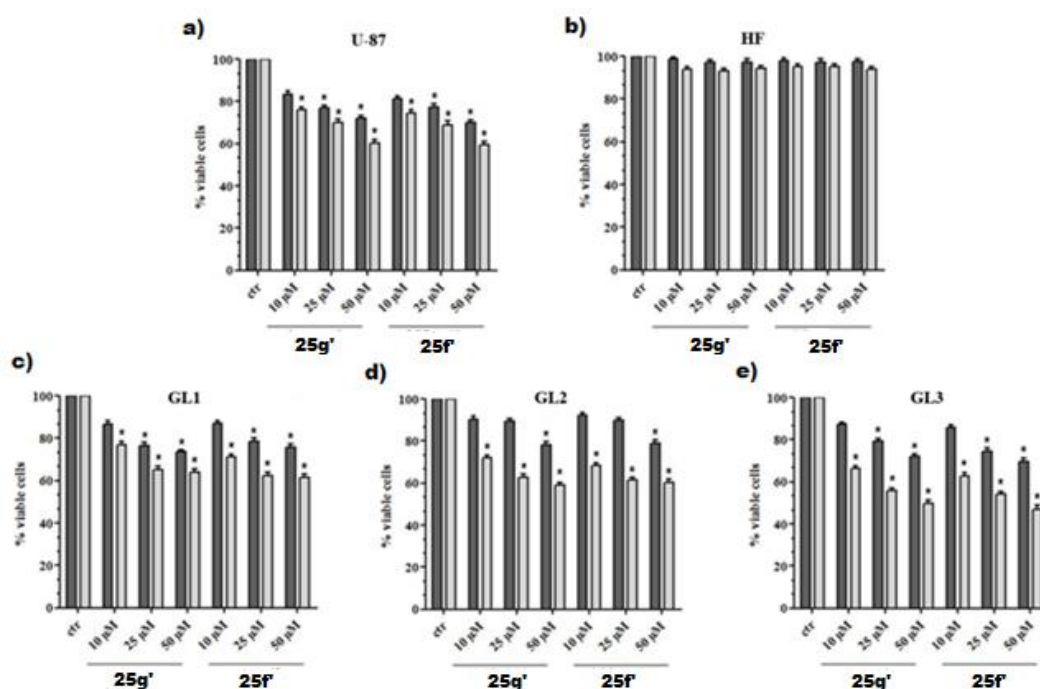


Figure 2.31. Cell viability of untreated (ctr) and **25f'** and **25g'** treated cultures expressed as percentage of alive cells after 48 h (dark grey bar) or 72 h (white bar). These data are expressed as the mean of at least 3 independent experiments. Standard deviation is reported in bars. Asterisks indicate the significant data.

Interestingly, after 72 h, none of the tested molecules had any negative effect on HF cell proliferation, suggesting that there was no unspecific cytotoxic effect (Figure 43 b). Based on these data, we decided to use **25f'** and **25g'** at the concentration of 25 μ M with an incubation time of 72 h for all the following experiments. In order to detect whether the effects on cell replication were connected to the specific inhibition of EZH2 activity, the levels of H3K27me3 were measured by western blot (Figure 2.32). Interestingly H3K27me3 levels were increased in GL1 cell lines if compared with U-87 cell line, while its levels in HF were not detectable (Figure 2.32). Treatment with **25f'** and **25g'** determined an evident reduction of H3K27me3 levels in

both glioblastoma cell cultures U-87 and GL1 (Figure 2.32), assessing that the tested compounds are really acting as EZH2i.

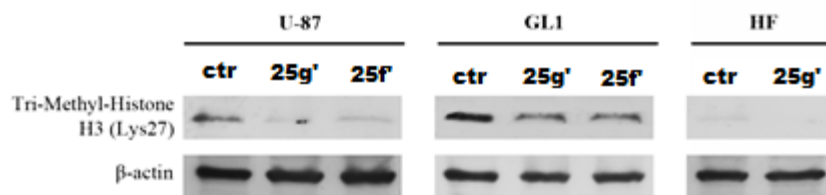


Figure 2.32. Western blot of untreated (ctr) and **25f'** and **25g'** treated U-87, GL1 and HF for tri-methyl-histone H3 and for actin.

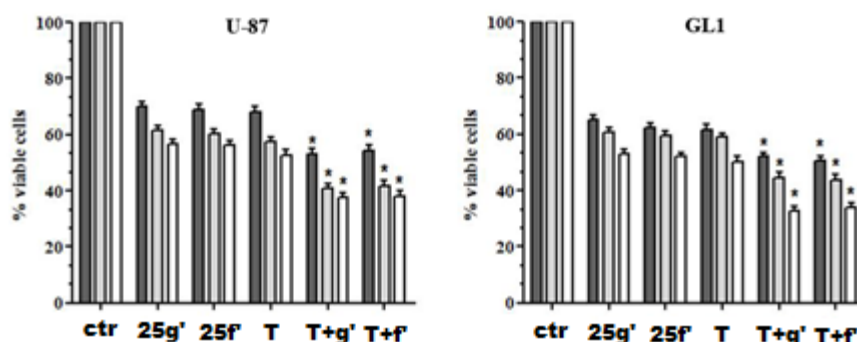


Figure 2.33. Cell viability of U-87 and GL1 untreated (ctr) and treated with **25f'**, **25g'**, and Temozolomide (T) expressed as percentage of alive cells. The three different bars indicate treatment at three different times: 24 h (dark gray), 48 h (light gray) and 72 h (white). These data are expressed as the mean of at least 3 independent experiments. Standard deviation is reported in bars. Asterisks indicate the significant data.

We next decided to compare the effects of the two novel EZH2 inhibitors with those of Temozolomide, the sole chemotherapeutic agent to date approved for the treatment of glioblastoma patients. Thus, we treated U-87 and GL1 cells with **25f'** (25 μ M), **25g'** (25 μ M), or Temozolomide (100 μ M), alone or in combination, for 72, 96 or 120 h. When used alone, the pyrrole-based EZH2 inhibitors and Temozolomide had equivalent effects on cell proliferation inhibition (Figure 2.33). Pleasingly, the combination of **25f'** or **25g'** and Temozolomide had much stronger, but not additive effects on cell proliferation inhibition already after 72 h (Figure 2.33).

2.2.5.1 In cell evaluation (2): conclusions and future perspectives

The fact that the treatment of glioblastomas remains difficult and that no contemporary treatments are curative, together with the growing number of evidences about EZH2 involvement in glioblastoma, call for a wider exploration of EZH2 inhibitors as potential therapeutic tools. In collaboration with the group of Prof. Scarpa, we started to study the effects of two novel EZH2 inhibitors **25f'** and **25g'** in different glioblastoma cell lines. Preliminary data show that both **25f'** and **25g'** were able to reduce cell proliferation after 48 h already at 10 μ M concentration. **25f'**

and **25g**' treatment determined an evident reduction of H3K27me3 levels in both glioblastoma U-87 and GL1 cells, assessing that the tested compounds are really acting as EZH2i. Finally, their association with Temozolomide produced much stronger effects on cell proliferation inhibition already after 72 h, than the treatment with single drugs.

2.3 General conclusions and future perspectives

The role of aberrant EZH2 activity in cancer is validated by several scientific evidences. In the last years, EZH2 inhibitors also entered the clinical arena.¹⁰³ This research project aimed to develop novel EZH2 inhibitors and validate their activity in different cancer cells. We started with a molecular simplification on compound **3** scaffold (GSK126, Figure 11), keeping fix the 4,6-dimethyl-3-methylamino-2-pyridinone moiety and replacing the indole central core with a pyrrole. We started then to build up a new scaffold, evaluating step by step the required or preferred substituents to improve the inhibition activity. In summary, the biochemical assays revealed an interesting structure activity relationship (SAR), that we can resemble as follows:

- a 2,5-dimethyl substitution on the pyrrole is the best combination: removing one or both the methyl groups, or replacing one of them with a more bulky and branched isopropyl group, caused a drop in inhibition potency;
- the pyrrole N(1) should be substituted, preferably with bulky and aromatic groups. The highest inhibition potency was obtained with an aromatic ring directly bound to the nitrogen;
- a substituent in *meta* or *para* on the phenyl ring can help to improve the activity. The *meta* isomers proved to be more potent than the *para* ones.

In this study, compounds **25x** and **25e'** were the most potent in the *in vitro* inhibition assay. With IC₅₀ values of 0.330 μ M and 0.138 μ M, respectively, they were 17 to 42 folds more potent than the lead **25c**. Selected compounds have been also screened against a panel of methyltransferases, in order to validate their target selectivity. Pleasingly, the tested compounds displayed no or slight inhibition activity against the methyltransferases DOT1L, DNMT1, G9a, MLL1 complex, PRMT1, SET7/9. Moreover, we found really interesting the EZH1 inhibition data. Our lead compound **25c** had a 42.8 μ M IC₅₀, with 7.4-fold selectivity for EZH2. Intriguingly, the *para*-substituted compound **25y** was completely inactive, while its *meta* isomer **25x**, as well as all the *meta*-substituted derivatives (**25t**, **d'**, and **e'**), displayed low μ M IC₅₀ values. So that we can conclude that the *meta*-substituted compounds can inhibit both EZH2 and EZH1.

Subsequently, compounds **25c**, **h**, **m**, **n**, **p-r**, **t**, **x**, **y**, **b'-e'**, **h'**, and **j'**, displaying enzymatic IC₅₀ values in the low μ M range, have been tested in U937, NB4, SHSY5Y, and MDA-MB231 cancer cell lines. In particular, we looked at their effect on cell proliferation, cell cycle progression and H3K27 methylation levels at a fixed dose (50 μ M) after 72 hours treatment. The preliminary results here reported are not exhaustive, but furnished us interesting information for further investigation. In some cases, we observed strong pro-apoptotic and cytotoxic effects, as for compound **25x**, that gave 100 % apoptosis in different cell lines. Considering the strong toxicity displayed by **25x** and **25y** it could be worth to explore their effects at lower (non-cytotoxic) doses, so to evaluate if it is possible to exclude any unspecific effect. Interestingly, **25h'** and **25j'** had relevant effects on cell cycle progression in different cell lines, increasing the G1 cell number

without strong cytotoxicity. In general, in most of the cases effects on H3K27 methylation levels were mild. In U937 cells H3K27 methylation levels were reduced only after **25b'** or **25d'** treatment. Instead, in NB4 leukemia cell line, we could not observe relevant effects on H3K27 methylation. Interestingly, the neuroblastoma SHSY5Y cell line was more sensitive to our compounds: H3K27me3 levels were reduced after 72 h treatment with **25c**, **m**, **n**, **p**, **r**, **t**, and **25b'-e'**. Also, in breast cancer MDA-MB231 cells we observed H3K27 demethylation after treatment with several of our compounds (**25h**, **m**, **t**, **y**, **b'**, **d'**, **h'**, **j'**). Overall **25b'** was the sole compound displaying a reduction of H3K27 methylation in all the tested cell lines, even if it was not the most effective in arresting cell cycle and cell proliferation. We speculate that this could be due to better pharmacokinetic (PK) features of this compound. However, longer time treatment is required to better evaluate the in-cell EZH2 inhibition activity of these compounds.

In parallel, in collaboration with the group of Prof. Scarpa, we started to study the effects of two novel EZH2 inhibitors **25f'** and **25g'** in different glioblastoma cell lines. Preliminary data show that both compounds were able to reduce cell proliferation after 48 h already at 10 μ M concentration. **25f'** and **25g'** treatment determined an evident reduction of H3K27me3 levels in both glioblastoma U-87 and GL1 cell lines, assessing that the tested compounds are really acting as EZH2i. Finally, their association with Temozolomide produced much stronger, but not additive effects on cell proliferation inhibition, than the treatment with single drugs already after 72 h treatment.

Considering the good profile in biochemical assays, we believe that, in order to better appreciate the activity of this series of compounds in cells, will be necessary to conjugate an improvement of substrate binding potency and a PK properties optimisation. The *meta* substitution could be further explored, inserting different size bulkier groups. We will investigate on the substitution with more lipophilic groups, that seem to be favored, and we will try to evaluate if the new substitutions will give us a different selectivity of inhibition for EZH2 over EZH1. Additionally, a main goal from the medicinal chemistry point of view will be the replacement of the 4,6-dimethyl-3-methylamino-2-pyridinone moiety with a completely different one. Looking at the known EZH2 inhibitors, what catches the eye is that all of the most potent compounds (including those in clinical studies) belong to the 2-pyridone-containing class. There have been already some attempts in replacing this groups with some analogues, but these manipulations mainly resulted in a drop of activity.¹⁰³ However, is always worth to remember that this moiety alone is not sufficient for the inhibition activity, as reported by Yang *et al.*,¹⁶⁸ and also confirmed in our study (see compounds **25e**, **f**). Probably, the best way to proceed, also considering that a crystal structure of PRC2 with inhibitor is now available,¹⁶⁷ will be a structure-based drug design. The data collected till now let us think that there might be a different sensitivity of the tested cancer cell lines towards EZH2 inhibition. This could be a point of interest for further investigation. We are planning to determine EZH2 and EZH1 expression levels in the different cancer cell lines we

are studying, to establish whether there is a different level of expression that can justify the different response, or we should look for more complex answers. In both cases, it is in our interest to better investigate about the mechanism of action of these compounds. We will evaluate them in SAM-competition experiments. In depth cell-based studies will focus on the identification of the targeted pathways.

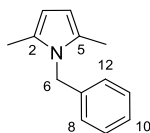
Concerning EZH2, it is worth to remember that there have been recently reported examples of development drug resistance to EZH2 inhibitors.¹⁸⁰ These findings have great implications for the clinical translation of EZH2 inhibitors and require the development of novel tools to target the resistant EZH2 mutants. Even though, we can always think about the design of novel and selective compounds, the investigation of a possible combination therapy between EZH2 inhibitors and other known or novel epi-drugs or standard drugs (polypharmacology) would be more intriguing.^{183,184} In these regards, the development of molecular hybrids could be an interesting strategy to evaluate. Finally, the growing number of evidences pushing for a deeper investigation on EZH1,^{179,233,234} together with the preliminary data collected in our biochemical screening, encourage for deeper investigation on this topic, including the development of proper chemical tools.

2.4 Experimental Section

2.4.1 Chemistry

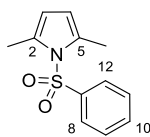
Melting points were determined on a Buchi 530 melting point apparatus and are uncorrected. ^1H NMR and ^{13}C NMR spectra were recorded at 400 and 100 MHz, respectively, on a Bruker AC 400 spectrometer; chemical shifts are reported in δ (ppm) units relative to the internal reference tetramethylsilane (Me_4Si). EIMS spectra were recorded with a Fisons Trio 1000 spectrometer; only molecular ions (M^+) and base peaks are given. All compounds were routinely checked by TLC and ^1H NMR. TLC was performed on aluminum-backed silica gel plates (Merck DC, Alufolien Kieselgel 60 F254) with spots visualized by UV light. All solvents were reagent grade and, when necessary, were purified and dried by standard methods. Concentration of solutions after reactions and extractions involved the use of a rotary evaporator operating at reduced pressure of ca. 20 Torr. Organic solutions were dried over anhydrous sodium sulfate. Elemental analysis has been used to determine purity of the described compounds, that is, $> 95\%$. Analytical results are within $\pm 0.40\%$ of the theoretical values. All chemicals were purchased from Sigma-Aldrich, Milan (Italy), or from Alfa Aesar, Karlsruhe (Germany), and were of the highest purity.

General procedure for the synthesis of pyrroles (26c-h, k-q, t, u, z, a'-e', k'). Example (method a): Synthesis of 1-benzyl-2,5-dimethyl-1H-pyrrole (26h)



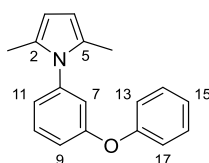
In a flame dried sealed tube, was prepared a solution of 2,5-hexanedione (8.50 mmol, 1.2 eq, 1 mL) in glacial acetic acid (3 mL). Benzyl amine (7.08 mmol, 1.0 eq, 1.20 g, 1.22 mL) was added to the solution. The reaction solution was stirred at 100 °C for 2 h. After this time the reaction was judged to be complete by TLC analysis. The acetic acid was removed *in vacuo* (azeotrope with toluene) and the residue was purified by silica gel chromatography, eluting with *n*-hexane: ethyl acetate 20:1. The product was obtained as a white solid (6.36 mmol, 1.18 g, 75 %). m.p. 41-45 °C (*n*-hexane). ^1H -NMR (d_6 -DMSO, 400 MHz, δ ; ppm): δ_{H} 2.24 (6H, s, C(2)CH₃, C(5)CH₃), 5.09 (2H, s, C(6)H₂), 5.95 (2H, s, C(3)H, C(4)H), 6.97 (2H, d, $J = 7.2$ Hz, C(8)H, C(12)H), 7.29 (1H, t, $J = 7.2$ Hz, C(10)H), 7.37 (2H, t, $J = 7.2$ Hz, C(9)H, C(11)H) ppm. ^{13}C NMR (d_6 -DMSO, 100 MHz, δ ; ppm) δ_{C} : 12.1 (2 C), 45.7, 105.6 (2 C), 125.5 (2 C), 126.9, 127.3, 128.4 (2 C), 138.7 ppm. MS (EI) m/z [M]⁺ calculated: 185.1204, found: 185.1209. The reported data are in good agreement with the literature.^{235,236}

Example (method b): Synthesis of 2,5-dimethyl-1-(phenylsulfonyl)-1H-pyrrole (26i)



In a sealed tube, was prepared a solution of 2,5-hexanedione (19.08 mmol, 3.0 eq, 2.24 mL) in glacial acetic acid (3 mL). Benzenesulfonamide (12.72 mmol, 1.0 eq, 2 g) and $\text{CoCl}_2 \times 6 \text{ H}_2\text{O}$ (0.64 mmol, 5 % mol, 0.151 g) were added to the solution. The reaction solution was stirred at 130 °C for 20 h. After this time, even if not complete (by TLC still 50 % of starting material), the reaction was stopped. The acetic acid was removed *in vacuo* (azeotrope with toluene) and the residue was purified by silica gel chromatography, eluting with *n*-hexane: ethyl acetate 15:1 (350.0 mg, 1.48 mmol, 12 %). m.p. 96-98 °C (cyclohexane). $^1\text{H-NMR}$ (CDCl_3 , 400 MHz, δ ; ppm): δ_{H} 2.41 (6H, s, C(2)CH₃, C(5)CH₃), 5.88 (2H, s, C(3)H, C(4)H), 7.53 (2H, t, J = 7.6 Hz, C(9)H, C(11)H), 7.60 (1H, t, J = 7.6 Hz, C(10)H), 7.67 (2H, d, J = 7.6 Hz, C(8)H, C(12)H) ppm. $^{13}\text{C NMR}$ (CDCl_3 , 100 MHz, δ ; ppm) δ_{C} : 12.4 (2 C), 107.1 (2C), 126.9 (2 C), 127.2 (2 C), 129.0 (2 C), 133.6, 138.2 ppm. MS (EI) m/z $[\text{M}]^+$ calculated: 235.0667, found: 235.0663. ²³⁷

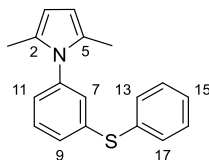
Synthesis of 2,5-dimethyl-1-(3-phenoxyphenyl)-1H-pyrrole (26h')



A flame dried sealed tube was loaded with 1-(3-bromophenyl)-2,5-dimethyl-1H-pyrrole **26d'** (1.99 mmol, 1.0 eq, 0.500 g), phenol (2.99 mmol, 1.5 eq, 0.282 g), Cs_2CO_3 (3.99 mmol, 2.0 eq, 1.303 g), CuI (0.20 mmol, 0.1 eq, 38.07 mg), and *N,N*-dimethylglycine hydrochloride (0.60 mmol, 0.3 eq, 83.75 mg), and dry dioxane (4 mL) was added. The system was degassed (N_2) and then stirred at 90 °C for 48 h. After this time TLC analysis indicated complete conversion of the starting material. The reaction was quenched by addition of H_2O (15 mL). The product was extracted with ethyl acetate ($3 \times 15 \text{ mL}$), the combined organic layers were washed with an aqueous saturated NaCl solution ($2 \times 5 \text{ mL}$), dried over Na_2SO_4 , filtered and concentrated *in vacuo*. The residue was further purified by silica gel chromatography eluting with petroleum ether: ethyl acetate 150:1, to obtain the pure 2,5-dimethyl-1-(3-phenoxyphenyl)-1H-pyrrole (1.25 mmol, 0.330 g, 63 %). m.p. 79-81 °C (cyclohexane). $^1\text{H-NMR}$ (CDCl_3 , 400 MHz, δ ; ppm): δ_{H} 1.96 (6H, s, C(2)CH₃, C(5)CH₃), 5.80 (2H, s, C(3)H, C(4)H), 6.74 (1H, t, J = 2.0 Hz, C(7)H), 6.85-6.88 (1H, m, C(11)H), 6.97-6.99 (3H, m, C(9)H, C(13)H, C(17)H) 7.07 (1H, t, J = 7.2 Hz, C(10)H), 7.26-7.34 (3H, m, C(14)H, C(15)H, C(16)H) ppm. $^{13}\text{C NMR}$ (CDCl_3 , 100 MHz, δ ;

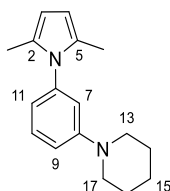
ppm) δ_C : 12.7 (2C), 107.1 (2C), 116.2, 118.4 (2C), 119.6, 124.0, 124.5, 126.7 (2C), 129.3 (2C), 130.2, 138.1, 156.8, 156.9 ppm. MS (EI) m/z $[M]^+$ calculated: 263.1310, found: 263.1314.

Synthesis of 2,5-dimethyl-1-(3-(phenylthio)phenyl)-1H-pyrrole (26i')



In a flame dried round bottom flask were added K_2CO_3 (2.72 mmol, 1.7 eq, 0.376 g), and dry *o*-xylene (3 mL), and the system was degassed (N_2), and cooled to 0 °C. Thiophenol (2.40 mmol, 1.5 eq, 0.264g, 0.246 mL) was added and the system was stirred at room temperature for 1 h. In a flame dried sealed tube was prepared a solution of 1-(3-bromophenyl)-2,5-dimethyl-1H-pyrrole (1.60 mmol, 1.0 eq, 0.400 g), $Pd_2(dba)_3$ (0.160 mmol, 10 % mol, 0.146 g), and xantphos (0.176 mmol, 11 % mol, 0.102 g) in *o*-xylene (8 mL). The solution was degassed (N_2) and stirred at room temperature for 20 mins. After this time, the thiophenolate suspension previously prepared was added to the reaction mixture. The system was heated to reflux for 20 h. After this time the reaction was judged to be complete by TLC analysis. The reaction was quenched by addition of H_2O (10 mL). The product was extracted with ethyl acetate (3×15 mL), the combined organic layers were washed with a 2 N aqueous solution of KOH (2×5 mL), and an aqueous saturated NaCl solution (2×5 mL), dried over Na_2SO_4 , filtered and concentrated *in vacuo*. The residue was further purified by silica gel chromatography eluting with *n*-hexane: ethyl acetate 40:1, obtaining the desired compound as a light-yellow solid (1.56 mmol, 0.435 g, 97 %). m.p. 75-78 °C (*n*-hexane). 1H -NMR ($CDCl_3$, 400 MHz, δ ; ppm): δ_H 2.02 (6H, s, C(2)CH₃, C(5)CH₃), 5.88 (2H, s, C(3)H, C(4)H), 7.05-7.09 (2H, m, C(10)H, C(15)H), 7.34-7.46 (7H, m, C(7)H, C(9)H, C(11)H, C(13)H, C(14)H, C(16)H, C(17)H) ppm. ^{13}C NMR ($CDCl_3$, 100 MHz, δ ; ppm) δ_C : 12.9 (2C), 106.7 (2C), 123.4, 126.3, 126.6 (2C), 127.0, 127.3, 128.6, 129.1 (2C), 130.2, 130.8 (2C), 133.1, 138.4 ppm. MS (EI) m/z $[M]^+$ calculated: 279.1082, found: 279.1085.

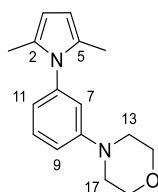
Synthesis of 1-(3-(2,5-dimethyl-1H-pyrrol-1-yl)phenyl)piperidine (26f')



In a flame dried sealed tube, 1-(3-bromophenyl)-2,5-dimethyl-1H-pyrrole (1.59 mmol, 1.0 eq, 0.400 g), piperidine (3.59 mmol, 2.0 eq, 0.272 g, 0.316 mL), $Pd(AcO)_2$ (0.024 mmol, 1.5 % mol, 5.4 mg), $PH^+(tBu)_3BF_3^-$ (0.019 mmol, 1.2 % mol, 5.6 mg), and $KOtBu$ (3.59 mmol, 2.25 eq,

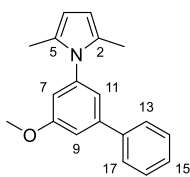
0.404 g) were added in sequence and suspended in dry toluene (4 mL). The system was degassed (N_2), and stirred at 80 °C for 4 h. After this time, TLC analysis indicated complete conversion of the starting material. The reaction was quenched with H_2O (10 mL). The product was extracted with ethyl acetate (3×15 mL), the combined organic layers were washed with an aqueous saturated NaCl solution (2×5 mL), dried over Na_2SO_4 , filtered and concentrated *in vacuo*. The crude was purified by silica gel chromatography eluting with *n*-hexane: ethyl acetate 5:1, to give 1-(3-(2,5-dimethyl-1H-pyrrol-1-yl)phenyl)piperidine as a colorless oil (1.27 mmol, 0.324 g, 80 %). 1H -NMR (d_6 -DMSO, 400 MHz, δ ; ppm): δ_H 1.59-1.60 (6H, m, C(14) H_2 , C(15) H_2 , C(16) H_2), 1.97 (6H, s, C(2)CH $_3$, C(5)CH $_3$), 3.17-3.20 (4H, m, C(13) H_2 , C(17) H_2), 5.70 (2H, s, C(3)H, C(4)H), 6.56 (1H, dd, J = 7.6 Hz, 2.0 Hz, C(11)H), 6.69 (1H, t, J =2.0 Hz, C(7)H), 6.97 (1H, dd, J = 7.6 Hz, 2.0 Hz, C(9)H), 7.29 (1H, t, J = 7.6 Hz, C(10)H) ppm. ^{13}C NMR (d_6 -DMSO, 100 MHz, δ ; ppm) δ_C : 12.8 (2C), 23.9, 26.3 (2C), 51.5 (2C), 106.8 (2C), 108.3, 113.2, 126.5, 127.2 (2C), 130.8, 139.0, 153.4 ppm. MS (EI) m/z $[M]^+$ calculated: 254.1783, found: 254.1782.

Synthesis of 4-(3-(2,5-dimethyl-1H-pyrrol-1-yl)phenyl)morpholine (26g')



In a flame dried sealed tube, 1-(3-bromophenyl)-2,5-dimethyl-1H-pyrrole (1.28 mmol, 1.1 eq, 0.320 g), morpholine (1.16 mmol, 1.0 eq, 0.101 g, 0.110 mL), $Pd(AcO)_2$ (0.012 mmol, 1 % mol, 2.6 mg), $PH^+(tBu)_3BF_3^-$ (0.009 mmol, 0.8 % mol, 2.7 mg), and $KOtBu$ (1.74 mmol, 1.5 eq, 0.196 g) were added in sequence and suspended in dry toluene (4 mL). The system was degassed (N_2), and left under stirring at 80 °C for 5 h. After this time, TLC analysis indicated complete conversion of the starting material. The reaction was quenched with H_2O (10 mL). The product was extracted with ethyl acetate (3×15 mL), the combined organic layers were washed with an aqueous saturated NaCl solution (2×5 mL), dried over Na_2SO_4 , filtered and concentrated *in vacuo*. The crude was purified by silica gel chromatography eluting with *n*-hexane: ethyl acetate 8:1, to give the pure 4-(3-(2,5-dimethyl-1H-pyrrol-1-yl)phenyl)morpholine as a light yellow oil (0.89 mmol, 0.227 g, 76 %). 1H -NMR (d_6 -DMSO, 400 MHz, δ ; ppm): δ_H 1.97 (6H, s, C(2)CH $_3$, C(5)CH $_3$), 3.16 (4H, t, J = 11.0 Hz, C(13) H_2 , C(17) H_2), 3.73 (4H, t, J = 11.0 Hz, C(14) H_2 , C(16) H_2), 5.76 (2H, s, C(3)H, C(4)H), 6.63 (1H, dd, J = 8.2 Hz, 2.0 Hz, C(11)H), 6.73 (1H, t, J = 2.0 Hz, C(7)H), 6.99 (1H, dd, J = 8.2 Hz, 2.0 Hz, C(9)H), 7.32 (1H, t, J = 8.0 Hz, C(10)H) ppm. ^{13}C NMR (d_6 -DMSO, 100 MHz, δ ; ppm) δ_C : 12.7 (2C), 48.2 (2C), 66.5 (2C), 106.8 (2C), 108.3, 113.1, 126.5, 126.9 (2C), 130.7, 139.0, 153.4 ppm. MS (EI) m/z $[M]^+$ calculated: 256.1576, found: 256.1578.

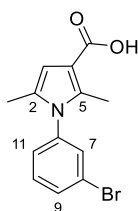
Synthesis of 1-(5-methoxy-[1,1'-biphenyl]-3-yl)-2,5-dimethyl-1H-pyrrole (26j')



A sealed tube was loaded with 1-(3-bromo-5-methoxyphenyl)-2,5-dimethyl-1H-pyrrole **26k'** (1.78 mmol, 1.0 eq, 0.500 g) and it was dissolved in a 3:1 mixture of THF (3.6 mL) and ethanol (1.2 mL). Phenylboronic acid (1.78 mmol, 1.0 eq, 0.217 g), a 2 M aqueous solution of Na₂CO₃ (3.74 mmol, 2.1 eq, 0.396 g), and Pd(Ph₃P)₄ (0.089 mmol, 5 % mol, 0.103 g) were added. The reaction mixture was stirred at 100 °C for 8 h. After this time the reaction was judged to be complete by TLC analysis, and it was quenched by addition of H₂O (7 mL). The product was extracted with ethyl acetate (3 × 15 mL), the combined organic layers were washed with an aqueous saturated NaCl solution (2 × 5 mL), dried over Na₂SO₄, filtered and concentrated *in vacuo*. The crude was purified by silica gel chromatography eluting with petroleum ether: ethyl acetate 90:1, giving the pure 1-(5-methoxy-[1,1'-biphenyl]-3-yl)-2,5-dimethyl-1H-pyrrole (1.33 mmol, 0.370 g, 75 %) m.p. 84-87 °C (cyclohexane). ¹H-NMR (*d*₆-DMSO, 400 MHz, δ; ppm): δ_H 2.03 (6H, s, C(2)CH₃, C(5)CH₃), 3.80 (3H, s, OCH₃), 5.85 (2H, s, C(3)H, C(4)H), 6.67 (1H, t, *J*= 2.0 Hz, C(9)H), 6.98 (1H, t, *J*= 1.6 Hz, C(7)H), 7.09 (1H, t, *J*= 2.0 Hz, C(11)H), 7.28-7.32 (1H, m, C(15)H), 7.36-7.40 (2H, m, (C(14)H, C(16)H), 7.51-7.54 (2H, m, C(13)H and C(17)H) ppm. ¹³C NMR (*d*₆-DMSO, 100 MHz, δ; ppm) δ_C: 12.9 (2C), 55.8, 106.8 (2C), 107.9, 108.7, 117.5, 126.6 (2C), 127.5, 127.9 (2C), 129.6 (2C), 138.8, 140.7, 142.4, 162.3 ppm. MS (EI) *m/z* [M]⁺ calculated: 277.1467, found: 277.1462.

General procedure for the synthesis of pyrroles-3-carboxylic acids (31c-h, k-q, t, u, z, a'-j').

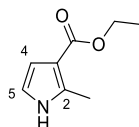
Example: Synthesis of 1-(3-bromophenyl)-2,5-dimethyl-1H-pyrrole-3-carboxylic acid (31d')



In a sealed tube, 1-(3-bromophenyl)-2,5-dimethyl-1H-pyrrole (1.60 mmol, 1.0 eq, 0.400 g) was dissolved in dichloroethane (5 mL) and the solution was cooled to 0 °C. Trichloroacetyl chloride (4.80 mmol, 3.0 eq, 0.536 mL) was added dropwise. The solution was stirred at 0 °C for 10 minutes, then let warm to room temperature and finally heat to 70 °C. The reaction was stirred at this temperature for 1 h. After this time, TLC analysis showed complete conversion of the starting material. The volatiles were removed *in vacuo*. The residue was dissolved in a 1:1 EtOH : THF mixture. The solution was cooled to 0 °C and a 2 M aqueous solution of KOH (16.0 mmol,

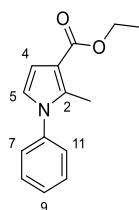
10 eq, 0.898 g) was added dropwise. The reaction mixture was stirred at room temperature for 1 h. After this time the reaction was judged to be complete by TLC analysis. The organic solvents were removed *in vacuo*. The byproducts were extracted from the basic aqueous layer with ethyl acetate (3×10 mL). The aqueous layer was then cooled to 0 °C and acidified till pH 2 by addition of a 2 M aqueous solution of HCl. The product precipitated, it was filtered, rinsed several times with distilled water and dried in oven (60 °C). Y 61 %. m.p. > 250 °C (ethanol). ¹H-NMR (*d*₆-DMSO, 400 MHz, δ ; ppm): δ_{H} 1.94 (3H, s, C(5)CH₃), 2.21 (3H, s, C(2)CH₃), 6.23 (1H, s, C(4)H), 7.34-7.37 (1H, dd, J = 7.2 Hz, 0.8 Hz, C(11)H), 7.52 (1H, t, J = 8 Hz, C(10)H), 7.62 (1H, t, J = 1.6 Hz, C(7)H), 7.72 (1H, dd, J = 8 Hz, 0.8 Hz, C(9)H), 11.68 (1H, bs, COOH) ppm. ¹³C NMR (*d*₆-DMSO, 100 MHz, δ ; ppm) δ_{C} : 12.1, 13.4, 107.1, 111.8, 120.5, 125.6, 126.1, 126.7, 130.5, 130.9, 136.0, 138.5, 165.5 ppm. MS (EI) m/z [M]⁺ calculated: 293.0051, 295.0031 found: 293.0050, 295.0029.

Synthesis of ethyl 2-methyl-1H-pyrrole-3-carboxylate (28)



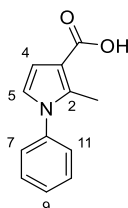
A mixture of ethyl acetoacetate (15.3 mmol, 1.0 eq, 2.0 g) and 2-chloroacetaldehyde (15.3 mmol, 1.0 eq, 1.96 mL) was cooled to 0 °C. A 17 M aqueous solution of NH₃ (46.2 mmol, 3.0 eq, 2.72 mL) was added dropwise. The reaction solution was left under stirring at room temperature for 20 h. After this time the reaction was quenched with H₂O (7 mL). The product was extracted with ethyl acetate (3×15 mL). The combined organic layers were washed with a 2N aqueous solution of HCl, (2×5 mL) and a saturated aqueous solution of NaCl (2×5 mL), dried over Na₂SO₄, filtered and concentrated *in vacuo*. (750 mg, 4.90 mmol, 32 %) m.p. 75-78 °C (*n*-hexane). ¹H-NMR (CDCl₃, 400 MHz, δ ; ppm): δ_{H} 1.36 (3H, t, J = 7.2 Hz, COOCH₂CH₃), 2.55 (3H, s, C(2)CH₃), 4.29 (2H, q, J = 7.2 Hz, COOCH₂CH₃), 6.57-6.59 (2H, m, C(4)H, C(5)H), 8.35 (1H, bs, NH) ppm. ¹³C NMR (CDCl₃, 100 MHz, δ ; ppm) δ_{C} : 13.7, 14.8, 59.2, 110.4, 111.7, 115.8, 134.9, 165.6 ppm. MS (EI) m/z [M]⁺ calculated: 153.0790, found: 153.0794. The reported data are in good agreement with the literature.^{238,239}

Synthesis of ethyl 2-methyl-1-phenyl-1H-pyrrole-3-carboxylate (29)



In a flame dried sealed tube was added ethyl 2-methyl-1H-pyrrole-3-carboxylate (1.31 mmol, 1.0 eq, 0.200 g), and it was solubilized in 1.5 mL of dry toluene and the system was degassed (N_2). K_3PO_4 (2.73 mmol, 2.1 eq, 0.579 g), *N, N'*-dimethylethylenediamine (0.26 mmol, 0.2 eq, 22.9 mg), and CuI (0.065 mmol, 0.05 eq, 12.4 mg) were added under N_2 flow. The reaction mixture was then left under stirring at 130 °C for 5 h. After this time, the reaction was judged complete by TLC analysis. The inorganic salts were removed by filtration, and the residue was purified by silica gel chromatography eluting with *n*-hexane: ethyl acetate 4:1, to obtain a light yellow oil. The product obtained was triturated with petroleum ether to give ethyl 2-methyl-1-phenyl-1H-pyrrole-3-carboxylate (1.23 mmol, 0.282 g, 94 %). m.p. 170-172 °C (toluene/acetonitrile). 1H -NMR ($CDCl_3$, 400 MHz, δ ; ppm): δ_H 1.38 (3H, t, J = 6.4 Hz, $COOCH_2CH_3$), 2.46 (3H, s, C(2)CH₃), 4.32 (2H, q, J = 6.4 Hz, $COOCH_2CH_3$), 6.69 (2H, s, C(4)H, C(5)H), 7.29 (2H, d, J = 7.6 Hz, C(7)H, C(11)H), 7.43-7.49 (3H, m, C(8)H, C(9)H, C(10)H) ppm. ^{13}C NMR ($CDCl_3$, 100 MHz, δ ; ppm) δ_C : 12.8, 14.5, 59.2, 109.9, 113.6, 121.4, 125.9 (2C), 127.9, 129.4 (2C), 136.1, 139.4, 165.6 ppm. MS (EI) m/z $[M]^+$ calculated: 229.1103, found: 229.1109. The reported data are in good agreement with the literature.²⁴⁰

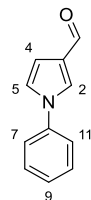
Synthesis of 2-methyl-1-phenyl-1H-pyrrole-3-carboxylic acid (31b)



A solution of ethyl 2-methyl-1-phenyl-1H-pyrrole-3-carboxylate (1.20 mmol, 1.0 eq, 0.280 mg) in ethanol (3 mL) was cooled to 0 °C and a 2 M aqueous solution of KOH (4.80 mmol, 4 eq, 0.269 g) was added dropwise to this solution. The reaction mixture was stirred at room temperature for 20 minutes and then heated to 70 °C for 4 h. After this time, 8 eq of KOH were added and the reaction was stirred at 70 °C for 20 h. Even if there was a residue of starting material, the reaction was stopped. The organic solvent was removed *in vacuo*, and the residue was diluted with H_2O . The residual starting material was extracted with CH_2Cl_2 from basic H_2O . The aqueous solution was then cooled to 0 °C and titrated by addition of a 2 M aqueous solution of HCl till pH 1. The product was then extracted with ethyl acetate (3×10 mL). The combined organic layers were washed with a saturated aqueous solution of NaCl (2×5 mL), dried over Na_2SO_4 , filtered and concentrated *in vacuo*. The compound was used without further purification (229 mg, 1.14 mmol, 95 %). m.p. 197-199 °C (acetonitrile). 1H -NMR (d_6 -DMSO, 400 MHz, δ ; ppm): δ_H 1.93 (3H, s, C(2)CH₃), 6.23 (1H, d, J = 7.5 Hz, C(4)H), 7.31 (2H, d, J = 7.2 Hz, C(7)H, C(11)H), 7.40 (1H, d, J = 7.5 Hz, C(5)H), 7.49-7.60 (3H, m, C(8)H, C(9)H, C(10)H), 11.95 (1H, bs, COOH) ppm. ^{13}C NMR (d_6 -DMSO, 100 MHz, δ ; ppm) δ_C : 12.8, 109.7, 114.2, 122.7, 125.9

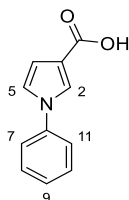
(2C), 128.1, 129.2 (2C), 136.8, 138.6, 166.2 ppm. MS (EI) m/z $[M]^+$ calculated: 201.0790, found: 201.0787.

Synthesis of 1-phenyl-1H-pyrrole-3-carbaldehyde (27 β)



In a flame dried round bottom flask was prepared a solution of dry DMF (1.40 mmol, 1.2 eq, 0.100 mL) in dry DCE (1.6 mL). The solution was cooled to 0 °C and oxalyl chloride (1.40 mmol, 1.2 eq, 0.118 mL) was added. The solution was stirred at 0 °C for 15 minutes. 1-phenylpyrrole (13.8 mmol, 1.0 eq, 2.0 g) was added dropwise, and the reaction mixture was let warm to room temperature and stirred for 2 h. After this time the reaction was quenched by adding a 2 M aqueous KOH solution. The product was extracted with ethyl acetate (3 × 15 mL), the combined organic layers were washed with a saturated aqueous solution of NaCl (2 × 5 mL), dried over Na₂SO₄, filtered and concentrated *in vacuo*. The product was further purified by silica gel chromatography eluting with *n*-hexane: ethyl acetate 5:1. The α and β formylated products were isolated. The β -formyl derivative was obtained in 32 % yield (yellow oil), where the α -formyl isomer was obtained with 48 % yield. ¹H-NMR (*d*₆-DMSO, 400 MHz, δ ; ppm): δ_H 6.69 (1H, d, J = 7.6 Hz, C(4)H), 7.05 (1H, t, C(9)H), 7.32 (1H, d, J = 7.6 Hz, C(5)H), 7.54 (2H, t, J = 7.6 Hz, C(8)H, C(10)H), 7.61 (1H, s, C(2)H), 7.76 (2H, d, J = 7.8 Hz, C(7)H, C(11)H), 9.81 (1H, s, CHO) ppm. ¹³C NMR (*d*₆-DMSO, 100 MHz, δ ; ppm) δ_C : 109.9, 119. 3, 121.0 (2C), 125.1, 127.3, 127.8, 129.6 (2C), 139.7, 185.2 ppm. MS (EI) m/z $[M]^+$ calculated: 171.0684, found: 171.0689.

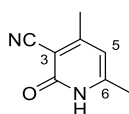
Synthesis of 1-phenyl-1H-pyrrole-3-carboxylic acid (31a)



To a solution of 1-phenyl-1H-pyrrole-3-carbaldehyde (3.60 mmol, 1.0 eq, 0.616 g) in methanol (3 mL), were added AgNO₃ (5.76 mmol, 1.6 eq, 0.0977 g) and a 6 M aqueous solution of NaOH (22.5 mmol, 6.25 eq, 0.899g). The reaction mixture was heated to reflux for 5 h. After this time the reaction was complete. The reaction mixture was cooled to 0 °C and the reaction was quenched by slow addition of a 2 M aqueous solution of HCl till pH 2. The product was extracted with ethyl acetate (3 × 15 mL), the combined organic layers were washed with a saturated

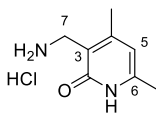
aqueous solution of NaCl (2×5 mL), dried over Na_2SO_4 , filtered and concentrated *in vacuo*. The extract was triturated with petroleum ether, filtered. The solid was rinsed several times with petroleum ether, and dried in oven (60°C). Y 62 %. m.p. $193\text{--}195^\circ\text{C}$ (acetonitrile). $^1\text{H-NMR}$ (d_6 -DMSO, 400 MHz, δ ; ppm): δ_{H} 6.61 (1H, bs, C(4)H), 7.34 (1H, t, $J=7.6$ Hz, C(9)H), 7.43 (1H, bs, C(5)H), 7.50 (2H, t, $J=7.6$ Hz, C(8)H, C(10)H), 7.67 (2H, d, $J=7.8$ Hz, C(7)H, C(11)H), 7.93 (1H, bs, C(2)H), 12.09 (1H, bs, COOH) ppm. $^{13}\text{C NMR}$ (d_6 -DMSO, 100 MHz, δ ; ppm) δ_{C} : 115.9, 116.3, 117.5, 120.6 (2C), 125.2, 126.7, 129.8 (2C), 139.7, 165.2 ppm. MS (EI) m/z $[\text{M}]^+$ calculated: 187.0633, found: 187.0635. The reported data are in good agreement with the literature.²⁴¹

Synthesis of 4,6-dimethyl-2-oxo-1,2-dihydropyridine-3-carbonitrile (32)



A solution of 2-cyanoacetamide (47.0 mmol, 1.0 eq, 4.0 g), and piperidine (6.20 mmol, 0.13 eq, 0.61 mL) in ethanol (30 mL) was stirred at 70°C for 40 min. After this time, the solution was let cool to room temperature, and 2,4-pentanedione (47.0 mmol, 1.0 eq, 4.9 mL) was added. The reaction was stirred at 70°C for 3 h. After this time the reaction was judged to be complete by TLC analysis. The product precipitated and it was filtered. The solid on the filter was rinsed with ethanol and diethyl ether, and then dried to give as a white solid (20.2 mmol, 3.0 g, 43 %). m.p. $288\text{--}290^\circ\text{C}$ (methanol). $^1\text{H-NMR}$ (d_6 -DMSO, 400 MHz, δ ; ppm): δ_{H} 2.22 (3H, s, C(4) H_3), 2.29 (3H, s, C(6) H_3), 6.14 (1H, bs, C(5)H), 12.29 (1H, bs, NH) ppm. $^{13}\text{C NMR}$ (d_6 -DMSO, 100 MHz, δ ; ppm) δ_{C} : 19.3, 19.6, 104.3, 110.1, 111.4, 150.6, 159.9, 160.8 ppm. MS (EI) m/z $[\text{M}]^+$ calculated: 148.0637, found: 148.0639.¹⁵⁹

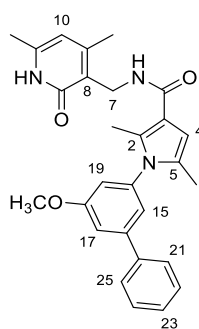
Synthesis of 3-(aminomethyl)-4,6-dimethylpyridin-2(1H)-one hydrochloride (33)



4,6-Dimethyl-2-oxo-1,2-dihydropyridine-3-carbonitrile (13.5 mmol, 1.0 eq, 2.0 g) was suspended in 5 mL of acetic acid and the system was degassed (N_2). Pd/C (1.35 mmol, 10 % mol, 0.144 mg) and PtO_2 (0.062 mmol, 0.05 eq, 14.11 mg) were added. H_2 gas (70 psi) was bubbled into the reaction mixture through a Paar-apparatus for 6 h at 40°C . After this time the reaction was judged complete by TLC analysis. The suspension was filtered and the acetic acid removed *in vacuo* (azeotrope with toluene). The residue was dissolved in ethanol (20 mL). The solution was cooled to 0°C and 3 mL of a 6 M aqueous solution of HCl were added dropwise. The product

immediately precipitated as hydrochloric salt. The system was left under stirring at 0 °C for 2 h. The product was then filtered, rinsed with ethanol and diethyl ether, to give the pure amine as a white solid. Y 69 %. m.p. 295-298 °C (ethanol). ¹H-NMR (*d*₆-DMSO, 400 MHz, δ; ppm): δ_H 2.16 (3H, s, C(4)CH₃), 2.21 (3H, s, C(6)CH₃), 3.77 (2H, bs, C(7)H₂), 5.97 (1H, s, C(5)H), 8.17 (2H, bs, NH₂), 11.58 (1H, bs, NHCO) ppm. ¹³C NMR (*d*₆-DMSO, 100 MHz, δ; ppm) δ_C: 18.8, 19.1, 38.2, 111.3, 116.7, 151.4, 156.1, 163.7 ppm. MS (EI) *m/z* [M-HCl]⁺ calculated: 152.0950, found: 152.0946. ¹⁵⁹

General procedure for the synthesis of pyrrole amides(25a-h, k-z, a'-j'). Example: Synthesis of N-((4,6-dimethyl-2-oxo-1,2-dihydropyridin-3-yl)methyl)-1-(5-methoxy-[1,1'-biphenyl]-3-yl)-2,5-dimethyl-1H-pyrrole-3-carboxamide (25j')

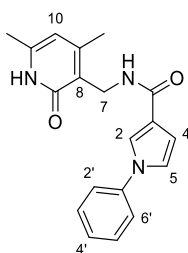


In a flame dried round bottom flask, 1-(5-methoxy-[1,1'-biphenyl]-3-yl)-2,5-dimethyl-1H-pyrrole-3-carboxylic acid (0.218 mmol, 1.0 eq, 70.0 mg) was solved in dry DMF (0.3 mL) under N₂ atmosphere. Triethylamine (1.53 mmol, 7.0 eq, 0.213 mL), and O-(benzotriazol-1-yl)-*N,N,N',N'*-tetramethyluronium tetrafluoroborate (TBTU) (0.262 mmol, 1.2 eq, 83.9 mg) were added to the reaction solution, and the system was left under stirring at room temperature for 40 minutes. After this time, the acid activation was confirmed by TLC analysis. 3-(Aminomethyl)-4,6-dimethylpyridin-2(1H)-one hydrochloride (0.239 mmol, 1.1 eq, 45.2 mg) was added to the solution and the reaction was stirred under N₂ at room temperature for 16 h. After this time, the reaction was judged complete by TLC analysis and it was quenched by addition of 3 mL of a saturated aqueous solution of NaCl. The product precipitated, and it was filtered and rinsed with distilled water. The solid was dried and further purified by silica gel chromatography eluting with ethyl acetate: methanol 40:1, to give **25j'** (0.142 mmol, 64.6 mg, 65 %). m.p. 140-145 °C (benzene). ¹H NMR (DMSO-*d*₆, 400 MHz, δ, ppm): δ_H 1.99 (3H, s, C(5)CH₃), 2.12 (3H, s, C(11)CH₃), 2.18 (3H, s, C(9)CH₃), 2.27 (3H, s, C(2)CH₃), 3.87 (3H, s, -OCH₃), 4.23 (2H, d, *J*= 5.2 Hz, C(7)H₂), 5.86 (1H, s, C(10)H), 6.31 (1H, s, C(4)H) 6.84 (1H, s, C(17)H), 7.11 (1H, s, C(19)H), 7.38 (1H, s, C(15)H), 7.32-7.49 (4H, m, C(22)H, C(23)H, C(24)H and -CH₂NHCO-), 7.75 (2H, d, *J*= 7.6 Hz, C(21)H, C(25)H), 11.48 (1H, bs, -NH- pyridone). ¹³C NMR (DMSO-*d*₆, 100 MHz, δ, ppm): δ_C 12.1, 13.4, 18.5, 19.6, 32.7, 55.7, 104.6, 108.1, 109.0, 110.9, 114.3, 116.1,

117.8, 127.7, 127.8 (2 C), 129.6 (2 C), 130.1, 131.5, 138.7, 140.7, 142.3, 151.6, 157.9, 162.1, 163.7, 167.6 ppm. MS (EI) m/z $[M]^+$ calculated: 455.2209, found: 455.2213.

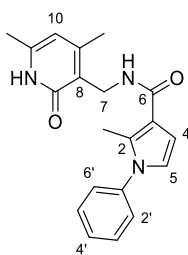
Chemical and Physical Data, ^1H NMR, ^{13}C NMR, and MS (EI) Data for Compounds 25a-h, k-z, a'-i'.

N-((4,6-dimethyl-2-oxo-1,2-dihydropyridin-3-yl)methyl)-1-phenyl-1H-pyrrole-3-carboxamide (25a)



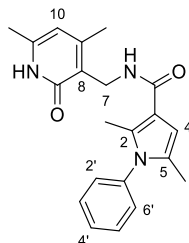
^1H NMR (DMSO- d_6 , 400 MHz, δ , ppm): δ 2.12 (3H, s, C(11) CH_3), 2.18 (3H, s, C(9) CH_3), 4.26 (2H, bs, C(7) H_2), 6.68 (1H, s, C(10) H), 7.30 (1H, t, J = 7.6 Hz, C(4') H), 7.35 (1H, bs, C(4) H), 7.48 (2H, t, J = 7.6 Hz, C(3') H and C(5') H), 7.59 (2H, d, J = 7.6 Hz, C(2') H and C(6') H), 7.75 (1H, bs, C(5) H), 7.97 (1H, s, C(2) H), 11.49 (1H, s, -NH- pyridone) ppm; ^{13}C NMR (DMSO- d_6 , 100 MHz, δ , ppm): δ 18.5, 19.1, 32.6, 106.5, 110.9, 115.7, 116.0, 120.4, 120.5, 120.8 (2C), 126.7, 129.8 (2C), 139.5, 151.7, 158.2, 163.6, 166.4 ppm; m.p. 115-120 $^\circ\text{C}$ (cyclohexane); Y = 56 %; MS (EI) m/z $[M]^+$ calculated: 321.1477, found: 321.1476.

N-((4,6-dimethyl-2-oxo-1,2-dihydropyridin-3-yl)methyl)-2-methyl-1-phenyl-1H-pyrrole-3-carboxamide (25b)



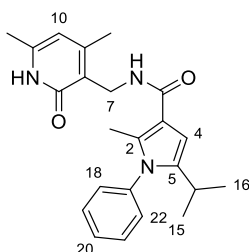
^1H NMR (DMSO- d_6 , 400 MHz, δ , ppm): δ_{H} 2.12 (3H, s, C(11) CH_3), 2.19 (3H, s, C(9) CH_3), 2.38 (3H, s, C(2) CH_3), 4.25 (2H, d, J = 5.6 Hz, C(7) H_2), 5.86 (1H, s, C(10) H), 6.61 (1H, d, J = 3.2 Hz, C(5) H), 6.80 (1H, d, J = 3.2 Hz, C(4) H), 7.36 (2H, d, J = 8 Hz, C(2') H and C(6') H), 7.44 (1H, t, J = 7.2 Hz, C(4') H), 7.52 (2H, t, J = 8 Hz, C(3') H and C(5') H), 7.58 (1H, t, J = 5.4 Hz, - CH_2NHCO -), 11.46 (1H, s, -NH- pyridone) ppm; ^{13}C NMR (DMSO- d_6 , 100 MHz, δ , ppm): δ_{C} 11.6, 18.5, 19.1, 32.8, 110.1, 111.3, 116.0, 120.2, 123.1, 125.3 (2C), 127.9, 129.3 (2C), 134.8, 137.7, 151.6, 157.9, 163.6, 167.3 ppm; m.p. 197-199 $^\circ\text{C}$ (acetonitrile); Y = 61 %; MS (EI) m/z $[M]^+$ calculated: 335.1634, found: 335.1639.

N-((4,6-dimethyl-2-oxo-1,2-dihydropyridin-3-yl)methyl)-2,5-dimethyl-1-phenyl-1H-pyrrole-3-carboxamide (25c)



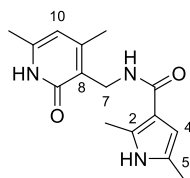
^1H NMR (DMSO- d_6 , 400 MHz, δ , ppm): δ_{H} 1.91 (3H, s, C(5) CH_3) 2.12 (3H, s, C(11) CH_3), 2.18 (3H, s, C(9) CH_3), 2.19 (3H, s, C(2) CH_3), 4.23 (2H, d, J = 5.2 Hz, C(7) H_2), 5.86 (1H, s, C(10) H), 6.29 (1H, s, C(4) H), 7.26 (2H, d, J = 7.2 Hz, C(2') H and C(6') H), 7.42 (1H, t, J = 5.6 Hz, - CH_2NHCO -), 7.49-7.56 (3H, m, C(3') H , C(4') H and C(5') H), 11.45 (1H, s, -NH- pyridone) ppm; ^{13}C NMR (DMSO- d_6 , 100 MHz, δ , ppm): δ_{C} 12.0, 13.3, 18.5, 19.1, 32.8, 104.7, 111.4, 114.2, 116.0, 127.8 (2C), 128.1, 129.1 (2C), 130.0, 131.4, 136.3, 151.5, 157.9, 163.6, 167.5 ppm; m.p. 220-225 $^{\circ}\text{C}$ (acetonitrile/methanol); Y= 58 %; MS (EI) m/z $[\text{M}]^+$ calculated: 349.1790, found: 349.1786.

N-((4,6-dimethyl-2-oxo-1,2-dihydropyridin-3-yl)methyl)-5-isopropyl-2-methyl-1-phenyl-1H-pyrrole-3-carboxamide (25d).



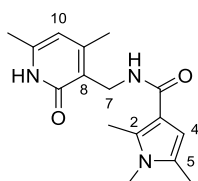
^1H NMR (DMSO- d_6 , 400 MHz, δ , ppm): δ_{H} 0.98 (6H, d, J = 6.4 Hz, C(15) CH_3 , C(16) CH_3), 2.12 (3H, s, C(9) CH_3), 2.16 (3H, s, C(11) CH_3), 2.18 (3H, s, C(2) CH_3), 2.49-2.51 (1H, m, C(14) H), 4.23 (2H, d, J = 5.2 Hz C(7) H_2), 5.87 (1H, s, C(10) H), 6.36 (1H, s, C(4) H), 7.28 (2H, d, J = 6.8 Hz, C(18) H , C(22) H), 7.46-7.55 (4H, m, C(19) H , C(20) H , C(21) H , and - CH_2NHCO -), 11.47 (1H, s, -NH- pyridone) ppm; ^{13}C NMR (DMSO- d_6 , 100 MHz, δ , ppm): δ_{C} 12.1, 18.5, 19.1, 20.8 (2C), 26.1, 32.8, 105.7, 111.1, 113.2, 116.0, 127.3 (2C), 128.1, 129.1 (2C), 132.1, 136.2, 143.8, 151.5, 157.9, 163.6, 167.5 ppm; m.p. 235-239 $^{\circ}\text{C}$ (acetonitrile/methanol); Y= 54 %. MS (EI) m/z $[\text{M}]^+$ calculated: 377.2103, found: 377.2108.

N-((4,6-dimethyl-2-oxo-1,2-dihydropyridin-3-yl)methyl)-2,5-dimethyl-1H-pyrrole-3-carboxamide (25e)



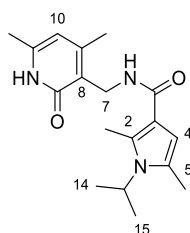
^1H NMR (DMSO- d_6 , 400 MHz, δ , ppm): δ_{H} 2.07 (3H, s, C(5) CH_3), 2.11 (3H, s, C(11) CH_3), 2.16 (3H, s, C(9) CH_3), 2.33 (3H, s, C(2) CH_3), 4.18 (2H, d, J = 4.8 Hz C(7) H_2), 5.84 (1H, s, C(10) H), 5.97 (1H, s, C(4) H), 7.19 (1H, t, J = 4.8 Hz, $-\text{CH}_2\text{NHCO}-$), 10.62 (1H, s, $-\text{NH}-$ pyrrole), 11.42 (1H, s, $-\text{NH}-$ pyridone) ppm; ^{13}C NMR (DMSO- d_6 , 100 MHz, δ , ppm): δ_{C} 13.3, 13.5, 18.4, 19.1, 32.8, 102.4, 110.4, 110.9, 116.0, 122.9, 133.7, 151.5, 157.9, 163.6, 168.0 ppm; m.p. 210-215 $^{\circ}\text{C}$ (acetonitrile/methanol); Y= 52 %; MS (EI) m/z $[\text{M}]^+$ calculated: 273.1477, found: 273.1480.

N-((4,6-dimethyl-2-oxo-1,2-dihydropyridin-3-yl)methyl)-1,2,5-trimethyl-1H-pyrrole-3-carboxamide (25f)



^1H NMR (DMSO- d_6 , 400 MHz, δ , ppm): δ 2.13 (6H, s, C(5) CH_3 and C(9) CH_3), 2.15 (3H, s, C(11) CH_3), 2.41 (3H, s, C(2) CH_3), 3.32 (3H, s, $-\text{NCH}_3$), 4.18 (2H, d, J = 5.2 Hz, C(7) H), 5.84 (1H, s, C(10) H), 6.07 (1H, s, C(4) H), 7.25 (1H, t, J = 5.2 Hz, $-\text{CH}_2\text{NHCO}-$), 11.46 (1H, s, $-\text{NH}-$ pyridone) ppm; ^{13}C NMR (DMSO- d_6 , 100 MHz, δ , ppm): δ 11.7, 12.5, 18.5, 19.1, 30.9, 32.8, 102.9, 111.2, 112.3, 116.0, 130.8, 133.1, 151.5, 157.9, 163.6, 167.4 ppm; m.p. 222-225 $^{\circ}\text{C}$ (acetonitrile/methanol); Y= 54 %; MS (EI) m/z $[\text{M}]^+$ calculated: 287.1634, found: 287.1635.

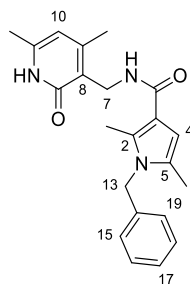
N-((4,6-dimethyl-2-oxo-1,2-dihydropyridin-3-yl)methyl)-1-isopropyl-2,5-dimethyl-1H-pyrrole-3-carboxamide (25g)



^1H NMR (DMSO- d_6 , 400 MHz, δ , ppm): δ_{H} 1.38 (6H, d, J = 6.8 Hz, C(14) H_3 and C(15) H_3), 2.11 (3H, s, C(5) CH_3), 2.16 (3H, s, C(9) CH_3), 2.19 (3H, s, C(11) CH_3), 2.50 (3H, s, C(2) CH_3), 4.18

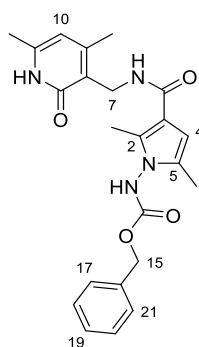
(2H, d, $J = 4.8$ Hz, C(7) H_2), 4.41-4.45 (1H, m, C(13) H), 5.84 (1H, s, -CH- pyridone), 6.03 (1H, s, C(4) H), 7.21 (1H, t, $J = 4.8$ Hz, -CH $_2$ NHCO-), 11.44 (1H, s, -NH- pyridone) ppm; ^{13}C NMR (DMSO- d_6 , 100 MHz, δ , ppm): δ_{C} 12.6, 14.1, 18.5, 19.1, 20.4 (2C), 32.8, 48.2, 103.8, 111.2, 114.3, 116.0, 125.4, 132.3, 151.5, 157.9, 163.6, 167.5 ppm; m.p. 180-185 °C (acetonitrile); Y= 63 %; MS (EI) m/z $[M]^+$ calculated: 315.1947, found: 315.1949.

1-benzyl-N-((4,6-dimethyl-2-oxo-1,2-dihydropyridin-3-yl)methyl)-2,5-dimethyl-1H-pyrrole-3-carboxamide (25h)



^1H NMR (DMSO- d_6 , 400 MHz, δ , ppm): δ_{H} 2.05 (3H, s, C(5) CH_3), 2.12 (3H, s, C(9) CH_3), 2.18 (3H, s, C(11) CH_3), 2.36 (3H, s, C(2) CH_3), 4.20 (2H, d, $J = 5.2$ Hz, C(7) H_2), 5.08 (2H, s, C(13) H_2), 5.86 (1H, s, C(10) H), 6.20 (1H, s, C(4) H), 6.87 (2H, d, $J = 7.2$ Hz, C(15) H , C(19) H), 7.24 (1H, t, $J = 7.2$ Hz, -CH $_2$ NHCO-), 7.30-7.37 (3H, m, C(16) H , C(17) H , C(18) H), 11.46 (1H, s, -NH- pyridone) ppm; ^{13}C NMR (DMSO- d_6 , 100 MHz, δ , ppm): δ_{C} 11.9, 12.3, 18.5, 19.1, 32.7, 48.8, 102.6, 111.3, 113.5, 116.0, 127.6 (2C), 127.8, 128.5 (2C), 129.5, 136.6, 151.5, 157.9, 163.6, 167.5 ppm; m.p. 205-208 °C (acetonitrile); Y= 50 %; MS (EI) m/z $[M]^+$ calculated: 363.1947, found: 363.1945.

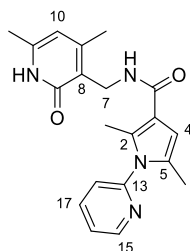
Benzyl (3-(((4,6-dimethyl-2-oxo-1,2-dihydropyridin-3-yl)methyl)carbamoyl)-2,5-dimethyl-1H-pyrrol-1-yl)carbamate (25k)



^1H NMR (DMSO- d_6 , 400 MHz, δ , ppm): δ_{H} 1.98 (3H, s, C(5) CH_3), 2.11 (3H, s, C(9) CH_3), 2.16 (3H, s, C(11) CH_3), 2.26 (3H, s, C(2) CH_3), 4.20 (2H, bs, C(7) H_2), 5.19 (2H, s, C(15) H_2), 5.85 (1H, s, C(10) H), 6.14 (1H, s, C(4) H), 7.38-7.42 (6H, m, C(17) H , C(18) H , C(19) H , C(20) H ,

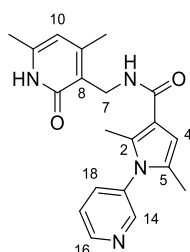
C(21)*H* and -CH₂NHCO-), 10.46 (1H, s, -NHCOOCH₂Ph), 11.43 (1H, s, -NH- pyridone) ppm; ¹³C NMR (DMSO-*d*₆, 100 MHz, δ, ppm): δ_C 11.3, 11.9, 18.5, 19.1, 32.8, 66.7, 103.1, 111.0, 113.2, 115.9, 127.9, 128.1 (2C), 128.3 (2C), 131.6, 132.6, 136.1, 151.5, 157.9, 158.2, 163.6, 167.5 ppm; m.p. 256-259 °C (methanol); Y= 60 %. MS (EI) *m/z* [M]⁺ calculated: 422.1954, found: 422.1956.

N-((4,6-dimethyl-2-oxo-1,2-dihydropyridin-3-yl)methyl)-2,5-dimethyl-1-(pyridin-2-yl)-1H-pyrrole-3-carboxamide (25l)



¹H NMR (DMSO-*d*₆, 400 MHz, δ, ppm): δ_H 1.97 (3H, s, C(5)CH₃), 2.12 (3H, s, C(9)CH₃), 2.18 (3H, s, C(11)CH₃), 2.26 (3H, s, C(2)CH₃), 4.23 (2H, d, *J*= 4.8 Hz, C(7)H₂), 5.86 (1H, s, C(10)*H*), 6.30 (1H, s, C(4)*H*), 7.44-7.53 (3H, m, C(15)*H*, C(16)*H* and -CH₂NHCO-), 8.03 (1H, t, *J*= 7.6 Hz, C(17)*H*), 8.64 (1H, d, *J*= 7.6 Hz, C(18)*H*), 11.46 (1H, s, -NH- pyridone) ppm; ¹³C NMR (DMSO-*d*₆, 100 MHz, δ, ppm): δ_C 12.0, 13.4, 18.5, 19.1, 32.8, 106.7, 111.2, 116.0, 119.8, 120.6, 122.5, 128.7, 130.3, 138.9, 148.4, 151.5, 152.7, 157.9, 163.6, 167.5 ppm; m.p. 230-233 °C (acetonitrile/methanol); Y= 57 %; MS (EI) *m/z* [M]⁺ calculated: 350.1743, found: 350.1748.

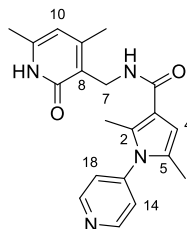
N-((4,6-dimethyl-2-oxo-1,2-dihydropyridin-3-yl)methyl)-2,5-dimethyl-1-(pyridin-3-yl)-1H-pyrrole-3-carboxamide (25m)



¹H NMR (DMSO-*d*₆, 400 MHz, δ, ppm): δ_H 1.92 (3H, s, C(5)CH₃), 2.12 (3H, s, C(9)CH₃), 2.18 (3H, s, C(11)CH₃), 2.21 (3H, s, C(2)CH₃), 4.23 (2H, d, *J*= 4.4 Hz, C(7)H₂), 5.86 (1H, s, C(10)*H*), 6.35 (1H, s, C(4)*H*), 7.49 (1H, t, *J*= 4.4 Hz, -CH₂NHCO-), 7.60 (1H, dd, *J*= 7 Hz, 4.4 Hz, C(17)*H*), 7.82 (1H, d, *J*= 7.6 Hz, C(18)*H*), 8.54 (1H, s, C(14)*H*), 8.68 (1H, d, *J*= 4.4 Hz, C(16)*H*), 11.47 (1H, s, -NH- pyridone) ppm; ¹³C NMR (DMSO-*d*₆, 100 MHz, δ, ppm): δ_C 12.0, 13.3, 18.5, 19.1, 32.8, 104.7, 111.3, 114.2, 115.9, 124.1, 127.8, 129.8, 131.4, 131.6, 143.8, 144.5, 151.5,

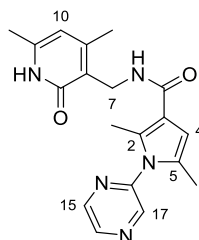
157.9, 163.6, 167.5 ppm; m.p. 183-185 °C (acetonitrile); Y= 61 %; MS (EI) m/z [M]⁺ calculated: 350.1743, found: 350.1746.

N-((4,6-dimethyl-2-oxo-1,2-dihydropyridin-3-yl)methyl)-2,5-dimethyl-1-(pyridin-4-yl)-1H-pyrrole-3-carboxamide (25n)



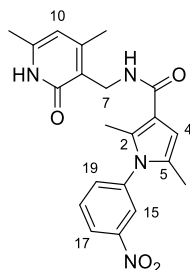
¹H NMR (DMSO-*d*₆, 400 MHz, δ , ppm): δ_{H} 1.97 (3H, s, C(5)CH₃), 2.12 (3H, s, C(9)CH₃), 2.17 (3H, s, C(11)CH₃), 2.25 (3H, s, C(2)CH₃), 4.22 (2H, d, *J*= 5.2 Hz, C(7)H₂), 5.86 (1H, s, C(10)H), 6.37 (1H, s, C(4)H), 7.40 (2H, d, *J*= 6 Hz, C(14)H, C(18)H), 7.53 (1H, t, *J*= 5.2 Hz, -CH₂NHCO-), 8.74 (2H, d, *J*= 6 Hz, C(15)H, C(17)H), 11.50 (1H, s, -NH- pyridone) ppm; ¹³C NMR (DMSO-*d*₆, 100 MHz, δ , ppm): δ_{C} 12.1, 13.4, 18.5, 19.2, 32.7, 104.6, 111.0, 113.9 (2C), 114.3, 116.0, 130.1, 131.5, 140.8, 150.4 (2C), 151.5, 157.9, 163.6, 167.5 ppm; m.p. 235-237 °C (acetonitrile/methanol); Y= 58 %; MS (EI) m/z [M]⁺ calculated: 350.1743, found: 350.1740.

N-((4,6-dimethyl-2-oxo-1,2-dihydropyridin-3-yl)methyl)-2,5-dimethyl-1-(pyrazin-2-yl)-1H-pyrrole-3-carboxamide (25o)



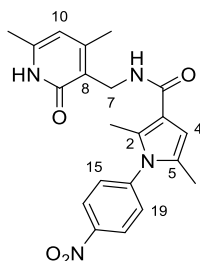
¹H NMR (DMSO-*d*₆, 400 MHz, δ , ppm): δ_{H} 2.02 (3H, s, C(5)CH₃), 2.12 (3H, s, C(9)CH₃), 2.18 (3H, s, C(11)CH₃), 2.30 (3H, s, C(2)CH₃), 4.23 (2H, d, *J*= 5.2 Hz, C(7)H₂), 5.86 (1H, s, C(10)H), 6.37 (1H, s, C(4)H), 7.56 (1H, t, *J*= 5.2 Hz, -CH₂NHCO-), 8.75-8.76 (1H, dd, *J*= 2.4 Hz, 1.6 Hz, C(16)H), 8.78 (1H, d, *J*= 2.4 Hz, C(15)H), 8.83 (1H, d, *J*= 1.6 Hz, C(17)H), 11.48 (1H, s, -NH- pyridone) ppm; ¹³C NMR (DMSO-*d*₆, 100 MHz, δ , ppm): δ_{C} 12.0, 13.3, 18.5, 19.1, 32.8, 106.7, 110.9, 116.1, 122.6, 128.5, 130.3, 133.8, 136.2, 137.9, 150.3, 151.5, 157.9, 163.6, 167.5 ppm; m.p. 200-205 °C (acetonitrile); Y= 52 %; MS (EI) m/z [M]⁺ calculated: 351.1695, found: 351.1697.

N-((4,6-dimethyl-2-oxo-1,2-dihydropyridin-3-yl)methyl)-2,5-dimethyl-1-(3-nitrophenyl)-1H-pyrrole-3-carboxamide (25p)



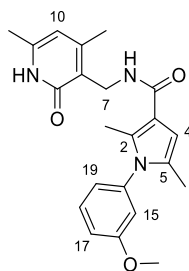
^1H NMR (DMSO- d_6 , 400 MHz, δ , ppm): δ_{H} 1.94 (3H, s, C(5) CH_3), 2.12 (3H, s, C(9) CH_3), 2.18 (3H, s, C(11) CH_3), 2.23 (3H, s, C(2) CH_3), 4.23 (2H, d, J = 4 Hz, C(7) H_2), 5.87 (1H, s, C(10) H), 6.37 (1H, s, C(4) H), 7.52 (1H, t, J = 7.6 Hz, C(18) H), 7.77-7.86 (2H, m, C(19) H and $-\text{CH}_2\text{NHCO}-$), 8.12 (1H, s, C(15) H), 8.34 (1H, d, J = 7.6 Hz, C(17) H), 11.49 (1H, s, $-\text{NH}-$ pyridone) ppm; ^{13}C NMR (DMSO- d_6 , 100 MHz, δ , ppm): δ_{C} 12.1, 13.3, 18.5, 19.2, 32.8, 104.8, 111.2, 114.2, 116.1, 121.9, 122.5, 129.6, 130.1, 130.3, 131.5, 136.4, 146.8, 151.5, 157.8, 163.6, 167.5 ppm; m.p. 137-139 °C (benzene); Y = 59 % MS (EI) m/z $[\text{M}]^+$ calculated: 394.1641, found: 394.1642.

N-((4,6-dimethyl-2-oxo-1,2-dihydropyridin-3-yl)methyl)-2,5-dimethyl-1-(4-nitrophenyl)-1H-pyrrole-3-carboxamide (25q)



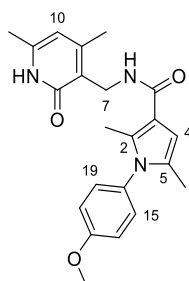
^1H NMR (DMSO- d_6 , 400 MHz, δ , ppm): δ_{H} 1.96 (3H, s, C(5) CH_3), 2.12 (3H, s, C(9) CH_3), 2.18 (3H, s, C(11) CH_3), 2.25 (3H, s, C(2) CH_3), 4.23 (2H, d, J = 5.2 Hz, C(7) H_2), 5.87 (1H, s, C(10) H), 6.38 (1H, s, C(4) H), 7.54 (1H, t, J = 5.2 Hz, $-\text{CH}_2\text{NHCO}-$), 7.62 (2H, d, J = 9.2 Hz, C(15) H , C(19) H), 8.37 (2H, d, J = 8.8 Hz, C(16) H , C(18) H), 11.49 (1H, s, $-\text{NH}-$ pyridone) ppm; ^{13}C NMR (DMSO- d_6 , 100 MHz, δ , ppm): δ_{C} 12.1, 13.2, 18.5, 19.2, 32.8, 104.7, 111.2, 114.3, 115.6, 123.7 (2 C), 125.1 (2 C), 130.0, 131.5, 142.4, 145.8, 151.5, 158.0, 163.7, 167.5 ppm; m.p. 243-246 °C (methanol); Y = 60 % MS (EI) m/z $[\text{M}]^+$ calculated: 394.1641, found: 394.1646.

N-((4,6-dimethyl-2-oxo-1,2-dihydropyridin-3-yl)methyl)-1-(3-methoxyphenyl)-2,5-dimethyl-1H-pyrrole-3-carboxamide (25t)



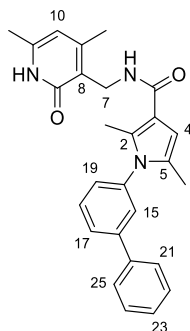
^1H NMR (DMSO- d_6 , 400 MHz, δ , ppm): δ_{H} 1.92 (3H, s, C(5) CH_3), 2.12 (3H, s, C(9) CH_3), 2.18 (3H, s, C(11) CH_3), 2.21 (3H, s, C(2) CH_3), 3.80 (3H, s, OCH_3), 4.23 (2H, $J = 5.2$ Hz, d, C(7) H_2), 5.86 (1H, s, C(10) H), 6.28 (1H, s, C(4) H), 6.81-6.83 (2H, m, C(15) H , C(18) H), 7.05 (1H, dd, $J = 2$ Hz, 8.2 Hz, C(17) H), 7.39-7.46 (2H, m, C(19) H and $-\text{CH}_2\text{NHCO}-$), 11.46 (1H, s, $-\text{NH}-$ pyridone) ppm; ^{13}C NMR (DMSO- d_6 , 100 MHz, δ , ppm): δ_{C} 12.2, 13.1, 18.5, 19.1, 32.8, 55.3, 104.9, 111.2, 114.3, 114.5, 115.5, 116.0, 124.7, 129.9, 130.1, 131.5, 139.0, 151.5, 157.9, 161.6, 163.5, 167.6 ppm; ,m.p. 202-204 $^{\circ}\text{C}$ (acetonitrile); Y= 65 %. MS (EI) m/z $[\text{M}]^+$ calculated: 379.1896, found: 379.1892.

N-((4,6-dimethyl-2-oxo-1,2-dihydropyridin-3-yl)methyl)-1-(4-methoxyphenyl)-2,5-dimethyl-1H-pyrrole-3-carboxamide (25u)



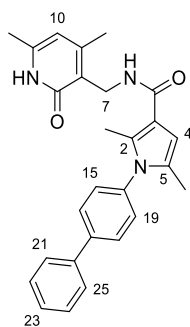
^1H NMR (DMSO- d_6 , 400 MHz, δ , ppm): δ_{H} 1.89 (3H, s, C(5) CH_3), 2.12 (3H, s, C(9) CH_3), 2.18 (6H, bs, C(11) CH_3 , C(2) CH_3), 3.82 (3H, s, OCH_3), 4.22 (2H, d, $J = 5.6$ Hz, C(7) H_2), 5.86 (1H, s, C(10) H), 6.25 (1H, s, C(4) H), 7.06 (2H, d, $J = 8.8$ Hz, C(16) H , C(18) H), 7.18 (2H, d, $J = 8.8$ Hz, C(15) H , C(19) H), 7.43 (1H, t, $J = 5.2$ Hz, $-\text{CH}_2\text{NHCO}-$), 11.46 (1H, s, $-\text{NH}-$ pyridone) ppm; ^{13}C NMR (DMSO- d_6 , 100 MHz, δ , ppm): δ_{C} 12.1, 13.2, 18.5, 19.1, 32.7, 55.4, 104.7, 111.2, 114.3, 115.4 (2 C), 115.8, 128.7 (2 C), 130.1, 131.6, 136.5, 151.6, 158.0, 159.4, 163.6, 167.5. ppm; m.p. 196-200 $^{\circ}\text{C}$ (acetonitrile); Y= 71 %. MS (EI) m/z $[\text{M}]^+$ calculated: 379.1896, found: 379.1894.

1-([1,1'-biphenyl]-3-yl)-N-((4,6-dimethyl-2-oxo-1,2-dihydropyridin-3-yl)methyl)-2,5-dimethyl-1H-pyrrole-3-carboxamide (25x)



^1H NMR (DMSO- d_6 , 400 MHz, δ , ppm): δ_{H} 1.96 (3H, s, C(5) CH_3), 2.12 (3H, s, C(9) CH_3), 2.19 (3H, s, C(11) CH_3), 2.25 (3H, s, C(2) CH_3), 4.23 (2H, d, J = 5.2 Hz, C(7) H_2), 5.87 (1H, s, C(10) H), 6.32 (1H, s, C(4) H), 7.26 (1H, d, J = 7.6 Hz, C(19) H), 7.40 (1H, t, J = 7.6 Hz, C(23) H), 7.45-7.50 (3H, m, C(22) H , C(24) H and $-\text{CH}_2\text{NHCO}-$), 7.54 (1H, s, C(15) H), 7.63 (1H, t, J = 7.6 Hz, C(18) H), 7.74 (2H, d, J = 7.6 Hz, C(21) H , C(25) H), 7.80 (1H, d, J = 8 Hz, C(17) H), 11.48 (1H, s, $-\text{NH}-$ pyridone) ppm; ^{13}C NMR (DMSO- d_6 , 100 MHz, δ , ppm): δ_{C} 12.1, 13.2, 18.5, 19.2, 32.7, 104.7, 111.1, 114.3, 116.1, 118.4, 121.2, 126.0, 126.9 (2 C), 127.8, 128.7 (2 C), 129.0, 130.1, 131.7, 139.9, 140.7, 141.1, 151.5, 157.9, 163.6, 167.5 ppm; m.p. 236-239 °C (methanol); Y= 67 % MS (EI) m/z $[\text{M}]^+$ calculated: 425.2103, found: 425.2107.

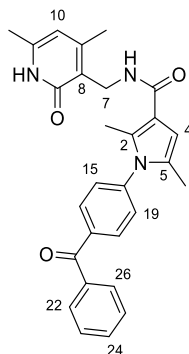
1-([1,1'-biphenyl]-4-yl)-N-((4,6-dimethyl-2-oxo-1,2-dihydropyridin-3-yl)methyl)-2,5-dimethyl-1H-pyrrole-3-carboxamide (25y)



^1H NMR (DMSO- d_6 , 400 MHz, δ , ppm): δ_{H} 1.96 (3H, s, C(5) CH_3), 2.12 (3H, s, C(9) CH_3), 2.19 (3H, s, C(11) CH_3), 2.25 (3H, s, C(2) CH_3), 4.24 (2H, d, J = 5.2 Hz, C(7) H_2), 5.86 (1H, s, C(10) H), 6.32 (1H, s, C(4) H), 7.36 (2H, d, J = 8.4 Hz, C(15) H , C(19) H), 7.40-7.46 (2H, m, C(23) H and $-\text{CH}_2\text{NHCO}-$), 7.51 (2H, t, J = 7.6 Hz, C(22) H , C(24) H), 7.75 (2H, d, J = 7.2 Hz, C(21) H , C(25) H), 7.82 (2H, d, J = 8.4 Hz, C(16) H , C(18) H), 11.48 (1H, s, $-\text{NH}-$ pyridone) ppm; ^{13}C NMR (DMSO- d_6 , 100 MHz, δ , ppm): δ_{C} 12.0, 13.3, 18.5, 19.1, 32.8, 104.7, 110.9, 114.2, 116.1, 126.3 (2C), 126.9 (2C), 127.7, 127.9 (2C), 128.8 (2C), 130.1, 131.5, 139.6, 140.9, 142.2, 151.4, 158.1, 163.6,

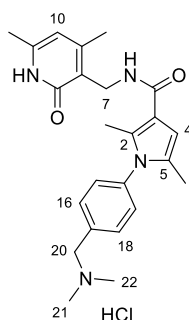
167.7 ppm; m.p. 203-205 °C (acetonitrile); Y= 56 %. MS (EI) m/z [M]⁺ calculated: 425.2103, found: 425.2100.

1-(4-benzoylphenyl)-N-((4,6-dimethyl-2-oxo-1,2-dihydropyridin-3-yl)methyl)-2,5-dimethyl-1H-pyrrole-3-carboxamide (25z)



¹H NMR (DMSO-*d*₆, 400 MHz, δ, ppm): δ_H 1.98 (3H, s, C(5)CH₃), 2.12 (3H, s, C(9)CH₃), 2.19 (3H, s, C(11)CH₃), 2.27 (3H, s, C(2)CH₃), 4.24 (2H, d, *J*= 5.2 Hz, C(7)H₂), 5.87 (1H, s, C(10)H), 6.36 (1H, s, C(4)H), 7.48-7.50 (3H, m, C(16)H, C(18)H and -CH₂NHCO-), 7.61 (2H, t, *J*= 7.6 Hz, C(23)H, C(25)H), 7.72 (1H, t, *J*= 7.6 Hz, C(24)H), 7.80 (2H, d, *J*= 7.4 Hz, C(22)H, C(26)H), 7.89 (2H, d, *J*= 8.4 Hz, C(15)H, C(19)H), 11.46 (1H, s, -NH- pyridone) ppm; ¹³C NMR (DMSO-*d*₆, 100 MHz, δ, ppm): δ_C 12.1, 13.3, 18.5, 19.1, 32.7, 104.8, 110.9, 114.3, 115.9, 125.3 (2 C), 128.2, 128.7 (2 C), 129.5 (2 C), 130.0, 130.6 (2 C), 131.5, 132.4, 138.1, 140.5, 151.5, 158.0, 163.6, 167.5, 195.2 ppm; m.p. 223-227 °C (acetonitrile/methanol); Y= 52 %. MS (EI) m/z [M]⁺ calculated: 453.2052, found: 453.2048.

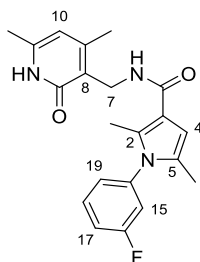
N-((4,6-dimethyl-2-oxo-1,2-dihydropyridin-3-yl)methyl)-1-(4-((dimethylamino)methyl)phenyl)-2,5-dimethyl-1H-pyrrole-3-carboxamide hydrochloride (25a')



¹H NMR (DMSO-*d*₆, 400 MHz, δ, ppm): δ_H 1.93 (3H, s, C(5)CH₃), 2.20 (3H, s, C(9)CH₃), 2.22 (3H, s, C(11)CH₃), 2.28 (3H, s, C(2)CH₃), 2.71 (3H, s, C(22)H₃), 2.73 (3H, s, C(21)H₃), 4.28 (2H, s, C(20)H₂), 4.36 (2H, d, *J*= 5.2 Hz, C(7)H₂), 6.15 (1H, s, C(10)H), 6.40 (1H, s, C(4)H), 7.39 (2H, d, *J*= 8.2 Hz, C(16)H, C(18)H), 7.75 (2H, d, *J*= 8.2 Hz, C(15)H, C(19)H), 8.03 (1H, t,

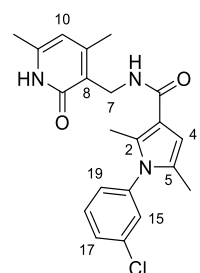
$J = 5.2$ Hz, $-\text{CH}_2\text{NHCO}-$), 10.92 (1H, s, $-\text{NH}-$ pyridone), 12.24 (1H, bs, $-\text{NH}^+(\text{CH}_3)_2\text{Cl}^-$) ppm. ^{13}C NMR ($\text{DMSO}-d_6$, 100 MHz, δ , ppm): δ_{C} 12.1, 13.3, 18.5, 19.1, 32.8, 45.1 (2C), 63.9, 104.7, 111.2, 114.2, 116.0, 126.3 (2C), 127.2 (2C), 130.1, 131.5, 139.0, 139.7, 151.6, 157.9, 163.6, 167.5 ppm; m.p. 159-164 °C (benzene); Y = 65 %. MS (EI) m/z $[\text{M}-\text{HCl}]^+$ calculated: 406.2369, found: 406.2367.

N-((4,6-dimethyl-2-oxo-1,2-dihydropyridin-3-yl)methyl)-1-(3-fluorophenyl)-2,5-dimethyl-1H-pyrrole-3-carboxamide (25b')



^1H NMR ($\text{DMSO}-d_6$, 400 MHz, δ , ppm): δ_{H} 1.92 (3H, s, $\text{C}(5)\text{CH}_3$), 2.11 (3H, s, $\text{C}(9)\text{CH}_3$), 2.17 (3H, s, $\text{C}(9)\text{CH}_3$), 2.21 (3H, s, $\text{C}(2)\text{CH}_3$), 4.22 (2H, d, $J = 5.2$ Hz, $\text{C}(7)\text{H}_2$), 5.86 (1H, s, $\text{C}(10)\text{H}$), 6.31 (1H, s, $\text{C}(4)\text{H}$), 7.14 (1H, d, $J = 8$ Hz, $\text{C}(19)\text{H}$), 7.27 (1H, d, $J = 9.6$ Hz, $\text{C}(17)\text{H}$), 7.33-7.37 (1H, t, $J = 5.2$ Hz, $-\text{CONHCH}_2-$), 7.46 (1H, t, $J = 4.8$ Hz, $\text{C}(15)\text{H}$), 7.56-7.61 (1H, q, $J = 8$ Hz, $\text{C}(18)\text{H}$), 11.47 (1H, bs, $-\text{NH}-$ pyridone). ^{13}C NMR ($\text{DMSO}-d_6$, 100 MHz, δ , ppm): δ_{C} 12.1, 13.2, 18.5, 19.2, 32.8, 104.7, 110.9, 114.2, 115.8, 116.1, 116.4, 124.7, 130.0, 130.6, 131.5, 136.2, 151.5, 158.0, 162.6, 163.7, 167.5 ppm; m.p. 215-218 °C (acetonitrile/methanol); Y = 59 %. MS (EI) m/z $[\text{M}]^+$ calculated: 367.1696, found: 367.1699.

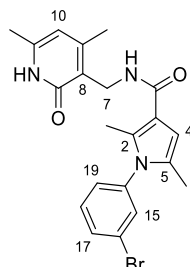
1-(3-chlorophenyl)-N-((4,6-dimethyl-2-oxo-1,2-dihydropyridin-3-yl)methyl)-2,5-dimethyl-1H-pyrrole-3-carboxamide (25c')



^1H NMR ($\text{DMSO}-d_6$, 400 MHz, δ , ppm): δ_{H} 1.92 (3H, s, $\text{C}(5)\text{CH}_3$), 2.11 (3H, s, $\text{C}(11)\text{CH}_3$), 2.17 (3H, s, $\text{C}(9)\text{CH}_3$), 2.21 (3H, s, $\text{C}(2)\text{CH}_3$), 4.22 (2H, d, $J = 5.2$ Hz, $\text{C}(7)\text{H}_2$), 5.86 (1H, s, $\text{C}(10)\text{H}$), 6.31 (1H, s, $\text{C}(4)\text{H}$), 7.26-7.28 (1H, m, $\text{C}(18)\text{H}$), 7.45-7.46 (2H, m, $\text{C}(15)\text{H}$, $\text{C}(17)\text{H}$), 7.56-7.58 (2H, m, CONHCH_2 and $\text{C}(19)\text{H}$), 11.48 (1H, bs, NH pyridone). ^{13}C NMR ($\text{DMSO}-d_6$, 100 MHz, δ , ppm): δ_{C} 12.1, 13.2, 18.5, 19.1, 32.8, 104.7, 111.2, 114.3, 116.0, 126.4, 127.6, 128.1, 130.2,

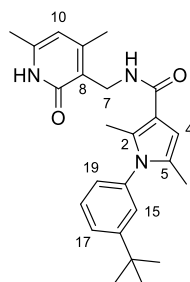
130.3, 131.5, 134.0, 137.8, 151.5, 157.9, 163.6, 167.5 ppm; m.p. 221-223 °C (acetonitrile/methanol); Y= 61 %. MS (EI) m/z [M]⁺ calculated: 383.1401, found: 383.1406.

1-(3-bromophenyl)-N-((4,6-dimethyl-2-oxo-1,2-dihydropyridin-3-yl)methyl)-2,5-dimethyl-1H-pyrrole-3-carboxamide (25d')



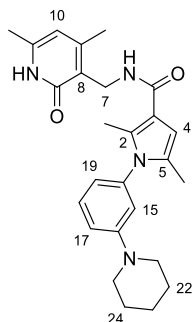
¹H NMR (DMSO-*d*₆, 400 MHz, δ, ppm): δ_H 1.92 (3H, s, C(5)CH₃), 2.11 (3H, s, C(11)CH₃), 2.17 (3H, s, C(9)CH₃), 2.21 (3H, s, C(2)CH₃), 4.22 (2H, d, *J*= 5.2 Hz, C(7)H₂), 5.86 (1H, s, C(10)H), 6.31 (1H, s, C(4)H), 7.30 (1H, m, C(18)H), 7.45-7.52 (2H, m, CH₂NHCO, C(19)H), 7.58 (1H, t, *J*= 2 Hz, C(15)H), 7.70 (1H, m, C(17)H), 11.48 (1H, bs, NH pyridone). ¹³C NMR (DMSO-*d*₆, 100 MHz, δ, ppm): δ_C 12.2, 13.3, 18.5, 19.1, 32.8, 104.8, 111.2, 114.4, 116.0, 120.5, 125.6, 125.9, 126.5, 129.9, 130.7, 131.5, 138.4, 151.5, 157.9, 163.6, 167.6. ppm; m.p. 163-165 °C (benzene); Y= 59 %. MS (EI) m/z [⁷⁹Br-M]⁺ calculated: 427.0895, found: 427.0893; [⁸¹Br-M]⁺ calculated: 429.0875, found: 429.0877.

1-(3-(tert-butyl)phenyl)-N-((4,6-dimethyl-2-oxo-1,2-dihydropyridin-3-yl)methyl)-2,5-dimethyl-1H-pyrrole-3-carboxamide (25e')



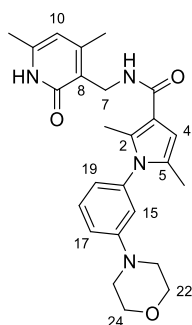
¹H NMR (DMSO-*d*₆, 400 MHz, δ, ppm): δ_H 1.30 (9H, s, C(16)C(CH₃)₃), 1.90 (3H, s, C(5)CH₃), 2.11 (3H, s, C(11)CH₃), 2.18 (3H, s, C(9)CH₃), 2.19 (3H, s, C(2)CH₃), 4.23 (2H, d, *J*= 5.2 Hz, C(7)H₂), 5.86 (1H, s, C(10)H), 6.28 (1H, s, C(4)H), 7.07 (1H, d, *J*= 7.2 Hz, C(17)H), 7.21 (1H, s, C(15)H), 7.41-7.50 (3H, m, C(18)H, C(19)H and CH₂NHCO), 11.47 (1H, bs, NH pyridone). ¹³C NMR (DMSO-*d*₆, 100 MHz, δ, ppm): δ_C 11.9, 13.2, 18.5, 19.2, 30.9 (3 C), 32.7, 34.8, 104.7, 111.2, 114.2, 116.1, 121.6, 123.2, 126.9, 129.8, 130.1, 131.6, 139.4, 148.3, 151.5, 158.0, 163.6, 167.6 ppm; m. p. 140-143 °C (benzene); Y= 66 %. MS (EI) m/z [M]⁺ calculated: 405.2416, found: 405.2414.

N-((4,6-dimethyl-2-oxo-1,2-dihydropyridin-3-yl)methyl)-2,5-dimethyl-1-(3-(piperidin-1-yl)phenyl)-1H-pyrrole-3-carboxamide (25f')



^1H NMR (DMSO- d_6 , 400 MHz, δ , ppm): δ_{H} 1.54-1.60 (6H, m, C(22) H_2 , C(23) H_2 , C(24) H_2), 1.92 (3H, s, C(5) CH_3), 2.11 (3H, s, C(11) CH_3), 2.18 (3H, s, C(9) CH_3), 2.21 (3H, s, C(2) CH_3), 3.18-3.20 (4H, m, C(21) H_2 , C(25) H_2), 4.22 (2H, d, J = 5.2 Hz, C(7) H_2), 5.86 (1H, s, C(10) H), 6.25 (1H, s, C(4) H), 6.55 (1H, d, J = 7.6 Hz, C(19) H), 6.70 (1H, bs, C(15) H), 7.01 (1H, dd, J = 2 Hz, 8.4 Hz, C(17) H), 7.34 (1H, t, J = 8 Hz, C(18) H), 7.40 (1H, t, J = 5.2 Hz, - CH_2NHCO -), 11.48 (1H, bs, -NH- pyridone). ^{13}C NMR (DMSO- d_6 , 100 MHz, δ , ppm): δ_{C} 12.1, 13.3, 18.5, 19.2, 24.6, 27.0 (2 C), 32.8, 51.4 (2 C), 104.7, 108.6, 111.2, 113.4, 114.2, 116.1, 126.8, 130.1, 130.5, 131.6, 139.3, 151.5, 153.4, 158.0, 163.6, 167.7 ppm; m.p. 135-137 °C (benzene); Y = 55 %. MS (EI) m/z $[\text{M}]^+$ calculated: 432.2525, found: 432.2521.

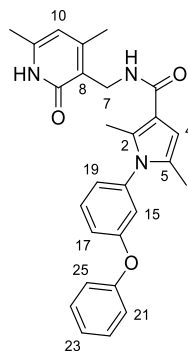
N-((4,6-dimethyl-2-oxo-1,2-dihydropyridin-3-yl)methyl)-2,5-dimethyl-1-(3-morpholinophenyl)-1H-pyrrole-3-carboxamide (25g')



^1H NMR (DMSO- d_6 , 400 MHz, δ , ppm): δ_{H} 1.92 (3H, s, C(5) CH_3), 2.12 (3H, s, C(11) CH_3), 2.18 (3H, s, C(9) CH_3), 2.21 (3H, s, C(2) CH_3), 3.16 (4H, t, J = 4.6 Hz, C(22) H_2 , C(24) H_2), 3.72 (4H, t, J = 4.6 Hz, C(21) H_2 , C(25) H_2), 4.22 (2H, d, J = 5.2 Hz, C(7) H_2), 5.86 (1H, s, C(10) H), 6.26 (1H, s, C(4) H), 6.64 (1H, d, J = 8 Hz, C(19) H), 6.76 (1H, s, C(15) H), 7.03 (1H, d, J = 7.2 Hz, C(17) H), 7.34-7.39 (2H, m, C(18) H and - CH_2NHCO -), 11.47 (1H, bs, -NH- pyridone) ppm. ^{13}C NMR (DMSO- d_6 , 100 MHz, δ , ppm): δ_{C} 12.1, 13.3, 18.5, 19.2, 32.8, 48.1 (2 C), 66.4 (2 C), 104.7, 108.6, 111.2, 113.4, 114.3, 116.0, 126.7, 130.1, 130.7, 131.5, 139.3, 151.5, 153.4, 158.0, 163.6,

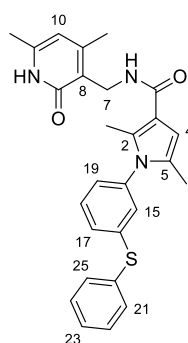
167.5 ppm; m.p. 178-180 °C (acetonitrile); Y= 53 %. MS (EI) m/z [M]⁺ calculated: 434.2318, found: 434.2321.

N-((4,6-dimethyl-2-oxo-1,2-dihydropyridin-3-yl)methyl)-2,5-dimethyl-1-(3-phenoxyphenyl)-1H-pyrrole-3-carboxamide (25h')



¹H NMR (DMSO-*d*₆, 400 MHz, δ, ppm): δ_H 1.96 (3H, s, C(5)CH₃), 2.19 (3H, s, C(11)CH₃), 2.25 (3H, s, C(9)CH₃), 2.29 (3H, s, C(2)CH₃), 4.46 (2H, d, *J*= 5.6 Hz, C(7)H₂), 5.94 (1H, s, C(10)H), 6.08 (1H, s, C(4)H), 6.75 (1H, s, C(15)H), 6.87 (1H, d, *J*= 7.2 Hz, C(17)H), 7.03-7.08 (3H, m, C(21)H, C(23)H, C(25)H), 7.12-7.17 (2H, m, C(22)H, C(24)H), 7.28 (1H, bs, -CH₂NHCO-), 7.34-7.42 (2H, m, C(18)H, C(19)H), 11.48 (1H, bs, -NH- pyridone). ¹³C NMR (DMSO-*d*₆, 100 MHz, δ, ppm): δ_C 12.1, 13.4, 18.5, 19.2, 32.8, 104.8, 111.2, 114.2, 115.9, 116.1, 118.2 (2 C), 119.6, 124.1, 124.4, 129.3 (2 C), 129.9, 130.0, 131.6, 138.3, 151.4, 156.8, 156.9, 158.0, 163.6, 167.5 ppm; m.p. 125-128 °C (cyclohexane); Y= 69 %. MS (EI) m/z [M]⁺ calculated: 441.2052, found: 441.2055.

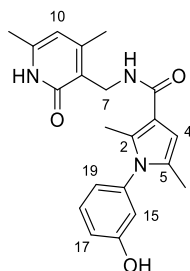
N-((4,6-dimethyl-2-oxo-1,2-dihydropyridin-3-yl)methyl)-2,5-dimethyl-1-(3-(phenylthio)phenyl)-1H-pyrrole-3-carboxamide (25i')



¹H NMR (DMSO-*d*₆, 400 MHz, δ, ppm): δ_H 1.87 (3H, s, C(5)CH₃), 2.11 (3H, s, C(11)CH₃), 2.15 (3H, s, C(9)CH₃), 2.16 (3H, s, C(2)CH₃), 4.20 (2H, d, *J*= 4.8 Hz, C(7)H₂), 5.85 (1H, s, C(10)H), 6.27 (1H, s, C(4)H), 7.00-7.53 (9H, m, C(15)H, C(17)H, C(18)H, C(19)H, C(21)H, C(22)H, C(23)H, C(24)H, C(25)H), 7.42 (1H, bs, -CH₂NHCO-), 11.47 (1H, s, -NH- pyridone). ¹³C NMR

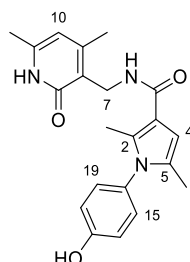
(DMSO-*d*₆, 100 MHz, δ , ppm): δ_c 12.2, 13.3, 18.5, 19.2, 32.7, 104.8, 111.0, 114.2, 115.9, 123.3, 126.2, 127.0, 127.5, 128.6, 129.2 (2 C), 129.9, 130.0, 131.2 (2 C), 131.7, 133.2, 138.6, 151.5, 157.9, 163.6, 167.6 ppm; m.p. 128-130 °C (benzene); Y= 75 %. MS (EI) *m/z* [M]⁺ calculated: 457.1824, found: 457.1822.

General procedure for the synthesis of the compounds 25v, w Example: Synthesis of N-((4,6-dimethyl-2-oxo-1,2-dihydropyridin-3-yl)methyl)-1-(3-hydroxyphenyl)-2,5-dimethyl-1H-pyrrole-3-carboxamide (25v)



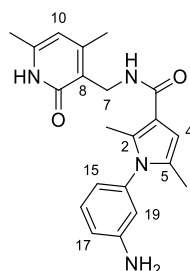
N-((4,6-dimethyl-2-oxo-1,2-dihydropyridin-3-yl)methyl)-1-(3-methoxyphenyl)-2,5-dimethyl-1H-pyrrole-3-carboxamide (**25t**) (0.0572 mmol, 1.0 eq, 21.7 mg) was solved in dry CH₂Cl₂ (1.5 mL) under N₂ atmosphere. The solution was cooled to -78 °C, and a 1 M solution of BBr₃ (0.114 mmol, 2.0 eq, 0.114 mL) in CH₂Cl₂ was added dropwise. The temperature was left slowly rise to -20 °C. After 2 h, 1.0 eq more of BBr₃ was added (-78 °C) and the solution was allowed to warm to room temperature and stirred for 3 h. After this time the reaction was complete, and it was quenched with H₂O (5 mL). The product was extracted with ethyl acetate (3 × 10 mL), the combined organic layers were washed with a saturated aqueous solution of NaCl (2 × 3 mL), dried over Na₂SO₄, filtered and concentrated *in vacuo*. The extract was triturated with a 1:1 mixture of petroleum ether: diethyl ether and filtered. The solid was rinsed several times with petroleum ether, and dried. Y= 73 %; m.p. 217-219 °C (acetonitrile/methanol); ¹H NMR (DMSO-*d*₆, 400 MHz, δ , ppm): δ_H 1.91 (3H, s, C(5)CH₃), 2.12 (3H, s, C(9)CH₃), 2.18 (3H, s, C(11)CH₃), 2.19 (3H, s, C(2)CH₃), 4.22 (2H, d, *J*= 5.2 Hz, C(7)H₂), 5.86 (1H, s, C(10)H), 6.25 (1H, s, C(4)H), 6.57 (1H, s, C(15)H), 6.63 (1H, d, *J*= 7.6 Hz, C(17)H), 6.87 (1H, t, *J*= 7.6 Hz, C(18)H), 7.31(1H, d, *J*= 7.6 Hz, C(19)H), 7.41(1H, t, *J*= 5.2 Hz, -CH₂NHCO-), 10.04 (1H, s, -OH), 11.46 (1H, s, -NH- pyridone) ppm; ¹³C NMR (DMSO-*d*₆, 100 MHz, δ , ppm): δ_c 12.1, 13.2, 18.6, 19.2, 32.7, 104.7, 111.2, 113.9, 114.2, 114.8, 115.9, 123.7, 129.8, 130.1, 131.5, 137.6, 151.5, 157.4, 157.9, 163.6, 167.6 ppm; MS (EI) *m/z* [M]⁺ calculated: 365.1739, found: 365.1737.

Chemical and Physical Data, ^1H NMR, ^{13}C NMR, and MS (EI) Data for Compound N-((4,6-dimethyl-2-oxo-1,2-dihydropyridin-3-yl)methyl)-1-(4-hydroxyphenyl)-2,5-dimethyl-1H-pyrrole-3-carboxamide (25w)



^1H NMR (DMSO- d_6 , 400 MHz, δ , ppm): δ_{H} 1.88 (3H, s, C(5) CH_3), 2.12 (3H, s, C(9) CH_3), 2.17 (3H, s, C(11) CH_3), 2.18 (3H, s, C(2) CH_3), 4.22 (2H, d, $J = 5.2$ Hz, C(7) H_2), 5.86 (1H, s, C(10) H), 6.23 (1H, s, C(4) H), 6.87 (2H, d, $J = 8.8$ Hz, C(16) H , C(18) H), 7.03 (2H, d, $J = 8.8$ Hz, C(15) H , C(19) H), 7.38 (1H, t, $J = 5.2$ Hz, $-\text{CH}_2\text{NHCO}-$), 9.79 (1H, s, $-\text{OH}$), 11.46 (1H, s, $-\text{NH}-$ pyridone) ppm; ^{13}C NMR (DMSO- d_6 , 100 MHz, δ , ppm): δ_{C} 12.1, 13.3, 18.5, 19.2, 32.8, 104.7, 111.2, 114.3, 116.0, 128.9 (2 C), 129.9, 130.0 (2 C), 131.5, 135.4, 151.5, 157.4, 158.0, 163.6, 167.4 ppm; m.p. 286-289 °C (methanol); Y= 55 % MS (EI) m/z $[\text{M}]^+$ calculated: 365.1739, found: 365.1740.

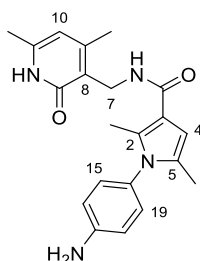
General procedure for the synthesis of the compounds 25r, s Example: Synthesis of 1-(3-aminophenyl)-N-((4,6-dimethyl-2-oxo-1,2-dihydropyridin-3-yl)methyl)-2,5-dimethyl-1H-pyrrole-3-carboxamide (25r)



A solution of N-((4,6-dimethyl-2-oxo-1,2-dihydropyridin-3-yl)methyl)-2,5-dimethyl-1-(3-nitrophenyl)-1H-pyrrole-3-carboxamide (**25p**) (0.127 mmol, 1.0 eq, 50.0 mg) in methanol (1 mL) was cooled to 0 °C, and $\text{SnCl}_2 \times 2 \text{H}_2\text{O}$ (0.643 mmol, 5.0 eq, 143.02 mg) and 37 % HCl (15 μL) were added. The reaction mixture was left to warm to room temperature and stirred for 30 h. After this time the reaction was judged to be complete by TLC analysis. The reaction was diluted with ethyl acetate (3 mL), cooled to 0 °C and quenched by addition of a $\text{Na}_2\text{CO}_3/\text{NaHCO}_3$ buffered solution (pH 8). The product was extracted with ethyl acetate (3×10 mL), dried over Na_2SO_4 , filtered and concentrated *in vacuo*. The extract was purified by silica gel chromatography eluting with ethyl acetate: methanol 10:1. Y= 53 %; m.p. decomposition at 210

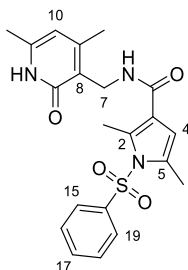
°C (acetonitrile/methanol); ^1H NMR (DMSO- d_6 , 400 MHz, δ , ppm): δ_{H} 1.91 (3H, s, C(5) CH_3), 2.12 (3H, s, C(9) CH_3), 2.18 (3H, s, C(11) CH_3), 2.20 (3H, s, C(2) CH_3), 4.22 (2H, d, J = 5.2 Hz, C(7) H_2), 5.36 (2H, s, PhNH_2), 5.86 (1H, s, C(10) H), 6.23 (1H, s, C(4) H), 6.30 (1H, d, J = 6.8 Hz, C(19) H), 6.34 (1H, t, J = 2 Hz, C(16) H), 6.63 (1H, dd, J = 2 Hz, 6.8 Hz, C(17) H), 7.14 (1H, t, J = 7.6 Hz, C(15) H), 7.39 (1H, t, J = 5.2 Hz, $-\text{CH}_2\text{NHCO}-$), 11.47 (1H, s, $-\text{NH}-$ pyridone) ppm; ^{13}C NMR (DMSO- d_6 , 100 MHz, δ , ppm): δ_{C} 12.1, 13.3, 18.5, 19.3, 32.7, 104.7, 109.6, 110.8, 111.0, 114.2, 116.0, 123.8, 129.9, 130.5, 131.4, 137.7, 148.2, 151.5, 157.9, 163.6, 167.4 ppm; MS (EI) m/z $[\text{M}]^+$ calculated: 364.1899, found: 364.1895.

Chemical and Physical Data, ^1H NMR, ^{13}C NMR, and MS (EI) Data for Compound 1-(4-aminophenyl)-N-((4,6-dimethyl-2-oxo-1,2-dihydropyridin-3-yl)methyl)-2,5-dimethyl-1H-pyrrole-3-carboxamide (25s)



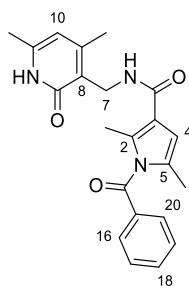
^1H NMR (DMSO- d_6 , 400 MHz, δ , ppm): δ_{H} 1.88 (3H, s, C(5) CH_3), 2.12 (3H, s, C(9) CH_3), 2.16 (3H, s, C(11) CH_3), 2.18 (3H, s, C(2) CH_3), 4.21 (2H, d, J = 5.2 Hz, C(7) H_2), 5.35 (2H, s, $-\text{PhNH}_2$), 5.86 (1H, s, C(10) H), 6.19 (1H, s, C(4) H), 6.63 (2H, d, J = 8.4 Hz, C(16) H , C(18) H), 6.84 (2H, d, J = 8.4 Hz, C(15) H , C(19) H), 7.34 (1H, t, J = 5.2 Hz, $-\text{CH}_2\text{NHCO}-$), 11.46 (1H, s, $-\text{NH}-$ pyridone) ppm; ^{13}C NMR (DMSO- d_6 , 100 MHz, δ , ppm): δ_{C} 12.3, 13.2, 18.5, 19.1, 32.8, 104.7, 110.9, 114.3, 115.9, 120.8 (2 C), 126.9 (2 C), 130.0, 131.5, 133.8, 145.7, 151.5, 158.0, 163.6, 167.5 ppm; m.p. decomposition at 200 °C (acetonitrile); Y= 55 % MS (EI) m/z $[\text{M}]^+$ calculated: 364.1899, found: 364.1898.

General procedure for the synthesis of the compounds 25i, j Example: Synthesis of N-((4,6-dimethyl-2-oxo-1,2-dihydropyridin-3-yl)methyl)-2,5-dimethyl-1-(phenylsulfonyl)-1H-pyrrole-3-carboxamide (25i)



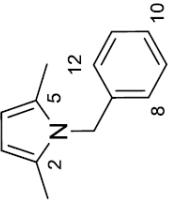
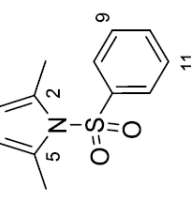
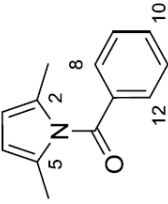
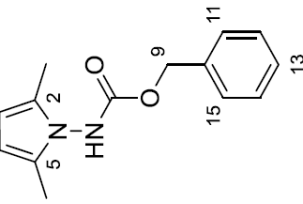
3-(aminomethyl)-4,6-dimethylpyridin-2(1H)-one hydrochloride (0.267 mmol, 1.5 eq, 50.41 mg) was suspended in acetonitrile (2 mL). Triethylamine (0.534 mmol, 3.0 eq, 0.0745 mL) was added and the reaction mixture was stirred at room temperature for 20 minutes. After this time, 2,2,2-trichloro-1-(2,5-dimethyl-1-(phenylsulfonyl)-1H-pyrrol-3-yl)ethan-1-one (0.178 mmol, 1.0 eq, 62.8 mg) was added and the reaction was stirred at room temperature for 16 h. After this time the reaction was quenched with H₂O (5 mL). The product was extracted with ethyl acetate (3 × 10 mL), the combined organic layers were washed with a saturated aqueous solution of NaHCO₃ (2 × 5 mL), and then with a saturated aqueous solution of NaCl (2 × 5 mL), dried over Na₂SO₄, filtered and concentrated *in vacuo*. The extract was purified by silica gel chromatography eluting with ethyl acetate: methanol 25:1. The product was triturated with a 1:1 mixture of petroleum ether: diethyl ether. Y= 56 %. m.p. 213-217 °C (acetonitrile/methanol); ¹H NMR (DMSO-*d*₆, 400 MHz, δ, ppm): δ_H 2.10 (3H, s, C(5)CH₃), 2.13 (3H, s, C(9)CH₃), 2.34 (3H, s, C(11)CH₃), 2.60 (3H, s, C(2)CH₃), 4.17 (2H, d, *J*= 5.2 Hz, C(7)H₂), 5.84 (1H, s, C(10)H), 6.41 (1H, s, C(4)H), 7.67 (2H, t, *J*= 7.6 Hz, C(16)H, C(18)H), 7.78 (4H, m, C(15)H, C(17)H, C(19)H and -CH₂NHCO-), 11.43 (1H, s, -NH- pyridone) ppm; ¹³C NMR (DMSO-*d*₆, 100 MHz, δ, ppm): δ_C 12.2, 14.3, 18.5, 19.1, 32.7, 106.4, 111.2, 114.4, 116.0, 127.1 (2 C), 128.9 (2 C), 133.8, 135.1, 135.7, 138.1, 151.5, 158.0, 163.6, 167.5 ppm; MS (EI) *m/z* [M]⁺ calculated: 413.1409, found: 413.1413.

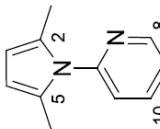
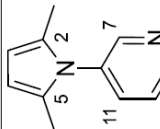
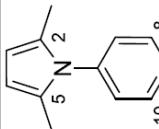
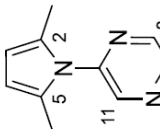
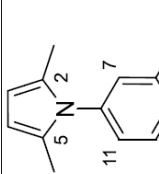
Chemical and Physical Data, ¹H NMR, ¹³C NMR, and MS (EI) Data for Compound 1-benzoyl-N-((4,6-dimethyl-2-oxo-1,2-dihydropyridin-3-yl)methyl)-2,5-dimethyl-1H-pyrrole-3-carboxamide (25j)

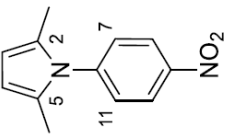
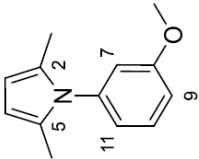
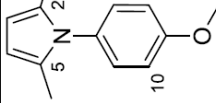
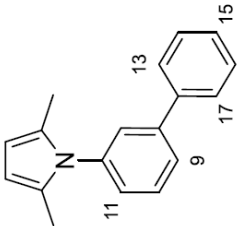


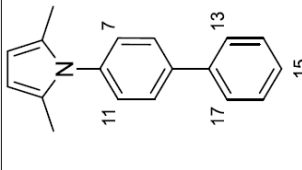
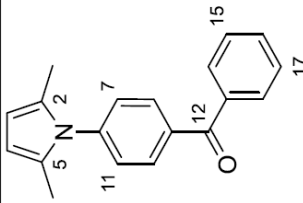
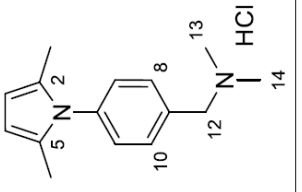
¹H NMR (CDCl₃, 400 MHz, δ, ppm): δ_H 2.08 (3H, s, C(5)CH₃), 2.31 (3H, s, C(9)CH₃), 2.35 (3H, s, C(11)CH₃), 2.40 (3H, s, C(2)CH₃), 4.51 (2H, d, *J*= 6 Hz, C(7)H₂), 5.97 (1H, s, C(10)H), 6.09 (1H, s, C(4)H), 7.47-7.51 (2H, m, C(17)H, C(19)H), 7.64-7.70 (3H, m, C(16)H, C(20)H and -CH₂NHCO-), 7.71-7.74 (1H, m, C(18)H), 11.48 (1H, s, -NH- pyridone) ppm; ¹³C NMR (CDCl₃, 100 MHz, δ, ppm): δ_C 12.4, 13.5, 18.5, 19.1, 32.8, 106.7, 111.2, 116.1, 119.9, 128.9 (2 C), 129.1 (2 C), 131.5, 131.7, 134.5, 136.4, 151.5, 158.0, 163.6, 167.5, 168.9 ppm; m.p. 118-122 °C (cyclohexane); Y= 63 %. MS (EI) *m/z* [M]⁺ calculated: 377.1739, found: 377.1735.

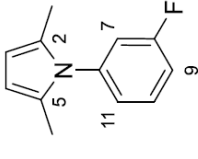
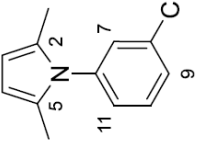
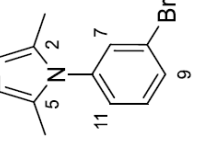
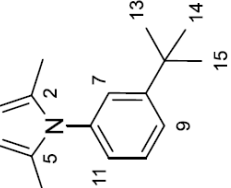
Table S1. Characterization of intermediates 26c-z , 26a'-k' , 27β , 28 , 29 .						
Cpd	Molecular structure	m.p. (°C)	Crystallization solvent	¹ H NMR	MS (ED) [M ⁺]	Ref
26c		46–48	<i>n</i> -hexane	¹ H-NMR (CDCl ₃ , 400 MHz, δ; ppm): δ _H 2.05 (6H, s, C(2)CH ₃ , C(5)CH ₃), 5.93 (2H, s, C(3)H ₂ , C(4)H ₂), 7.23–7.25 (2H, dd, <i>J</i> = 8.2 Hz, 1.2 Hz, C(7)H, C(11)H), 7.39–7.43 (1H, m, C(9)H), 7.46–7.50 (2H, m, C(8)H, C(10)H) ppm.	Calculated: 171.1048; found: 171.1050	242, 243
26d		58–60	<i>n</i> -hexane	¹ H-NMR (CDCl ₃ , 400 MHz, δ; ppm): δ _H 1.10 (6H, d, <i>J</i> = 7.2 Hz, C(13)H ₃ , C(14)H ₃), 2.02 (3H, s, C(5)H ₃), 2.68–2.75 (1H, m, C(12)H), 5.97 (2H, s, C(3)H, C(4)H), 7.27 (2H, d, <i>J</i> = 8.0 Hz, C(7)H, C(11)H), 7.42–7.51 (3H, m, C(8)H, C(9)H, C(10)H) ppm.	Calculated: 199.1361; found: 199.1358	243
26f		oil	-	¹ H-NMR (CDCl ₃ , 400 MHz, δ; ppm): δ _H 2.32 (6H, s, C(2)H ₃ , C(5)H ₃), 3.51 (3H, s, C(6)H ₃), 5.76 (2H, s, C(3)H, C(4)H) ppm.	Calculated: 109.0891; found: 109.0889	244
26g		oil	-	¹ H-NMR (CDCl ₃ , 400 MHz, δ; ppm): δ _H 1.50 (6H, d, <i>J</i> = 7.2 Hz, C(7)H ₃ , C(8)H ₃), 2.32 (6H, s, C(2)H ₃ , C(5)H ₃), 4.41–4.48 (1H, m, C(6)H), 5.77 (2H, s, C(3)H, C(4)H) ppm.	Calculated: 137.1204; found: 137.1206	243

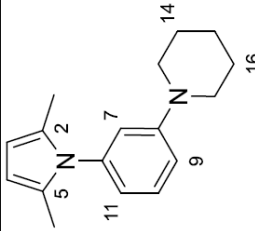
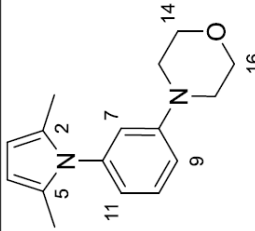
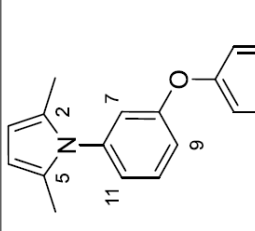
26h		41-45	<i>n</i> -hexane	¹ H-NMR (<i>d</i> ₆ -DMSO, 400 MHz, δ; ppm): δ _H 2.24 (6H, s, C(2)CH ₃ , C(5)CH ₃), 5.09 (2H, s, C(6)H ₂), 5.95 (2H, s, C(3)H, C(4)H), 6.97 (2H, d, <i>J</i> = 7.2 Hz, C(8)H, C(12)H), 7.29 (1H, t, <i>J</i> = 7.2 Hz, C(10)H), 7.37 (2H, t, <i>J</i> = 7.2 Hz, C(9)H, C(11)H) ppm.	Calculated: 185.1204; found: 185.1209.	235,236
26i		96-98	cyclohexane	¹ H-NMR (CDCl ₃ , 400 MHz, δ; ppm): δ _H 2.41 (6H, s, C(2)CH ₃ , C(5)CH ₃), 5.88 (2H, s, C(3)H, C(4)H), 7.53 (2H, t, <i>J</i> = 7.6 Hz, C(9)H, C(11)H), 7.60 (1H, t, <i>J</i> = 7.6 Hz, C(10)H), 7.67 (2H, d, <i>J</i> = 7.6 Hz, C(8)H, C(12)H) ppm.	Calculated: 235.0667; found: 235.0663	-
26j		38-39	<i>n</i> -hexane	¹ H-NMR (CDCl ₃ , 400 MHz, δ; ppm): δ _H 2.09 (6H, s, C(2)H ₃ , C(5)H ₃), 5.89 (2H, s, C(3)H, C(4)H), 7.50 (2H, t, <i>J</i> = 7.6 Hz, C(9)H, C(11)H), 7.62 (1H, tt, <i>J</i> = 7.1 Hz, 1.2 Hz, C(10)H), 7.71 (2H, dd, <i>J</i> = 7.8 Hz, 1.2 Hz, C(8)H, C(12)H) ppm	Calculated: 199.0997; found: 199.0994	245,246
26k		117-119	cyclohexane	¹ H-NMR (CDCl ₃ , 400 MHz, δ; ppm): δ _H 2.13 (6H, s, C(2)H ₃ , C(5)H ₃), 5.25 (2H, s, C(9)H ₂), 5.80 (2H, s, C(3)H, C(4)H), 7.05-7.13 (1H, m, C(13)H), 7.36-7.49 (5H, m, NH, C(11)H, C(12)H, C(14)H, C(15)H) ppm	Calculated: 244.1212; found: 244.1215	247

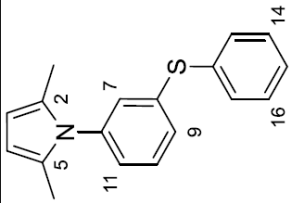
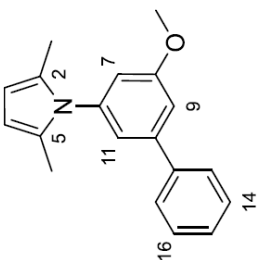
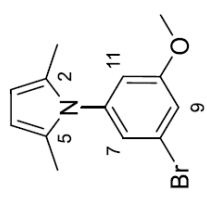
26l		oil		¹ H-NMR (CDCl ₃ , 400 MHz, δ; ppm): δ _H 2.15 (6H, s, C(2)CH ₃ , C(5)CH ₃), 5.93 (2H, s, C(3)H, C(4)H), 7.25 (1H, d, <i>J</i> = 8.0 Hz, C(11)H), 7.31-7.34 (1H, m, C(9)H), 7.83-7.87 (1H, td, <i>J</i> = 7.6 Hz, 2.0 Hz, C(10)H), 8.63-8.65 (1H, m, C(8)H) ppm.	Calculated: 172.1000; found: 172.1004	248 249
26m		oil		¹ H-NMR (CDCl ₃ , 400 MHz, δ; ppm): δ _H 2.07 (6H, s, C(2)CH ₃ , C(5)CH ₃), 5.97 (2H, s, C(3)H, C(4)H), 7.44-7.47 (1H, dd, <i>J</i> = 8.0 Hz, 4.8 Hz, C(10)H), 7.58-7.61 (1H, dq, <i>J</i> = 6.8 Hz, 1.6 Hz, C(11)H), 8.55 (1H, d, <i>J</i> = 2.4 Hz, C(7)H), 8.67-8.68 (1H, dd, <i>J</i> = 4.8, 1.2 Hz, C(9)H) ppm.	Calculated: 172.1000; found: 172.0998	235
26n		113-115	cyclohexane	¹ H-NMR (CDCl ₃ , 400 MHz, δ; ppm): δ _H 2.11 (6H, s, C(2)CH ₃ , C(5)CH ₃), 5.97 (2H, s, C(3)H, C(4)H), 7.19-7.20 (2H, dd, <i>J</i> = 4.6 Hz, 1.6 Hz, C(7)H, C(11)H), 8.74-8.75 (2H, dd, <i>J</i> = 4.6 Hz, 1.6 Hz, C(8)H, C(10)H) ppm.	Calculated: 172.1000; found: 172.1002	235
26o		60-62	<i>n</i> -hexane	¹ H-NMR (CDCl ₃ , 400 MHz, δ; ppm): δ _H 2.19 (6H, s, C(2)CH ₃ , C(5)CH ₃), 5.98 (2H, s, C(3)H, C(4)H), 8.58-8.61 (3H, m, C(8)H, C(9)H, C(11)H) ppm.	Calculated: 173.0953; Found: 173.0957	250
26p		75-80	<i>n</i> -hexane	¹ H-NMR (CDCl ₃ , 400 MHz, δ; ppm): δ _H 2.09 (6H, s, C(2)CH ₃ , C(5)CH ₃), 5.76 (2H, s, C(3)H, C(4)H), 7.60 (1H, d, <i>J</i> = 8 Hz, C(11)H), 7.69 (1H, t, <i>J</i> = 8 Hz, C(10)H), 8.14 (1H, t, <i>J</i> = 2.0 Hz, C(7)H), 8.30 (1H, dd, <i>J</i> = 8.2 Hz, 0.8 Hz, C(9)H) ppm.	Calculated: 216.0899; found: 216.0901	251

26q		78-81	<i>n</i> -hexane	¹ H-NMR (CDCl ₃ , 400 MHz, δ; ppm): δ _H 2.10 (6H, s, C(2)CH ₃ , C(5)CH ₃), 5.98 (2H, s, C(3)H, C(4)H), 7.41 (2H, d, <i>J</i> = 9.2 Hz, C(7)H, C(11)H), 8.37 (2H, d, <i>J</i> = 9.2 Hz, C(8)H, C(10)H) ppm.	Calculated: 216.0899; found: 216.0895	251
26t		55-56	<i>n</i> -hexane	¹ H-NMR (CDCl ₃ , 400 MHz, δ; ppm): δ _H 2.10 (6H, s, C(2)CH ₃ , C(5)CH ₃), 3.85 (3H, s, OCH ₃), 5.92 (2H, s, C(3)H, C(4)H), 6.81 (1H, dt, <i>J</i> = 7.6 Hz, 1.6 Hz, C(9)H), 6.84 (1H, t, <i>J</i> = 1.6 Hz, C(7)H), 7.5 (1H, td, <i>J</i> = 7.6 Hz, 1.6 Hz, C(10)H), 7.37-7.42 (1H, m, C(11)H) ppm.	Calculated: 201.1154; found: 201.1155	235, 252
26u		57-59	<i>n</i> -hexane	¹ H-NMR (CDCl ₃ , 400 MHz, δ; ppm): δ _H 2.05 (6H, s, C(2)CH ₃ , C(5)CH ₃), 3.89 (3H, s, OCH ₃), 5.91 (2H, s, C(3)H, C(4)H), 6.99-7.00 (2H, d, <i>J</i> = 8.8 Hz, C(7)H, C(11)H), 7.15-7.17 (2H, d, <i>J</i> = 8.8 Hz, C(8)H, C(10)H) ppm.	Calculated: 201.1154; found: 201.1157	253, 252
26x		55-57	<i>n</i> -hexane	¹ H-NMR (CDCl ₃ , 400 MHz, δ; ppm): δ _H 2.11 (6H, s, C(2)CH ₃ , C(5)CH ₃), 5.96 (2H, s, C(3)H, C(4)H), 7.22 (1H, d, <i>J</i> = 8.0 Hz, C(9)H), 7.40 (1H, t, <i>J</i> = 7.2 Hz, C(15)H), 7.49 (3H, t, <i>J</i> = 8.0 Hz, C(11)H, C(14)H, C(16)H), 7.55 (1H, t, <i>J</i> = 7.2 Hz, C(10)H), 7.63-7.67 (3H, m, C(7)H, C(13)H, C(17)H) ppm.	Calculated: 274.1361; found: 274.1365.	-

26y		74-76	<i>n</i> -hexane	¹ H-NMR (CDCl ₃ , 400 MHz, δ; ppm): δ _H 2.12 (6H, s, C(2)CH ₃ , C(5)CH ₃), 5.98 (2H, s, C(3)H, C(4)H), 7.32 (2H, d, <i>J</i> = 8.2 Hz, C(8)H, C(10)H), 7.42 (1H, t, <i>J</i> = 7.2 Hz, C(15)H), 7.51 (2H, t, <i>J</i> = 7.6 Hz, C(14)H, C(16)H), 7.67 (2H, d, <i>J</i> = 7.6 Hz, C(13)H, C(17)H), 7.71 (2H, d, <i>J</i> = 8.2 Hz, C(7)H, C(11)H) ppm.	Calculated: 274.1361; found: 274.1359.	254
26z		133-135	cyclohexane	¹ H-NMR (CDCl ₃ , 400 MHz, δ; ppm): δ _H 2.01 (6H, s, C(2)CH ₃ , C(5)CH ₃), 5.92 (2H, s, C(3)H, C(4)H), 7.45 (2H, t, <i>J</i> = 7.6 Hz, C(15)H, C(17)H), 7.53-7.57 (1H, m, C(16)H), 7.65 (2H, d, <i>J</i> = 7.6 Hz, C(14)H, C(18)H), 7.78 (2H, d, <i>J</i> = 7.8 Hz, C(8)H, C(10)H), 7.85 (2H, d, <i>J</i> = 7.8 Hz, C(7)H, C(11)H) ppm.	Calculated: 275.1310; found: 275.1308	-
26a'		323-325	methanol	¹ H-NMR (d ₆ -DMSO, 400 MHz, δ; ppm): δ _H 1.95 (6H, s, C(13)H ₃ , C(14)H ₃), 2.17 (6H, s, C(2)CH ₃ , C(5)CH ₃), 3.44 (2H, s, C(12)H ₂), 5.78 (2H, s, C(6)H ₂), 7.18 (2H, d, <i>J</i> = 6.4 Hz, C(8)H, C(10)H), 7.40 (2H, d, <i>J</i> = 6.4 Hz, C(7)H, C(11)H) ppm.	Calculated [M-HCl] ⁺ : 228.1626; found: 228.1630	235

26b'		62-63	<i>n</i> -hexane	¹ H-NMR (CDCl ₃ , 400 MHz, δ; ppm): δ _H 2.07 (6H, s, C(2)CH ₃ , C(5)CH ₃), 5.93 (2H, s, C(3)H, C(4)H), 6.98 (1H, dt, <i>J</i> = 9.6 Hz, 2.4 Hz, C(11)H), 7.04 (1H, dt, <i>J</i> = 8 Hz, 1.2 Hz, C(9)H), 7.12-7.16 (1H, tdd, <i>J</i> = 8.4 Hz, 2.4 Hz, 0.8 Hz, C(10)H), 7.42-7.48 (1H, m, C(7)H) ppm.	Calculated: 189.0954; found: 189.0957	252
26c'		41-42	<i>n</i> -hexane	¹ H-NMR (CDCl ₃ , 400 MHz, δ; ppm): δ _H 1.97 (6H, s, C(2)CH ₃ , C(5)CH ₃), 5.83 (2H, s, C(3)H, C(4)H), 7.02-7.10 (1H, m, C(10)H), 7.16 (1H, t, <i>J</i> = 1.6 Hz, C(7)H), 7.30-7.35 (2H, m, C(9)H, C(11)H) ppm.	Calculated: 205.0658; found: 205.0656	255
26d'		84-85	<i>n</i> -hexane	¹ H-NMR (CDCl ₃ , 400 MHz, δ; ppm): δ _H 1.96 (6H, s, C(2)CH ₃ , C(5)CH ₃), 5.82 (2H, s, C(3)H, C(4)H), 7.08-7.11 (1H, ddd, <i>J</i> = 7.6 Hz, 1.8 Hz, 0.8 Hz, C(11)H), 7.26 (1H, t, <i>J</i> = 8 Hz, C(10)H), 7.32 (1H, t, <i>J</i> = 1.6 Hz, C(7)H), 7.45-7.48 (1H, ddd, <i>J</i> = 8 Hz, 1.8, 1.2 Hz, C(9)H) ppm.	Calculated: 249.0153, 251.0133; found: 249.0150, 251.0131	256, 257
26e'		59-61	<i>n</i> -hexane	¹ H-NMR (CDCl ₃ , 400 MHz, δ; ppm): δ _H 1.26 (9H, s, C(13)H ₃ , C(14)H ₃ , C(15)H ₃), 1.97 (6H, s, C(2)CH ₃ , C(5)CH ₃), 5.84 (2H, s, C(3)H, C(4)H), 6.94-6.97 (1H, dt, <i>J</i> = 7.2 Hz, 1.6 Hz, C(11)H), 7.16 (1H, t, <i>J</i> = 2.0 Hz, C(7)H), 7.28-7.35 (2H, m, C(9)H, C(10)H) ppm.	Calculated: 227.1674; found: 227.1678	-

26f		oil	-	¹ H-NMR (<i>d</i> ₆ -DMSO, 400 MHz, δ ; ppm): δ_{H} 1.59-1.60 (6H, m, C(14)H ₂ , C(15)H ₂ , C(16)H ₂), 1.97 (6H, s, C(2)CH ₃ , C(5)CH ₃), 3.17-3.20 (4H, m, C(13)H ₂ , C(17)H ₂), 5.70 (2H, s, C(3)H, C(4)H), 6.56 (1H, dd, <i>J</i> =7.6 Hz, 2.0 Hz, C(11)H), 6.69 (1H, t, <i>J</i> =2.0 Hz, C(7)H), 6.97 (1H, dd, <i>J</i> =7.6 Hz, 2.0 Hz, C(9)H), 7.29 (1H, t, <i>J</i> =7.6 Hz, C(10)H) ppm.	Calculated: 254.1783, found: 254.1782	-
26g'		oil	-	¹ H-NMR (<i>d</i> ₆ -DMSO, 400 MHz, δ ; ppm): δ_{H} 1.97 (6H, s, C(2)CH ₃ , C(5)CH ₃), 3.16 (4H, t, <i>J</i> =11.0 Hz, C(13)H ₂ , C(17)H ₂), 3.73 (4H, t, <i>J</i> =11.0 Hz, C(14)H ₂ , C(16)H ₂), 5.76 (2H, s, C(3)H, C(4)H), 6.63 (1H, dd, <i>J</i> =8.2 Hz, 2.0 Hz, C(11)H), 6.73 (1H, t, <i>J</i> =2.0 Hz, C(7)H), 6.99 (1H, dd, <i>J</i> =8.2 Hz, 2.0 Hz, C(9)H), 7.32 (1H, t, <i>J</i> =8.0 Hz, C(10)H) ppm.	Calculated: 256.1576, found: 256.1578	-
26h'		79-82	<i>n</i> -hexane	¹ H-NMR (CDCl ₃ , 400 MHz, δ ; ppm): δ_{H} 1.96 (6H, s, C(2)CH ₃ , C(5)CH ₃), 5.80 (2H, s, C(3)H, C(4)H), 6.74 (1H, t, <i>J</i> =2.0 Hz, C(7)H), 6.85-6.88 (1H, m, C(11)H), 6.97-6.99 (3H, m, C(9)H, C(13)H, C(17)H), 7.07 (1H, t, <i>J</i> =7.2 Hz, C(10)H), 7.26-7.34 (3H, m, C(14)H, C(15)H, C(16)H) ppm.	Calculated: 263.1310, found: 263.1314	-

26i'		75-78	<i>n</i> -hexane	¹ H-NMR (CDCl ₃ , 400 MHz, δ, ppm): δ _H 2.02 (6H, s, C(2)CH ₃ , C(5)CH ₃), 5.88 (2H, s, C(3)H, C(4)H), 7.05-7.09 (2H, m, C(10)H, C(15)H), 7.34-7.46 (7H, m, C(7)H, C(9)H, C(11)H, C(13)H, C(14)H, C(16)H, C(17)H) ppm.	Calculated: 279.1082, found: 279.1085.	-
26j'		84-87	cyclohexane	¹ H-NMR (d ₆ -DMSO, 400 MHz, δ, ppm): δ _H 2.03 (6H, s, C(2)CH ₃ , C(5)CH ₃), 3.80 (3H, s, OCH ₃), 5.85 (2H, s, C(3)H, C(4)H), 6.67 (1H, t, <i>J</i> = 2.0 Hz, C(9)H), 6.98 (1H, t, <i>J</i> = 1.6 Hz, C(7)H), 7.09 (1H, t, <i>J</i> = 2.0 Hz, C(11)H), 7.28-7.32 (1H, m, C(15)H), 7.36-7.40 (2H, m, C(14)H, C(16)H), 7.51-7.54 (2H, m, C(13)H and C(17)H) ppm.	Calculated: 277.1467, found: 277.1462	-
26k'		115-116	cyclohexane	¹ H-NMR (d ₆ -DMSO, 400 MHz, δ, ppm): δ _H 2.02 (6H, s, C(2)CH ₃ , C(5)CH ₃), 3.81 (3H, s, OCH ₃), 5.85 (2H, s, C(3)H, C(4)H), 6.93 (1H, t, <i>J</i> = 1.6 Hz, C(11)H), 7.03 (1H, t, <i>J</i> = 2.0 Hz, C(9)H), 7.15 (1H, t, <i>J</i> = 2.0 Hz, C(7)H) ppm.	Calculated: 279.0259; found: 279.0261	-

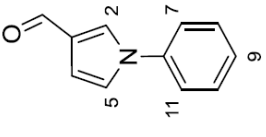
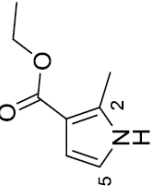
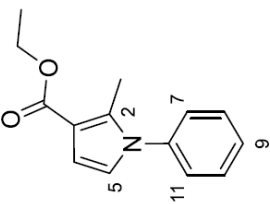
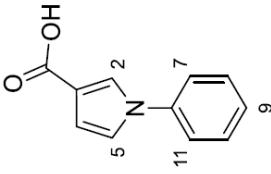
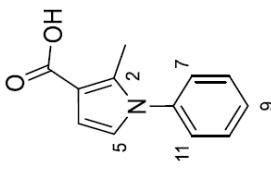
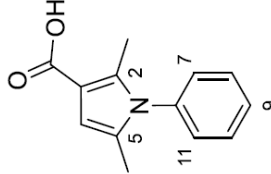
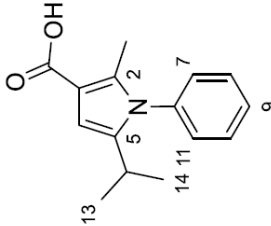
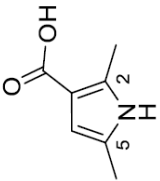
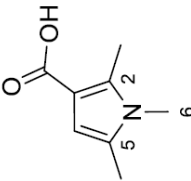
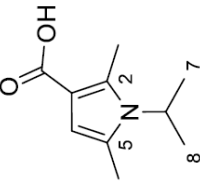
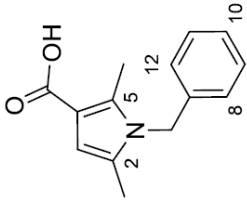
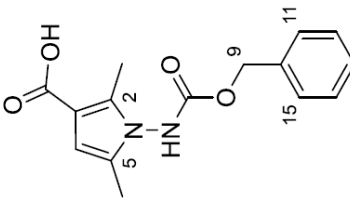
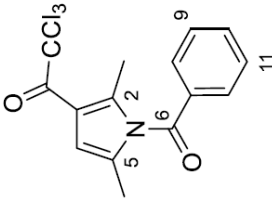
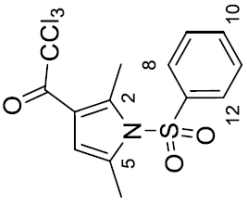
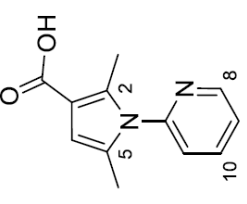
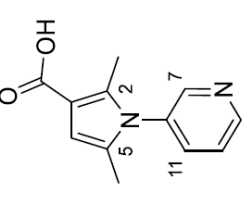
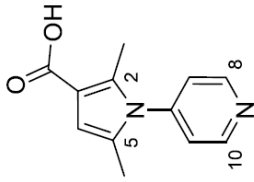
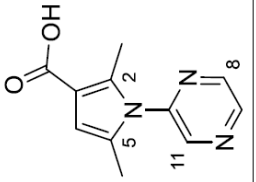
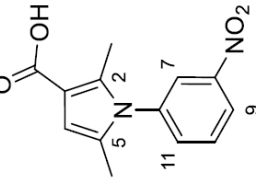
27β		oil	-	¹ H-NMR (<i>d</i> ₆ -DMSO, 400 MHz, δ; ppm): δ _H 6.69 (1H, d, <i>J</i> = 7.6 Hz, C(4)H), 7.05 (1H, t, C(9)H), 7.32 (1H, d, <i>J</i> = 7.6 Hz, C(5)H), 7.54 (2H, t, <i>J</i> = 7.6 Hz, C(8)H, C(10)H), 7.61 (1H, s, C(2)H), 7.76 (2H, d, <i>J</i> = 7.8 Hz, C(7)H, C(11)H), 9.81 (1H, s, CHO) ppm	Calculated: 171.0684; found: 171.0687	258
28		75-78	<i>n</i> -hexane	¹ H-NMR (CDCl ₃ , 400 MHz, δ; ppm): δ _H 1.36 (3H, t, <i>J</i> = 7.2 Hz, COOCH ₂ CH ₃), 2.55 (3H, s, C(2)CH ₃), 4.29 (2H, q, <i>J</i> = 7.2 Hz, COOCH ₂ CH ₃), 6.57-6.59 (2H, m, C(4)H, C(5)H), 8.35 (1H, bs, NH) ppm.	Calculated: 153.0790; found: 153.0794	238
29		170-172	toluene/acetonitrile	¹ H-NMR (CDCl ₃ , 400 MHz, δ; ppm): δ _H 1.38 (3H, t, <i>J</i> = 6.4 Hz, COOCH ₂ CH ₃), 2.46 (3H, s, C(2)CH ₃), 4.32 (2H, q, <i>J</i> = 6.4 Hz, COOCH ₂ CH ₃), 6.69 (2H, s, C(4)H, C(5)H), 7.29 (2H, d, <i>J</i> = 7.6 Hz, C(7)H, C(11)H), 7.43-7.49 (3H, m, C(8)H, C(9)H, C(10)H) ppm.	Calculated: 229.1103; found: 229.1109	259

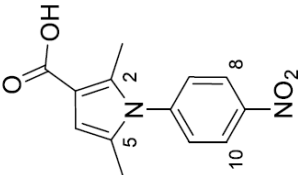
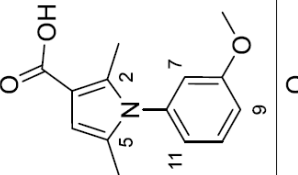
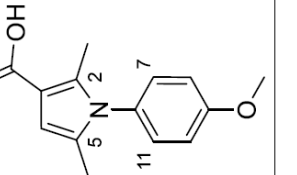
Table S2. Characterization data for intermediates 31a-z , 31a'-j' .					
Cpd	Molecular structure	m.p. (°C)	Crystallization solvent	¹ H NMR	MS (ED) [M] ⁺ Ref
31 a		193-195	acetonitrile	¹ H-NMR (<i>d</i> ₆ -DMSO, 400 MHz, δ; ppm): δ _H 6.61 (1H, bs, C(4)H), 7.34 (1H, t, <i>J</i> = 7.6 Hz, C(9)H), 7.43 (1H, bs, C(5)H), 7.50 (2H, t, <i>J</i> = 7.6 Hz, C(8)H, C(10)H), 7.67 (2H, d, <i>J</i> = 7.8 Hz, C(7)H, C(11)H), 7.93 (1H, bs, C(2)H), 12.09 (1H, bs, COOH) ppm	calculated: 187.0633, found: 187.0635. 241
31b		197-199	acetonitrile	¹ H-NMR (<i>d</i> ₆ -DMSO, 400 MHz, δ; ppm): δ _H 1.93 (3H, s, C(2)CH ₃), 6.23 (1H, s, C(4)H), 7.31 (2H, d, <i>J</i> = 7.6 Hz, C(7)H, C(11)H), 7.40 (1H, bs, C(5)H), 7.49-7.60 (3H, m, C(8)H, C(9)H, C(10)H), 11.95 (1H, bs, COOH) ppm	calculated: 201.0790, found: 201.0787 -
31c		210-215	acetonitrile	¹ H-NMR (<i>d</i> ₆ -DMSO, 400 MHz, δ; ppm): δ _H 1.92 (3H, s, C(5)CH ₃), 2.20 (3H, s, C(2)CH ₃), 6.23 (1H, s, C(4)H), 7.31 (2H, d, <i>J</i> = 7.2 Hz, C(7)H, C(11)H), 7.48-7.59 (3H, m, C(8)H, C(9)H, C(10)H), 11.61 (1H, bs, COOH) ppm	Calculated: 215.0946, found: 215.0949 260

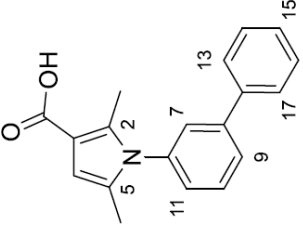
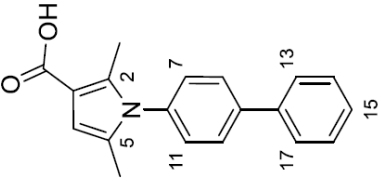
31d		230-232	methanol	¹ H-NMR (DMSO- <i>d</i> ₆ , 400 MHz, δ , ppm): δ_{H} 0.98 (6H, d, J = 7.2 Hz, C(13)CH ₃ , C(14)CH ₃), 2.05 (1H, m, C(12)H), 2.18 (3H, s, C(2)CH ₃), 6.36 (1H, s, C(4)H), 7.33 (2H, d, J = 7.6 Hz, C(7)H, C(11)H), 7.47-7.54 (3H, m, C(8)H, C(9)H, C(10)H), 12.03 (1H, bs, COOH) ppm	Calculated: 243.1259, found: 243.1262	-
31e		210-213	acetonitrile	¹ H-NMR (<i>d</i> ₆ -DMSO, 400 MHz, δ ; ppm): δ_{H} 2.09 (3H, s, C(5)CH ₃), 2.34 (3H, s, C(2)CH ₃), 5.95 (1H, s, C(4)H), 10.84 (1H, s, NH), 11.35 (1H, bs, COOH) ppm	Calculated: 139.0633, found: 139.0635	261
31f		223-225	acetonitrile/methanol	¹ H-NMR (<i>d</i> ₆ -DMSO, 400 MHz, δ ; ppm): δ_{H} 1.97 (3H, s, C(5)H ₃), 2.33 (3H, s, C(2)CH ₃), 3.32 (3H, s, NCH ₃), 5.87 (1H, s, C(4)H), 11.56 (1H, bs, COOH) ppm	Calculated: 153.0790, found: 153.0787	-
31g		183-183	acetonitrile	¹ H-NMR (<i>d</i> ₆ -DMSO, 400 MHz, δ ; ppm): δ_{H} 1.40 (6H, d, J = 6.8 Hz, C(7)H, C(8)H), 2.22 (3H, s, C(5)H ₃), 2.51 (3H, s, C(2)CH ₃), 4.47 (1H, m, C(6)H), 6.04 (1H, s, C(4)H), 11.39 (1H, bs, COOH) ppm	Calculated: 181.1103, found: 181.1101	-

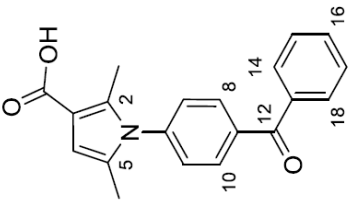
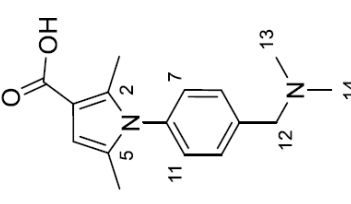
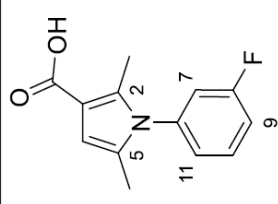
31h		195-198	acetonitrile	¹ H-NMR (DMSO- <i>d</i> ₆ , 400 MHz, δ , ppm): δ 2.03 (3H, s, C(2)H ₃), 2.4 (3H, s, C(5)H ₃), 5.12 (2H, s, C(6)H ₂), 6.17 (1H, s, C(3)H), 6.90 (2H, d, J = 7.2 Hz, C(8)H, C(12)H), 7.25 (1H, t, J = 7.2 Hz, C(10)H) 7.32 (2H, t, J = 7.2 Hz, C(9)H, C(11)H), 11.5 (1H, bs, COOH) ppm	Calculated: 229.1103, found: 229.1106	262
31k		190-192	acetonitrile	¹ H-NMR (<i>d</i> ₆ -DMSO, 400 MHz, δ , ppm): δ 1.99 (3H, s, C(5)H ₃), 2.26 (3H, s, C(2)CH ₃), 5.20 (2H, s, C(9)H ₂), 6.08 (1H, s, C(4)H), 7.38-7.47 (5H, m, aromatic protons), 10.60 (1H, bs, NH), 11.75 (1H, bs, COOH) ppm	Calculated: 288.1110, found: 288.1107	-
30j		oil	-	¹ H-NMR (CDCl ₃ , 400 MHz, δ , ppm): δ 2.14 (3H, s, C(5)H ₃), 2.44 (3H, s, C(2)CH ₃), 6.70 (1H, s, C(4)H), 7.56 (2H, t, J = 7.8 Hz, C(9)H, C(11)H), 7.72-7.77 (3H, m, C(8)H, C(10)H, C(12)H) ppm	Calculated: 342.9934, found: 342.9931	-

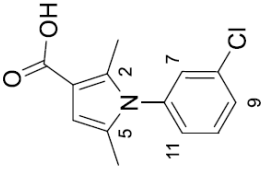
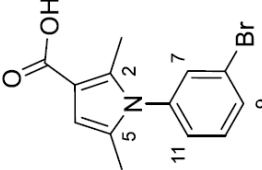
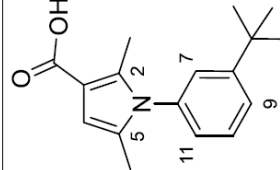
30i		oil	-	¹ H-NMR (CDCl ₃ , 400 MHz, δ: ppm): δ _H 2.51 (3H, s, C(5)H ₃), 2.80 (3H, s, C(2)CH ₃), 6.65 (1H, s, C(4)H), 7.60 (2H, t, J= 7.6 Hz, C(9)H, C(11)H), 7.70 (1H, t, J= 7.6 Hz, C(10)H), 7.82 (2H, d, J= 7.6 Hz, C(8)H, C(12)H) ppm	Calculated: 378.9603, found: 378.9608	-
31l		178-180	toluene/acetonitrile	¹ H-NMR (d ₆ -DMSO, 400 MHz, δ: ppm): δ _H 1.98 (3H, s, C(5)H ₃), 2.26 (3H, s, C(2)CH ₃), 6.23 (1H, s, C(4)H), 7.50 (1H, d, J= 8 Hz, C(11)H), 7.53-7.56 (1H, ddd, J= 7.2 Hz, 4.8 Hz, 0.8 Hz, C(9)H), 8.03-8.08 (1H, td, J= 7.8 Hz, 2 Hz, C(10)H), 8.65-8.66 (1H, dd, J= 4.8 Hz, 0.8 Hz, C(8)H), 12.03 (1H, bs, COOH) ppm	Calculated: 216.0899, found: 216.0901	-
31m		oil	-	¹ H-NMR (d ₆ -DMSO, 400 MHz, δ: ppm): δ _H 1.93 (3H, s, C(5)H ₃), 2.23 (3H, s, C(2)CH ₃), 6.20 (1H, s, C(4)H), 7.57-7.61 (1H, dd, J= 8 Hz, 4.8 Hz, C(9)H), 7.82 (1H, d, J= 8.8 Hz, C(11)H), 8.53 (1H, d, J= 2.4 Hz, C(7)H), 8.67 (1H, d, J= 4.8 Hz, C(10)H), 12.52 (1H, bs, COOH) ppm	Calculated: 216.0899, found: 216.0897	-

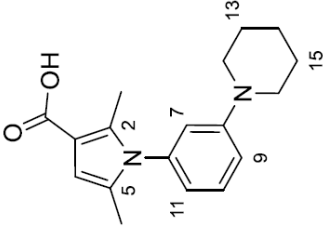
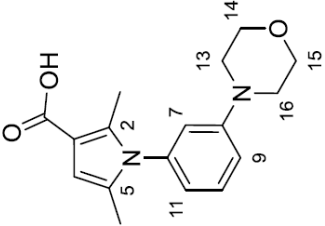
31n		240-245	methanol	¹ H-NMR (<i>d</i> ₆ -DMSO, 400 MHz, δ, ppm): δ _H 1.98 (3H, s, C(5)H ₃), 2.26 (3H, s, C(2)CH ₃), 6.28 (1H, s, C(4)H), 7.45 (2H, d, <i>J</i> = 5.6 Hz, C(7)H, C(11)H), 8.77 (2H, d, <i>J</i> = 5.6 Hz, C(8)H, C(10)H), 11.81 (1H, bs, COOH) ppm	Calculated: 216.0899, found: 216.0898	-
31o		oil	-	¹ H-NMR (<i>d</i> ₆ -DMSO, 400 MHz, δ, ppm): δ _H 2.03 (3H, s, C(5)H ₃), 2.32 (3H, s, C(2)CH ₃), 6.23 (1H, s, C(4)H), 8.76 (2H, d, <i>J</i> = 8.4 Hz, C(8)H, C(9)H), 8.83 (1H, s, C(11)H), 12.45 (1H, bs, COOH) ppm	Calculated: 217.0851, found: 217.0853	-
31p		255-260	methanol	¹ H-NMR (<i>d</i> ₆ -DMSO, 400 MHz, δ, ppm): δ _H 1.83 (3H, s, C(5)CH ₃), 2.16 (3H, s, C(2)CH ₃), 6.28 (1H, s, C(4)H), 7.57 (1H, t, <i>J</i> = 7.6 Hz, C(10)H), 7.93 (1H, d, <i>J</i> = 7.6 Hz, C(11)H), 8.22 (1H, dt, <i>J</i> = 7.6 Hz, 1.6 Hz, C(9)H), 8.45 (1H, t, <i>J</i> = 1.6 Hz, C(7)H), 11.91 (1H, bs, COOH) ppm	Calculated: 260.0797, found: 260.0799	-

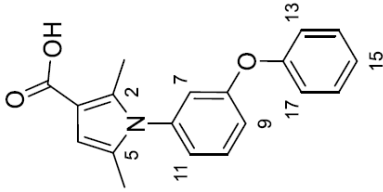
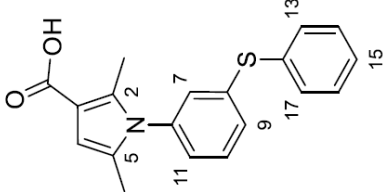
31q		275-276	methanol	¹ H-NMR (<i>d</i> ₆ -DMSO, 400 MHz, δ , ppm): δ_{H} 1.98 (3H, s, C(5)CH ₃), 2.25 (3H, s, C(2)CH ₃), 6.30 (1H, s, C(4)H), 7.67 (2H, d, <i>J</i> = 8.8 Hz, C(7)H), 8.38 (2H, d, <i>J</i> = 8.8 Hz, C(8)H), 11.82 (1H, bs, COOH) ppm	Calculated: 260.0797, found: 260.0795	262
31t		241-244	methanol	¹ H-NMR (<i>d</i> ₆ -DMSO, 400 MHz, δ , ppm): δ_{H} 1.78 (3H, s, C(5)CH ₃), 2.21 (3H, s, C(2)CH ₃), 3.80 (3H, s, OCH ₃), 6.22 (1H, s, C(4)H), 6.85-6.87 (2H, m, C(7)H, C(9)H), 7.06-7.09 (1H, dd, <i>J</i> = 8.4 Hz, 2 Hz, C(11)H), 7.46 (1H, t, <i>J</i> = 8 Hz, C(10)H), 11.60 (1H, bs, COOH) ppm	Calculated: 245.1052, found: 245.1049	-
31u		243-245	methanol	¹ H-NMR (<i>d</i> ₆ -DMSO, 400 MHz, δ , ppm): δ_{H} 1.88 (3H, s, C(5)CH ₃), 2.34 (3H, s, C(2)CH ₃), 3.83 (3H, s, OCH ₃), 6.20 (1H, s, C(4)H), 7.08 (2H, d, <i>J</i> = 8.8 Hz, C(7)H, C(11)H), 7.22 (2H, d, <i>J</i> = 8.8 Hz, C(8)H, C(10)H), 11.62 (1H, bs, COOH) ppm	Calculated: 245.1052, found: 245.1054	262

31x		160-162	toluene/acetonitrile	¹ H-NMR (<i>d</i> ₆ -DMSO, 400 MHz, δ ; ppm): δ_{H} 1.98 (3H, s, C(5)CH ₃), 2.26 (3H, s, C(2)CH ₃), 6.25 (1H, s, C(4)H), 7.30 (1H, d, <i>J</i> = 6 Hz, C(11)H), 7.41 (1H, t, <i>J</i> = 7.2 Hz, C(15)H), 7.49 (2H, t, <i>J</i> = 7.6 Hz, C(14)H, C(16)H), 7.60 (1H, s, C(7)H), 7.65 (1H, t, <i>J</i> = 7.6 Hz, C(10)H), 7.77 (2H, d, <i>J</i> = 7.6 Hz, C(13)H, C(17)H), 7.82 (1H, d, <i>J</i> = 7.8 Hz, C(9)H), 11.81 (1H, bs, COOH) ppm	Calculated 291.1259; found: 291.1256	-
31y		235-237	methanol	¹ H-NMR (<i>d</i> ₆ -DMSO, 400 MHz, δ ; ppm): δ_{H} 1.97 (3H, s, C(5)CH ₃), 2.25 (3H, s, C(2)CH ₃), 6.26 (1H, s, C(4)H), 7.39-7.43 (3H, m, C(15)H, C(8)H, C(10)H), 7.51 (2H, t, <i>J</i> = 7.6 Hz, C(14)H, C(16)H), 7.75 (2H, d, <i>J</i> = 7.2 Hz, C(13)H, C(17)H), 7.84 (2H, d, <i>J</i> = 8.4 Hz, C(7)H, C(11)H), 11.85 (1H, bs, COOH) ppm	Calculated: 291.1259, found: 291.1262	-

31z		290-292	methanol	¹ H-NMR (<i>d</i> ₆ -DMSO, 400 MHz, δ : ppm): δ_H 2.00 (3H, s, C(5)CH ₃), 2.27 (3H, s, C(2)CH ₃), 6.29 (1H, s, C(4)H), 7.53 (2H, d, <i>J</i> = 8.4 Hz, C(8)H, C(10)H), 7.61 (2H, t, <i>J</i> = 7.4 Hz, C(15)H, C(17)H), 7.72 (1H, t, <i>J</i> = 7.4 Hz, C(16)H), 7.81 (2H, d, <i>J</i> = 7.2 Hz, C(14)H, C(18)H), 7.90 (2H, d, <i>J</i> = 8.4 Hz, C(7)H, C(11)H), 11.79 (1H, bs, COOH) ppm	Calculated: 319.1208, found: 319.1210	-
31a'		178-180	toluene/acetonitrile	¹ H-NMR (<i>d</i> ₆ -DMSO, 400 MHz, δ : ppm): δ_H 1.92 (3H, s, C(5)CH ₃), 2.19 (3H, s, C(2)CH ₃), 2.23 (6H, s, C(13)H ₃ , C(14)H ₃), 3.55 (2H, s, C(12)H ₂), 6.23 (1H, s, C(4)H), 7.26 (2H, d, <i>J</i> = 6.4 Hz, C(7)H, C(11)H), 7.48 (2H, d, <i>J</i> = 6.4 Hz, C(8)H, C(10)H), 12.10 (1H, bs, COOH) ppm	Calculated: 272.1525, found: 272.1528	-
31b'		220-226	methanol	¹ H-NMR (<i>d</i> ₆ -DMSO, 400 MHz, δ : ppm): δ_H 1.95 (3H, s, C(5)CH ₃), 2.22 (3H, s, C(2)CH ₃), 6.24 (1H, s, C(4)H), 7.19 (1H, dd, <i>J</i> = 7.6 Hz, 0.8 Hz, C(11)H), 7.31-7.41 (2H, m, C(7)H, C(9)H), 7.59-7.63 (1H, m, C(8)H), 11.54 (1H, bs, COOH) ppm	Calculated: 233.0852, found: 233.0849	-

31c'		240-245	methanol	¹ H-NMR (<i>d</i> ₆ -DMSO, 400 MHz, δ; ppm): δ _H 1.94 (3H, s, C(5)CH ₃), 2.21 (3H, s, C(2)CH ₃), 6.24 (1H, s, C(4)H), 7.30-7.33 (1H, m, C(10)H), 7.51 (1H, s, C(7)H), 7.58-7.61 (2H, m, C(9)H, C(11)H), 11.65 (1H, bs, COOH) ppm	Calculated: 249.0557, found: 249.0559	-
31d'		> 250	methanol	¹ H-NMR (<i>d</i> ₆ -DMSO, 400 MHz, δ; ppm): δ _H 1.94 (3H, s, C(5)CH ₃), 2.21 (3H, s, C(2)CH ₃), 6.23 (1H, s, C(4)H), 7.34-7.37 (1H, dd, <i>J</i> = 7.2 Hz, 0.8 Hz, C(11)H), 7.52 (1H, t, <i>J</i> = 8 Hz, C(10)H), 7.62 (1H, t, <i>J</i> = 1.6 Hz, C(7)H), 7.72 (1H, dd, <i>J</i> = 8 Hz, 0.8 Hz, C(9)H), 11.68 (1H, bs, COOH) ppm	calculated: 293.0051, 295.0031 found: 293.0050, 295.0029.	-
31e'		148-150	toluene	¹ H-NMR (<i>d</i> ₆ -DMSO, 400 MHz, δ; ppm): δ _H 1.32 (9H, s, C(CH ₃) ₃), 1.93 (3H, s, C(5)CH ₃), 2.20 (3H, s, C(2)CH ₃), 6.23 (1H, s, C(4)H), 7.10-7.12 (1H, dt, <i>J</i> = 7.6 Hz, 1.6 Hz, C(11)H), 7.26 (1H, t, <i>J</i> = 1.6 Hz, C(7)H), 7.47 (1H, t, <i>J</i> = 7.6 Hz, C(10)H), 7.52 (1H, dt, <i>J</i> = 7.6 Hz, 1.6 Hz, C(9)H), 11.62 (1H, bs, COOH) ppm	Calculated: 271.1572, found: 271.1570	-

31f		178-180	toluene/acetonitrile	¹ H-NMR (<i>d</i> ₆ -DMSO, 400 MHz, δ; ppm): δ _H 1.56 (6H, m, C(13)H ₃ , C(14)H ₂ , C(15)H ₂), 1.94 (3H, s, C(5)CH ₃), 2.21 (3H, s, C(2)CH ₃), 3.19-3.21 (4H, m, C(12)H ₂ , C(16)H ₂), 6.20 (1H, s, C(4)H), 6.59 (1H, d, <i>J</i> = 7.6 Hz, C(11)H), 6.75 (1H, bs, C(7)H), 7.30 (1H, dd, <i>J</i> = 8 Hz, 2 Hz, C(9)H), 7.33 (1H, t, <i>J</i> = 8 Hz, C(10)H), 11.56 (1H, bs, COOH) ppm	Calculated: 298.1681, found: 298.1684	-
31g'		173-175	toluene/acetonitrile	¹ H-NMR (<i>d</i> ₆ -DMSO, 400 MHz, δ; ppm): δ _H 1.94 (3H, s, C(5)CH ₃), 2.23 (3H, s, C(2)CH ₃), 3.15-3.18 (4H, m, C(13)H ₂ , C(16)H ₂), 3.71-3.74 (4H, m, C(14)H ₂ , C(15)H ₂), 6.21 (1H, s, C(4)H), 6.76 (1H, s, C(7)H), 7.02 (1H, d, <i>J</i> = 7.6 Hz, C(9)H), 7.13 (1H, d, <i>J</i> = 7.6 Hz, C(11)H), 7.41 (1H, t, <i>J</i> = 7.6 Hz, C(10)H), 11.66 (1H, bs, COOH) ppm	Calculated: 300.1474, found: 300.1478	-

<p>31h'</p>		<p>172-173</p>	<p>toluene/acetonitrile</p>	<p>¹H-NMR (<i>d</i>₆-DMSO, 400 MHz, δ; ppm): δ_{H} 1.95 (3H, s, C(5)CH₃), 2.23 (3H, s, C(2)CH₃), 6.21 (1H, s, C(4)H), 6.92 (1H, t, J= 2.4 Hz, C(7)H), 7.07-7.14 (4H, m, C(9)H, C(11)H, C(13)H, C(17)H), 7.20 (1H, t, J= 7.2 Hz, C(15)H), 7.44 (2H, t, J= 7.2 Hz, C(14)H, C(16)H), 7.56 (1H, t, J= 8 Hz, C(10)H), 11.50 (1H, bs, COOH) ppm</p>	<p>-</p> <p>Calculated: 307.1208, found: 307.1211</p>
<p>31i'</p>		<p>172-174</p>	<p>toluene/acetonitrile</p>	<p>¹H-NMR (<i>d</i>₆-DMSO, 400 MHz, δ; ppm): δ_{H} 1.89 (3H, s, C(5)CH₃), 2.17 (3H, s, C(2)CH₃), 6.20 (1H, s, C(4)H), 7.06 (1H, t, J= 1.6 Hz, C(7)H), 7.22 (1H, dd, J= 8 Hz, 1.6 Hz, C(11)H), 7.37-7.48 (5H, m, aromatic protons), 7.54 (1H, t, J= 8 Hz, C(10)H), 11.70 (1H, bs, COOH) ppm</p>	<p>-</p> <p>Calculated: 323.0980, found: 323.0978</p>

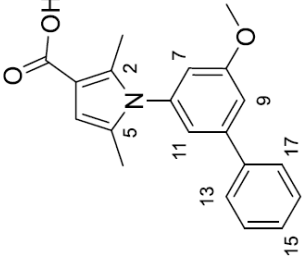
3lj'		168-170	toluene/acetonitrile	¹ H-NMR (<i>d</i> ₆ -DMSO, 400 MHz, δ ; ppm): δ_{H} 2.00 (3H, s, C(5)CH ₃), 2.28 (3H, s, C(2)CH ₃), 3.88 (3H, s, OCH ₃), 6.24 (1H, s, C(4)H), 6.89 (1H, t, <i>J</i> = 2 Hz, C(7)H), 7.16 (1H, t, <i>J</i> = 1.6 Hz, C(9)H), 7.35 (1H, t, <i>J</i> = 1.8 Hz, C(11)H), 7.40 (1H, t, <i>J</i> = 7.2 Hz, C(15)H), 7.48 (2H, t, <i>J</i> = 7.6 Hz, C(14)H, C(16)H), 7.76 (2H, d, <i>J</i> = 7.6 Hz, C(13)H, C(17)H), 11.70 (1H, bs, COOH) ppm	Calculated: 321.1365, found: 321.1367 -
-------------	---	---------	----------------------	--	---

Table S3. Elemental Analyses for Compounds 25a-z, 25a'-j' .									
compd	MW	calculated, %				found, %			
		C	H	N	other	C	H	N	other
25a	321.38	71.10	5.96	13.08	9.96 (O)	71.23	5.87	13.05	9.85 (O)
25b	335.41	71.62	6.31	12.53	9.54 (O)	71.54	6.28	12.61	9.57 (O)
25c	349.43	72.18	6.63	12.03	9.16 (O)	72.25	6.54	12.06	9.15 (O)
25d	377.49	73.18	7.21	11.13	8.48 (O)	73.08	7.30	11.21	8.41 (O)
25e	273.34	65.91	7.01	15.37	11.71 (O)	65.84	7.12	15.44	11.60 (O)
25f	287.36	66.88	7.37	14.62	11.14 (O)	66.83	7.46	14.54	11.17 (O)
25g	315.42	68.54	7.99	13.32	10.14 (O)	68.49	7.84	13.46	10.21 (O)
25h	363.46	72.70	6.93	11.56	8.80 (O)	72.64	6.90	11.62	8.84 (O)
25i	413.49	61.00	5.61	10.16	15.48 (O) 7.75 (S)	61.07	5.73	10.24	15.33 (O) 7.63 (S)
25j	377.44	70.01	6.14	11.13	12.72 (O)	70.10	6.21	11.09	12.60 (O)
25k	422.49	65.39	6.20	13.26	15.15 (O)	65.44	6.14	13.21	15.21 (O)
25l	350.42	68.55	6.33	15.99	9.13 (O)	68.65	6.27	15.87	9.21 (O)
25m	350.42	68.55	6.33	15.99	9.13 (O)	68.52	6.30	15.94	9.24 (O)
25n	350.42	68.55	6.33	15.99	9.13 (O)	68.58	6.27	15.91	9.24 (O)
25o	351.41	64.94	6.02	19.93	9.11 (O)	64.92	6.07	19.97	9.04 (O)
25p	394.43	63.95	5.62	14.20	16.22 (O)	63.90	5.71	14.29	16.10 (O)
25q	394.43	63.95	5.62	14.20	16.22 (O)	63.88	5.68	14.16	16.28 (O)
25r	364.45	69.21	6.64	15.37	8.78 (O)	69.16	6.71	15.39	8.74 (O)
25s	364.45	69.21	6.64	15.37	8.78 (O)	69.32	6.74	15.42	8.52 (O)
25t	379.46	69.64	6.64	11.07	12.65 (O)	69.59	6.52	11.12	12.77 (O)
25u	379.46	69.64	6.64	11.07	12.65 (O)	69.61	6.56	11.16	12.67 (O)
25v	365.43	69.02	6.34	11.50	13.13 (O)	69.08	6.25	11.46	13.21 (O)
25w	365.43	69.02	6.34	11.50	13.13 (O)	69.12	6.29	11.54	13.05 (O)
25x	425.53	76.21	6.40	9.87	7.52 (O)	76.18	6.46	9.74	7.62 (O)
25y	425.53	76.21	6.40	9.87	7.52 (O)	76.24	6.47	9.85	7.44 (O)
25z	453.54	74.15	6.00	9.27	10.58 (O)	74.31	5.94	9.33	10.42 (O)
25a'	422.99	65.07	7.05	12.65	8.00 (Cl) 7.22 (O)	65.01	7.13	12.44	8.09 (Cl) 7.33 (O)
25b'	367.42	68.65	6.04	11.44	5.17 (F) 8.71 (O)	68.72	6.01	11.52	5.11 (F) 8.64 (O)
25c'	383.88	65.71	5.78	10.95	9.23 (Cl) 8.34 (O)	65.88	5.64	10.92	9.11 (Cl) 8.45 (O)

25d'	428.33	58.89	5.18	9.81	18.65 (Br) 7.47 (O)	58.81	5.03	9.94	18.73 (Br) 7.49 (O)
25e'	405.54	74.04	7.71	10.36	7.89 (O)	74.12	7.68	10.44	7.76 (O)
25f'	432.57	72.19	7.46	12.95	7.40 (O)	72.24	7.33	12.97	7.46 (O)
25g'	434.54	69.10	6.96	12.89	11.05 (O)	69.28	6.84	12.75	11.13 (O)
25h'	441.53	73.45	6.16	9.52	10.87 (O)	73.52	6.21	9.63	10.64 (O)
25i'	457.59	70.87	5.95	9.18	6.99 (O) 7.01 (S)	70.93	6.02	9.26	6.87 (O) 6.92 (S)
25j'	455.56	73.82	6.42	9.22	10.54	73.96	6.51	9.15	10.38

2.4.2 Biochemistry

EZH2/PRC2 assays. (Reaction Biology Corporation, USA) The EZH2 substrate (0.05 mg/mL Core Histone or 5 μ M H3/H4 Octamer, H3/H4 Tetramer, or Histone H3) was added in freshly prepared reaction buffer (50 mM Tris-HCl (pH 8), 50 mM NaCl, 1 mM EDTA, 1 mM DTT, 1 mM PMSF, 1% DMSO). The PRC2 complex [complex of human EZH2, human EED, human SUZ12, human AEBP2, and human RbAp48] was delivered into the substrate solution and the mixture was mixed gently. Afterwards, the tested compounds dissolved in DMSO were delivered into the enzyme/substrate reaction mixture by using Acoustic Technology (Echo 550, LabCyte Inc. Sunnyvale, CA) in nanoliter range, and 3 H-SAM was added into the reaction mixture to initiate the reaction. The reaction mixture was incubated for 1 h at 30 °C and then it was delivered to filter-paper for detection. The data were analyzed using Excel and GraphPad Prism software for IC₅₀ curve fits.

EZH1 complex, DOT1L, G9a, MLL1 complex, SET7/9, PRMT1, and DNMT1 assays. (Reaction Biology Corporation, USA) The appropriate methyltransferase substrate (0.05 mg/mL core histone for EZH1 complex, 0.05 mg/mL oligonucleosomes for DOT1L, 5 μ M histone H3 (1-21) peptide for G9a, 0.05 mg/mL nucleosomes for MLL1 complex, 0.05 mg/mL core histone for SET7/9, 5 μ M histone H4 for PRMT1, and 0.001 mg/mL poly(dI-dC) for DNMT1) was added in freshly prepared reaction buffer (50 mM Tris-HCl (pH 8.5), 5 mM MgCl₂, 50 mM NaCl, 0.01 % Brij35, 1 mM DTT, 1 % DMSO). The MT enzyme was delivered into the substrate solution and the mixture was mixed gently. Afterwards, the tested compounds dissolved in DMSO were delivered into the enzyme/substrate reaction mixture by using Acoustic Technology (Echo 550, LabCyte Inc. Sunnyvale, CA) in nanoliter range, and 1 μ M 3 H-SAM was also added into the reaction mixture to initiate the reaction. The reaction mixture was incubated for 1 h at 30 °C and then it was delivered to filter-paper for detection. The data were analyzed using Excel and GraphPad Prism software for IC₅₀ curve fits.

2.4.3 In cell evaluation (1)

(Prof. Lucia Altucci, Department of Biochemistry, Biophysics and General Pathology, Second University of Naples)

Cells culture (DCC). SHSY5Y and MDA-MB231 cells (purchased by ATCC) were cultured in Dulbecco's Modified Eagle Medium (DMEM) (EuroClone), supplemented with 10% heat-inactivated fetal bovine serum FBS (Sigma-Aldrich), antibiotics (100 U/mL penicillin, 100 μ g/mL streptomycin and 250 ng/mL amphotericin-B) and 2 mM L-glutamine (Euroclone).

U937 and NB4 cells were cultured in RPMI supplemented with 10 % heat-inactivated fetal bovine serum (FBS) (Sigma-Aldrich), antibiotics (100 U/mL penicillin, 100 μ g/mL streptomycin and 250 ng/mL amphotericin-B), and 2 mM L-glutamine (Euroclone).

Cell viability analysis. Cells were treated with **25c, h, m, n, p-r, t, x, y, b'-e', h', and j'** (stock

solution 10 mM in dimethylsulfoxide (DMSO)) and reference compound **3**. Then the cells were incubated with trypan blue (Euroclone) at a ratio of 1:1. Trypan blue-positive cells (dead cells) as well as total cell population were counted (burker chamber) using an optical microscope to calculate the percentage of viable cells.

Cell cycle. 2.0×10^5 cells were collected, washed with PBS once and resuspended in hypotonic buffer (0.1% NP-40, 0.1% sodium citrate, 50 $\mu\text{g}/\mu\text{L}$ propidium iodide (PI) in phosphate buffered saline). Cells were then incubated in the dark for at least 30 minutes and measured on FACS Calibur flow cytometer (Becton Dickinson). Flow cytometric data were analysed using ModFit (Verity) and Cell Quest (Becton Dickinson) technologies. Apoptosis was measured as pre-G1 analyzed by FACS with Cell Quest software (BD Biosciences). Cell death was measured as sub-G1 DNA fragmentation. All experiments were performed in triplicate and values expressed in mean \pm SD.

Antibodies, Plasmids and chemicals. Primary antibodies used: anti-acetylated tubulin (SIGMA), anti-H3K27me3 (Abcam); anti-H4 (Abcam) was used as loading control. Antibodies were used according to the manufacturer's instructions.

Total proteins extraction. Cells were harvested and washed once with cold PBS and lysed in a lysis buffer containing 50 mM Tris-HCl pH 7.4, 150 mM NaCl, 1 % NP40, 10 mM NaF, 1 mM PMSF and protease inhibitor cocktail (Roche). The lysates were centrifuged at 13000 r.p.m. for 30 min at 4 °C. Protein concentrations were estimated by Bradford assay (Bio-Rad).

Western blot analyses. 50 μg of total protein and 10 μg of histone extracts, were denatured boiling samples in buffer (0.25 M Tris-HCl pH 6.8, 8 % SDS, 40 % glycerol, 5 % 2-mercaptoethanol, bromophenol blue 0.05 %) for 3 min before electrophoresis. Proteins were subjected to SDS-PAGE (8 %-10 %-15 % polyacrylamide) in Tris-glycine-SDS (25 mM Tris, 192 mM glycine, 0.1 % SDS). After electrophoresis, proteins were transferred to nitrocellulose membranes (Schleicher e Schuell, Germany) in a buffer containing Tris-glycine (25 mM Tris, 192 mM glycine) (Bio-Rad, Italy) and 20 % methanol. The complete transfer was assessed using Ponceau red (Sigma Aldrich, USA) staining. After blocking with 5 % non-fat dry milk in TBS 1 \times / Tween 0.1 % (10 mM Tris-HCl pH 8.0, 150 mM NaCl, 0.1 % Tween-20), the membrane was incubated with the primary antibody overnight at 4 °C. After washing with TBS 1 \times / Tween 0.1 %, membranes were incubated with the horseradish peroxidase-conjugated secondary antibody (1:5000) for 60 min at room temperature and the reaction was detected with chemiluminescence detection system (Amersham Biosciences, UK).

2.4.4 In cell evaluation (2)

(Prof. Susanna Scarpa, Department of Experimental Medicine, Sapienza University, Rome)

Cell cultures and treatments. The human glioblastoma multiform cell line U-87 MG (here indicated as U-87) has been utilized (ATCC). Three primary cell cultures (GL1, GL2, GL3) were

established from surgical tissues of patients with glioblastoma, plus one human dermal fibroblast primary culture, HF, as previously described. U-87 were grown in EMEM medium supplemented with 10 % fetal calf serum (FCS), 2 mM glutamine, 50 U/mL penicillin-streptomycin, 1 mM non-essential amino acid, 1 mM sodium pyruvate; the primary cell cultures and HF were grown in DMEM medium supplemented with 10 % fetal calf serum (FCS), 2 mM glutamine, 50 U/mL penicillin-streptomycin.

The two EZH2 inhibitors (**25f'** and **25g'**) were solubilized in dimethylsulfoxide (DMSO) at 10 mM stock solution and utilized to final concentrations from 10 μ M to 50 μ M. Temozolomide was solubilized in DMSO at 100 mM stock solution and utilized to final concentration of 100 μ M.

Cytotoxicity assay. To determine cytotoxicity, sulforhodamine B colorimetric assay was performed: 1.5×10^4 cells were plated on 96 well plates, grown for 24 h and treated with different concentrations of **25f'**, **g'** (10 μ M, 25 μ M, 50 μ M), and with 100 μ M temozolomide, for 48 or 72 h. Control cells were treated with equivalent amounts of DMSO. Cells were then fixed with 50 % trichloroacetic acid for 1 h at 4 °C and stained for 30 min at room temperature with 0.4 % sulforhodamine B in 1 % acetic acid. Excess dye was removed by washing four times with 1 % acetic acid. Protein-bound dye was dissolved in 10 mM TRIS pH 10, and optical density (OD) was determined at 510 nm using a microplate reader.

Western blot. Cell lysates were obtained scraping the cells in lysis buffer 1 % Triton, 0.1 % SDS, 150 mM NaCl, 50 mM TRIS-HCl pH 7.4, 2 mM EDTA plus protease inhibitor cocktail tablet (Roche Applied Sciences) for 30 min at 4 °C, lysates were then centrifuged at 12,000 rpm for 15 min at 4 °C. Protein concentration was evaluated by Bio-Rad Protein Concentration Assay. Samples of lysate (100 μ g) were separated by molecular weight on 10 or 12 % SDS-PAGE and then transferred into a nitrocellulose membrane. Blots were blocked for 1 hour at room temperature in 5 % non-fat dry milk and then incubated overnight at 4 °C with antibody to Tri-Methyl-Histone H3 (Lys27) (Cell Signaling Technology) diluted 1:1000 in 5 % BSA, 0.1 % Tween 20 TRIS-buffered saline or alternatively for 1 hour at room temperature with anti- β -actin (Sigma Aldrich) diluted 1:1000 in TRIS-buffered saline. Blots were washed in TRIS-buffered saline with 0.1 % Tween 20 and then incubated with horseradish peroxidase conjugated anti-rabbit or anti-mouse antibodies (1:5000 diluted) (Sigma-Aldrich). The filters were then developed by enhanced chemiluminescence (Super Signal West Pico Chemiluminescent Substrate, Thermo Scientific) using Kodak X-Omat films. The densitometry quantitation of the bands was performed using Image J software (NIH).

Immunofluorescence. The cells were grown directly on Labteck chamber slides (Nunc) for 24 hours. Cells were then washed with PBS with Ca/Mg and fixed with absolute cold methanol for 5 min (for nestin staining) or with 4 % buffered paraformaldehyde for 20 minutes at 4 °C (for GFAP staining). The cells were incubated with 3 % bovine serum albumin for 1 hour at room

temperature and then with anti glial fibrillary acidic protein (GFAP) antibody (Abcam) for 1 hour at room temperature, and with anti-nestin antibody (Abcam) overnight at 4 °C. Cells were then washed twice with PBS with Ca/Mg and then incubated with the secondary anti rabbit antibody Alexa Fluor 594 conjugated (1:400 diluted) for 1 hour at room temperature. The cells were finally washed twice with PBS with Ca/Mg, mounted with Prolong Antifade reagent (Life Technologies) and analyzed by a fluorescence microscope (Olympus BX52), image acquisition and processing were conducted by IAS 2000 software. Fluorescence intensity of 3 randomly selected fields was acquired by densitometric quantitation using ImageJ software and the mean was determined (NIH).

Statistical analysis and graphic programs. All results were analyzed by ANOVA, and the significance was evaluated by the Tukey HSD post hoc test (Honestly Significant Difference). All figures were elaborated with Adobe Photoshop CS5 and all graphs with Graph Pad Prism 5.0.

3 Development of Pyrazole-based Inhibitors of EZH2 able to Induce Apoptosis and Autophagy in Cancer Cells, reduce cell stemness in SHH medulloblastoma cancer stem cells, and impair of tumour growth *in vivo**

3.1 Research project

As previously mentioned, in parallel with the pyrrole-based EZH2i project, we developed a second project on design and synthesis of pyrazole-based EZH2i. This project started with a structural simplification and modification on the indazole scaffold described by GSK and Epyzime companies (2, 4 Figure 1.5). Our approach was based on:

- ring opening of the indazole aromatic bicycle to get the pyrazole heterocycle;
- shifting of the dimethylpyridone amide group from C(4) indazole position to the C(4) pyrazole position;
- N(1) pyrazole substitutions with alkyl (isopropyl, cyclopentyl), arylalkyl (benzyl) and aryl (phenyl) groups;
- addition of alkyl (methyl, *n*-propyl) and of different aromatic (phenyl, pyrrolyl, styryl) substituents at C(5) pyrazole position (Figure 3.1).

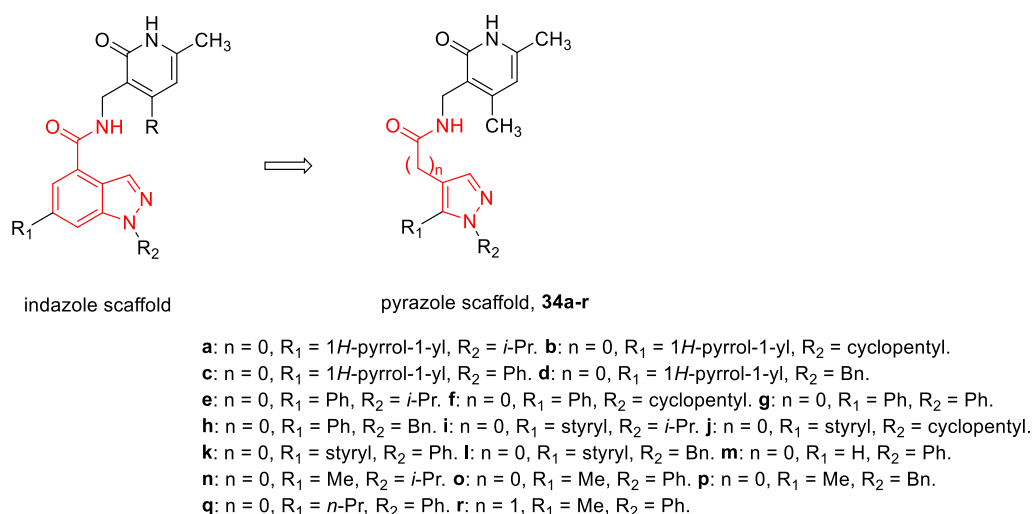


Figure 3.1. Design of novel Pyrazole-based EZH2 inhibitors (**34a-r**).

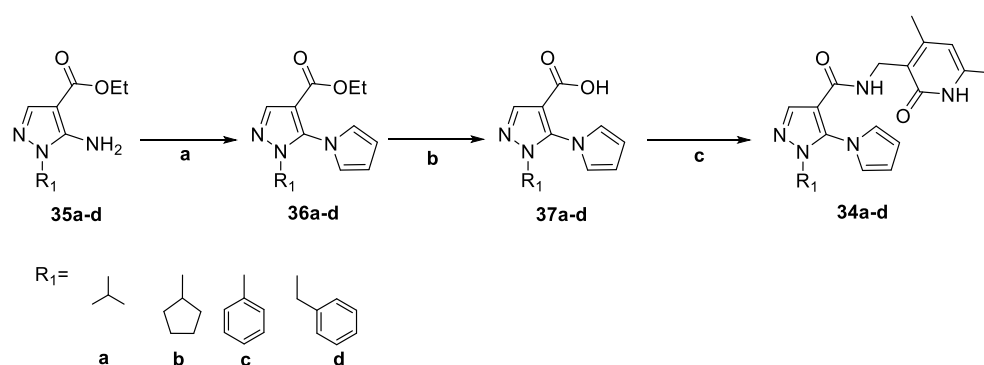
All the newly obtained derivatives **34a-r** have been screened by Reaction Biology Corporation (PA, USA) against the EZH2 methyltransferase activity by using the PRC2 multicomponent protein in order to determine their inhibition activity (IC₅₀ values or percent of inhibition at fixed dose). Next, we have tested the capability of the most active compound **34o** (IC₅₀ 15.4 μM) to decrease the histone H3K27me3 levels by western blot, as well as to arrest proliferation by MTS assay in four different cancer cell lines (human breast cancer MDA-MB231, myelogenous leukemia K562, prostate cancer PC3, and neuroblastoma SK-N-BE). Finally, we investigated the cell death mechanism (apoptosis, autophagy) in the most responsive cell lines (K562, SK-N-BE).

Additionally, **34o** served as a tool in a biological study by the group of Prof. Elisabetta Ferretti, where EZH2 has been validated as an attractive target for SHH MB cancer and cancer stem cell impairment. In this study, EZH2 pharmacological inhibition by **34o** proved to be effective also in medulloblastoma xenografted mouse models.²⁶⁴

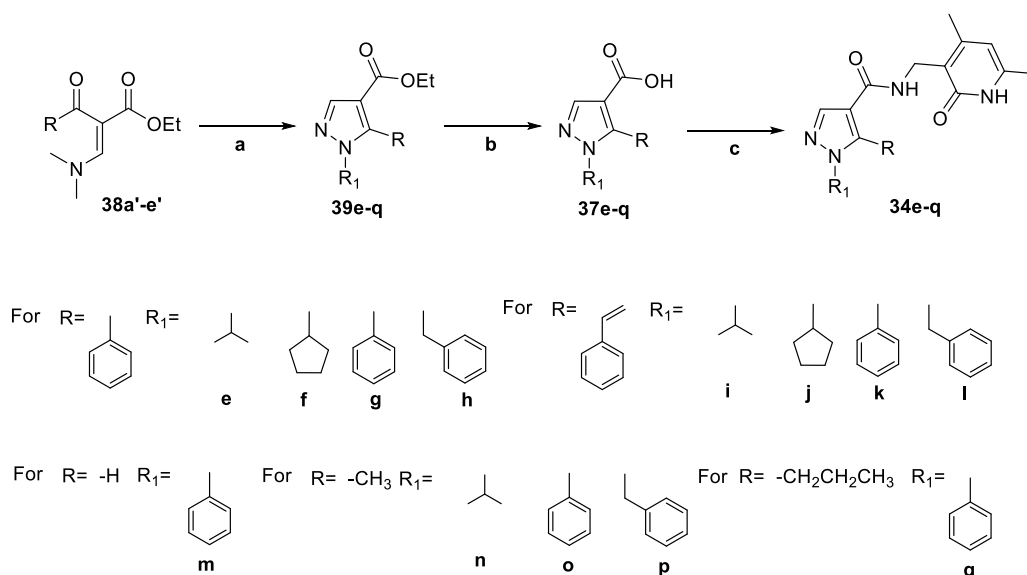
3.2 Results and Discussion

3.2.1 Chemistry

Compounds **34a-d** were prepared starting from a Clauson-Kaas reaction between 5-amino-pyrazole esters **35a-d** (previously prepared according to the literature)²⁶⁵ and 2,5-dimethoxytetrahydrofuran in acetic acid at 80 °C, providing the 5-pyrrolyl-pyrazole derivatives **36a-d** (Scheme 8). The esters **36a-d** were hydrolyzed in basic conditions with 2 N potassium hydroxide in ethanol to give the corresponding pyrazole acid derivatives **37a-d**.

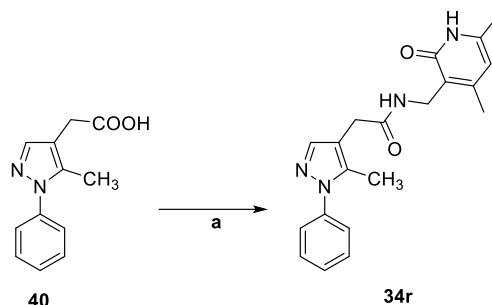


Scheme 8. Reagents and conditions: **a)** 2,5-dimethoxytetrahydrofuran, CH₃COOH, 80°C, 1-6 h; **b)** 2N KOH, EtOH, r. t., 16 h; **c)** **33**, TBTU, Et₃N, dry DMF, N₂, r. t., 16 h.



Scheme 9. Reagents and conditions: **a)** appropriate hydrazine, EtOH, 80 °C or r. t.; **b)** 2 N KOH, EtOH, r. t., 16 h; **c)** **33**, TBTU, Et₃N, dry DMF, N₂, r. t., 16 h.

The coupling between the acids **37a-d** and the amine **33** (prepared as described in chapter 2), in presence of triethylamine, *N,N,N',N'*-tetramethyl-O-(benzotriazol-1-yl)uronium tetrafluoroborate (TBTU), dry *N,N*-dimethylformamide, yielded the final amides **34a-d** (Scheme 8). The synthesis of the pyrazole derivatives **34e-q** started from the appropriate enamine **38a'-e'** (prepared according to the literature)²⁶⁶, which underwent cyclo-condensation with the appropriate hydrazines (all commercially available) in EtOH at 80 °C to obtain pyrazole esters **39e-q**. The latter intermediates were hydrolyzed in the same conditions as described for **36a-d**, to provide the corresponding pyrazole acid derivatives **37e-q**, which were finally converted into the amides **34e-q** by using the same methodology as described for **34a-d** (Scheme 8 and 9). The amide **34r** was obtained from the acid **40** (prepared according to the literature)²⁶⁷, following the same procedure as above described for final compounds **34a-q** (Scheme 10).

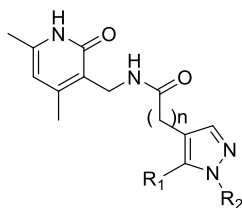


Scheme 10. Reagents and conditions: **a**) **33**, TBTU, Et₃N, dry DMF, N₂, r. t., 16 h.

3.2.2 Biochemical EZH2 enzymatic inhibition assay and structure activity relationship (SAR)

All new synthesized compounds have been tested against the human histone five component complex Polycomb Repressive Complex 2 (PRC2) containing the catalytic methyltransferase EZH2, Embryonic Ectoderm Differentiation (EED), Suppressor of Zeste 12 protein homolog (SUZ12), Histone-binding protein RBBP4 (Rbap48) and Zinc finger protein AEBP2 (AEBP2). Moreover, Histone H3 at 5 µM and SAM at 250 nM as substrate and cofactor, respectively, were used. SAH was used as a positive control compound. As a part of our molecular pruning approach, we first decided to synthesize compounds in which the indazole nucleus was replaced by a 5-arylpyrazole ring. First, we inserted at the pyrazole-C(5) position a 1*H*-pyrrol-1-yl (**34a-d**), phenyl (**34e-h**) or styryl (**34i-l**) group, and an *iso*-propyl, cyclopentyl, phenyl or benzyl substituent at N(1), obtaining compounds displaying very low EZH2 inhibition activity (Table 4). The shift of the phenyl ring from pyrazole C(5) to N(1) position (**34m**) led to the first pyrazole analog with > 25 % of inhibition at 50 µM (Table 4). However, its negligible IC₅₀ value (> 400 µM) suggested that additional structural modifications were required.

Table 4. Inhibiting activity against PRC2 (IC₅₀^a, μM or % inhibition at fixed dose, 50 μM) Compounds were tested in 10-dose IC₅₀ mode with 2-fold serial dilution starting from 200 μM solutions or in two independent experiments at the fixed 50 μM concentration.



34a-r

cpd	n	R ₁	R ₂	% inhibition at 50 μM	IC ₅₀ , μM
34a	0	1 <i>H</i> -pyrrol-1-yl	<i>iso</i> -propyl	0	
34b	0	1 <i>H</i> -pyrrol-1-yl	cyclopentyl	4.7	
34c	0	1 <i>H</i> -pyrrol-1-yl	phenyl	0	
34d	0	1 <i>H</i> -pyrrol-1-yl	benzyl	5.8	
34e	0	phenyl	<i>iso</i> -propyl	0	
34f	0	phenyl	cyclopentyl	2.7	
34g	0	phenyl	phenyl	6.9	
34h	0	phenyl	benzyl	20	
34i	0	styryl	<i>iso</i> -propyl	0	
34j	0	styryl	cyclopentyl	2.9	
34k	0	styryl	phenyl	0	
34l	0	styryl	benzyl	11.8	
34m	0	H	phenyl	25.3	>400
34n	0	methyl	<i>iso</i> -propyl	16.7	342.7
34o	0	methyl	phenyl	71.5	15.4
34p	0	methyl	benzyl	68.3	19.6
34q	0	<i>n</i> -propyl	phenyl	29.0	151
34r	1	methyl	phenyl	4.5	>400
SAH					34.7
3					0.009

The introduction of a methyl group at the pyrazole C(5) with compound **34o** turned in a nice improvement of the inhibitory potency against EZH2 (IC₅₀= 15.4 μM). The replacement of the

phenyl group at the N(1) of **34o** with a benzyl group gave the equipotent analog **34p** (IC_{50} = 19.6 μ M). Conversely, replacing the N(1) phenyl with an *iso*-propyl group (**34n**), elongating the C(5) substituent of **34o**, from methyl to *n*-propyl (**34q**), or homologating its carboxamide to acetamide linkage (**34r**), caused a severe drop or complete loss in inhibition activity (Table 4). Based on these data, compound **34o** was chosen for further evaluation.

3.2.3 Compound 34o activity validation: biochemical screening in presence of different substrates, SAM-competition experiments and screening against a panel of methyltransferases (EZH1, DOT1L, DNMT1, G9a, MLL1 complex, PRMT1, SET7/9)

Further experiments on **34o** using different substrates (H3/H4 octamer, H3/H4 tetramer, and histone H3) confirmed its inhibitory ability against EZH2/PRC2 (IC_{50} values = 6.3, 5.3, and 5.7 μ M, respectively), as well as its SAM-dependent mechanism of action (Figure 3.2).

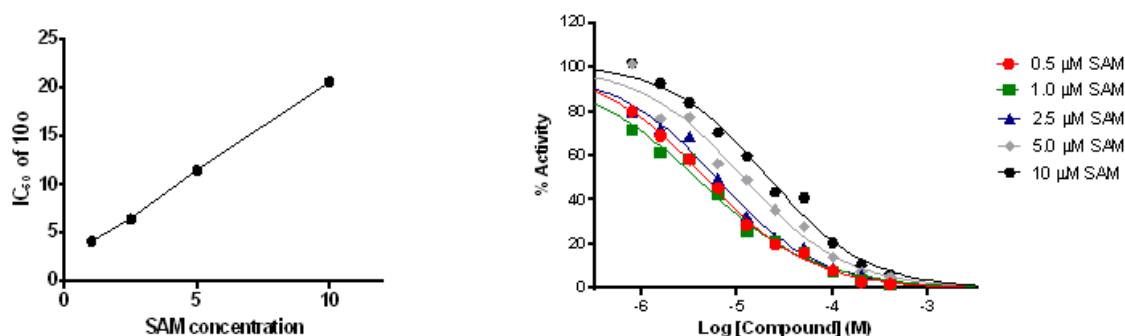


Figure 3.2. SAM competition experiments. Left, dependence of **34o** IC_{50} values with increasing SAM concentration. Right, inhibitory effects of **34o** vs EZH2/PRC2 at increasing SAM concentrations.

Table 5. IC_{50} or percentage of Inhibition of **34o** against a panel of methyltransferases.

MT	IC_{50} , μ M	% inhibition at 100 μ M	% inhibition at 200 μ M
EZH1 complex	138.5	43	-
DOT1L		6	3
G9a		7	5
MLL1 complex		7	21
SET7/9		0.8	5
PRMT1		8	6
DNMT1		0	0

Moreover, **34o** was screened against a panel of methyltransferases (MTs) and proved to be a selective inhibitor of EZH2. Indeed, **34o** was 22-fold less potent against the closely related EZH1

complex, and practically inactive against the other MTs, including the arginine methyltransferase PRMT1, and the DNA methyltransferase DNMT1 (Table 5).

3.2.4 Effects of **34o** in a panel of cancer cells

(Group Prof. Marco Tafani, Department of Experimental Medicine, Sapienza University of Rome, Italy).

We evaluated the capability of **34o** to arrest proliferation (MTS assay) on four different cancer cell lines, including: human breast cancer MDA-MB231, myelogenous leukemia K562, prostate cancer PC3 and neuroblastoma SK-N-BE. **34o** was tested at three different concentrations (1, 10 and 25 μ M), and up to 5 days of treatment (Figure 3.3).

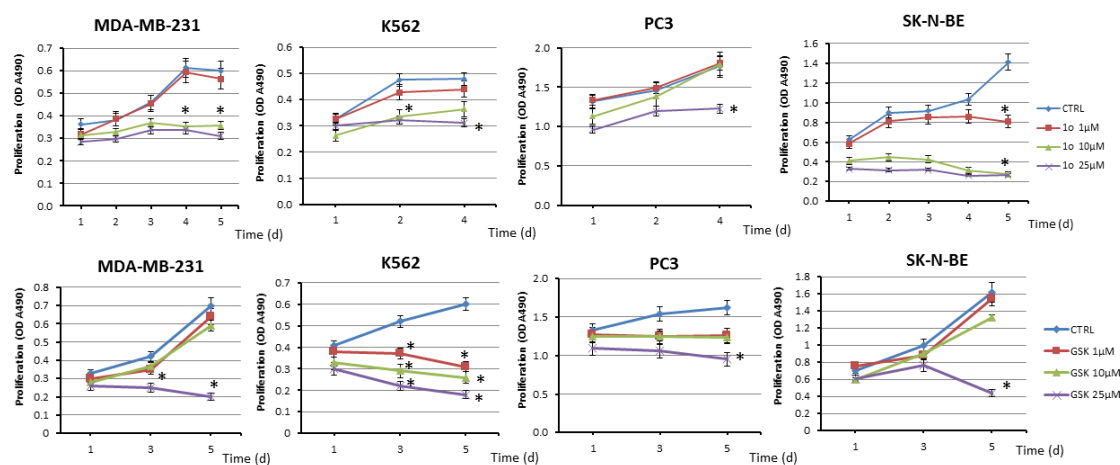


Figure 3.3. Antiproliferative effect of **34o** (Top line) or **3** (bottom line) on different cancer cell lines after 1, 2 and 4 days of treatment (K562 and PC3), or after 1, 2, 3, 4 and 5 days of treatment (MDA-MB-231 and SK-N-BE). The effect of **34o** was determined by MTS cell proliferation assay after treatment with 1, 10 and 25 μ M of compound.

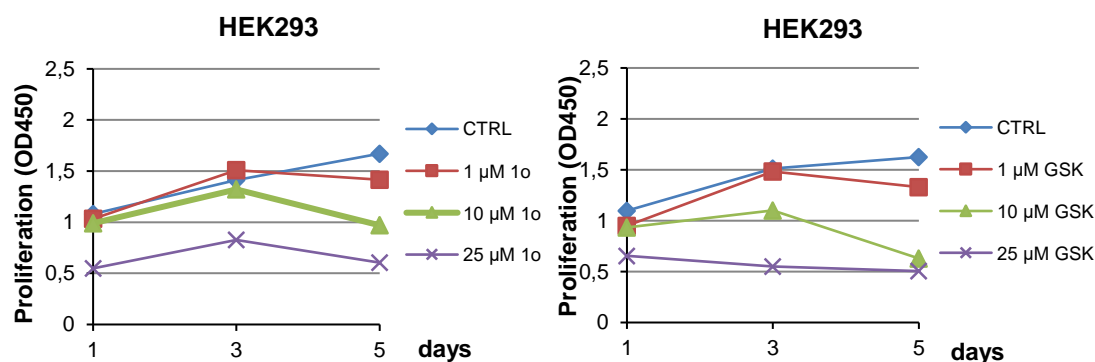


Figure 3.4. Cytotoxicity of **34o** and **3** in non-cancer cells. Antiproliferative effects of **34o** (left) and of **3** (right) in human embryonic kidney HEK293 cells treated with 1, 10 and 25 μ M of the compound for 5 days (MTS Cell Proliferation Assay).

The effects of **34o** on cell growth and morphology were assessed in SK-N-BE and K562 cells, chosen as representative of non-adherent and adherent cell lines, respectively. **3** was used as

reference drug. Respect to the control, **34o** increased cell detachment in SK-N-BE and reduced cell growth in K562 cells. Similar results were obtained with **3** at 1 μ M (Figure 3.5).

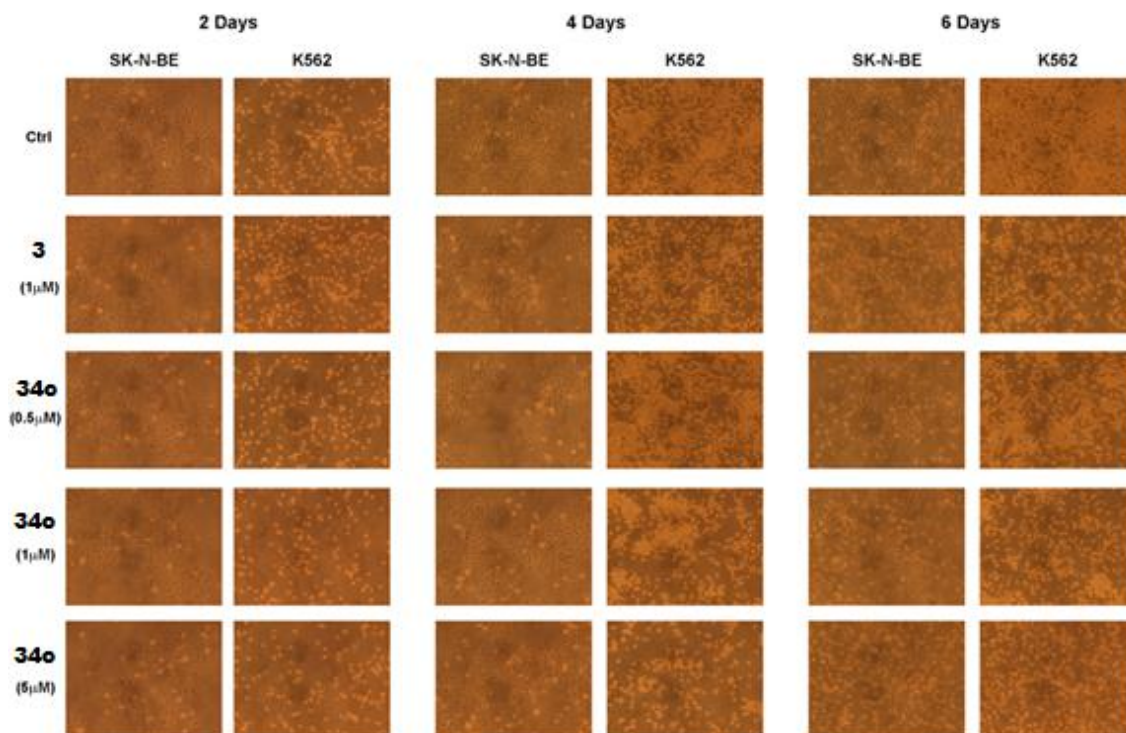


Figure 3.5. SK-N-BE and K562 cells were either left untreated or treated with 0.5, 1 and 5 μ M **34o** for 2, 4 and 6 days. **3** (1 μ M) was used as a reference. Cell morphology was evaluated by optical microscopy and picture taken.

With the sole exception of PC3 cancer cell line, **34o** displayed a dose- and time-dependent reduction of proliferation, detectable from 1 μ M in SK-N-BE, and from 10 μ M in MDA-MB231 and in K562 cells. Instead, in PC3 cells, **34o** showed proliferation arrest only at 25 μ M. Differently, **3** (GSK126, Figure 1.5) was very potent against the leukemia K562 cells, but displayed significant effects in the tested solid tumor cells only at 25 μ M (Figure 3.3). Interestingly, when tested in non-cancer human embryonic kidney cells HEK293, **34o** proved to be less toxic than **3** showing only moderate toxicity after 5 days at 10 μ M (Figure 3.4).

3.2.5 Intracellular inhibition of H3K27 methylation

(Group Prof. Marco Tafani, Department of Experimental Medicine, Sapienza University of Rome, Italy)

As a functional read-out of EZH2 inhibition in cells, we determined the levels of H3K27me3 in SK-N-BE and in K562 cells treated with **34o** (0.5 and 1 μ M) for 6 days, in comparison with **3** (1 μ M). β -Actin was used for equal loading. Western blots in Figure 3.6 shows a dose-dependent reduction of the H3K27me3 levels after treatment of with **34o**, particularly in SK-N-BE cells, where **34o** was more effective than **3** (over 80 % against 40 % of H3K27me3 demethylation). As expected, **3** displayed the strongest effect in K562 cells (see Figure 3.6 B for quantization by

densitometry analysis). We have also shown that, in both cell lines, neither **34o** nor **3** reduced H3 levels after 6 days of treatment at 1 μ M (Figure 3.7).

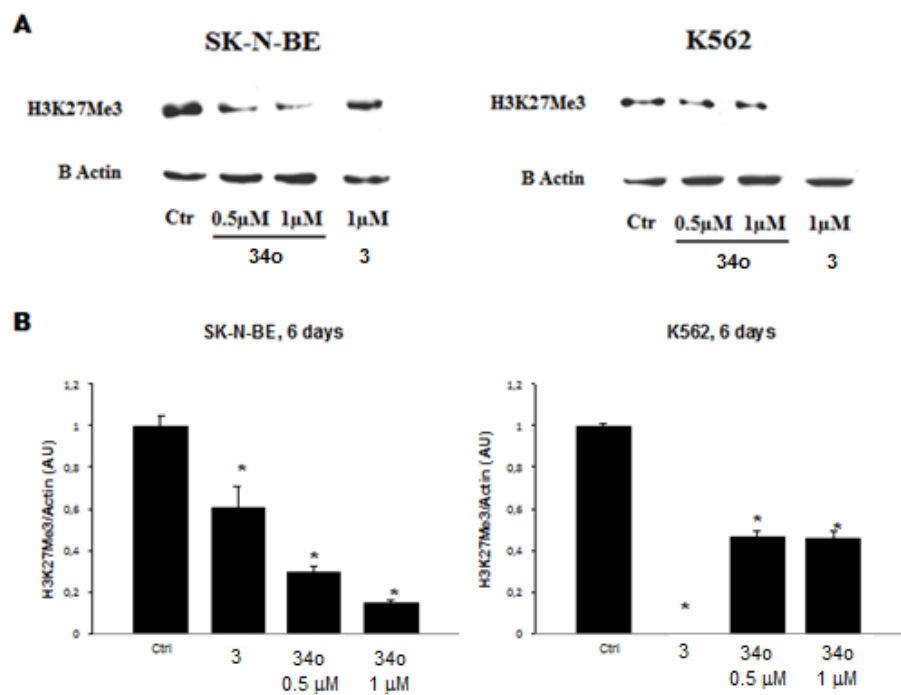


Figure 3.6. (A) Western blotting showing reduction of H3K27 trimethylation by **34o** in neuroblastoma (SK-N-BE) and leukemia (K562) cells, and (B) relative densitometric analysis. B-Actin was used for normalization.

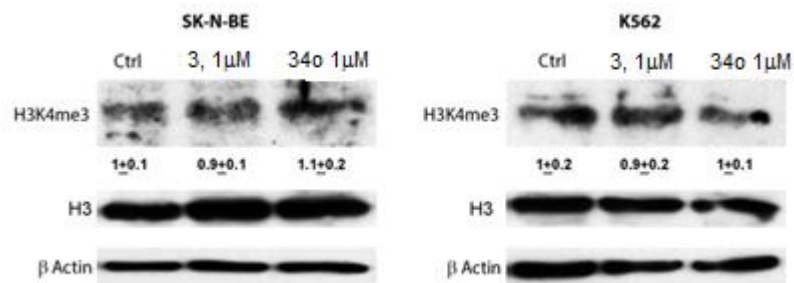


Figure 3.7. Western blot analysis showing the levels of H3K4me3 and histone H3 after treatment with **3** and **34o** (both at 1 μ M) in SK-N-BE and K562 cells. The relative densitometry for H3K4me3 (arbitrary units) is reported. β -Actin was used for normalization.

3.2.6 Autophagy induction of 34o in myelogenous leukemia K562 and neuroblastoma SK-N-BE cell lines

(Group Prof. Marco Tafani, Department of Experimental Medicine, Sapienza University of Rome, Italy)

Autophagy represents a physiological mechanism used by cells to recycle intracellular components or remove damaged organelles. However, excessive autophagy activation can result in cell death. EZH2 has been recently reported to epigenetically repress negative regulators of the mTOR pathway, such as TSC2, leading to inhibition of autophagy.²⁶⁸ Accordingly, the EZH2

inhibitors GSK343 (**4**, Figure 1.5)¹⁵⁹ and UNC1999 (**6**, Figure 1.5)¹⁶¹ have been shown to induce autophagic cell death in MDA-MB-231 cells.²⁶⁹ Additionally, co-inhibition of both EGFR and EZH2 has been studied in colon cancer HT-29 and HCT-15 cell lines, using the small molecules gefitinib and **6**. The association of these two drugs yielded not only a significant decrease in cell number and increased apoptosis compared to the single target inhibition, but also significantly induced autophagy, indicating that autophagy may play a role in the observed synergy. From a molecular point of view, induction of autophagy can be evaluated by studying the expression of proteins that represent markers of such a process. The most studied and used marker of autophagy is the protein called MAP1LC3A, or microtubule associated protein 1 light chain 3 alpha, or LC3. In fact, during this process, the full-length form of LC3 is cleaved to give the smaller LC3-II, that is then lipidated and associates with the forming autophagosome. Therefore, accumulation of LC3-II is used as an indicator of autophagy induction.

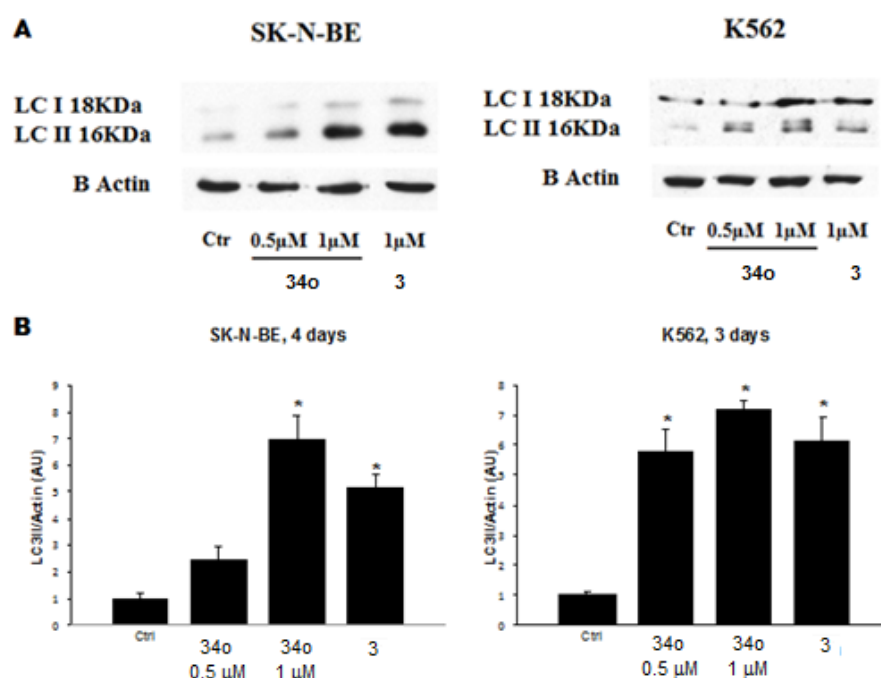


Figure 3.8. Effect of **34o** on autophagy induction. **(A)** Western blot analysis for LC3-II protein accumulation in SKN-BE (after 4 days treatment) and K562 (after 3 days treatment) by using **34o** at 0.5 and 1 μM in comparison with **3** at 1 μM. **(B)** Densitometric analysis. β-Actin was used for normalization.

Thus, we have investigated the capability of **34o** to induce autophagy (LC3-II protein accumulation) in SK-N-BE and K562 cells. Western blot analysis, after treatment of SK-N-BE (4 days) and K562 (3 days) with **34o**, showed a clear dose dependent (from 0.5 to 1 μM) induction of LC3-II protein (Figure 3.8 A), even stronger than the reference compound **3** (used at 1 μM) in both cell lines (Figure 3.8 A). Quantization of these data by densitometric analysis is shown in Figure 3.8 B.

3.2.7 Effects of **34o** on apoptosis induction in neuroblastoma SK-N-BE cell lines

(Group of Prof. Marco Tafani, Department of Experimental Medicine, Sapienza University of Rome, Italy)

To further investigate about the induction of apoptosis by **34o** in neuroblastoma SK-N-BE cells, the levels poly(ADP-ribose)polymerase (PARP) cleavage, a mark of late event in apoptosis, and caspase 3 induction were determined by western blot followed by densitometric analysis. (Figure 3.9 A) Tested in a dose range from 0.5 to 5 μ M for 4 days, **34o** induced detectable dose-dependent PARP-cleavage (determined by antibody anti-PARP) as well as caspase 3 induction, nevertheless it was less effective than **3** (able to give a similar result already at 1 μ M, Figure 3.9).

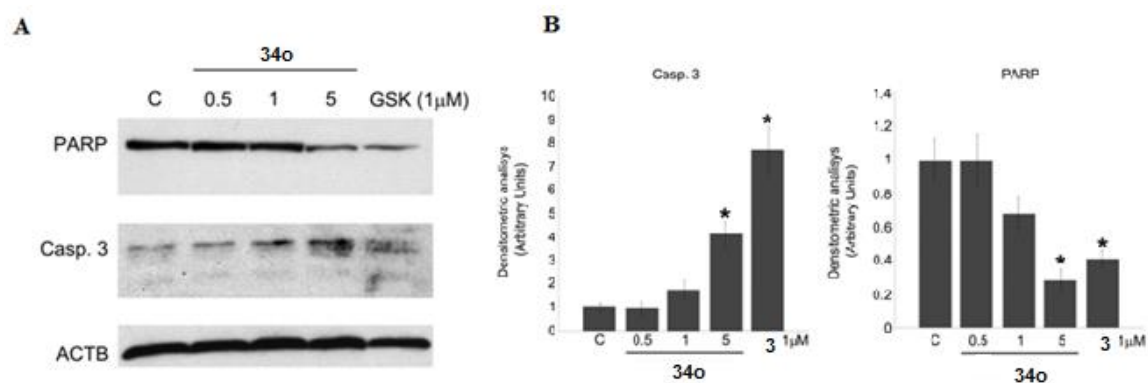


Figure 3.9. (A) Western blot and related densitometric analysis (B) for PARP cleavage and caspase 3 induction by **34o** at 0.5, 1 and 5 μ M for 4 days in SK-N-BE cells. **3** was used as reference compound (1 μ M), β -actin as loading control.

3.2.8 Effects of 34o in SHH medulloblastoma cancer stem cells

(Group of Prof. Elisabetta Ferretti, Department of Experimental Medicine, Sapienza University of Rome, Italy)

The group of Prof. Ferretti is investigating about medulloblastoma (MB) pediatric brain cancer, and medulloblastoma cell stemness in relation with EZH2 overexpression.^{270,271} In this context, they have found that both mouse and human MB-SLCs (medulloblastoma stem like cells) display high levels of EZH2 when grown in stem cell-medium (SM) and lower levels in cells grown in FBS-supplemented medium (DFM). A similar effect was observed also in MB DAOY cells. Stemness and differentiation markers were evaluated in all the mentioned cell lines, and the DMF cultured cells acquired a more “differentiated” phenotype, with a reduced expression of the stemness markers.²⁶⁴

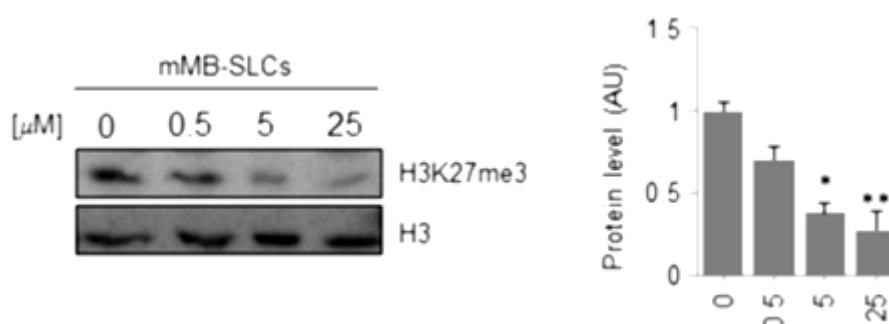


Figure 3.10. Representative Western Blot (up) and densitometric analysis (down) of H3K27me3 protein levels in mMB SLCs treated for 48 h with 0.5, 5 and 25 μ M of **34o**. * $p < 0.05$, ** $p < 0.01$.

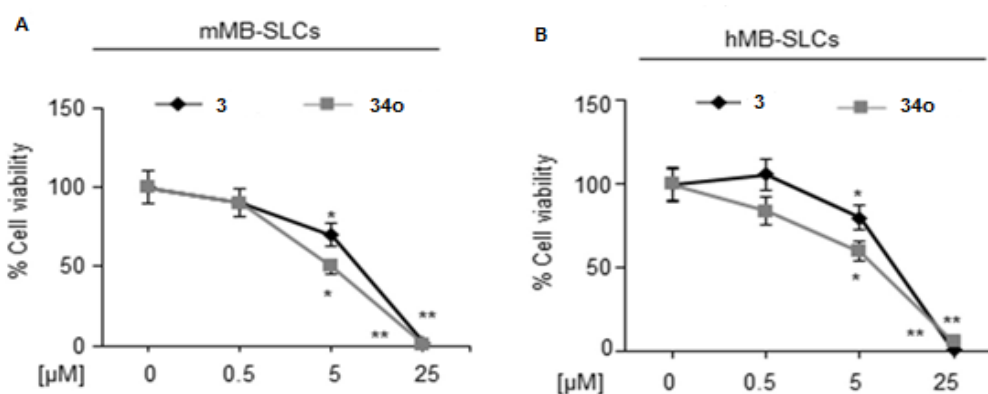


Figure 3.11. Evaluation of cell viability, measured with MTS assay, of mMB-SLCs (A) and hMB-SLCs (B) treated with increasing concentrations of **34o** and **3** at 48 h. p value versus untreated cells: * $p < 0.05$, ** $p < 0.01$.

Moreover, through lentiviral-mediated short hairpin EZH2 silencing technique, they proved that EZH2 plays a critical role in the maintenance of MB cells including stem-like cells (SLCs).²⁶⁴ They wanted to validate these effects also after EZH2 pharmacological inhibition, and they used compound **34o** as a pharmacological tool to validate these results. First of all, the ability of **34o** (at 0.5, 5, and 25 μ M) to inhibit the EZH2 enzymatic activity was validated in an *in vitro* cell-

based assay. The lowest dose that significantly decreased H3K27me3 level in MB-SLCs was 5 μ M (Figure 3.10).

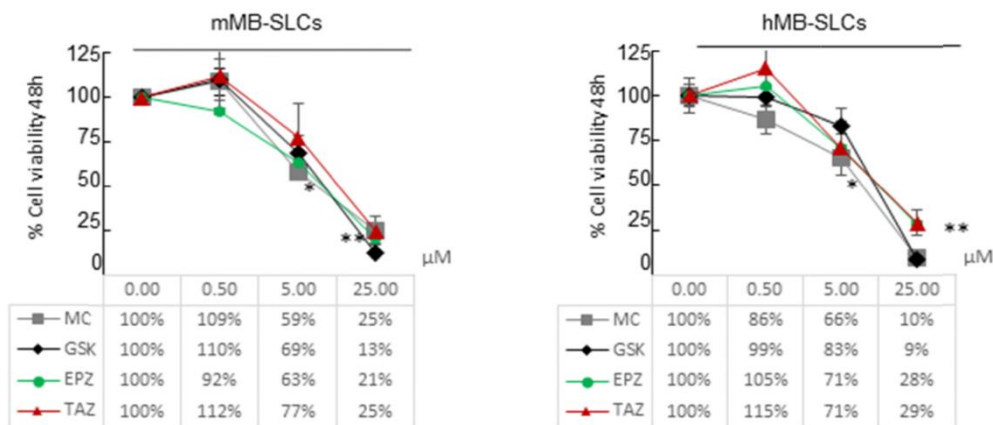


Figure 3.12. Evaluation of cell viability, measured with MTS assay, of mMB-SLCs and hMB-SLCs treated for 48 h with 0.5, 5, 25 μ M of **34o** (MC, gray), **3** (GSK, black), **2** (EPZ, green) and **7** (TAZ, red). *p<0.05, **p<0.01.

The effects of **34o** on murine and human MB-SLCs were evaluated in dose- and time-dependent experiments, using **3** (GSK126, Figure 1.5) as a reference drug. In both cell lines, we were able to define the lowest effective dose of **34o** at 5 μ M, and the minimum effective time as 48 h (Figure 3.11). The dose selection was further confirmed by cell viability experiments on MB-SLCs in comparison with known EZH2is, including EPZ5687 (**2**, Figure 1.5), and tazemetostat (**7**, Figure 1.5) (Figure 3.12).

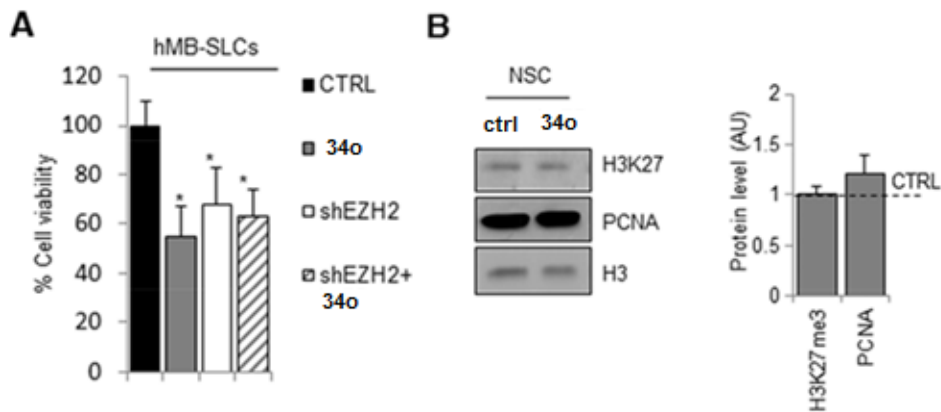


Figure 3.13. (A) Evaluation of cell viability, measured with MTS assay, of hMB-SLCs treated for 48 h with 5 μ M of **34o** and shEZH2 alone or in combination. Bars represent mean \pm S.D. *p<0.05. **(B)** Western Blot (left) and densitometric analysis (right) of H3K27me3 and PCNA, in Neural Stem Cells (NSC) treated for 48 h with 5 μ M **34o**. H3: loading control. *p<0.05.

Interestingly, the combination treatment of hMB-SLCs with **34o** (5 μ M) and shEZH2 did not display any additive effect on cell viability respect to the shEZH2 treatment alone, thus assessing the target specificity of our compound (Figure 3.13 A). In order to exclude any nonspecific toxic effect by **34o**, it was tested on neural stem cells (NSC), used as a model of non-transformed cells.

²⁷² In NSCs, compound **34o** had no significant effect on H3K27me3 and PCNA protein levels (Figure 3.13 B).

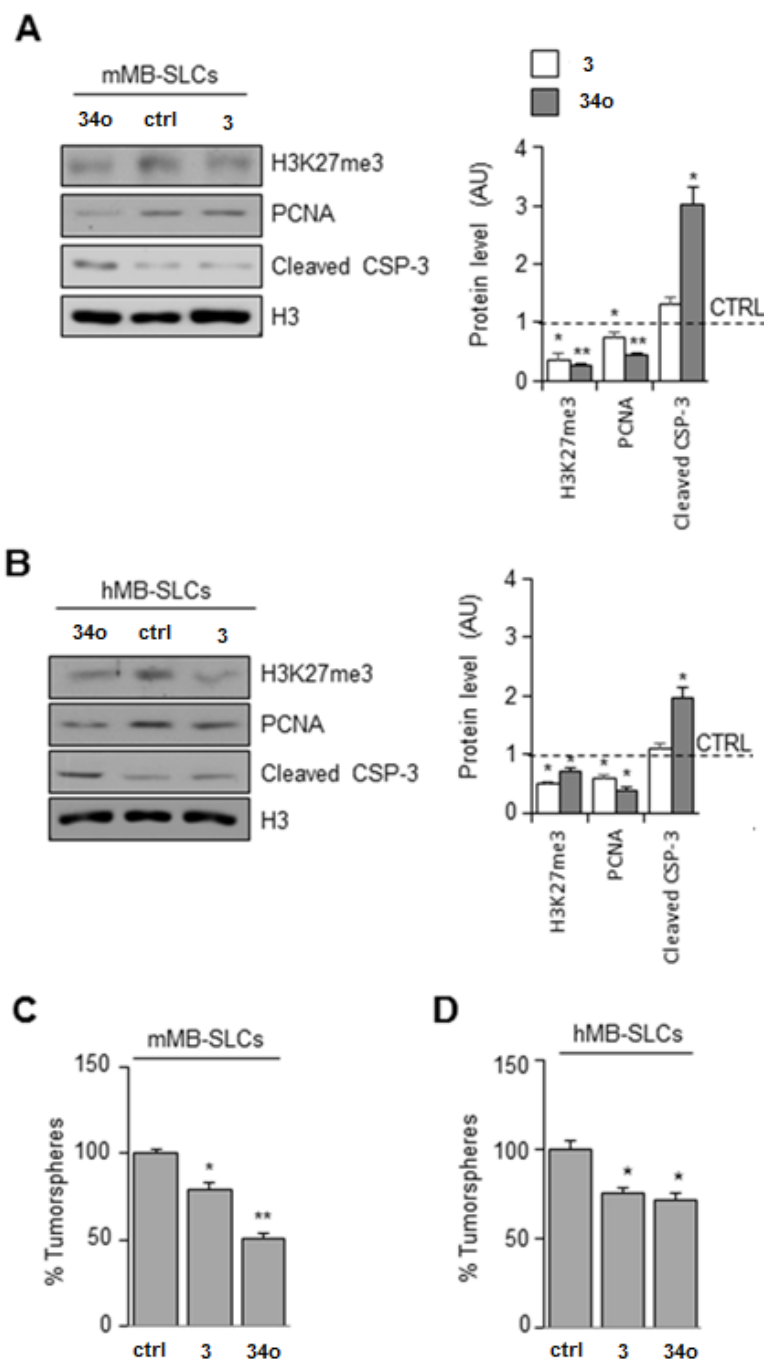


Figure 3.14. Biological effects of EZH2 inhibition in SHH MB-SLCs. **(A-B)** mMB-SLCs and hMB-SLCs were treated for 48 h with 5 μ M of **34o** or **3**. Representative images of Western Blot (left) and densitometric analysis (right) of H3K27me3, PCNA, and cleaved caspase 3 (cleaved CSP-3). H3: loading control. Dashed bars represent DMSO-treated cells (CTRL). * $p < 0.05$, ** $p < 0.01$. **(C-D)** Self-renewal measured by clonogenic assay. * $p < 0.05$, ** $p < 0.01$.

The effects of **34o** treatment in mMB-SLCs and hMB-SLCs, and in DAOY and DAOY-SLCs were evaluated more in depth. In mMB-SLCs and hMB-SLCs both **34o** and **3** significantly

reduced H3K27me3 and PCNA protein levels. In these cell lines, compound **34o** induced apoptosis (caspase 3 cleavage) (Figure 3.14 A and B), and significantly reduced mMB-SLC and hMB-SLC self-renewal, measured as clonogenic potential (stemness impairment) (Figure 3.14 C and D). In DAOY cells, H3K27me3 and PCNA levels resulted impaired only by **34o**, while in DAOY-SLCs, both drugs down affected H3K27me3 and PCNA levels (Figure 3.15 A). Such effects were confirmed by cell viability assays: **34o** impaired cell viability in both cell systems after 48 h, while **3** was able to significantly impair only DAOY-SLCs viability after 72 h of treatment (Figure 3.15 B). Additionally, **34o** induced cell death in DAOY-SLCs (Figure 3.15 C). In this way we demonstrated that EZH2 pharmacological inhibition in medulloblastoma can impair cell proliferation and stemness, and induce apoptosis.

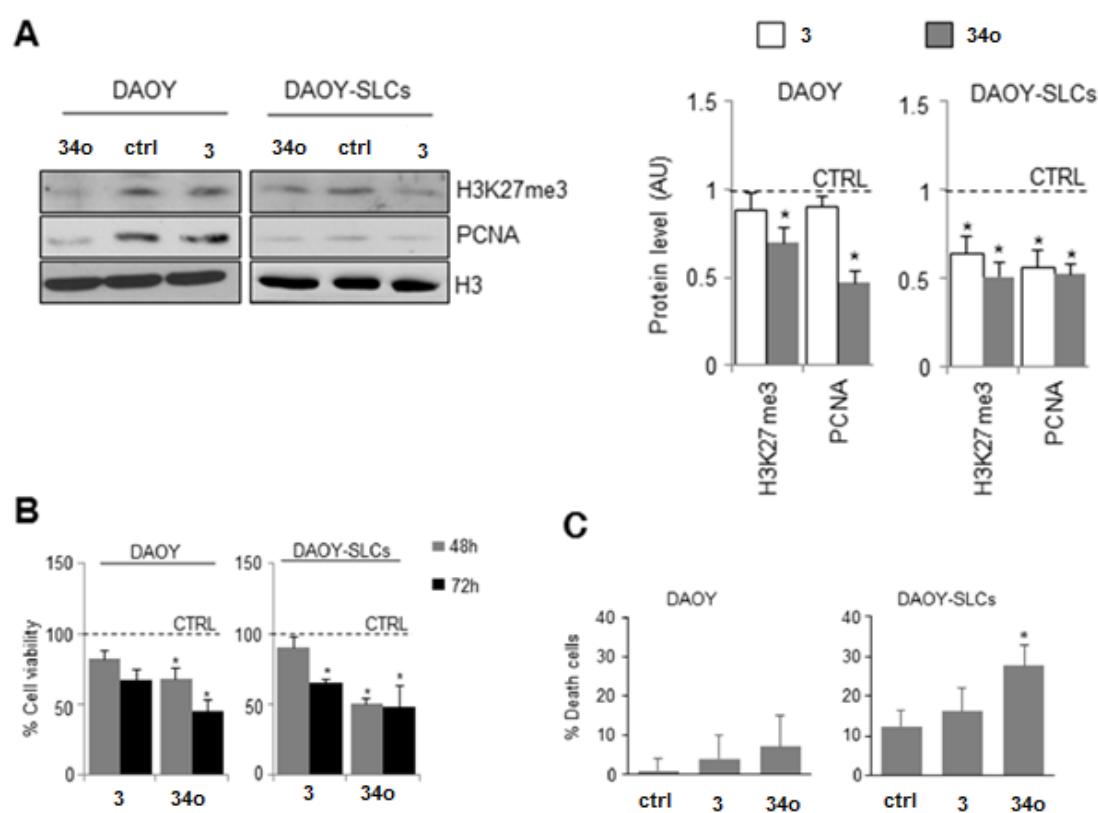


Figure 3.15. Biological effects of EZH2 inhibition in DAOY cells and DAOY-SLCs. **(A)** DAOY cells and DAOY-SLCs were treated for 48 h with 5 μ M of **34o** or **3**. Representative images of Western Blot (left) and densitometric analysis (right) of H3K27me3 and PCNA. H3: loading control. Dashed bars represent DMSO-treated cells (CTRL). * $p < 0.05$. **(B)** Evaluation of cell viability, measured with MTS assay, of DAOY and DAOY-SLCs treated for 48 h and 72 h with 5 μ M of **34o** or **3**. * $p < 0.05$. **(C)** Percentage of cell death assessed in DAOY and in DAOY-SLCs treated with both compounds for 72 h. Bars represent the mean of at least three independent experiments performed in triplicate mean \pm S.D. * $p < 0.05$.

3.2.9 Effects of **34o** in an *in vivo* mouse model of medulloblastoma

(Group of Prof. Elisabetta Ferretti, Department of Experimental Medicine, Sapienza University of Rome, Italy)

Before going on with further experiments, considering the existing reports regarding limitation to *in vivo* use of EZH2i due to poor bio-distribution and scarce BBB penetration,^{273,274} in collaboration with the group of Prof. Sabrina Castellano, we tested both **34o** and **3** in the parallel artificial membrane permeability assay for the BBB (PAMPA-BBB). Propranolol and furosemide were used as positive and negative controls, respectively. In this assay, **34o** displayed a closer capability to permeate the lipid membrane to propranolol than **3**. (Table 5) Thus, **34o** was judged eligible for *in vivo* experiments on medulloblastoma mouse model.

Table 5. Log Pe values of tested compounds in the PAMPA-BBB.

Compound	Log P _e	Δ (respect to propranolol)
3	-5.41 ± 0.04	-0.20
34o	-5.33 ± 0.01	-0.12
Propranolol (positive control)	-5.21 ± 0.06	
Furosemide (negative control)	Under detection limit	

Twice/week intra-peritoneal injection of **34o** at 20 μM/ Kg in 6-day old mice led to a significant reduction of H3K27me3 levels in cerebella and in brains (Figure 3.16 A), further confirming that **34o** crosses the BBB. Next, in nude mice have been generated xenograft DAOY-SLCs orthotopic tumors (XT-MB), that grew as tumor masses with the characteristics of MBs. Mice treatment with **34o** significantly impaired XT-MB growth (Figure 3.16 B). A dose dependent reduction of H3K27me3 in treated mice was revealed by western blot analysis of tumor xenografts (Figure 3.16 C and 3.17 A). Interestingly, tumors from treated mice also showed significantly lower levels of NANOG protein (Figure 3.16 C), and a significant reduction of proliferating Ki67-positive cells as well (Figure 3.16 D). Finally, an increased level of cleaved caspase 3 in treated mice suggested apoptosis induction. (Figure 3.17 B). Taken together, these data show that **34o** is effective in hampering MB-SLCs growth *in vivo*.

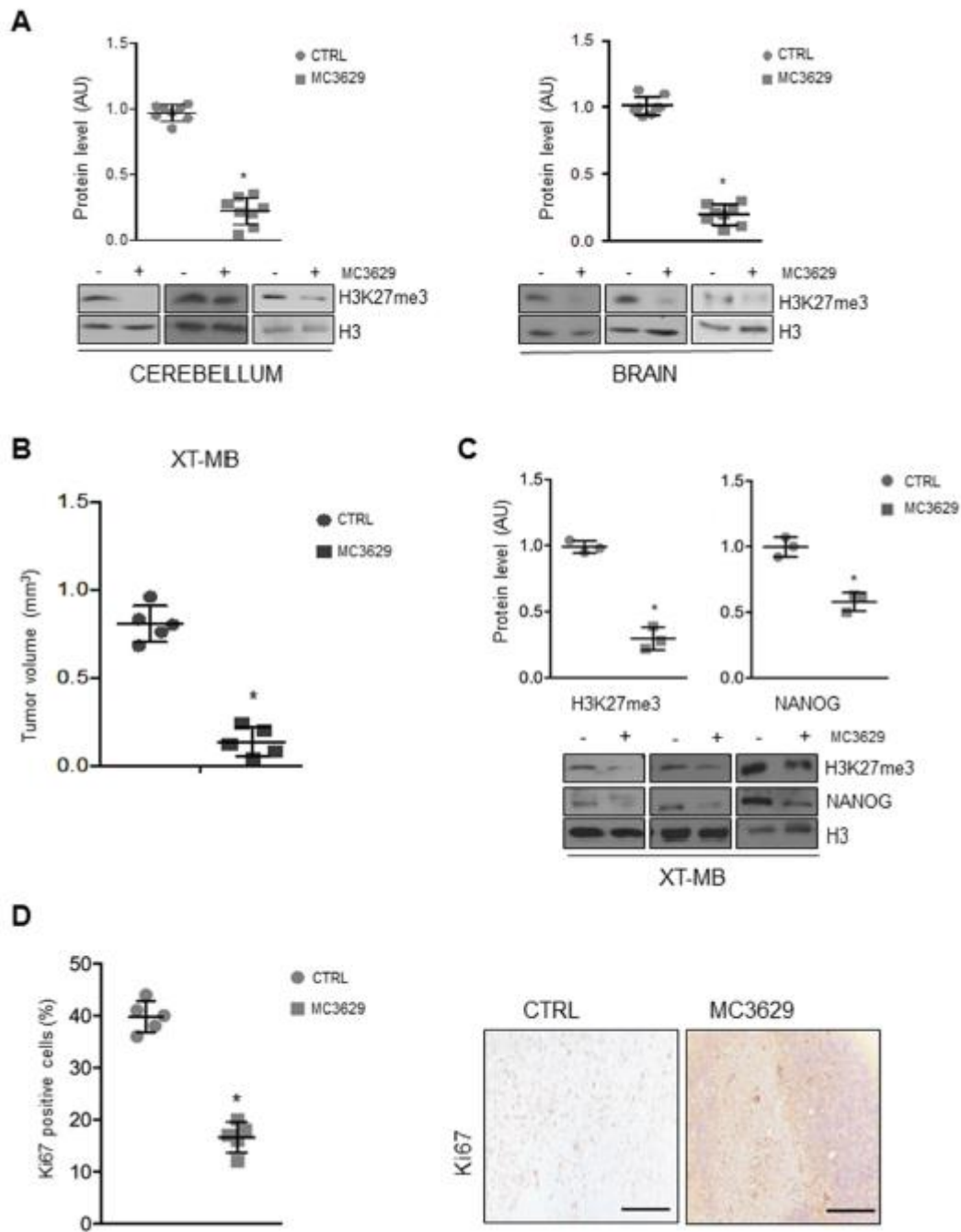


Figure 3.16: Biological effects of **340** (MC3629) *in vivo*. **(A)** Representative Western Blots show H3K27me3 levels in cerebellum and brain from wild type mice treated with **340** or vehicle (CTRL). Dot plots represent densitometric analysis of all samples. * $p < 0.05$. **(B-D)** Xenograft tumors (XT-MB) were generated in mice, after 10 days **340** was administered twice a week for 3 weeks; control mice were treated with vehicle (CTRL). **(B)** Xenograft volume (mm³) evaluated at the maximum diameter; dot plot represents mean \pm S.D. * $p < 0.05$. **(C)** Representative images of Western Blot and densitometric analysis of H3K27me3 and NANOG. H3: loading control * $p < 0.05$. **(D)** Xenograft sections were immunostained for the proliferation marker Ki67: on the left, dot plot shows Ki67 levels of proliferating cells; on the right, representative images of the staining. * $p < 0.05$.

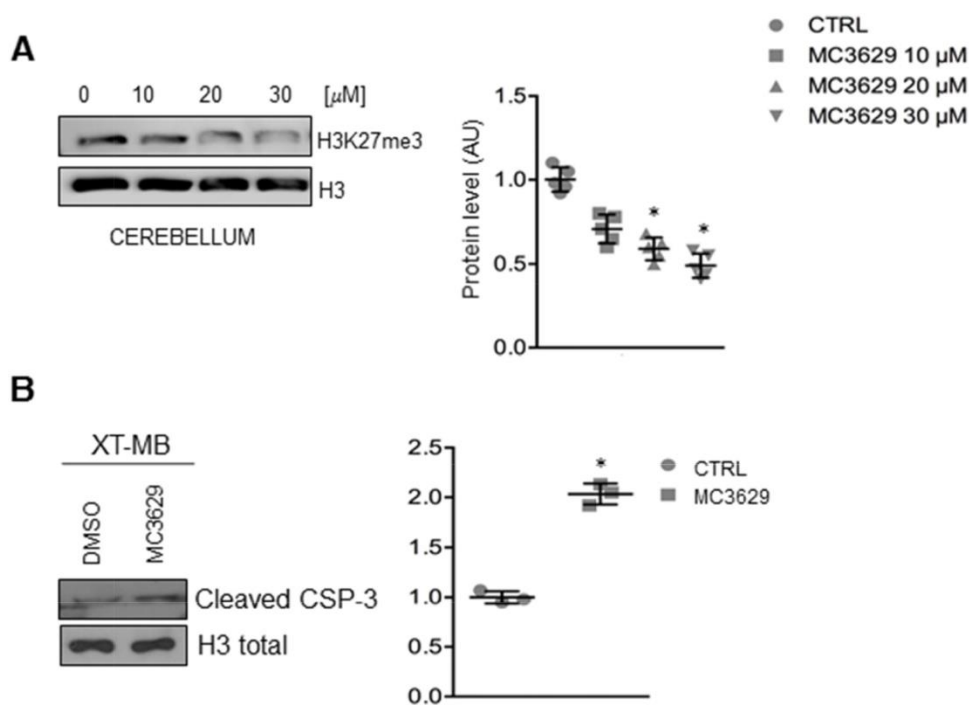


Figure 3.17: (A) Representative western Blot (left) and densitometric analysis (right) of H3K27me3 for dose finding in *in vivo* experiments. H3: loading control, * $p < 0.05$. (B) Representative Western Blot (left) and densitometric analysis (right) of cleaved-CSP-3 for evaluation of apoptosis in XT-MB treated with **34o** (MC3629). H3: loading control. * $p < 0.05$.

3.3 Conclusions

This research project yielded the design, synthesis and biological validation of a class of novel pyrazole-based EZH2 inhibitors **34a-r**. Our molecular design was based on the replacement of the indole/indazole bicyclic ring, contained in known EZH2i (**2**, **4**, Figure 5), with the simpler pyrazole group, and we found the insertion of a phenyl or benzyl portion at the N(1) and the methyl group at the C(5) position of the pyrazole ring as the best substitutions to afford the highest inhibition potency *in vitro*. The most potent compound in biochemical assays, **34o** (IC_{50} values = 5.3-15.4 μM), was tested in cell-based assays. Compound **34o** displayed arrest of cell proliferation in SK-N-BE neuroblastoma, MDA-MB231 breast cancer, and K562 leukemia cells during 4/5 days of treatment. **3** (GSK126), used as the reference drug, was more potent against K562 but less efficient against solid tumor cell lines. Western blot analysis performed in K562 and SK-N-BE cells treated with **34o** revealed a reduction of the levels of H3K27me3, and induction of autophagy (increase of the LC3 II levels) stronger than that obtained after **3** treatment. When tested in SK-N-BE cells for induction of apoptosis, **34o** determined PARP cleavage and induction of caspase 3, in this case lower than those obtained with **3**, suggesting that in this cell line autophagy rather than apoptosis induction may be involved in the arrest of proliferation.

The group of Prof. Ferretti proved that the genetic silencing of EZH2 in MB-SLCs, derived from patients affected by SHH MB or from SHH MB murine model, led to reduction of H3K27me3 levels, reduction of proliferation, and self-renewal impairment. To evaluate if pharmacological EZH2 inhibition could have the same effects, **34o** has been tested in the same cellular models. This compound at 5 μ M displayed significant biological activity, impairing cell proliferation and self-renewal, and inducing apoptosis. When co-administered with shEZH2 to hMB-SLCs, **34o** did not show any additive effect on cell viability, thus confirming its selective action on the methyltransferase target. We then assessed the capability of **34o** to cross the BBB *in vitro*, in a PAMPA-BBB assay. Moreover, we observed the ability of **34o** to reduce H3K27me3 levels in brain and cerebellum *in vivo*. Finally, we treated MB xenografted mice with **34o**. *In vivo* experiments showed a significant decrease of tumor volume, a reduction of stemness and cell proliferation, and induction of apoptosis in treated mice. Thank to this study we validated EZH2 as an attractive target for SHH MB cancer and cancer stem cell impairment. We also demonstrated that EZH2 pharmacological inhibition by **34o** is effective in MB cells and in MB xenografted mouse models.

3.4 Experimental Section

3.4.1 Chemistry

Melting points were determined on a Buchi 530 melting point apparatus and are uncorrected. ^1H NMR and ^{13}C NMR spectra were recorded at 400 and 100 MHz, respectively, on a Bruker AC 400 spectrometer; chemical shifts are reported in δ (ppm) units relative to the internal reference tetramethylsilane (Me_4Si). EIMS spectra were recorded with a Fisons Trio 1000 spectrometer; only molecular ions (M^+) and base peaks are given. All compounds were routinely checked by TLC and ^1H NMR. TLC was performed on aluminum-backed silica gel plates (Merck DC, Alufolien Kieselgel 60 F254) with spots visualized by UV light. All solvents were reagent grade and, when necessary, were purified and dried by standard methods. Concentration of solutions after reactions and extractions involved the use of a rotary evaporator operating at reduced pressure of ca. 20 Torr. Organic solutions were dried over anhydrous sodium sulfate. Elemental analysis has been used to determine purity of the described compounds, that is, $> 95\%$. Analytical results are within $\pm 0.40\%$ of the theoretical values. All chemicals were purchased from Sigma-Aldrich, Milan (Italy), or from Alfa Aesar, Karlsruhe (Germany), and were of the highest purity.

General procedure for the synthesis of pyrazole esters 35a-d and 39e-q. Example: Ethyl 1-isopropyl-5-phenyl-1H-pyrazole-4-carboxylate (39e)

To a solution of ethyl -2-benzoyl-3-(dimethylamino)acrylate (**38e**) (1.011 mmol, 1.0 eq, 0.250 g) in ethanol (5 mL), isopropylhydrazine hydrochloride (1.011 mmol, 1.0 eq, 0.112 g) and triethylamine (2.022 mmol, 2.0 eq, 0.28 mL) were added and the reaction mixture was refluxed for 2 h. After the completion of the reaction, the solvent was evaporated (by 90 %) and H_2O (20 mL) was added to the residue. The aqueous phase was extracted with CH_2Cl_2 (3×50 mL), the combined organic layers were washed with a saturated solution of NaHCO_3 (2×15 mL), and a saturated solution of NaCl (2×10 mL), dried over Na_2SO_4 and concentrated *in vacuo*, to obtain ethyl 1-isopropyl-5-phenyl-1H-pyrazole-4-carboxylate as a pure colourless solid, which was used in the following step without further purification. Y = 66 %. ^1H NMR (CDCl_3 , 400 MHz, δ , ppm): δ_{H} 1.15 (3H, t, $-\text{COOCH}_2\text{CH}_3$), 1.45 (6H, d, $-\text{CH}(\text{CH}_3)_2$), 4.14 (2H, q, $-\text{COOCH}_2\text{CH}_3$), 4.34 (1H, m, $-\text{CH}(\text{CH}_3)_2$), 7.36 (2H, m, aromatic protons), 7.50 (3H, m, aromatic protons), 8.05 (1H, s, pyrazole proton) ppm; ^{13}C NMR (CDCl_3 , 100 MHz, δ , ppm): δ_{C} 14.26, 21.74 (2C), 53.12, 61.21, 115.65, 128.52 (2C), 128.61, 128.91 (2C), 130.80, 139.82, 152.04, 163.24 ppm; MS (EI) m/z $[\text{M}]^+$ calculated: 258.1368, found: 258.1373.

General procedure for the synthesis of 5-pyrrolyl-pyrazole esters 36a-d. Example: synthesis of ethyl 1-cyclopentyl-5-(1H-pyrrol-1-yl)-1H-pyrazole-4-carboxylate (36b)

To a solution of ethyl 1-cyclopentyl-5-amino-1H-pyrazole-4-carboxylate (**35b**) (4.478 mmol, 1.0 eq, 1 g) in acetic acid (6 mL), 2,5-dimethoxytetrahydrofuran (6.718 mmol, 1.5 eq, 0.870 mL) was

added and the reaction mixture was refluxed for 1 h. Then 5 mL of toluene were added and the yellow solution was concentrated under reduced pressure, the residue was purified by silica gel chromatography eluting with *n*-hexane: ethyl acetate 8:1, to furnish ethyl 1-cyclopentyl-5-(1H-pyrrol-1-yl)-1H-pyrazole-4-carboxylate (**10b**) as a light-yellow oil. Y= 88 %. ¹H NMR (CDCl₃, 400 MHz, δ , ppm): δ_{H} 1.20 (3H, t, -COOCH₂CH₃), 1.64 (2H, m, cyclopentane protons), 1.93-2.03 (4H, m, cyclopentane protons), 2.07 (2H, m, cyclopentane protons), 4.18 (2H, q, -COOCH₂CH₃), 4.33 (1H, m, cyclopentane proton), 6.40 (2H, d, pyrrole protons), 6.78 (2H, m, pyrrole protons), 7.99 (1H, s, pyrazole proton) ppm; ¹³C NMR (CDCl₃, 100 MHz, δ , ppm): δ_{C} 14.26, 24.58 (2C), 33.37 (2C), 59.74, 62.16, 101.03, 112.92 (2C), 121.59 (2C), 139.21, 142.64, 163.88 ppm; MS (EI) *m/z* [*M*]⁺ calculated: 273.1477, found: 273.1479.

General procedure for the synthesis of pyrazole acids 37a-q. Example: synthesis of 1-phenyl-5-styryl-1H-pyrazole-4-carboxylic acid (37k)

Ethyl 1-phenyl-5-styryl-1H-pyrazole-4-carboxylate (**39k**) (1.818 mmol, 1.0 eq, 0.579 g) was suspended in ethanol (6 mL), then a 2 N aqueous solution of KOH (7.280 mmol, 4.0 eq, 3.64 mL) was added, and the resulting mixture was left stirring at room temperature. After 16 h the reaction was complete, the ethanol was removed *in vacuo*. The residue was diluted with H₂O and cooled to 0 °C. A 2 N aqueous solution of HCl was added dropwise till pH= 2. The obtained precipitate was filtered, rinsed with distilled water (3 × 3 mL) and dried in oven at 60 °C to give **37k** as a colourless solid. Yield 93 %. ¹H NMR (DMSO-*d*₆, 400 MHz, δ , ppm): δ_{H} 7.01 (d, 1H, -CH=CHPh), 7.24 (d, 1H, -CH=CHPh), 7.35 (m, 5H, aromatic protons), 7.57 (m, 5H, aromatic protons), 8.09 (s, 1H, pyrazole proton), 12.63 (bs, 1H, -COOH) ppm; ¹³C NMR (DMSO-*d*₆, 100 MHz, δ , ppm): δ_{C} 24.6 (2C), 33.4 (2C), 62.2, 99.5, 112.9 (2C), 121.6 (2C), 138.8, 142.0, 166.1; MS (EI) *m/z* [*M*]⁺ calculated: 290.1055, found: 290.1058.

General procedure for the synthesis of amides 34a-r. Example: synthesis of N-((4,6-dimethyl-2-oxo-1,2-dihydropyridin-3-yl)methyl)-5-methyl-1-phenyl-1H-pyrazole-4-carboxamide (34o)

To a solution of 5-methyl-1-phenyl-1H-pyrazole-4-carboxylic acid (**15o**) (0.742 mmol, 1.0 eq, 0.150 g) in anhydrous *N,N*-dimethylformamide (5 mL), TBTU (*N,N,N',N'*-Tetramethyl-O-(benzotriazol-1-yl)uronium tetrafluoroborate) (0.890 mmol, 1.2 eq, 0.463 g) and triethylamine (5.194 mmol, 7.0 eq, 0.720 mL) were added under N₂ atmosphere and the solution was left under stirring at room temperature for 25 minutes. After this time, 3-(aminomethyl)-4,6-dimethylpyridin-2(1*H*)-one hydrochloride (**33**) (0.890 mmol, 1.2 eq, 0.167 g) was added and the mixture was stirred at room temperature overnight. The reaction was quenched by a saturated solution of NaCl (20 mL) and the precipitate was filtered, rinsed with H₂O (3 × 3 mL) and *n*-hexane (3 × 3 mL). The resulting light-yellow solid was purified by recrystallization (acetonitrile: methanol 1:1) to provide pure **34o** as a colorless solid. Y= 60 %; m.p. 225-227 °C; ¹H NMR

(DMSO-*d*₆, 400 MHz, δ , ppm): δ_{H} 2.13 (s, 3H, 4,6-dimethylpyridone -CH₃), 2.19 (s, 3H, 4,6-dimethylpyridone -CH₃), 2.51 (s, 3H, 5-methylpyrazole -CH₃), 4.27 (d, 2H, -CH₂NH, *J* = 4.8 Hz), 5.87 (s, 1H, -CH pyridone proton), 7.53 (m, 5H, aromatic protons), 7.96 (t, 1H, -CH₂NH, *J* = 4.8 Hz), 8.13 (s, 1H, pyrazole proton), 11.48 (br s, 1H, pyridone NH) ppm; ¹³C NMR (DMSO-*d*₆, 100 MHz, δ , ppm): δ_{C} 11.1, 18.5, 19.1, 32.8, 111.1, 116.0, 123.3 (2C), 126.9, 127.2, 129.1 (2C), 139.2, 142.6, 146.6, 151.5, 158.0, 163.6, 165.9 ppm; MS (EI) *m/z* [M]⁺ calculated: 336.1586, found: 336.1590.^{275,276}

Chemical and Physical Data, ¹H NMR, ¹³C NMR, and MS (EI) Data for Compounds 34a-r.
N-((4,6-dimethyl-2-oxo-1,2-dihydropyridin-3-yl)methyl)-1-isopropyl-5-(1H-pyrrol-1-yl)-1H-pyrazole-4-carboxamide (34a)

¹H NMR (DMSO-*d*₆, 400 MHz, δ , ppm): δ_{H} 1.32 (d, 6H, (CH₃)₂CH-, *J* = 6.4 Hz), 2.09 (s, 3H, 4,6 dimethylpyridone -CH₃), 2.10 (s, 3H, 4,6 dimethylpyridone -CH₃), 3.88 (m, 1H, (CH₃)₂CH-), 4.13 (d, 2H, -CH₂NH-, *J* = 3.6 Hz), 5.82 (s, 1H, -CH- pyridone proton), 6.29 (dd, 2H, pyrrole protons, *J* = 5.6 Hz), 6.95 (dd, 2H, pyrrole protons, *J* = 2.0 Hz), 7.14 (d, 1H, -CH₂NH-, *J* = 3.6 Hz), 8.00 (s, 1H, pyrazole proton), 11.46 (s, 1H, pyridone -NH) ppm; ¹³C NMR (DMSO-*d*₆, 100 MHz, δ , ppm): δ_{C} 18.5, 19.1, 21.7 (2C), 32.8, 51.4, 100.2, 111.1, 112.9 (2C), 116.0, 121.6 (2C), 138.1, 147.3, 151.6, 158.0, 163.6, 165.1 ppm; Y = 66 %; m.p. 229-231 °C (methanol); MS (EI) *m/z* [M]⁺ calculated: 353.1852, found: 353.1845.

1-cyclopentyl-N-((4,6-dimethyl-2-oxo-1,2-dihydropyridin-3-yl)methyl)-5-(1H-pyrrol-1-yl)-1H-pyrazole-4-carboxamide (34b)

¹H NMR (DMSO-*d*₆, 400 MHz, δ , ppm): δ_{H} 1.53 (m, 2H, cyclopentyl protons), 1.78 (m, 2H, cyclopentyl protons), 1.87 (m, 4H, cyclopentyl protons), 2.09 (s, 3H, 4,6 dimethylpyridone -CH₃), 2.10 (s, 3H, 4,6 dimethylpyridone -CH₃), 4.07 (m, 1H, cyclopentyl (CH₂)₂CH-), 4.12 (d, 2H, -CH₂NH-, *J* = 4.8 Hz), 5.82 (s, 1H, -CH- pyridone proton), 6.29 (d, 2H, pyrrole protons, *J* = 5.4 Hz), 6.94 (d, 2H, pyrrole protons, *J* = 2.0 Hz), 7.15 (t, 1H, -CH₂NH-, *J* = 3.6 Hz), 7.98 (s, 1H, pyrazole proton), 11.46 (s, 1H, pyridone -NH) ppm; ¹³C NMR (DMSO-*d*₆, 100 MHz, δ , ppm): δ_{C} 18.5, 19.1, 24.6 (2C), 32.8, 33.4 (2C), 62.2, 99.8, 111.1, 112.9 (2C), 116.0, 121.6 (2C), 139.1, 146.4, 151.6, 158.0, 163.6, 165.1 ppm; Y = 61 %; m.p. 208-210 °C (acetonitrile/ methanol); MS (EI) *m/z* [M]⁺ calculated: 379.2008, found: 379.2011.

N-((4,6-dimethyl-2-oxo-1,2-dihydropyridin-3-yl)methyl)-1-phenyl-5-(1H-pyrrol-1-yl)-1H-pyrazole-4-carboxamide (34c)

¹H NMR (DMSO-*d*₆, 400 MHz, δ , ppm): δ_{H} 2.11 (s, 3H, 4,6 dimethylpyridone -CH₃), 2.50 (s, 3H, 4,6 dimethylpyridone -CH₃), 4.17 (d, 2H, -CH₂NH-, *J* = 4.8 Hz), 5.84 (s, 1H, -CH- pyridone proton), 6.17 (d, 2H, aromatic protons, *J* = 1.6 Hz), 6.85 (d, 2H, aromatic protons, *J* = 1.6 Hz), 7.11 (d, 2H, aromatic protons, *J* = 8.0 Hz), 7.36 (d, 2H, aromatic protons, *J* = 6.4 Hz), 7.49 (t, 1H,

-CH₂NH-, $J = 4.0$ Hz), 8.24 (s, 1H, pyrazole proton), 11.48 (s, 1H, pyridone -NH) ppm; ¹³C NMR (DMSO-*d*₆, 100 MHz, δ , ppm): δ_c 18.5, 19.1, 32.8, 101.3, 111.1, 112.9 (2C), 116.0, 121.6 (2C), 125.2 (2C), 127.2, 129.5 (2C), 138.5, 139.6, 141.7, 151.6, 158.0, 163.6, 165.1 ppm; Y= 68 %; m.p. 232-235 °C (methanol); MS (EI) m/z [M]⁺ calculated: 387.1695, found: 387.1699.

1-benzyl-N-((4,6-dimethyl-2-oxo-1,2-dihydropyridin-3-yl)methyl)-5-(1H-pyrrol-1-yl)-1H-pyrazole-4-carboxamide (34d)

¹H NMR (DMSO-*d*₆, 400 MHz, δ , ppm): δ_H 2.09 (s, 3H, 4,6 dimethylpyridone -CH₃), 2.10 (s, 3H, 4,6 dimethylpyridone -CH₃), 4.13 (d, 2H, -CH₂NH-, $J = 4.8$ Hz), 5.01 (s, 2H, -NCH₂Ph), 5.82 (s, 1H, -CH- pyridone proton), 6.26 (s, 2H, pyrrole protons), 6.87 (s, 2H, pyrrole protons, $J = 1.6$ Hz), 6.96 (d, 2H, aromatic protons, $J = 6.8$ Hz), 7.27 (m, 3H, aromatic protons), 7.36 (t, 1H, -CH₂NH-, $J = 4.0$ Hz), 8.02 (s, 1H, pyrazole proton), 11.46 (s, 1H, pyridone -NH) ppm; ¹³C NMR (DMSO-*d*₆, 100 MHz, δ , ppm): δ_c 18.5, 19.1, 32.8, 51.1, 100.5, 111.1, 112.9 (2C), 116.0, 121.6 (2C), 127.6, 128.4 (2C), 129.0 (2C), 136.3, 139.6, 141.5, 151.6, 158.0, 163.6, 165.1 ppm; Y= 65 %; m.p. 187-189 °C (acetonitrile); MS (EI) m/z [M]⁺ calculated: 401.1852, found: 401.1845.

N-((4,6-dimethyl-2-oxo-1,2-dihydropyridin-3-yl)methyl)-1-isopropyl-5-phenyl-1H-pyrazole-4-carboxamide (34e)

¹H NMR (DMSO-*d*₆, 400 MHz, δ , ppm): δ_H 1.31 (d, 6H, (CH₃)₂CH-, $J = 5.6$ Hz), 2.07 (s, 3H, 4,6 dimethylpyridone -CH₃), 2.10 (s, 3H, 4,6 dimethylpyridone -CH₃), 4.15 (d, 2H, -CH₂NH-, $J = 4.8$ Hz), 4.17 (m, 1H, (CH₃)₂CH-), 5.82 (s, 1H, -CH- pyridone proton), 7.28 (t, 1H, -CH₂NH-, $J = 4.0$ Hz), 7.35 (m, 2H, aromatic protons), 7.48 (m, 3H, aromatic protons), 7.96 (s, 1H, pyrazole proton), 11.44 (s, 1H, pyridone -NH) ppm; ¹³C NMR (DMSO-*d*₆, 100 MHz, δ , ppm): δ_c 18.5, 19.1, 21.7 (2C), 32.8, 53.1, 111.1, 116.0, 124.5, 128.5 (2C), 128.6, 128.9 (2C), 130.8, 141.5, 151.6, 153.9, 158.0, 163.6, 165.3 ppm; Y= 67 %; m.p. 211-213 °C (acetonitrile/ methanol); MS (EI) m/z [M]⁺ calculated: 364.1899, found: 364.1901.

1-cyclopentyl-N-((4,6-dimethyl-2-oxo-1,2-dihydropyridin-3-yl)methyl)-5-phenyl-1H-pyrazole-4-carboxamide (34f)

¹H NMR (DMSO-*d*₆, 400 MHz, δ , ppm): δ_H 1.51 (m, 2H, cyclopentyl protons), 1.80 (m, 2H, cyclopentyl protons), 1.89 (m, 4H, cyclopentyl protons), 2.07 (s, 3H, 4,6 dimethylpyridone -CH₃), 2.10 (s, 3H, 4,6 dimethylpyridone -CH₃), 4.10 (d, 2H, -CH₂NH-, $J = 5.2$ Hz), 4.33 (m, 1H, cyclopentyl proton -N-CH-), 5.82 (s, 1H, -CH- pyridone proton), 7.30 (t, 1H, -CH₂NH-, $J = 4.8$ Hz), 7.34 (m, 2H, aromatic protons), 7.48 (m, 3H, aromatic protons), 7.95 (s, 1H, pyrazole proton), 11.44 (s, 1H, pyridone -NH) ppm; ¹³C NMR (DMSO-*d*₆, 100 MHz, δ , ppm): δ_c 18.5, 19.1, 24.6 (2C), 32.8, 33.4 (2C), 64.1, 111.1, 116.0, 122.8, 128.5 (2C), 128.6, 128.9 (2C), 130.8, 142.0, 151.6, 154.1, 158.0, 163.6, 165.3 ppm; Y= 59 %; m.p. 213-215 °C (acetonitrile/ methanol); MS (EI) m/z [M]⁺ calculated: 390.2056, found: 390.2060.

N-((4,6-dimethyl-2-oxo-1,2-dihydropyridin-3-yl)methyl)-1,5-diphenyl-1H-pyrazole-4-carboxamide (34g)

¹H NMR (DMSO-*d*₆, 400 MHz, δ , ppm): δ_{H} 2.10 (s, 3H, 4,6 dimethylpyridone -CH₃), 2.11 (s, 3H, 4,6 dimethylpyridone -CH₃), 4.17 (d, 2H, -CH₂NH-, *J* = 5.2 Hz), 5.84 (s, 1H, -CH- pyridone proton), 7.17 (d, 2H, aromatic protons, *J* = 6.4 Hz), 7.24 (d, 2H, aromatic protons, *J* = 6.4 Hz), 7.32 (m, 6H, aromatic protons), 7.60 (t, 1H, -CH₂NH-, *J* = 4.8 Hz), 8.15 (s, 1H, pyrazole proton), 11.46 (s, 1H, pyridone -NH) ppm; ¹³C NMR (DMSO-*d*₆, 100 MHz, δ , ppm): δ_{C} 18.5, 19.1, 32.8, 111.1, 116.0, 124.1 (2C), 125.8, 127.1, 128.4 (2C), 128.6, 128.9 (2C), 129.1 (2C), 130.6, 139.6, 140.2, 146.0, 151.6, 158.0, 163.6, 165.3 ppm; Y = 57 %; m.p. 206-208 °C (acetonitrile/methanol); MS (EI) *m/z* [M]⁺ calculated: 398.1743, found: 398.1740.

1-benzyl-N-((4,6-dimethyl-2-oxo-1,2-dihydropyridin-3-yl)methyl)-5-phenyl-1H-pyrazole-4-carboxamide (34h)

¹H NMR (DMSO-*d*₆, 400 MHz, δ , ppm): δ 2.08 (s, 3H, 4,6 dimethylpyridone -CH₃), 2.10 (s, 3H, 4,6 dimethylpyridone -CH₃), 4.11 (d, 2H, -CH₂NH-, *J* = 4.0 Hz), 5.14 (s, 2H, -NCH₂Ph), 5.82 (s, 1H, -CH- pyridone proton), 6.90 (d, 2H, aromatic protons, *J* = 5.6 Hz), 7.27 (m, 5H, aromatic protons), 7.43 (m, 4H, aromatic protons and -CH₂NH-), 8.01 (s, 1H, pyrazole proton), 11.45 (s, 1H, pyridone -NH) ppm; ¹³C NMR (DMSO-*d*₆, 100 MHz, δ , ppm): δ 18.5, 19.1, 32.8, 52.9, 111.1, 116.0, 120.6, 127.6, 128.0 (2C), 128.4 (2C), 128.6 (3C), 128.9 (2C), 130.9, 136.0, 140.6, 142.5, 151.6, 158.0, 163.6, 165.3 ppm; Y = 62 %; m.p. 181-183 °C (acetonitrile); MS (EI) *m/z* [M]⁺ calculated: 412.1899, found: 412.1893.

(E)-N-((4,6-dimethyl-2-oxo-1,2-dihydropyridin-3-yl)methyl)-1-isopropyl-5-styryl-1H-pyrazole-4-carboxamide (34i)

¹H NMR (DMSO-*d*₆, 400 MHz, δ , ppm): δ_{H} 1.40 (d, 6H, (CH₃)₂CH-, *J* = 5.6 Hz), 2.10 (s, 3H, 4,6 dimethylpyridone -CH₃), 2.15 (s, 3H, 4,6 dimethylpyridone -CH₃), 4.24 (d, 2H, -CH₂NH-, *J* = 4.0 Hz), 4.82 (m, 1H, (CH₃)₂CH-), 5.84 (s, 1H, -CH- pyridone proton), 7.18 (d, 1H, vinyl proton, *J* = 16.8 Hz), 7.38 (m, 4H, aromatic protons and vinyl proton), 7.59 (m, 2H, aromatic protons), 7.83 (t, 1H, -CH₂NH-, *J* = 5.0 Hz), 7.87 (s, 1H, pyrazole proton), 11.46 (s, 1H, pyridone -NH) ppm; ¹³C NMR (DMSO-*d*₆, 100 MHz, δ , ppm): δ_{C} 18.5, 19.1, 21.7 (2C), 32.8, 52.3, 111.1, 116.0, 121.8, 122.0, 126.3 (2C), 129.0 (2C), 129.8, 131.6, 136.6, 143.8, 145.3, 151.6, 158.0, 163.6, 165.4 ppm; Y = 64 %; m.p. 223-225 °C (methanol); MS (EI) *m/z* [M]⁺ calculated: 390.2056, found: 390.2058.

(E)-1-cyclopentyl-N-((4,6-dimethyl-2-oxo-1,2-dihydropyridin-3-yl)methyl)-5-styryl-1H-pyrazole-4-carboxamide (34j)

¹H NMR (DMSO-*d*₆, 400 MHz, δ , ppm): δ_{H} 1.64 (m, 2H, cyclopentyl protons), 1.83 (m, 2H, cyclopentyl protons), 1.97 (m, 2H, cyclopentyl protons), 2.06 (m, 2H, cyclopentyl protons), 2.10

(s, 3H, 4,6 dimethylpyridone –CH₃), 2.16 (s, 3H, 4,6 dimethylpyridone –CH₃), 4.24 (d, 2H, –CH₂NH–, *J*= 5.2 Hz), 4.98 (m, 1H, cyclopentyl proton –N–CH–), 5.84 (s, 1H, –CH– pyridone proton), 7.20 (d, 1H, vinyl proton, *J*= 16.8 Hz), 7.38 (m, 4H, aromatic protons and vinyl proton), 7.34 (m, 1H, aromatic proton), 7.41 (m, 3H, aromatic and vinyl protons), 7.60 (d, 2H, aromatic protons, *J*= 7.2 Hz), 7.85 (t, 1H, –CH₂NH– *J*= 5.1 Hz), 7.87 (s, 1H, pyrazole proton), 11.45 (s, 1H, pyridone –NH) ppm; ¹³C NMR (DMSO-*d*₆, 100 MHz, δ, ppm): δ_C 18.5, 19.1, 24.6 (2C), 32.8, 33.4 (2C), 63.9, 111.1, 116.0, 120.6, 122.1, 126.3 (2C), 129.0 (2C), 129.8, 131.6, 136.6, 143.4, 144.3, 151.6, 158.0, 163.6, 165.4 ppm; Y= 63 %; m.p. 192-194 °C (acetonitrile); MS (EI) *m/z* [M]⁺ calculated: 416.2212, found: 416.2215.

(E)-N-((4,6-dimethyl-2-oxo-1,2-dihydropyridin-3-yl)methyl)-1-phenyl-5-styryl-1H-pyrazole-4-carboxamide (34k)

¹H NMR (DMSO-*d*₆, 400 MHz, δ, ppm): δ_H 2.12 (s, 3H, 4,6 dimethylpyridone –CH₃), 2.19 (s, 3H, 4,6 dimethylpyridone –CH₃), 4.31 (d, 2H, –CH₂NH–, *J*= 4.0 Hz), 5.87 (s, 1H, –CH– pyridone proton), 6.85 (d, 1H, vinyl proton, *J*= 16.8 Hz), 7.32 (m, 6H, aromatic protons and vinyl proton), 7.53 (m, 5H, aromatic protons), 8.09 (t, 1H, –CH₂NH–, *J*= 5.1 Hz), 8.12 (s, 1H, pyrazole proton), 11.47 (s, 1H, pyridone –NH) ppm; ¹³C NMR (DMSO-*d*₆, 100 MHz, δ, ppm): δ_C 18.5, 19.1, 32.8, 111.1, 116.0, 117.9, 122.2, 123.0 (2C), 126.3 (2C), 127.2, 129.0 (2C), 129.1 (2C), 129.8, 132.6, 136.6, 136.7, 139.5, 141.8, 151.6, 158.0, 163.6, 165.4 ppm; Y= 62 %; m.p. 231-233 °C (methanol); MS (EI) *m/z* [M]⁺ calculated: 424.1899, found: 424.1903.

(E)-1-benzyl-N-((4,6-dimethyl-2-oxo-1,2-dihydropyridin-3-yl)methyl)-5-styryl-1H-pyrazole-4-carboxamide (34l)

¹H NMR (DMSO-*d*₆, 400 MHz, δ, ppm): δ_H 2.11 (s, 3H, 4,6 dimethylpyridone –CH₃), 2.18 (s, 3H, 4,6 dimethylpyridone –CH₃), 4.27 (d, 2H, –CH₂NH–, *J*= 4.4 Hz), 5.57 (s, 2H, –NCH₂–Ph), 5.86 (s, 1H, –CH– pyridone proton), 7.14 (d, 2H, aromatic protons), 7.24-7.40 (m, 7H, aromatic protons and vinyl protons), 7.47 (d, 3H, aromatic protons, *J*= 7.6 Hz), 7.95 (s, 1H, pyrazole proton), 7.97 (t, 1H, –CH₂NH–, *J*= 5.8 Hz), 11.46 (s, 1H, pyridone –NH) ppm; ¹³C NMR (DMSO-*d*₆, 100 MHz, δ, ppm): δ_C 18.5, 19.1, 32.8, 52.8, 111.1, 116.0, 118.8, 121.7, 126.3 (2C), 127.6, 128.0 (2C), 128.4 (2C), 129.0 (2C), 129.8, 131.1, 136.0, 136.6, 140.7, 142.8, 151.6, 158.0, 163.6, 165.4 ppm; Y= 58 %; m.p. 195-197 °C (acetonitrile); MS (EI) *m/z* [M]⁺ calculated: 438.2056, found: 438.2051.

N-((4,6-dimethyl-2-oxo-1,2-dihydropyridin-3-yl)methyl)-1-phenyl-1H-pyrazole-4-carboxamide (34m)

¹H NMR (DMSO-*d*₆, 400 MHz, δ, ppm): δ_H 2.13 (s, 3H, 4,6 dimethylpyridone –CH₃), 2.19 (s, 3H, 4,6 dimethylpyridone –CH₃), 4.28 (d, 2H, –CH₂NH–, *J*= 4.8 Hz), 5.88 (s, 1H, –CH– pyridone proton), 7.35 (t, 1H, aromatic proton), 7.52 (m, 2H, aromatic protons), 7.82 (d, 2H, aromatic

protons, $J = 7.6$ Hz), 8.05 (t, 1H, $-\text{CH}_2\text{NH}-$, $J = 4.8$ Hz), 8.15 (s, 1H, pyrazole proton), 8.98 (s, 1H, pyrazole proton), 11.50 (s, 1H, pyridone $-\text{NH}$) ppm; ^{13}C NMR (DMSO- d_6 , 100 MHz, δ , ppm): δ_{C} 18.5, 19.1, 32.8, 111.1, 116.0, 119.2 (2C), 119.4, 127.5, 129.4 (2H), 132.3, 136.8, 139.4, 151.6, 158.0, 162.3, 163.61 ppm; Y= 67 %; m.p. > 250 °C (methanol); MS (EI) m/z $[\text{M}]^+$ calculated: 322.1430, found: 322.1433.

N-((4,6-dimethyl-2-oxo-1,2-dihydropyridin-3-yl)methyl)-1-isopropyl-5-methyl-1H-pyrazole-4-carboxamide (34n)

^1H NMR (DMSO- d_6 , 400 MHz, δ , ppm): δ_{H} 1.33 (d, 6H, $(\text{CH}_3)_2\text{CH}-$, $J = 4.4$ Hz), 2.11 (s, 3H, 4,6 dimethylpyridone $-\text{CH}_3$), 2.15 (s, 3H, 4,6 dimethylpyridone $-\text{CH}_3$), 2.50 (s, 3H, 5 methylpyrazole $-\text{CH}_3$), 4.22 (d, 2H, $-\text{CH}_2\text{NH}-$, $J = 4.8$ Hz), 4.51 (m, 1H, $(\text{CH}_3)_2\text{CH}-$), 5.85 (s, 1H, $-\text{CH}-$ pyridone proton), 7.76 (t, 1H, $-\text{CH}_2\text{NH}-$, $J = 7.6$ Hz), 7.87 (s, 1H, pyrazole proton), 11.47 (s, 1H, pyridone $-\text{NH}$) ppm; ^{13}C NMR (DMSO- d_6 , 100 MHz, δ , ppm): δ_{C} 11.9, 18.5, 19.1, 21.7 (2C), 32.8, 51.0, 111.1, 116.0, 125.9, 147.2, 148.8, 151.6, 158.0, 163.6, 165.9 ppm; Y= 57 %; m.p. 194-196 °C (acetonitrile); MS (EI) m/z $[\text{M}]^+$ calculated: 302.1743, found: 302.1744.

1-benzyl-N-((4,6-dimethyl-2-oxo-1,2-dihydropyridin-3-yl)methyl)-5-methyl-1H-pyrazole-4-carboxamide (34p)

^1H NMR (DMSO- d_6 , 400 MHz, δ , ppm): δ_{H} 2.11 (s, 3H, 4,6 dimethylpyridone $-\text{CH}_3$), 2.16 (s, 3H, 4,6 dimethylpyridone $-\text{CH}_3$), 2.44 (s, 3H, 5 methylpyrazole $-\text{CH}_3$), 4.22 (d, 2H, $-\text{CH}_2\text{NH}-$, $J = 5.2$ Hz), 5.31 (s, 2H, $-\text{NCH}_2\text{-Ph}$), 5.85 (s, 1H, $-\text{CH}-$ pyridone proton), 7.09 (d, 2H, aromatic protons, $J = 6.8$ Hz), 7.31 (m, 3H, aromatic protons), 7.84 (t, 1H, $-\text{CH}_2\text{NH}-$, $J = 4.8$ Hz), 7.94 (s, 1H, pyrazole proton), 11.47 (s, 1H, pyridone $-\text{NH}$) ppm; ^{13}C NMR (DMSO- d_6 , 100 MHz, δ , ppm): δ_{C} 11.8, 18.5, 19.1, 32.8, 52.6, 111.1, 116.0, 123.6, 127.6, 128.4 (2C), 128.7 (2C), 136.1, 147.4, 150.1, 151.6, 158.0, 163.6, 165.9 ppm; Y= 51 %; m.p. 219-221 °C (methanol); MS (EI) m/z $[\text{M}]^+$ calculated: 350.1743, found: 350.1739.²⁷⁵

N-((4,6-dimethyl-2-oxo-1,2-dihydropyridin-3-yl)methyl)-1-phenyl-5-propyl-1H-pyrazole-4-carboxamide (34q)

^1H NMR (DMSO- d_6 , 400 MHz, δ , ppm): δ_{H} 0.72 (t, 3H, $\text{CH}_3\text{CH}_2\text{CH}_2-$, $J = 7.2$ Hz), 1.40 (m, 2H, $\text{CH}_3\text{CH}_2\text{CH}_2-$), 2.13 (s, 3H, 4,6 dimethylpyridone $-\text{CH}_3$), 2.17 (s, 3H, 4,6 dimethylpyridone $-\text{CH}_3$), 2.92 (t, 2H, $\text{CH}_3\text{CH}_2\text{CH}_2-$), 4.28 (d, 2H, $-\text{CH}_2\text{NH}-$, $J = 7.6$ Hz), 5.87 (s, 1H, $-\text{CH}-$ pyridone proton), 7.50 (m, 5H, aromatic protons), 7.95 (t, 1H, $-\text{CH}_2\text{NH}-$, $J = 4.0$ Hz), 8.11 (s, 1H, pyrazole proton), 11.50 (s, 1H, pyridone $-\text{NH}$) ppm; ^{13}C NMR (DMSO- d_6 , 100 MHz, δ , ppm): δ_{C} 13.6, 18.5, 19.1, 21.8, 25.0, 32.8, 111.1, 116.0, 119.9, 124.2 (2C), 127.2, 128.9 (2C), 139.8, 145.7, 146.6, 151.6, 158.0, 163.6, 165.6 ppm; Y= 60 %; m.p. 204-206 °C (acetonitrile/ methanol); MS (EI) m/z $[\text{M}]^+$ calculated: 364.1899, found: 364.1904.

N-((4,6-dimethyl-2-oxo-1,2-dihydropyridin-3-yl)methyl)-2-(5-methyl-1-phenyl-1H-pyrazol-4-yl)acetamide (34r)

¹H NMR (DMSO-*d*₆, 400 MHz, δ, ppm): δ_H 2.11 (s, 3H, 4,6 dimethylpyridone –CH₃), 2.13 (s, 3H, 4,6 dimethylpyridone –CH₃), 2.27 (s, 3H, pyrazole –CH₃), 3.26 (s, 2H, –CH₂CONH–), 4.09 (d, 2H, –CH₂NH–, *J*= 5.2 Hz), 5.85 (s, 1H, –CH– pyridone proton), 7.39 (t, 1H, aromatic proton, *J*= 7.6 Hz), 7.42-7.54 (m, 5H, aromatic and pyrazole protons), 7.91 (t, 1H, –CH₂NH–, *J*= 4.4 Hz), 11.47 (s, 1H, pyridone –NH) ppm; ¹³C NMR (DMSO-*d*₆, 100 MHz, δ, ppm): δ_C 10.3, 18.5, 19.1, 30.3, 33.0, 109.1, 111.1, 116.0, 123.3 (2C), 127.2, 129.1 (2C), 136.6, 138.0, 139.3, 151.6, 158.0, 163.6, 170.8 ppm; Y= 66 %; m.p. 215-217 °C (acetonitrile/ methanol); MS (EI) *m/z* [M]⁺ calculated: 350.1743, found: 350.1747

Table S4. Chemical and Physical Data of the Intermediates **38a'-e'**.

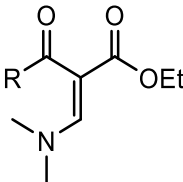
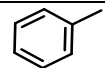
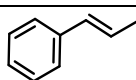
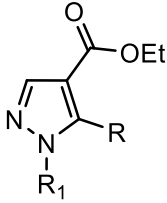
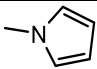
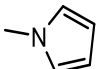
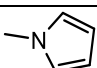
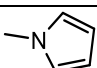
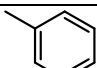
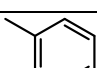
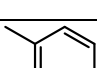
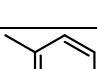
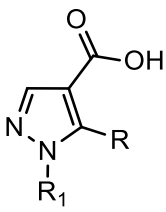
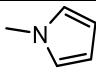
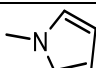
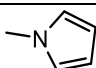
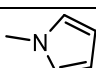
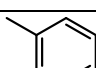
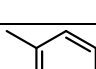
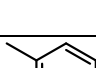
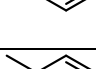
<div style="text-align: center;"> 38a'-e'</div>				
Cpd	R	m. p. (°C)	recrystallization solvent	yield (%)
38a' ²⁷⁷		64-66	cyclohexane	78
38b' ²⁷⁸		oil	-	72
38c' ²⁷⁹	-H	150-152	toluene	65
38d' ²⁶⁶	-CH ₃	43-45	<i>n</i> -hexane	77
38e' ²⁷⁸	-CH ₂ CH ₂ CH ₃	112-114	cyclohexane	69

Table S5. Chemical and Physical Data of the Intermediates **35a-d**, **36a-d**, and **39e-q**.

<div style="text-align: center;">  <p>35a-d, 36a-d, 39e-q</p> </div>					
Cpd	R	R ₁	m. p. (°C)	recrystallization solvent	yield (%)
35a ²⁸⁰	-NH ₂	<i>i</i> -Pr	62-63	cyclohexane	92
35b ²⁸¹	-NH ₂	cyclopentyl	oil	-	95
35c ²⁸²	-NH ₂	Ph	107-109	cyclohexane	81
35d ²⁶⁵	-NH ₂	Bn	109-111	cyclohexane	82
36a		<i>i</i> -Pr	oil	-	67
36b		cyclopentyl	oil	-	77
36c ²⁸³		Ph	111-113	cyclohexane	88
36d		Bn	44-45	<i>n</i> -hexane	77
39e		<i>i</i> -Pr	oil	-	75
39f		cyclopentyl	oil	-	68
39g ²⁸⁴		Ph	113-115	cyclohexane	66
39h ²⁸⁵		Bn	68-70	<i>n</i> -hexane	73
39i	-CH=CHPh	<i>i</i> -Pr	oil	-	70
39j	-CH=CHPh	cyclopentyl	oil	-	67

39k ²⁸⁶	-CH=CHPh	Ph	oil	-	69
39l ²⁸⁷	-CH=CHPh	Bn	oil	-	65
39m ²⁸⁸	-H	Ph	98-100	cyclohexane	66
39n ²⁸⁹	-CH ₃	<i>i</i> -Pr	oil	-	70
39o ²⁹⁰	-CH ₃	Ph	56-58	<i>n</i> -hexane	88
39p	-CH ₃	Bn	oil	-	82
39q ²⁸⁴	- CH ₂ CH ₂ CH 3	Ph	112-114	cyclohexane	92

Table S6. Chemical and Physical Data of the Intermediates 37a-q .					
 <p style="text-align: center;">37a-q</p>					
Cpd	R	R ₁	m. p. (°C)	recrystallization solvent	yield (%)
37a		<i>i</i> -Pr	138-140	toluene	87
37b		cyclopentyl	167-168	toluene/acetonitrile	93
37c ²⁹¹		Ph	184-186	acetonitrile	89
37d		Bn	170-172	toluene/acetonitrile	77
37e		<i>i</i> -Pr	164-166	toluene/acetonitrile	73
37f		cyclopentyl	196-197	acetonitrile	68
37g ²⁹⁰		Ph	177-178	toluene/acetonitrile	83
37h ²⁹²		Bn	166-168	toluene/acetonitrile	76
37i	-CH=CHPh	<i>i</i> -Pr	167-170	toluene/acetonitrile	80
37j	-CH=CHPh	cyclopentyl	191-193	acetonitrile	85
37k	-CH=CHPh	Ph	176-177	toluene/acetonitrile	83
37l	-CH=CHPh	Bn	136-140	toluene	78
37m ²⁹³	-H	Ph	225-227	methanol	88
37n ²⁸⁹	-CH ₃	<i>i</i> -Pr	151-153	toluene	92
37o ²⁹⁰	-CH ₃	Ph	163-165	toluene/acetonitrile	86

37p ²⁷⁵	-CH ₃	Bn	167-169	toluene/acetonitrile	77
37q ²⁹⁰	- CH ₂ CH ₂ CH 3	Ph	111-113	cyclohexane	71

Table S7. Elemental Analyses for Compounds 34a-r.							
cmpd	MW	calculated, %			found, %		
		C	H	N	C	H	N
34a	353.43	64.57	6.56	19.82	64.78	6.67	19.59
34b	379.46	66.47	6.64	18.46	66.23	6.51	18.72
34c	387.44	68.20	5.46	18.08	68.04	5.55	18.32
34d	401.47	68.81	5.77	17.44	68.59	5.65	17.69
34e	364.45	69.21	6.64	15.37	69.44	6.75	15.19
34f	390.49	70.75	6.71	14.35	70.98	6.84	14.11
34g	398.47	72.34	5.57	14.06	72.59	5.68	13.82
34h	412.49	72.80	5.86	13.58	73.04	5.99	13.27
34i	390.49	70.75	6.71	14.35	70.57	6.59	14.52
34j	416.53	72.09	6.78	13.45	71.88	6.70	13.64
34k	424.50	73.56	5.70	13.20	73.82	5.88	12.95
34l	438.53	73.95	5.98	12.78	74.17	6.08	12.54
34m	322.37	67.07	5.63	17.38	67.29	5.74	17.17
34n	302.38	63.55	7.33	18.53	63.89	7.45	18.28
34o	336.40	67.84	5.99	16.66	68.02	6.10	16.39
34p	350.42	68.55	6.33	15.99	68.36	6.29	16.17
34q	364.45	69.21	6.64	15.37	69.44	6.79	15.08
34r	350.42	68.55	6.33	15.99	68.42	6.39	16.13

3.4.2 Biochemistry

EZH2/PRC2 assays. (Reaction Biology Corporation, USA) The EZH2 substrate (0.05 mg/mL core histone, or 5 μ M H3/H4 octamer, or 5 μ M H3/H4 tetramer, or 5 μ M histone H3) was added in the freshly prepared reaction buffer (50 mM Tris-HCl (pH 8.0), 50 mM NaCl, 1 mM EDTA, 1 mM DTT, 1 mM PMSF, 1 % DMSO). The PRC2 complex [complex of human EZH2, human EED, human SUZ12, human AEBP2, and human RbAp48] was delivered into the substrate solution and the mixture was mixed gently. Afterwards, the tested compounds dissolved in DMSO were delivered into the enzyme/substrate reaction mixture by using Acoustic Technology (Echo 550, LabCyte Inc. Sunnyvale, CA) in nanoliter range, and 3 H-SAM was added into the reaction mixture to initiate the reaction. The reaction mixture was incubated for 1 h at 30°C and then it was delivered to filter-paper for detection. The data were analyzed using Excel and GraphPad Prism software for IC₅₀ curve fits. For SAM competition experiments, the same procedure was used with different SAM concentration (1, 2.5, 5, and 10 μ M) and H3/H4 octamer as the substrate.

EZH1 complex, DOT1L, G9a, MLL1 complex, SET7/9, PRMT1, and DNMT1 assays. (Reaction Biology Corporation, USA) The appropriate methyltransferase substrate (0.05 mg/mL core histone for EZH1 complex, 0.05 mg/mL oligonucleosomes for DOT1L, 5 μ M histone H3 (1-21) peptide for G9a, 0.05 mg/mL nucleosomes for MLL1 complex, 0.05 mg/mL core histone for SET7/9, 5 μ M histone H4 for PRMT1, and 0.001 mg/mL poly(dI-dC) for DNMT1) was added in freshly prepared reaction buffer (50 mM Tris-HCl (pH 8.5), 5 mM MgCl₂, 50 mM NaCl, 0.01 % Brij35, 1 mM DTT, 1% DMSO). The MT enzyme was delivered into the substrate solution and the mixture was mixed gently. Afterwards, the tested compounds dissolved in DMSO were delivered into the enzyme/substrate reaction mixture by using Acoustic Technology (Echo 550, LabCyte Inc. Sunnyvale, CA) in nanoliter range, and 1 μ M 3 H-SAM was also added into the reaction mixture to initiate the reaction. The reaction mixture was incubated for 1 h at 30 °C and then it was delivered to filter-paper for detection. The data were analyzed using Excel and GraphPad Prism software for IC₅₀ curve fits.

3.4.3 In cell evaluation

(Groups of Prof. Elisabetta Ferretti, and Dott. Marco Tafani, Department of Experimental Medicine, Sapienza University of Rome, Italy)

Cell cultures. The MDA-MB-231 human breast carcinoma cell line, the human neuroblastoma cell line SK-N-BE, and the human chronic myelogenous leukemia cell line K562 were maintained in RPMI 1640 medium (Sigma-Aldrich, St. Louis, MO, USA). The human prostate adenocarcinoma cell line PC-3 was maintained in DMEM medium (Sigma-Aldrich). Both media were supplemented with 100 units/mL penicillin, 0.1 mg/mL streptomycin, and 10 % heat-

inactivated fetal bovine serum (FBS) (Sigma-Aldrich). All the cells were maintained at 37 °C in a humidified atmosphere of 5 % CO₂ and 95 % air.

DAOY cells were obtained from ATCC and cultured in MEM medium (Gibco, Invitrogen), supplemented with 10 % heat-inactivated fetal bovine serum, 1 % sodium pyruvate, 1 % non-essential amino acid solution, 1 % L-glutamine and penicillin/streptomycin. Human and mouse stem-like cells (hMB-SLC and mMB-SLC) were derived, as previously described from primary human SHH-MBs and from spontaneous tumors arisen in Ptc^{+/-} mice.²⁷⁴ DAOY-SLCs were obtained as described in Alimova *et al.*²⁷⁰ All SLCs were maintained in DMEM/F12 supplemented with 0.6% glucose, 25 mg/mL insulin, 60 mg/ml *N*-acetyl-L-cystein, 2 mg/mL heparin, 20 ng/mL EGF, 20 ng/mL bFGF (Peprotech, Rocky Hill, NJ), 1X penicillin-streptomycin and B27 supplement without vitamin A (Gibco). For differentiation experiments, hMB-SLCs and mMB-SLC were mechanically dissociated and plated for 48 h on D-poly-lysine coated dishes in differentiation medium (DMEM/F12 with N2 supplement and 2 mg/mL heparin, 0,6 % glucose, 60 mg/mL *N*-acetyl-L-cysteine, 1% FBS). For self-renewal assessment, clonogenic assay was performed as previously described.²⁷⁴ Briefly: oncospheres were disaggregated with non-enzymatic cell dissociation buffer (Sigma) and cells were plated at clonal density (1-2 cells/mm²) into 96-well plates and cultured for an appropriate number of days (7-15) until oncospheres were countable.

Cell Viability. Cells were seeded in a 96 well plate. The day after cells were treated as described and cell viability was measured by using the CellTiter 96 AQueous One Solution Cell Proliferation Assay (MTS) (Promega, Milan, Italy) and following manufacturer's instructions. Cell viability was also assessed by Trypan blue exclusion. Following treatment, cells were stained by addition of Trypan Blue. Cells were then visualized and counted with a phase contrast microscopy (NIKON Eclipse TE2000U). Finally, cell viability and morphology was also documented by taking pictures of the cells after 2, 4 and 6 days of treatment by using a digital camera mounted on an EclipseNet 2000 microscope (Nikon Instruments, Florence, Italy).

Protein Extraction and Western Blot Assays. **3** was dissolved in DMSO and added to a final concentration of 1 μM. Compound **34o** was dissolved in DMSO and added to a final concentration of 0.5, 1 and 5 μM for the indicated times. Cells were harvested, washed twice in PBS and resuspended in lysis buffer (50 mM Tris pH 7.4, 5 mM EDTA, 250 mM NaCl, 50 mM NaF, 0.1 % Triton X-100, 10 μg/mL leupeptin and 1 mM phenyl-methylsulfonyl fluoride). After 30 min on ice, the lysates were clarified by centrifugation (10 min at 4 °C) and the supernatant fraction collected. Protein concentration was measured by the Bradford assay (Bio-Rad Laboratories, Hercules, CA, USA). Proteins were applied to SDS-polyacrylamide gels. The gels were blotted (1.5 h at 230 mA) onto a Hybond-ECL nitrocellulose filter (Amersham Life science, Inc.). A Dual Color prestained protein solution (Bio-Rad Laboratories) was used as a molecular weight standard. The filter was washed twice with TBS-0.1 % Tween-20 buffer (TBS-T), before

blocking non-specific binding sites with 5 % milk/TBS-T for 1 h. The filter was then incubated with the specific primary antibody [mouse anti-human H3K27me3, anti-human H3K4me3, anti-human H3, anti-caspase 3 antibody (Abcam, Cambridge, UK), rabbit anti-human LC3I/II (Novus Biologicals, Abingdon, UK), mouse anti- β -actin (Sigma), or rabbit anti-PARP (Santa Cruz Biotechnology, Santa Cruz, CA, USA)] diluted in 5 % milk/TBS-T overnight at 4 °C. The nitrocellulose filter was washed twice and incubated with horseradish peroxidase-conjugated appropriate secondary antibody [mouse anti-rabbit HRP, goat anti-mouse HRP (Amersham Biosciences, Piscataway, NJ, USA)]. Detection was performed at room temperature using the enhanced chemiluminescent detection system (ECL kit) purchased from Euroclone (Milan, Italy). Experiments were repeated three times. Densitometric analysis of the bands relative to β -actin was performed using Image J software (NIH).

Western blot (medulloblastoma). Western blots were performed according to standard procedures.²⁹⁴ Briefly, protein lysates were prepared using RIPA buffer with fresh protease inhibitors. Lysates were separated on SDS polyacrylamide gels. Proteins were transferred on nitrocellulose membrane (0.45 μ m) (PerkinElmer). Membranes were blocked for 1 h at room temperature in 5 % nonfat dry milk and incubated overnight at 4 °C with antibodies against EZH2 (4905S Cell signaling), H3K27me3 (07-449 Millipore), PCNA (2586 Cell signaling), ACTIN (I-19 sc-1616; Santa Cruz Biotechnology), GAPDH (ab9484, Abcam), cleaved CSP-3 (D-175 9661S; Cell Signaling) and H3 (ab1971, Abcam). HRP-conjugated secondary antibodies (Santa Cruz Biotechnology) were used in combination with enhanced chemiluminescence (ECL Amersham).

Fluorescence-activated cell sorting. Cells were sorted based on CD133 expression levels using a FACSARIAIII (BD Biosciences) equipped with a 633 nm laser and FACSDiva software (BD Biosciences version 6.1.3). Briefly, cells were immunostained with APC-conjugated anti-CD133 (Miltenyi Biotec) according to manufacturer's protocol, and were then subjected to cell sorting. Cells were gated using forward and side scatter (FSC-A and SSC-A) plot to identify live cells (average 65%), and were then detected in the APC channel for CD133 expression. Following this gate strategy, cells were sorted for expression of CD133 (APC- and APC+ cells) and subsequently checked for purity.

PAMPA-BBB. Donor solution (500 μ M or 250 μ M) was prepared by diluting 10 or 5 mM DMSO compound stock solution using phosphate buffer (pH 7.4, 0.01 M). Filter membrane was coated with 5 μ L of BBB-specific lipid solution prepared dissolving 16 mg of PBL (Avanti Lipids Polar, 141101P) in 600 μ L of *n*-dodecane. Donor solution (150 μ L) was added to each well of the filter plate. To each well of the acceptor plate 300 μ L of solution (5% DMSO in phosphate buffer) were added. Each compound was tested in triplicate. The sandwich was incubated for 24 h at room temperature under gentle shaking. After the incubation time, the sandwich plates were separated and 250 μ L of the acceptor plate were transferred to a UV quartz

microtiter plate and measured by UV spectroscopy, using a Multiskan GO microplate spectrophotometer (Thermo Scientific) at 250–500 nm at step of 5 nm. Reference solutions (250 µL) were prepared diluting the sample stock solutions to the same concentration as that with no membrane barrier. The BBB permeability value Log *Pe* is determined applying the equation:

$$\log Pe = \log \left\{ C \times \left(-\ln \left(1 - \frac{[drug]_{acceptor}}{[drug]_{equilibrium}} \right) \right) \right\}$$

$$C = \left(\frac{Vd \times Va}{(Vd + Va) \times area \times time} \right)$$

In this equation, *VA* is the volume of the acceptor compartment (0.3 cm³), *VD* is the donor volume (0.15 cm³), *area* is the accessible filter area (0.24 cm²), and *time* is the incubation time in seconds.

3.4.4 Mice experiments

Mice were purchased from Charles River Laboratories and maintained in the Animal Facility at Sapienza University of Rome. All procedures were performed in accordance with the Guidelines for Animal Care and Use of the National Institutes of Health with the approval of the Ethics Committee for Animal Experimentation (Prot. N 03/2013) of Sapienza University of Rome.

In vivo treatment. CD1 wild-type mice were treated intra-peritoneally with 20 µMoles/Kg of **34o** (n=8 for each group). Treatment was performed at the age of 8 and 10 days post-natal and mice were sacrificed at 12 days post-natal. Brain and cerebellum tissues were collected for analysis.

Medulloblastoma xenografts. DAOY-SLCs were stereotactically implanted into the cerebellum of nude mice by using the following coordinates according to the atlas of Franklin and Paxinos: 6.6 mm posterior to the bregma; 1 mm lateral to the midline; and 2 mm ventral from the surface of skull of mice, under ketamine (100 mg/kg, i.p.)/xylazine (10 mg/kg, i.p.) anesthesia. Cells (2 × 10⁵ per 3 µL) were implanted at an infusion rate of 1 µL/min. Mice were separated into two groups. Group 1 (n=8) was intraperitoneally treated with **34o** (20 µMoles/Kg) suspended in 10 % (2-Hydroxypropyl)-β-cyclodextrin +1 % DMSO (Sigma), Group 2 (n= 8) was treated with 10 % (2-Hydroxypropyl)- β-cyclodextrin +1 % DMSO (Sigma). After 21 days of treatment, animals were sacrificed and brains were formalin fixed and paraffin embedded. Serial thick coronal sections (2 µm) starting from mesencephalon to the end of cerebellum were performed. The analysis was performed on 20 sections, sampled every 40 µm on the horizontal plan of the cerebellum, in which the tumor was identified and outlined at 2.5 X magnification.

Every 40 µm of brain slice, hematoxylin and eosin (H&E) staining was performed. Tumor area of every slice was evaluated with a microscope (Axio Imager M1 microscope) equipped with a motorized stage and software Image Pro Plus 6.2. The following formula was used to calculate

brain tumor volume: tumor volume = sum of (measured area for each slice x slice thickness x sampling frequency).²⁹⁵

Immunohistochemistry. Paraffin-embedded sections were deparaffinized, and stained with either H&E or immunohistochemical stains as specified. Heat-induced epitope retrieval was performed with citrate buffer pH 6. Sections were incubated with ki67 primary antibody (*Thermo Scientific*) for 1 h. Ki67 expression was expressed as percentages of total cells with labeled nuclei.

* Adapted with the permission of the authors from:

- Mellini P, Marrocco B, Borovika D, Polletta L, Carnevale I, Saladini S, Stazi G, Zwergel C, Trapencieris P, Ferretti E, Tafani M, Valente S, and Mai A. Pyrazole-based inhibitors of Enhancer of Zeste Homolog 2 induce apoptosis and autophagy in cancer cells. *Phil. Trans. R. Soc. B*. doi: 10.1098/rstb.2017.0150 (ACCEPTED in September 2017, now in Press)
- Miele E, Valente S, Alfano V, Silvano M, Mellini P, Borovika D, Marrocco B, Po A, Besharat ZM, Catanzaro G, Battaglia G, Abballe L, Zwergel C, Stazi G, Milite C, Castellano S, Tafani M, Trapencieris P, Mai A, Ferretti E. The histone methyltransferase EZH2 as a druggable target in SHH medulloblastoma cancer stem cells. *Oncotarget*. 2017 Aug 2;8(40):68557-68570. doi: 10.18632/oncotarget.19782. PubMed PMID: 28978137.

4 Design, synthesis and characterization of novel Astemizole analogues as potential PRC2 disruptors

4.1 Research project

The catalytic methyltransferase activity of EZH2, as previously mentioned, only takes place in co-presence of at least two other protein subunits of the PRC2 complex: EED and SUZ12.⁷³⁻⁷⁵ Furthermore, it has been demonstrated that the catalytic activity of EZH2 is impaired by the disruption of the interaction with its partner EED.^{70,169} These evidences, together with the need to develop a new class of PRC2-targeting molecules, led to the application of the protein-protein interaction (PPI) disruption as a strategy to target the PRC2.

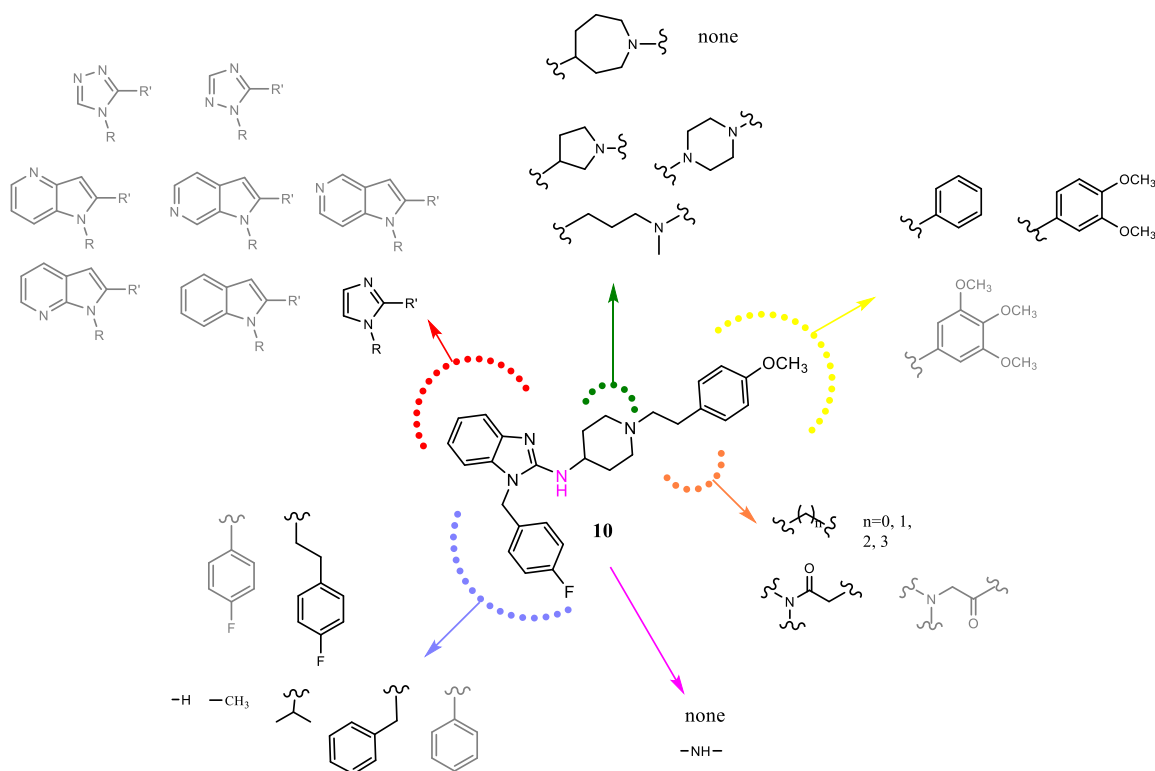


Figure 4.1. Molecular design study on Astemizole **10**. In black are reported the modifications that have been applied on final compounds, in grey are reported those modifications that have not been yet included in final compounds.

During the last part of my PhD, I worked on the development of PRC2 disruptors. The starting point of our project was a paper published by Kong *et al.* in 2014. The authors reported the well-known antihistamine drug Astemizole (**10**, Figure 1.6 and 4.1) as EZH2-EED disruptor.¹⁷¹ Knowing that **10**, other than antihistamine (H₁) activity, is cardio toxic, we decided to manipulate its scaffold, so to try to dissect the anti-H₁ and cardio toxic effects from the PRC2 disruption activity. Compound **10** looks as a nice scaffold to work on for a medicinal chemist: figure 63 resembles our molecular design study. In black are reported the modifications that have been

applied, in gray those that we included in our design, but we still did not apply to any final compound.

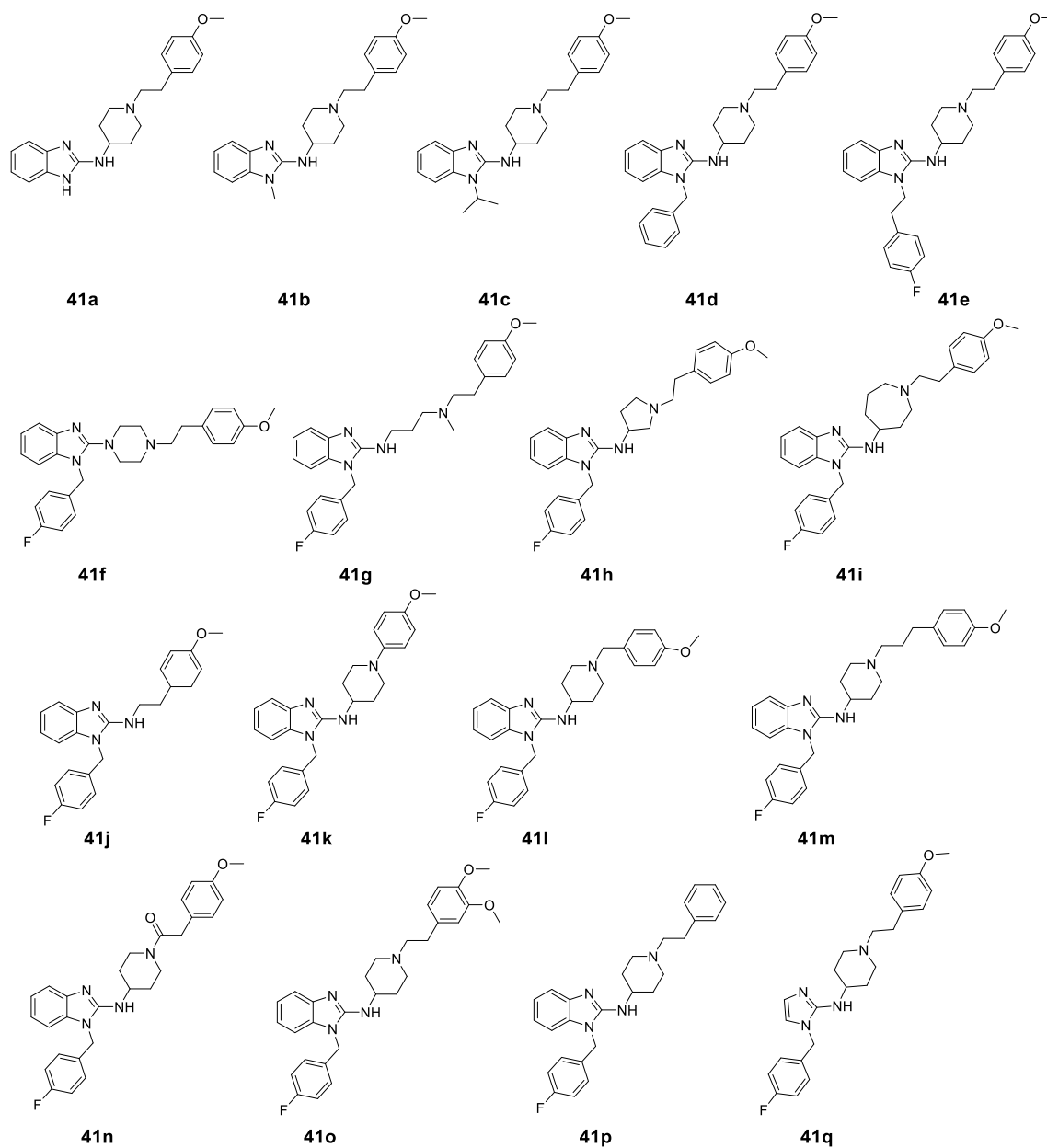


Figure 4.2. Novel Astemizole (**10**) analogues **41a-q**.

We started our molecular design study breaking up **10** in six different portions:

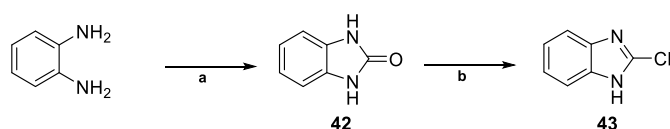
- benzimidazole core,
- benzimidazole N(1) substitution,
- NH linker,
- piperidine ring,
- ethylene spacer,
- 4-methoxyphenyl ring.

We, then, focused on each single portion and evaluated if it was possible to remove it, or how to replace it. We started with the benzoimidazole core, and we thought that it could be replaced with a nitrogen-containing monocycle (imidazole or triazole), or with an indole or different fused bicycles (red arrow, Figure 4.1). The benzoimidazole N(1) of **10** is substituted with a 4-fluorobenzyl group. We questioned whether this group was essential for PRC2 disruption, thus we removed or replaced it with different aliphatic or aromatic substituents, such as methyl, isopropyl, benzyl, or 4-fluorophenethyl (light blue arrow, Figure 4.1). We also wanted to evaluate the importance of the NH linker between the benzoimidazole and the piperidine. Thus, we tried to remove this flexible linker, including the nitrogen in the piperidine ring generating a piperazine (pink and green arrows, Figure 4.1). We then decided to expand our investigation also to the piperidine portion. More in detail, we completely removed this ring, or replace it with inferior or superior cyclic homologues, or cut it giving a linear, nitrogen-containing spacer (green arrow, Figure 4.1). Also, the ethylene spacer between the piperidine and 4-methoxyphenyl ring was an element of investigation. We thought to remove, shorten or elongate it, or to replace one of the two methylene with a carbonyl group (orange arrow, Figure 4.1). Finally, we questioned about the importance of the 4-methoxy substitution, removing or doubling it (yellow arrow, Figure 4.1). Figure 4.2 will resemble all the final compounds obtained so far.

4.2 Results and discussion

4.2.1 Chemistry

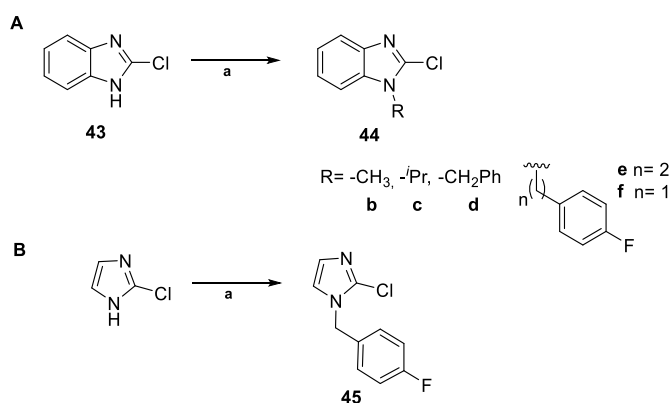
For the synthesis of compounds **41a-p** we started building the 2-chlorobenzimidazole (**43**, Scheme 11) from 2-aminoaniline, reacted with 1,1'-carbonyldiimidazole in *N,N*-dimethylformamide to give benzoimidazolone (**42**, Scheme 11).



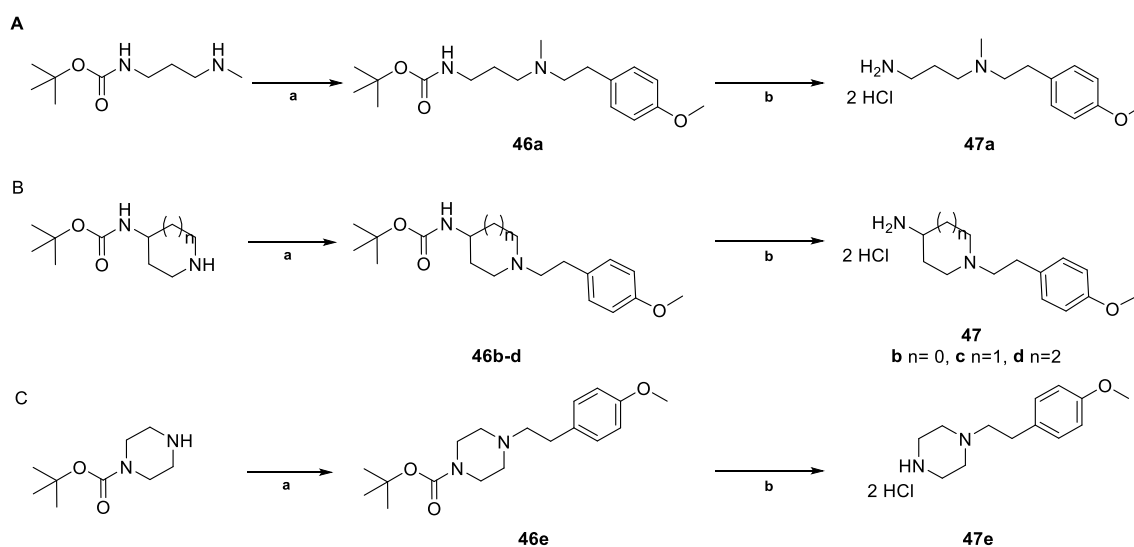
Scheme 11. Reagents and conditions **a**) CDI, dry DMF, 75 °C, 3 h (78 %); **b**) POCl₃, Reflux, 2 h (60 %).

Compound **42** was then involved in a reaction with phosphoryl chloride to give **43** in good yield (Scheme 11). The N-alkylation of the 2-chlorobenzimidazole (**43**), or 2-chloroimidazole (commercially available) central core was performed in presence of sodium hydride with the appropriate alkyl or benzyl halide, yielding the intermediates **44b-f** and **45** (Scheme 12). The amines **47a-e** were obtained in two steps starting from the commercially available tert-butyl (3-(methylamino)propyl)carbamate, tert-butyl pyrrolidin-3-ylcarbamate, tert-butyl piperidin-4-ylcarbamate, tert-butyl azepan-4-ylcarbamate, or tert-butyl piperazine-1-carboxylate. In these cases, potassium carbonate was sufficient to promote the NH deprotonation and thus the subsequent S_N on the 1-(2-bromoethyl)-4-methoxybenzene substrate. The tert-butyloxycarbonyl-

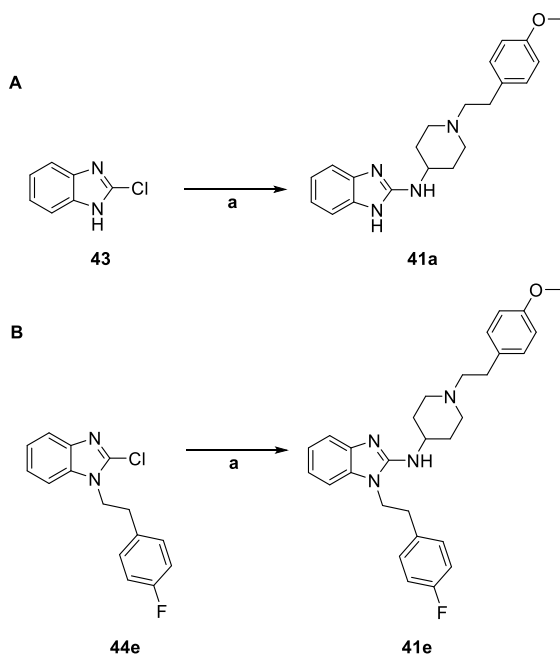
protected intermediates **46a-e** underwent cleavage in acidic media, to give the corresponding amine hydrochlorides **47a-e** (Scheme 13). The amines **47a-e**, or the commercially available 2-(4-methoxyphenyl)ethan-1-amine, were then involved in a S_N with compounds **43**, **44e**, or **44f** as nucleophiles, using *N*-methyl-2-pyrrolidone as solvent and 4-dimethylaminopyridine as a catalyst when required, to give the final compounds **41a, e-k** (Scheme 14 and 15).



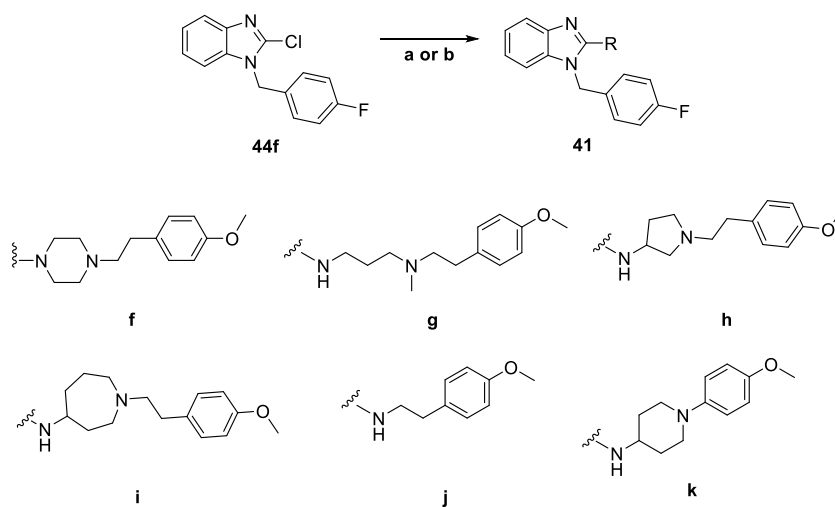
Scheme 12. Reagents and conditions **a**) iodomethane, or 2-iodopropane, or benzylbromide, or 4-fluorobenzylbromide, or (2-bromoethyl)benzene, NaH 60 %, dry THF/ dry DMF, 0 °C to r.t., 1-6 h (65-99 %)



Scheme 13. Reagents and conditions **a**) 1-(2-bromoethyl)-4-methoxybenzene, dry K₂CO₃, dry CH₃CN, 60-80 °C, 4 h (60-70 %); **b**) 4 N HCl in THF, dry THF, 0 °C to r.t., 5 h (83-95 %)

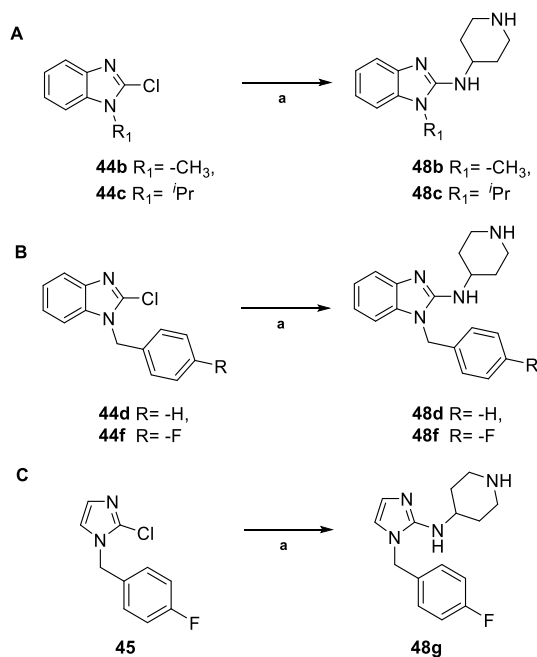


Scheme 14. Reagents and conditions **a)** **47c**, NMP, sealed tube, 175 °C, 4-14 h (39-75 %)

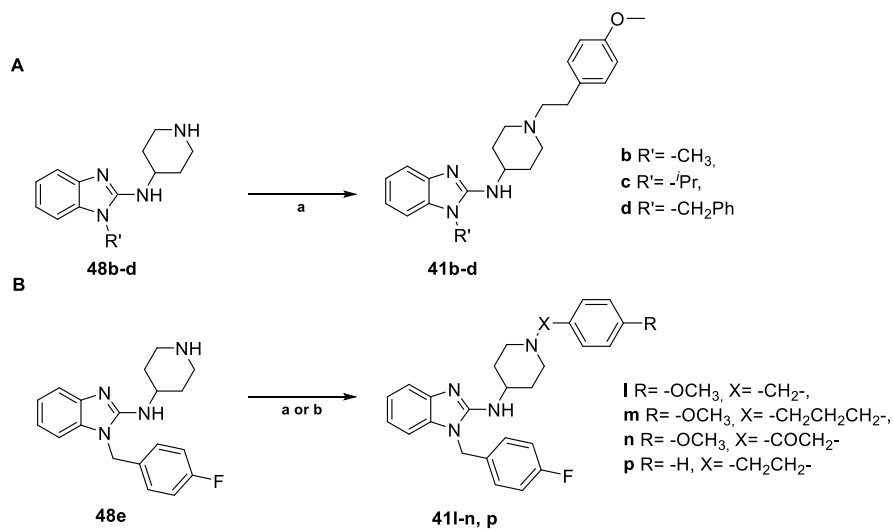


Scheme 15. Reagents and conditions **a)** 2-(4-methoxyphenyl)ethan-1-amine, or **47e**, NMP, sealed tube, 175 °C, 16 h (36-64 %); **b)** **47a**, **b**, or **d**, DIPEA, NMP, sealed tube, 175 °C (30-45 %)

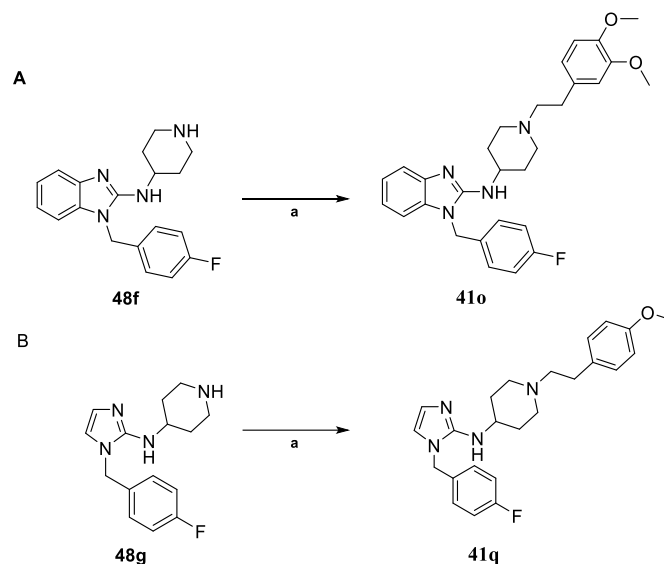
In the same conditions, reacting the 2-chloro substituted intermediates **44b-d** and **45** with 4-aminopiperidine, we obtained the amines **48b-d**, **f**, **g** (Scheme 16). Finally, reacting these amines with the appropriate alkyl halide in presence of potassium carbonate we obtained the final compounds **41b-d**, **l**, **m**, **p-r**. Whereas, an amide coupling of **48e** with 2-(4-methoxyphenyl)acetic acid in presence of 1, 1'-carbonyldiimidazole yielded compound **41n** (Scheme 17 B, method b). We tried to synthesise the β -carbonyl amine isomer, but, even though the reaction worked, the product proved unstable, and we were not able to isolate it.



Scheme 16. Reagents and conditions **a**) 4-aminopiperidine, NMP, sealed tube, 175 °C, 2-3 h (26-88 %)



Scheme 17. Reagents and conditions **a**) 1-(bromomethyl)-4-methoxybenzene, or 1-(3-bromopropyl)-4-methoxybenzene, or 4-(2-bromoethyl)-1,2-dimethoxybenzene, or 1-(2-bromoethyl)-4-methoxybenzene, or (2-bromoethyl)benzene, dry K_2CO_3 , dry CH_3CN , r.t to 60-80 °C, 4 h (24-72 %); **b**) 2-(4-methoxyphenyl)acetic acid, CDI, dry THF, r.t., 5 h (75 %)



Scheme 18. Reagents and conditions **a**) 1-(bromomethyl)-4-methoxybenzene, or 1-(3-bromopropyl)-4-methoxybenzene, or 4-(2-bromoethyl)-1,2-dimethoxybenzene, or 1-(2-bromoethyl)-4-methoxybenzene, or (2-bromoethyl)benzene, dry K_2CO_3 , dry CH_3CN , r.t to 60-80 °C, 4 h (24-72 %).

4.3 Conclusions and future perspectives

During the last part of my PhD, I directed my research toward the development of PRC2 disruptors. This research project started with the idea of manipulating compound **10**, recently reported as PRC2 disruptor, but known since a long time as antihistamine (H_1) drug with cardio-toxic side effects. By means of chemical manipulation on this known scaffold, we aimed to dissect the antihistamine and cardio-toxic effects from the PRC2 disruption activity of compound **10**. So far, this research project yielded the synthesis and characterization of a series of 17 compounds as Astemizole (**10**) analogues (**41a-r**). We validated a facile and fast synthetic route for this series of compounds.

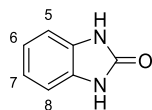
The synthesized derivatives will be evaluated as PRC2 disruptors, as well as anti- H_1 . We hope that some of the modifications that we applied will give the desired selectivity and guide us for further optimization.

4.4 Experimental Section

4.4.1 Chemistry

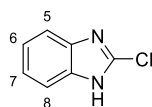
Melting points were determined on a Buchi 530 melting point apparatus and are uncorrected. ^1H NMR and ^{13}C NMR spectra were recorded at 400 and 100 MHz, respectively, on a Bruker AC 400 spectrometer; chemical shifts are reported in δ (ppm) units relative to the internal reference tetramethylsilane (Me_4Si). EIMS spectra were recorded with a Fisons Trio 1000 spectrometer; only molecular ions (M^+) and base peaks are given. All compounds were routinely checked by TLC and ^1H NMR. TLC was performed on aluminum-backed silica gel plates (Merck DC, Alufolien Kieselgel 60 F254) with spots visualized by UV light. All solvents were reagent grade and, when necessary, were purified and dried by standard methods. Concentration of solutions after reactions and extractions involved the use of a rotary evaporator operating at reduced pressure of ca. 20 Torr. Organic solutions were dried over anhydrous sodium sulfate. Elemental analysis has been used to determine purity of the described compounds, that is, > 95%. Analytical results are within $\pm 0.40\%$ of the theoretical values. All chemicals were purchased from Sigma-Aldrich, Milan (Italy), or from Alfa Aesar, Karlsruhe (Germany), and were of the highest purity.

Synthesis of 1,3-dihydro-2H-benzo[d]imidazol-2-one (42)



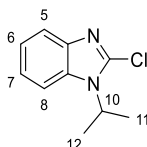
2-aminoaniline (27.74 mmol, 1.0 eq, 3.0 g) was dissolved in dry DMF (3 mL) and *N,N'*-carbonyldiimidazole (30.51 mmol, 1.1 eq, 4.94 g) was added. The solution was stirred at 75 °C for 3 h. After this time, TLC analysis indicated complete conversion of the starting material. The solution was cooled to 0 °C, and it was quenched by adding a 0.5 M aqueous solution of HCl. The product precipitated and the solid was filtered, rinsed with distilled H_2O , then dried in oven (60 °C) resulting in 78 % yield (2.90 g, 21.60 mmol, 78 %). m.p. > 300 °C (methanol); ^1H NMR ($\text{DMSO}-d_6$, 400 MHz, δ , ppm): δ_{H} 6.92 (2H, d, $J = 7.6$ Hz, C(6)H, C(7)H), 7.41 (2H, d, $J = 7.6$ Hz, C(5)H, C(8)H), 7.85 (2H, s, 2(NH)) ppm; ^{13}C NMR ($\text{DMSO}-d_6$, 100 MHz, δ , ppm): δ_{C} 108.4 (2C), 120.2 (2C), 128.9 (2C), 155.4 ppm; MS (EI) m/z $[\text{M}]^+$ calculated: 134.0480, found: 134.0476.

Synthesis of 2-chloro-1H-benzo[d]imidazole (43)



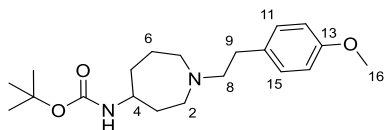
1,3-dihydro-2H-benzo[d]imidazol-2-one **42** (21.6 mmol, 1.0 eq, 2.9 g) was refluxed in absolute POCl₃ (3 mL) for 2 h. After this time all the starting material was converted into product. The reaction was cooled to 0 °C and quenched by slow addition of H₂O (5 mL). NH₄OH solution was added till pH = 8. The product precipitated, it was filtered, rinsed with distilled H₂O, and dried in oven (60 °C). The solid was further purified on column chromatography eluting with chloroform: ethyl acetate 10: 1, to give the desired product in 60 % yield (1.92 g, 12.9 mmol, 60 %). m.p. 205-210 °C (acetonitrile); ¹H NMR (DMSO-*d*₆, 400 MHz, δ, ppm): δ_H 7.15 (2H, d, *J*= 7.8 Hz, C(6)H, C(7)H), 7.51 (2H, d, *J*= 7.8 Hz, C(5)H, C(8)H), 12.61 (1H, bs, NH) ppm; ¹³C NMR (DMSO-*d*₆, 100 MHz, δ, ppm): δ_C 112.4, 118.3, 123.2 (2C), 138.9, 139.5 (2C). ppm; MS (EI) *m/z* [M]⁺ calculated: 152.0151, found: 152.0154.

General procedure for the synthesis of the intermediates 44b-e and 45. Example: synthesis of 2-chloro-1-isopropyl-1H-benzo[d]imidazole (44c)



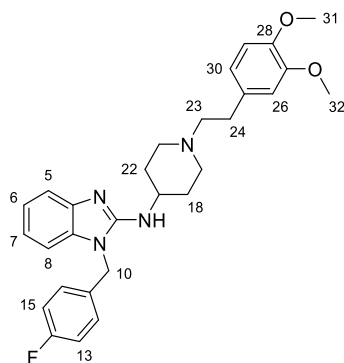
A suspension of NaH (60 % dispersion in mineral oil) (3.94 mmol, 1.2 eq, 94.46 mg) in dry DMF (2 mL) was cooled to 0 °C, and a solution of 2-chlorobenzimidazole (3.28 mmol, 1.0 eq, 500 mg) in dry DMF (2 mL) was added dropwise. The reaction mixture was stirred at 0 °C for 20 minutes. After this time, 2-iodopropane (3.94 mmol, 1.2 eq, 669 mg, 0.39 mL) was added and the system was stirred at room temperature for 6 h. Then, since there was still a large amount of residual starting material, the system was cooled to 0 °C, and 1.3 eq of NaH were added. After 20 minutes, 0.8 eq of 2-iodopropane were added and the reaction was stirred at room temperature for 3 h. The reaction was judged to be complete by TLC analysis. The reaction mixture was cooled to 0 °C, diluted by adding CH₂Cl₂ (10 mL), then quenched with water (15 mL). The product was extracted with CH₂Cl₂ (3 × 15 mL), the combined organic layers were washed with an aqueous saturated NaCl solution (2 × 5 mL), dried over Na₂SO₄, filtered and concentrated *in vacuo*. The crude was purified by silica gel chromatography eluting with *n*-hexane: ethyl acetate 2:1, to give 2-chloro-1-isopropyl-1H-benzo[d]imidazole (530 mg, 2.72 mmol, 83 %). m.p. 69-70 °C (cyclohexane); ¹H NMR (CDCl₃, 400 MHz, δ, ppm): δ_H 1.63 (6H, d, *J*= 6.4 Hz, C(11)H₃, C(12)H₃), 4.83-4.86 (1H, m, C(10)H), 7.13-7.17 (2H, m, C(6)H, C(7)H), 7.41 (1H, d, *J*= 7.6 Hz, C(8)H), 7.64 (1H, d, *J*= 7.6 Hz, C(5)H) ppm; ¹³C NMR (CDCl₃, 100 MHz, δ, ppm): δ_C 20.4 (2 C), 47.7, 111.6, 121.2, 122.8, 124.5, 136.1, 138.3, 140.8. ppm; MS (EI) *m/z* [M]⁺ calculated: 194.0611, found: 194.0607. The reported data are in good agreement with the literature.²⁹⁶

l-m, o-q Example 1: tert-butyl (1-(4-methoxyphenethyl)azepan-4-yl)carbamate (46e)



To a solution of tert-butyl azepan-4-ylcarbamate (1.14 mmol, 1.0 eq, 245.1 mg) in dry CH₃CN (4 mL) was added dry K₂CO₃ (1.482 mmol, 1.3 eq, 204.8 mg). Then, 1-(2-bromoethyl)-4-methoxybenzene (1.14 mmol, 1.0 eq, 246.0 mg) was added and the reaction mixture was stirred at 80 °C for 5 h. After this time CH₃CN was removed *in vacuo*, and the residue was dissolved in CH₂Cl₂ (5 mL). Then water (20 mL) was added. The product was extracted with CH₂Cl₂ (3 × 10 mL), the combined organic layers were washed with an aqueous saturated NaCl solution (2 × 5 mL), dried over Na₂SO₄, filtered and concentrated *in vacuo*. The crude was purified by silica gel chromatography eluting with chloroform: methanol 15:1, to give tert-butyl (1-(4-methoxyphenethyl)azepan-4-yl)carbamate (0.798 mmol, 278 mg, 70 %). m.p. - (oil); ¹H NMR (CDCl₃, 400 MHz, δ, ppm): δ_H 1.47 (9H, s, COOC(CH₃)₃), 1.62-1.97 (6H, m, C(3)H₂, C(5)H₂, C(6)H₂), 2.62-2.67 (2H, m, C(9)H₂), 2.74-2.84 (6H, m, C(2)H₂, C(7)H₂, C(8)H₂), 3.80 (3H, s, C(16)H₃), 3.80-3.85 (1H, m, C(4)H), 4.90 (1H, bs, CONH), 6.85 (2H, d, *J*= 8.6 Hz, C(12)H, C(14)H), 7.13 (2H, d, *J*= 8.6 Hz, C(11)H, C(15)H) ppm; ¹³C NMR (CDCl₃, 100 MHz, δ, ppm): δ_C 23.7, 28.4 (3C), 32.8, 34.4, 35.7, 51.8, 53.7, 54.3, 54.7, 55.6, 79.3, 113.8 (2C), 129.5 (2C), 131.9, 157.1, 157.8 ppm; MS (EI) *m/z* [M]⁺ calculated: 348.2413, found: 348.2410.

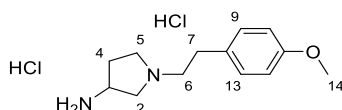
Example 2: synthesis of N-(1-(3,4-dimethoxyphenethyl)piperidin-4-yl)-1-(4-fluorobenzyl)-1H-benzo[d]imidazol-2-amine (41o)



In a flame dried round bottom flask, was prepared a solution of 1-(4-fluorobenzyl)-N-(piperidin-4-yl)-1H-benzo[d]imidazol-2-amine (0.208 mmol, 1.0 eq, 67.4 mg) in dry CH₃CN (2 mL), and dry K₂CO₃ (0.270 mmol, 1.3 eq, 37.37 mg), and 3,4-dimethoxyphenethyl bromide (0.208 mmol, 1.0 eq, 50.93 mg) were added. The system was stirred at 80 °C for 5 h. After this time, since there was still a large residue of amine, 0.2 eq of K₂CO₃, and 0.2 eq of 3,4-dimethoxyphenethyl

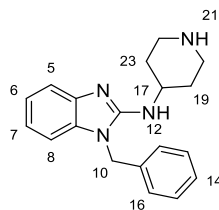
bromide were added and the reaction was heated to 100 °C for 4 h. The reaction was then stopped. The excess of K₂CO₃ was removed by filtration. The filtrate was concentrated *in vacuo* and purified by silica gel chromatography eluting with chloroform: methanol 20:1, to give 41 mg of pure compound (0.084 mmol, 40%). m.p.- (oil) ¹H NMR (CDCl₃, 400 MHz, δ, ppm): δ_H 1.51-1.98 (4H, m, C(18)H₂, C(22)H₂), 2.69-2.73 (1H, m, C(17)H), 2.80-2.94 (4H, dm, C(19)H₂, C(21)H₂), 3.02 (2H, t, *J*= 12 Hz, C(24)H₂), 3.46 (2H, d, *J*= 12.4 Hz, C(23)H₂), 3.87 (6H, s, C(31)H₃, C(32)H₃), 5.16 (2H, s, C(10)H₂), 6.75-6.83 (3H, m, C(26)H, C(29)H, C(30)H), 7.01 (3H, m, aromatic protons), 7.09-7.22 (4H, m, aromatic protons), 7.28 (1H, bs, NH), 7.63 (1H, d, *J*= 8 Hz, C(8)H) ppm; ¹³C NMR (CDCl₃, 100 MHz, δ, ppm): δ_C 31.9 (2C), 32.8, 46.2, 49.3, 51.7 (2C), 55.9 (2C), 59.4, 108.5, 111.3, 112.1, 115.6 (2C), 116.4, 119.8, 120.3, 120.6, 129.1 (2C), 131.7, 132.6, 134.5, 141.4, 147.8, 148.1, 148.9, 161.2 ppm; MS (EI) *m/z* [M]⁺ calculated: 488.2588, found: 488.2591.

General procedure for the synthesis of the intermediates 47a-e. Example: synthesis of 1-(4-methoxyphenethyl)pyrrolidin-3-amine hydrochloride



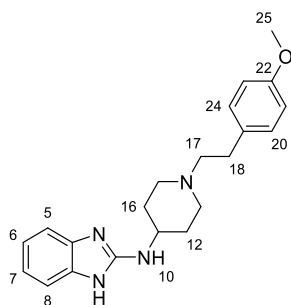
A solution of tert-butyl (1-(4-methoxyphenethyl)pyrrolidin-3-yl)carbamate (0.798 mmol, 1.0 eq, 255.7 mg) in dry THF (6 mL) was cooled to 0 °C, and a 4 N solution of HCl (7.98 mmol, 10 eq, 1.99 mL) in dioxane was added dropwise. The solution was stirred at 0 °C for 10 minutes, and then let warm to room temperature. After 6 h, 10 eq more of 4 N HCl were added and the reaction was stirred at room temperature for 6 h. After this time the reaction was complete. The volatiles were removed *in vacuo*. Diethyl ether was added to the residue, and the product precipitated, it was filtered, rinsed with diethyl ether, and dried (0.662 mmol, 194.2 mg, 83 %). m.p. 165-170 °C (toluene/acetonitrile); ¹H NMR (*d*₆DMSO, 400 MHz, δ, ppm): δ_H 1.31-1.39 (1H, m, C(4)H), 1.95-2.03 (1H, m C(4)H'), 2.07-2.13 (1H, m, C(2)H), 2.15-2.19 (1H, m, C(5)H), 2.60-2.64 (1H, m, C(2)H'), 2.67-2.71 (2H, m, C(6)H₂), 2.74 (2H, d, C(7)H₂), 2.95-3.01 (1H, m, C(5)H'), 3.27-3.35 (1H, m, C(1)H), 3.79 (3H, s, C(14)H₃), 6.7 (2H, d, *J*= 8 Hz, C(10)H, C(12)H), 7.15 (2H, d, *J*= 8 Hz, C(9)H, C(13)H) ppm; ¹³C NMR (CDCl₃, 100 MHz, δ, ppm): δ_C 31.6, 33.1, 50.6, 54.4, 54.9, 55.3, 64.2, 114.1 (2C), 129.3 (2C), 132.0, 157.6 ppm; MS (EI) *m/z* [M-HCl]⁺ calculated: 220.1576, found: 220.1577.

General procedure for the synthesis of the intermediates 48b-d, f, g and the final compounds 41a, e-k. Example 1 (method a): synthesis of 1-benzyl-N-(piperidin-4-yl)-1H-benzo[d]imidazol-2-amine (48d)



In a sealed tube, 1-benzyl-2-chloro-1H-benzo[d]imidazole (1.607 mmol, 1.0 eq, 0.390 g) and 4-aminopiperidine (2.411 mmol, 1.5 eq, 0.241 g, 0.25 mL) were dissolved in 1 mL of NMP. The reaction was heated to 175 °C for 3 h. After this time TLC analysis showed complete conversion of the starting material. The reaction was diluted with CH₂Cl₂ (5 mL), then quenched with water (5 mL). The product was extracted with CH₂Cl₂ (3 × 7 mL), the combined organic layers were washed with an aqueous saturated NaCl solution (2 × 5 mL), dried over Na₂SO₄, filtered and concentrated *in vacuo*. The crude was purified by silica gel chromatography eluting with chloroform: methanol: ammonia 15: 1: 0.1, to give the pure 1-benzyl-N-(piperidin-4-yl)-1H-benzo[d]imidazol-2-amine (0.153 g, 0.499 mmol, 31 %). m.p. 79-84 °C (cyclohexane); ¹H NMR (CDCl₃, 400 MHz, δ, ppm): δ_H 1.53 (2H, q, *J*= 12 Hz, C(19)H, C(23)H), 1.88-1.91 (2H, m, C(19)H, C(23)H), 2.87-2.89 (1H, m, C(18)H), 3.04 (2H, t, *J*= 12.4 Hz, C(20)H, C(22)H), 3.47-3.50 (2H, d, *J*= 12.4 Hz, C(20)H, C(22)H), 5.22 (2H, s, C(10)H₂), 7.03 (1H, d, *J*= 7.6 Hz, aromatic proton), 7.10 (1H, t, *J*= 7.2 Hz, C(6)H), 7.19-7.20 (3H, m, aromatic protons), 7.28-7.37 (3H, m, aromatic protons), 7.64 (1H, d, *J*= 7.2 Hz, C(8)H) ppm; ¹³C NMR (CDCl₃, 100 MHz, δ, ppm): δ_C 32.9 (2C), 46.2, 47.6 (2C), 49.7, 108.5, 116.5, 120.2, 120.7, 126.9 (2C), 127.5, 128.4 (2C), 134.6, 137.1, 141.3, 147.9 ppm; MS (EI) *m/z* [M]⁺ calculated: 306.1844, found: 306.1849.

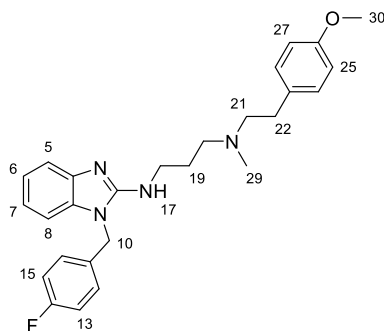
Example 2 (method a): synthesis of N-(1-(4-methoxyphenethyl)piperidin-4-yl)-1H-benzo[d]imidazol-2-amine (41a)



A sealed tube was loaded 2-chlorobenzimidazole (1.97 mmol, 1.0 eq, 300 mg) and 1-(4-methoxyphenethyl)piperidin-4-amine (2.96 mmol, 1.5 eq, 692 mg), and they were dissolved in

1.5 mL of NMP. The system was stirred at 175 °C for 3.5 h. After this time, the reaction was judged to be complete by TLC analysis. The reaction was diluted with CH₂Cl₂ (5 mL), then quenched with water (5 mL). The product was extracted with CH₂Cl₂ (3 × 7 mL), the combined organic layers were washed with an aqueous saturated NaCl solution (2 × 5 mL), dried over Na₂SO₄, filtered and concentrated *in vacuo*. The crude was purified by silica gel chromatography eluting with chloroform: methanol 10:1, to obtain 516 mg of pure compound (1.47 mmol, 75 %). m.p. 229-231 °C (acetonitrile/methanol). ¹H NMR (*d*₆-DMSO, 400 MHz, δ, ppm): δ_H 1.73-1.77 (2H, m, C(12)H, C(16)H), 2.08-2.11 (2H, m, C(12)H, C(16)H), 2.69-2.72 (2H, m, C(13)H, C(15)H), 2.87-2.90 (2H, m, C(18)H₂), 2.92-2.95 (2H, m, C(19)H₂), 3.16-3.19 (2H, m, C(13)H, C(15)H), 3.49-3.52 (1H, m, C(11)H), 3.73 (3H, s, C(25)H₃), 6.88-6.91 (4H, m, C(6)H, C(7)H, C(20)H, C(24)H), 7.00 (1H, d, *J* = 4.8 Hz, N(10)H), 7.15-7.20 (4H, m, C(5)H, C(8)H, C(21)H, C(23)H) ppm; ¹³C NMR (*d*₆-DMSO, 100 MHz, δ, ppm): δ_C 32.1 (2C), 32.9, 49.2, 51.8 (2C), 55.4, 59.1, 113.2, 113.4, 113.8 (2C), 121.5 (2C), 129.4 (2C), 131.9, 135.4, 136.0, 150.6, 157.8 ppm; MS (EI) *m/z* [M]⁺ calculated: 350.2107, found: 350.2104.

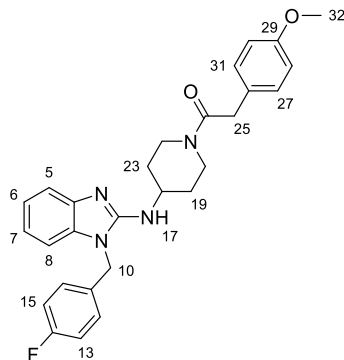
Example 3 (method b): synthesis of N1-(1-(4-fluorobenzyl)-1H-benzo[d]imidazol-2-yl)-N3-(4-methoxyphenethyl)-N3-methylpropane-1,3-diamine (41g)



In a sealed tube, 2-chloro-1-(4-fluorobenzyl)-1H-benzo[d]imidazole (0.402 mmol, 1.0 eq, 104.8 mg) was dissolved in NMP (2.6 mL), N1-(4-methoxyphenethyl)-N1-methylpropane-1,3-diamine dihydrochloride (0.603 mmol, 1.5 eq, 178.2 mg) and DIPEA (1.407 mmol, 3.5 eq, 181.8 mg, 0.24 mL) were added. The reaction was stirred at 175 °C for 6.5 h. After this time, even if there was still a small residue of starting material, the reaction was quenched with water (5 mL). The product was extracted with CH₂Cl₂ (3 × 7 mL), the combined organic layers were washed with an aqueous saturated NaCl solution (2 × 5 mL), dried over Na₂SO₄, filtered and concentrated *in vacuo*. The crude was purified by silica gel chromatography eluting with chloroform: methanol: ammonia 20:1:0.1, to obtain 35 mg of pure compound (0.078 mmol, 19 %). m.p. – (oil) ¹H NMR (CDCl₃, 400 MHz, δ, ppm): δ_H 1.87-1.91 (2H, m, C(19)H₂), 2.18 (3H, s, C(29)H₃), 2.63-2.65 (6H, m, C(20)H₂, C(21)H₂, C(22)H₂), 3.64-3.67 (5H, m, C(18)H₂, C(30)H₃), 4.84 (2H, s, C(10)H₂), 6.76-6.79 (2H, d, *J* = 8.8 Hz, C(25)H, C(27)H), 6.84-7.17 (9H, m, C(6)H, C(7)H,

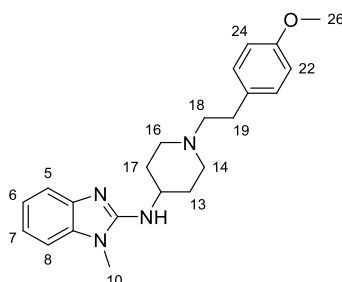
C(5)H, C(12)H, C(13)H, C(15)H, C(16)H, C(24)H, C(28)H), 7.50 (1H, d, J = 7.6 Hz, C(8)H) ppm; ^{13}C NMR (CDCl_3 , 100 MHz, δ , ppm): δ_{C} 27.1, 39.5, 42.5, 43.8, 46.2, 55.4, 55.7, 59.5, 108.4, 113.8 (2C), 115.5 (2C), 116.4, 119.9, 120.4, 129.1 (2C), 129.7 (2C), 131.8, 132.3, 134.6, 141.5, 148.7, 157.8, 162.5 ppm; MS (EI) m/z $[\text{M}]^+$ calculated: 446.2482, found: 446.2487.

Synthesis of the final compound 1-(4-((1-(4-fluorobenzyl)-1H-benzo[d]imidazol-2-yl)amino)piperidin-1-yl)-2-(4-methoxyphenyl)ethan-1-one (41n)



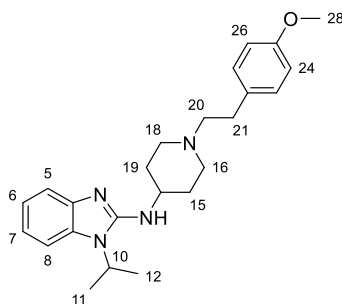
In a flame dried round bottom flask, 2-(4-methoxyphenyl)acetic acid (0.154 mmol, 1.0 eq, 26 mg) and CDI (1.85 mmol, 1.2 eq, 30 mg) were dissolved in dry THF (1 mL). The solution was stirred at room temperature for 30 minutes. After this time, the amine **48f** (1.54 mmol, 1.0 eq, 50 mg) was added. The reaction was stirred at room temperature for 5 h, when it was judged complete by TLC analysis. The organic solvent was removed *in vacuo*. The reaction was quenched with H_2O (3 mL) and the product extracted with CH_2Cl_2 (3×5 mL), the combined organic layers were washed with an aqueous 2 N HCl solution (3 mL), and an aqueous saturated NaCl solution (2×3 mL), dried over Na_2SO_4 , filtered and concentrated *in vacuo*. The extract was triturated in petroleum ether. The solid was filtered and rinsed several times with petroleum ether, then dried *in vacuo*. (54.6 mg, 0.116 mmol, 75 %). m.p. 165-168 °C (toluene/acetonitrile). ^1H NMR (CDCl_3 , 400 MHz, δ , ppm): δ_{H} 1.57-1.61 (2H, m, C(19) H_2 , C(23) H_2), 1.93-1.95 (2H, m, C(19) H_2 , C(23) H_2), 3.23-3.65 (4H, dm, C(20) H_2 , C(22) H_2), 3.52 (2H, s, C(25) H_2), 3.82 (3H, s, C(32) H_3), 4.01-4.05 (1H, m, C(18)H), 5.18 (2H, s, C(10) H_2), 6.89 (2H, d, J = 8 Hz, C(28)H, C(30)H), 7.01-7.18 (8H, m, aromatic protons), 7.26-7.28 (2H, m, C(5)H, N(17)H), 7.74 (1H, d, J = 8 Hz, C(8)H) ppm; ^{13}C NMR (CDCl_3 , 100 MHz, δ , ppm): δ_{C} 31.9 (2C), 39.2, 44.2 (2C), 46.3, 49.2, 55.3, 108.5, 113.4 (2C), 115.5 (2C), 116.3, 119.8, 120.5, 127.7, 129.1 (2C), 129.2 (2C), 131.8, 134.6, 141.3, 148.1, 158.4, 162.3, 169.01 ppm; MS (EI) m/z $[\text{M}]^+$ calculated: 472.2275, found: 472.2278.

Chemical and Physical Data, ^1H NMR, ^{13}C NMR, and MS (EI) Data for Compounds 41b-f, h-k.
N-(1-(4-Methoxyphenethyl)piperidin-4-yl)-1-methyl-1H-benzo[d]imidazol-2-amine (41b)



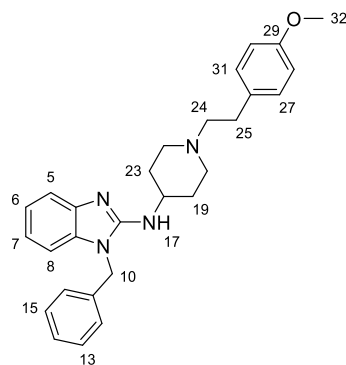
^1H NMR (CDCl_3 , 400 MHz, δ , ppm): δ_{H} 1.60-2.06 (4H, dm, C(13) H_2 , C(17) H_2), 2.72-2.75 (1H, m, C(11)H), 2.82 (2H, t, J = 7 Hz, C(22) H_2 , C(24) H_2), 2.96 (2H, t, J = 7 Hz, C(22) H_2 , C(24) H_2), 3.01-3.07 (2H, td, J = 2 Hz, 12 Hz, C(20) H_2 , C(22) H_2), 3.58-3.62 (5H, m, C(10) H_3 , C(20) H_2 , C(22) H_2), 3.81 (3H, s, C(26) H_3), 6.87 (2H, d, J = 8.4 Hz, C(22)H, C(24)H), 7.15-7.20 (5H, m, aromatic protons), 7.59-7.61 (1H, m, C(8)H) ppm; ^{13}C NMR (CDCl_3 , 100 MHz, δ , ppm): δ_{C} 28.9, 31.9 (2C), 32.7, 49.3, 51.7 (2C), 55.4, 59.0, 108.9, 113.8 (2C), 116.6, 120.7, 121.6, 129.5 (2C), 132.1, 134.7, 139.6, 152.9, 157.8 ppm; m.p. – (oil). MS (EI) m/z $[\text{M}]^+$ calculated: 364.2263, found: 364.2268.

1-Isopropyl-N-(1-(4-methoxyphenethyl)piperidin-4-yl)-1H-benzo[d]imidazol-2-amine (41c)



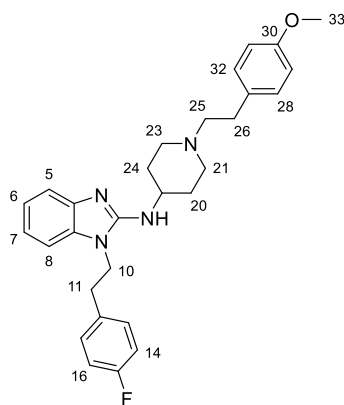
^1H NMR (CDCl_3 , 400 MHz, δ , ppm): δ_{H} 1.59 (8H, d, J = 6.4 Hz, C(11) H_3 , C(12) H_3 , C(15)H, C(19)H), 2.03 (2H, d, J = 11.2 Hz, C(15)H, C(19)H), 2.69-2.75 (1H, m, C(14)H), 2.80 (2H, t, J = 7.2 Hz, C(20)H), 2.95 (2H, t, J = 7.2 Hz, C(20)H, C(21)H), 3.03 (2H, t, J = 10.8 Hz, C(16)H, C(18)H), 3.41-3.43 (2H, m, C(16)H, C(18)H), 3.81 (3H, s, C(28) H_3), 4.62-4.66 (1H, m, C(10)H), 6.87 (2H, d, J = 8.4 Hz, C(24)H, C(26)H), 7.11-7.19 (4H, m, aromatic protons), 7.42 (1H, d, J = 7.4 Hz, C(5)H), 7.63 (1H, d, J = 7.8 Hz, C(8)H) ppm; ^{13}C NMR (CDCl_3 , 100 MHz, δ , ppm): δ_{C} 20.3 (2C), 31.9 (2C), 32.7, 46.5, 49.3, 51.8 (2C), 55.4, 59.0, 110.3, 113.8 (2C), 117.6, 121.9, 122.3, 129.5 (2C), 132.1, 134.2, 141.6, 151.2, 157.6 ppm; m.p. 93-96 °C (cyclohexane). MS (EI) m/z $[\text{M}]^+$ calculated: 329.2576, found: 329.2579.

1-Benzyl-N-(1-(4-methoxyphenethyl)piperidin-4-yl)-1H-benzo[d]imidazol-2-amine (41d)



^1H NMR (CDCl_3 , 400 MHz, δ , ppm): δ_{H} 1.53-1.56 (2H, m, C(19) H_2 , C(23) H_2), 1.93-1.96 (2H, m, C(19) H_2 , C(23) H_2), 2.66-2.71 (1H, m, C(18)H), 2.79 (2H, t, J = 6.8 Hz, C(24) H_2), 2.89 (2H, t, J = 6.8 Hz, C(24) H_2 , C(25) H_2), 2.97-3.03 (2H, m, C(20) H_2 , C(22) H_2), 3.45-3.49 (2H, m, C(20) H_2 , C(22) H_2), 3.81 (3H, s, C(32) H_3), 5.21 (2H, s, C(10)H), 6.86 (2H, d, J = 8.8 Hz, C(28)H, C(30)H), 7.02-7.22 (7H, m, aromatic protons), 7.65 (1H, d, J = 8 Hz, C(8)H) ppm; ^{13}C NMR (CDCl_3 , 100 MHz, δ , ppm): δ_{C} 31.9 (2C), 32.7, 46.2, 49.3, 51.8 (2C), 55.4, 59.1, 108.4, 113.7 (2C), 116.4, 119.8, 120.5, 126.9 (2C), 127.4, 128.5 (2C), 129.4 (2C), 132.1, 134.6, 137.1, 141.3, 148.2, 157.8 ppm; m.p. – (oil). MS (EI) m/z $[\text{M}]^+$ calculated: 440.2576, found: 440.2578.

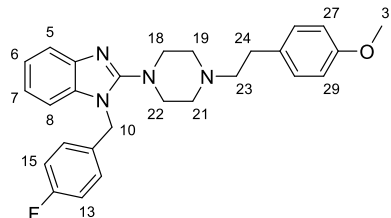
1-(4-Fluorophenethyl)-N-(1-(4-methoxyphenethyl)piperidin-4-yl)-1H-benzo[d]imidazol-2-amine (41e)



^1H NMR (CDCl_3 , 400 MHz, δ , ppm): δ_{H} 1.22-1.30 (2H, m, C(20)H, C(24)H), 1.85-1.88 (2H, m, C(20)H, C(24)H), 2.16 (2H, t, J = 10.4 Hz, C(21)H, C(23)H), 2.49-2.53 (2H, m, C(25) H_2 , C(26) H_2), 2.67-2.71 (2H, m, C(25) H_2 , C(26) H_2), 2.82-2.85 (2H, m, C(21)H, C(23)H), 2.96 (2H, t, J = 6.4 Hz, C(11) H_2), 3.10 (1H, d, J = 7.2 Hz, NH), 3.71-3.73 (4H, m, C(33) H_3 , C(19)H), 4.00 (2H, t, J = 6.4 Hz, C(10)H), 6.76 (2H, d, J = 8.8 Hz, C(29)H, C(31)H), 6.90 (4H, d, J = 7.2 Hz, C(13)H, C(17)H, C(28)H, C(32)H), 6.99-7.01 (2H, m, C(6)H, C(7)H), 7.04-7.08 (3H, m, C(5)H, C(14)H, C(16)H), 7.41 (1H, d, J = 7.6 Hz, C(8)H) ppm; ^{13}C NMR (CDCl_3 , 100 MHz, δ , ppm): δ_{C} 31.8 (2C), 32.7, 35.4, 43.6, 49.4, 51.7 (2C), 55.2, 59.1, 110.4, 113.7 (2C), 115.1 (2C), 116.5,

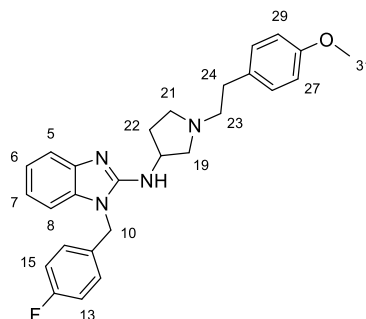
119.8, 124.1, 129.5 (2C), 130.3 (2C), 131.9, 133.3, 135.7, 141.0, 148.9, 157.8, 161.3 ppm; m.p. 147-150 °C (toluene). MS (EI) m/z $[M]^+$ calculated: 472.2638, found: 472.2633.

1-(4-Fluorobenzyl)-2-(4-(4-methoxyphenethyl)piperazin-1-yl)-1H-benzo[d]imidazole (41f)



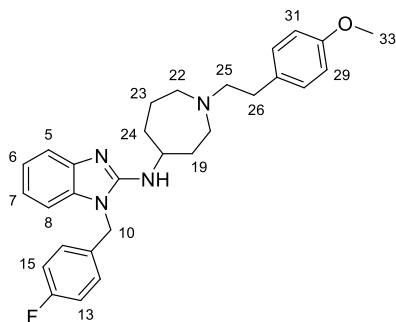
^1H NMR (CDCl_3 , 400 MHz, δ , ppm): δ_{H} 2.61-2.80 (8H, m, C(19) H_2 , C(21) H_2 , C(23) H_2 , C(24) H_2), 3.31-3.34 (4H, m, C(18) H_2 , C(22) H_2), 3.81 (3H, s, C(31) H_3), 5.21 (2H, s, C(10) H_2), 6.85 (2H, d, J = 8.8 Hz, C(27)H, C(29)H), 7.00-7.22 (9H, m, aromatic protons), 7.67 (1H, d, J = 7.6 Hz, C(8)H) ppm; ^{13}C NMR (CDCl_3 , 100 MHz, δ , ppm): δ_{C} 32.7, 46.1, 47.9 (2C), 52.4 (2C), 55.3, 59.7, 108.6, 113.6 (2C), 115.5 (2C), 116.4, 119.8, 120.5, 129.1 (2C), 129.6 (2C), 131.8, 132.1, 135.4, 141.2, 155.4, 157.7, 162.3 ppm; m.p. 140-142 °C (toluene). MS (EI) m/z $[M]^+$ calculated: 444.2325, found: 444.2322.

1-(4-fluorobenzyl)-N-(1-(4-methoxyphenethyl)pyrrolidin-3-yl)-1H-benzo[d]imidazol-2-amine (41h)



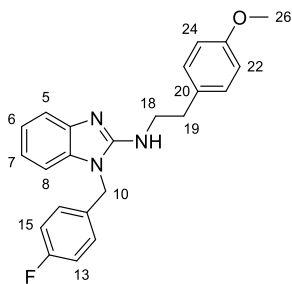
^1H NMR (CDCl_3 , 400 MHz, δ , ppm): δ_{H} 1.65-1.73 (1H, m, C(22)H), 2.24 (1H, q, J = 8.8 Hz, C(19)H), 2.37-2.45 (1H, m, C(22)H'), 2.57 (1H, dd, J = 6 Hz, 10 Hz, C(21)H), 2.56-2.76 (4H, m, C(19)H', C(21)H', C(23)H, C(24)H), 2.91 (1H, d, J = 10 Hz, C(24)H'), 2.95-2.98 (1H, m, C(23)H'), 3.80 (3H, s, C(31) H_3), 5.05 (2H, s, C(10) H_2), 6.84 (2H, d, J = 8.4 Hz, C(27)H, C(29)H), 7.01-7.05 (4H, m, C(6)H, C(7)H, C(26)H, C(30)H), 7.11-7.17 (5H, m, C(5)H, C(12)H, C(13)H, C(15)H, C(16)H), 7.54 (1H, d, J = 8 Hz, C(8)H) ppm; ^{13}C NMR (CDCl_3 , 100 MHz, δ , ppm): δ_{C} 30.9, 33.1, 46.2, 51.1, 52.7, 54.9, 55.4, 62.5, 108.4, 113.8 (2C), 115.4, 115.7, 116.4, 119.8, 120.5, 129.0, 129.2, 129.6 (2C), 131.8, 132.1, 134.5, 141.3, 148.1, 157.7, 162.1 ppm; m.p. 140-143 °C (toluene). MS (EI) m/z $[M]^+$ calculated: 444.2325, found: 444.2326.

1-(4-Fluorobenzyl)-N-(1-(4-methoxyphenethyl)azepan-4-yl)-1H-benzo[d]imidazol-2-amine (41i)



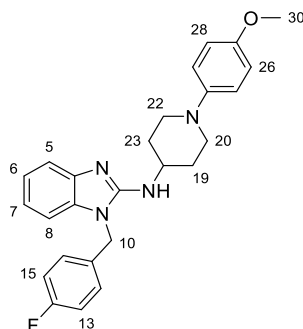
^1H NMR (CDCl_3 , 400 MHz, δ , ppm): δ_{H} 1.37 (1H, m, C(24)H), 1.51-1.79 (5H, m, C(19)H₂, C(24)H', C(25)H₂), 2.14-2.23 (2H, m, C(22)H, C(25)H), 2.38-2.53 (2H, m, C(20)H₂), 2.61 (1H, t, J = 6 Hz, C(26)H), 2.80 (1H, t, J = 6 Hz, C(26)H'), 2.83-2.95 (2H, m, C(22)H', C(25)H'), 3.19-3.23 (1H, m, C(20)H), 3.80 (3H, s, C(33)H₃), 5.75 (2H, s, C(10)H₂), 6.82 (2H, d, J = 7.6 Hz, C(29)H, C(31)H), 7.03-7.07 (4H, m, C(6)H, C(7)H, C(28)H, C(32)H), 7.11-7.17 (5H, m, C(5)H, C(12)H, C(13)H, C(15)H, C(16)H), 7.58 (1H, d, J = 8 Hz, C(8)H) ppm; ^{13}C NMR (CDCl_3 , 100 MHz, δ , ppm): δ_{C} 23.6, 32.8, 34.2, 35.9, 46.2, 51.8, 54.3 (2C), 54.7, 55.4, 108.5, 113.8 (2C), 115.4, 115.6, 116.4, 119.8, 120.4, 129.1 (2C), 129.5 (2C), 131.7, 132.1, 134.6, 141.3, 148.1, 157.8, 162.3 ppm; m.p. 96-99 °C (cyclohexane). MS (EI) m/z $[\text{M}]^+$ calculated: 472.2638, found: 472.2637.

1-(4-Fluorobenzyl)-N-(4-methoxyphenethyl)-1H-benzo[d]imidazol-2-amine (41j)



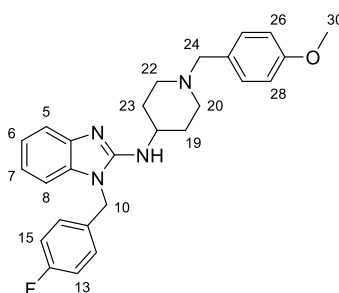
^1H NMR (CDCl_3 , 400 MHz, δ , ppm): δ_{H} 2.80 (2H, t, J = 6 Hz, C(19)H₂), 3.66 (2H, q, J = 6 Hz, C(18)H₂), 3.72 (3H, s, C(26)H₃), 4.86 (2H, s, C(10)H₂), 6.69 (2H, d, J = 8.4 Hz, C(22)H, C(24)H), 6.86-6.99 (8H, m, aromatic protons), 7.06-7.09 (1H, m, C(7)H), 7.47 (1H, d, J = 7.6 Hz, C(8)H) ppm; ^{13}C NMR (CDCl_3 , 100 MHz, δ , ppm): δ_{C} 35.2, 43.4, 46.2, 55.3, 108.5, 113.8 (2C), 115.4 (2C), 116.4, 119.8, 120.4, 128.9 (2C), 129.1 (2C), 131.6, 131.7, 134.5, 141.4, 148.6, 157.8, 162.3 ppm; m.p. 130-132 °C (cyclohexane). MS (EI) m/z $[\text{M}]^+$ calculated: 375.1747, found: 375.1744.

**1-(4-Fluorobenzyl)-N-(1-(4-methoxyphenyl)piperidin-4-yl)-1H-benzo[d]imidazol-2-amine
(41k)**



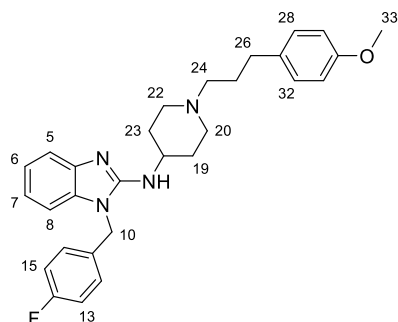
^1H NMR (CDCl_3 , 400 MHz, δ , ppm): δ_{H} 1.52-1.62 (2H, m, C(19)H, C(23)H), 2.20-2.24 (2H, m, C(20)H, C(22)H), 2.86-2.92 (2H, m, C(19)H, C(23)H), 3.35-3.39 (2H, m, C(20)H, C(22)H), 3.79 (3H, s, C(30)H₃), 3.81 (1H, d, J = 12.8 Hz, NH), 4.06-4.11 (1H, m, C(18)H), 5.10 (2H, s, C(10)H₂), 6.84 (2H, d, J = 9.2 Hz, C(26)H, C(28)H), 6.91 (2H, d, J = 9.2 Hz, C(25)H, C(29)H), 7.04-7.10 (4H, m, C(12)H, C(13)H, C(15)H, C(16)H), 7.15-7.19 (3H, m, C(5)H, C(6)H, C(7)H), 7.56 (1H, d, J = 8 Hz, C(8)H) ppm; ^{13}C NMR (CDCl_3 , 100 MHz, δ , ppm): δ_{C} 32.1 (2C), 46.3, 49.2, 50.4 (2C), 55.3, 108.4, 115.4 (2C), 115.6 (2C), 116.4, 118.9 (2C), 120.1, 120.6, 129.1 (2C), 131.7, 134.6, 141.3, 146.1, 148.2, 154.4, 162.3 ppm; m.p. 164-165 °C (toluene/acetonitrile). MS (EI) m/z $[\text{M}]^+$ calculated: 430.2169, found: 430.2173.

**1-(4-Fluorobenzyl)-N-(1-(4-methoxybenzyl)piperidin-4-yl)-1H-benzo[d]imidazol-2-amine
(41l)**



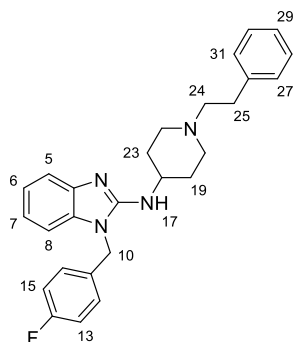
^1H NMR (CDCl_3 , 400 MHz, δ , ppm): δ_{H} 1.48-1.52 (2H, m, C(19)H, C(23)H), 1.98-2.04 (2H, m, C(19)H, C(23)H), 2.72-2.79 (1H, m, C(18)H), 3.03 (2H, t, J = 11.6 Hz, C(20)H, C(22)H), 3.47-3.51 (2H, m, C(20)H, C(22)H), 3.79 (2H, s, C(24)H₂), 3.82 (3H, s, C(30)H₃), 5.19 (2H, s, C(10)H₂), 6.89 (2H, d, J = 8.4 Hz, C(26)H, C(28)H), 7.02-7.25 (9H, m, aromatic protons), 7.65 (1H, d, J = 7.6 Hz, C(8)H) ppm; ^{13}C NMR (CDCl_3 , 100 MHz, δ , ppm): δ_{C} 31.8 (2C), 46.2, 49.3, 51.9 (2C), 55.4, 61.8, 108.5, 113.9 (2C), 115.4 (2C), 116.3, 119.8, 120.4, 124.5, 128.9 (2C), 129.7 (2C), 131.7, 134.5, 141.4, 148.1, 158.7, 162.4 ppm; m.p. - (oil). MS (EI) m/z $[\text{M}]^+$ calculated: 444.2325, found: 444.2321.

1-(4-Fluorobenzyl)-N-(1-(3-(4-methoxyphenyl)propyl)piperidin-4-yl)-1H-benzo[d]imidazol-2-amine (41m)



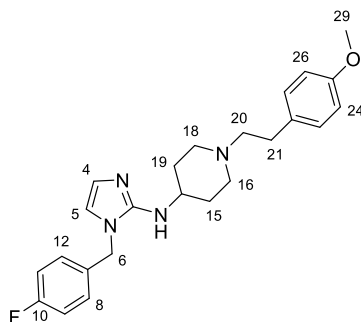
^1H NMR (CDCl_3 , 400 MHz, δ , ppm): δ_{H} 1.61-1.66 (2H, m, C(19)H, C(23)H), 1.88-1.92 (2H, m, C(19)H, C(23)H), 1.98-2.02 (2H, m, C(25)H₂), 2.63 (2H, t, J = 9.6 Hz, C(20)H, C(22)H), 2.74 (3H, m, C(18)H, C(20)H, C(22)H), 3.00 (2H, t, J = 12 Hz, C(24)H₂), 3.43-3.48 (2H, m, C(26)H), 3.77 (3H, s, C(33)H₃), 5.17 (2H, s, C(10)H₂), 6.83 (2H, d, J = 8.4 Hz, C(29)H, C(31)H), 7.01-7.05 (3H, m, aromatic protons), 7.10-7.23 (6H, m, aromatic protons), 7.65 (1H, d, J = 8 Hz, C(8)H) ppm; ^{13}C NMR (CDCl_3 , 100 MHz, δ , ppm): δ_{C} 28.7, 31.8 (2C), 33.5, 46.2, 49.3, 52.2 (2C), 55.3, 58.1, 108.4, 113.6 (2C), 115.4 (2C), 116.5, 119.9, 120.4, 128.9 (2C), 129.3 (2C), 131.7, 134.6, 136.7, 141.4, 148.1, 157.8, 162.5 ppm; m.p. 40 °C (*n*-hexane). MS (EI) m/z $[\text{M}]^+$ calculated: 472.2638, found: 472.2641.

1-(4-Fluorobenzyl)-N-(1-phenethylpiperidin-4-yl)-1H-benzo[d]imidazol-2-amine (41p).



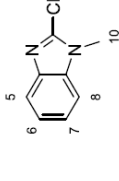
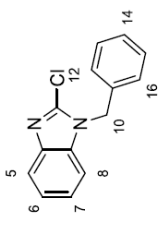
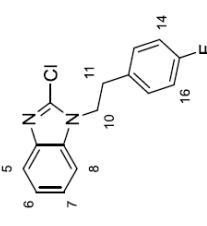
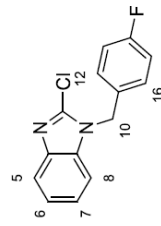
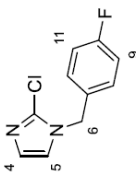
^1H NMR (CDCl_3 , 400 MHz, δ , ppm): δ_{H} 1.50-1.58 (2H, m, C(19)H₂, C(23)H₂), 1.93-1.98 (2H, m, C(19)H₂, C(23)H₂), 2.68-2.73 (1H, m, C(18)H), 2.83-2.86 (2H, m, C(24)H₂, C(25)H₂), 2.94-2.98 (2H, m, C(24)H₂, C(25)H₂), 3.02-3.05 (2H, d, J = 12.4 Hz, C(20)H₂, C(22)H₂), 3.45-3.48 (2H, d, J = 12.4 Hz, C(20)H₂, C(22)H₂), 5.16 (2H, s, C(10)H), 7.00-7.33 (12H, m, aromatic protons), 7.65 (1H, d, J = 8 Hz, C(8)H) ppm; ^{13}C NMR (CDCl_3 , 100 MHz, δ , ppm): δ_{C} 31.7 (2C), 32.5, 46.2, 49.3, 51.8 (2C), 59.6, 108.5, 115.4 (2C), 116.3, 119.7, 120.4, 126.2, 128.4 (2C), 128.7 (2C), 129.1 (2C), 131.7, 134.5, 139.0, 141.3, 148.1, 161.6 ppm; m.p. - (oil). MS (EI) m/z $[\text{M}]^+$ calculated: 428.2376, found: 428.2379.

N-(1-(4-Fluorobenzyl)-1H-imidazol-2-yl)-1-(4-methoxyphenethyl)piperidin-4-amine (41q).



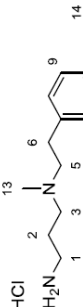
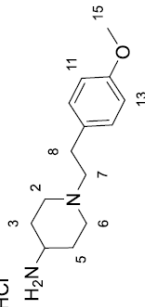
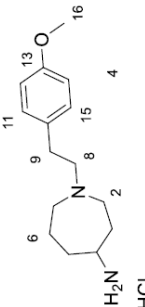
^1H NMR (CDCl_3 , 400 MHz, δ , ppm): δ_{H} 1.35-1.37 (2H, m, C(15)H, C(19)H), 1.87-1.90 (2H, m, C(15)H, C(19)H), 2.61-2.71 (1H, m, C(16)H), 2.75-2.81 (4H, m, C(16)H, C(18)H, C(21) H_2), 2.93 (2H, t, J = 7.2 Hz, C(20) H_2), 3.57-3.60 (2H, m, C(16)H, C(18)H), 3.72 (3H, s, C(29) H_3), 4.90 (2H, s C(6)H), 6.76-6.86 (6H, m, aromatic protons), 7.01 (2H, d, J = 8 Hz, C(8)H, C(12)H), 7.06 (2H, d, J = 8 Hz, C(23)H, C(27)H) ppm; ^{13}C NMR (CDCl_3 , 100 MHz, δ , ppm): δ_{C} 31.7 (2C), 32.8, 49.3, 50.4, 51.7 (2C), 55.4, 59.1, 113.7 (2C), 114.8, 115.2 (2C), 118.9, 129.4 (2C), 130.1 (2C), 132.2, 132.8, 148.5, 157.8, 162.4 ppm; m.p. 85-87 °C (cyclohexane). MS (EI) m/z $[\text{M}]^+$ calculated: 408.2325, found: 408.2324.

Table S8. Characterization data for compounds **44b-e, 45**.

cpd	Molecular structure	m.p. (°C)	Recrystallization solvent	¹ H NMR	HRMS (EI)	Ref.
44b		115-117	cyclohexane	¹ H NMR (CDCl ₃ , 400 MHz, δ, ppm): δ _H 3.79 (3H, s, C(10)H ₃), 7.27 (2H, m, C(6)H, C(7)H), 7.60 (2H, m, C(5)H, C(8)H) ppm.	Calculated: 166.0298; Found: 166.0295	296
44d		103-105	cyclohexane	¹ H NMR (CDCl ₃ , 400 MHz, δ, ppm): δ _H 5.37 (2H, s, C(10)H ₂), 7.09 (2H, d, C(12)H, C(16)H), 7.24-7.36 (6H, m, C(5)H, C(6)H, C(7)H, C(8)H, C(13)H, C(15)H), 7.52 (1H, m, C(14)H) ppm.	Calculated: 242.0611; Found: 242.0609	296
44e		75-80	<i>n</i> -hexane	¹ H NMR (CDCl ₃ , 400 MHz, δ, ppm): δ _H 3.10 (2H, t, C(11)H), 4.40 (2H, d, C(10)H), 6.95 (2H, t, C(14)H, C(16)H), 7.03 (2H, m, C(13)H, C(17)H), 7.20 (1H, m, C(8)H), 7.28 (2H, m, C(6)H, C(7)H), 7.71 (1H, d, C(5)H) ppm	Calculated: 274.0673; Found: 274.0677	-
44f		89-90	cyclohexane	¹ H NMR (CDCl ₃ , 400 MHz, δ, ppm): δ _H 5.21 (2H, s, C(10)H ₂), 7.03 (2H, m, C(13)H, C(15)H), 7.16 (2H, d, C(12)H, C(15)H), 7.32 (2H, m, C(6)H, C(7)H), 7.60 (2H, m, C(5)H, C(8)H) ppm.	Calculated: 260.0517; Found: 260.0520	297,298
45		60-62	<i>n</i> -hexane	¹ H NMR (CDCl ₃ , 400 MHz, δ, ppm): δ _H 5.09 (2H, s, C(6)H ₂), 6.89 (1H, d, C(5)H), 7.00 (1H, d, C(4)H), 7.07 (2H, t, C(9)H, C(11)H), 7.16-7.19 (2H, m, C(8)H, C(12)H) ppm.	Calculated: 210.0360; Found: 210.0355	-

cpd	Molecular structure	¹ H NMR	HRMS (EI)	Ref.
46a		¹ H NMR (CDCl ₃ , 400 MHz, δ, ppm): δH 1.45 (9H, s, COOC(CH ₃) ₃), 1.87 (2H, m, C(2)H ₂), 2.18 (3H, s, C(13)H ₃), 2.64 (6H, m, C(3)H ₂ , C(5)H ₂ , C(6)H ₂), 3.65-3.68 (5H, m, C(1)H ₃ , C(14)H ₃), 6.73 (2H, d, C(8)H, C(12)H), 7.08 (2H, d, C(9)H, C(11)H) ppm.	Calculated: 322.2256; Found: 322.2260	-
46b		¹ H NMR (CDCl ₃ , 400 MHz, δ, ppm): δH 1.47 (9H, s, COOC(CH ₃) ₃), 1.71 (1H, m, C(4)H), 2.19 (1H, m, C(4)H'), 2.23 (1H, m, C(5)H), 2.31 (1H, m, C(2)H), 2.44 (1H, m, C(6)H), 2.99 (1H, m, C(2)H'), 3.10 (1H, m, C(5)H'), 3.18 (1H, m, C(6)H'), 3.79 (3H, s, C(14)H ₃), 3.81 (1H, m, C(3)H), 4.90 (1H, d, CONH), 6.85 (2H, d, C(10)H, C(12)H), 7.13 (2H, d, C(9)H, C(13)H) ppm.	Calculated: 320.2100; Found: 320.2098	-
46c		¹ H NMR (CDCl ₃ , 400 MHz, δ, ppm): δH 1.47 (9H, s, COOC(CH ₃) ₃), 1.62-1.97 (4H, m, C(3)H ₂ , C(5)H ₂), 2.62-2.67 (2H, m, C(8)H ₂), 2.71-2.82 (6H, m, C(2)H ₂ , C(6)H ₂ , C(7)H ₂), 3.79 (3H, s, C(15)H ₃), 3.81 (1H, m, C(4)H), 4.90 (1H, d, CONH), 6.85 (2H, d, C(11)H, C(13)H), 7.13 (2H, d, C(10)H, C(14)H) ppm.	Calculated: 334.2256; Found: 334.2253	299
46e		¹ H NMR (CDCl ₃ , 400 MHz, δ, ppm): δH 1.46 (9H, s, COOC(CH ₃) ₃), 2.46 (4H, t, C(2)H ₂ , C(6)H ₂), 2.54-2.59 (2H, m, C(8)H ₂), 2.72-2.77 (2H, m, C(7)H ₂), 3.46 (4H, t, C(3)H ₂ , C(5)H ₂), 3.79 (3H, s, C(15)H ₃), 6.83 (2H, d, C(10)H, C(14)H), 7.11 (2H, d, C(11)H, C(13)H) ppm.	Calculated: 320.2100; Found: 320.2105	-

Table S9. Characterization data for compounds **47a-e**.

cpd	Molecular structure	m.p.	Recrystallization solvent	¹ H NMR	HRMS (EI)	Ref.
47a		95-100	cyclohexane	¹ H NMR (<i>d</i> ₆ DMSO, 400 MHz, δ, ppm): δ _H 1.91 (2H, m, C(2)H ₂), 2.21 (3H, s, C(13)H ₃), 2.51 (2H, t, C(3)H ₂), 2.62 (4H, m, C(1)H ₂ , C(5)H ₂), 2.73 (2H, m, C(6)H ₂), 3.79 (3H, s, C(14)H ₃), 6.78 (2H, d, C(8)H, C(12)H), 7.08 (2H, d, C(9)H, C(11)H) ppm.	Calculated: 222.1732; Found: 222.1730	300
47c		263-265	methanol	¹ H NMR (<i>d</i> ₆ DMSO, 400 MHz, δ, ppm): δ _H 1.46 (2H, m, C(3)H, C(5)H), 1.63 (2H, m, C(3)H', C(5)H'), 2.05 (2H, m, C(2)H, C(6)H), 2.74-2.81 (5H, m, C(4)H, C(7)H, C(8)H), 2.87 (2H, m, C(2)H', C(6)H'), 3.81 (3H, s, C(15)H ₃), 6.78 (2H, d, C(11)H, C(13)H), 7.11 (2H, d, C(10)H, C(14)H) ppm	Calculated: 234.1732; Found: 234.1735.	-
47d		264-265	methanol	¹ H NMR (<i>d</i> ₆ DMSO, 400 MHz, δ, ppm): δ _H 1.32 (1H, m, C(5)H), 1.45-1.59 (3H, m, C(3)H, C(5)H', C(6)H), 1.63-1.67 (2H, m, C(3)H', C(6)H'), 2.12-2.18 (2H, m, C(2)H, C(8)H), 2.40 (1H, m, C(7)H), 2.48 (1H, m, C(7)H'), 2.61 (1H, m, C(9)H), 2.74 (1H, m, C(9)H'), 2.83 (1H, m, C(8)H'), 2.87 (1H, m, C(2)H'), 3.81 (3H, s, C(16)H ₃), 6.80 (2H, d, C(12)H, C(14)H), 7.13 (2H, d, C(11)H, C(15)H) ppm	Calculated: 248.1889; Found: 248.1891.	-

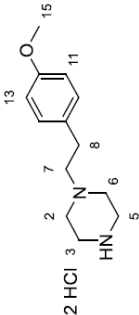
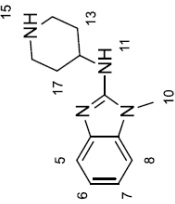
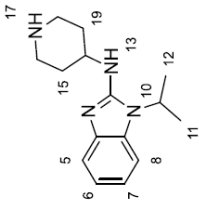
47e		257-258	methanol	¹ H NMR (<i>d</i> ₆ DMSO, 400 MHz, δ , ppm): δ_{H} 2.45 (4H, t, C(2)H ₂ , C(4)H ₂), 2.56 (2H, t, C(7)H ₂), 2.59 (4H, t, C(3)H ₂ , C(5)H ₂), 2.73 (2H, t, C(8)H ₂), 3.79 (3H, s, C(15)H ₃), 6.83 (2H, d, C(11)H, C(13)H), 7.10 (2H, d, C(10)H, C(14)H) ppm	Calculated: 220.1576; Found: 220.1574.	301
------------	---	---------	----------	---	---	-----

Table S10. Characterization data for compounds **48b-g**.

cpd	Molecular structure	m.p. (°C)	Recrystallization solvent	¹ H NMR	HRMS (EI)	Ref.
48b		154-155	toluene	¹ H NMR (CDCl ₃ , 400 MHz, δ , ppm): δ_{H} 1.61 (2H, q, C(13)H, C(17)H), 1.98 (2H, m, C(13)H, C(17)H), 2.93 (1H, m, C(12)H), 3.07 (2H, t, C(14)H, C(16)H), 3.57 (2H, m, C(14)H, C(16)H), 3.61 (3H, s, C(10)H ₃), 7.19 (3H, m, C(5)H, C(6)H, C(7)H), 7.60 (1H, d, C(8)H) ppm.	Calculated: 230.1531; Found: 230.1533	302
48c		79-80	cyclohexane	¹ H NMR (CDCl ₃ , 400 MHz, δ , ppm): δ_{H} 1.61 (8H, m, C(11)H ₃ , C(12)H ₃ , C(13)H, C(17)H), 1.99 (2H, m, C(13)H, C(17)H), 2.94 (1H, m, C(12)H), 3.06 (2H, t, C(14)H, C(16)H), 3.42 (2H, m, C(14)H, C(16)H), 4.66 (1H, m, C(10)H), 7.16 (2H, m, C(6)H, C(7)H), 7.43 (1H, d, C(5)H), 7.63 (1H, d, C(8)H) ppm.	Calculated: 258.1844; Found: 258.1842	303

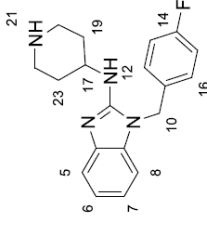
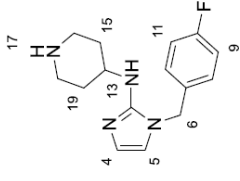
48f		90-94	cyclohexane	¹ H NMR (CDCl ₃ , 400 MHz, δ , ppm): δ_{H} 1.48 (2H, m, C(19)H, C(23)H), 1.89 (2H, m, C(19)H, C(23)H), 2.89 (1H, m, C(17)H), 3.03 (2H, td, C(20)H, C(22)H), 3.43-3.48 (2H, m, C(20)H, C(22)H), 5.17 (1H, s, C(10)H), 6.89-7.21 (7H, m, aromatic protons), 7.63 (1H, d, C(8)H) ppm.	Calculated: 324.1750; Found: 324.1754	304
48g		85-87	cyclohexane	¹ H NMR (CDCl ₃ , 400 MHz, δ , ppm): δ_{H} 1.54 (2H, m, C(15)H, C(19)H), 1.92 (2H, m, C(15)H, C(19)H), 2.56 (1H, m, C(14)H), 2.96 (2H, td, C(16)H, C(18)H), 3.15 (2H, m, C(16)H, C(18)H), 5.25 (1H, s, C(6)H), 6.86 (1H, d, C(4)H), 7.08 (2H, m, C(9)H, C(11)H), 7.11-7.15 (2H, d, C(8)H, C(12)H), 7.22 (2H, d, C(5)H) ppm.	Calculated: 274.1594; Found: 274.1597	305

Table S11. Elemental Analyses for Compounds 41a-q .									
compd	MW	calculated, %				found, %			
		C	H	N	other	C	H	N	other
41a	350.47	71.97	7.48	15.99	4.57 (O)	71.84	7.53	15.86	4.77 (O)
41b	364.49	72.50	7.74	15.37	4.39 (O)	72.63	7.81	15.32	4.24 (O)
41c	392.55	73.43	8.22	14.27	4.08 (O)	73.29	8.31	14.29	4.11 (O)
41d	440.59	76.33	7.32	12.72	3.63 (O)	76.39	7.26	12.81	3.54 (O)
41e	472.61	73.70	7.04	11.86	4.02 (F) 3.39 (O)	73.54	7.21	11.73	4.08 (F) 3.44 (O)
41f	444.55	72.95	6.58	12.60	4.27 (F) 3.60 (O)	72.88	6.46	12.74	4.23 (F) 3.69 (O)
41g	446.57	72.62	7.00	12.55	4.25 (F) 3.58 (O)	72.74	7.03	12.39	4.38 (F) 3.46 (O)
41h	444.55	72.95	6.58	12.60	4.27 (F) 3.60 (O)	73.08	6.71	12.43	4.13 (F) 3.65 (O)
41i	472.61	73.70	7.04	11.86	4.02 (F) 3.39 (O)	73.59	7.13	11.75	4.09 (F) 3.44 (O)
41j	375.45	73.58	5.91	11.19	5.06 (F) 4.26 (O)	73.39	6.02	11.10	5.00 (F) 4.49 (O)
41k	430.53	72.54	6.32	13.01	4.41 (F) 3.72 (O)	72.63	6.45	12.97	4.35 (F) 3.60 (O)
41l	444.55	72.95	6.58	12.60	4.27 (F) 3.60 (O)	72.89	6.66	12.45	4.51 (F) 3.49 (O)
41m	472.61	73.70	7.04	11.86	4.02 (F) 3.39 (O)	73.45	7.15	11.74	4.14 (F) 3.52 (O)
41n	472.56	71.17	6.19	11.86	4.02 (F) 6.77 (O)	71.24	6.32	11.73	3.89 (F) 6.82 (O)
41o	488.61	71.29	6.81	11.47	3.89 (F) 6.55 (O)	71.36	6.74	11.33	3.82 (F) 6.75 (O)
41p	428.55	75.67	6.82	13.07	4.43 (F)	75.51	6.69	13.02	4.78 (F)
41q	408.52	70.56	7.16	13.71	4.65 (F) 3.92 (O)	70.68	7.22	13.63	4.49 (F) 3.98 (O)

5 Development Of Photoaffinity Probes For BET Bromodomains

Project realized in collaboration with Prof. Stuart Conway during a visiting period in his group, Organic Chemistry Department, University of Oxford)

5.1 Activity-based protein profiling (ABPP)

After the development of the first activity-based probe (ABP) in 1961,³⁰⁶ activity-based protein profiling (ABPP) proved to be a powerful tool to study enzyme activity in complex contexts. This technique aims to selectively visualize the active forms of particular enzymes using chemical probes defined activity-based probes (ABPs), directed to the active site. Niphakis, 2014 #1719} Considering all the processes a protein can undergo, and all the different forms it can exist, this technique should be regarded as complementary to the classical methods used for protein or mRNA quantification, that could lead to misinterpretation. The applications of ABPs in time have been numerous. They have been used to identify unknown functions of known proteins, to study up- and down-regulation of catalytic activity in several diseases, to identify protein targets of certain chemical entities, to study proteins in complex biological samples (cell cultures, and living organisms),^{307,308} or to study protein-protein interactions,³⁰⁹

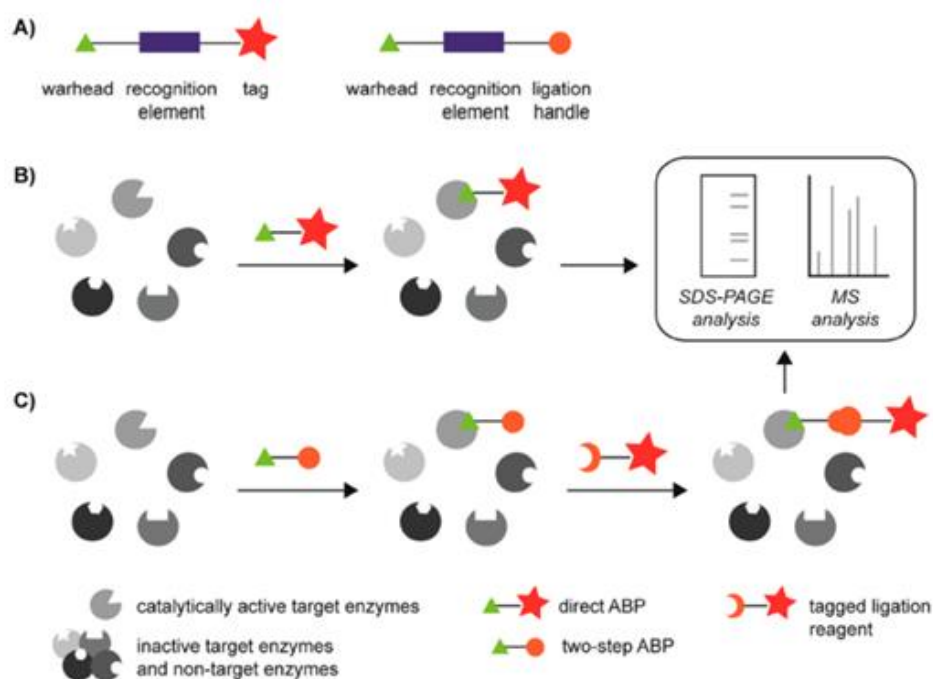


Figure 5.1. One and two step ABPs. **A)** A scheme resembling the composition of one and two step ABPs. **B)** Direct ABP labelling, and **C)** two step ABP labelling.³⁰⁷

In order to be functional, ABPs should contain three elements (Figure 5.1 A):

- a recognition element, which confers selectivity for a particular protein or protein class;
- a reactive group or “warhead”, which reacts with the target enzyme. Generally, a photoaffinity element able to react upon irradiation at a certain wavelength;

- a tag (direct ABP, Figure 5.1 B) or a ligation handle (two step ABP, Figure 5.1 C).

Different tags can be used, based on the detection techniques. Fluorescent tags enable visualization of the labeled proteins via SDS-PAGE or by fluorescence microscopy. Affinity tags (e.g. biotin), instead, are ideal for blotting detection, or pull-down experiments followed by mass spectrometry analysis. As previously mentioned, there are direct or two steps ABPs. In the direct ABPs, the tag is directly bound to the ABP (Figure 5.1 B). Instead, in the two-step labeling, the ABP is first modified with a small bio-orthogonal chemical group, that allows the modification with the tag-containing group (Figure 5.1 C). The advantage of a two-steps ABP is to have a smaller modular probe, that is less prone to unspecific interaction with the target protein, but it can be still selectively functionalized after target binding. Additionally, cell permeability of two-steps ABP is generally improved.³⁰⁷ In the design and development of ABPs one of the main challenges is the balance between selectivity and reactivity. To find a good equilibrium and have a functional probe, it is necessary to use the appropriate recognition element and reactive group.³⁰⁷

5.1.1 Photoaffinity labelling and photoreactive groups

Photoaffinity labelling (PAL) is a powerful technique used to study protein-ligand interactions. It can be useful to elucidate the unknown target of a ligand, to elucidate protein structure, function and conformational changes, as well as to identify alternative binding sites.³¹⁰ Also medicinal chemistry and drug discovery benefit of this technique.³¹¹ PAL is realized using chemical probes able to irreversibly bind a target protein, after activation by light irradiation.³¹² To do that it is necessary to incorporate in the probe a photoreactive group, which, upon irradiation at the proper wavelength, is able to form a reactive intermediate that rapidly reacts with and binds to the nearest molecule, being ideally the target protein. As nicely summarized by Smith and Collins, the ideal features of a photoaffinity probe include high degree similarity, activity, and affinity level comparable to the parent compound, stability in the dark in a range of pHs, activation at wavelengths that do not damage the biological samples. The newly formed bond should be stable in the isolation and detection conditions.³¹³ The most common photoreactive groups used for PAL are phenylazides, benzophenones and phenyldiazirines (Figure 5.2). Other used functional groups include diazo groups, diazocarbonyls, enones, sulfur radicals, halogenated substrates, nitrobenzenes, diazonium salts, and alkyl derivatives of azides and diazirines.^{314,315} Phenylazides form a reactive phenylnitrene upon loss of nitrogen (Figure 5.2 a). They are easily synthesized and commercially available.³¹² However, the use of phenylazides has many drawbacks. First of all, they need to be irradiated at high energy (250-280 nm), with the risk of damaging biological samples. The photo-crosslinking reaction with nitrenes gives not high yields, when compared with carbenes.³¹⁶ One possible reason is that

nitrenes can give side reactions, rearranging to form benzazirines and dehydroazepines/ketenimines (Figure 5.2 a).^{312,317}

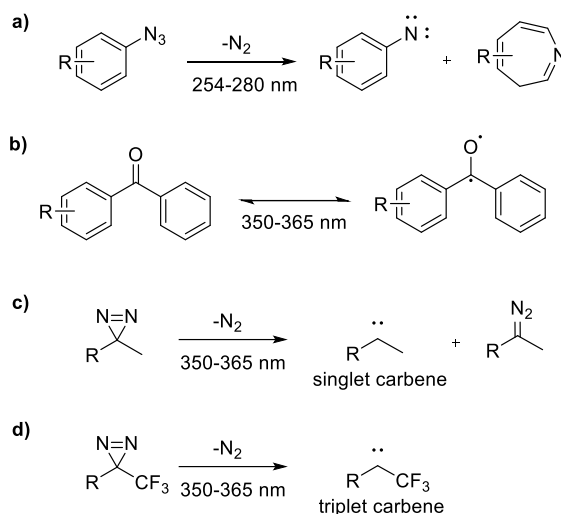


Figure 5.2. The most common photo-crosslinking group used in ABPs and their products after irradiation.

Generating the photo-reactive species upon irradiation at 350-370 nm (wavelength not dangerous for proteins), benzophenones and diazirines should be preferred as photo-reactive groups. Benzophenones form a reactive triplet diradical when irradiated with light (Figure 5.2 b). They are quite stable and easy to prepare. Nevertheless, they require long irradiation periods, that negatively affect labelling specificity.³¹⁸ Finally, the most commonly used photoaffinity group is represented by aryldiazirines, and specially the trifluoromethyl derivative, endowed with a great chemical stability. Upon irradiation, diazirines form a carbenes, that are extremely reactive and have a short half-life, which guarantees a rapid crosslink (Figure 5.2 c, d). However, due to this high reactivity, carbenes can give nonspecific binding, or they can be quenched by water, thus reducing ligation yields. Irradiation of diazirines possessing electron-donating substituents also generates diazo intermediate, that can itself form a carbene, but the process is really slow. Instead, electron-withdrawing groups favor the formation of a triplet carbene, unable to give such byproducts, for this reason the trifluoromethyl derivative is often preferred.

5.1.2 Two step ABP and ligation chemistry

In case of two step ABPs, once the protein has been crosslinked, it will be necessary to functionalize it with a proper tag. Ligation chemistry is often used to this purpose, and a number of bio-orthogonal reactions have been applied.³¹⁹ In the ligation handle ABP design, one should take in account that the ligation step should be selective, high yielding and suitable for use in aqueous solution. Click chemistry best satisfy these requirements.³²⁰ The copper-catalysed alkyne azide cycloaddition (CuAAC) developed by Sharpless *et al.* is broadly applied. Indeed,

this reaction is fast and efficient in physiological conditions, and compatible with different functional groups. Nevertheless, the copper catalyst is toxic to cells,³²¹ thus copper-free click chemistry has been developed. Bertozzi *et al.* proposed to use strain as driving force to promote alkyne-azide cycloaddition (SPAAC: strain-promoted alkyne azide cycloaddition).^{322,323} They show that cyclooctanynes and azides can react rapidly and efficiently in aqueous media, without any metal catalyst. A step forward in the optimization of SPAAC has been the insertion of a *gem*-difluoro substitution in α of the alkyne of the cyclooctyne, proved to be useful also *in vivo*.³²⁴ Other click-reaction variants have been developed in time including the strain-promoted alkyne-nitrone cycloaddition,^{325,326} and the photo-click cycloaddition.³²⁷⁻³²⁹ Additionally, the traceless Staudinger ligation, cross-metathesis reactions, Pd-catalyzed cross-coupling, Diels-Alder cycloadditions between strained alkenes/alkynes and tetrazines, 1,2-aminothiol-CBT condensations, and ketone-hydroxylamine condensation are other possible biorthogonal reactions to be applied in ligation chemistry.³¹⁹ Obviously, each of these reactions has a range of preferred conditions that could limit its application to certain experimental conditions.³¹⁹

5.2 Rationale

During the last five months of my PhD, I have been working in the laboratory of Prof. Conway in Oxford Chemistry Research Laboratory on the development of photoaffinity probes for BET bromodomains. Recently, in the Conway group have been developed photoaffinity labelling probes for BET bromodomains. Benzophenone- and diazirine-based probes have been designed based on the potent bromodomain ligand **24**.^{330,331} The synthesised probes have been validated and studied at various levels. This work is already at its second round of optimisation (Figure 5.3), and has yielded a useful second-generation modular probe (**49**).

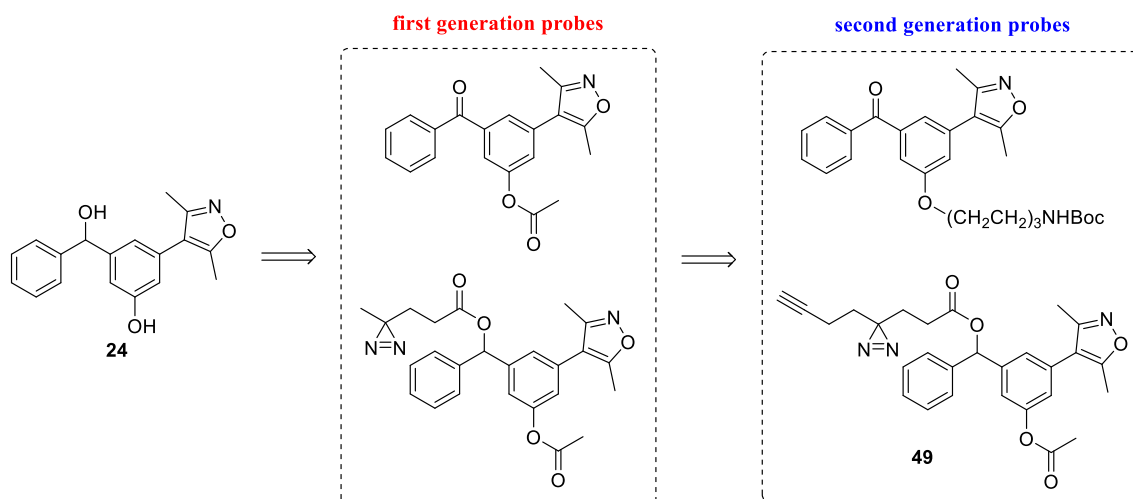


Figure 5.3. From the ligand to the probes: development of photoaffinity labelling probes for bromodomains, first and second step of optimization.

Compound **49** shows 30 % cross-linking efficiency to the BRD4(1) bromodomain and, weak, but noteworthy, binding to the bromodomains of CREBBP, WDR9(2) (a non-canonical bromodomain), and the parasitic *TcBDF3* bromodomain was detected.³³² However, cross-linking experiments on cell lysates revealed potential cellular stability issues for the probe.

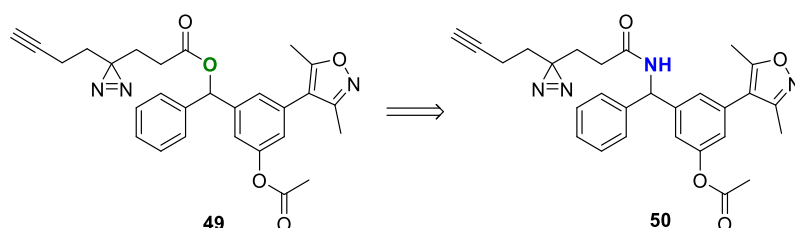


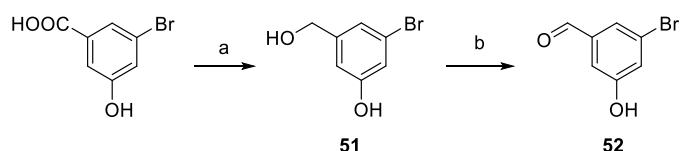
Figure 5.4. Overcoming cell lysates instability: design of a third-generation probe.

Prompted by these results, the first goal of my project was the synthesis and characterisation of a probe with an increased stability in cell lysate. Looking at the structure of compound **49** was quite immediate to identify the ester linkage between the BRD-binding core and the probe side chain as a liable bond that could be responsible of the instability of the probe in cell lysates.

Thus, in a first attempt, we thought to replace the aforementioned ester linkage with an amide one (Figure 5.4).

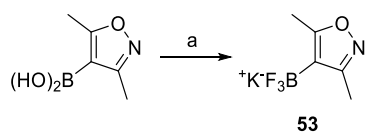
5.2.1 Synthesis of the third-generation probe

The synthesis of 3-benzoyl-5-(3,5-dimethylisoxazol-4-yl)phenyl acetate (**57**) was performed according to the literature³³¹ and following the optimisation previously reported in the group.³³² The aldehyde **52** was obtained starting from commercially available 3-bromo-5-hydroxybenzoic acid (Scheme 19).



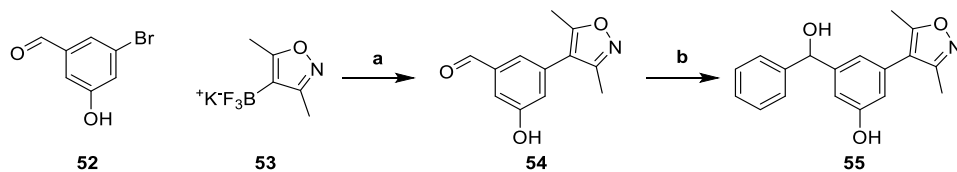
Scheme 19. Reagents and conditions: **a**) BH_3 1M in THF, dry THF, Ar, rt, 3h, (92 %); **b**) MnO_2 , CHCl_3 , 70 °C, 2h, (71 %).

The bi-substituted benzoic acid was first reduced, by using borane tetrahydrofuran complex, to the corresponding benzylic alcohol (**51**), which was then involved in a mild oxidation with manganese(IV)oxide. The oxidation was performed in chloroform under reflux as previously optimised (Scheme 19).³³²



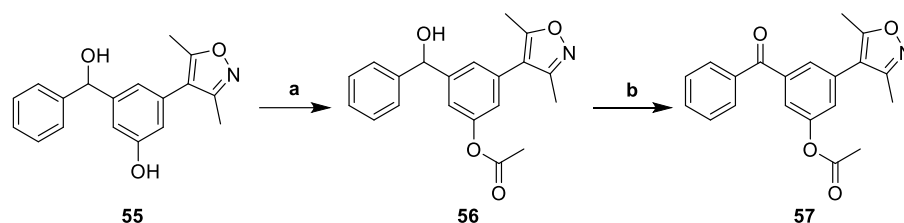
Scheme 20. Reagents and conditions: **a**) **I.** KF (aq), CH_3CN ; **II.** L-(+)-tartaric acid, THF, (73 %).

Potassium (3,5-dimethylisoxazol-4-yl)trifluoroborate (**53**) was obtained with a good yield (73 %) starting from the corresponding boronic acid, following the procedure described by Lennox and Lloyd-Jones (Scheme 20).³³³ The Suzuki coupling between **52** and **53** worked in a 83 % yield (Scheme 21). **54** was then involved in a Grignard reaction with phenylmagnesium bromide to give **55** in a good yield (85 %) (Scheme 21). Compound **55** was selectively acetylated on the phenolic hydroxyl group in presence of sodium hydroxide and acetic anhydride, yielding **56** (Scheme 22).



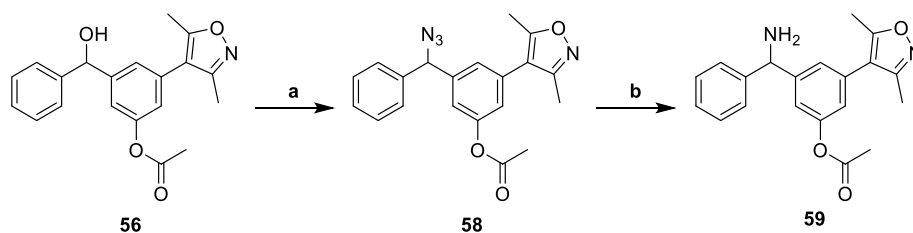
Scheme 21. Reagents and conditions: **a**) $\text{Pd}(\text{OAc})_2$, RuPhos, Na_2CO_3 , EtOH, sealed tube, 80°C, overnight (83 %); **b**) PhMgBr 1 M in THF, dry THF, Ar atm, RT, 1h, (85 %).

The oxidation of this compound to the corresponding benzophenone derivative was performed with manganese(IV)oxide applying the same conditions used for the oxidation of the alcohol **51** (Scheme 22). In this case, a larger amount of oxidising agent was required to observe complete conversion of the starting material. The reaction took longer than reported using the more powerful, but toxic reagent pyridinium chlorochromate. Considering the good yield (79 %), it would be preferable to use this less toxic alternative.



Scheme 22. Reagents and conditions: **a)** acetic anhydride, NaOH (aq), i PrOH, rt, 1h (81 %); **b)** MnO₂, CHCl₃, 70 °C, 26 h (79 %).

The synthesis of the amine **59** (a-b) proved challenging. Different strategies have been applied before finding a convenient synthetic route. A summary of the strategies applied with the relative results is provided by Table 6.



Scheme 23. Reagents and conditions: **a)** (CH₃)₃SiN₃, Cu(CF₃SO₃)₂, dry CH₂Cl₂, N₂, 0 °C to 40 °C, overnight (70 %); **b)** Ph₃P, THF/H₂O, 40 °C, overnight.

Finally, the synthesis of the azide **58** has been found to be the most convenient and high yielding approach. Compound **58** was obtained from the reaction of compound **56** with trimethylsilyl azide in presence of copper triflate in anhydrous dichloromethane at 40 °C (Scheme 23).

Subsequently, different strategies have been applied for the reduction of the azide **58** to the amine **59**. The mildest method was tried first: a Staudinger reduction in presence of triphenylphosphine and water at 40 °C. Even though the starting material was fully converted into the product without any major byproduct formation, it was found quite challenging to purify the amine **59** from the triphenylphosphin oxide byproduct. Thus, the same reaction was carried also in presence of polymer supported triphenylphosphine, but the overall reaction resulted less clean. Additionally, an hydrogenation using Pd/C (10 %) as catalyst yielded the desired product together with an over-reduced byproduct that was not possible to purify.

Finally, a classical Staudinger reduction was found the most convenient method to apply for this reduction.

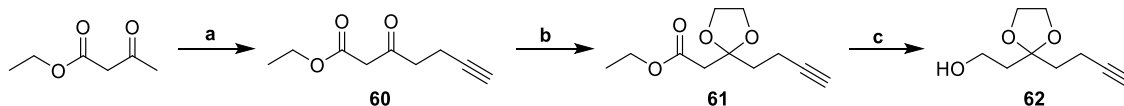
Table 6. Summary of the applied strategies for the synthesis of the amine **59** or the azide **58**. SM= starting material

SM	Reaction conditions	Result
57	I. $\text{NH}_2\text{OH} \times \text{HCl}$ (1.2 eq) CH_3COONa (2 eq), CH_3OH , reflux;	Isoxazole unstable.
	II. 25% NH_4OH , $\text{NH}_4\text{CH}_3\text{COO}$ (25 eq), Zn dust (25 eq), 70 °C, EtOH	
57	$\text{NH}_4\text{CH}_3\text{COO}$ (10 eq), $\text{NaBH}(\text{OAc})_3$ (1 eq), dry DCE, N_2 , 70 °C.	Deacetylation.
De-acetyl-57	I. $\text{Ti}(\text{OiPr})_4$ (2 eq), $\text{NH}_4\text{CH}_3\text{COO}$ (15 eq), dry THF, rt, 6 h.	The reaction did not go to completion. 11b isolated in 11% yield
	II. NaBH_4 (2 eq), rt, overnight.	
56	PPh_3 (1.5 eq), phthalimide (1.5 eq), DIAD (1.6 eq), dry THF, N_2 .	Mitsunobu product isolated 11% yield
56	a. DPPA (1.2 eq), DBU (1.2 eq), dry THF, 0 °C to RT.	SM completely consumed, but no azide formation observed.
	b. DPPA (1.2 eq), DBU (1.2 eq), dry DMF, 0 °C to 45 °C.	
56	I. $\text{CH}_3\text{SO}_2\text{Cl}$ (1.2 eq), dry Et_3N (1.5 eq), dry CH_2Cl_2 , 0 °C to RT, 1 h;	The azide product formation observed, but the reaction was very slow and did not go to completion.
	II. NaN_3 (2 eq), dry DMF, rt, 48 h.	
56	$(\text{CH}_3)_3\text{SiN}_3$ (3 eq), $\text{Cu}(\text{CF}_3\text{SO}_3)_2$ (10 % mol), dry CH_2Cl_2 , N_2 , 40 °C, overnight	58 isolated with 70% yield, a small amount of -OTMS intermediate residual even after addition of $(\text{CH}_3)_3\text{SiN}_3$ and long hours reaction.

The amine **59** proved to be unstable, thus, the extract was used in the next step without further purification. For future investigation, an alternative way to reduce the azide **58** could be an hydrogenation in presence of Lindlar catalyst.

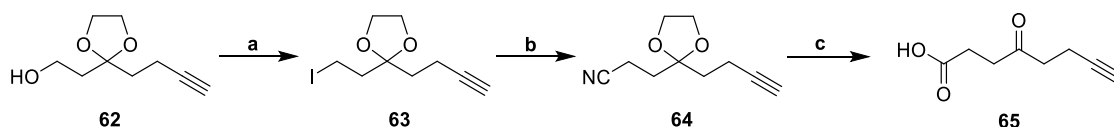
The synthesis of the diazirine cross linker was based on the procedures reported by Li *et al.*³³⁴ and the optimisation applied in the group.³³² Ethylacetoacetate underwent double lithiation with

freshly prepared lithium diisopropylamide, followed by selective C(4) alkylation with propargyl bromide to give **60**. The protected acetal derivative **61** was obtained heating **60** under reflux with ethylene glycol in presence of sub-stoichiometric amount of *para*-toluensulfonic acid in toluene, ensuring the removal of the water by a Dean-Stark apparatus (Scheme 24).



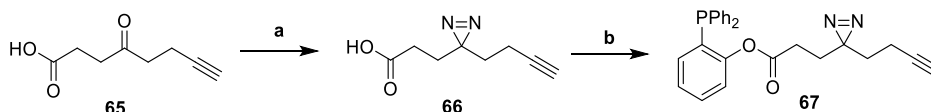
Scheme 24. Reagents and conditions: **a)** **I.** Diisopropylamine, *n*-BuLi, 30 min, -78°C , **II.** ethyl acetoacetate, -78°C - 0°C , 1 h, **III.** propargyl bromide, 1 h, 0°C , (68 %); **b)** 4-TsOH, ethylene glycol, toluene, Dean-Stark apparatus, 20 h, 130°C ; **c)** LiAlH_4 , THF, 3 h, (48% over 2 steps).

Compound **61** was then involved in a reduction with lithium aluminium hydride to give the alcohol **62** (Scheme 24). Through an Appel reaction **62** was converted into the corresponding iodo-alkane **63**, used as starting material for a nucleophilic substitution with potassium cyanide that allowed to increase the carbon chain length giving **64**. The basic hydrolysis of the nitrile, followed by an acidic acetal hydrolysis gave the carboxylic acid **65** (Scheme 25).



Scheme 25. Reagents and conditions: **a)** 1*H*-Imidazole, PPh_3 , I_2 , CH_2Cl_2 , 40°C , 1 h (88 %); **b)** KCN, DMF, 70°C , 3 h (83 %); **c)** **I.** 10 % NaOH (aq.), 1 h, 100°C ; **II.** 2 M HCl (aq) adjusted pH to 1, 15 h, rt (75 %).

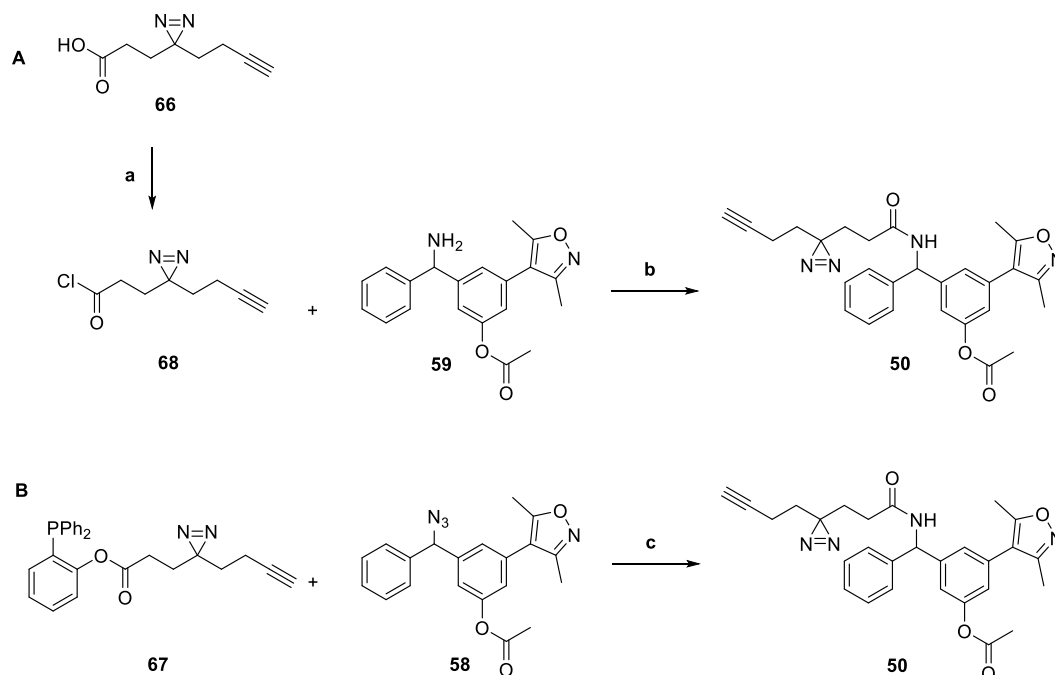
The diazirine derivative **66** was synthesised by applying the conditions reported in the literature.³³⁵ The diphenylphosphanyl-phenyl ester **67** was obtained from the esterification of the acyl chloride of the carboxylic acid **66** with *o*-diphenylphosphinophenol (Scheme 26).³³⁶



Scheme 26. Reagents and conditions: **a)** **I.** 7N NH_3 in MeOH, overnight, 0°C to rt, **II.** $\text{H}_2\text{N-OSO}_3\text{H}$, dry MeOH, -40°C to 0°C , **III.** I_2 , Et_3N , Et_2O , 0°C , 1 h (23 %); **b)** **I.** SOCl_2 , 40°C , 30 min, **II.** dry Et_3N , *o*-diphenylphosphinophenol, dry CH_2Cl_2 , Ar, rt (45 % over two steps).

The final compound **50** was first synthesized through a coupling of the amine **59** with acyl chloride **68**, freshly prepared from the acid **66** (Scheme 27A). This classical way gave compound **50** with a 38 % yield. Additionally, once we had proved that the azido-intermediate **58** was reduced in the Staudinger conditions in presence of triphenylphosphine, we found it

convenient and interesting to investigate the traceless Staudinger ligation conditions to get compound **50**.



Scheme 27. Reagents and conditions: **a**) SOCl_2 , 40 °C, 30 min; **b**) dryEt_3N , $\text{dryCH}_2\text{Cl}_2$, 0 °C to rt, 1 h (38 % over two steps) ; **c**) **1**. dry DMF, **2**. H_2O .

For this purpose, the azide **58** was reacted with the diphenylphospanyl-phenyl ester **67** (Scheme 27B). In these conditions we were able to obtain the final compound. This strategy was considered particularly attractive to skip one synthetic step and avoid isolating the amine intermediate which is difficult to purify and unstable. Moreover, to the best of our knowledge, this is the first time that this reaction is applied for the synthesis of such kind of small molecules. Nonetheless, further optimisation of the traceless Staudinger ligation is ongoing.

5.2.2 BRD(4)1 affinity of compound 50

(Larissa See and Amy Scolah, Group of Prof. Stuart Conway, CRL, Oxford)

Before proceeding with compound **50** testing in crosslinking experiments, we confirmed its ability to bind the target BRD4(1) in Alpha Screen assay. The compound have been tested in triplicate in presence of BRD4(1) and the H4(KAc)₄ peptide as competitor.

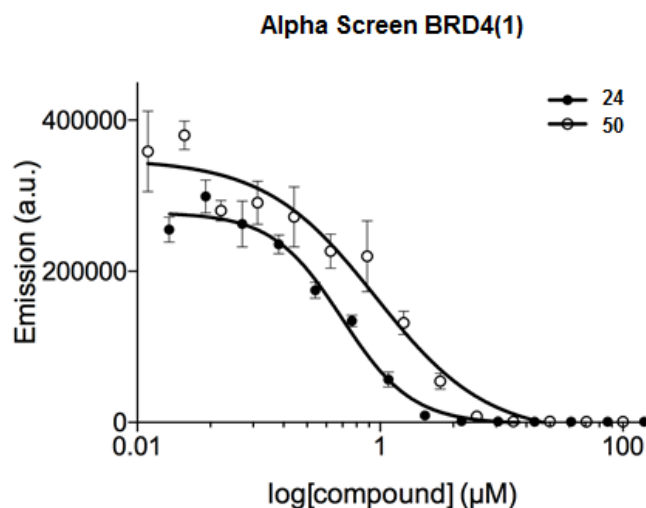


Figure 5.5. BRD4(1) Alpha Screen for compounds **24** and **50**. Data were fitted using Prism software, using the four-parameter sigmoidal log[inhibitor] vs response equation.

Table 7. BRD4(1) Alpha Screen IC₅₀ values for compounds **24**, **49**, and **50**. In brackets are reported 95 % confidence intervals. *result obtained in an independent experiment performed in the same conditions.³³²

Cpd	Molecular structure	IC ₅₀ on BRD4(1)
24		0.48 μM (0.38-0.61)
49		0.91 μM (0.62-1.24)*
50		0.92 μM (0.51-1.66)

Compound **50** have been tested at the highest concentration of 100 μM, and 1:2 serial dilutions have been done for a total of 14 points. The known BRD4 ligand **24** has been used as positive control. The obtained results are recapitulated in Figure 5.5 and Table 7. The Alpha Screen data

show that compound **50** retained the IC₅₀ value of its close analogue **49**.³³² In light of these data, we proceeded with compound **50** testing.

5.2.3 Photo crosslinking experiments with compound **50**

UV/VIS spectra of compound **50** were recorded in triplicates scanning in a range between 150 and 600 nm. However, a characteristic absorption was observed only between 250 and 450 nm (Figure 5.6). At least three main transitions can be appreciated. Around 360 nm the n to π^* transition of the diazirine is observed. The molar extinction coefficient at 360 nm is 60 M⁻¹ cm⁻¹, in agreement with literature data for aliphatic diazirines.³³⁷

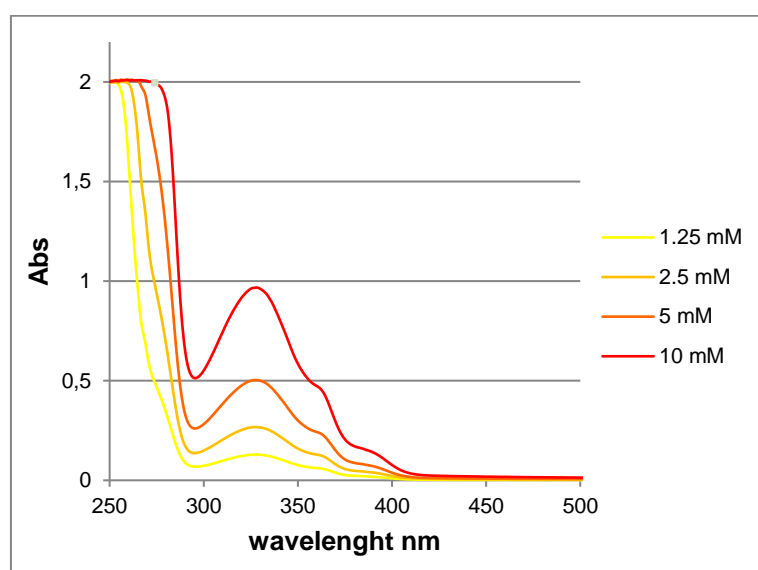


Figure 5.6. UV/VIS spectra of 10 mM, 5 mM, 2.5 mM, and 1.25 mM solutions of **50** in MeOH.

Crosslinking experiments between the diazirine **50** and purified BRD4(1) bromodomain were performed by irradiating the samples in a photoreactor at 350 nm, to selectively activate the diazirine. The samples were first analyzed by protein LC-MS. Incubation of purified BRD4(1) with the probe **50** in absence of UV irradiation did not result in any crosslinking (Figure 5.7 c). However, already after 2 min irradiation the crosslinking reaction occurred with about 20 % efficiency (Figure 5.7 d). Time course experiments showed an irradiation time dependent increase of crosslinking efficiency (CE), reaching a maximum of about 50 %. Interestingly, long irradiation time did not improve the CE, and artifacts were observed. Finally, we concluded that the best compromise in terms of incubation time, was 20 minutes. Pleasingly, the crosslinking efficiency was superior to the previous probe. Moreover, an optimization of the irradiation conditions was achieved running the photo-crosslinking reaction in 3 mm NMR tubes, rather than in glass vials. In this way the exposed surface was maximized and a better CE was observed. A competition experiment confirmed the selective binding in the KAc binding site of the probe **50**, since no crosslinking was observed in presence of 10 equivalents of known BRD4 ligands **21** or **24** (Figure 5.7 g-h; see Figure 1.10 for molecular structures).

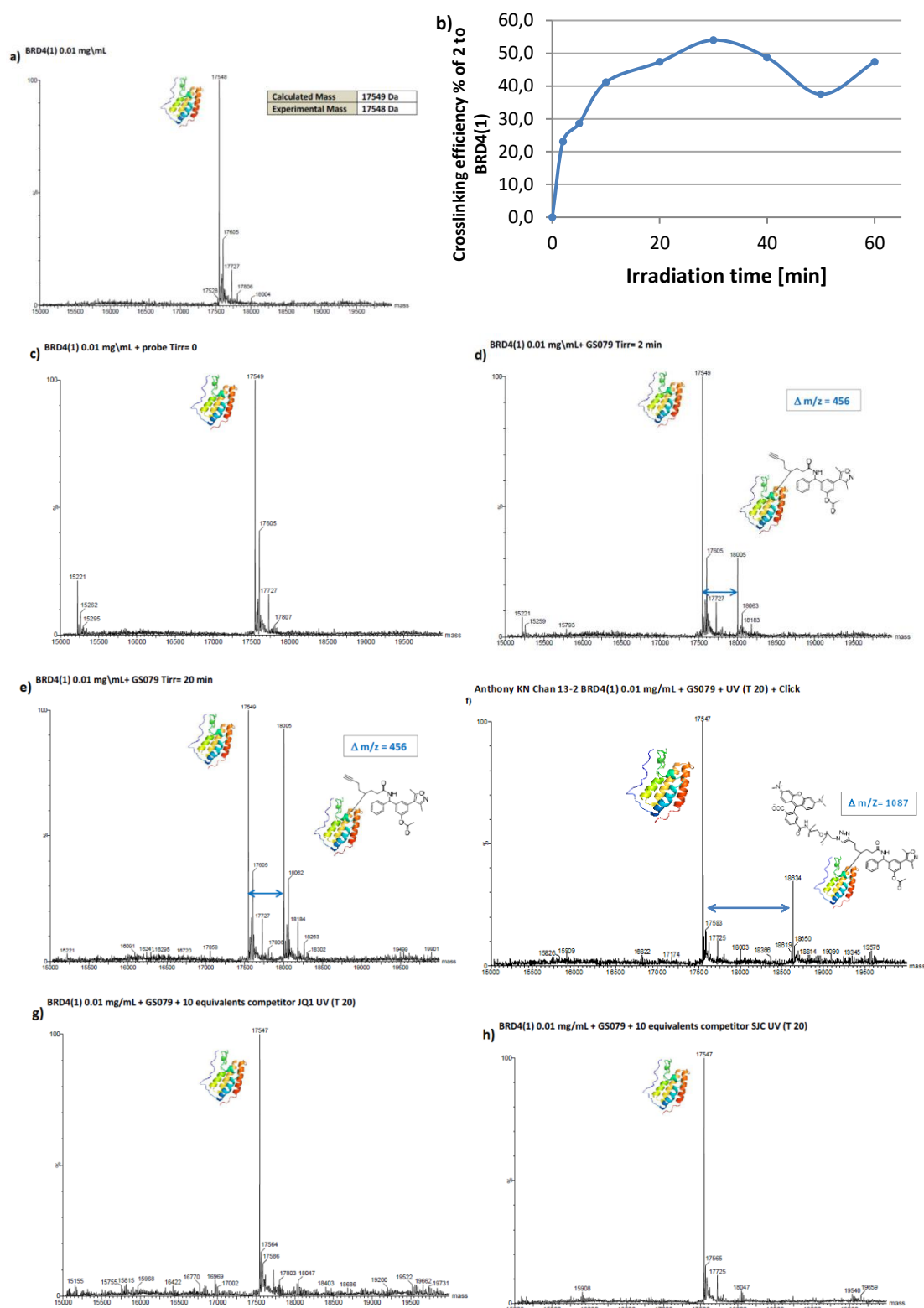


Figure 5.7. (a) Deconvoluted protein mass spectrum of the BRD4(1) bromodomain; (b) Time course of the crosslinking efficiency of the probe **50** to BRD4(1) bromodomain; Deconvoluted protein mass spectrum of (c) BRD4(1) incubated with diazirine probe **50** without UV irradiation; (d) with 2 min UV irradiation (e) with 20 min UV irradiation. (f) CuAAC between the cross linked protein and TAMRA-PEG3 azide. (g) Competition experiment with 10 eq of **21** and 20 min UV irradiation. (h) Competition experiment with 10 eq of **24** and 20 min UV irradiation.

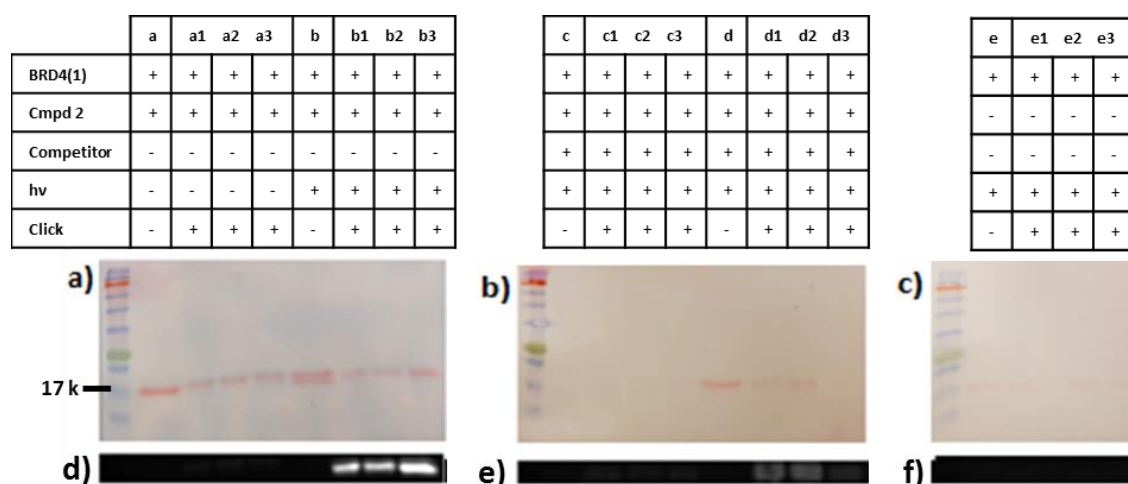


Figure 5.8. SDS-PAGE gel of purified BRD4(1) bromodomain crosslinked with probe **50** (for each condition the experiment was performed in triplicates). a), b) and c) The membrane was visualized with Ponceau stain. d), e), f) Fluorescence (Ex 532 nm, Em: 605 nm) visualization.



Figure 5.9. SDS-PAGE gel of purified BRD4(1) bromodomain crosslinked with probe **50** (for each condition the experiment was performed in triplicates). a), b) and c) The membrane was visualized through fluorescence (Ex 532 nm, Em: 605 nm). The relative fluorescence intensity is reported below, and it was determined with Image J software.

In further investigations, the crosslinked protein was reacted in a copper catalysed alkyne azide cyclisation (CuAAC) with TAMRA-PEG-azide (Figure 5.7 f). The click chemistry was performed using copper sulphate, the reducing agent tris(2-carboxyethyl)phosphine (TCEP) and the ligand tris[(1-benzyl-1H-1,2,3-triazol-4-yl)methyl]amine (TBTA).³³⁸ One hour incubation at room temperature was sufficient to show the mass corresponding to the TAMRA labelled BRD4(1) bromodomain (Figure 5.7 f). This experiment demonstrates a functional *in vitro* probe, which is able to crosslink to BRD4(1) bromodomain, and subsequently the linker can be modified by using CuAAC chemistry to attach not only a fluorophore as TAMRA, but also other linkers, useful for further experiments. The TAMRA-labelled BRD4(1) bromodomain protein was also visualized on a PVDF (polyvinylidene difluoride) membrane through fluorescence (Ex 532 nm, Em: 605 nm). An intense band on lane B1-3 confirmed the CuAAC chemistry worked with TAMRA-PEG-azide (Figure 5.8 d). The negative controls in lane C 1-3 (competitor **24**) and D 1-3 (competitor **21**) show very faint bands, indicating the probe might have slightly crosslinked, despite the competition (Figure 5.8 e). It is worth to remark that **21** proved poorly soluble in the assay conditions, thus the crosslinking observed in this case could be due to an effective competitor concentration lower than what expected. Noteworthy, the crosslinking observed in the competition experiment with the more soluble compound **24** is comparable with that observed with the non-irradiated samples (Figure 5.9 a-c). The poor chemical-physical

properties of **21** could explain also the higher internal variability between the triplicates (Figure 5.9 a-c). Additionally, the BSA control showed crosslinking. Considering the unspecific mechanism of the photo-catalyzed reaction, this is not surprising. However, in the next future could be interesting to perform competition experiments with BRD4 inhibitors in presence of BSA, as well as a photo-crosslinking reaction in presence of both BRD(4)1 and BSA. Taken together, the data obtained with the competition experiment and the BSA-control experiment, suggest that an optimization of the conditions of the experiment, and in detail of the probe concentration, is required. It could be particularly useful to repeat the crosslinking reaction in presence of a dose- range of the probe. This experiment will allow to identify the lowest effective concentration of the probe, aimed also to gain selectivity.

5.3 Conclusions and perspectives

This project yielded the validation of a synthetic route to obtain compound **50**, as well as its synthesis and characterisation. The probe has been already tested and proved to be efficient in preliminary *in vitro* enzymatic assays. To the best of our knowledge, for the first time in this study the traceless Staudinger ligation was proved to be an attractive strategy also in the synthesis of such kind of small molecules. This synthetic route allowed us to skip one step and, noteworthy, to prepare the amine **59**, not easy to purify and unstable. Nonetheless, additional experiments are ongoing, aimed to better investigate and optimize the conditions for the traceless Staudinger ligation.

Preliminary biochemical *in vitro* experiments showed that the probe **50** is efficiently crosslinked to BRD4(1) only after UV-irradiation. The CE is increasing in a time dependent way, but the most convenient irradiation time has been judged to be 20 minutes (CE 47 %). To prove the selective binding in the KAc binding site of the probe **50**, a competition experiment in presence of 10 equivalents of the known BRD4 ligands **21** or **24** (Figure 1.10) was performed. While from LC-MS no crosslinked protein was detected, after click reaction a small amount of the crosslinked protein was visualized by fluorescence detection, revealing that the probe might have slightly crosslinked. It is worth to remark that **21** proved poorly soluble in the assay conditions, thus the crosslinking observed in this case could be due to an effective competitor concentration lower than what expected. Noteworthy, the crosslinking observed in the competition experiment with the more soluble compound **49** is comparable with that observed with the non-irradiated samples. Interestingly, in the photoreaction conditions the probe **50** was able to crosslink also to BSA. Those evidences suggest that for further investigations may be worth to optimize the probe concentration in the crosslinking reaction mixture. The low specificity could be due to the high concentration with respect to the target protein. Once the assay conditions will be optimized, the probe selectivity will be assessed in cross linking experiments with several human and parasitic bromodomains. Finally, the validated probe will be tested in cross-linking and pull-down experiments on cell lysates, after confirming its stability in the assay conditions. This experiment will be performed using cell lysates derived from cells expressing/overexpressing BRD4(1). In these more complex media, the selectivity of the probe over other bromodomains, as well as other different cellular targets will be evaluated. The results obtained will be essential for further development of photoaffinity probes for bromodomains, thus providing new tools for a better understanding of the role of bromodomains, not only in humans, but also in parasites. Figure 5.9 resembles some of the possible future chemical manipulations to be applied in the design of novel photoaffinity probes. Considering the comparable potency of the BRD4(1) ligands **69** and **70** (Figure 5.10), the probes could be evaluated either in the acetylated form on the phenolic-OH, or containing the

free -OH. (Figure 5.9). This aspect could be interesting especially in terms of chemical-physical properties of the probes.

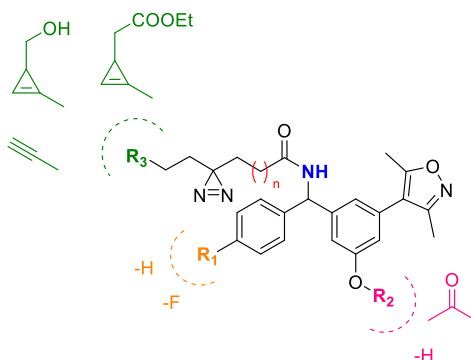


Figure 5.9. Probing the probe: future perspectives.

Hewings *et al.* demonstrated that a fluorine is tolerated in the *meta* or *para* position of the bromodomain ligand **71** (Figure 5.10),^{330,331} therefore fluorine-substituted probes should be considered as well. According to Hewings *et al.*, the fluorine substituted derivatives display a similar activity against BRD4(1), but the *para* fluoro substituted compound is more selective for BRD4(1) over CREBBP.³³¹ Thus, could be interesting to evaluate first the *para*-fluoro substitution (Figure 5.10).

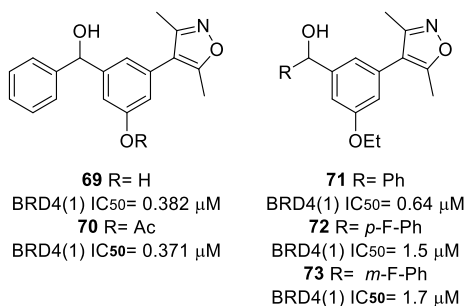


Figure 5.10. 3,5-dimethylisoxazole BRD4(1) ligands. IC₅₀ values obtained in an ALPHA assay.

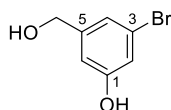
Moreover, it could be worth evaluating the effect of different lengths of the probe side chain on potency and selectivity (Figure 5.9). Finally, different copper-free click tags could be applied. For example, Li *et al.* have described the use of cyclopropane-containing copper-free clickable photo-crosslinkers, useful for protein labelling, as well as imaging in live cells.³³⁹ Hence, a different series of clickable cyclopropane-containing probes could be evaluated (Figure 5.9).

5.4 Experimental section

5.4.1 Chemistry

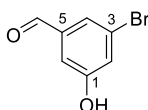
All dry reactions were carried out using standard techniques under an argon or nitrogen atmosphere with flame-dried glassware. Anhydrous solvents were purchased from Sigma Aldrich. Commercially available diisopropylamine (DIPA) was purified according to the standard procedure (refluxed on KOH for 3 hours and then distilled). All the other commercially available reagents were used as supplied without further purification. Petroleum ether refers to the fraction boiling at 40–60 °C. Analytical thin-layer chromatography (TLC) analysis was carried out on Merck silica gel 60 F254 pre-coated aluminium-backed plates and visualised by UV light ($\lambda_{\text{max}} = 254 \text{ nm}$) and stained with aqueous basic potassium permanganate solution or ninhydrin solution. Flash column chromatography was carried out on silica gel (60 Å, 240–400 mesh) under positive pressure of nitrogen. ^1H NMR spectra were recorded on a Bruker AVIII HD 400 (400 MHz) spectrometer or Bruker AVII 500 (500 MHz) spectrometer in CDCl_3 (unless otherwise stated). Chemical shifts δ are quoted in parts per million (ppm) relative to tetramethylsilane ($\delta = 0.00 \text{ ppm}$), to the nearest 0.01 ppm. ^1H NMR spectra is reported as follows: chemical shift (number of protons, multiplicity (s = singlet, d = doublet, t = triplet, q = quartet, m = multiplet, br = broadened), coupling constant J (to the nearest 0.1 Hz), assignment). Residual protic solvent was used as the internal reference: CHCl_3 ($\delta_{\text{H}} = 7.26 \text{ ppm}$). ^{13}C NMR spectra were recorded on Bruker AVIII HD 400 (101 MHz) spectrometer or Bruker AVII 500 (126 MHz) spectrometer in CDCl_3 (unless otherwise stated). Chemical shifts δ are quoted in parts per million (ppm) relative to tetramethylsilane ($\delta = 0.00 \text{ ppm}$), to the nearest 0.1 ppm. The multiplicity of each signal is singlet unless otherwise stated. Residual protic solvent was used as the internal reference: CHCl_3 ($\delta_{\text{C}} = 77.2 \text{ ppm}$). NMR data was processed using Mestrenova 11.0 software. Spectra were assigned using HSQC and HMBC experiments as necessary. Electrospray ionisation mass spectra were obtained using an Agilent 6120 spectrometer for low resolution or Bruker MicroTOF spectrometer for high resolution, where m/z values are reported in Daltons. Infrared spectra were recorded from neat samples on a Bruker Tensor 27 spectrometer with a diamond ATR Spectrometer. Absorption maxima (ν_{max}) are reported in wavenumbers (cm^{-1}) where s = strong, m = medium, w = weak, br = broad. Melting points were obtained using a Gallenkamp MF-370 capillary tube melting point apparatus and are uncorrected. Analytical high-performance liquid chromatography (HPLC) was performed on a PerkinElmer Flexar system with a Binary LC Pump and UV/VIS LC Detector set at 254 nm. For determination of purity, a Dionex Acclaim® 120 C18 column [$5 \mu\text{m}$, 12 Å , $150 \text{ mm} \times 4.6 \text{ mm}$] reverse phase column was used with a constant flow rate of 1.5 mL min^{-1} and gradient method of 10 min from 95:5 H_2O :acetonitrile to 5:95 H_2O :acetonitrile with a 5 min hold. Samples injected were prepared by dissolving in methanol or acetonitrile and filtered.

Synthesis of 3-bromo-5-(hydroxymethyl)phenol (**51**)



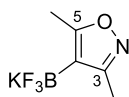
A solution of 3-bromo-5-hydroxybenzoic acid (0.100 g, 0.461 mmol, 1.0 eq) in dry THF (4 mL) was cooled to 0 °C. BH_3 in THF (1 M, 1.38 mL, 1.38 mmol, 3.0 eq) was added dropwise over a period of 30 minutes. After the addition was complete the reaction solution was warmed to room temperature and stirred for 5 h after which time TLC analysis indicated complete consumption of the starting material. The solution was cooled to 0 °C and quenched with a 2 M aqueous solution of HCl (0.7 mL). The solvent was removed *in vacuo*. The residue was suspended in H_2O (5 mL) and extracted with EtOAc (3×5 mL). The combined organic layers were washed with saturated aqueous solution of NaHCO_3 (2×5 mL), and brine (5 mL), dried over MgSO_4 , filtered, and concentrated *in vacuo*. The residue was purified by silica gel chromatography, eluting with ethyl acetate: petroleum ether 1:2, to afford **3** as a colourless solid (0.0825 g, 0.406 mmol, 88.1 %): Rf: 0.15 (petroleum ether: EtOAc 2:1); mp 85-90 °C (EtOAc); ^1H NMR (400 MHz, $(\text{CD}_3)_2\text{SO}$) δ_{H} : 9.83 (1H, br. s, C(1)OH), 6.91 (1H, m, C(6)H), 6.79 (1H, dd, J 2.1, 2.1, C(2)H), 6.72 (1H, m, C(4)H), 5.26 (1H, br. s, CH_2OH), 4.40 (2H, d, J 4.0 CH_2OH); LRMS m/z (ES-) 201 ($[\text{M}^{79}\text{Br}-\text{H}]^-$, 100%), 203 ($[\text{M}^{81}\text{Br}-\text{H}]^-$, 93.68%). These data are in good agreement with the literature.³³¹

Synthesis of 3-Bromo-5-hydroxybenzaldehyde (**52**)



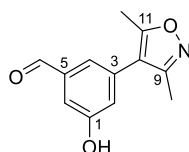
To a solution of 3-bromo-5-(hydroxymethyl)phenol **51** (1.78 g, 8.77 mmol, 1.0 eq) in CHCl_3 (15 mL) activated MnO_2 (5.34 g, 61.37 mmol, 7 eq) was added. The reaction mixture was heated under reflux for 3 h after which time the reaction was judged to be complete by TLC analysis. The suspension was cooled to room temperature, then filtered through Celite®, and concentrated *in vacuo*. The residue was purified by silica gel chromatography, eluting with ethyl acetate: petroleum ether 1:3, to afford **52** as a yellow solid (1.39 g, 6.91 mmol, 79 %): Rf: 0.26 (petroleum ether: EtOAc 3:1); mp 138-140 °C (CHCl_3); ^1H NMR (400 MHz, $(\text{CD}_3)_2\text{SO}$) δ_{H} 10.48 (1H, s, CHO), 9.88 (1H, s, C(1)OH), 7.52 (1H, dd, J 1.4, 1.4, C(2')H), 7.27-7.25 (2H, m, C(4')H and C(6')H); LRMS m/z (ES-) 198.9 ($[\text{M}^{79}\text{Br}-\text{H}]^-$, 82.6%), 200.9 ($[\text{M}^{81}\text{Br}-\text{H}]^-$, 78.3%). These data are in accordance with the literature.³³¹

Synthesis of potassium (3,5-dimethylisoxazol-4-yl)trifluoroborate (**53**)



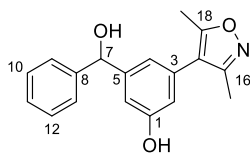
To a suspension of (3,5-dimethylisoxazol-4-yl)boronic acid (2.5 g, 17.74 mmol, 1.0 eq) in CH₃CN (15 mL), were added 7 mL of a 10 M aqueous solution of KF (4.12 g, 70.96 mmol, 4.0 eq). The reaction mixture was stirred at room temperature until complete dissolution of the boronic acid. A solution of *L*-(+)-tartaric acid (5.46 g, 36.37 mmol, 2.05 eq) in THF (27 mL) was added dropwise to the reaction mixture over a period of 10 minutes. A colourless precipitate formed instantly. The suspension was stirred at room temperature for 20 minutes. After this time the reaction mixture was filtered. The filter cake was rinsed several times with CH₃CN, the combined filtrates were concentrated *in vacuo* to give **53** as a colourless solid (2.62 g, 12.9 mmol, 73 %). Rf: 0.10 (petroleum ether: Et₂O 1:1); mp >300 °C (acetone) [Lit:59 > 200 °C]; ¹H NMR (400 MHz, (CD₃)₂SO) δ_H: 2.20 (3H, s, C(3)CH₃), 2.05 (3H, s, C(5)CH₃); ¹⁹F NMR (376 MHz, (CD₃)₂SO) δ_F: -134.20, -134.96 (3F, m); LRMS m/z (ES-) 164.1 ([M-K]⁻ 100 %). These data are in accordance with the literature.³³¹

Synthesis of 3-(3,5-dimethylisoxazol-4-yl)-5-hydroxybenzaldehyde (**54**)



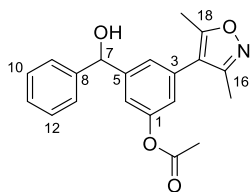
In a flame dried Schlenk tube, 3-bromo-5-hydroxybenzaldehyde **52** (1.00 g, 4.98 mmol, 1.0 eq) was solubilized in degassed EtOH (15 mL). Potassium (3,5-dimethylisoxazol-4-yl)trifluoroborate **53** (1.11 g, 5.47 mmol, 1.1 eq), Pd(OAc)₂ (0.067 g, 0.29 mmol, 0.06 eq), RuPhos (0.279 g, 0.59 mmol, 0.12 eq), and Na₂CO₃ (1.05 g, 9.95 mmol, 2.0 eq) were added to the solution and the reaction mixture was stirred at 80 °C, for 3 h. After this time the reaction was judged to be complete by TLC analysis. After cooling to rt the suspension was filtered through Celite®. The Celite® was rinsed with CH₂Cl₂ and the filtrate was concentrated *in vacuo*. The residue was triturated in a mixture of petroleum ether: diethyl ether 10:1 for 20 minutes. The suspension was filtered and rinsed with petroleum ether to give **54** as a colourless solid (0.893 g, 4.11 mmol, 83 %). Rf: 0.21 (petroleum ether: EtOAc 3:1); mp 189-191 °C (CHCl₃) [Lit 184-187 °C]; ¹H NMR (400 MHz, (CD₃)₂SO) δ_H: 10.19 (1H, s, CHO), 9.97 (1H, s, OH), 7.37 (1H, m, C(4)H), 7.25 (1H, m, C(2)H), 7.09 (1H, m, C(6)H), 2.43 (3H, s, C(9)CH₃), 2.24 (3H, s, C(11)CH₃); LRMS m/z (ES-):216.1 ([M-H]⁻100 %) These data are in accordance with the literature.³³¹

Synthesis of 3-(3,5-dimethylisoxazol-4-yl)-5-(hydroxy(phenyl)methyl)phenol (**55**)



A solution of 3-(3,5-dimethylisoxazol-4-yl)-5-hydroxybenzaldehyde **54** (50 mg, 0.23 mmol, 1.0 eq) in dry THF (4 mL) was cooled to 0 °C. A 1 M solution of phenylmagnesium bromide in THF (0.69 mL, 0.69 mmol, 3.0 eq) was added dropwise over 15 minutes. As the phenylmagnesium bromide was added, an off-white precipitate formed instantly. The suspension was warmed to room temperature and stirred for 1 h, when the reaction was judged to be complete by TLC analysis. The suspension was cooled to 0 °C and the reaction was quenched by addition of 0.5 mL of a 1 M aqueous solution of HCl and concentrated *in vacuo*. The residue was suspended in H₂O (5 mL) and extracted with Et₂O (3 × 5 mL). The combined organic extracts were washed with a saturated aqueous solution of NaHCO₃ (2 × 5 mL), brine (2 × 5 mL), dried over MgSO₄, filtered and concentrated *in vacuo*. The extract was purified by silica gel chromatography eluting with petroleum ether: ethyl acetate 1.5:1 to afford **7** as a colourless solid (61 mg, 0.206 mmol, 90 %). Rf: 0.12 (petroleum ether: EtOAc 2:1); mp 180-185 °C (CHCl₃) [Lit: 59 187-188 °C]; ¹H NMR (400 MHz, (CD₃)₂SO) δ_H: 9.54 (1H, s, OH), 7.40 (2H, m, C(9)H and C(13)H), 7.31 (2H, m, C(10)H and C(12)H), 7.21 (1H, m, C(11)H), 6.79 (2H, m, C(6)H and C(4)H), 6.57 (1H, dd, J 1.8, 1.8, C(2)H), 5.90-5.89 (1H, d, J 4.0, C(7)H), 5.66-5.65 (1H, d, J 4.0, CHOH), 2.36 (3H, s, C(16)CH₃), 2.18 (3H, s, C(18)CH₃); LRMS m/z (EI-) 294.1 ([M-H]⁻ 100%). These data are in accordance with the literature.³³¹

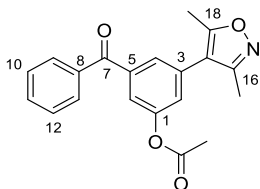
Synthesis of 3-(3,5-dimethylisoxazol-4-yl)-5-(hydroxy(phenyl)methyl)phenyl acetate (**56**)



To a solution of 3-(3,5-dimethylisoxazol-4-yl)-5-(hydroxy(phenyl)methyl)phenol **55** (0.200 g, 0.677 mmol, 1.0 eq) in iPrOH (10 mL) was added a solution of NaOH (0.0731 g, 1.83 mmol, 2.7 eq) in water (0.2 mL). After the completed addition, acetic anhydride (170 μL, 1.83 mmol, 2.7 eq) was added dropwise, and the suspension was stirred for 1 h at room temperature. After this time TLC analysis indicated complete conversion of the starting material. The suspension was adsorbed onto Celite®, and concentrated *in vacuo*. The residue was purified by silica gel chromatography, eluting with CHCl₃: EtOAc 5:1, to afford **56** as a colourless oil (0.184 g, 0.545 mmol, 81 %). Rf: 0.16 (CHCl₃: EtOAc 5:1); ¹H NMR (400 MHz, CDCl₃) δ_H: 7.42-7.37 (4H, m,

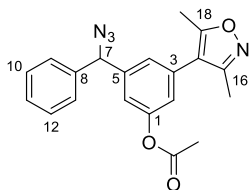
C(9)*H*, C(10)*H*, C(12')*H* and C(13)*H*), 7.35-7.32 (1*H*, m, C(11)*H*), 7.17-7.16 (1*H*, m, C(6)*H*), 7.13 (1*H*, m, C(4)*H*), 6.92 (1*H*, dd, *J* 1.8, 1.8, C(2)*H*), 5.89 (1*H*, s, C(7)*H*), 2.39 (3*H*, s, C(18)*CH*₃), 2.33 (3*H*, s, CO*CH*₃), 2.25 (3*H*, s, C(16)*CH*₃); LRMS *m/z* (ES⁺) 338.2 ([*M*+*H*]⁺ 100 %). These data are in accordance with the literature.³³¹

Synthesis of 3-benzoyl-5-(3,5-dimethylisoxazol-4-yl)phenyl acetate (**57**)



To a solution of 3-(3,5-dimethylisoxazol-4-yl)-5-(hydroxy(phenyl)methyl)phenyl acetate **56** (0.184 g, 0.545 mmol, 1.0 eq) in CHCl₃ (5 mL) was added MnO₂ (0.474 g, 5.45 mmol, 10 eq) and the reaction mixture was heated under reflux for 15 h. After this time 10 eq of MnO₂ (0.474 g, 5.45 mmol) were added and the reaction mixture was stirred for additional 3.5 h. After this time the reaction was judged to be complete by TLC analysis. After cooling to room temperature, the suspension was filtered through Celite®, and concentrated *in vacuo*. The crude material was purified by silica gel chromatography, eluting with CHCl₃: EtOAc 30:1, to afford **57** as a colourless solid (0.144 g, 0.429 mmol, 79 %). R_f: 0.19 (CHCl₃: EtOAc 30:1); mp 119-121 °C (acetone) [Michael Brand 136-138°C]; ¹H NMR (400 MHz, CDCl₃) δ_H: 7.76 (2*H*, m, C(9)*H* and C(13)*H*), 7.56 (1*H*, dddd, *J* 7.4, 7.4, 1.2, 1.2, C(11)*H*), 7.49 (1*H*, dd, *J* 1.5, 1.5, C(6)*H*), 7.47-7.43 (3*H*, m, C(10)*H*, C(12)*H*, C(4)*H*), 7.17 (1*H*, dd, *J* 1.7, 2.1, C(2)*H*), 2.38 (3*H*, s, C(16)*CH*₃), 2.29 (3*H*, s, CO*CH*₃), 2.24 (3*H*, s, C(18)*CH*₃); LRMS *m/z* (ES⁺) 336.2 ([*M*+*H*]⁺, 100%). These data are in accordance with what reported in the group.³³²

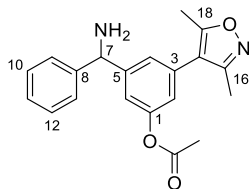
Synthesis of 3-(azido(phenyl)methyl)-5-(3,5-dimethylisoxazol-4-yl)phenyl acetate (**58**)



A solution of 3-(3,5-dimethylisoxazol-4-yl)-5-(hydroxy(phenyl)methyl)phenyl acetate (**57**) (250 mg, 0.741 mmol, 1.0 eq) in dry CH₂Cl₂ (1.5 mL) under N₂ atmosphere was cooled at 0 °C. Trimethylsilyl azide (295 µL, 2.22 mmol, 3 eq) was added dropwise to the solution and it was stirred at 0 °C for 5 minutes. After this time Cu(CF₃SO₃)₂ (26.8 mg, 0.0741 mmol, 0.1 eq) was added to the solution. The solution was stirred at 0 °C for 10 minutes and then was allowed to warm to room temperature and stirred at this temperature for one hour. After this time all the

alcohol starting material was converted into the –OTMS protected derivative. The solution was then heated to 40 °C and stirred under N₂ atmosphere for 20 hours. After this time the reaction was judged complete by TLC analysis and it was quenched with water. The product was extracted with CH₂Cl₂ (3 × 5 mL). The combined organic layers were washed with brine (2 × 4 mL), dried over MgSO₄, filtered and concentrated *in vacuo*. The extract was purified by silica gel chromatography eluting with a gradient of 7 % to 35 % EtOAc in petroleum ether to afford 3-(azido(phenyl)methyl)-5-(3,5-dimethylisoxazol-4-yl)phenyl acetate (**58**) (204 mg, 0.563 mmol, 76 %) as a colourless oil. R_f: 0.42 petroleum ether: EtOAc 2: 1. ν_{max} (thin film)/cm⁻¹ 2101 (N₃), 1767 (C=O), 1202 (C-O), 706 (m). ¹H NMR (500 MHz, CDCl₃) δ_{H} : 7.43 - 7.30 (m, 5H, C(9)H, C(10)H, C(11)H, C(12)H, and C(13)H), 7.07 - 7.05 (m, 1H, C(4)H), 7.05 - 7.02 (m, 1H, C(6)H), 6.95 (t, 1H, J = 1.9 Hz, C(2)H), 5.74 (s, 1H, C(7)H), 2.38 (s, 3H, C(16)H₃), 2.30 (s, 3H, COCH₃), 2.23 (s, 3H, C(18)H₃). ¹³C NMR (126 MHz, CDCl₃) δ : 169.2 (OCOCH₃), 165.8 (C(16)), 158.5 (C(18)), 151.2 (C(1)), 142.0 (C(5)), 138.9 (C(8)), 132.2 (C(3)), 129.1 (C(9) and C(13)), 128.7 (C(11)), 127.6 (C(10) and C(12)), 125.2 (C(4)), 121.8 (C(2)), 119.7 (C(6)), 115.7 (C(17)), 67.9 (C(7)), 21.3 (OCOCH₃), 11.8 (C(16)), 10.9 (C(18)). LRMS: m/z (ES+) 363.2 ([M+H]⁺, 100%); 385.2 ([M+Na]⁺ 43%), HRMS: m/z (ES+) 363.14526 [M+H]⁺ (requires 363.14517).

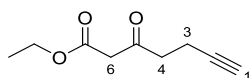
Synthesis of 3-(amino(phenyl)methyl)-5-(3,5-dimethylisoxazol-4-yl)phenyl acetate (**59**)



3-(azido(phenyl)methyl)-5-(3,5-dimethylisoxazol-4-yl)phenyl acetate (63 mg, 0.174 mmol, 1.0 eq) was solubilised in wet THF (2.9 mL). Triphenylphosphine (136.8 mg, 0.521 mmol, 3.0 eq) and water (320 μ L) were added to the solution and the system was stirred at room temperature for one hour. After this time, TLC analysis indicated the complete conversion of the starting material to give the iminophosphorane intermediate. The reaction was then heated to 40 °C for 16 h. After this time the reaction was judged complete by TLC analysis. The solvent was removed *in vacuo*, the residue was dissolved in toluene (7 mL) and the product extracted with a 2M HCl solution (3 × 3 mL). The combined acidic aqueous layers were titrated by addition of a 1M solution of K₂CO₃. The product was then extracted from the basic aqueous layer with EtOAc (3 × 5 mL). The combined organic layers were washed with brine (1 × 5 mL), dried over MgSO₄, filtered and concentrated *in vacuo* to give 3-(amino(phenyl)methyl)-5-(3,5-dimethylisoxazol-4-yl)phenyl acetate as a colourless oil (53.5 mg) that was used in the next step without further purification. R_f: 0.21 chloroform: methanol 30: 1. ¹H NMR (400 MHz, CDCl₃) δ_{H} 7.42 - 7.29

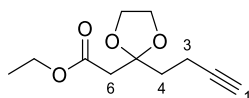
(5H, m, C(9), C(10), C(11), C(12), C(13)), 7.17 (1H, ddd, $J = 2.2, 1.5, 0.7$ Hz, C(4)), 7.12 (1H, ddd, $J = 1.6, 0.6$ Hz, C(6)), 6.86 (1H, dd, $J = 2.2, 1.6$ Hz, C(2)), 5.24 (1H, s, C(7)), 2.37 (3H, s, C(16)H₃), 2.30 (3H, s, COCH₃), 2.23 (3H, s, C(18)H₃), 2.21 (2H, d, $J = 0.8$ Hz, -NH₂). ¹³C NMR (100 MHz, CDCl₃) δ_c : 169.5 (OCOCH₃), 165.7 (C(16)), 158.6 (C(18)), 151.1 (C(1)), 148.0 (C(5)), 145.0 (C(5)), 132.2 (C(3)), 128.8 (C(9) and C(13)), 128.7 (C(11)), 126.9 (C(10) and C(12)), 125.2 (C(4)), 120.8 (C(2)), 119.3 (C(6)), 116.0 (C(17)), 59.5 (C(7)), 21.3 (OCOCH₃), 11.8 (C(16)CH₃), 10.9 (C(18)CH₃). LRMS: m/z (ES⁺) 320.2 (100 %, [M+H-NH₃]⁺), HRMS: m/z (ES⁺) 337.15472 [M+H]⁺ (requires 337.15467).

Synthesis of ethyl 3-oxohept-6-ynoate (60)



A solution of distilled diisopropyl amine (1.56 g, 2.16 mL, 15.37 mmol, 2.0 eq) in dry THF (15 mL) was cooled to -78 °C. *n*-BuLi in hexanes (2.5 M, 6.15 mL, 15.37 mmol, 2.0 eq) was added dropwise over 5 minutes. After the completed addition the solution was warmed to 0 °C and stirred for 30 minutes. After this time the solution was cooled to -78 °C. A solution of distilled ethyl acetoacetate (1.0 g, 0.97 mL, 7.68 mmol, 1.0 eq) in dry THF (0.97 mL) was added over 5 minutes. After the completed addition the solution was warmed to 0 °C and stirred for 1 h. After this time, propargyl bromide (80% in toluene, 0.914 g, 1.14 mL, 7.68 mmol, 1.0 eq) was added, and the solution was stirred for 1 h, at 0 °C. After this time the reaction was quenched by slow addition of glacial acetic acid (0.9 mL). The suspension was concentrated *in vacuo*, and the residue was suspended in H₂O (10 mL) and extracted with EtOAc (3×10 mL). The combined organic layers were washed with brine (2×3 mL), dried over MgSO₄, filtered, and concentrated *in vacuo*. The residual oil was purified by silica gel chromatography, eluting with CHCl₃:EtOAc 20:1, to afford **12** as pale yellow oil (0.877 g, 5.21 mmol, 67.9 %). Rf: 0.56 (CHCl₃:EtOAc 10:1); ¹H NMR (400 MHz, CDCl₃) δ_H : 4.23 (2H, q, J 7.2, OCH₂), 3.49 (2H, s, C(6)H₂), 2.84 (2H, t, J 7.4, C(4)H₂), 2.50 (2H, td, J 7.5, 2.7, C(3)H₂), 1.98 (1H, t, J 2.7, C(1)CH), 1.31 (3H, t, J 7.2, CH₃CH₂O); GC-HRMS m/z (CI⁺) [Found: (M+H)⁺ 169.0861 requires 169.0859]. These data are in good agreement with the literature.³⁴⁰

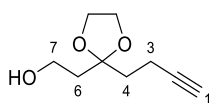
Synthesis of ethyl 2-(2-(but-3-yn-1-yl)-1,3-dioxolan-2-yl)acetate (61)



To a solution of ethyl 3-oxohept-6-ynoate **60** (0.877 g, 5.21 mmol, 1.0 eq) in toluene (37 mL) were added ethylene glycol (0.356 g, 0.32 mL, 5.73 mmol, 1.1 eq), and 4-toluenesulfonic acid

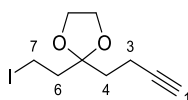
monohydrate (0.0496 g, 0.260 mmol, 0.05 eq). The solution was heated under reflux, for 19 h in a Dean-Stark apparatus. After this time the reaction was judged to be complete by TLC analysis. After cooling to ambient temperature, the organic layer was washed with a 1 M aqueous solution of K_2CO_3 (3×10 mL), brine (10 mL), dried (MgSO_4), filtered and concentrated *in vacuo*. The residual oil (0.782 g) was used without further purification. Rf: 0.21 (petroleum ether: EtOAc 4:1); ^1H NMR (400 MHz, CDCl_3) δ_{H} : 4.08 (2H, q, J 7.2, OCH_2), 3.95-3.90 (4H, m, $\text{O}(\text{CH}_2)_2\text{O}$), 2.59 (2H, s, $\text{C}(6)\text{H}_2$), 2.27-2.21 (2H, m, $\text{C}(3)\text{H}_2$), 2.07-2.04 (2H, m, $\text{C}(4)\text{H}_2$), 1.87 (1H, t, J 2.6, $\text{C}(1)\text{CH}$), 1.20 (3H, t, J 7.2, $\text{CH}_3\text{CH}_2\text{O}$); MS m/z (GCMS) 213.1127 (100 % $[\text{M}+\text{H}]^+$) (requires 213.1121). These data are in good agreement with the literature.³⁴⁰

Synthesis of 2-(2-(but-3-yn-1-yl)-1,3-dioxolan-2-yl)ethan-1-ol (62)



To a solution ethyl 2-(2-(but-3-yn-1-yl)-1,3-dioxolan-2-yl)acetate **61** (0.782 g, 3.68 mmol, 1.0 eq) in dry THF (15 mL) was added LiAlH_4 (1 M in THF, 4.23 mL, 4.23 mmol, 1.15 eq) dropwise at 0 °C. The reaction solution was let under stirring at room temperature for 2 h. After this time the reaction was judged to be complete by TLC analysis. The reaction mixture was cooled to 0 °C and 337 μL of H_2O were added. The system was stirred at 0 °C for 10 minutes, then let warm to room temperature. After this time to the reaction mixture were added 337 μL of a 10 % w/v NaOH solution, and 1010 μL of H_2O in three portions. The obtained solution was stirred at room temperature for 10 minutes, then dried over MgSO_4 , filtered, and concentrated *in vacuo* to afford yellow oil. The crude was purified by silica gel chromatography, eluting with petroleum ether: EtOAc 1:1, to afford 2-(2-(but-3-yn-1-yl)-1,3-dioxolan-2-yl)ethan-1-ol as pale yellow oil (1.04 g, 6.82 mmol, 78%). Rf: 0.10 (petroleum ether: EtOAc 2:1); ^1H NMR (400 MHz, CDCl_3) δ_{H} : 3.98-3.89 (4H, m, $\text{O}(\text{CH}_2)_2\text{O}$), 3.71-3.67 (2H, dt, J 5.3, 5.3, $\text{C}(7)\text{H}_2$), 2.59 (1H, t, J 5.3, OH), 2.21 (2H, td, J 7.0, 2.4, $\text{C}(3)\text{H}_2$), 1.89-1.86 (5H, m, $\text{C}(1)\text{H}$, $\text{C}(4)\text{H}_2$ and $\text{C}(6)\text{H}_2$). GC-HRMS m/z (CI^+) [Found: $(\text{M}+\text{H})^+$ 171.1016 requires 171.1016]. These data are in good agreement with the literature.³⁴⁰

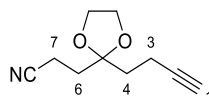
Synthesis of 2-(but-3-yn-1-yl)-2-(2-iodoethyl)-1,3-dioxolane (63)



A solution of PPh_3 (0.720 g, 2.75 mmol, 1.1 eq) and 1H-imidazole (0.510 g, 7.49 mmol, 3.0 eq) in CH_2Cl_2 (17 mL) was cooled at 0 °C and iodine (0.761 g, 2.99 mmol, 1.2 eq) was added. The dark solution was stirred for 15 min at room temperature. 2-(2-(But-3-yn-1-yl)-1,3-dioxolan-2-

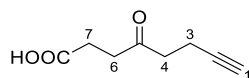
yl)ethan-1-ol **62** (0.425 g, 2.49 mmol, 1.0 eq) in CH₂Cl₂ (4.5 mL) was added dropwise at 0 °C. After the completed addition the reaction mixture was stirred under reflux for 1 h where TLC analysis indicated complete conversion of the alcohol. After cooling to ambient temperature the brown solution was quenched with 10% w/v aqueous Na₂S₂O₃ (20 mL). The product was extracted with CH₂Cl₂ (3 × 10 mL). The combined organic layers were washed with brine (2 × 10 mL), dried (MgSO₄), filtered and concentrated *in vacuo*. The residual solid was triturated in petroleum ether : Et₂O 10:1 for 5 min, filtered and concentrated *in vacuo* to afford a yellow oil (2.30 g) which was further purified by silica gel chromatography, eluting with petroleum ether: EtOAc 4:1, to afford **63** as a colourless oil (0.610 g, 2.18 mmol, 88 %). Rf: 0.56 (petroleum ether: EtOAc 4:1); ¹H NMR (400 MHz, CDCl₃) δ_H: 3.89 (4H, s, O(CH₂)₂O), 3.09-3.06 (2H, m, C(7)H₂), 2.23-2.17 (4H, m, C(4)H₂ and C(6)H₂), 1.88 (1H, t, *J* 2.7, C(1)H), 1.82-1.78 (2H, m, C(3)H₂); MS *m/z* (GSMS) 281.0025 ([M+H]⁺). These data are in accordance with what reported.³³²

Synthesis of 3-(2-(but-3-yn-1-yl)-1,3-dioxolan-2-yl)propanenitrile (**64**)



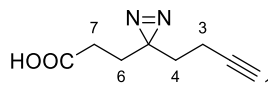
To a solution of 2-(but-3-yn-1-yl)-2-(2-iodoethyl)-1,3-dioxolane **63** (0.610 g, 2.177 mmol, 1.0 eq) in DMF (5 mL) was added potassium cyanide (0.149 mg, 2.287 mmol, 1.05 eq). The solution was stirred at 70 °C for 3 hours. After this time the reaction was judged to be complete by TLC analysis. The reaction was stirred overnight at room temperature. The next morning, the reaction was quenched by adding saturated aqueous NaHCO₃ solution (15 mL). The product was extracted with EtOAc (3 × 5 mL). The combined organic layers were washed with LiCl (0.5 M, 2 × 5 mL), brine (5 mL), dried (MgSO₄), filtered, and concentrated *in vacuo*. The residue was purified by silica gel chromatography, eluting with petroleum ether: ethyl acetate 4:1, to afford **64** as a colourless oil (0.351 g, 1.953 mmol, 90 %). Rf: 0.21 (petroleum ether: EtOAc 4:1); ¹H NMR (400 MHz, CDCl₃) δ_H: 3.92 (4H, s, O(CH₂)₂O), 2.35 (2H, t, *J* 7.6, C(7)H₂), 2.21 (2H, td, *J* 7.4, 2.8 C(3)H₂), 1.98 (2H, t, *J* 7.6, C(6)H₂), 1.90 (1H, t, *J* 2.8, C(1)H), 1.80 (2H, t, *J* 7.4 C(4)H₂); LRMS *m/z* (ES⁺) 202 ([M+Na]⁺, 100%). These data are in accordance with what reported in the group.³³²

Synthesis of 4-oxooct-7-ynoic acid (**65**)



A solution of 3-(2-(but-3-yn-1-yl)-1,3-dioxolan-2-yl)propanenitrile **64** (0.316 g, 1.76 mmol, 1.0 eq) in 10% aqueous NaOH (3 mL) was heated under reflux for 2 hours. After this time the TLC analysis indicated complete consumption of the starting material. After cooling to room temperature, the aqueous layer was washed with Et₂O (3 mL). The pH of the aqueous solution was adjusted to pH 1 by adding a 2M aqueous HCl solution. The acid solution was stirred at room temperature for three hours. After this time the product was extracted with CH₂Cl₂ (5 × 5 mL). The combined organic layers were washed with brine (5 mL), dried (MgSO₄), filtered, and concentrated *in vacuo*. The residue was purified by silica gel chromatography, eluting with petroleum ether: ethyl acetate 5:1 and 2% acetic acid, to afford **65** as a colourless solid (0.204 g, 1.32 mmol, 75 %); m.p. 55-57 °C (EtOAc). R_f: 0.10 (petroleum ether: EtOAc 5:1:2% acetic acid); ¹H NMR (400 MHz, d₆-DMSO) δ_H: 12.12 (s, 1H, -COOH), 2.76 (t, *J* = 2.7 Hz, 1H, C(1)*H*), 2.71 – 2.62 (m, 4H, C(4)*H*₂ C(6)*H*₂), 2.40 (t, *J* = 6.5 Hz, 2H, C(7) *H*₂), 2.31 (td, *J* = 7.3, 2.7 Hz, 2H, C(3)*H*₂). LRMS: *m/z* (ES⁻) 153.0 ([M-H]⁻, 100%). These data are in accordance with what reported in the group.³³²

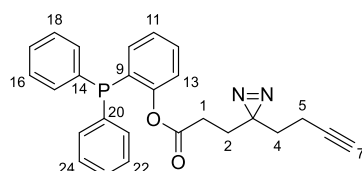
Synthesis of 3-(3-(But-3-yn-1-yl)-3H-diazirin-3-yl)propanoic acid (**66**)



4-Oxo-oct-7-ynoic acid **65** (250 mg, 1.62 mmol, 1.0 eq) was solubilized in dry MeOH (1 mL) and the solution was cooled to 0 °C. A 7 M solution of NH₃ in MeOH was added (5 mL) and the reaction solution was stirred at 0 °C for 5 h. After this time a solution of hydroxylamine-O-sulfonic acid (367 mg, 3.24 mmol, 1.6 eq) in dry MeOH (2 mL) was added dropwise at 0 °C. After one hour at 0 °C the suspension was warmed to room temperature and stirred overnight. The suspension was diluted with MeOH (5 mL), filtered, rinsed (MeOH), and concentrated *in vacuo*. The residue was dissolved in Et₂O (2 mL), triethylamine (565 μL, 4.05 mmol, 2.5 eq) was added and the solution was cooled to 0 °C. A solution of I₂ (617 mg, 2.43, 1.5 eq) was added in 5 portions until the brown colour persist. After 30 minutes the solution was diluted with EtOAc (10 mL), washed with a 1 M aqueous solution of HCl (10 mL), 10% w/v aqueous solution of Na₂S₂O₃ (10 mL), 1 M aqueous HCl (10 mL), dried over MgSO₄, filtered and concentrated *in vacuo*. The crude material was purified by silica gel chromatography, eluting with 20% EtOAc in petroleum ether and 1% AcOH, to afford 3-(3-(But-3-yn-1-yl)-3H-diazirin-3-yl)propanoic acid as a yellow oil (54 mg, 0.325 mmol, 20 %). R_f: 0.14 (EtOAc 40 % in petroleum ether + 2% acetic acid); ν_{max} (thin film)/cm⁻¹ 3500-2500 (br w) (COOH), 3296 (w) (C≡C-H), 2925 (w), 1712 (s) (C=O), 1434 (w) (diazirine), 1289 (w), 1220 (w), 925 (w), 647

(m); ^1H NMR (400 MHz, $d_6\text{DMSO}$) δ_{H} 12.17 (1H, s, COOH), 2.84 (1H, t, $J = 2.7$ Hz, C(1)H), 2.04 (2H, t, $J = 7.5$ Hz, C(7) H_2), 1.99 (2H, td, $J = 7.3, 2.7$ Hz, C(3) H_2), 1.66 (2H, t, $J = 7.5$ Hz, C(6) H_2), 1.58 (2H, t, $J = 7.3$ Hz, C(4) H_2); LRMS m/z (ES-) 165.1 (100% $[\text{M}+\text{H}]^+$). These data are in good agreement with what previously reported in the group.³³²

Synthesis of 2-(diphenylphosphaneyl)phenyl 3-(3-(but-3-yn-1-yl)-3H-diazirin-3-yl)propanoate (67)

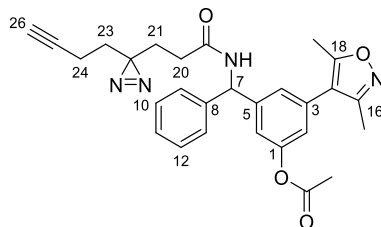


Step 1: 3-(3-(But-3-yn-1-yl)-3H-diazirin-3-yl)propanoic acid (22 mg, 0.132 mmol, 1.5 eq) was dissolved in 1 mL of SOCl_2 and stirred at 40 °C for 30 minutes. After this time the SOCl_2 was removed *in vacuo* and the residue was dissolved in dry CH_2Cl_2 (N_2 atmosphere).

Step 2: 2-(diphenylphosphanyl)phenol (24.6 mg, 0.088 mmol, 1.0 eq) was solubilised in 0.5 mL of dry CH_2Cl_2 (N_2 atmosphere) and Et_3N (37 μL , 0.265 mmol, 3.0 eq) was added. The solution was cooled at 0 °C and stirred for 5 minutes. After this time a solution of 3-(3-(But-3-yn-1-yl)-3H-diazirin-3-yl)propionyl chloride in dry CH_2Cl_2 (see step 1) was added dropwise over 5 minutes. The solution was stirred at 0 °C for 10 minutes and then let warm to room temperature and stirred for one hour. After this time the reaction was judged to be complete by TLC analysis. The reaction was quenched by water (5 mL). The product was extracted with CH_2Cl_2 (3×4 mL). The combined organic layers were washed with a 1 M aqueous solution of K_2CO_3 (5 mL), a 1 M aqueous solution of HCl (5 mL), and brine (5 mL), dried over MgSO_4 , filtered, and concentrated *in vacuo*. The extract was purified by column chromatography eluting with EtOAc : petroleum ether 1: 15 to afford 2-(diphenylphosphaneyl)phenyl 3-(3-(but-3-yn-1-yl)-3H-diazirin-3-yl)propanoate as a colourless oil (17 mg, 0.03986 mmol, Y 45 %, 98.4 % HPLC pure). R_f : 0.14 (EtOAc: petroleum ether 1:10). ν_{max} (thin film) cm^{-1} 3296 (wb) ($\text{C}\equiv\text{C}-\text{H}$), 3055 (w) 2921 (w) (C-H), 2300 (w) ($\text{C}\equiv\text{C}$), 1760 (s) ($\text{C}=\text{O}$), 16 1587 (w), 1466, 1434 (m), 1191 (m), 1132 (s), 746, 697. ^1H NMR (500 MHz, CDCl_3) δ_{H} : 7.41 – 7.28 (11H, m, C(10)H, C(15)H, C(16)H, C(17)H, C(18)H, C(19)H, C(21)H, C(22)H, C(23)H, C(24)H, C(25)H), 7.19 – 7.10 (2H, m, C(11)H, C(12)H), 6.81 (1H, ddd, $J = 7.6, 4.4, 1.6$ Hz, C(13)H), 2.08 – 2.02 (2H, t, $J = 7.9$ Hz, C(1)H $_2$), 2.01 – 1.93 (3H, m, C(5)H $_2$, C(7)H), 1.59 (4H, q, $J = 7.9$ Hz, C(2)H $_2$, C(4)H $_2$); ^{13}C NMR (126 MHz, CDCl_3) δ_{C} 170.2 (C=O), 152.7 (C(8), $J = 17.1$ Hz), 135.5 (C(14), C(20), $J = 9.6$ Hz), 134.1 (C(15), C(19), C(21), C(25), $J = 20.2$), 133.8 (C(10)), 133.8 (C(13)), 130.3 (C(9)), 129.3 (C(17), C(23)), 128.8 (C(16), C(18), C(22), C(24), $J = 7.5$ Hz), 126.4 (C(12)), 122.6 (C(11)), 82.7 (C(6)), 69.4 (C(7)), 32.2 (C(4)), 28.4 (C(1)), 27.9 (C(2)), 27.5 (C(3)), 13.4

(C(5)); ^{31}P NMR (202 MHz, CDCl_3) δ -15.88 (+37.94 oxide). LRMS: m/z (ES^+) 427.2 ($[\text{M}+\text{H}]^+$, 100%); HRMS: m/z (ES^+) 427.15723 ($[\text{M}+\text{H}]^+$) (requires 427.15699).

Synthesis of 3-((3-(3-(but-3-yn-1-yl)-3H-diazirin-3-yl)propanamido)(phenyl)methyl)-5-(3,5-dimethylisoxazol-4-yl)phenyl acetate (50)



Step 1: 3-(3-(But-3-yn-1-yl)-3H-diazirin-3-yl)propanoic acid (29.6 mg, 0.178 mmol, 1.5 eq) was dissolved in 1.5 mL of SOCl_2 and stirred at 40 °C for 30 minutes. After this time the SOCl_2 was removed *in vacuo* and the residue was dissolved in dry CH_2Cl_2 (N_2 atmosphere).

Step 2: 3-(Amino(phenyl)methyl)-5-(3,5-dimethylisoxazol-4-yl)phenyl acetate (40 mg, 0.119 mmol, 1.0 eq) was solubilised in 1 mL of dry CH_2Cl_2 (N_2 atmosphere) and Et_3N (49.7 μL , 0.357 mmol, 3.0 eq) was added. The solution was cooled at 0 °C and stirred for 5 minutes. After this time a solution of 3-(3-(But-3-yn-1-yl)-3H-diazirin-3-yl)propionyl chloride in dry CH_2Cl_2 (see step 1) was added dropwise over 5 minutes. The solution was stirred at 0 °C for 10 minutes and then let warm to room temperature and stirred for one hour. After this time the reaction was judged to be complete by TLC analysis. The reaction was quenched by water (5 mL). The product was extracted with CH_2Cl_2 (3 \times 4 mL). The combined organic layers were washed with a 1 M aqueous solution of K_2CO_3 (5 mL), a 1 M aqueous solution of HCl (5 mL), and brine (5 mL), dried over MgSO_4 , filtered, and concentrated *in vacuo*. The extract was purified by column chromatography eluting with a gradient of 10% to 15% of EtOAc in Toluene to afford 3-((3-(3-(but-3-yn-1-yl)-3H-diazirin-3-yl)propanamido)(phenyl)methyl)-5-(3,5-dimethylisoxazol-4-yl)phenyl acetate as a colourless oil (22 mg, 45.4 μmol , Y 38 %, 97% HPLC pure). R_f : 0.39 (EtOAc : petroleum ether 1:1). ν_{max} (thin film)/ cm^{-1} 3293 (wb) (NH amide and $\text{C}\equiv\text{C-H}$), 2924 (w) (C-H), 1766 (m) (C=O), 1645 (m) (C=O amide), 1535 (m), 1204 (s). ^1H NMR (500 MHz, CDCl_3) δ_H : 7.36 (2H, tt, J = 8.1, 1.7 Hz, C(10)*H* and C(12)*H*), 7.33 - 7.29 (m, 1H, C(11)*H*), 7.25 (2H, d, C(9)*H* and C(13)*H*), 6.99 (1H, m, C(4)*H*), 6.94 - 6.90 (2H, m, C(6)*H* and C(2)*H*), 6.26 (1H, d, J = 7.8 Hz, C(7)*H*), 6.06 (1H, d, J = 7.8 Hz, NHCO), 2.35 (3H, s, C(16) H_3), 2.29 (3H, s, COCH_3), 2.20 (3H, s, C(18) H_3), 2.05 - 1.97 (4H, m, C(20)*H* and C(24)*H*), 1.95 (1H, t, J = 2.6 Hz, C(26)*H*), 1.92 - 1.87 (2H, t, C(23)*H*), 1.62 (2H, t, J = 7.4 Hz, C(21)*H*). ^{13}C NMR (126 MHz, CDCl_3) δ : 170.4 (C(19)), 169.4 (OCOCH_3), 165.8 (C(16)), 158.5 (C(18)), 151.3 (C(1)), 143.8 (C(5)), 140.6 (C(8)), 132.2 (C(3)), 129.1 (C(9) and C(13)), 128.2 (C(11)), 127.6 (C(10) and C(12)), 125.7 (C(4)), 121.4 (C(2)), 119.6 (C(6)), 115.8 (C(17)), 82.8 (C(25)), 69.4 (C(26)),

56.8 (C(7)), 32.6 (C(21)), 30.4 (C(20)), 28.3 (C(23)), 27.9 (C(22)), 21.3 (OCOCH₃), 13.4 (C(24)), 11.8 (C(16)CH₃), 10.9 (C(18) CH₃). LRMS: m/z (ES+) 485.2 ([M+H]⁺, 89%); 507.2 ([M+Na]⁺ 51%), HRMS: m/z (ES+) 507.20035 [M+Na]⁺ (requires 507.20028).

5.4.2 Biochemical methods

Protein expression and purification (Dr Anthony K. N. Chan, Group of Prof. Stuart Conway, CRL, Oxford). The BRD4(1) bromodomain (Addgene plasmid # 38942) construct was transformed into E. coli BL21 (DE3) cells for expression. The protein was purified using Immobilized Metal Affinity Chromatography with a HisTrap™ column (GE Healthcare) followed by gel filtration chromatography with Superdex 75 resin (GE Healthcare). The protein purity was assessed by SDS-PAGE.

Alpha Screen assay (Larissa See and Amy Scorah, Group of Prof. Stuart Conway, CRL, Oxford). Assay buffer (25 mM HEPES, 100 mM NaCl, 0.05 % (w/v) CHAPS, 0.1 % (w/v) BSA, pH 7.6) was freshly prepared and filter sterilised through a 0.22 µm filter. For incubation steps, the plate was sealed, shaken for 10 seconds at 600 rpm on a plate oscillator and kept at room temperature in the dark. Compounds, protein, and peptides were dispensed into a ProxiPlate-384 Plus (Perkin Elmer) using a Thermo-Fisher electronic multi-channel pipette. The plate was read using a Synergy™ 2 MultiMode Microplate Reader using the built-in AlphaScreen 384 ProxiPlate function: excitation 680 nm, 0.18 sec; emission 570 nm, 0.37 sec. Ni²⁺ chelate acceptor and streptavidin donor beads were prepared as a mixture in a 1:400 dilution (0.005 mg/mL final assay concentration). Compounds (5 µL) were dispensed into wells as serial dilutions from the specified concentrations from 50 mM (24) and 10 mM (50) DMSO stock solutions. Protein-peptide mixes (7 µL) for each combination were prepared then dispensed into wells and incubated for 30 minutes. BRD4 protein and biotinylated H4(KAc)₄ were used at 10 nM and 4 nM final assay concentration (FAC) respectively. Assay beads (8 µL) were added to attain a final assay volume of 20 µL and incubated in the dark for 1 hour. Dose response curves were obtained for compounds in triplicate, from 150 µM (24) and 100 µM (50) with serial 1:2 dilutions. DMSO concentration was maintained at 0.5 % FAC. Data was processed by fitting a four-parameter equation to calculate IC₅₀ values using Prism software.

Crosslinking experiments on purified bromodomains: The crosslinking reaction was performed in 3mm Microsample NMR tubes in a total volume of 100 µL.

The protein was centrifuged to remove aggregates. Protein concentration were determined by measuring the absorbance at 280 nm using a NanoDrop Lite spectrophotometer (Nanodrop® Technologies Inc.) by using the predicted protein absorbance (BRD4(1): ϵ_{280} : 28545 M⁻¹ cm⁻¹).

Time course experiment: All the samples were prepared with a final volume of 100 µL in SEC Buffer (50 mM Hepes, 500 mM NaCl, pH 7.6). Purified BRD4(1) final concentration: 10 µM; probe final concentration: 20 µM (from a 10 mM stock solution in DMSO); final DMSO 0.2 %. The samples were pre-incubated at 4 °C for 30 min. Subsequently, the mixtures were irradiated in a Luzchem LZC-5 photoreactor equipped with eight 8 Watt lamps (Hitachi FL8BL-8, ~350 nm) for 0 to 60 minutes at 4 °C.

Competition experiment: All the samples were prepared with a final volume of 100 μL in SEC Buffer (50 mM Hepes, 500 mM NaCl, pH 7.6). An excess (10 equivalents) of the competitor (JQ-1 or **1**) was added to a solution of 10 μM purified BRD4(1) and 20 μM compound **2**. The DMSO concentration was normalized to 1 %. The samples were pre-incubated at 4 $^{\circ}\text{C}$ for 30 min. Subsequently, the mixtures were irradiated in a Luzchem LZC-5 photoreactor equipped with eight 8 Watt lamps (Hitachi FL8BL-8, ~ 350 nm) for 20 minutes at 4 $^{\circ}\text{C}$. Purified BRD4(1) final concentration: 10 μM ; probe final concentration: 20 μM (from a 10 mM stock solution in DMSO); competitor final concentration: 200 μM (JQ-1 from a 30 mM stock solution in DMSO; **1** from a 50 mM stock solution in DMSO); final DMSO 1 %.

Crosslinking efficiencies: The crosslinking efficiencies of the probe to purified BRD4(1) bromodomains were determined by protein liquid chromatography-mass spectrometry (LC-MS). A Waters LCT Premier XE (ESI-TOF-MS) coupled to a Waters 1525 μ Binary HPLC system using a Merck Cromolith RP18e guard cartridge as the column (5 x 2 mm) was used. Mobile Phase: Solvent A: Water + 0.1% formic acid; Solvent B: Acetonitrile

Step length (min)	Flow rate (mL/min)	Elapsed time (min)	%A	%B
1	0.4	1	95	5
4	0.4	5	0	100
3	1	8	0	100
0.1	1	8.1	95	5

Total mass spectra were reconstructed from the ion series using the MaxEnt1 algorithm on MassLynx software (Version 4.1, Waters Inc.) by deconvolution between 15000 and 20000 Da. Crosslinking efficiencies (CE) were calculated by comparing the peak heights of the signal from crosslinked BRD4(1) to the signal from unreacted BRD4(1) displayed in MassLynx (Equation 1).

$$CE [\%] = \frac{CP}{BRD4(1) + CP} \times 100$$

Equation 1 The equation used to determine the crosslinking efficiency (CE), where CP is the peak height of crosslinked BRD4(1) protein and BRD4(1) is the peak height of unreacted BRD4(1) protein.

CuAAC of the crosslinked protein: 50 μL of the solutions of the crosslinked protein were mixed with 50 μL of freshly prepared click mix solution and 1 μL of a 10 mM stock solution (DMSO) of TAMRA-PEG-azide and incubated at room temperature for 2 h. The click mix solution contains 1 mM CuSO_4 , 1 mM *tris*(2-carboxyethyl)phosphine hydrochloride (TCEP HCl), 0.1 mM *tris*(benzyltriazolylmethyl)amine (TBTA) (from a 5 mM DMSO stock solution) dissolved in Milli-Q water. All chemicals were purchased from Sigma-Aldrich.

SDS-PAGE: Sodium dodecyl sulfate polyacrylamide gel was cast using Mini-PROTEAN® 3 Cell (Bio-Rad). Sodium dodecyl sulfate polyacrylamide gel electrophoresis (SDS-PAGE) was performed using Mini-PROTEAN® 3 Electrophoresis Module (Bio-Rad). The Tris-Glycine discontinuous buffer system was used in the SDS-PAGE experiments. Protein samples for SDS-PAGE was first prepared in 4× Laemmli sample buffer containing 0.355 M β -mercaptoethanol, and then denatured at 100 °C for 10 min. Chemicals for SDS-PAGE, Trizma® base, 30% acrylamide/bis-acrylamide solution, sodium dodecyl sulfate dust-free pellets, *N,N,N',N'*-tetramethylethane-1,2-diamine (TEMED) and ammonium persulfate (APS), were purchased from Sigma-Aldrich. Glycine was purchased from Fisher Scientific.

Protein staining: After SDS-PAGE proteins transferred onto PVDF membranes were stained with Ponceau S Stain (Amresco Inc.) for 15 min. Subsequently, the membranes were rinsed with Milli-Q water to allow protein visualisation. The proteins crosslinked and clicked with TAMRA-PEG-azide were visualised on the SDS PAGE gel using ChemiDoc™ MP System (Bio-Rad) (Ex. 532 nm, Em. 605 nm).

PART 2: Ether Lipids Metabolism

6 Introduction (2)

6.1 Lipid metabolism and cancer

Aggressive metastatic tumors exhibit an altered cell metabolism favoring high cell proliferation rate and invasiveness. Already in 1920s, Warburg's discoveries pointed out a relation between cancer and aberrant metabolism.³⁴¹ During the last years, scientists put efforts to define the metabolic pathways driving normal cells to a deviant tumorigenic state.³⁴² Among the biochemical nodes that contribute to cancer development, dysregulated lipid metabolism and enhanced *de novo* lipogenesis are established hallmarks of cancer.³⁴³⁻³⁴⁵ Remarkably, in cancer cells lipids are required not only as cell membrane building blocks and to the formation of lipid rafts, essential for cellular trafficking and migration, but also for generation of signalling molecules, critical for cancer progression, and for lipid-mediated proteins post-translational modifications.³⁴⁶ Among the numerous lipid-modulated signalling pathways, phosphatidyl inositol, lysophosphatidic acid (LPA), sphingosine-1-phosphate, and prostaglandin signalling pathways have been shown to play a role in cancer.³⁴⁷⁻³⁵³ The discovery in 1994 of the oncogenic protein fatty acid synthase (FASN) fostered the research on understanding dysregulated lipid metabolism in cancer cells.³⁵⁴ Thus, the discovery by Kuhajda *et al.* was followed by a number of studies proving that both genetic or pharmacological ablation of FASN are able to reduce cancer pathogenicity. Several mechanisms have been proposed to explain this evidence, including phospholipids depletion, lipid rafts alterations, DNA replication inhibition, malonyl-CoA build up and associated toxicity, and inhibition of anti-apoptotic proteins such as Akt.³⁵⁵ Notwithstanding the fact that FASN is an attractive target in oncology, its druggability proved challenging. Early FASN inhibitors, including cerulenin and its derivative C75, epigallocatechin-3-gallate, triclosan, and orlistat target different regions of the FASN complex and induce apoptotic cell death in cancer cells. However, none of them is selective enough for FANS to be used for clinical development.³⁵⁶ More recently, the resolution of FASN crystal structure allowed a structure-based development of various tool compounds.^{357,358} To date, TVB-2640 is the first and sole FASN inhibitor that successfully acceded the clinical phase (NCT02223247, NCT02980029, NCT03032484, NCT03179904). In the last years, several studies pointed out that the endogenous production (via FASN) is not the only way for cancer cells to increase fatty acids production. More in detail, also the release of esterified fatty acids (via monoacylglycerol lipase, MAGL), or the release and absorption of fatty acids from dietary sources (via lipoprotein lipase, LPL and fatty acid binding protein 4, FABP4) have been implied in this process.³⁵⁹⁻³⁶¹ Accordingly, Nomura *et al.* showed how an increase in dietary fat intake could drive cancer cell pathogenesis.³⁶² Targeting fatty acids metabolism could be much more selective for highly proliferative cells than targeting glucose metabolism.

6.2 Ether lipids and cancer

Ether phospholipids constitute a particular class of phospholipids, characterized by one or more ether linkage, rather than an ester linkage, at the sn-1 position of the glycerol backbone (Figure 6.1 B-C). They constitute approximately the 20 % of the total phospholipid mass in healthy humans and their distribution varies greatly among the different tissues (particularly abundant in brain, heart, and white blood cells).^{363,364} Two types of ether bonds occur in ether phospholipids: the alkyl-ether bond and the vinyl-ether bond. A major subgroup of ether phospholipids is those of plasmalogens, characterized by a vinyl-ether bond at sn-1.

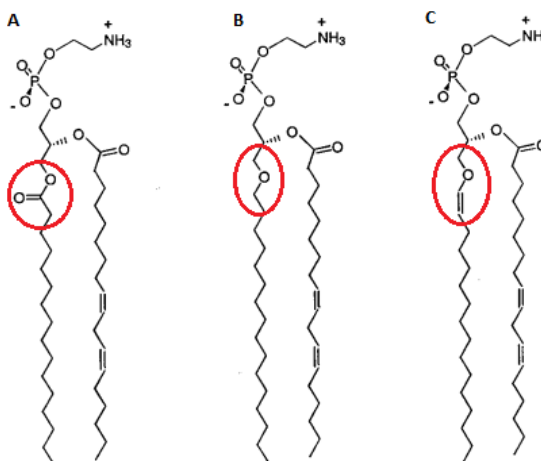


Figure 6.1. Classical phospholipids (A), alkyl ether lipids (B), and plasmalogens or vinyl-ether lipids (C). The red circles highlight the different type of bond present at the sn-1 position of the glycerol backbone.

Even though the role of intracellular and circulating ether lipids is not fully understood, their physical properties are crucial in many aspect of cell biology. Ether lipids contribute to cellular structure definition, membrane fusion and vesicle formation, free radical scavenging, storage of lipid second messengers.^{364,365} Additionally, some ether lipids, including platelet-activating factor-ether (PAFe) and lysophosphatidic acid-ether (LPAe), have been regarded as pro-oncogenic signalling molecules.^{349,366-369}

For the first time in the 1960s, Snyder and Wood documented an aberrant ether lipid metabolism across different types of cancer.^{370,371} Later, the serine hydrolase KIAA1363, involved in ether lipids metabolism, was found to be upregulated in different human aggressive cancers.^{369,372} In 2011, a study by Chang *et al.* contributed to the target validation, showing that both genetic silencing or selective pharmacological inhibition of KIAA1363 lowered ether lipids and oncogenic signalling lipids, such as alkyl lysophosphatidic acid, impairing cancer cell migration, invasion, and *in vivo* tumorigenicity.³⁷³ The broad spectrum of functions covered by lipids at cellular and supra-cellular level, along with the interplay between lipid metabolism and oncogenic signalling, call for a deeper investigation on the alterations in cancer lipid metabolism. Lipid metabolism could be a new target in cancer therapy.

6.2.1 Ether lipids biosynthesis

The ether lipids biosynthesis is initiated in the peroxisomes to be concluded in the endoplasmic reticulum (ER) (Figure 6.2).³⁷⁴ Two substrates, namely dihydroxyacetone phosphate (DHAP) and a long-chain ($C > 10$) fatty acyl-CoA ester, are involved in the first step: an esterification catalysed by the acyl-transferase called glyceronephosphate O-acyl transferase (GNPAT; also known as dihydroxyacetonephosphate acyltransferase (DHAPAT), Figure 6.2).

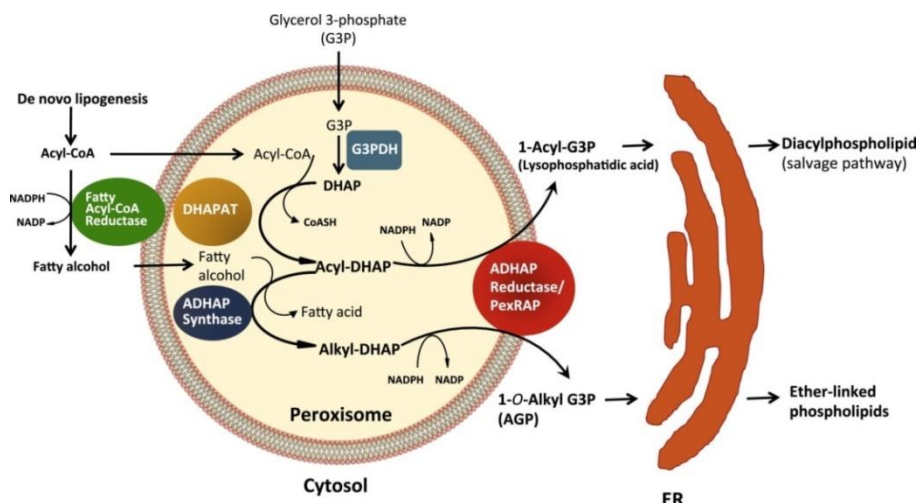


Figure 6.2. Ether lipids biosynthesis in peroxisomes.

The DHAPAT thus generates an acyl-DHAP, substrate of the enzyme alkylglycerone phosphate synthase (AGPS; also known as alkyl-dihydroxyacetone phosphate synthase (AGPS), Figure 6.2). AGPS is responsible for the replacement of a fatty acid with a fatty alcohol generating an alkyl-DHAP.³⁷⁵⁻³⁷⁷ The alkyl-DHAP is translocated to the cytosol, where it is either reduced to alkyl-glycerol phosphate (alkyl-GP) or is transported to the ER as such and then reduced to alkyl-GP by the ER enzymes (Figure 6.2).

6.2.2 AGPS crystal structure

The key step in the ether phospholipids synthesis is clearly the exchange of a fatty acid chain in acyl-DHAP with a fatty alcohol chain, catalysed by AGPS enzyme.

AGPS is a 130 kDa peroxisomal flavoenzyme, using flavin adenine dinucleotide (FAD) as a cofactor. Interestingly, the FAD acts through an unusual non-redox catalytic mechanism. Indeed, it covalently binds the DHAP moiety of acyl-DHAP, acting as a trap to immobilize the substrate in AGPS active site, promoting the acyl-alkyl exchange and forming the precursor of all ether lipid species.³⁷⁷ The crystal structure of *Cavia porcellus* AGPS (displaying a 93 % sequence identity with the human enzyme) was reported in this work. The AGPS crystal structure shows that this enzyme is a dimer of identical subunits, each composed by three domains: N-terminal, FAD-binding and cap domains (Figure 6.3). AGPS has a V-shaped active site located at the interface between the FAD and cap domains in front of the flavin ring. More in detail, the active site runs across the cap-FAD domain interface from the gating helix to

Arg419 (Figure 6.3). The active site is built to perfectly host the tripartite substrate acyl-DHAP, composed by a fatty chain hydrophobic tail, the central three-carbon unit of DHAP, and the negatively charged phosphate group.

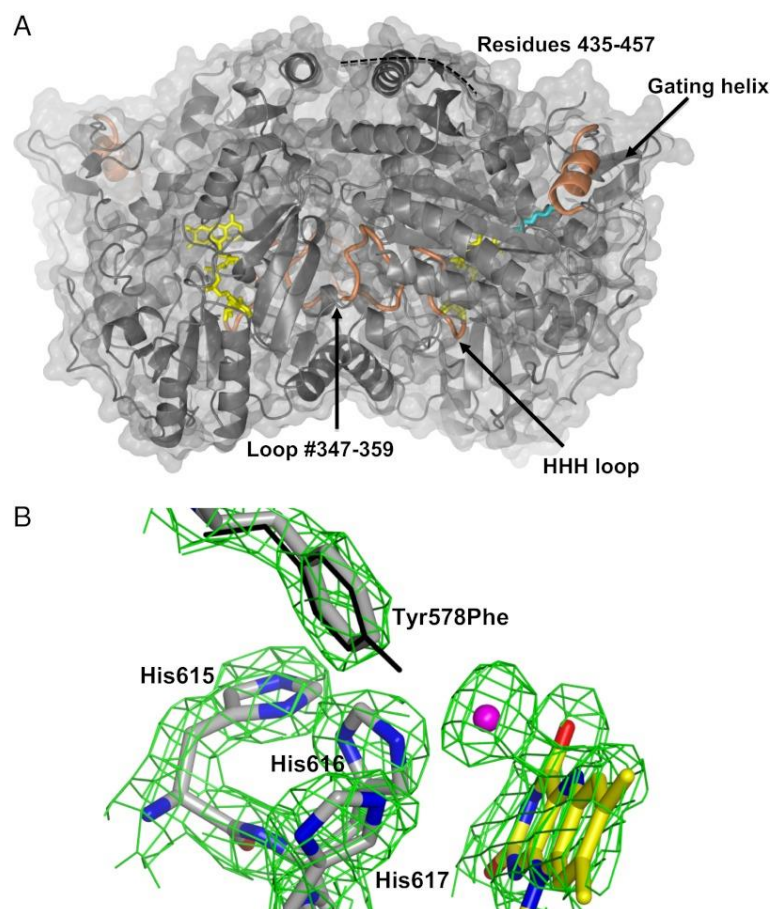


Figure 6.3. Crystal structure of AGPS. **(A)** The dimer with the molecular twofold axis vertical in the plane of the paper. The FAD is shown in yellow; the bound aliphatic ligand, in cyan. Loop 347–359, the “HHH loop” (615–622), and the gating α -helix (126–137) are shown in orange. # indicates that loop 347–359 is part of the active site of the twofold related subunit. AGPS is associated to the inner side of the peroxisomal membrane. **(B)** The final 2Fo-Fc-weighted electron density map (contoured at the 1.4 σ level) of the active site in the Tyr578Phe mutant. Protein carbons are shown in gray; flavin carbons, in yellow; oxygens, in red; nitrogens, in blue; and chloride, in magenta. The Tyr578 side chain of the WT protein is superimposed and shown with thin bonds.³⁷⁷

In detail, the longest arm of the V-shaped active site is rich in hydrophobic residues, hosting the hydrophobic aliphatic portion of the substrate. The second, shorter, and spherical arm comprises several hydrophilic residues including Arg419 and two Thr residues, enabling the substrate phosphate group anchoring. The two arms are connected by a small constriction where His616, His617, Tyr576 and the FAD flavin ring are located (Figure 6.3 B).³⁷⁷ Based on these evidences, the catalytic cycle of AGPS has been described by Nenci *et al.* as here reported (Figure 6.4). The acyl-DHAP substrate, in its enol form, first attacks the flavin N(5). The substrate tautomerization is most likely enabled by Tyr578, involved in acid/base catalysis. This

hypothesis is supported by the evidence that the Tyr578Phe AGPS mutant is catalytically inactive. Additionally, the negatively charged enolate is stabilised by interaction with the His615-617 residues in the HHH loop. Indeed, the His616Ala or H617Ala mutants are inactive. The formation of the C(1) acyl-DHAP to N(5) flavin covalent adduct is followed by the release of a fatty acid, generating the covalent intermediate between hydroxyacetone phosphate and the flavin. Finally, the fatty alcohol, probably deprotonated by Tyr578, attacks the hydroxyacetone phosphate C(1) exchanging with the flavin to obtain the ether-containing product (Figure 6.4).³⁷⁷ Nenci *et al.* studied five active-site mutations (Thr309Ile, Arg419His, Leu469Pro, Arg515Leu, and Tyr578Phe), three of them found in patients affected by rhizomelic chondrodysplasia punctata.^{378,379} All the studied mutations inactivate the enzyme. Three of them (Thr309Ile, Leu469Pro, and Arg515Leu) prevent the enzyme to bind FAD, whereas the two others (Arg419His and Tyr578Phe), although exhibiting normal stability, were enzymatically inactive. These results contributed to define the crucial residues for substrate binding and catalytic activity.

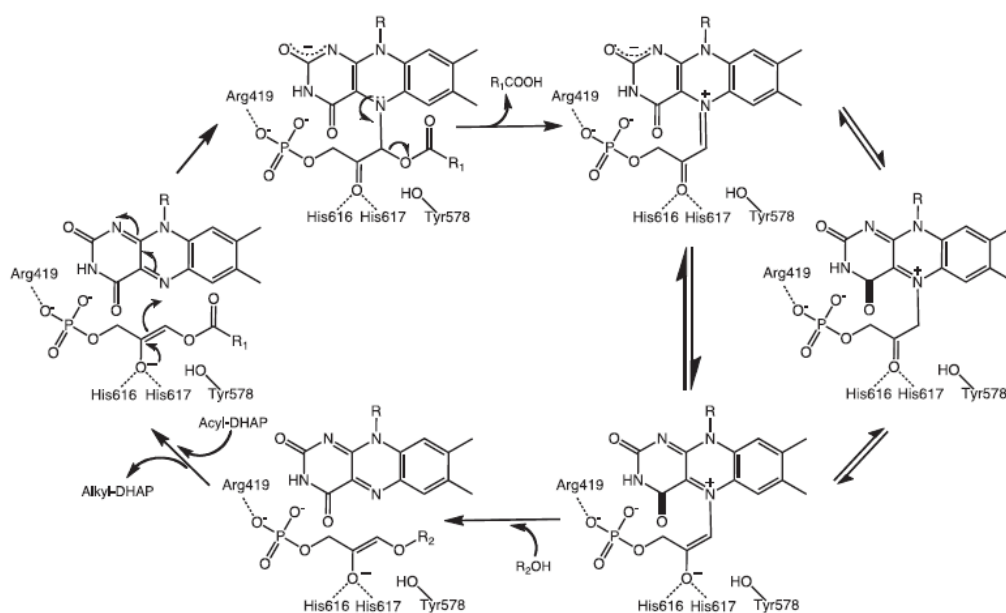


Figure 6.4. Mechanistic proposal for the AGPS reaction.³⁷⁷

6.2.3 AGPS and Cancer

The crucial role of AGPS is highlighted by the the devastating consequences of its inactivating mutations, related with serious and invalidating diseases. Benjamin *et al.* reported that AGPS is up-regulated across different types of aggressive and metastatic tumors, such as human breast (231MFP), melanoma (C8161) and prostate cancer (PC3) compared with less aggressive cancer cells (MCF7, MUM2C, and LNCaP, respectively).³⁸⁰ In this context, AGPS overexpression determines an increase in the level of ether lipids and controls cellular utilization of fatty acid, eicosanoid and acylglycerophospholipid metabolism to promote cell proliferation, motility and,

therefore, tumor growth and metastasis formation.^{349,376,377,381} Benjamin *et al.* documented that AGPS gene expression is enhanced in ER(+)/PR(+) and ER(-)/PR(-), and in Nottingham grade 1, 2, and 3 primary human breast tumors compared with normal breast tissues, as measured by quantitative PCR (qPCR). These findings suggest that AGPS overexpression can occur in early stages of breast cancer development. Interestingly, AGPS overexpression in grade 1, 2, and 3 primary human breast tumors, and in aggressive breast and melanoma cancer cells was significantly correlated with transforming Harvey-Rat sarcoma oncogene (HRAS) expression, showing that transformation of cells by HRAS is a way to up-regulate AGPS expression. Metabolomic profiling of aggressive human breast 231MFP, melanoma C8161 and prostate PC3 cancer cells, as well as HRAS-transformed MCF10A cells, revealed that they display largely higher ether lipid levels compared with less aggressive or empty vector-transfected MCF10A control cells. More in detail, the lipid species whose levels are increased upon AGPS overexpression include: phosphatidic acid-ether (PAe), LPAe, phosphatidyl inositol-ether (PIe), phosphatidylcholine-ether (PCe), lysophosphatidylcholine-ether (LPCe), phosphatidylserine-ether (PSe), phosphatidylglycerol-ether (PGe), lysophosphatidylglycerol-ether (LPGe) lipids, and plasmalogen ether lipids, such as phosphatidylethanolamine-plasmalogen (PEp).³⁸⁰ Interestingly, several of those lipids are known oncogenic signaling molecules which contribute to the inflammatory microenvironment.³⁸²

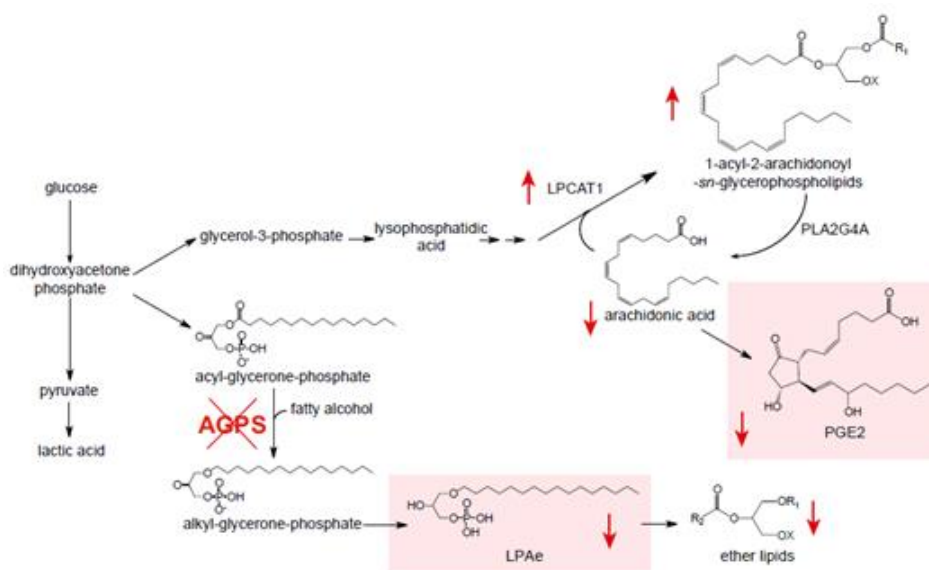


Figure 6.5. Model depicting the metabolic role of AGPS in exerting control over ether lipid metabolism, fatty acid metabolism, and glycerophospholipid metabolism.

To further elucidate the contribution of AGPS to cancer pathogenicity, AGPS was genetically silenced in breast 231MFP and melanoma C8161 cancer cells.³⁸⁰ Its inactivation led to an overall reduced level of multiple structural ether lipids, as well as, oncogenic signaling molecules, also reducing breast 231MFP and melanoma C8161 tumor xenograft growth in immune-deficient mice.³⁸⁰ Accordingly, AGPS overexpression in less aggressive breast (MCF7)

and melanoma (MUM2C) cancer cells lead to an increase in cell migration and cell survival *in situ*, and tumor xenograft growth *in vivo*, suggesting that the sole AGPS is sufficient to establish an aggressive phenotype in less aggressive human cancer cells.³⁸⁰ The effects of AGPS were also investigated in human glioma U87 and hepatic carcinoma HepG2 cell lines.³⁸³ Zhu *et al.* found that AGPS silencing resulted in a decreased the expression of oncogenic signalling molecules, affecting adhesion and invasion potential of these cell lines. Furthermore, AGPS depletion was shown to cause cell cycle arrest in G0/G1 phase, suggesting that AGPS could play a role also as a cell-cycle regulator in cancer proliferation. In this study, the authors found that cell levels of invasion-related genes (such as Mmp-2/9, E-cadherin and CD44) were strongly affected by AGPS knock-down.³⁸³ Finally, AGPS affected the activity of MAPK signaling pathway and the transcriptional activity of Twist, AP-1, and Snail.³⁸³

6.3 Discovery and development of the first in class AGPS inhibitor

The increasing number of evidences proving AGPS implication in cancer rise and evolution, called for the development of small molecules able to target this enzyme, potentially useful as tools for further biological investigation and target validation, with the aim to exploit it as target against metastatic tumors. Recently, we reported the discovery of the first class AGPS inhibitors through an in-house established ligand binding assay (ThermoFAD).^{384,385} We started with screening an initial set of 1360 small molecules from the Prestwick Chemical Library that encompasses 1280 approved drugs and a subset of the ZINC database.³⁸⁶ AGPS from *Cavia porcellus* was chosen as a suitable system for inhibitor screening because of its stability and suitability for crystallographic studies. We identified lead compounds that affected the thermal stability of AGPS, increasing the melting temperature of the protein by 4 °C (Figure 6.6). They included the antifungal agent antimycin A (from Prestwick Chemical Library, **74** Figure 6.6),³⁸⁷ and (3-(2-fluorophenyl)-N-(1-(2-oxo-2,3-dihydro-1H-benzoimidazol-5-yl)ethyl)butanamide (ZINC-69435460, **75** Figure 6.6).

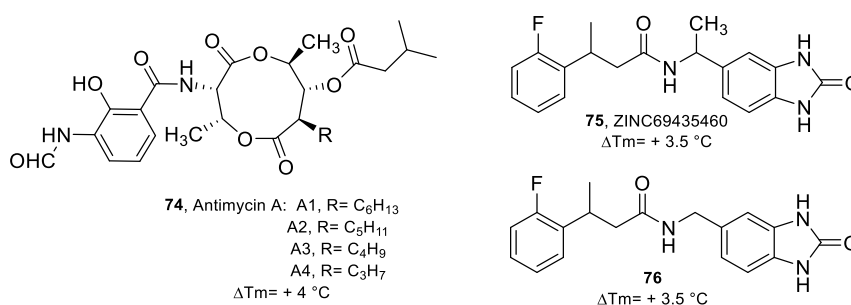


Figure 6.6. Structure and effect on AGPS thermal stability of the identified inhibitors

To confirm whether these lead compounds inhibited AGPS activity, we used a radioactivity-based enzymatic assay, using palmitoyl-DHAP and [1-¹⁴C]- hexadecanol as substrates. This assay is based on the detection of [1-¹⁴C]hexadecyl-DHAP formation as a function of time in the presence of an excess of inhibitor (180 μM). Even though we were not able to calculate K_i values, due to limitations of our enzymatic assay (poor solubility of the substrates and low sensitivity of the radioactive detection), we were able to demonstrate that the two lead compounds inhibit AGPS enzymatic activity (Figure 6.7).³⁸⁵ The attempts to measure the inhibitors binding through surface plasmon resonance and isothermal calorimetry failed due to insolubility of the compounds. Nonetheless, the affinity constants were estimated as 200–700 nM for both compounds through thermal shift assay following the procedures established by Matulis *et al.*³⁸⁸ To explore the binding mechanisms between AGPS and the identified inhibitors, the crystal structures of AGPS in complex with **74** and **75** were determined by X-ray crystallography at 2.0–2.2 Å resolution, enabling a detailed view of the inhibitor binding (Figure 6.8). Both inhibitors resided in the V-shaped active site, whose vertex is the putative substrate cavity, in front of the FAD.

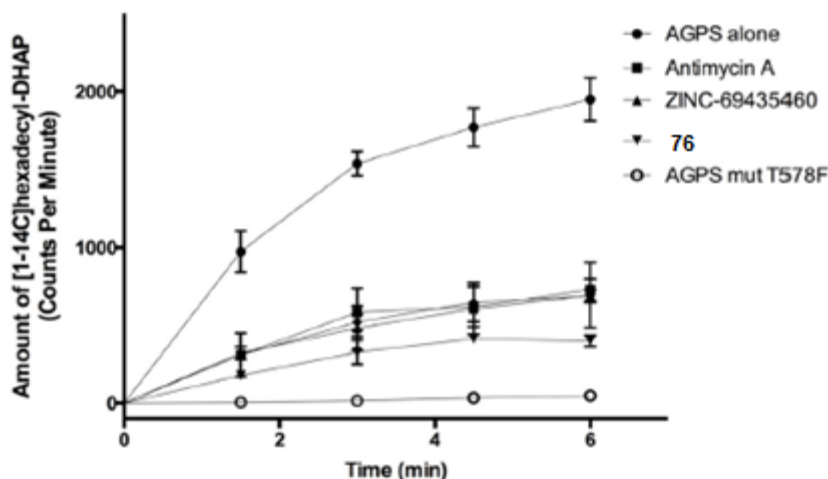


Figure 6.7. AGPS functional role and inhibition of AGPS activity by lead inhibitors. Inhibition of *Cavia porcellus* AGPS activity was assessed by a radioactivity assay using 100 μ M palmitoyl-DHAP, 96 μ M [1- 14 C]hexadecanol, and 180 μ M inhibitor and detecting the formation of [1- 14 C]hexadecyl-DHAP as a function of time. The controls were performed using AGPS alone and the catalytically inactive AGPS mutant T578F. Measurements were performed at least in triplicate.³⁸⁵

Most importantly, both inhibitors establish specific interactions with the protein residues, but their binding mode and location in the active site are significantly different (Figure 6.8 B, C). The two molecules, binding two, only partly overlapping, druggable sites within the protein, were therefore considered as distinct lead compounds. The crystal structure of **75** (ZINC-69435460) shows that the dihydrobenzimidazole moiety occupies the hydrophilic DHAP site, making π -stacking interactions with the FAD isoalloxazine ring, thus preventing the access of the substrate to the active site (Figure 6.8 B). In this region, several H-bonds, including those with His616 and His617, belonging to the HHH loop, contribute to the binding. The amidic substituent points with the fluorophenyl ring toward the hydrophobic tunnel that hosts the acyl chain of the substrate. Here binding is mediated mainly by hydrophobic interactions. Conversely, compound **74** (antimycin A) locates outside of the active site and do not establish direct contact with the flavin (Figure 6.8 C). Basically, whereas **75** binds deeper into the active site, **74** acts as a plug that obstructs access of the substrate. In both cases, the inhibitor binding does not cause dramatic changes in the protein conformation, but only small changes. Even though, the investigation on **74** was interesting to better understand its mode of binding and to identify druggable sites in the protein, it was not considered an attractive lead for further optimisation, considering the high synthetic challenges and its known activity as inhibitor of cytochrome C reductase.³⁸⁹ Along this line, we focused our efforts on the synthesis and evaluation of several structurally related analogues of **75**.

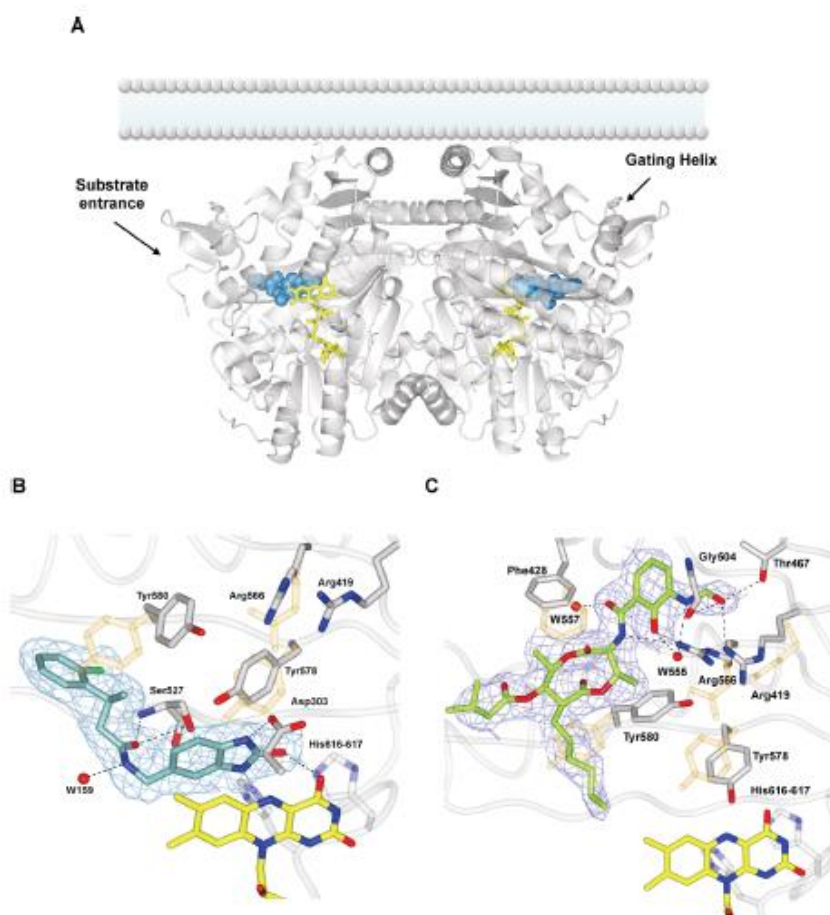


Figure 6.8. Structural studies on *Cavia porcellus* AGPS in complex with the inhibitors **74** and **75**. (A) Overall view of the dimeric enzyme bound to **75** (in blue). The inhibitor is extended along the hydrophobic substrate tunnel, delimited by the “gating helix” (residues 126–137). AGPS is known to be associated with the luminal side of the peroxisomal membrane as outlined in the figure. FAD is shown in yellow. (B) Weighted 2Fo – Fc final electron density map contoured at the 1.2 σ level for **75** in the same orientation of the left subunit shown in part A. Binding involves specific H bonds (black dashed lines) with the catalytic residues Asp303, Ser527, His616, and His617. The position and the distance of the inhibitor suggest also π interactions with the cofactor isoalloxazine ring. A few side chains change their conformation with respect to the unbound enzyme (light orange). (C) Final weighted 2Fo– Fc map (1.2 σ contour level) for the antimycin A–enzyme complex. Commercial **74** is a mixture of four compounds, differing in the length of the alkyl chain. From the crystal structure in complex with AGPS, it is evident that antimycin A1 is binding to the enzyme as its bulky six-carbon side chain nicely fits the electron density. The electron density is fully consistent with antimycin A1 (6-carbon alkyl moiety) being bound to the protein. Inhibitor binding causes the rearrangement of several residues around the active site (in orange superposition with native AGPS residues).³⁸⁵

Next, an exploration of a small series of **75** analogues, yielded the identification of compound **76** (Figure 6.6). Compound **76**, lacking the methyl group at β -carbon of amide moiety, showed higher binding affinity and the same effect on AGPS enzymatic activity compared to **75**.

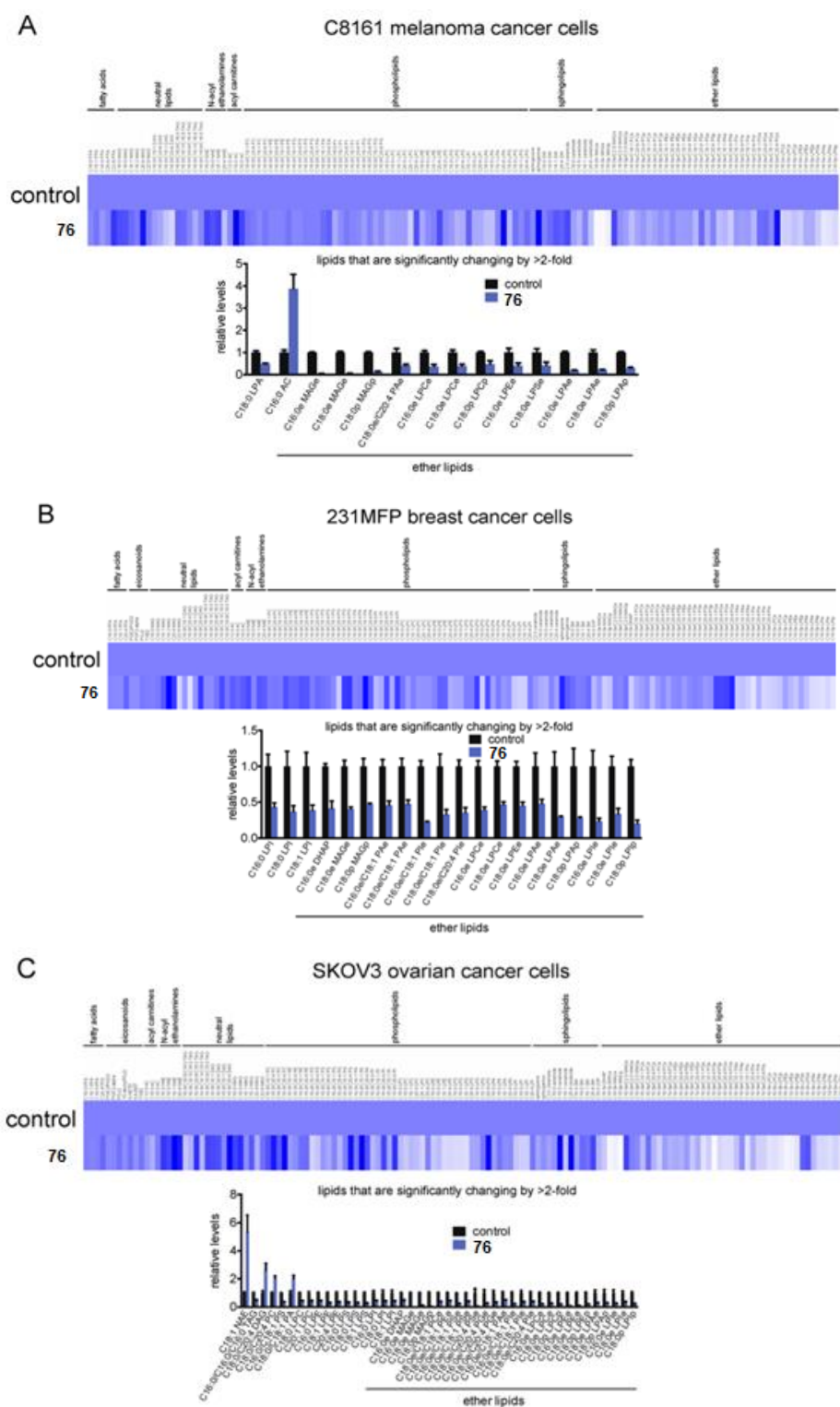


Figure 6.9. Lipidomic profiling data from C8161 melanoma (**A**), 231MFP breast (**B**), and SKOV3 ovarian (**C**) cancer cells treated with vehicle (DMSO) or **76** (500 μ M) for 24 h. Shown in heat maps are relative levels compared to control for each lipid measured by targeted SRM-based LC-MS/MS lipidomics. Darker and lighter blue compared to control indicates elevated or reduced levels, respectively, upon **76** treatment. Bar graphs show lipid species that were significantly ($p < 0.05$) changed >2-fold upon **76** treatment compared to vehicle-treated controls. Data in bar graphs are shown as average \pm SEM. ³⁸⁵

Considering also that compound **76** was lacking one of the two chiral centers of **75**, it was chosen as “hit” for further biological evaluation.³⁸⁵ Lipidomic analysis on C8161 melanoma, 231MFP breast, and SKOV3 ovarian cancer cells treated with **76** (500 μ M), showed that **76** primarily lowers the levels of ether lipids across all three cancer cell lines, largely without affecting the levels of lipids from other classes (Figure 6.9). Interestingly, the levels of the oncogenic signalling lipid LPAe were also lowered upon **76** treatment (Figure 6.9). Unfortunately, no effects were observed after treatment of cancer cells with a lower concentration of **76** (50 μ M). We believe that this could be due to cell/peroxisome permeability issues. We also investigated about the effects of **76** on cell survival and migration (Figure 6.10). In C8161 melanoma, 231MFP breast, and SKOV3 ovarian cancer cell, treatment with **76** (500 μ M) impairs serum-free cell survival and migration rate down to 50 % (Figure 6.10 A-F).³⁸⁵ These results recapitulate what previously observed after AGPS genetic knockdown in cancer cells.³⁸⁰ The results obtained in this first study are promising. The development of *in vivo* efficacious AGPS inhibitors will be crucial for the future application of AGPS inhibitors for cancer therapy. They will also be valuable tools for further investigations on the biology of ether phospholipids.

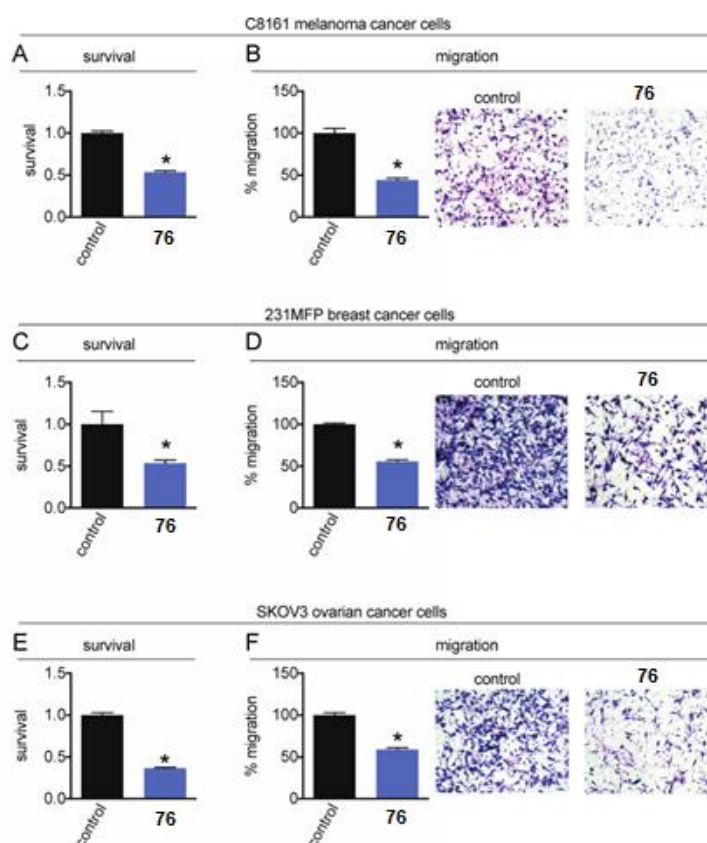


Figure 6.10. AGPS inhibitor **76** impairs cancer cell pathogenicity. Shown are effects of **76** upon cell survival and migration in C8161 melanoma (**A**, **B**), 231MFP breast (**C**, **D**), and SKOV3 ovarian (**E**, **F**) cancer cells. Data shown as average \pm SEM, $n = 3-4$ /group. Significance is represented as * $p < 0.05$ in relation to control groups.³⁸⁵

7 Development of Alkyl Glycerone Phosphate Synthase Inhibitors: Structure-Activity Relationship and Effects on Ether Lipids and Epithelial-Mesenchymal Transition in Cancer Cells

7.1 Research project

Prompted by these results we decided to pursue an in-depth SAR investigation on compound **76** scaffold, aimed to pinpoint the essential pharmacophore group for the inhibitory activity, and to increase the potency. Thus, we divided our scaffold in different portions, and started to manipulate them one by one, keeping fix the others. We first focused our attention on the phenylpropionamide moiety of our lead compound. More in detail, we performed a series of chemical manipulations including:

- introduction of more bulky groups on the β carbon (**77j-k**, Figure 7.1),
- shift of the methyl group from β to α carbon (**77l**, Figure 7.1),
- shift of the fluorine substituent to *meta* or *para* position of the phenyl ring (**77b-c**, Figure 7.1),
- exploration of different substitutions at the *ortho* position of the phenyl ring, including the removal of the fluorine (**77a**, Figure 7.1) or its replacement with other halogens (**77d-e**, Figure 7.1), electron withdrawing groups or electron donating groups (**77f-g**, figure 7.1),
- doubling of the fluorine substitution on the phenyl ring (**77h-i**, Figure 7.1).

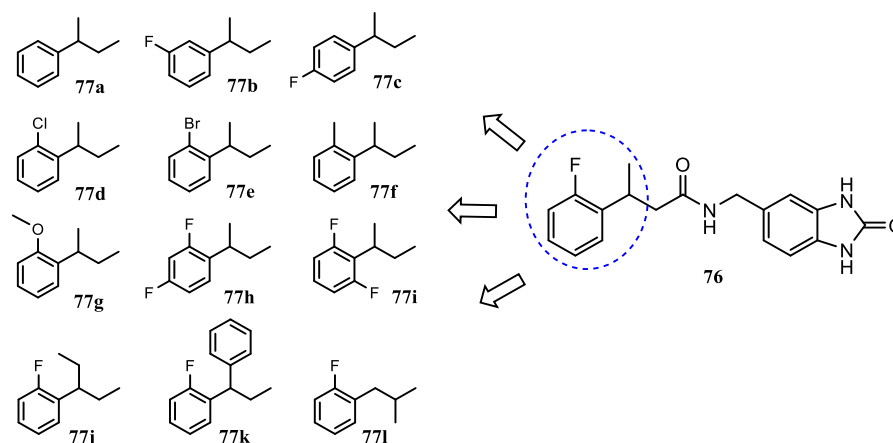


Figure 7.1. Development of novel analogues (**77a-l**) of AGPS inhibitor **76**.

The first SAR data showed that the 2,6-difluoro substitution of compound **77i** was the most favorable to improve the target binding and inhibitory activity. Thus, we also investigated about the effect of different modifications on compound **77i**, including:

- shortening of the length of the chain connecting the two aromatic moieties (**77m-n**, Figure 7.2),

- replacement of the benzoimidazolone with a benzoimidazole (**77o**, Figure 7.2),
- substitution of the two ureidic nitrogens of the benzoimidazolone with methyl groups (**77p**, Figure 7.2)
- homologation of the benzoimidazolone ring and its replacement with a 3,4-dihydroquinoxalin-2-one (**77q**, Figure 7.2).

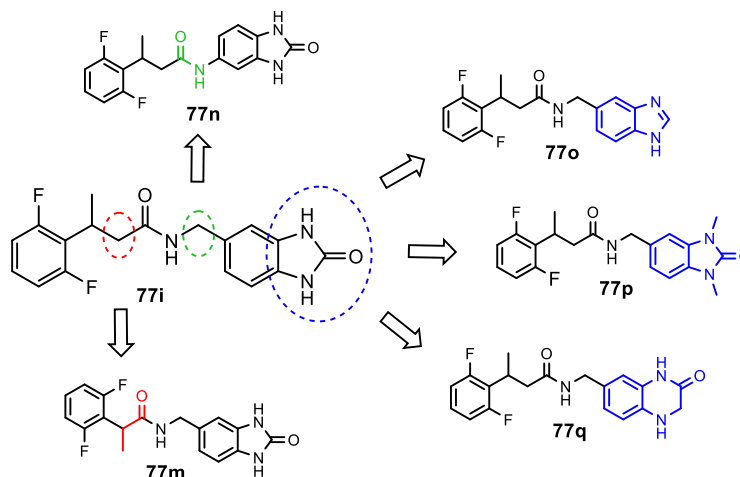
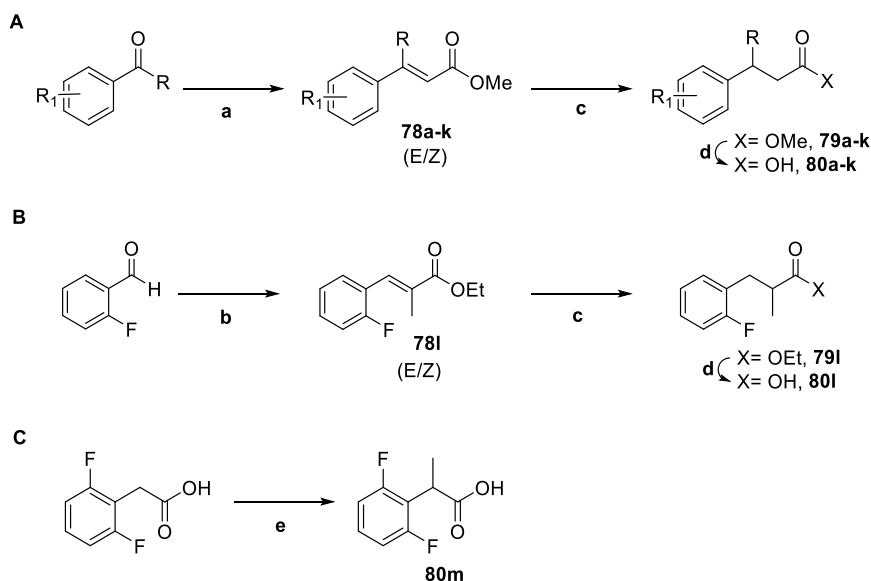


Figure 7.2. Further structural investigation on AGPS inhibitor **77i**: derivatives **77m-q**.

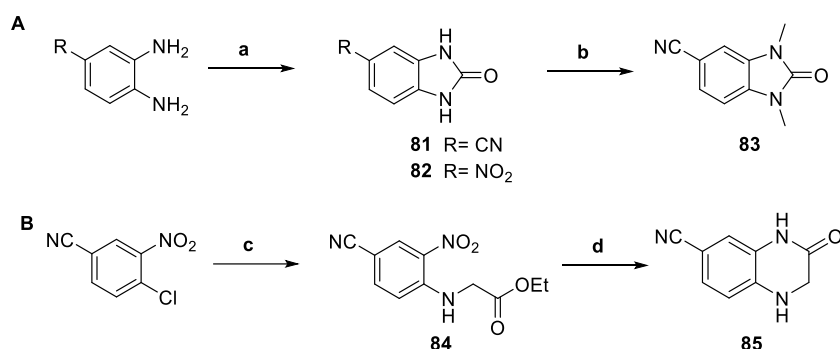
7.2 Results and discussion

7.2.1 Chemistry

The synthesis of derivatives **77a-k**, **77n-q** started from Wittig-Horner condensation between differently substituted ketones and trimethylphosphonoacetate, by using 60 % sodium hydride in tetrahydrofuran at 0 °C to afford unsaturated esters **78a-k** (Scheme 28A). Differently, the Wittig-Horner reaction between 2-fluorobenzaldehyde and triethyl 2-phosphonopropionate in presence of anhydrous potassium carbonate in ethanol at 80 °C provided the unsaturated ester **78l** (Scheme 28B). The esters **78a-l** underwent palladium catalyzed hydrogenation, by using a ThalesNano H-Cube Reactor, to afford the esters **79a-l**, which were converted to the corresponding acids **80a-l** through a basic hydrolysis by using 2 N potassium hydroxide in ethanol (Scheme 28A-B). The acid **80m** was prepared as previously reported in the group (Scheme 28C).³⁹⁰ The synthesis of the amines **86-88** started reacting the 3,4-diaminobenzonitrile or 4-nitrobenzene-1,2-diamine in presence of *N, N'* carbonyldiimidazole to give the benzoimidazolones **81** and **82** (Scheme 29). A double N-alkylation of **81** in presence of sodium hydride and iodomethane gave compound **83** (Scheme 29). Compound **85** was synthesized starting from 4-chloro-3-nitrobenzonitrile that was first involved in a S_N in presence of ethyl glycinate hydrochloride to give the intermediate **84** (Scheme 29). A one-pot reaction on the nitro-derivative **84**, including reduction of the nitro-group and cyclization, yielded compound **85** (Scheme 29).

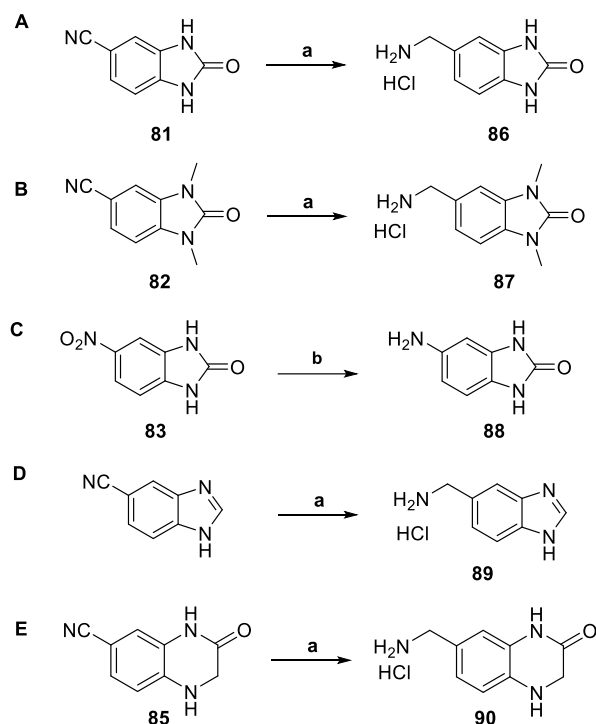


Scheme 28. Reagents and conditions: **a**) trimethylphosphonoacetate, 60 % NaH, dry THF, 0 °C to r. t., N₂ atmosphere, overnight (41-79 %) ; **b**) triethyl-2-fosfonopropionato, dry K₂CO₃, dry EtOH, 80 °C, 2 h; **c**) MeOH, 10% Pd/C, P_{H2}=10 bar, v=1 ml/min, 30 °C (79-83 %) ; **d**) 2N KOH, EtOH, r. t., overnight (94-97 %) **e**) I. 2.5 M *n*-BuLi in hexane, dry THF, -10 °C to r.t., 1h; II. Methyl iodide, -10 °C to r.t., 15 min (77 %).

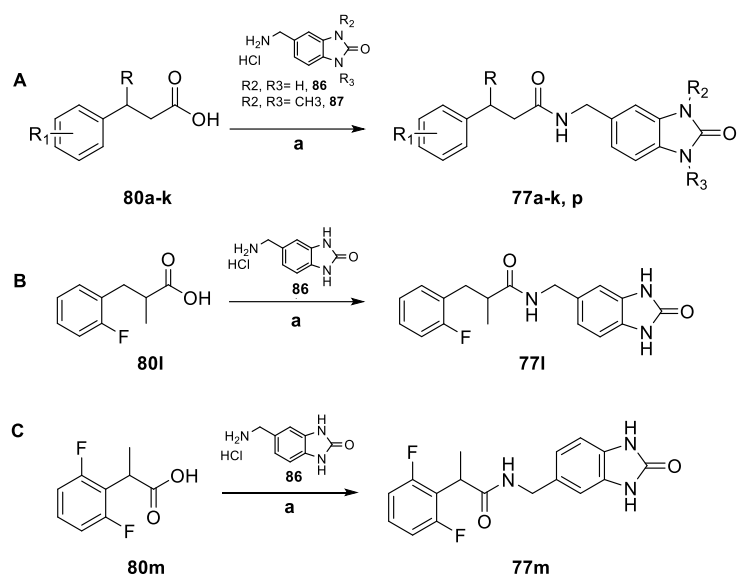


Scheme 29. Reagents and conditions: **a**) *N,N'*-carbonyldiimidazole, dry THF, 75 °C, 2 h (90-92 %); **b**) I. 60% NaH, dry THF, 0 °C, 30 min; II. CH₃I, dry THF r. t., N₂ atmosphere, overnight (97 %); **c**) ethyl glycinate hydrochloride, K₂CO₃, dry DMF, 90 °C, sealed tube (94 %); **d**) SnCl₂ × 2 H₂O, 37 % HCl, r. t (61 %).

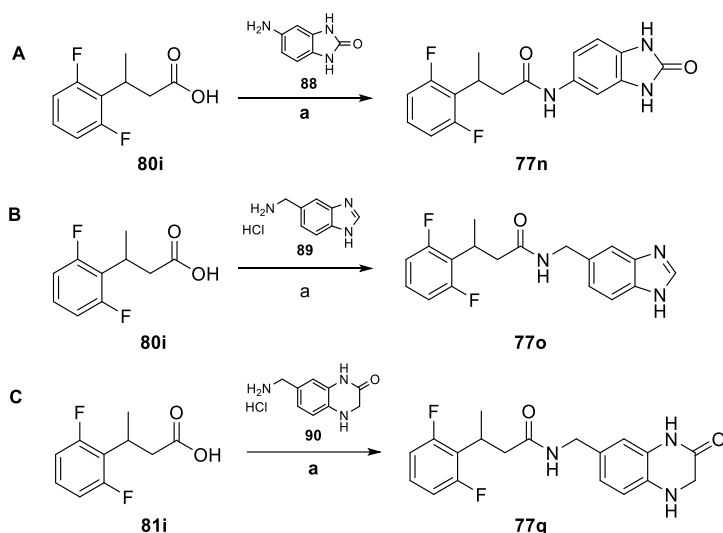
The amines **86**, **87**, **89**, and **90** were obtained from the corresponding nitriles through 10 % palladium on carbon catalyzed hydrogenation in acetic acid with a ThalesNano H-Cube Reactor (Scheme 30A, B, D, E). The amine **88** was obtained by reduction of the nitro derivative **83** in presence of tin(II)chloride and concentrated hydrochloric acid in ethanol (Scheme 30C). In the last step, the acids **80a-m** were coupled with the opportune amines in presence of *N,N*-carbonyldiimidazole and triethylamine in anhydrous *N,N*-dimethylformamide to obtain final amides **77a-q** (Schemes 31, 32).



Scheme 30. Reagents and conditions: **a**) glacial CH_3COOH , Pd/C 10 %, P_{H_2} =50 bar, v =1.5ml/min, 50 °C (77- 91 %); **b**) $\text{SnCl}_2 \times 2 \text{H}_2\text{O}$, 37 % HCl, EtOH, r. t (44 %).



Scheme 31. Reagents and conditions **a**) N,N -carbonyldiimidazole, dry DMF, r. t. or 70 °C, overnight (73- 85 %).



Scheme 32. Reagents and conditions **a**) *N,N*-carbonyldiimidazole, dry DMF r. t. or 70 °C, overnight (73-85 %).

7.2.2 ThermoFAD based screening of compounds 77a-q

(Group of Prof. Andrea Mattevi, Dr. Valentina Piano, Department of Biology and Biotechnology, University of Pavia)

As previously showed, ThermoFAD was a reliable assay to screen molecules binding to AGPS, therefore, we took advantage of this medium-throughput screening to test the novel analogues (**77a-q**) of compound **76**.³⁸⁵ From the effects of the tested compounds on AGPS thermal stability (Table 8), it is evident that increasing the steric hindrance at the β carbon of the phenylpropionamide moiety with an ethyl (**77j**) or with a phenyl substituent (**77k**), caused respectively a decrease or a complete loss in AGPS binding. Looking at the effect of the substitution of the phenyl ring of phenylpropionamide moiety, we observed that the elimination of the fluorine at C(2) position resulted in a reduction of the target binding (ΔT_m 1.5 °C, **77a**), whereas its replacement with other halogens, such as chlorine (**77d**), bromine (**77e**) or with a methyl group (**77f**) was well tolerated, showing thermal shift values similar to the reference **76**. Nevertheless, when the fluorine atom was replaced with an electron releasing group, such as a methoxy group (**77g**), the binding was abrogated (Table 8). We also investigated on the fluorine-substituted isomers of compound **76**. Thus, the fluorine was repositioned to the *meta* or *para* position of the phenyl ring. Although the *meta* substitution yielded a slight decrease in binding affinity (ΔT_m 3 °C, **77b**), the *para* substituted isomer displayed an increase of AGPS T_m up to 4 °C (**77c**). Prompted by these results, we synthesized also 2,4- and 2,6-difluoro analogues. Among them the 2,6-difluoro derivative (**77i**) induced an increase of AGPS T_m up to 5 °C. The additional attempts to shorten the distance between the phenyl (**77m**) or benzoimidazolone (**77n**) moieties and the amide group resulted in poor or none binding, thus showing that the length of the molecule and, in particular, the distance between the two

aromatic rings is essential for the binding. Furthermore, the double methylation of the urea moiety of the benzoimidazolone, such as its replacement with a benzoimidazole or with a superior homologue ring were not tolerated (**77o-q**, Table 8).

Table 8. Effect of the novel Inhibitors (**77a-q**) on AGPS Thermal Stability. The shift in T_m (ΔT_m) is considered in comparison with the unbound enzyme. Measurements were performed at least in triplicate; standard deviations are included in ± 10 %. * ΔT_m : increase in melting temperature (+, °C).

Cpd	Molecular structure	ΔT_m *	Cpd	Molecular structure	ΔT_m *
76		3.5	77i		5
77a		1.5	77j		1
77b		3.0	77k		0
77c		4.0	77l		3.0
77d		3.5	77m		1
77e		3.5	77n		0
77f		3.0	77o		0
77g		0	77p		0
77h		3.5	77q		0

7.2.3 Radioactivity assay of compounds **76**, **77a-f**, **77h-p**

(Group of Prof. Andrea Mattevi, Dr. Valentina Piano, Department of Biology and Biotechnology, University of Pavia)

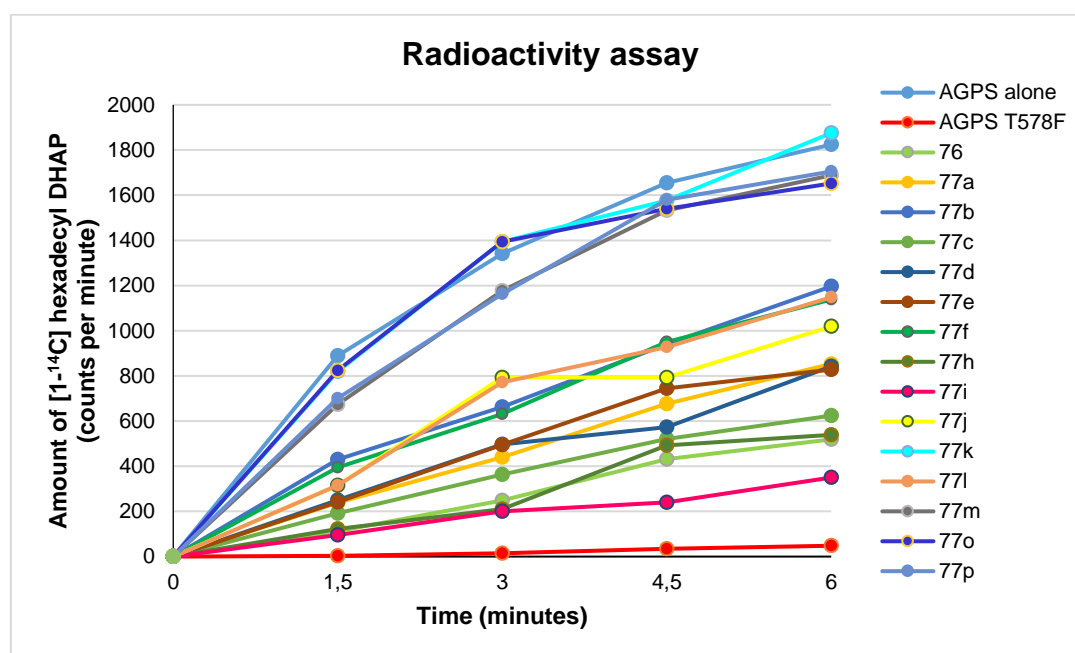


Figure 7.3. Inhibition of *Cavia porcellus* AGPS enzymatic activity was detected by a radioactivity assay using 100 μ M palmitoyl-DHAP, 96 μ M [1-¹⁴C]hexadecanol, and 180 μ M inhibitor and detecting the formation of [1-¹⁴C]hexadecyl-DHAP as a function of time. Controls were performed using AGPS alone and the catalytically inactive AGPS mutant T578F.³⁷⁷ Measurements were performed at least in triplicate and standard deviations are included in $\pm 10\%$.

To assess whether the compounds **77** had an effect on AGPS catalytic activity, we performed a radioactivity-based enzymatic assay. Palmitoyl-DHAP and [1-¹⁴C]-hexadecanol were used as substrates and the formation of [1-¹⁴C]-hexadecyl-DHAP was measured as a function of time in presence of the compounds **76**, **77a-f**, **77h-p**. Pleasingly, the inhibitory effect (Figure 7.3) was observed only with the compounds showing binding in ThermoFAD assay (**77d-f**, **77h-l**, **77n**, **77o**). Indeed, compounds **77o** and **77p**, showing no binding, did not show AGPS inhibition (Figure 7.3). Interestingly, the 2,6-difluoro substituted compound (**77i**), which gave the highest AGPS thermal shift, showed also the highest inhibition potency, even when compared to the lead compound **76** (Figure 7.3).

7.2.4 Three-dimensional structure of AGPS in complex with **77i**

(Group of Prof. Andrea Mattevi, Dr. Valentina Piano, Department of Biology and Biotechnology, University of Pavia)

To determine whether **77i** retained the same binding mode of the parent inhibitor **76**, the crystal structure of AGPS in complex with **77i** was determined by X-ray crystallography at high resolution (2.0-2.2 Å).

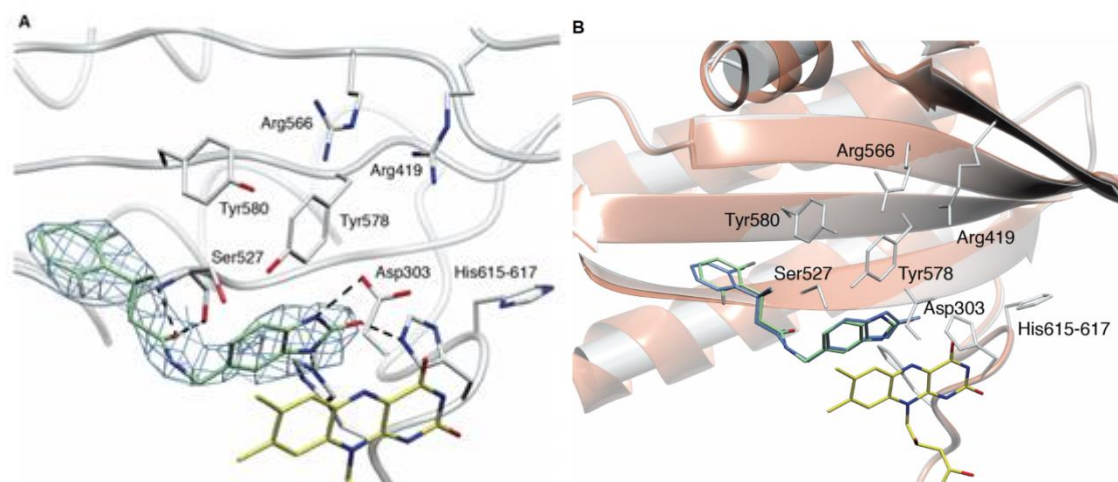


Figure 7.4. Crystal structure of *Cavia porcellus* AGPS in complex with inhibitor **77i**. **(A)** Weighted 2Fo – Fc final electron density map contoured at the 1.2 σ level for **77i**. The binding is mediated by specific H bonds (black dashed lines) with the active site residues Asp303, Ser527, His616, and His617, which force the benzoimidazolone moiety in front of the FAD cofactor, suggesting a π interactions with the cofactor isoalloxazine ring. **(B)** Superposition of the crystal structures of unbound AGPS (black), AGPS (grey) in complex with **77i** (green) and AGPS (coral) in complex with **76** (light blue). The binding of both **77i** and **76** results in the same conformational changes in the side chains of the catalytic residues Tyr580, Tyr578, Arg566 and Arg419, compared to the unbound enzyme. The superposition of **77i** and **76** shows that the binding site of the two inhibitors is perfectly conserved.

Although the quality of the collected data is not optimal, due to the low solubility of the inhibitor that damages the crystals (both in soaking and co-crystallization procedures), it is clear that **77i** binds in AGPS active site as expected (Figure 7.4 A). Indeed, the binding mode of the parent compound **76** is perfectly conserved, including the pattern of rearrangements in the side chains of the active site residues, compared to the unbound enzyme (Figure 7.4 B). The benzoimidazolone moiety is placed in the hydrophilic vertex of the V-shaped substrate cavity, where it establishes multiple H bonds with catalytic residues. The presence of the second fluorine on the phenyl ring most likely enhances the hydrophobic interactions of the **77i** side chain with the aliphatic residues surrounding the tunnel hosting the acyl-chain of the substrate.

7.2.5 Effect of AGPS inhibitor **77i** on ether lipids levels and on migration rate in 231MFP breast cancer cells

(Group of Prof Daniel K. Nomura, Department of Nutritional Sciences and Toxicology, University of California, Berkeley)

Next, we started to investigate whether compound **77i** was more effective than the lead compound **76** also in a cellular context. Therefore, compound **77i** was tested in the 231MFP breast cancer cell line, to study its effects on lipid metabolism, and cell migration

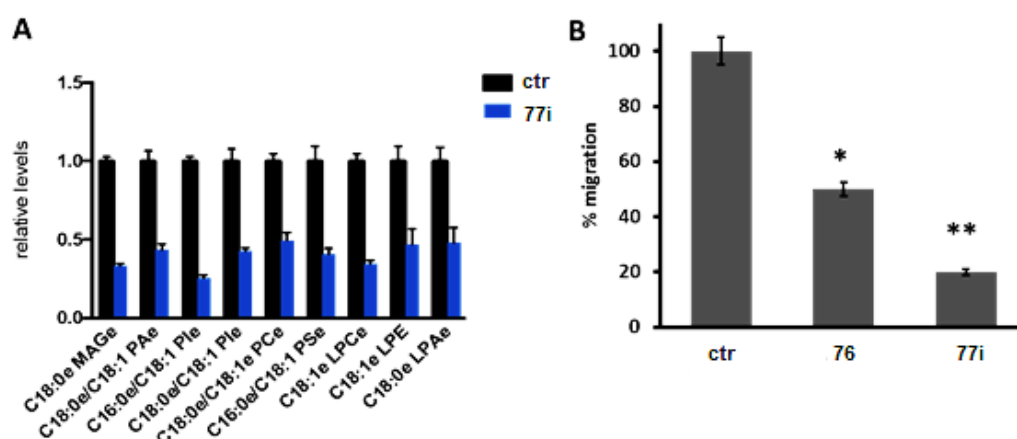


Figure 7.5. (A) AGPS inhibitor **77i** lowers ether lipid levels in 231MFP breast cancer cells. Shown are lipidomic profiling data from 231MFP breast cancer cells treated with vehicle (DMSO) or **77i** (500 μ M) for 24 h. Data in bar graphs are shown as average \pm SEM. Lipid abbreviations are included in the Abbreviations list. Lower case “e” and “p” letters indicate ether and plasmalogen phospholipids, respectively; (B) AGPS inhibitor **77i** effect upon cell migration rate in 231MFP breast cancer cells. Vehicle (DMSO) or **77i** or **76** (used as reference positive control) were preincubated with cancer cells before seeding cells into serum-free survival or migration assays. Data shown as average \pm SEM, n =3–4/group. Significance is represented as *p < 0.05 and as **p < 0.01 related to control groups

Compound **77i** decreased the level of ether phospholipids synthesis, ranging from 50 % (PLe, LPE and LPAe) to 75 % (PLe) (Figure 7.5 A). Moreover, **77i** was able to reduce of 80 % the migration of 231MFP breast cancer cells, while compound **76** showed only a 50 % decrease (Figure 7.5 B). These data further confirmed **77i** to be more efficient even in a cellular context. However, in this assay we were not able to observe such effects treating cells with lower concentration than 500 μ M (data not shown).

7.2.6 Compound **77i**, but not its analogue **77p**, increases E-cadherin and reduces Snail and Mmp2 expression in PC3 and MDA-MB231 cancer cells

(Group of Prof. Marco Tripodi, Dr. Raffaele Strippoli, Dr. Cecilia Battistelli, Department of cellular Biotechnology and Hematology, “Sapienza” University of Rome)

In the tumor development and progression, invasion represents a crucial step associated with an altered gene and cellular lipids expression. The development of an invasive phenotype has been

associated with cancer aggravation.³⁹¹ In particular, invasiveness is typically associated with the epithelial-mesenchymal transition (EMT) process accompanied by a downregulation of adhesion molecules expression (E-cadherin), as well as an increase of factors as metalloproteinases (MMP-2/9), involved in the degradation of basement membrane components.³⁹²⁻³⁹⁵ In 2014, Zhu *et al.* published a study where they investigated on the role of AGPS in regulating the invasion potential in glioma (U-87) and hepatic carcinoma cells (HepG2),³⁸³ thus disclosing the existing link between AGPS and invasiveness. The authors found that AGPS-*knock-down* improved the expression of E-cadherin, regulated MMP2/9 gene, and reduced activity of the MAPK signaling pathway and transcription activity of Twist, AP-1, and Snail.³⁸³

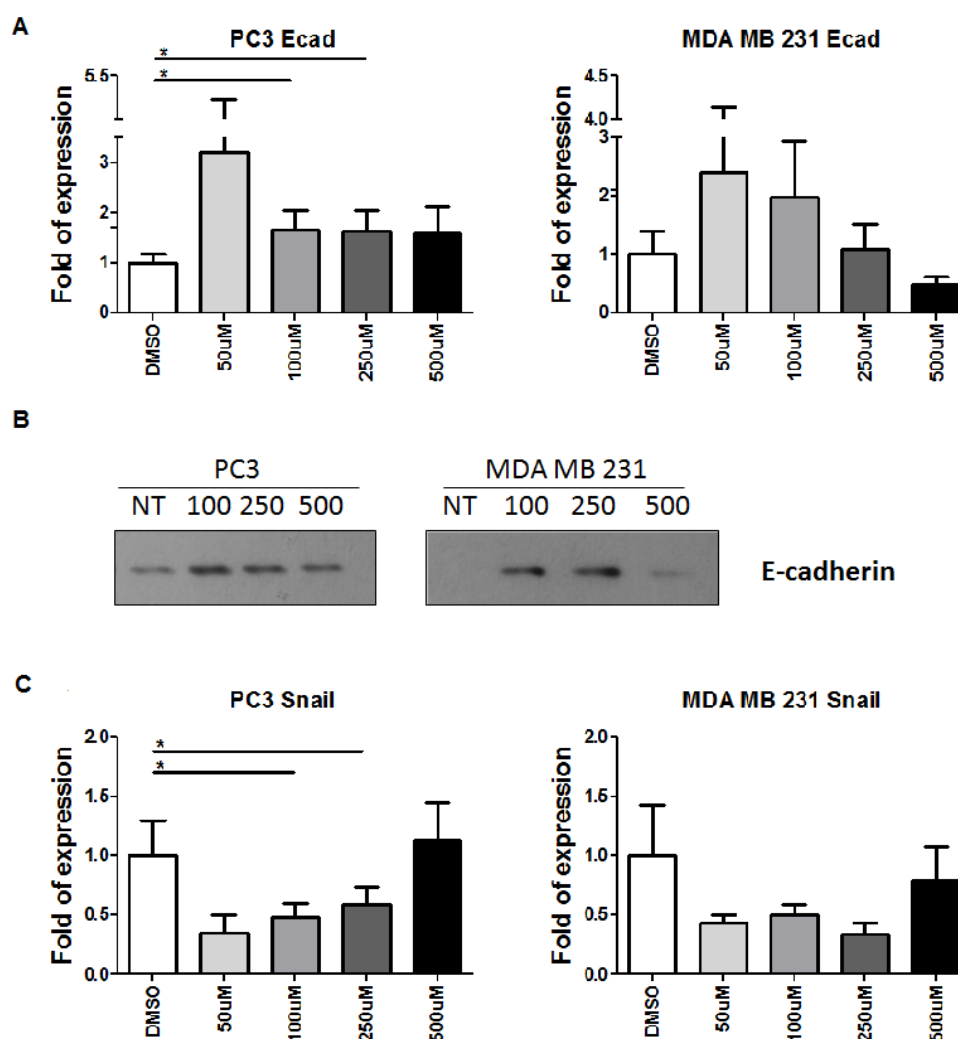


Figure 7.6. Effects of **77i** (50, 100, 250, 500 μM) on PC3 and MDA-MB231 cancer cells after 24 hours treatment. Vehicle (DMSO) treated cells have been used as control. (A) E-cadherin transcript quantification via RT-PCR in PC3 and MDA-MB231 cancer cells; (B) a typical western blot showing the effect of **77i** (50, 100, 250 μM) on E-cadherin protein levels in PC3 and MDA-MB231 cancer cells; (C) Snail transcript quantification via RT-PCR in PC3 and MDA-MB231 cancer cells. Each data is the mean of at least three independent experiments. Error bars are shown.

Based on these scientific evidences, we decided to better investigate about the mechanism of compound **77i**, and check if AGPS pharmacological inhibition could reproduce the effects observed by Zhu *et al.* with genetic *knock-down*. In collaboration with the group of Prof. Tripodi, having a long experience and a good know-how in EMT investigation, we looked at the effects of compound **77i** in human prostate cancer (PC3) and breast adenocarcinoma (MDA-MB231) cell lines. First, we measured the levels of E-cadherin (protein and mRNA), Snail (mRNA) and MMP2 (mRNA) after 24 hours treatment with **77i** (Figure 91, 92). Considering what previously observed for 231MFP breast cancer cells, we decided to use **77i** in a dose range, being 500 μ M the highest dose. Vehicle (DMSO) treated cells have been used as control. The preliminary results showed that **77i** is able to increase E-cadherin expression and protein levels in PC3 and MDA-MB231 cancer cells when compared to the vehicle treated control (Figure 7.6 A, B). In MDA-MB231 after treatment with 500 μ M of **77i** we observed a reduction of E-cadherin levels, we could speculate that it could be due to cytotoxic effects related to the high dosage (see cell proliferation experiments). Accordingly, **77i** reduced Snail expression when compared to the vehicle treated control, with the sole exception of the 500 μ M treated PC3 cells, where an increase in Snail levels was observed (Figure 7.6 C). Similarly, a reduction in MMP2 expression was observed in both treated cell lines (Figure 7.7). The fact that we are not able to see a dose-dependent effect, once again, could be related to cytotoxic effects of high doses treatment.

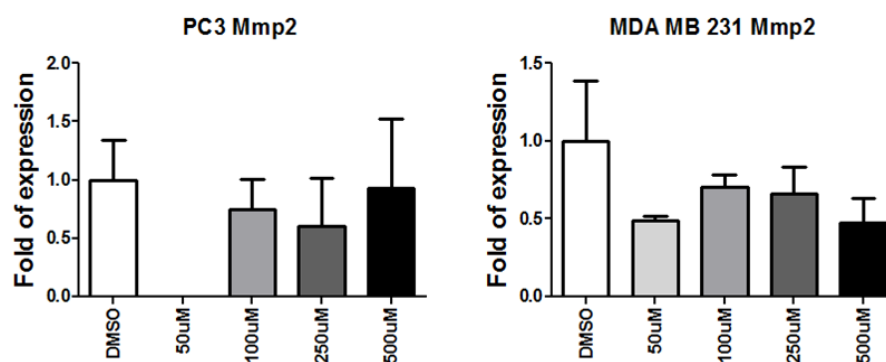


Figure 7.7. Effects of **77i** (50, 100, 250, 500 μ M) on PC3 and MDA-MB231 cancer cells after 24 hours treatment. Vehicle (DMSO) treated cells have been used as control. Mmp2 transcript quantification via RT-PCR in PC3 and MDA-MB231 cancer cells. Each data is the mean of at least two independent experiments. Error bars are shown.

In order to better validate these results, we decided to evaluate the effects of **77i** in comparison with our previous lead **76** and with the bis-methylated inactive analogue **77p** (negative control), all tested in a dose range (50, 100, 250 μ M) in PC3 and MDA-MB231 cancer cell lines (Figure 7.8). **77i** was confirmed to increase E-cadherin, and reduce Snail and MMP2 expression levels in both tested cell lines (Figure 7.8).

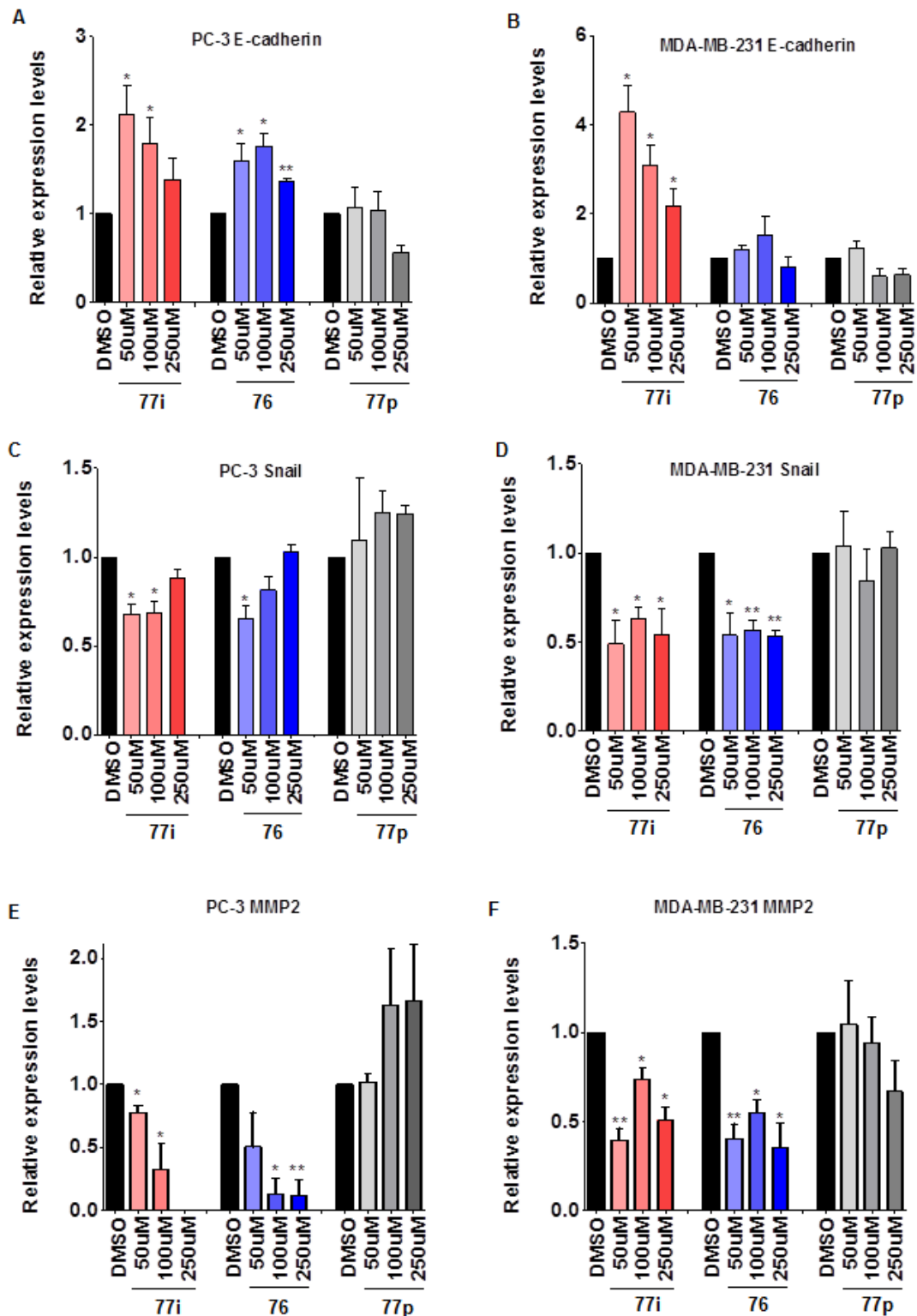


Figure 7.8. Effects of **76**, **77i**, and **77p** (negative control) in a dose range (50, 100, 250 μ M) on PC3 and MDA-MB231 cancer cells after 24 hours treatment. Vehicle (DMSO) treated cells have been used as control. **(A-B)** E-cadherin transcript quantification via RT-PCR in PC3 and MDA-MB231 cancer cells; **(C-D)** Snail transcript quantification via RT-PCR in PC3 and MDA-MB231 cancer cells. **(E-F)** MMP2 transcript quantification via RT-PCR in PC3 and MDA-MB231 cancer cells. The results represent the average \pm SEM of at least three independent experiments performed in triplicates. Significance is represented as * $p < 0.05$ and as ** $p < 0.01$ related to control groups.

Also compound **76** displayed a similar trend if compared to **77i**. Pleasingly, compound **77p**, previously shown not to bind AGPS, and inactive as AGPS inhibitor, had no significant effect on E-cadherin, Snail and MMP2 expression (Figure 7.8). These preliminary data are a starting point for further target validation, and furnished important information about the mechanism of action of AGPS inhibitors. We proved for the first time that AGPS pharmacological inhibition can reduce cancer cell invasiveness, directly influencing E-cadherin, MMP2 and Snail expression. The reported data suggest that there may be a different sensitivity of these two cell lines to AGPS inhibition. In order to find an explanation to this evidence, we measured the AGPS mRNA expression levels in these cell lines. As shown in Figure 7.9A, the expression level of AGPS in MDA-MB 231 cell line is more than double, if compared to PC-3 cells. Thus, justifying the different response of the two cell lines to AGPS inhibitors. In further investigation we also studied the effect of compound **77i** on PC-3 and MDA-MB 231 cancer cell lines. Interestingly, compound **77i** had no strong antiproliferative effects till the dose of 100 μM , however at 250 μM we started to see antiproliferative activity, that could explain what observed for EMT markers expression.

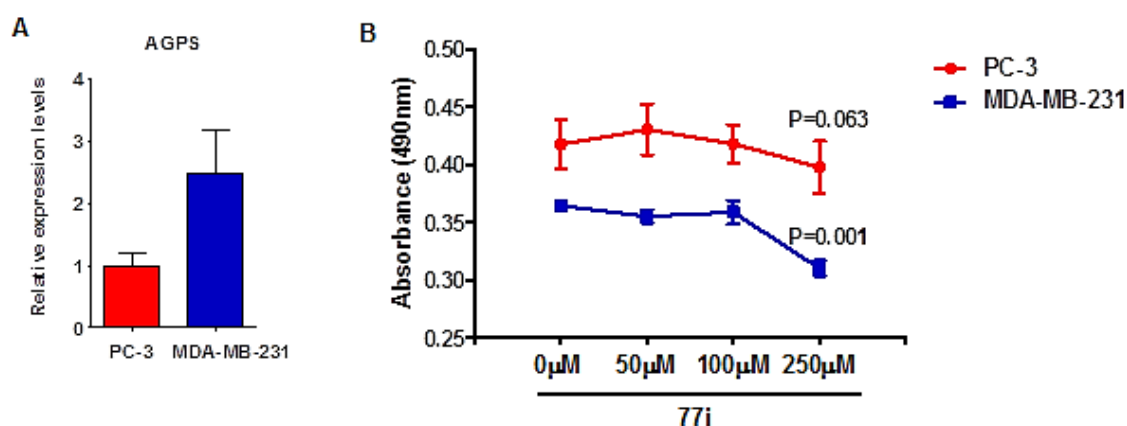


Figure 7.9. (A) mRNA expression of AGPS in PC-3 and MDA-MB-231 cells. Quantitative RT-PCR was performed on total RNA. L32 levels were used for normalization. Bars represent \pm SEM of seven independent experiments. (B) Dose-response curves for antiproliferative activity of **77i**, in a dose range (50, 100, 250 μM) on PC-3 and MDA-MB-231 cancer cells after 24 h treatment. The results represent the average \pm SEM of two independent experiments performed in triplicate. Significance is represented as * $p < 0.05$ and as ** $p < 0.01$ related to control groups.

7.3 Conclusions and future perspectives

The FAD-dependent enzyme AGPS recently became an interesting potential target against aggressive metastatic tumors, as it has been found to be up-regulated across different types of aggressive cancer cell lines, such as human breast 231 MFP, melanoma C8161, and prostate PC3 cancers.³⁸⁰ AGPS knockdown led to an overall reduction of ether lipid levels, as well as oncogenic signaling molecules, such as LPAe, PAFe and eicosanoids, and it showed to lower

tumor growth rate in xenograft mice.³⁸⁰ The newly established small-molecule screening (ThermoFAD) allowed us to identify and characterize the first AGPS inhibitor, compound **76**, which recapitulates the features of AGPS knockdown. In this study, we presented the design and development of compound **76** derivatives, aimed to highlight structure-activity relationship and define the pharmacophore elements, and to increase the inhibition potency both *in vitro* and in cancer cells. We applied several structural manipulations on compound **76**, like the modulation of the steric hindrance at the α or β carbon or the insertion of different substituents on the phenyl ring of phenylpropionamide moiety, shortening the distance in turn between the phenyl or benzimidazolone moiety and the amide link, the bis methylation of urea moiety of the benzimidazolone scaffold, its replacement with a benzoimidazolone or with a superior cyclic homologue. Among all mentioned chemical manipulations, the sole 2,6-difluoro-substitution (**77i**) resulted in an improvement of the activity (confirmed by binding and enzymatic assay). The co-crystal structure of AGPS with **77i** revealed that this compound retained the binding mode observed for **76**. We speculate that the second fluorine on the phenyl ring of **77i** enhances the hydrophobic interactions with the aliphatic residues surrounding the substrate tunnel. When tested in 231MFP breast cancer cell, compound **77i** lowered from 50% (PCe, LPE and LPAe) to 75% (PLE) ether lipid levels, and reduced up to 80% the cell migration rate. Once tested in prostate cancer PC3 and breast adenocarcinoma MDA-MB231 cell lines, compound **77i** was able to increase E-cadherin expression, while reducing Snail and MMP2 transcript levels. Pleasingly, the bis-methylated analogue **77p**, that displayed no target binding and inhibition activity *in vitro*, had no effects on the expression of these markers.

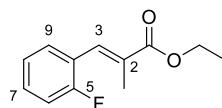
This study allowed us to accumulate further evidences about the potential role of benzoimidazolone based AGPS inhibitors and their structural requisites for binding. The collected results show that the inhibitor identified in the initial screening **76** engages so specific interactions with the catalytic residues of AGPS active site, that only minor changes in the scaffold are tolerated. Even though biochemical and crystallography data, as well as preliminary cell-based data are quite promising, an improvement of the pharmacokinetic properties, such as solubility and cell permeability, is still required. It is in our interest to better investigate about the cellular mechanism of action of this class of compounds. More in detail, we will try to better discern the relation between AGPS and invasiveness, reconstructing the molecular pathways involved. To the best of our knowledge, there are no other AGPS inhibitors reported in the literature. Compound **77i** will serve as a tool for any further investigation.

7.4 Experimental section

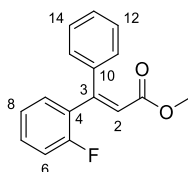
7.4.1 Chemistry

Melting points were determined on a Buchi 530 melting point apparatus and are uncorrected. ^1H NMR and ^{13}C NMR spectra were recorded at 400 and 100 MHz, respectively, on a Bruker AC 400 spectrometer; chemical shifts are reported in δ (ppm) units relative to the internal reference tetramethylsilane (Me_4Si). EIMS spectra were recorded with a Fisons Trio 1000 spectrometer; only molecular ions (M^+) and base peaks are given. All compounds were routinely checked by TLC and ^1H NMR. TLC was performed on aluminum-backed silica gel plates (Merck DC, Alufolien Kieselgel 60 F254) with spots visualized by UV light. All solvents were reagent grade and, when necessary, were purified and dried by standard methods. Concentration of solutions after reactions and extractions involved the use of a rotary evaporator operating at reduced pressure of ca. 20 Torr. Organic solutions were dried over anhydrous sodium sulfate. Elemental analysis has been used to determine purity of the described compounds, that is, >95%. Analytical results are within $\pm 0.40\%$ of the theoretical values. All chemicals were purchased from Sigma-Aldrich, Milan (Italy), or from Alfa Aesar, Karlsruhe (Germany), and were of the highest purity.

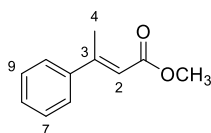
General procedure for the ester intermediates 78a-l. Example: Synthesis of ethyl 3-(2-fluorophenyl)-2-methylacrilate (78l)



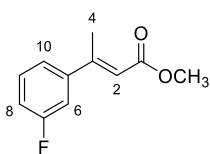
To a suspension of anhydrous K_2CO_3 (8.06 mmol, 2 eq, 1.11 g) in dry EtOH (10 mL) were added in sequence triethyl-2-phosphonopropionate (4.83 mmol, 1.2 eq, 1.04 mL) and 2-fluorobenzaldehyde (4.03 mmol, 1.0 eq, 0.42 mL). The reaction mixture was kept stirring at 80 °C for 7 h. After this time reaction was quenched with water (10 mL), concentrated *in vacuo*, and the residue was extracted with ethyl acetate (3 x 10 mL). The organic layer was dried over Na_2SO_4 , filtered and concentrated *in vacuo*. The crude has been purified by column chromatography on silica gel eluting with *n*-hexane: ethyl acetate 50:1 to get the compound **78l** as a light yellow oil as a mixture of the two isomers cis:trans=1:2 (205 mg, 0.984 mmol, 41 %). ^1H -NMR (CDCl_3 , 400 MHz, δ ; ppm): δ_{H} 1.11 (3H, t, $J = 7.2$ Hz, $\text{COOCH}_2\text{CH}_3$ CIS), 1.38 (6H, $J = 7.2$ Hz, $2 \times$ (3H), t, $\text{COOCH}_2\text{CH}_3$ TRANS), 2.06 (6H, $2 \times$ (3H), s, $\text{C}(2)\text{CH}_3$ TRANS), 2.15 (3H, s, $\text{C}(2)\text{CH}_3$ CIS), 4.12 (2H, q, $J = 6.8$ Hz, $\text{COOCH}_2\text{CH}_3$ CIS), 4.30 (4H, $2 \times$ (2H), q, $J = 7.2$ Hz, $\text{COOCH}_2\text{CH}_3$ TRANS), 6.75 (1H, s, $\text{C}(3)\text{H}$ CIS), 7.04-7.39 (12 H, m, aromatic protons CIS e TRANS), 7.72 (2H, s, $\text{C}(3)\text{H}$ TRANS) ppm. ^{13}C NMR (CDCl_3 , 100 MHz, δ ; ppm) δ_{C} : 13.4, 14.7, 60.5, 115.8, 121.9, 124.9, 130.6, 131.0, 132.0, 132.9, 158.6, 169.2 ppm. MS (EI) m/z [M] $^+$ calculated: 208.0900, found: 208.0896.³⁹⁶

Example: Synthesis of methyl 3-(2-fluorophenyl)-3-phenylacrylate (78k)

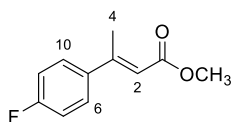
Trimethyl phosphonacetate (5.21 mmol, 1.25 eq, 0.505 mL) was added dropwise to a suspension of NaH (5.21 mmol, 1.25 eq, 0.125 g) in dry THF (8 mL) at 0 °C under inert atmosphere (N₂). After 30 minutes, 2-fluorobenzophenone (4.17 mmol, 1.0 eq, 0.42 mL) was added to the reaction mixture. The reaction mixture was let to warm slowly to room temperature. The system was kept stirring at room temperature for 19 h. After this time, the reaction was complete and it was quenched by addition of 10 mL of a 1 M solution of NH₄Cl and the product was extracted with Et₂O. The combined organic layers were dried over Na₂SO₄, filtered, and concentrated *in vacuo*. The crude was purified by silica gel chromatography eluting with *n*-hexane: ethyl acetate, 50 :1 to give the pure **78k** as a colourless oil (500 mg, 1.95 mmol, 78 %). ¹H-NMR (CDCl₃, 400 MHz, δ; ppm): δ_H 3.56 (3H, s, COOCH₃); 6.27 (1H, s, C(2)H); 6.93-7.09 (3H, m, C(9)H, C(11)H, C(15)H); 7.15 (2H, m, C(7)H, C(13)H); 7.22-7.30 (4H, m, C(6)H, C(8)H, C(12)H, C(14)H) ppm. ¹³C NMR (CDCl₃, 100 MHz, δ; ppm) δ_C: 52.2, 114.3, 119.8, 123.7, 126.2 (2C), 127.3, 128.1, 128.3 (2C), 129.1, 130.8, 136.6, 152.1, 158.5, 166.9 ppm. MS (EI) m/z [M]⁺ calculated: 256.0900, found: 256.0903.³⁹⁷

Chemical and Physical Data, ¹H NMR, melting points, and MS (EI) Data for Compounds 78a-j.

Methyl-3-phenylbut-2-enoate (78a). ¹H NMR (CDCl₃, 400 MHz, δ, ppm): δ_H 2.41 (3H, d, *J* = 1.2 Hz, C(4)H₃), 3.73 (3H, s, COOCH₃), 6.10 (1H, d, *J* = 1.2 Hz, C(2)H), 7.39-7.48 (5H, m, aromatic protons) ppm. m.p.: oil. MS (EI) m/z [M]⁺ calculated: 176.0837; found: 176.0842.³⁹⁸

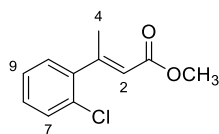


Methyl-3-(3-fluorophenyl)but-2-enoate (78b). ¹H NMR (CDCl₃, 400 MHz, δ, ppm): δ_H 2.49 (3H, d, *J* = 1.2 Hz, C(4)H₃), 3.69 (3H, s, COOCH₃), 6.07 (1H, d, *J* = 1.2 Hz, C(2)H), 6.97-7.02 (1H, tdd, *J* = 1.2 Hz, 2.2 Hz, 8.2 Hz, C(9)H), 7.09 (1H, dt, *J* = 2 Hz, 10.4 Hz, C(10)H), 7.16-7.19 (1H, m, C(8)H), 7.25-7.30 (1H, m, C(6)H) ppm. (TRANS only). m.p.: oil. MS (EI) m/z [M]⁺ calculated: 194.0743; found: 194.0740.

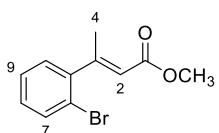


Methyl-3-(4-fluorophenyl)but-2-enoate (78c). ¹H NMR (CDCl₃, 400 MHz, δ, ppm): δ_H 2.58 (3H, d, *J* = 1.2 Hz, C(4)H₃), 3.78 (3H, s, COOCH₃), 6.12 (1H, d, *J* = 1.2 Hz, C(2)H), 7.09 (2H, t, *J* = 7.8 Hz, C(6)H, C(10)H),

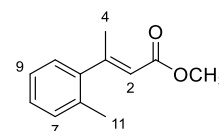
7.46-7.50 (2H, m, C(7)H, C(9)H) ppm. (TRANS only). m.p.: oil. MS (EI) m/z [M]⁺ calculated: 194.0743; found: 194.0739.³⁹⁸



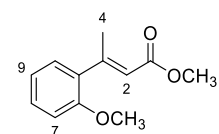
Methyl-3-(2-chlorophenyl)but-2-enoate (78d). ¹H NMR (CDCl₃, 400 MHz, δ, ppm): δ_H 2.19 (3H, d, *J* = 1.2 Hz, C(4)H₃ TRANS), 2.52 (3H (2), d, *J* = 1.2 Hz, C(4)H₃ CIS), 3.57 (3H, s, COOCH₃ TRANS), 3.78 (3H (2), s, COOCH₃ CIS), 5.86 (1H (0.6), d, *J* = 1.6 Hz, C(2)H CIS) 6.04 (1H, d, *J* = 1.6 Hz, C(2)H TRANS), 7.09 (1H, dd *J* = 2.4 Hz, 6.1 Hz, aromatic proton), 7.18-7.20 (1H, m, aromatic proton), 7.24-7.31 (4H, m, aromatic protons CIS+TRANS), 7.39-7.43 (2H, m, aromatic protons CIS+TRANS) ppm. m.p.: oil. MS (EI) m/z [M]⁺ calculated: 210.0448; found: 210.0450.³⁹⁹



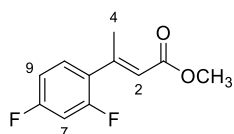
Methyl-3-(2-bromophenyl)but-2-enoate (78e). ¹H NMR (CDCl₃, 400 MHz, δ, ppm): δ_H 2.18 (3H, d, *J* = 1.2 Hz, C(4)H₃ TRANS), 2.50 (3H (2), d, *J* = 1.2 Hz, C(4)H₃ CIS), 3.57 (3H, s, COOCH₃ TRANS), 3.78 (3H (2), s, COOCH₃ CIS), 5.84 (1H (0.7), d, *J* = 1.2 Hz, C(2)H CIS), 6.03 (1H, d, *J* = 1.2 Hz, C(2)H TRANS), 7.09 (1H, dd, *J* = 1.6 Hz, 7.6 Hz, aromatic proton), 7.16-7.21 (3H, m, aromatic protons CIS+TRANS), 7.30-7.36 (2H, m, aromatic protons CIS+TRANS), 7.60 (2H, d, *J* = 8 Hz, aromatic protons) ppm. m.p.: oil. MS (EI) m/z [M]⁺ calculated: 253.9942; found: 253.9945.



Methyl-3-(o-tolyl)but-2-enoate (78f). ¹H NMR (CDCl₃, 400 MHz, δ, ppm): δ_H 2.21 (3H, s, C(11)H₃), 2.38 (3H, d, *J* = 1.2 Hz, C(4)H₃), 3.68 (3H, s, COOCH₃), 5.70 (1H, d, *J* = 1.2 Hz, C(2)H), 6.99 (1H, d, *J* = 6.8 Hz, C(7)H), 7.08-7.17 (3H, m, C(8)h, C(9)H, C(10)H) ppm. (TRANS only). m.p.: oil. MS (EI) m/z [M]⁺ calculated: 190.0994; found: 190.0992.³⁹⁸

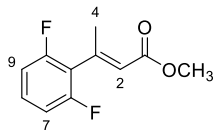


Methyl-3-(2-methoxyphenyl)but-2-enoate (78g). ¹H NMR (CDCl₃, 400 MHz, δ, ppm): δ_H 2.18 (3H, d, *J* = 1.2 Hz, C(4)H₃ TRANS), 2.52 (3H (2), d, *J* = 1.2 Hz, C(4)H₃ CIS), 3.56 (3H, s, COOCH₃ TRANS), 3.68 (3H (2.4), s, COOCH₃ CIS), 3.83 (3H, s, OCH₃ TRANS), 3.86 (3H (2.5), s, OCH₃ CIS), 5.93 (1H (0.7), d, *J* = 1.2 Hz, C(2)H CIS), 5.99 (1H, d, *J* = 1.2 Hz, C(2)H TRANS), 6.92-7.06 (5H, m, aromatic protons CIS+TRANS), 7.15-7.17 (1H (0.76), dd, *J* = 1.6 Hz, 7.6 Hz, aromatic proton CIS) 7.28-7.35 (2H, m, aromatic protons CIS+TRANS) ppm. m.p.: oil. MS (EI) m/z [M]⁺ calculated: 206.0943; found: 206.0941.⁴⁰⁰

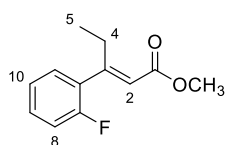


Methyl-3-(2,4-difluorophenyl)but-2-enoate (78h). ¹H NMR (CDCl₃, 400 MHz, δ, ppm): δ_H 2.09 (3H (2.5), d, *J* = 1.2 Hz, C(4)H₃ TRANS), 2.44 (3H, d, *J* = 1.2 Hz, C(4)H₃ CIS), 3.52 (3H, s, COOCH₃ TRANS), 3.69 (3H (2.5), s, COOCH₃ CIS), 5.91 (1H (0.8), d, *J* = 1.2 Hz, C(2)H CIS), 5.96 (1H, d, *J* = 1.2 Hz, C(2)H

TRANS), 6.73-6.83 (4H, m, aromatic protons, CIS+TRANS), 7.01-7.06 (1H, m, aromatic proton), 7.16-7.22 (1H, m, aromatic proton) ppm. m.p.: oil. MS (EI) m/z [M]⁺ calculated: 212.0649; found: 212.0651.

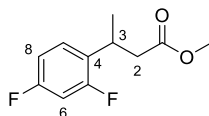


Methyl-3-(2,6-difluorophenyl)but-2-enoate (78i). ¹H NMR (CDCl₃, 400 MHz, δ, ppm): δ_H 2.40 (3H, d, *J* = 1.2 Hz, C(4)H₃), 3.69 (3H, s, COOCH₃), 5.87 (1H, t, *J* = 0.8 Hz, C(2)H), 6.82-6.86 (2H, m, C(7)H, C(9)H), 7.14-7.20 (1H, m, C(8)H) ppm. m.p.: oil. MS (EI) m/z [M]⁺ calculated: 212.0649; found: 212.0647.



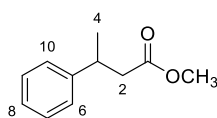
Methyl-3-(2-fluorophenyl)pent-2-enoate (78j). ¹H NMR (CDCl₃, 400 MHz, δ, ppm): δ_H 1.08-1.11 (3H, t, *J* = 7.2 Hz, C(5)H₃), 2.47-2.52 (2H, q, *J* = 7.2 Hz, C(4)H₂), 3.59 (3H, s, COOCH₃), 6.03 (1H, bs, C(2)H), 7.07-7.18 (3H, m, aromatic protons), 7.31-7.35 (1H, m, aromatic proton) ppm. m.p.: oil. MS (EI) m/z [M]⁺ calculated: 208.0900; found: 208.0903.

General procedure for the arylpropionic esters intermediates 79a-l. Example: Synthesis of methyl 3-(2,4-difluorophenyl)butanoate (79h)



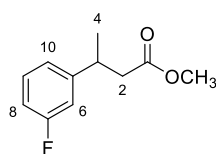
A 0.05 M solution of methyl-3-(2,4-difluorophenyl)but-2-enoate (279 mg, 1.31 mmol) (**78h**) in methanol has been reduced under flow conditions (1 mL/min) on Pd/C 10 % catalyst in presence of an H₂ pressure of 10 bar by using H-Cube® (Thales Nano) to give **79h**. The solvent has been removed *in vacuo*, to give the pure product. No further purification was required (222.8 mg, 1.04 mmol, 80 %). m.p.: oil. ¹H-NMR (CDCl₃, 400 MHz, δ; ppm): δ_H 1.30 (3H, d, *J* = 6.8 Hz, C(3)CH₃), 2.54-2.60 (2H, dd, *J* = 15.4 Hz, 7.6 Hz, C(2)H), 2.63-2.69 (2H, dd, *J* = 15.4 Hz, 7.6 Hz, C(2)H'), 3.47-3.56 (1H, m, C(2)H), 3.63 (1H, s, COOCH₃), 6.74-6.84 (2H, m, C(6)H, C(8)H), 7.14-7.20 (1H, m, C(7)H) ppm. ¹³C NMR (CDCl₃, 100 MHz, δ; ppm) δ_C: 20.2, 33.0, 38.9, 51.6, 103.6, 111.6, 129.3, 131.1, 153.9, 163.3, 172.1 ppm. MS (EI) m/z [M]⁺ calculated: 214.0805, found: 214.0799.

Chemical and Physical Data, ¹H NMR, melting points, and MS (EI) Data for Compounds 79a-g, 79i-k.



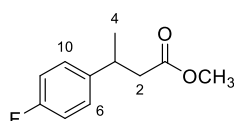
Methyl 3-phenylbutanoate (79a). ¹H NMR (CDCl₃, 400 MHz, δ, ppm): δ_H 1.30 (3H, d, *J* = 6.8 Hz, C(4)H₃), 2.47-2.52 (1H, dd, *J* = 15.4 Hz, 7.6 Hz, C(2)H), 2.59-2.64 (1H, dd, *J* = 15.4 Hz, 7.6 Hz, C(2)H'), 3.39-3.43 (1H, m,

C(3)H), 3.68 (3H, s, COOCH₃), 7.14-7.18 (1H, m, C(8)H), 7.24 (2H, t, *J* = 7.6 Hz, C(7)H, C(9)H), 7.35 (2H, dd, *J* = 7.6 Hz, C(6)H, C(10)H) ppm. m.p.: oil. MS (EI) *m/z* [M]⁺ calculated: 178.0994; found: 178.0990.⁴⁰¹



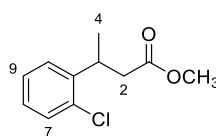
Methyl 3-(3-fluorophenyl)butanoate (79b). ¹H NMR (CDCl₃, 400 MHz, δ, ppm): δ_H 1.39-1.40 (3H, d, *J* = 4 Hz, C(4)H), 2.62-2.67 (1H, dd, *J* = 12 Hz, 8 Hz, C(2)H), 2.69-2.74 (1H, dd, *J* = 12 Hz, 8 Hz, C(2)H'), 3.36-3.41 (1H, m, C(3)H), 3.73 (3H, s, COOCH₃), 6.97-7.04 (2H, m, C(6)H, C(8)H),

7.10 (1H, d, *J* = 8 Hz, C(10)H), 7.33-7.38 (1H, q, *J* = 8 Hz, C(9)H) ppm. m.p.: oil. MS (EI) *m/z* [M]⁺ calculated: 196.0900; found: 196.0897.



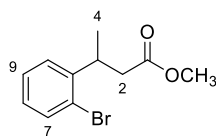
Methyl 3-(4-fluorophenyl)butanoate (79c). ¹H NMR (CDCl₃, 400 MHz, δ, ppm): δ_H 1.39 (3H, d, *J* = 8 Hz, C(4)H), 2.62-2.71 (2H, m, C(2)H₂), 3.36-3.40 (1H, m, C(3)H), 3.72 (3H, s, COOCH₃), 7.08 (2H, t, *J* = 8 Hz, C(6)H, C(10)H), 7.26-7.29 (2H, m, C(7)H, C(9)H) ppm. m.p.: oil. MS (EI) *m/z* [M]⁺ calculated:

196.0900; found: 196.0904.³⁹⁸

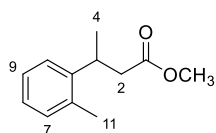


Methyl 3-(2-chlorophenyl)butanoate (79d). ¹H NMR (CDCl₃, 400 MHz, δ, ppm): δ_H 1.30 (3H, d, *J* = 6.8 Hz, C(4)H₃), 2.50-2.56 (1H, dd, *J* = 8.8 Hz, 15.2 Hz, C(2)H), 2.68-2.73 (1H, dd, *J* = 8.8 Hz, 15.2 Hz, C(2)H'), 3.65 (3H, s, COOCH₃), 3.77-3.82 (1H, m, C(3)H), 7.12-7.25 (4H, m, aromatic protons) ppm. m.p.: oil.

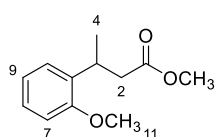
MS (EI) *m/z* [M]⁺ calculated: 212.0604; found: 212.0607.⁴⁰¹



Methyl 3-(2-bromophenyl)butanoate (79e). ¹H NMR (CDCl₃, 400 MHz, δ, ppm): δ_H 1.30 (3H, d, *J* = 6.8 Hz, C(4)H₃), 2.52-2.58 (1H, dd, *J* = 8.4 Hz, 15.2 Hz, C(2)H), 2.60-2.66 (1H, dd, *J* = 8.4 Hz, 15.2 Hz, C(2)H'), 3.24-3.33 (1H, m, C(3)H), 3.62 (3H, s, COOCH₃), 7.18-7.23 (3H, m, C(7)H, C(9)H, C(10)H), 7.29-7.32 (1H, m, C(8)H) ppm. m.p.: oil. MS (EI) *m/z* [M]⁺ calculated: 256.0099; found: 256.0095.⁴⁰¹

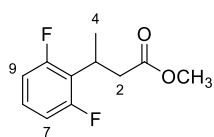


Methyl 3-(o-tolyl)butanoate (79f). ¹H NMR (CDCl₃, 400 MHz, δ, ppm): δ_H 1.25 (3H, d, *J* = 6.8 Hz, C(4)H₃), 2.38 (3H, s, C(11)H₃), 2.50-2.56 (1H, dd, *J* = 8.8 Hz, 15.4 Hz, C(2)H), 2.61-2.66 (1H, dd, *J* = 8.8 Hz, 15.4 Hz, C(2)H'), 3.49-3.58 (1H, m, C(3)H), 3.63 (3H, s, COOCH₃), 7.07-7.17 (4H, m, aromatic protons) ppm. m.p.: oil. MS (EI) *m/z* [M]⁺ calculated: 192.1150; found: 192.1147.⁴⁰²

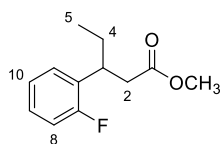


Methyl 3-(2-methoxyphenyl)butanoate (79g). ¹H NMR (CDCl₃, 400 MHz, δ, ppm): δ_H 1.27 (3H, d, *J* = 6.8 Hz, C(4)H₃), 2.48-2.54 (1H, dd, *J* = 9.2 Hz, 15 Hz, C(2)H), 2.67-2.72 (1H, dd, *J* = 9.2 Hz, 15 Hz, C(2)H'), 3.62-

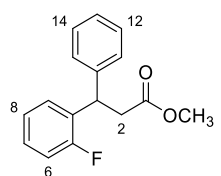
3.67 (4H, m, C(3)H, C(11)H₃), 3.83 (3H, s, COOCH₃), 6.86 (1H, d, *J* = 8 Hz, C(7)H), 6.91 (1H, t, *J* = 7.6 Hz, C(9)H), 7.16-7.21 (2H, m, C(8)H, C(10)H) ppm. m.p.: oil. MS (EI) *m/z* [M]⁺ calculated: 208.1099; found: 208.1098.⁴⁰¹



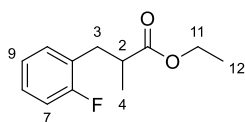
Methyl 3-(2,6-difluorophenyl)butanoate (79i). ¹H NMR (CDCl₃, 400 MHz, δ, ppm): δ_H 1.46-1.47 (3H, d, *J* = 4 Hz, C(4)H₃), 2.85 (2H, t, *J* = 6 Hz, C(2)H₂), 3.73 (3H, s, COOCH₃), 3.83-3.87 (1H, m, C(3)H), 6.94 (2H, t, *J* = 8 Hz, C(7)H, C(9)H), 7.21-7.26 (1H, m, C(8)H) ppm. m.p.: oil. MS (EI) *m/z* [M]⁺ calculated: 214.0805; found: 214.0808.



Methyl 3-(2-fluorophenyl)pentanoate (79j). ¹H NMR (CDCl₃, 400 MHz, δ, ppm): δ_H 0.83 (3H, t, *J* = 8 Hz, C(5)H₃), 1.67-1.80 (2H, m, C(4)H₂), 2.62-2.76 (2H, m, C(2)H₂), 3.35 (1H, m, C(3)H), 3.61 (3H, s, COOCH₃), 6.99-7.17 (2H, m, aromatic protons), 7.18-7.24 (2H, m, aromatic protons) ppm. m.p.: oil. MS (EI) *m/z* [M]⁺ calculated: 210.1056; found: 210.1061.

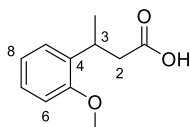


Methyl 3-(2-fluorophenyl)-3-phenylpropanoate (79k). ¹H NMR (CDCl₃, 400 MHz, δ, ppm): δ_H 3.10 (2H, d, *J* = 8 Hz, C(2)H₂), 3.60 (3H, s, COOCH₃), 4.85 (1H, t, *J* = 8 Hz, C(3)H), 7.11 (1H, t, *J* = 8 Hz, aromatic proton), 7.19 (1H, t, *J* = 8 Hz, aromatic proton), 7.26-7.35 (7H, m, aromatic protons) ppm. m.p.: oil. MS (EI) *m/z* [M]⁺ calculated: 258.1056; found: 258.1054.



Ethyl 3-(2-fluorophenyl)-2-methylpropanoate (79l). ¹H NMR (CDCl₃, 400 MHz, δ, ppm): δ_H 1.18-1.22 (6H, m, C(4)H₃, C(12)H₃), 2.77-2.83 (2H, m, C(3)H₂), 2.97-3.06 (1H, m, C(2)H), 4.10 (2H, q, *J* = 8 Hz, C(11)H₂), 7.00-7.09 (2H, m, aromatic protons), 7.16-7.25 (2H, m, aromatic protons) ppm. m.p.: oil. MS (EI) *m/z* [M]⁺ calculated: 210.1056; found: 210.1059.⁴⁰³

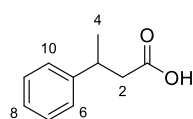
General procedure for the arylpropionic acids intermediates 80a-l. Example: Synthesis of 3-(2-methoxyphenyl)butanoic acid (80g)



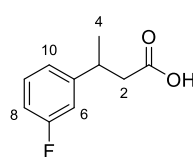
The ester **79g** (1.04 mmol, 1.0 eq, 0.220 g) was solubilized in EtOH (2 mL). The system was cooled to 0 °C and a 2 M aqueous solution of KOH (4.16 mmol, 4.0 eq, 0.220 g) was added dropwise. The reaction mixture was allowed to warm to room temperature and kept stirring for 1 h. After this time the reaction was judged to be complete by TLC analysis. The EtOH was removed *in vacuo*. The residual aqueous solution was cooled to 0 °C titrated with 1 M HCl, till

pH = 1. The product was extracted with ethyl acetate (3×10 mL). The combined organic layers were washed with brine (10 mL) and then dried over Na_2SO_4 , filtered and concentrated *in vacuo* to give the pure compound **80g** as a colorless oil (0.183 g, 0.94 mmol, 90 %). ^1H -NMR (d_6 -DMSO, 400 MHz, δ ; ppm): δ_{H} 1.15 (2H, d, $J = 7.2$ Hz, C(3) CH_3), 2.38-2.44 (1H, dd, $J = 8.8$ Hz, 15.2 Hz, C(2)H), 2.51-2.55 (1H, dd, $J = 8.8$ Hz, 15.2 Hz, C(2)H'), 3.46-3.53 (1H, m, C(3)H), 3.79 (3H, s, OCH_3), 6.89 (1H, t, $J = 7.2$ Hz, C(7)H), 6.95 (1H, d, $J = 8$ Hz, C(9)H), 7.17 (2H, m, C(6)H, C(8)H), 12.15 (1H, bs, COOH) ppm. ^{13}C NMR (d_6 -DMSO, 100 MHz, δ ; ppm) δ_{C} : 20.2, 32.7, 40.4, 55.6, 111.0, 121.5, 127.3, 127.9, 136.1, 158.1, 176.3 ppm. MS (EI) m/z $[\text{M}]^+$ calculated: 194.0943, found: 194.0947. ⁴⁰¹

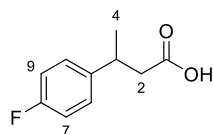
Chemical and Physical Data, ^1H NMR, melting points, and MS (EI) Data for Compounds 80a-f, 80h-k.



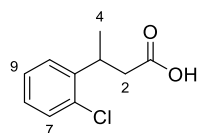
3-Phenylbutanoic acid (80a). ^1H NMR (d_6 -DMSO, 400 MHz, δ , ppm): δ_{H} 1.24 (3H, d, $J = 7.2$ Hz, C(4) H_3), 2.47-2.52 (1H, dd, $J = 8$ Hz, 15.2 Hz C(2)H), 2.65-2.70 (1H, dd, $J = 8$ Hz, 15.2 Hz, C(2)H'), 3.14 (1H, m, C(3)H), 7.16-7.20 (1H, m, C(8)H), 7.25 (2H, t, $J = 7.2$ Hz, C(7)H, C(9)H), 7.35 (2H, d, $J = 7.2$ Hz, C(6)H, C(10)H), 12.09 (1H, bs, COOH) ppm. m.p.: oil. MS (EI) m/z $[\text{M}]^+$ calculated: 164.0837; found: 164.0840. ⁴⁰¹



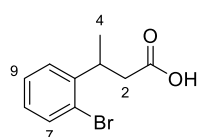
3-(3-Fluorophenyl)butanoic acid (80b). ^1H NMR (d_6 -DMSO, 400 MHz, δ , ppm): δ_{H} 1.21 (3H, d, $J = 6.8$ Hz, C(4) H_3), 2.47-2.53 (2H, m, C(2) H_2), 3.13-3.22 (1H, m, C(3)H), 6.98-7.03 (1H, m, C(8)H), 7.09-7.12 (2H, m, C(6)H, C(10)H), 7.30-7.35 (1H, m, C(9)H), 12.12 (1H, bs, COOH) ppm. m.p.: oil. MS (EI) m/z $[\text{M}]^+$ calculated: 182.0743; found: 182.0746. ⁴⁰⁴



3-(4-Fluorophenyl)butanoic acid (80c). ^1H NMR (d_6 -DMSO, 400 MHz, δ , ppm): δ_{H} 1.19 (3H, d, $J = 6.8$ Hz, C(4) H_3), 2.46-2.50 (2H, m, C(2) H_2), 3.12-3.19 (1H, m, C(3)H), 7.10 (2H, d, $J = 8.8$ Hz, C(6)H, C(10)H), 7.27-7.31 (2H, m, C(7)H, C(9)H), 12.08 (1H, bs, COOH) ppm. m.p.: 70-72 °C (cyclohexane). MS (EI) m/z $[\text{M}]^+$ calculated: 182.0743; found: 182.0739. ⁴⁰⁵

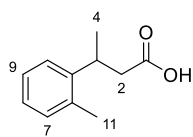


3-(2-Chlorophenyl)butanoic acid (80d). ^1H NMR (d_6 -DMSO, 400 MHz, δ , ppm): δ_{H} 1.27 (3H, d, $J = 7.2$ Hz, C(4) H_3), 2.53-2.56 (1H, dd, $J = 8$ Hz, 15.2 Hz, C(2)H), 2.62-2.67 (1H, dd, $J = 8$ Hz, 15.2 Hz, C(2)H'), 3.45-3.49 (1H, m, C(3)H), 7.17-7.20 (2H, m, C(8)H, C(9)H), 7.27 (1H, dd, C(10)H), 7.39 (1H, dd, C(7)H), 12.09 (1H, bs, COOH) ppm. m.p.: oil. MS (EI) m/z $[\text{M}]^+$ calculated: 198.0448; found: 198.0451. ⁴⁰¹

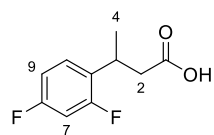


3-(2-Bromophenyl)butanoic acid (80e). ^1H NMR (d_6 -DMSO, 400 MHz, δ , ppm): δ_{H} 1.19 (3H, d, $J = 7.2$ Hz, C(4) H_3), 2.49-2.52 (2H, m, C(2) H_2), 3.09-3.18 (1H, m, C(3)H), 7.18 (1H, t, $J = 6.8$ Hz, C(9)H), 7.24-7.31 (3H, m,

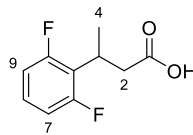
C(7)H, C(8)H, C(10)H), 12.07 (1H, bs, COOH) ppm. m.p.: oil. MS (EI) m/z $[M]^+$ calculated: 241.9942; found: 241.9942.⁴⁰¹



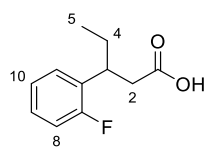
3-(*o*-Tolyl)butanoic acid (80f). ^1H NMR (d_6 -DMSO, 400 MHz, δ , ppm): δ_{H} 1.16 (3H, d, J = 6.8 Hz, C(4)H₃), 2.31 (3H, s, C(11)H₃), 2.47-2.53 (2H, m, C(2)H₂), 3.37 (1H, m, C(3)H), 7.06 (1H, t, J = 7.6 Hz, C(8)H), 7.11-7.16 (2H, m, C(7)H, C(9)H), 7.22 (1H, d, J = 7.6 Hz, C(10)H), 12.16 (1H, bs, COOH) ppm. m.p.: oil. MS (EI) m/z $[M]^+$ calculated: 178.0994; found: 178.0998.⁴⁰¹



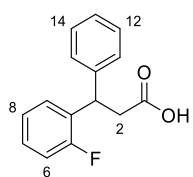
3-(2,4-Difluorophenyl)butanoic acid (80h). ^1H NMR (d_6 -DMSO, 400 MHz, δ , ppm): δ_{H} 1.20 (3H, d, J = 6.8 Hz, C(4)H₃), 2.55-2.56 (2H, dd, J = 1.2 Hz, 7.6 Hz, C(2)H₂), 3.35-3.44 (1H, m, C(3)H), 7.03 (1H, td, J = 2.4 Hz, 8.4 Hz, C(7)H), 7.13-7.18 (1H, m, C(9)H), 7.40 (1H, m, C(10)H), 12.06 (1H, bs, COOH) ppm. m.p.: 72-74 °C (cyclohexane). MS (EI) m/z $[M]^+$ calculated: 200.0649; found: 200.0651.



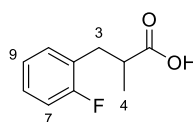
3-(2,6-Difluorophenyl)butanoic acid (80i). ^1H NMR (d_6 -DMSO, 400 MHz, δ , ppm): δ_{H} 1.26 (3H, d, J = 7.2 Hz, C(4)H₃), 2.65 (2H, d, J = 7.6 Hz, C(2)H₂), 3.53-3.63 (1H, m, C(3)H), 7.04 (2H, t, J = 8.8 Hz, C(7)H, C(9)H), 7.26-7.33 (1H, m, C(8)H), 12.14 (1H, bs, COOH) ppm. m.p.: oil. MS (EI) m/z $[M]^+$ calculated: 200.0649; found: 200.0647.



3-(2-Fluorophenyl)pentanoic acid (80j). ^1H NMR (d_6 -DMSO, 400 MHz, δ , ppm): δ_{H} 0.73 (3H, t, J = 7.6 Hz, C(5)H₃), 1.48-1.59 (1H, m, C(4)H), 1.62-1.72 (1H, m, C(4)H'), 2.51-2.55 (1H, dd, J = 6.8 Hz, 15.8 Hz, C(2)H), 2.57-2.66 (1H, dd, J = 6.8 Hz, 15.8 Hz, C(2)H'), 3.13-3.28 (1H, m, C(3)H), 7.09-7.16 (2H, m, C(8)H, C(10)H), 7.21-7.27 (1H, m, C(9)H), 7.30-7.34 (1H, m, C(11)H), 12.11 (1H, bs, COOH) ppm. MS (EI) m/z $[M]^+$ calculated: 196.0900; found: 196.0904.

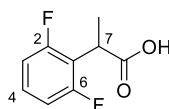


3-(2-Fluorophenyl)-3-phenylpropanoic acid (80k). ^1H NMR (d_6 -DMSO, 400 MHz, δ , ppm): δ_{H} 3.05 (2H, d, J = 7.2 Hz, C(2)H₂), 4.69 (1H, t, J = 8 Hz, C(3)H), 7.09-7.29 (8H, m, aromatic protons), 7.49 (1H, td, J = 1.6 Hz, 7.6 Hz, C(7)H), 12.28 (1H, bs, COOH) ppm. m.p.: 122-124 (cyclohexane/benzene). MS (EI) m/z $[M]^+$ calculated: 244.0900; found: 244.0903.



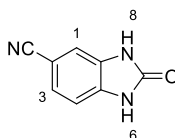
3-(2-Fluorophenyl)-2-methylpropanoic acid (80l). ^1H NMR (d_6 -DMSO, 400 MHz, δ , ppm): δ_{H} 1.04 (3H, d, J = 6.8 Hz, C(4)H₃), 2.62-2.69 (2H, m, C(3)H₂), 2.89-2.93 (1H, m, C(2)H), 7.11-7.17 (2H, m, C(7)H, C(9)H), 7.24-7.30 (2H, m, C(8)H, C(10)H), 12.33 (1H, bs, COOH) ppm. m.p.: oil. MS (EI) m/z $[M]^+$ calculated: 182.0743; found: 182.0741.

Synthesis of 2-(2,6-difluorophenyl)propanoic acid (80m)

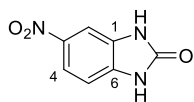


2,6-Difluorophenylacetic acid (5.81 mmol, 1.0 eq, 1.0 g) was dissolved in dry THF (16 mL). The solution was cooled to -10 °C. A 2.5 M solution of *n*-buthyl lithium in hexane (5.81 mmol, 1.0 eq, 2.32 mL) was added dropwise. The system was stirred for 15 minutes at the same temperature. After this time, a second portion of *n*-buthyl lithium (6.97 mmol, 1.2 eq, 2.79 mL) was added dropwise. The resulting mixture was stirred for 1 h at room temperature. After this time, the reaction solution was cooled to -10 °C and methyl iodide (6.97 mmol, 1.2 eq, 0.61 mL) was added dropwise. The reaction was stirred at room temperature for 15 minutes. The clear solution was then poured into cold water (40 mL) and 2 N HCl solution (4 mL) was added. The product was extracted with ethyl acetate (3 × 10 mL). The combined organic layers were washed with brine (2 × 10 mL) and then dried over Na₂SO₄, filtered and concentrated *in vacuo*. The residue was purified by silica gel chromatography eluting with EtOAc : chloroform 1:1 to obtain the pure acid **80m** as a white solid (4.42 mmol, 0.822 g, 76 %). m.p.: 50-53 °C (*n*-hexane). ¹H-NMR (CDCl₃, 400 MHz, δ; ppm): δ_H 1.51 (3H, d, *J*= 6.8 Hz C(7)HCH₃), 4.12 (1H, q, *J*= 6.8 Hz C(7)H), 6.79-6.85 (2H, m, C(3)H, C(5)H), 7.20-7.24 (1H, m, C(4)H) ppm. ¹³C NMR (CDCl₃, 100 MHz, δ; ppm) δ_C 15.9, 42.1, 113.3 (2C), 119.4, 130.2, 161.9, 164.5, 178.8 ppm. MS (EI) *m/z* [M]⁺ calculated: 186.0492, found: 186.0488. ³⁹⁰

General procedure for the synthesis of the benzoimidazolones **81 and **82**. Example: 2-oxo-2,3-dihydro-1H-benzo[d]imidazole-5-carbonitrile (**81**)**

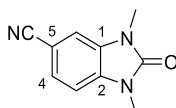


To a solution of 3,4-diaminobenzonitrile (7.51 mmol, 1.0 eq., 1 g) in dry THF (15 mL), was added *N,N'*-carbonyldiimidazole (11.26 mmol, 1.5 eq., 1.83 g) and the system was stirred at 75 °C for 2 h. After this time the reaction was judged to be complete by TLC analysis. The reaction was quenched by addition of 15 mL of water. The product precipitated. The suspension was filtered and the solid on the filter was rinsed with a 1 M aqueous HCl solution, with distilled water, and dried in oven (60 °C). The solid was then triturated in pure petroleum ether, filtered and dried, to give the pure compound **81** as a light brown solid (7.28 mmol, 1.16 g, 97 %). m.p. 295-299 °C (ethanol) ¹H-NMR (*d*₆-DMSO, 400 MHz, δ; ppm) δ_H 7.07 (1H, d, *J*= 8 Hz C(5)H), 7.32 (1H, s, C(1)H), 7.40 (1H, dd, *J*= 0.8 Hz, 8 Hz, C(3)H), 11.07 (1H, s, N(8)H), 11.20 (1H, s, N(6)H) ppm. ¹³C NMR (*d*₆-DMSO, 100 MHz, δ; ppm) δ_C: 108.1, 112.9, 114.4, 118.3, 130.1, 130.9, 131.0, 156.3 ppm. MS (EI) *m/z* [M]⁺ calculated: 159.0433, found: 159.0436. ^{406,407}



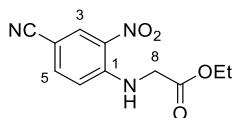
5-nitro-1,3-dihydro-2H-benzo[d]imidazol-2-one (82) $^1\text{H-NMR}$ (d_6 -DMSO, 400 MHz, δ ; ppm) δ_{H} 7.10 (1H, d, J = 8.4 Hz C(5)H), 7.71 (1H, d, J = 2 Hz C(2)H), 7.93-7.96 (1H, dd, J = 2 Hz, 8.4 Hz, C(4)H), 11.30 (2H, bs, N(7)H, N(9)H) ppm. $^{13}\text{C NMR}$ (d_6 -DMSO, 100 MHz, δ ; ppm) δ_{C} : 108.0, 111.3, 117.9, 130.5, 131.2, 141.2, 155.6 ppm. MS (EI) m/z $[\text{M}]^+$ calculated: 179.0331, found: 179.0334. m.p. 300-305 °C (ethanol) ^{408,409}

Synthesis of 1,3-dimethyl-2-oxo-2,3-dihydro-1H-benzo[d]imidazo-5-carbonitrile (83)



2-oxo-2,3-dihydro-1H-benzo[d]imidazole-5-carbonitrile (1.88 mmol, 1.0 eq, 0.3 g) was solubilized in anhydrous THF (10 mL). The solution was cooled to 0 °C and NaH (4.52 mmol, 2.4 eq, 0.18 g) was added. The reaction mixture was stirred at 0 °C for 20 minutes. After this time methyl iodide (4.52 mmol, 2.4 eq, 0.64 g) was added dropwise and the system was allowed to warm to room temperature and stirred for 19 h. After this time the reaction was judged to be complete by TLC analysis and it was quenched with water (8 mL). The product was extracted with ethyl acetate (3 \times 10 mL). The combined organic layers were washed with saturated aqueous solution of NaCl (2 \times 5 mL), dried over Na_2SO_4 and filtered. The extract was then purified by silica gel chromatography eluting with *n*-hexane: ethyl acetate 1: 5 to give compound **7** (229 mg, 1.60 mmol, 85 %), m.p. 204-205 °C (ethanol). $^1\text{H-NMR}$ (d_6 -DMSO, 400 MHz, δ ; ppm) δ_{H} : 3.36 (3H, s, -N(1) CH_3), 3.37 (3H, s, -N(2) CH_3), 7.33 (1H, d, J = 8.4 Hz C(3)H), 7.55 (1H, dd, J = 1.2 Hz, 8 Hz, C(4)H), 7.69 (1H, d, J = 1.2 Hz, C(6)H) ppm. $^{13}\text{C NMR}$ (d_6 -DMSO, 100 MHz, δ ; ppm) δ_{C} : 26.8, 27.5, 107.7, 111.3, 113.1, 118.3, 128.2, 132.7, 133.5, 155.5 ppm. MS (EI) m/z $[\text{M}]^+$ calculated: 187.0746, found: 187.0751. ⁴¹⁰

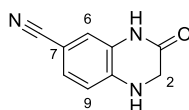
Synthesis of ethyl (4-cyano-2-nitrophenyl)glycinate (84)



In a sealed tube, 4-chloro-3-nitrobenzonitrile (2.70 mmol, 1.0 eq., 0.5 g) was dissolved in dry DMF (6 mL), K_2CO_3 (13.7 mmol, 5 eq., 1.89 g) and ethyl glycinate hydrochloride (8.2 mmol, 3.0 eq., 1.15 g) were added. The reaction mixture was stirred at 90 °C for 1 h. After this time the reaction was judged to be complete by TLC analysis. The reaction was quenched by addition of 10 mL of a saturated solution of NaCl. The product precipitated and it was filtered. The solid on the filter was rinsed with distilled water, and dried to give the pure compound **84** (2.56 mmol,

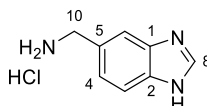
0.64 g, 94 %). m.p. 95-99 °C (cyclohexane). ¹H-NMR (*d*₆-DMSO, 400 MHz, δ; ppm) δ_H 1.33 (3H, t, *J*= 7.2 Hz, COOCH₂CH₃), 4.12 (2H, d, *J*= 5.2 Hz, C(8)H), 4.31 (2H, q, *J*= 7.2 Hz, COOCH₂CH₃), 6.76 (2H, d, *J*= 8.8 Hz, C(6)H), 7.63-7.66 (1H, dd, *J*= 8.8 Hz, 1.6 Hz, C(5)H), 8.55 (1H, d, *J*= 1.6 Hz, C(3)H), 8.81 (1H, t, *NH*) ppm. ¹³C NMR (*d*₆-DMSO, 100 MHz, δ; ppm) δ_C: 14.1, 45.0, 60.9, 101.3, 116.9, 120.8, 129.4, 134.2, 135.6, 143.0, 171.2 ppm. MS (EI) *m/z* [M]⁺ calculated: 249.0750, found: 249.0748.

Synthesis of 3-oxo-1,2,3,4-tetrahydroquinoxaline-6-carbonitrile (**85**)



Ethyl (4-cyano-2-nitrophenyl)glycinate (1.00 mmol, 1.0 eq, 0.25 g) was dissolved in EtOH (3 mL) and the solution was cooled to 0 °C. SnCl₂ (5.01 mmol, 5.0 eq, 1.13 g) and 37 % HCl (0.83 mL) were added. The reaction mixture was stirred at 0 °C for 10 minutes, then let warm to room temperature and left under stirring for 16 h. After this time, the reaction was judged to be complete by TLC analysis. The solvent was removed *in vacuo*. The residue was suspended in 20 mL of ethyl acetate and an aqueous saturated solution of Na₂CO₃ was added dropwise till pH=8. The product was extracted with ethyl acetate (3 × 10 mL). The combined organic layers were washed with a saturated aqueous solution of NaCl (2 × 5 mL), dried over Na₂SO₄, filtered and concentrated *in vacuo*. The obtained solid was triturated in petroleum ether, filtered and dried to give **85** as pure compound (0.613 mmol, 0.106 mg, Y 61 %). m.p. 190-192 °C (acetonitrile). ¹H-NMR (*d*₆-DMSO, 400 MHz, δ; ppm): δ_H 3.91 (2H, d, *J*= 1.2 Hz, C(2)H₂), 6.69 (1H, d, *J*= 8 Hz, C(9)H), 6.94 (1H, bs, -NHCH₂CONH-), 6.95 (1H, d, *J*= 1.6 Hz, C(6)H), 7.17 (1H, dd, *J*= 1.6 Hz, 8 Hz, C(8)H), 10.51 (1H, s, -NHCH₂CONH-) ppm. ¹³C NMR (*d*₆-DMSO, 100 MHz, δ; ppm) δ_C: 42.6, 105.8, 115.9, 117.9, 118.4, 125.8, 130.5, 138.5, 163.3 ppm. MS (EI) *m/z* [M]⁺ calculated: 173.0589, found: 173.0587. ⁴¹¹

General procedure for the Synthesis of amines **86**, **87**, **89** and **90**. Example: Synthesis of (1H-benzo[d]imidazol-5-yl)methylamine hydrochloride (**89**)



A 0.05 M solution of 5-cyanobenzimidazole (3.49 mmol, 1 eq, 0.5 g) in glacial acetic acid has been let flow (1.5 mL/min) on Pd/C 10 % catalyst in presence of an H₂ pressure of 50 bar by using H-Cube® (Thales Nano). The acetic acid was removed under reduced pressure to give the

corresponding acetate salt of compound **89**. The crude was suspended in dry THF and 10 eq. of HCl (2 M in THF) were added dropwise to such suspension. The reaction mixture was left under stirring for 2 h. After this time the suspension was filtered, the solid was rinsed with petroleum ether to give the pure compound **89** as a white solid (2.69 mmol, 0.494 g, 77 %). m.p. > 300 °C (ethanol). ¹H-NMR (*d*₆-DMSO, 400 MHz, δ; ppm) δ_H: 4.21 (2H, d, *J*= 5.6 Hz, C(10)H₂), 7.65 (1H, d, *J*= 8.4 Hz, C(4)H), 7.86 (1H, d, *J*= 8.4 Hz, C(3)H), 8.02 (1H, s, C(6)H), 8.56-8.60 (3H, m, CH₂NH₂ and C(8)H), 9.42 (1H, s, benzimidazole -NH-) ppm. ¹³C NMR (*d*₆-DMSO, 100 MHz, δ; ppm) δ_C: 45.9, 114.2, 117.7, 124.8, 136.8, 137.1, 138.0, 143.8 ppm. MS (EI) *m/z* [M-HCl]⁺ calculated: 147.0796, found: 147.0798. ⁴¹²

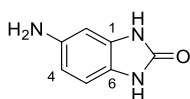
Chemical and Physical Data, ¹H NMR, ¹³C NMR, and MS (EI) Data for Compounds 86, 87 and 90.

5-(aminomethyl)-1,3-dihydro-2H-benzo[d]imidazol-2-one hydrochloride (86) ¹H-NMR (*d*₆-DMSO, 400 MHz, δ; ppm) δ_H: 3.96 (2H, q, *J*= 5.6 Hz, C(9)H₂), 6.94 (1H, d, *J*= 8 Hz, C(5)H), 7.04 (1H, d, *J*= 8 Hz, C(4)H), 7.10 (1H, s, C(2)H), 8.33 (3H, bs, NH₃⁺), 10.74 (1H, s, N(7)H), 10.82 (1H, s, N(9)H) ppm. ¹³C NMR (*d*₆-DMSO, 100 MHz, δ; ppm) δ_C: 45.9, 107.3, 112.5, 125.0, 128.7, 130.1, 135.9, 156.2 ppm. m.p. > 300 °C (methanol) MS (EI) *m/z* [M-HCl]⁺ calculated: 163.0746, found: 163.0742. ^{385,413}

5-(aminomethyl)-1,3-dimethyl-1,3-dihydro-2H-benzo[d]imidazol-2-one hydrochloride (87) ¹H-NMR (*d*₆-DMSO, 400 MHz, δ; ppm) δ_H: 3.30 (6H, s, N(7)CH₃, N(9)CH₃), 3.76 (2H, m, C(9)H₂), 7.04-7.07 (2H, m, C(4)H, C(5)H), 7.14 (1H, s, C(2)H), 8.45 (3H, bs, NH₃⁺) ppm. ¹³C NMR (*d*₆-DMSO, 100 MHz, δ; ppm) δ_C: 27.3, 27.6, 45.8, 109.8, 110.9, 125.7, 131.9, 133.4, 136.1, 155.8 ppm. m.p. 295-300 °C (methanol). MS (EI) *m/z* [M-HCl]⁺ calculated: 191.1059, found: 191.1063. ⁴¹⁴

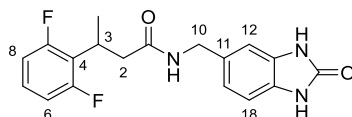
7-(aminomethyl)-3,4-dihydroquinoxalin-2(1H)-one hydrochloride (90) ¹H-NMR (*d*₆-DMSO, 400 MHz, δ; ppm) δ_H: 3.83 (4H, s, C(2)H₂, C(10)H₂), 7.27-7.29 (2H, m, C(6)H, C(8)H), 7.70 (1H, d, *J*= 8 Hz, C(9)H), 8.11 (2H, s, NH₂), 10.25 (1H, bs, NHCO) ppm. ¹³C NMR (*d*₆-DMSO, 100 MHz, δ; ppm) δ_C: 43.1, 45.7, 115.6, 117.9, 124.8, 126.6, 131.7, 136.2, 165.5 ppm. m.p. 200-205 °C (acetonitrile/methanol). MS (EI) *m/z* [M-HCl]⁺ calculated: 177.0902, found: 177.0903.

Synthesis of 5-amino-1,3-dihydro-2H-benzo[d]imidazol-2-one (88)



5-nitro-1,3-dihydro-2H-benzo[d]imidazol-2-one (0.837 mmol, 1 eq, 0.15 g) was dissolved in ethanol (5 mL). To the solution was added $\text{SnCl}_2 \times 2 \text{H}_2\text{O}$ (4.187 mmol, 5 eq, 0.94 g) and the system was cooled to 0 °C. Then, 37 % HCl (0.5 mL) was added dropwise. The reaction mixture was stirred at 0 °C for 10 minutes, then let warm to room temperature and then heated to 75 °C. The reaction mixture was stirred at this temperature for 3 h and then left overnight (10 h) at room temperature. The next morning the reaction was judged to be complete by TLC analysis. The reaction was cooled to 0 °C, and quenched by dropwise addition of a saturated aqueous solution of NaHCO_3 till pH 7-8. The product was extracted with ethyl acetate (3×10 mL). The combined organic layers were washed with a saturated aqueous solution of NaCl (2×5 mL) and then dried over Na_2SO_4 , filtered and concentrated *in vacuo*. The extract was purified by silica gel chromatography eluting with chloroform: methanol 8 : 1, to give 5-amino-1,3-dihydro-2H-benzo[d]imidazol-2-one (0.365 mmol, 54.5 mg, Y 44 %). m.p. 253-256 °C (methanol). ^1H -NMR (d_6 -DMSO, 400 MHz, δ ; ppm) δ_{H} : 6.21-6.24 (1H, dd, $J = 2$ Hz, 8.2 Hz, C(4)H), 6.29 (1H, d, $J = 2$ Hz, C(2)H), 6.63 (1H, d, $J = 8$ Hz, C(5)H), 10.08 (1H, bs, N(1)H), 10.23 (1H, bs, N(2)H) ppm. ^{13}C NMR (d_6 -DMSO, 100 MHz, δ ; ppm) δ_{C} : 95.4, 106.7, 108.6, 119.9, 130.2, 143.1, 156.4 ppm. MS (EI) m/z $[\text{M}]^+$ calculated: 149.0589, found 149.0586. ⁴¹⁵

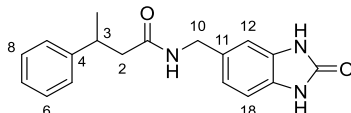
General procedure for the amides 77a-1. Example: Synthesis of 3-(2,6-difluorophenyl)-N-((2-oxo-2,3-dihydro-1H-benzo[d]imidazol-5-yl)methyl)butanamide (77i)



Compound **80i** (0.399 mmol, 1.0 eq, 0.08 g) was dissolved in dry DMF (3 mL). 1.1 eq of 1,1'-carbonyldiimidazole (0.439 mmol, 1.1 eq, 0.06 g) were added and the system was stirred at room temperature for 40 minutes. After this time triethylamine (1.19 mmol, 3 eq, 0.15 mL) and **86** (0.599 mmol, 1.5 eq, 0.12 g) were added and the system was left under stirring at room temperature overnight (16 h). The next morning the reaction was judged to be complete by TLC analysis. The reaction was quenched by addition of 10 mL of a saturated solution of NaCl. The product was then extracted with ethyl acetate (3×10 mL). The combined organic layers were washed with a saturated aqueous solution of Na_2CO_3 (2×5 mL), a 2N HCl aqueous solution (2×5 mL), and saturated aqueous solution of NaCl (2×5 mL), dried over Na_2SO_4 , filtered and concentrated *in vacuo*. The obtained white solid was triturated in diethyl ether, filtered and dried to give **77i** as pure compound (0.103 g, 0.299 mmol, 75%). m.p. 197-199 °C (acetonitrile/methanol). ^1H NMR (d_6 -DMSO, 400 MHz, δ ; ppm) δ_{H} : 1.24 (3H, d, $J = 6.8$ Hz, C(3) CH_3), 2.46-2.61 (2H, m, C(2) H_2), 3.63-3.68 (1H, m, C(3) H), 4.17 (2H, d, $J = 5.6$ Hz, C(10) H_2), 6.68 (1H, d, $J = 7.6$ Hz, C(18) H), 6.78 (2H, t, $J = 7.6$ Hz, C(6) H , C(8) H), 7.02 (2H, t, $J = 8.8$ Hz, C(12) H , C(16) H), 7.28 (1H, m, $J = 7.6$ Hz, C(7) H), 8.37 (1H, t, $J = 5.2$ Hz, -NHCH₂),

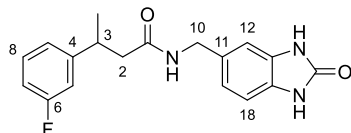
10.53 (1H, s, -NHCONH-), 10.55 (1H, s, -NHCONH-) ppm. ^{13}C NMR (d_6 -DMSO, 100 MHz, δ ; ppm) δ_{C} : 19.4, 30.0, 42.5, 43.9, 110.9, 111.5 (2C), 111.7, 120.0, 124.9, 128.4, 129.5, 130.2, 134.6, 155.5, 161.0 (2C), 173.2 ppm. MS (EI) m/z $[\text{M}]^+$ calculated: 345.1289, found: 345.1285.

Chemical and Physical Data, ^1H NMR, ^{13}C NMR, and MS (EI) Data for Compounds 77a-q. N-((2-oxo-2,3-dihydro-1H-benzo[d]imidazol-5-yl)methyl)-3-phenylbutanamide (77a)



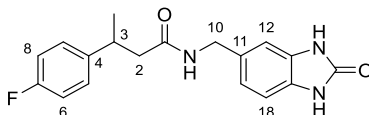
^1H NMR (d_6 -DMSO, 400 MHz, δ ; ppm) δ_{H} : 1.18 (3H, d, $J = 6.8$ Hz, C(3) CH_3), 3.01-3.04 (2H, m, C(2) H_2), 3.17-3.22 (1H, m, C(3) H), 4.18 (2H, d, $J = 5.6$ Hz, C(10) H_2), 6.67 (1H, d, $J = 8.8$ Hz, C(18) H), 6.79 (2H, d, $J = 8$ Hz, C(5) H , C(9) H), 7.16-7.30 (5H, m, C(6) H , C(7) H , C(8) H , C(12) H , C(16) H), 8.27 (1H, t, $J = 5.6$ Hz, -NHCH $_2$), 10.54 (1H, s, -NHCONH-), 10.56 (1H, s, -NHCONH-) ppm. ^{13}C NMR (d_6 -DMSO, 100 MHz, δ ; ppm) δ_{C} : 21.3, 42.1, 43.0, 43.8, 110.9, 111.9, 124.9, 126.1, 126.7 (2C), 128.4, 128.5 (2C), 130.3, 134.6, 146.2, 155.6, 173.0 ppm. MS (EI) m/z $[\text{M}]^+$ calculated: 309.1477, found 309.1481. Y = 78 %. m.p. 252-254 °C (methanol).

3-(3-fluorophenyl)-N-((2-oxo-2,3-dihydro-1H-benzo[d]imidazol-5-yl)methyl)butanamide (77b)



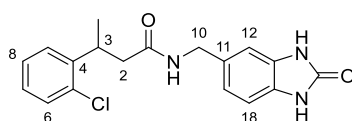
^1H NMR (d_6 -DMSO, 400 MHz, δ ; ppm) δ_{H} : 1.19 (3H, d, $J = 7.2$ Hz, C(3) CH_3), 2.33-2.45 (2H, m, C(2) H_2), 3.20-3.24 (1H, m, C(3) H), 4.17 (2H, d, $J = 6$ Hz, C(10) H_2), 6.65 (1H, d, $J = 8.8$ Hz, C(18) H), 6.79 (2H, d, $J = 8$ Hz, C(5) H , C(9) H), 6.98-7.08 (3H, m, C(8) H , C(12) H , C(19) H), 7.29-7.35 (1H, m, C(7) H), 8.24 (1H, t, $J = 6$ Hz, -NHCH $_2$), 10.51 (1H, s, -NHCONH-), 10.53 (1H, s, -NHCONH-) ppm. ^{13}C NMR (d_6 -DMSO, 100 MHz, δ ; ppm) δ_{C} : 21.4, 39.5, 42.2, 44.0, 110.9, 111.9, 113.8, 114.1, 124.8, 125.4, 128.5, 129.1, 130.3, 134.6, 145.1, 155.4, 159.6, 172.9 ppm. MS (EI) m/z $[\text{M}]^+$ calculated: 327.1383, found: 327.1385. Y = 81 %. m.p. 250-252 °C (methanol).

3-(4-fluorophenyl)-N-((2-oxo-2,3-dihydro-1H-benzo[d]imidazol-5-yl)methyl)butanamide (77c)



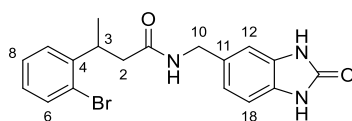
^1H NMR (d_6 -DMSO, 400 MHz, δ ; ppm) δ_{H} : 1.18 (3H, d, J = 6.8 Hz, C(3) CH_3), 2.32-2.41 (2H, m, C(2) H_2), 3.18-3.24 (1H, m, C(3) H), 4.17 (2H, d, J = 5.2 Hz, C(10) H_2), 6.63 (1H, d, J = 9 Hz, C(18) H), 6.78 (2H d, J = 7.6 Hz, C(5) H , C(9) H), 7.09 (2H, t, J = 8.8 Hz, C(12) H , C(19) H), 7.23-7.27 (2H, m, C(6) H , C(8) H), 8.23 (1H, t, J = 6 Hz, - NHCH_2), 10.51 (1H, s, - NHCONH-), 10.54 (1H, s, - NHCONH-) ppm. ^{13}C NMR (d_6 -DMSO, 100 MHz, δ ; ppm) δ_{C} : 21.4, 42.0, 43.1, 44.0, 110.9, 111.8, 115.4 (2C), 125.0, 128.4 (2C), 128.4, 130.3, 134.5, 145.1, 155.6, 160.2, 173.2 ppm. MS (EI) m/z $[\text{M}]^+$ calculated: 327.1383, found: 327.1387. Y= 79 %. m.p. 250-252 °C (methanol).

3-(2-chlorophenyl)-N-((2-oxo-2,3-dihydro-1H-benzo[d]imidazol-5-yl)methyl)butanamide (77d)



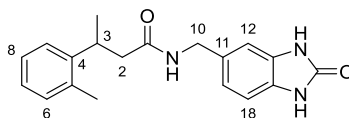
^1H NMR (d_6 -DMSO, 400 MHz, δ ; ppm) δ_{H} : 1.18 (3H, d, J = 6.8 Hz, C(3) CH_3), 2.32-2.43 (2H, m, C(2) H_2), 3.17-3.24 (1H, m, C(3) H), 4.18 (2H, d, J = 5.6 Hz, C(10) H_2), 6.68 (1H, d, J = 8 Hz, C(18) H), 6.81 (2H, d, J = 7.6 Hz, C(9) H , C(19) H), 7.16-7.33 (4H, m, C(6) H , C(7) H , C(8) H , C(12) H), 8.26 (1H, t, J = 5.6 Hz, - NHCH_2 -), 10.53 (1H, s, - NHCONH-), 10.55 (1H, s, - NHCONH-) ppm. ^{13}C NMR (d_6 -DMSO, 100 MHz, δ ; ppm) δ_{C} : 20.3, 35.3, 42.4, 44.0, 110.9, 111.9, 124.9, 126.4, 127.9, 128.2, 128.5, 129.1, 130.2, 133.5, 134.7, 144.8, 156.0, 173.1 ppm. MS (EI) m/z $[\text{M}]^+$ calculated: 343.1088, found: 343.1085. Y= 73 %. m.p. 251-253 °C (methanol).

3-(2-bromophenyl)-N-((2-oxo-2,3-dihydro-1H-benzo[d]imidazol-5-yl)methyl)butanamide (77e)



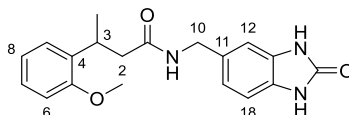
^1H NMR (d_6 -DMSO, 400 MHz, δ ; ppm) δ_{H} : 1.18 (3H, d, J = 6.8 Hz, C(3) CH_3), 2.32-2.43 (2H, m, C(2) H_2), 3.17-3.23 (1H, m, C(3) H), 4.18 (2H, d, J = 5.6 Hz, C(10) H_2), 6.68 (1H, d, J = 8 Hz, C(18) H), 6.79 (2H, d, J = 8 Hz, C(9) H , C(19) H), 7.16-7.30 (4H, m, C(6) H , C(7) H , C(8) H , C(12) H), 8.26 (1H, t, J = 5.6 Hz, - NHCH_2 -), 10.52 (1H, s, - NHCONH-), 10.55 (1H, s, - NHCONH-) ppm. ^{13}C NMR (d_6 -DMSO, 100 MHz, δ ; ppm) δ_{C} : 20.3, 36.6, 42.3, 44.0, 110.9, 111.8, 123.0, 124.9, 126.9, 128.0, 128.5, 129.4, 130.2, 133.6, 134.7, 146.0, 155.6, 173.2 ppm. MS (EI) m/z $[\text{M}]^+$ calculated: 387.0582, found: 387.0579. Y= 80 %. m.p. 250-252 °C (methanol).

N-((2-oxo-2,3-dihydro-1H-benzo[d]imidazol-5-yl)methyl)-3-(o-tolyl)butanamide (77f)



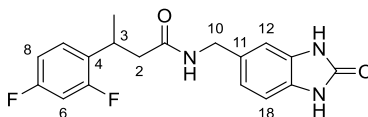
^1H NMR (d_6 -DMSO, 400 MHz, δ ; ppm) δ_{H} : 1.14 (3H, d, J = 6.8 Hz, C(3) CH_3), 2.31 (3H, s, C(5) CH_3), 2.34-2.39 (2H, m, C(2) H_2), 3.40-3.47 (1H, m, C(3) H), 4.18 (2H, t, J = 5.2 Hz, C(10) H_2), 6.66 (1H, d, J = 8.4 Hz, C(18) H), 6.79 (2H, d, J = 7.2 Hz, C(9) H , C(19) H), 7.05-7.21 (4H, m, C(6) H , C(7) H , C(8) H , C(12) H), 8.27 (1H, t, J = 5.2 Hz, - NHCH_2 -), 10.52 (1H, s, - NHCONH -), 10.55 (1H, s, - NHCONH -) ppm. ^{13}C NMR (d_6 -DMSO, 100 MHz, δ ; ppm) δ_{C} : 19.5, 20.3, 35.6, 42.3, 43.9, 110.9, 111.8, 125.0, 126.4, 127.4, 127.8, 128.3, 130.2, 130.4, 134.7, 136.5, 145.5, 155.6, 173.2 ppm. MS (EI) m/z $[\text{M}]^+$ calculated: 323.1634, found: 323.1637. Y= 85 %. m.p. 237-239 $^{\circ}\text{C}$ (methanol).

3-(2-methoxyphenyl)-N-((2-oxo-2,3-dihydro-1H-benzo[d]imidazol-5-yl)methyl)butanamide (77g)



^1H NMR (d_6 -DMSO, 400 MHz, δ ; ppm) δ_{H} : 1.11 (3H, d, J = 6.4 Hz, C(3) CH_3), 2.34 (1H, dd, J = 5.2 Hz, 13.6 Hz, C(2) H), 2.40 (2H, dd, J = 5.2 Hz, 13.6 Hz, C(2) H'), 3.54-3.57 (1H, m, C(3) H), 3.78 (3H, s, - OCH_3), 4.15-4.26 (2H, m, C(10) H_2), 6.75 (1H, d, J = 8 Hz, C(18) H), 6.79-6.82 (2H, m, C(9) H , C(19) H), 6.89 (1H, t, J = 7.6 Hz, C(7) H), 6.94 (1H, d, J = 7.6 Hz, C(6) H), 7.14-7.19 (2H, m, C(8) H , C(12) H), 8.27 (1H, t, J = 5.2 Hz, - NHCH_2 -), 10.53 (1H, s, - NHCONH -), 10.56 (1H, s, - NHCONH -) ppm. ^{13}C NMR (d_6 -DMSO, 100 MHz, δ ; ppm) δ_{C} : 20.3, 32.8, 42.3, 43.9, 55.5, 111.0, 111.2, 112.3, 121.5, 125.0, 127.6, 127.9, 128.4, 130.3, 134.6, 136.2, 155.6, 158.0, 173.2 ppm. MS (EI) m/z $[\text{M}]^+$ calculated: 339.1583, found: 339.1588. Y= 77 %. m.p. 213-215 $^{\circ}\text{C}$ (acetonitrile/methanol).

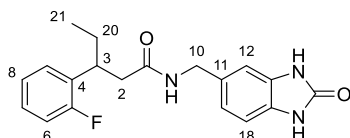
3-(2,4-difluorophenyl)-N-((2-oxo-2,3-dihydro-1H-benzo[d]imidazol-5-yl)methyl)butanamide (77h)



^1H NMR (d_6 -DMSO, 400 MHz, δ ; ppm) δ_{H} : 1.18 (3H, d, J = 6.8 Hz, C(3) H_3), 2.42-2.44 (2H, m, C(2) H_2), 3.45-3.47 (1H, m, C(3) H), 4.17 (2H, d, J = 5.2 Hz, C(10) H_2), 6.66 (1H, d, J = 8 Hz, C(18) H), 6.77-6.79 (2H, m, C(9) H , C(19) H), 7.02 (1H, td, J = 2.4 Hz, 8.4 Hz, C(8) H), 7.14 (1H,

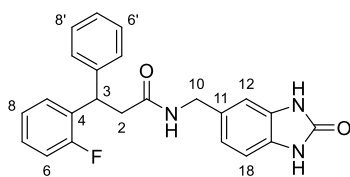
td, $J = 2.4$ Hz, 10.4 Hz, C(12) H), 7.34 (1H, q, $J = 8.8$ Hz, C(6) H), 8.31 (1H, t, $J = 5.6$ Hz, -NHCH₂-), 10.53 (1H, s, -NHCONH-), 10.56 (1H, s, -NHCONH-) ppm. ¹³C NMR (*d*₆-DMSO, 100 MHz, δ ; ppm) δ_c : 20.3, 35.4, 42.3, 43.9, 103.5, 110.9, 111.4, 111.8, 125.0, 128.4, 129.3, 130.2, 131.1, 134.6, 153.9, 155.6, 163.3, 173.2 ppm. MS (EI) m/z [M]⁺ calculated: 345.1289, found: 345.1291. Y= 85 %. m.p. 244-246 °C (methanol).

3-(2-fluorophenyl)-N-((2-oxo-2,3-dihydro-1H-benzo[d]imidazol-5-yl)methyl)pentanamide (77j)



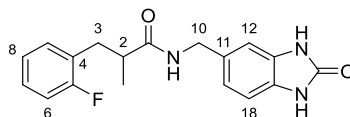
¹H NMR (*d*₆-DMSO, 400 MHz, δ ; ppm) δ_H : 0.71 (3H, t, $J = 7.2$ Hz, C(21) H_3), 1.47-1.54 (1H, m, C(20) H_2), 1.60-1.67 (1H, m, C(3) H), 2.43 (1H, dd, $J = 8$ Hz, 14.2 Hz, C(2) H), 2.49 (1H, dd, $J = 8$ Hz, 14.2 Hz, C(2) H'), 4.15 (2H, d, $J = 6$ Hz, C(10) H_2), 6.62 (1H, d, $J = 8$ Hz, C(18) H), 6.74-6.78 (2H, m, C(9) H , C(19) H), 7.09-7.16 (2H, m, C(7) H , C(8) H), 7.21-7.29 (2H, m, C(6) H , C(12) H), 8.27 (1H, t, $J = 5.6$ Hz, -NHCH₂), 10.52 (1H, s, -NHCONH), 10.54 (1H, s, -NHCONH) ppm. ¹³C NMR (*d*₆-DMSO, 100 MHz, δ ; ppm) δ_c : 13.1, 25.7, 39.3, 43.8, 44.2, 110.9, 112.2, 117.3, 124.9, 125.4, 127.9, 128.4, 128.6, 130.0, 130.3, 137.1, 156.2, 159.9, 173.1 ppm. MS (EI) m/z [M]⁺ calculated: 341.1540, found: 341.1543. Y= 73 %. m.p. 201-203 °C (acetonitrile/methanol).

3-(2-fluorophenyl)-N-((2-oxo-2,3-dihydro-1H-benzo[d]imidazol-5-yl)methyl)-3-phenylpropanamide (77k)



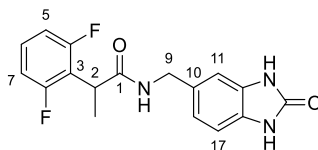
¹H NMR (*d*₆-DMSO, 400 MHz, δ ; ppm) δ_H : 2.91 (2H, d, $J = 7.6$ Hz, C(2) H_2), 4.14 (2H, d, $J = 4.4$ Hz, C(10) H_2), 4.78 (1H, t, $J = 7.6$ Hz, C(3) H), 6.55 (1H, d, $J = 7.6$ Hz, C(18) H), 6.71-6.74 (2H, m, C(9), C(19)), 7.09-7.28 (8H, m, C(6) H , C(7) H , C(5') H , C(6') H , C(7') H , C(8') H , C(9') H , C(12) H), 7.41 (1H, t, $J = 7.2$ Hz, C(8) H), 8.38 (1H, t, $J = 4.4$ Hz, -NHCH₂-), 10.53 (1H, s, -NHCONH-), 10.56 (1H, s, -NHCONH-) ppm. ¹³C NMR (*d*₆-DMSO, 100 MHz, δ ; ppm) δ_c : 37.9, 42.9, 43.8, 110.9, 112.0, 116.2, 124.0, 125.4, 126.8, 127.9 (2C), 128.3, 128.7 (2C), 129.0, 129.4, 130.3, 133.0, 134.8, 143.5, 154.9, 159.9, 169.9 ppm. MS (EI) m/z [M]⁺ calculated: 389.1540, found: 389.1538. Y= 75 %. m.p. 230-232 °C (methanol).

3-(2-fluorophenyl)-2-methyl-N-((2-oxo-2,3-dihydro-1H-benzo[d]imidazol-5-yl)methyl)propanamide (77l)



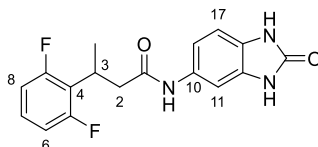
^1H NMR (d_6 -DMSO, 400 MHz, δ ; ppm) δ_{H} : 1.03 (3H, d, J = 6.4 Hz, C(2) CH_3), 2.59-2.67 (2H, m, C(3) H_2), 2.83 (1H, m, C(2) H), 4.13 (1H, dd, J = 5.6 Hz, 14.8 Hz, C(10) H), 4.21 (1H, dd, J = 5.6 Hz, 14.8 Hz, C(10) H_2), 6.65 (1H, d, J = 7.6 Hz, C(18) H), 6.75-6.80 (2H, m, C(9), C(19)), 7.06-7.15 (2H, m, C(7), C(8)), 7.20-7.27 (2H, m, C(6), C(12)), 8.25 (1H, t, J = 5.6 Hz, - NHCH_2), 10.52 (1H, s, - NHCONH-), 10.54 (1H, s, - NHCONH-) ppm. ^{13}C NMR (d_6 -DMSO, 100 MHz, δ ; ppm) δ_{C} : 18.3, 36.2, 41.0, 42.9, 110.9, 111.9, 115.7, 124.6, 125.0, 125.9, 128.5, 129.4, 130.2, 132.3, 134.7, 155.5, 160.0, 171.0 ppm. MS (EI) m/z $[\text{M}]^+$ calculated: 327.1383, found: 327.1388. Y= 73 %. m.p. 231-233 $^{\circ}\text{C}$ (methanol).

2-(2,6-difluorophenyl)-N-((2-oxo-2,3-dihydro-1H-benzo[d]imidazol-5-yl)methyl)propanamide (77m)



^1H NMR (d_6 -DMSO, 400 MHz, δ ; ppm) δ_{H} : 1.42 (3H, d, J = 7.2 Hz, C(2) CH_3), 3.93 (1H, q, J = 7.2 Hz, C(2) H), 4.22 (2H, d, J = 6 Hz, C(9) H_2), 6.78-6.83 (3H, m, C(11) H , C(17) H , C(18) H), 7.06 (2H, t, J = 8.4 Hz, (C5) H , C(7) H), 7.30-7.37 (1H, m, C(6) H), 8.22 (1H, t, J = 6 Hz, - NHCH_2 -), 10.53 (1H, s, - NHCONH-), 10.56 (1H, s, - NHCONH-) ppm. ^{13}C NMR (d_6 -DMSO, 100 MHz, δ ; ppm) δ_{C} : 17.5, 42.9, 47.0, 110.9, 111.7, 112.4 (2C), 115.3, 124.9, 128.4, 129.7, 130.2, 134.6, 155.5, 162.4 (2C), 175.7 ppm. MS (EI) m/z $[\text{M}]^+$ calculated: 331.1132, found: 331.1137. Y= 75 %. m.p. 217-219 $^{\circ}\text{C}$ (acetonitrile/methanol).

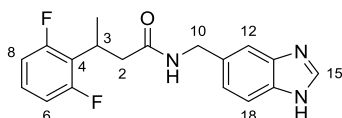
3-(2,6-difluorophenyl)-N-(2-oxo-2,3-dihydro-1H-benzo[d]imidazol-5-yl)butanamide (77n)



^1H NMR (d_6 -DMSO, 400 MHz, δ ; ppm) δ_{H} : 1.29 (3H, d, J = 6.8 Hz, C(3) CH_3), 2.66 (1H, m, C(2) H), 2.64-2.79 (1H, m, C(2) H), 3.71-3.74 (1H, m, C(3) H), 6.79 (1H, d, J = 8.4 Hz, C(17) H), 6.94 (1H, d, J = 8 Hz, C(18) H), 7.04 (2H, t, J = 8.4 Hz, C(6) H , C(8) H), 7.27-7.31 (1H, m,

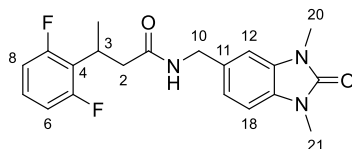
C(7)*H*), 7.40 (1H, s, C(11)*H*), 9.82 (1H, s, -NHCO-), 10.46 (1H, s, -NHCONH-), 10.51 (1H, s, -NHCONH-) ppm. ¹³C NMR (*d*₆-DMSO, 100 MHz, δ; ppm) δ_C: 19.3, 30.1, 41.9, 104.7, 109.3, 111.5 (2C), 116.4, 122.0, 125.9, 129.5, 130.8, 135.9, 155.4, 161.0 (2C), 171.6 ppm. MS (EI) *m/z* [M]⁺ calculated: 331.1132, found: 331.1129. Y= 78 %. m.p. > 250 °C (methanol).

N-((1H-benzo[d]imidazol-5-yl)methyl)-3-(2,6-difluorophenyl)butanamide (77o)



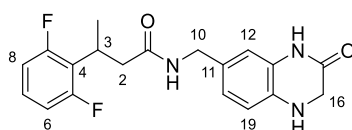
¹H NMR (MeOD, 400 MHz, δ, ppm) δ_H: 1.36 (3H, d, *J*= 7.2 Hz, C(3)CH₃), 2.68 (2H, d, *J*= 8 Hz, C(2)H₂), 3.76-3.86 (1H, m, C(3)*H*), 4.35 (1H, d, *J*= 14.4 Hz, C(10)*H*), 4.46 (1H, d, *J*= 14.4 Hz, C(10)*H*'), 6.86 (2H, t, *J*= 8.8 Hz, C(6)*H*, C(8)*H*), 7.05 (1H, d, *J*= 8.4 Hz, C(19)*H*), 7.15-7.22 (1H, m, C(7)*H*), 7.45 (1H, s, C(12)*H*), 7.51 (1H, d, *J*= 8.4 Hz, C(18)*H*), 8.15 (1H, s, C(15)*H*) ppm. ¹³C NMR (MeOD, 100 MHz, δ, ppm) δ_C: 19.4, 30.1, 42.4, 43.9, 111.6 (2C), 113.9, 118.8, 122.0, 125.3, 129.5, 135.5, 136.9, 138.3, 143.8, 161.1 (2C), 173.2 ppm. MS (EI) *m/z* [M]⁺ calculated: 329.1340, found: 329.1335. Y= 77 %. m.p. - (oil).

3-(2,6-difluorophenyl)-N-((1,3-dimethyl-2-oxo-2,3-dihydro-1H-benzo[d]imidazol-5-yl)methyl)butanamide (77p)



¹H NMR (*d*₆-DMSO, 400 MHz, δ; ppm) δ_H: 1.25 (3H, d, *J*= 7.2 Hz, C(3)CH₃), 2.52-2.58 (2H, m, C(2)H₂), 3.30 (6H, s, C(20)H₃, C(21)H₃), 3.62-3.68 (1H, m, C(3)*H*), 4.22-4.27 (2H, m, C(10)H₂), 6.68 (1H, d, *J*= 7.6 Hz, C(18)*H*), 6.78 (2H, d, *J*= 7.2 Hz, C(6)*H*, C(8)*H*), 7.00-7.04 (2H, m, C(12)*H*, C(19)*H*), 7.24-7.29 (1H, m, C(7)*H*), 8.37 (1H, t, *J*= 6 Hz, -NHCH₂) ppm. ¹³C NMR (*d*₆-DMSO, 100 MHz, δ; ppm) δ_C: 19.3, 26.9, 27.4, 30.1, 42.4, 44.0, 110.9, 111.3, 111.6 (2C), 122.1, 125.4, 129.5, 132.8, 133.9, 135.1, 155.4, 161.1 (2C), 173.3 ppm. MS (EI) *m/z* [M]⁺ calculated: 373.1602, found: 373.1607. Y= 82 %. m.p. 220-222 °C (acetonitrile/methanol).

3-(2,6-difluorophenyl)-N-((3-oxo-1,2,3,4-tetrahydroquinoxalin-6-yl)methyl)butanamide (77q)



^1H NMR (d_6 -DMSO, 400 MHz, δ ; ppm) δ_{H} : 1.26 (3H, d, J = 7.2 Hz, C(3) H_3), 2.56 (1H, dd, J = 8 Hz, 27 Hz, C(2) H), 2.65 (1H, dd, J = 8 Hz, 27 Hz, C(2) H'), 3.65-3.70 (1H, m, C(3) H), 4.29 (2H, d, J = 5.6 Hz, C(16) H_2), 6.97-7.04 (3H, m, C(6) H , C(8) H , C(19) H), 7.13 (1H, s, NHC(16) H_2), 7.25-7.32 (1H, m, C(7) H), 7.65 (1H, d, J = 8.4 Hz, C(20) H), 8.11 (1H, s, C(12) H), 8.57 (1H, t, J = 6 Hz, -CONHCH $_2$), 12.4 (1H, bs, NHCOCH $_2$) ppm. ^{13}C NMR (d_6 -DMSO, 100 MHz, δ ; ppm) δ : 19.3, 29.9, 42.4, 42.7, 44.0, 111.5 (2C), 117.2, 117.8, 122.0, 125.9, 126.6, 129.5, 131.7, 135.3, 161.1 (2C), 163.4, 173.3. ppm. MS (EI) m/z $[\text{M}]^+$ calculated: 359.1445, found: 359.1451. Y= 83 %. m.p. 252-255 °C (methanol).

Table S12. Elemental analysis for compounds 77a-q .									
Cmpd	MW	calculated, %				found, %			
		C	H	N	other	C	H	N	other
77a	309.37	69.88	6.19	13.58		70.06	6.28	13.30	
77b	327.36	66.04	5.54	12.84	5.80 (F)	65.84	5.41	13.09	5.95 (F)
77c	327.36	66.04	5.54	12.84	5.80 (F)	66.18	5.71	12.65	5.67 (F)
77d	343.81	62.88	5.28	12.22	10.31 (Cl)	63.12	5.37	11.96	10.22 (Cl)
77e	388.27	55.68	4.67	10.82	20.58 (Br)	55.77	4.78	10.59	20.44 (Br)
77f	323.40	70.57	6.55	12.99		70.70	6.72	12.74	
77g	339.40	67.24	6.24	12.38		67.52	6.39	12.11	
77h	345.35	62.60	4.96	12.17	11.00 (F)	62.45	4.76	12.31	11.12 (F)
77i	345.35	62.60	4.96	12.17	11.00 (F)	62.78	5.11	11.94	10.84 (F)
77j	341.39	66.85	5.91	12.31	5.57 (F)	66.59	6.07	12.19	5.65 (F)
77k	389.43	70.94	5.18	10.79	4.88 (F)	71.21	5.27	10.52	4.74 (F)
77l	327.36	66.04	5.54	12.84	5.80 (F)	66.17	5.62	12.59	5.68 (F)
77m	331.32	61.63	4.56	12.68	11.47 (F)	61.54	4.45	12.83	11.59 (F)
77n	331.32	61.63	4.56	12.68	11.47 (F)	61.44	4.42	12.92	11.58 (F)
77o	329.35	65.64	5.20	12.76	11.54 (F)	65.78	5.36	12.52	11.44 (F)
77p	373.40	64.33	5.67	11.25	10.18 (F)	64.57	5.72	11.02	10.32 (F)
77q	359.38	63.50	5.33	11.69	10.57 (F)	63.77	5.45	11.41	10.45 (F)

7.4.2 Biochemical and crystallographic methods. Protein Production and Crystallization

(Dr. Valentina Piano, Group of Prof. Andrea Mattevi, Department of Biology and Biotechnology, University of Pavia). *Cavia porcellus* AGPS expression and purification were performed according to the methods previously described.³⁷⁷ Crystals of AGPS in complex with **77i** were obtained by co-crystallization, pre-incubating AGPS (12 mg mL⁻¹) and **77i** (1 mM) on ice 5 min before setting the plates. The crystal of AGPS/**77i** complex were obtained by sitting-drop vapor diffusion at 20 °C mixing the pre-incubated AGPS/**77i** solution and 2–6% wt/vol PEG 1500 in 100 mM 4-(2-hydroxyethyl)-1-piperazineethanesulfonic acid (Hepes) at pH 7.0–7.5 and washed in cryo-protectant solution (30 wt %/vol PEG 1500 in 100 mM Hepes, pH 7.0–7.5) without inhibitor before freezing.

ThermoFAD-based screening (Dr. Valentina Piano, Group of Prof. Andrea Mattevi, Department of Biology and Biotechnology, University of Pavia). ThermoFAD experiments were performed with 5 µM AGPS, 180 µM inhibitors, 50 mM HEPES buffer at pH 7.5, 50 mM NaCl, 5% glycerol, and 20 µL final volume. The temperature gradient was set to 25–70 °C with fluorescence detection every 0.2 °C at 485 ± 30 nm excitation and 625 ± 30 nm emission for 5 s (BioRad MiniOpticon Real-Time PCR System). To estimate the binding of the identified compounds, the same ThermoFAD protocol was applied by using serial dilutions of the compounds from 500 µM to 10 nM.³⁸⁵

Enzymatic assays (Dr. Valentina Piano, Group of Prof. Andrea Mattevi, Department of Biology and Biotechnology, University of Pavia). Activity assays were performed under the same conditions previously described using radioactive [1-¹⁴C]-hexadecanol.^{416,417} The final concentrations were the following: 500 nM AGPS, 50 mM Tris/HCl at pH 8.2, 50 mM NaF, 0.1% (w/v) Triton X-100, 100 µM palmitoyl-DHAP (Echelon Bioscience), 96 µM [1-¹⁴C]-hexadecanol (Sigma; specific radioactivity adjusted to 13000 dpm/nmol) in a total volume of 100 µL at 36 °C. When appropriate, an inhibitor or the vehicle (DMSO) was added to the reaction mixture to a final concentration of 180–200 µM after pre-incubation with the protein for 30 min at 4 °C.

7.4.3 Cell based methods.

Targeted Lipidomic Analyses (Sharon Louie, Daniel K. Nomura, Department of Nutritional Sciences and Toxicology, University of California, Berkeley). Metabolite measurements were conducted using modified previous procedures.³⁸⁰ Cancer cells were grown in serum-free media for 24 h to minimize the contribution of serum-derived metabolites to the cellular profiles. Cells were treated with **77i** (500 µM) for 24 h. Cancer cells (1 × 10⁶ cells/6 cm dish or 2 × 10⁶ cells/6 cm dish) were washed twice with phosphate buffer saline (PBS), harvested by scraping, and isolated by centrifugation at 1400 g at 4 °C, and cell pellets were flash frozen and stored at - 80 °C until metabolome extractions. Lipid metabolites were extracted in 4 mL of a 2:1:1 mixture of

chloroform:methanol/phosphate (buffered saline, pH 7.4, 50 mM) with inclusion of internal standards C12:0 dodecylglycerol (10 nmol) and pentadecanoic acid (10 nmol). Organic and aqueous layers were separated by centrifugation at 1000 g for 5 min, and the organic layer was collected. The aqueous layer was acidified (for metabolites such as LPA) by adding 0.1% formic acid, followed by the addition of 2 mL of chloroform. The mixture was vortexed, and the organic layers were combined, dried down under N₂, and dissolved in 120 µL of chloroform, of which 10 µL was analyzed by both single reaction monitoring (SRM)-based LC-MS/MS or untargeted LC-MS. LC separation was achieved with a Luna reverse-phase C5 column (50 mm × 4.6 mm with 5 µm diameter particles, Phenomenex). MS analysis was performed with an electrospray ionization (ESI) source on an Agilent 6430 QQQ LC-MS/MS. Representative metabolites were quantified by SRM of the transition from precursor to product ions at associated collision energies.

Cell Migration Studies (Sharon Louie, Group of Prof. Daniel K. Nomura, Department of Nutritional Sciences and Toxicology, University of California, Berkeley). Migration assays were performed as previously described in Transwell chambers (Corning) coated with collagen. 231MFP migration was measured after 8 h of 500 µM **76** and **77i** treatment.³⁸⁰

Cell Culture. (Dr. Raffaele Strippoli, Dr. Cecilia Battistelli, Group of Prof. Marco Tripodi, Department of cellular Biotechnology and Hematology, “Sapienza” University of Rome) PC3 and MDA-MB 231 cells were grown in D-MEM supplemented with 10 % fetal bovine serum (Gibco Life Technology Monza Italy) and antibiotics. 24 hours after seeding, cells were treated with 50 µM, 100 µM, 250 µM or 500 µM **76**, **77i** or **77p** for 24 hours. DMSO vehicle was used as control. 24 hours after treatment cells were washed once with PBS and collected in RNA lysis buffer (Qiagen GmbH, Hilden, Germany) for RNA extraction and gene expression analysis or in Laemmli buffer for protein detection by western blot.

Western blot analysis (Dr. Raffaele Strippoli, Dr. Cecilia Battistelli, Group of Prof. Marco Tripodi, Department of cellular Biotechnology and Hematology, “Sapienza” University of Rome) Cells were lysed in Laemmli buffer (62.5 mM Tris-HCl at pH 6.8, 2 % SDS, 10 % glycerol, 5 % β-mercaptoethanol). Proteins from either cell lysates were resolved on SDS-PAGE and transferred to Nitrocellulose filters (GE Healthcare). Blots were probed with specific antibodies after blocking non-specific reactivity with TBS-Tween plus 5 % milk powder and the immune complexes were detected with horseradish peroxidase-conjugated species-specific secondary antiserum (Bio-Rad Laboratories, Hercules, CA) followed by enhanced chemiluminescence reaction (Cyanagen). The following primary antibody was used: E-cadherin (BD).

RNA extraction, reverse transcription, reverse transcription and real-time polymerase chain reaction. (Dott. Raffaele Strippoli, Dott. Cecilia Battistelli, Group of Prof. Marco Tripodi, Department of cellular Biotechnology and Hematology, “Sapienza” University of Rome) RNAs were extracted by RNeasy Mini Kit (Qiagen GmbH, Hilden, Germany) and reverse transcribed with iScript™ c-DNA Synthesis Kit (Bio-Rad Laboratories Inc., Hercules, CA, USA). cDNAs were amplified by qPCR reaction using GoTaq qPCR Master Mix (Promega, Madison, WI, USA). Relative amounts, obtained with $2^{(-\Delta Ct)}$ method, were normalized with respect to the housekeeping gene L34 rRNA. List of primers is reported in Table A:

	Forward Primer	Reverse Primer
L34	GTCCCGAACCCCTGGTAATAG	GGCCCTGCTGACATGTTTCTT
Mmp2	ATGCCGCCTTTAACTGGAG	GGAAAGCCAGGATCCATTTT
Snail	CACTATGCCGCGCTCTTTC	GCTGGAAGGTAAACTCTGGATTAGA
E-Cad	TACGCCTGGGACTCCACCTA	CCAGAAACGGAGGCCTGAT

References

- 1 Waddington, C. H. The epigenotype. 1942. *Int J Epidemiol* **41**, 10-13, doi:10.1093/ije/dyr184 (2012).
- 2 Goldberg, A. D., Allis, C. D. & Bernstein, E. Epigenetics: a landscape takes shape. *Cell* **128**, 635-638, doi:10.1016/j.cell.2007.02.006 (2007).
- 3 Foley, D. L. *et al.* Prospects for epigenetic epidemiology. *Am J Epidemiol* **169**, 389-400, doi:10.1093/aje/kwn380 (2009).
- 4 Arrowsmith, C. H., Bountra, C., Fish, P. V., Lee, K. & Schapira, M. Epigenetic protein families: a new frontier for drug discovery. *Nat Rev Drug Discov* **11**, 384-400, doi:10.1038/nrd3674 (2012).
- 5 Luger, K., Mader, A. W., Richmond, R. K., Sargent, D. F. & Richmond, T. J. Crystal structure of the nucleosome core particle at 2.8 Å resolution. *Nature* **389**, 251-260, doi:10.1038/38444 (1997).
- 6 Narlikar, G. J., Sundaramoorthy, R. & Owen-Hughes, T. Mechanisms and functions of ATP-dependent chromatin-remodeling enzymes. *Cell* **154**, 490-503, doi:10.1016/j.cell.2013.07.011 (2013).
- 7 Zhou, C. Y., Johnson, S. L., Gamarra, N. I. & Narlikar, G. J. Mechanisms of ATP-Dependent Chromatin Remodeling Motors. *Annu Rev Biophys* **45**, 153-181, doi:10.1146/annurev-biophys-051013-022819 (2016).
- 8 Rhee, H. S., Bataille, A. R., Zhang, L. & Pugh, B. F. Subnucleosomal structures and nucleosome asymmetry across a genome. *Cell* **159**, 1377-1388, doi:10.1016/j.cell.2014.10.054 (2014).
- 9 Weber, C. M. & Henikoff, S. Histone variants: dynamic punctuation in transcription. *Genes Dev* **28**, 672-682, doi:10.1101/gad.238873.114 (2014).
- 10 Strahl, B. D. & Allis, C. D. The language of covalent histone modifications. *Nature* **403**, 41-45, doi:10.1038/47412 (2000).
- 11 Kouzarides, T. Chromatin modifications and their function. *Cell* **128**, 693-705, doi:10.1016/j.cell.2007.02.005 (2007).
- 12 Bird, A. Perceptions of epigenetics. *Nature* **447**, 396-398, doi:10.1038/nature05913 (2007).
- 13 Sterner, D. E. & Berger, S. L. Acetylation of histones and transcription-related factors. *Microbiol Mol Biol Rev* **64**, 435-459 (2000).
- 14 Zhang, Y. & Reinberg, D. Transcription regulation by histone methylation: interplay between different covalent modifications of the core histone tails. *Genes Dev* **15**, 2343-2360, doi:10.1101/gad.927301 (2001).
- 15 Nowak, S. J. & Corces, V. G. Phosphorylation of histone H3: a balancing act between chromosome condensation and transcriptional activation. *Trends Genet* **20**, 214-220, doi:10.1016/j.tig.2004.02.007 (2004).
- 16 Shilatifard, A. Chromatin modifications by methylation and ubiquitination: implications in the regulation of gene expression. *Annu Rev Biochem* **75**, 243-269, doi:10.1146/annurev.biochem.75.103004.142422 (2006).
- 17 Nathan, D. *et al.* Histone sumoylation is a negative regulator in *Saccharomyces cerevisiae* and shows dynamic interplay with positive-acting histone modifications. *Genes Dev* **20**, 966-976, doi:10.1101/gad.1404206 (2006).
- 18 Hassa, P. O., Haenni, S. S., Elser, M. & Hottiger, M. O. Nuclear ADP-ribosylation reactions in mammalian cells: where are we today and where are we going? *Microbiol Mol Biol Rev* **70**, 789-829, doi:10.1128/MMBR.00040-05 (2006).
- 19 Cuthbert, G. L. *et al.* Histone deimination antagonizes arginine methylation. *Cell* **118**, 545-553, doi:10.1016/j.cell.2004.08.020 (2004).
- 20 Nelson, C. J., Santos-Rosa, H. & Kouzarides, T. Proline isomerization of histone H3 regulates lysine methylation and gene expression. *Cell* **126**, 905-916, doi:10.1016/j.cell.2006.07.026 (2006).
- 21 Jenuwein, T. & Allis, C. D. Translating the histone code. *Science* **293**, 1074-1080, doi:10.1126/science.1063127 (2001).

- 22 Gaspar-Maia, A., Alajem, A., Meshorer, E. & Ramalho-Santos, M. Open chromatin in pluripotency and reprogramming. *Nat Rev Mol Cell Biol* **12**, 36-47, doi:10.1038/nrm3036 (2011).
- 23 Margueron, R., Trojer, P. & Reinberg, D. The key to development: interpreting the histone code? *Curr Opin Genet Dev* **15**, 163-176, doi:10.1016/j.gde.2005.01.005 (2005).
- 24 Nightingale, K. P., O'Neill, L. P. & Turner, B. M. Histone modifications: signalling receptors and potential elements of a heritable epigenetic code. *Curr Opin Genet Dev* **16**, 125-136, doi:10.1016/j.gde.2006.02.015 (2006).
- 25 Krietenstein, N. *et al.* Genomic Nucleosome Organization Reconstituted with Pure Proteins. *Cell* **167**, 709-721 e712, doi:10.1016/j.cell.2016.09.045 (2016).
- 26 Whitehouse, I., Rando, O. J., Delrow, J. & Tsukiyama, T. Chromatin remodelling at promoters suppresses antisense transcription. *Nature* **450**, 1031-1035, doi:10.1038/nature06391 (2007).
- 27 Yen, K., Vinayachandran, V., Batta, K., Koerber, R. T. & Pugh, B. F. Genome-wide nucleosome specificity and directionality of chromatin remodelers. *Cell* **149**, 1461-1473, doi:10.1016/j.cell.2012.04.036 (2012).
- 28 Yen, K., Vinayachandran, V. & Pugh, B. F. SWR-C and INO80 chromatin remodelers recognize nucleosome-free regions near +1 nucleosomes. *Cell* **154**, 1246-1256, doi:10.1016/j.cell.2013.08.043 (2013).
- 29 de Dieuleveult, M. *et al.* Genome-wide nucleosome specificity and function of chromatin remodellers in ES cells. *Nature* **530**, 113-116, doi:10.1038/nature16505 (2016).
- 30 Hartley, P. D. & Madhani, H. D. Mechanisms that specify promoter nucleosome location and identity. *Cell* **137**, 445-458, doi:10.1016/j.cell.2009.02.043 (2009).
- 31 Zentner, G. E. & Henikoff, S. Regulation of nucleosome dynamics by histone modifications. *Nat Struct Mol Biol* **20**, 259-266, doi:10.1038/nsmb.2470 (2013).
- 32 Shivaswamy, S. *et al.* Dynamic remodeling of individual nucleosomes across a eukaryotic genome in response to transcriptional perturbation. *PLoS Biol* **6**, e65, doi:10.1371/journal.pbio.0060065 (2008).
- 33 de la Serna, I. L., Ohkawa, Y. & Imbalzano, A. N. Chromatin remodelling in mammalian differentiation: lessons from ATP-dependent remodellers. *Nat Rev Genet* **7**, 461-473, doi:10.1038/nrg1882 (2006).
- 34 Vassileva, I., Yanakieva, I., Peycheva, M., Gospodinov, A. & Anachkova, B. The mammalian INO80 chromatin remodeling complex is required for replication stress recovery. *Nucleic acids research* **42**, 9074-9086, doi:10.1093/nar/gku605 (2014).
- 35 Lai, W. K. M. & Pugh, B. F. Understanding nucleosome dynamics and their links to gene expression and DNA replication. *Nat Rev Mol Cell Biol* **18**, 548-562, doi:10.1038/nrm.2017.47 (2017).
- 36 Ambler, R. P. & Rees, M. W. Epsilon-N-Methyl-lysine in bacterial flagellar protein. *Nature* **184**, 56-57 (1959).
- 37 Murray, K. The Occurrence of Epsilon-N-Methyl Lysine in Histones. *Biochemistry* **3**, 10-15 (1964).
- 38 Shi, Y. *et al.* Histone demethylation mediated by the nuclear amine oxidase homolog LSD1. *Cell* **119**, 941-953, doi:10.1016/j.cell.2004.12.012 (2004).
- 39 Biggar, K. K. & Li, S. S. Non-histone protein methylation as a regulator of cellular signalling and function. *Nat Rev Mol Cell Biol* **16**, 5-17, doi:10.1038/nrm3915 (2015).
- 40 Morin, R. D. *et al.* Frequent mutation of histone-modifying genes in non-Hodgkin lymphoma. *Nature* **476**, 298-303, doi:10.1038/nature10351 (2011).
- 41 Martin, C. & Zhang, Y. The diverse functions of histone lysine methylation. *Nat Rev Mol Cell Biol* **6**, 838-849, doi:10.1038/nrm1761 (2005).
- 42 Shi, Y. & Whetstine, J. R. Dynamic regulation of histone lysine methylation by demethylases. *Mol Cell* **25**, 1-14, doi:10.1016/j.molcel.2006.12.010 (2007).
- 43 Kouzarides, T. Histone methylation in transcriptional control. *Curr Opin Genet Dev* **12**, 198-209 (2002).

- 44 Sims, R. J., 3rd, Nishioka, K. & Reinberg, D. Histone lysine methylation: a signature for chromatin function. *Trends Genet* **19**, 629-639, doi:10.1016/j.tig.2003.09.007 (2003).
- 45 Blanc, R. S. & Richard, S. Arginine Methylation: The Coming of Age. *Mol Cell* **65**, 8-24, doi:10.1016/j.molcel.2016.11.003 (2017).
- 46 Kirmizis, A. *et al.* Arginine methylation at histone H3R2 controls deposition of H3K4 trimethylation. *Nature* **449**, 928-932, doi:10.1038/nature06160 (2007).
- 47 Guccione, E. *et al.* Methylation of histone H3R2 by PRMT6 and H3K4 by an MLL complex are mutually exclusive. *Nature* **449**, 933-937, doi:10.1038/nature06166 (2007).
- 48 Fuhrmann, J., Clancy, K. W. & Thompson, P. R. Chemical biology of protein arginine modifications in epigenetic regulation. *Chem Rev* **115**, 5413-5461, doi:10.1021/acs.chemrev.5b00003 (2015).
- 49 Gayatri, S. & Bedford, M. T. Readers of histone methylarginine marks. *Biochim Biophys Acta* **1839**, 702-710, doi:10.1016/j.bbagr.2014.02.015 (2014).
- 50 McCabe, M. T., Mohammad, H. P., Barbash, O. & Kruger, R. G. Targeting Histone Methylation in Cancer. *Cancer J* **23**, 292-301, doi:10.1097/PPO.0000000000000283 (2017).
- 51 Yang, Y. & Bedford, M. T. Protein arginine methyltransferases and cancer. *Nat Rev Cancer* **13**, 37-50, doi:10.1038/nrc3409 (2013).
- 52 Lewis, E. B. A gene complex controlling segmentation in *Drosophila*. *Nature* **276**, 565-570 (1978).
- 53 Whitcomb, S. J., Basu, A., Allis, C. D. & Bernstein, E. Polycomb Group proteins: an evolutionary perspective. *Trends Genet* **23**, 494-502, doi:10.1016/j.tig.2007.08.006 (2007).
- 54 Scheuermann, J. C. *et al.* Histone H2A deubiquitinase activity of the Polycomb repressive complex PR-DUB. *Nature* **465**, 243-247, doi:10.1038/nature08966 (2010).
- 55 Klymenko, T. *et al.* A Polycomb group protein complex with sequence-specific DNA-binding and selective methyl-lysine-binding activities. *Genes Dev* **20**, 1110-1122, doi:10.1101/gad.377406 (2006).
- 56 Simon, J. A. & Kingston, R. E. Mechanisms of polycomb gene silencing: knowns and unknowns. *Nat Rev Mol Cell Biol* **10**, 697-708, doi:10.1038/nrm2763 (2009).
- 57 Schuettengruber, B. & Cavalli, G. Recruitment of polycomb group complexes and their role in the dynamic regulation of cell fate choice. *Development* **136**, 3531-3542, doi:10.1242/dev.033902 (2009).
- 58 Cao, R. *et al.* Role of histone H3 lysine 27 methylation in Polycomb-group silencing. *Science* **298**, 1039-1043, doi:10.1126/science.1076997 (2002).
- 59 Fischle, W. *et al.* Molecular basis for the discrimination of repressive methyl-lysine marks in histone H3 by Polycomb and HP1 chromodomains. *Genes Dev* **17**, 1870-1881, doi:10.1101/gad.1110503 (2003).
- 60 Min, J., Zhang, Y. & Xu, R. M. Structural basis for specific binding of Polycomb chromodomain to histone H3 methylated at Lys 27. *Genes Dev* **17**, 1823-1828, doi:10.1101/gad.269603 (2003).
- 61 Blackledge, N. P. *et al.* Variant PRC1 complex-dependent H2A ubiquitylation drives PRC2 recruitment and polycomb domain formation. *Cell* **157**, 1445-1459, doi:10.1016/j.cell.2014.05.004 (2014).
- 62 Cooper, S. *et al.* Targeting polycomb to pericentric heterochromatin in embryonic stem cells reveals a role for H2AK119u1 in PRC2 recruitment. *Cell Rep* **7**, 1456-1470, doi:10.1016/j.celrep.2014.04.012 (2014).
- 63 Holoch, D. & Margueron, R. Mechanisms Regulating PRC2 Recruitment and Enzymatic Activity. *Trends Biochem Sci* **42**, 531-542, doi:10.1016/j.tibs.2017.04.003 (2017).
- 64 Margueron, R. & Reinberg, D. The Polycomb complex PRC2 and its mark in life. *Nature* **469**, 343-349, doi:10.1038/nature09784 (2011).

- 65 Cooper, S. *et al.* Jarid2 binds mono-ubiquitylated H2A lysine 119 to mediate crosstalk between Polycomb complexes PRC1 and PRC2. *Nat Commun* **7**, 13661, doi:10.1038/ncomms13661 (2016).
- 66 Kim, H., Kang, K. & Kim, J. AEBP2 as a potential targeting protein for Polycomb Repression Complex PRC2. *Nucleic acids research* **37**, 2940-2950, doi:10.1093/nar/gkp149 (2009).
- 67 Moritz, L. E. & Trievel, R. C. Structure, mechanism, and regulation of polycomb repressive complex 2. *J Biol Chem*, doi:10.1074/jbc.R117.800367 (2017).
- 68 Ciferri, C. *et al.* Molecular architecture of human polycomb repressive complex 2. *Elife* **1**, e00005, doi:10.7554/eLife.00005 (2012).
- 69 Rinn, J. L. *et al.* Functional demarcation of active and silent chromatin domains in human HOX loci by noncoding RNAs. *Cell* **129**, 1311-1323, doi:10.1016/j.cell.2007.05.022 (2007).
- 70 Han, Z. *et al.* Structural basis of EZH2 recognition by EED. *Structure* **15**, 1306-1315, doi:10.1016/j.str.2007.08.007 (2007).
- 71 Margueron, R. *et al.* Role of the polycomb protein EED in the propagation of repressive histone marks. *Nature* **461**, 762-767, doi:10.1038/nature08398 (2009).
- 72 Margueron, R. *et al.* Ezh1 and Ezh2 maintain repressive chromatin through different mechanisms. *Mol Cell* **32**, 503-518, doi:10.1016/j.molcel.2008.11.004 (2008).
- 73 Cao, R. & Zhang, Y. SUZ12 is required for both the histone methyltransferase activity and the silencing function of the EED-EZH2 complex. *Mol Cell* **15**, 57-67, doi:10.1016/j.molcel.2004.06.020 (2004).
- 74 Ketel, C. S. *et al.* Subunit contributions to histone methyltransferase activities of fly and worm polycomb group complexes. *Mol Cell Biol* **25**, 6857-6868, doi:10.1128/MCB.25.16.6857-6868.2005 (2005).
- 75 Pasini, D., Bracken, A. P., Jensen, M. R., Lazzerini Denchi, E. & Helin, K. Suz12 is essential for mouse development and for EZH2 histone methyltransferase activity. *EMBO J* **23**, 4061-4071, doi:10.1038/sj.emboj.7600402 (2004).
- 76 He, A. *et al.* PRC2 directly methylates GATA4 and represses its transcriptional activity. *Genes Dev* **26**, 37-42, doi:10.1101/gad.173930.111 (2012).
- 77 Vasanthakumar, A. *et al.* A non-canonical function of Ezh2 preserves immune homeostasis. *EMBO Rep* **18**, 619-631, doi:10.15252/embr.201643237 (2017).
- 78 Kim, K. H. & Roberts, C. W. Targeting EZH2 in cancer. *Nat Med* **22**, 128-134, doi:10.1038/nm.4036 (2016).
- 79 Agger, K. *et al.* UTX and JMJD3 are histone H3K27 demethylases involved in HOX gene regulation and development. *Nature* **449**, 731-734, doi:10.1038/nature06145 (2007).
- 80 Hong, S. *et al.* Identification of JmjC domain-containing UTX and JMJD3 as histone H3 lysine 27 demethylases. *Proc Natl Acad Sci U S A* **104**, 18439-18444, doi:10.1073/pnas.0707292104 (2007).
- 81 Lee, M. G. *et al.* Demethylation of H3K27 regulates polycomb recruitment and H2A ubiquitination. *Science* **318**, 447-450, doi:10.1126/science.1149042 (2007).
- 82 Lan, F. *et al.* A histone H3 lysine 27 demethylase regulates animal posterior development. *Nature* **449**, 689-694, doi:10.1038/nature06192 (2007).
- 83 De Santa, F. *et al.* The histone H3 lysine-27 demethylase Jmjd3 links inflammation to inhibition of polycomb-mediated gene silencing. *Cell* **130**, 1083-1094, doi:10.1016/j.cell.2007.08.019 (2007).
- 84 Antonyamy, S. *et al.* Structural context of disease-associated mutations and putative mechanism of autoinhibition revealed by X-ray crystallographic analysis of the EZH2-SET domain. *PLoS One* **8**, e84147, doi:10.1371/journal.pone.0084147 (2013).
- 85 Wu, H. *et al.* Structure of the catalytic domain of EZH2 reveals conformational plasticity in cofactor and substrate binding sites and explains oncogenic mutations. *PLoS One* **8**, e83737, doi:10.1371/journal.pone.0083737 (2013).

- 86 Jiao, L. & Liu, X. Structural basis of histone H3K27 trimethylation by an active polycomb repressive complex 2. *Science* **350**, aac4383, doi:10.1126/science.aac4383 (2015).
- 87 Justin, N. *et al.* Structural basis of oncogenic histone H3K27M inhibition of human polycomb repressive complex 2. *Nat Commun* **7**, 11316, doi:10.1038/ncomms11316 (2016).
- 88 Zhang, Y., Justin, N., Wilson, J. R. & Gamblin, S. J. Comment on "Structural basis of histone H3K27 trimethylation by an active polycomb repressive complex 2". *Science* **354**, 1543, doi:10.1126/science.aaf6236 (2016).
- 89 Cao, R. & Zhang, Y. The functions of E(Z)/EZH2-mediated methylation of lysine 27 in histone H3. *Curr Opin Genet Dev* **14**, 155-164, doi:10.1016/j.gde.2004.02.001 (2004).
- 90 Lee, T. I. *et al.* Control of developmental regulators by Polycomb in human embryonic stem cells. *Cell* **125**, 301-313, doi:10.1016/j.cell.2006.02.043 (2006).
- 91 Bracken, A. P. *et al.* EZH2 is downstream of the pRB-E2F pathway, essential for proliferation and amplified in cancer. *EMBO J* **22**, 5323-5335, doi:10.1093/emboj/cdg542 (2003).
- 92 Bruggeman, S. W. *et al.* Ink4a and Arf differentially affect cell proliferation and neural stem cell self-renewal in Bmi1-deficient mice. *Genes Dev* **19**, 1438-1443, doi:10.1101/gad.1299305 (2005).
- 93 Cao, Q. *et al.* Repression of E-cadherin by the polycomb group protein EZH2 in cancer. *Oncogene* **27**, 7274-7284, doi:10.1038/onc.2008.333 (2008).
- 94 Chang, C. J. *et al.* EZH2 promotes expansion of breast tumor initiating cells through activation of RAF1-beta-catenin signaling. *Cancer Cell* **19**, 86-100, doi:10.1016/j.ccr.2010.10.035 (2011).
- 95 Du, J. *et al.* FOXC1, a target of polycomb, inhibits metastasis of breast cancer cells. *Breast Cancer Res Treat* **131**, 65-73, doi:10.1007/s10549-011-1396-3 (2012).
- 96 Koh, C. M. *et al.* Myc enforces overexpression of EZH2 in early prostatic neoplasia via transcriptional and post-transcriptional mechanisms. *Oncotarget* **2**, 669-683, doi:10.18632/oncotarget.327 (2011).
- 97 Muller, H. *et al.* E2Fs regulate the expression of genes involved in differentiation, development, proliferation, and apoptosis. *Genes Dev* **15**, 267-285, doi:10.1101/gad.864201 (2001).
- 98 Neri, F. *et al.* Myc regulates the transcription of the PRC2 gene to control the expression of developmental genes in embryonic stem cells. *Mol Cell Biol* **32**, 840-851, doi:10.1128/MCB.06148-11 (2012).
- 99 Benetatos, L., Voulgaris, E., Vartholomatos, G. & Hatzimichael, E. Non-coding RNAs and EZH2 interactions in cancer: long and short tales from the transcriptome. *Int J Cancer* **133**, 267-274, doi:10.1002/ijc.27859 (2013).
- 100 Caretti, G., Palacios, D., Sartorelli, V. & Puri, P. L. Phosphoryl-EZH-ion. *Cell Stem Cell* **8**, 262-265, doi:10.1016/j.stem.2011.02.012 (2011).
- 101 Cakouros, D. *et al.* Twist-1 induces Ezh2 recruitment regulating histone methylation along the Ink4A/Arf locus in mesenchymal stem cells. *Mol Cell Biol* **32**, 1433-1441, doi:10.1128/MCB.06315-11 (2012).
- 102 Corvetta, D. *et al.* Physical interaction between MYCN oncogene and polycomb repressive complex 2 (PRC2) in neuroblastoma: functional and therapeutic implications. *J Biol Chem* **288**, 8332-8341, doi:10.1074/jbc.M113.454280 (2013).
- 103 Stazi, G., Zwergel, C., Mai, A. & Valente, S. EZH2 inhibitors: a patent review (2014-2016). *Expert Opin Ther Pat* **27**, 797-813, doi:10.1080/13543776.2017.1316976 (2017).
- 104 Chang, C. J. & Hung, M. C. The role of EZH2 in tumour progression. *Br J Cancer* **106**, 243-247, doi:10.1038/bjc.2011.551 (2012).
- 105 Chase, A. & Cross, N. C. Aberrations of EZH2 in cancer. *Clin Cancer Res* **17**, 2613-2618, doi:10.1158/1078-0432.CCR-10-2156 (2011).
- 106 Wang, C. *et al.* EZH2 Mediates epigenetic silencing of neuroblastoma suppressor genes CASZ1, CLU, RUNX3, and NGFR. *Cancer Res* **72**, 315-324, doi:10.1158/0008-5472.CAN-11-0961 (2012).

107 Kim, J. & Yu, J. Interrogating genomic and epigenomic data to understand prostate
cancer. *Biochim Biophys Acta* **1825**, 186-196, doi:10.1016/j.bbcan.2011.12.003 (2012).

108 Fujikawa, D. *et al.* Polycomb-dependent epigenetic landscape in adult T-cell leukemia.
Blood **127**, 1790-1802, doi:10.1182/blood-2015-08-662593 (2016).

109 Varambally, S. *et al.* The polycomb group protein EZH2 is involved in progression of
prostate cancer. *Nature* **419**, 624-629, doi:10.1038/nature01075 (2002).

110 Kleer, C. G. *et al.* EZH2 is a marker of aggressive breast cancer and promotes
neoplastic transformation of breast epithelial cells. *Proc Natl Acad Sci U S A* **100**,
11606-11611, doi:10.1073/pnas.1933744100 (2003).

111 Bachmann, I. M. *et al.* EZH2 expression is associated with high proliferation rate and
aggressive tumor subgroups in cutaneous melanoma and cancers of the endometrium,
prostate, and breast. *J Clin Oncol* **24**, 268-273, doi:10.1200/JCO.2005.01.5180 (2006).

112 Sauvageau, M. & Sauvageau, G. Polycomb group proteins: multi-faceted regulators of
somatic stem cells and cancer. *Cell Stem Cell* **7**, 299-313,
doi:10.1016/j.stem.2010.08.002 (2010).

113 Nichol, J. N., Dupere-Richer, D., Ezponda, T., Licht, J. D. & Miller, W. H., Jr. H3K27
Methylation: A Focal Point of Epigenetic Deregulation in Cancer. *Adv Cancer Res* **131**,
59-95, doi:10.1016/bs.acr.2016.05.001 (2016).

114 Kamminga, L. M. *et al.* The Polycomb group gene Ezh2 prevents hematopoietic stem
cell exhaustion. *Blood* **107**, 2170-2179, doi:10.1182/blood-2005-09-3585 (2006).

115 Herrera-Merchan, A. *et al.* Ectopic expression of the histone methyltransferase Ezh2 in
haematopoietic stem cells causes myeloproliferative disease. *Nat Commun* **3**, 623,
doi:10.1038/ncomms1623 (2012).

116 Tanaka, S. *et al.* Ezh2 augments leukemogenicity by reinforcing differentiation
blockage in acute myeloid leukemia. *Blood* **120**, 1107-1117, doi:10.1182/blood-2011-
11-394932 (2012).

117 Vo, B. T. *et al.* Inactivation of Ezh2 Upregulates Gfi1 and Drives Aggressive Myc-
Driven Group 3 Medulloblastoma. *Cell Rep* **18**, 2907-2917,
doi:10.1016/j.celrep.2017.02.073 (2017).

118 Luo, H. *et al.* EZH2 promotes invasion and metastasis of laryngeal squamous cells
carcinoma via epithelial-mesenchymal transition through H3K27me3. *Biochem Biophys
Res Commun* **479**, 253-259, doi:10.1016/j.bbrc.2016.09.055 (2016).

119 Cardenas, H., Zhao, J., Vieth, E., Nephew, K. P. & Matei, D. EZH2 inhibition promotes
epithelial-to-mesenchymal transition in ovarian cancer cells. *Oncotarget*,
doi:10.18632/oncotarget.11497 (2016).

120 Honma, K. *et al.* Interferon regulatory factor 4 negatively regulates the production of
proinflammatory cytokines by macrophages in response to LPS. *Proc Natl Acad Sci U S
A* **102**, 16001-16006, doi:10.1073/pnas.0504226102 (2005).

121 Yoshida, H., Nadanaka, S., Sato, R. & Mori, K. XBP1 is critical to protect cells from
endoplasmic reticulum stress: evidence from Site-2 protease-deficient Chinese hamster
ovary cells. *Cell Struct Funct* **31**, 117-125 (2006).

122 Turner, C. A., Jr., Mack, D. H. & Davis, M. M. Blimp-1, a novel zinc finger-containing
protein that can drive the maturation of B lymphocytes into immunoglobulin-secreting
cells. *Cell* **77**, 297-306 (1994).

123 Sciammas, R. & Davis, M. M. Modular nature of Blimp-1 in the regulation of gene
expression during B cell maturation. *J Immunol* **172**, 5427-5440 (2004).

124 Alzrigat, M. *et al.* EZH2 inhibition in multiple myeloma downregulates myeloma
associated oncogenes and upregulates microRNAs with potential tumor suppressor
functions. *Oncotarget*, doi:10.18632/oncotarget.14378 (2016).

125 Yan, J. *et al.* EZH2 overexpression in natural killer/T-cell lymphoma confers growth
advantage independently of histone methyltransferase activity. *Blood* **121**, 4512-4520,
doi:10.1182/blood-2012-08-450494 (2013).

126 Xu, K. *et al.* EZH2 oncogenic activity in castration-resistant prostate cancer cells is
Polycomb-independent. *Science* **338**, 1465-1469, doi:10.1126/science.1227604 (2012).

- 127 Kim, E. *et al.* Phosphorylation of EZH2 activates STAT3 signaling via STAT3
methylation and promotes tumorigenicity of glioblastoma stem-like cells. *Cancer Cell*
23, 839-852, doi:10.1016/j.ccr.2013.04.008 (2013).
- 128 Morin, R. D. *et al.* Somatic mutations altering EZH2 (Tyr641) in follicular and diffuse
large B-cell lymphomas of germinal-center origin. *Nat Genet* **42**, 181-185,
doi:10.1038/ng.518 (2010).
- 129 McCabe, M. T. *et al.* Mutation of A677 in histone methyltransferase EZH2 in human B-
cell lymphoma promotes hypertrimethylation of histone H3 on lysine 27 (H3K27). *Proc*
Natl Acad Sci U S A **109**, 2989-2994, doi:10.1073/pnas.1116418109 (2012).
- 130 Majer, C. R. *et al.* A687V EZH2 is a gain-of-function mutation found in lymphoma
patients. *FEBS Lett* **586**, 3448-3451, doi:10.1016/j.febslet.2012.07.066 (2012).
- 131 Sneeringer, C. J. *et al.* Coordinated activities of wild-type plus mutant EZH2 drive
tumor-associated hypertrimethylation of lysine 27 on histone H3 (H3K27) in human B-
cell lymphomas. *Proc Natl Acad Sci U S A* **107**, 20980-20985,
doi:10.1073/pnas.1012525107 (2010).
- 132 Nikoloski, G. *et al.* Somatic mutations of the histone methyltransferase gene EZH2 in
myelodysplastic syndromes. *Nat Genet* **42**, 665-667, doi:10.1038/ng.620 (2010).
- 133 Ntziachristos, P. *et al.* Genetic inactivation of the polycomb repressive complex 2 in T
cell acute lymphoblastic leukemia. *Nat Med* **18**, 298-301, doi:10.1038/nm.2651 (2012).
- 134 Ernst, T. *et al.* Inactivating mutations of the histone methyltransferase gene EZH2 in
myeloid disorders. *Nat Genet* **42**, 722-726, doi:10.1038/ng.621 (2010).
- 135 Boyer, L. A. *et al.* Polycomb complexes repress developmental regulators in murine
embryonic stem cells. *Nature* **441**, 349-353, doi:10.1038/nature04733 (2006).
- 136 Ezhkova, E. *et al.* Ezh2 orchestrates gene expression for the stepwise differentiation of
tissue-specific stem cells. *Cell* **136**, 1122-1135, doi:10.1016/j.cell.2008.12.043 (2009).
- 137 Shan, Y. *et al.* PRC2 specifies ectoderm lineages and maintains pluripotency in primed
but not naive ESCs. *Nat Commun* **8**, 672, doi:10.1038/s41467-017-00668-4 (2017).
- 138 Piunti, A. & Pasini, D. Epigenetic factors in cancer development: polycomb group
proteins. *Future Oncol* **7**, 57-75, doi:10.2217/fon.10.157 (2011).
- 139 Karantanos, T., Chistofides, A., Barhdan, K., Li, L. & Boussiotis, V. A. Regulation of T
Cell Differentiation and Function by EZH2. *Front Immunol* **7**, 172,
doi:10.3389/fimmu.2016.00172 (2016).
- 140 Caretti, G., Di Padova, M., Micales, B., Lyons, G. E. & Sartorelli, V. The Polycomb
Ezh2 methyltransferase regulates muscle gene expression and skeletal muscle
differentiation. *Genes Dev* **18**, 2627-2638, doi:10.1101/gad.1241904 (2004).
- 141 Sher, F. *et al.* Differentiation of neural stem cells into oligodendrocytes: involvement of
the polycomb group protein Ezh2. *Stem Cells* **26**, 2875-2883,
doi:10.1634/stemcells.2008-0121 (2008).
- 142 Hwang, W. W. *et al.* Distinct and separable roles for EZH2 in neurogenic astroglia.
Elife **3**, e02439, doi:10.7554/eLife.02439 (2014).
- 143 Pereira, J. D. *et al.* Ezh2, the histone methyltransferase of PRC2, regulates the balance
between self-renewal and differentiation in the cerebral cortex. *Proc Natl Acad Sci U S*
A **107**, 15957-15962, doi:10.1073/pnas.1002530107 (2010).
- 144 Acharyya, S. *et al.* TNF inhibits Notch-1 in skeletal muscle cells by Ezh2 and DNA
methylation mediated repression: implications in duchenne muscular dystrophy. *PLoS*
One **5**, e12479, doi:10.1371/journal.pone.0012479 (2010).
- 145 Palacios, D. *et al.* TNF/p38alpha/polycomb signaling to Pax7 locus in satellite cells
links inflammation to the epigenetic control of muscle regeneration. *Cell Stem Cell* **7**,
455-469, doi:10.1016/j.stem.2010.08.013 (2010).
- 146 Chen, H. *et al.* Polycomb protein Ezh2 regulates pancreatic beta-cell Ink4a/Arf
expression and regeneration in diabetes mellitus. *Genes Dev* **23**, 975-985,
doi:10.1101/gad.1742509 (2009).
- 147 Zhou, J. X. *et al.* Combined modulation of polycomb and trithorax genes rejuvenates
beta cell replication. *J Clin Invest* **123**, 4849-4858, doi:10.1172/JCI69468 (2013).

- 148 Wei, Y. *et al.* CDK1-dependent phosphorylation of EZH2 suppresses methylation of H3K27 and promotes osteogenic differentiation of human mesenchymal stem cells. *Nat Cell Biol* **13**, 87-94, doi:10.1038/ncb2139 (2011).
- 149 Chen, Y. H. *et al.* Myocyte enhancer factor-2 interacting transcriptional repressor (MITR) is a switch that promotes osteogenesis and inhibits adipogenesis of mesenchymal stem cells by inactivating peroxisome proliferator-activated receptor gamma-2. *J Biol Chem* **286**, 10671-10680, doi:10.1074/jbc.M110.199612 (2011).
- 150 Wang, L., Jin, Q., Lee, J. E., Su, I. H. & Ge, K. Histone H3K27 methyltransferase Ezh2 represses Wnt genes to facilitate adipogenesis. *Proc Natl Acad Sci U S A* **107**, 7317-7322, doi:10.1073/pnas.1000031107 (2010).
- 151 Tanaka, M., Roberts, J. M., Qi, J. & Bradner, J. E. Inhibitors of emerging epigenetic targets for cancer therapy: a patent review (2010-2014). *Pharm Pat Anal* **4**, 261-284, doi:10.4155/ppa.15.16 (2015).
- 152 Glazer, R. I., Knode, M. C., Tseng, C. K., Haines, D. R. & Marquez, V. E. 3-Deazaneplanocin A: a new inhibitor of S-adenosylhomocysteine synthesis and its effects in human colon carcinoma cells. *Biochem Pharmacol* **35**, 4523-4527 (1986).
- 153 Miranda, T. B. *et al.* DZNep is a global histone methylation inhibitor that reactivates developmental genes not silenced by DNA methylation. *Mol Cancer Ther* **8**, 1579-1588, doi:10.1158/1535-7163.MCT-09-0013 (2009).
- 154 Tan, J. *et al.* Pharmacologic disruption of Polycomb-repressive complex 2-mediated gene repression selectively induces apoptosis in cancer cells. *Genes Dev* **21**, 1050-1063, doi:10.1101/gad.1524107 (2007).
- 155 Sun, F. *et al.* Preclinical pharmacokinetic studies of 3-deazaneplanocin A, a potent epigenetic anticancer agent, and its human pharmacokinetic prediction using GastroPlus. *Eur J Pharm Sci* **77**, 290-302, doi:10.1016/j.ejps.2015.06.021 (2015).
- 156 Knutson, S. K. *et al.* A selective inhibitor of EZH2 blocks H3K27 methylation and kills mutant lymphoma cells. *Nature chemical biology* **8**, 890-896, doi:10.1038/nchembio.1084 (2012).
- 157 Morera, L., Lubbert, M. & Jung, M. Targeting histone methyltransferases and demethylases in clinical trials for cancer therapy. *Clin Epigenetics* **8**, 57, doi:10.1186/s13148-016-0223-4 (2016).
- 158 Yap, T. A. *et al.* A Phase I Study of GSK2816126, an Enhancer of Zeste Homolog 2(EZH2) Inhibitor, in Patients (pts) with Relapsed/Refractory Diffuse Large B-Cell Lymphoma (DLBCL), Other Non-Hodgkin Lymphomas (NHL), Transformed Follicular Lymphoma (tFL), Solid Tumors and Multiple Myeloma (MM). *Blood* **128**, 4203 (2016).
- 159 Verma, S. K. *et al.* Identification of Potent, Selective, Cell-Active Inhibitors of the Histone Lysine Methyltransferase EZH2. *ACS medicinal chemistry letters* **3**, 1091-1096, doi:10.1021/ml3003346 (2012).
- 160 Qi, W. *et al.* Selective inhibition of Ezh2 by a small molecule inhibitor blocks tumor cells proliferation. *Proc Natl Acad Sci U S A* **109**, 21360-21365, doi:10.1073/pnas.1210371110 (2012).
- 161 Konze, K. D. *et al.* An orally bioavailable chemical probe of the Lysine Methyltransferases EZH2 and EZH1. *ACS Chem Biol* **8**, 1324-1334, doi:10.1021/cb400133j (2013).
- 162 Knutson, S. K. *et al.* Durable tumor regression in genetically altered malignant rhabdoid tumors by inhibition of methyltransferase EZH2. *Proc Natl Acad Sci U S A* **110**, 7922-7927, doi:10.1073/pnas.1303800110 (2013).
- 163 Ribrag, V. *et al.* Phase 1 study of tazemetostat (EPZ-6438), an inhibitor of enhancer of zeste-homolog 2 (EZH2): preliminary safety and activity in relapsed or refractory non-Hodgkin lymphoma (NHL) patients. *Blood* **126**, 473-473 (2015).
- 164 Nasveschuk, C. G. *et al.* Discovery and Optimization of Tetramethylpiperidiny Benzamides as Inhibitors of EZH2. *ACS medicinal chemistry letters* **5**, 378-383, doi:10.1021/ml400494b (2014).

- 165 Gehling, V. S. *et al.* Discovery, design, and synthesis of indole-based EZH2 inhibitors. *Bioorg Med Chem Lett* **25**, 3644-3649, doi:10.1016/j.bmcl.2015.06.056 (2015).
- 166 Vaswani, R. G. *et al.* Identification of (R)-N-((4-Methoxy-6-methyl-2-oxo-1,2-dihydropyridin-3-yl)methyl)-2-methyl-1-(1-(2,2,2-trifluoroethyl)piperidin-4-yl)ethyl)-1H-indole-3-carboxamide (CPI-1205), a Potent and Selective Inhibitor of Histone Methyltransferase EZH2, Suitable for Phase I Clinical Trials for B-Cell Lymphomas. *J Med Chem* **59**, 9928-9941, doi:10.1021/acs.jmedchem.6b01315 (2016).
- 167 Brooun, A. *et al.* Polycomb repressive complex 2 structure with inhibitor reveals a mechanism of activation and drug resistance. *Nat Commun* **7**, 11384, doi:10.1038/ncomms11384 (2016).
- 168 Yang, X. *et al.* Structure-Activity Relationship Studies for Enhancer of Zeste Homologue 2 (EZH2) and Enhancer of Zeste Homologue 1 (EZH1) Inhibitors. *J Med Chem* **59**, 7617-7633, doi:10.1021/acs.jmedchem.6b00855 (2016).
- 169 Kim, W. *et al.* Targeted disruption of the EZH2-EED complex inhibits EZH2-dependent cancer. *Nature chemical biology* **9**, 643-650, doi:10.1038/nchembio.1331 (2013).
- 170 Walensky, L. D. Stabilized EZH2 peptides for treatment of cancer. WO2014151369A2 (2014).
- 171 Kong, X. *et al.* Astemizole arrests the proliferation of cancer cells by disrupting the EZH2-EED interaction of polycomb repressive complex 2. *J Med Chem* **57**, 9512-9521, doi:10.1021/jm501230c (2014).
- 172 Chen, H. *et al.* Wedelolactone disrupts the interaction of EZH2-EED complex and inhibits PRC2-dependent cancer. *Oncotarget* **6**, 13049-13059, doi:10.18632/oncotarget.3790 (2015).
- 173 Li, L. *et al.* Discovery and Molecular Basis of a Diverse Set of Polycomb Repressive Complex 2 Inhibitors Recognition by EED. *PLoS One* **12**, e0169855, doi:10.1371/journal.pone.0169855 (2017).
- 174 Lingel, A. *et al.* Structure-Guided Design of EED Binders Allosterically Inhibiting the Epigenetic Polycomb Repressive Complex 2 (PRC2) Methyltransferase. *J Med Chem* **60**, 415-427, doi:10.1021/acs.jmedchem.6b01473 (2017).
- 175 Huang, Y. *et al.* Discovery of First-in-Class, Potent and Orally Bioavailable EED inhibitor with Robust Anti-cancer Efficacy. *J Med Chem*, doi:10.1021/acs.jmedchem.6b01576 (2017).
- 176 He, Y. *et al.* The EED protein-protein interaction inhibitor A-395 inactivates the PRC2 complex. *Nature chemical biology*, doi:10.1038/nchembio.2306 (2017).
- 177 Qi, W. *et al.* An allosteric PRC2 inhibitor targeting the H3K27me3 binding pocket of EED. *Nature chemical biology*, doi:10.1038/nchembio.2304 (2017).
- 178 Barnash, K. D. *et al.* Discovery of Peptidomimetic Ligands of EED as Allosteric Inhibitors of PRC2. *ACS Comb Sci* **19**, 161-172, doi:10.1021/acscmbosci.6b00174 (2017).
- 179 Xu, B. *et al.* Selective inhibition of EZH2 and EZH1 enzymatic activity by a small molecule suppresses MLL-rearranged leukemia. *Blood* **125**, 346-357, doi:10.1182/blood-2014-06-581082 (2015).
- 180 Gibaja, V. *et al.* Development of secondary mutations in wild-type and mutant EZH2 alleles cooperates to confer resistance to EZH2 inhibitors. *Oncogene* **35**, 558-566, doi:10.1038/onc.2015.114 (2016).
- 181 Baude, A., Lindroth, A. M. & Plass, C. PRC2 loss amplifies Ras signaling in cancer. *Nat Genet* **46**, 1154-1155, doi:10.1038/ng.3124 (2014).
- 182 De Raedt, T. *et al.* Exploiting cancer cell vulnerabilities to develop a combination therapy for ras-driven tumors. *Cancer Cell* **20**, 400-413, doi:10.1016/j.ccr.2011.08.014 (2011).
- 183 Benedetti, R., Conte, M., Iside, C. & Altucci, L. Epigenetic-based therapy: From single- to multi-target approaches. *Int J Biochem Cell Biol* **69**, 121-131, doi:10.1016/j.biocel.2015.10.016 (2015).

184 de Lera, A. R. & Ganesan, A. Epigenetic polypharmacology: from combination therapy
to multitargeted drugs. *Clin Epigenetics* **8**, 105, doi:10.1186/s13148-016-0271-9 (2016).

185 Knutson, S. K. *et al.* Synergistic Anti-Tumor Activity of EZH2 Inhibitors and
Glucocorticoid Receptor Agonists in Models of Germinal Center Non-Hodgkin
Lymphomas. *PLoS One* **9**, e111840, doi:10.1371/journal.pone.0111840 (2014).

186 Kirk, J. S. *et al.* Top2a identifies and provides epigenetic rationale for novel
combination therapeutic strategies for aggressive prostate cancer. *Oncotarget* **6**, 3136-
3146, doi:10.18632/oncotarget.3077 (2015).

187 Johnson, D. P. *et al.* HDAC1,2 inhibition impairs EZH2- and BBAP-mediated DNA
repair to overcome chemoresistance in EZH2 gain-of-function mutant diffuse large B-
cell lymphoma. *Oncotarget* **6**, 4863-4887, doi:10.18632/oncotarget.3120 (2015).

188 Grinshtein, N. *et al.* Small molecule epigenetic screen identifies novel EZH2 and
HDAC inhibitors that target glioblastoma brain tumor-initiating cells. *Oncotarget* **7**,
59360-59376, doi:10.18632/oncotarget.10661 (2016).

189 Allfrey, V. G., Faulkner, R. & Mirsky, A. E. Acetylation and Methylation of Histones
and Their Possible Role in the Regulation of Rna Synthesis. *Proc Natl Acad Sci U S A*
51, 786-794 (1964).

190 Shahbazian, M. D. & Grunstein, M. Functions of site-specific histone acetylation and
deacetylation. *Annu Rev Biochem* **76**, 75-100,
doi:10.1146/annurev.biochem.76.052705.162114 (2007).

191 Groth, A., Rocha, W., Verreault, A. & Almouzni, G. Chromatin challenges during DNA
replication and repair. *Cell* **128**, 721-733, doi:10.1016/j.cell.2007.01.030 (2007).

192 Benton, C. B., Fiskus, W. & Bhalla, K. N. Targeting Histone Acetylation: Readers and
Writers in Leukemia and Cancer. *Cancer J* **23**, 286-291,
doi:10.1097/PPO.0000000000000284 (2017).

193 Bassett, S. A. & Barnett, M. P. The role of dietary histone deacetylases (HDACs)
inhibitors in health and disease. *Nutrients* **6**, 4273-4301, doi:10.3390/nu6104273
(2014).

194 Gu, W. & Roeder, R. G. Activation of p53 sequence-specific DNA binding by
acetylation of the p53 C-terminal domain. *Cell* **90**, 595-606 (1997).

195 Hyndman, K. A. & Knepper, M. A. Dynamic regulation of lysine acetylation: the
balance between acetyltransferase and deacetylase activities. *Am J Physiol Renal
Physiol* **313**, F842-F846, doi:10.1152/ajprenal.00313.2017 (2017).

196 Haynes, S. R. *et al.* The bromodomain: a conserved sequence found in human,
Drosophila and yeast proteins. *Nucleic acids research* **20**, 2603 (1992).

197 Li, Y. *et al.* AF9 YEATS domain links histone acetylation to DOT1L-mediated H3K79
methylation. *Cell* **159**, 558-571, doi:10.1016/j.cell.2014.09.049 (2014).

198 Filippakopoulos, P. & Knapp, S. Targeting bromodomains: epigenetic readers of lysine
acetylation. *Nat Rev Drug Discov* **13**, 337-356, doi:10.1038/nrd4286 (2014).

199 Fujisawa, T. & Filippakopoulos, P. Functions of bromodomain-containing proteins and
their roles in homeostasis and cancer. *Nat Rev Mol Cell Biol* **18**, 246-262,
doi:10.1038/nrm.2016.143 (2017).

200 Wilhelm, M. *et al.* Mass-spectrometry-based draft of the human proteome. *Nature* **509**,
582-587, doi:10.1038/nature13319 (2014).

201 Wang, C. Y. & Filippakopoulos, P. Beating the odds: BETs in disease. *Trends Biochem
Sci* **40**, 468-479, doi:10.1016/j.tibs.2015.06.002 (2015).

202 Belkina, A. C. & Denis, G. V. BET domain co-regulators in obesity, inflammation and
cancer. *Nat Rev Cancer* **12**, 465-477, doi:10.1038/nrc3256 (2012).

203 Muller, S., Filippakopoulos, P. & Knapp, S. Bromodomains as therapeutic targets.
Expert Rev Mol Med **13**, e29, doi:10.1017/S1462399411001992 (2011).

204 Owen, D. J. *et al.* The structural basis for the recognition of acetylated histone H4 by
the bromodomain of histone acetyltransferase gcn5p. *EMBO J* **19**, 6141-6149,
doi:10.1093/emboj/19.22.6141 (2000).

205 Jacobson, R. H., Ladurner, A. G., King, D. S. & Tjian, R. Structure and function of a
human TAFII250 double bromodomain module. *Science* **288**, 1422-1425 (2000).

- 206 Dhalluin, C. *et al.* Structure and ligand of a histone acetyltransferase bromodomain. *Nature* **399**, 491-496, doi:10.1038/20974 (1999).
- 207 Perez-Salvia, M. & Esteller, M. Bromodomain inhibitors and cancer therapy: From structures to applications. *Epigenetics* **12**, 323-339, doi:10.1080/15592294.2016.1265710 (2017).
- 208 Yang, Z., He, N. & Zhou, Q. Brd4 recruits P-TEFb to chromosomes at late mitosis to promote G1 gene expression and cell cycle progression. *Mol Cell Biol* **28**, 967-976, doi:10.1128/MCB.01020-07 (2008).
- 209 Feng, Q. *et al.* An epigenomic approach to therapy for tamoxifen-resistant breast cancer. *Cell Res* **24**, 809-819, doi:10.1038/cr.2014.71 (2014).
- 210 Zou, Z. *et al.* Brd4 maintains constitutively active NF-kappaB in cancer cells by binding to acetylated RelA. *Oncogene* **33**, 2395-2404, doi:10.1038/onc.2013.179 (2014).
- 211 Delmore, J. E. *et al.* BET bromodomain inhibition as a therapeutic strategy to target c-Myc. *Cell* **146**, 904-917, doi:10.1016/j.cell.2011.08.017 (2011).
- 212 Yang, Z. *et al.* Recruitment of P-TEFb for stimulation of transcriptional elongation by the bromodomain protein Brd4. *Mol Cell* **19**, 535-545, doi:10.1016/j.molcel.2005.06.029 (2005).
- 213 Smith, S. G. & Zhou, M. M. The Bromodomain: A New Target in Emerging Epigenetic Medicine. *ACS Chem Biol* **11**, 598-608, doi:10.1021/acschembio.5b00831 (2016).
- 214 Vidler, L. R., Brown, N., Knapp, S. & Hoelder, S. Druggability analysis and structural classification of bromodomain acetyl-lysine binding sites. *J Med Chem* **55**, 7346-7359, doi:10.1021/jm300346w (2012).
- 215 Filippakopoulos, P. *et al.* Selective inhibition of BET bromodomains. *Nature* **468**, 1067-1073, doi:10.1038/nature09504 (2010).
- 216 Nicodeme, E. *et al.* Suppression of inflammation by a synthetic histone mimic. *Nature* **468**, 1119-1123, doi:10.1038/nature09589 (2010).
- 217 Ceribelli, M. *et al.* A Druggable TCF4- and BRD4-Dependent Transcriptional Network Sustains Malignancy in Blastic Plasmacytoid Dendritic Cell Neoplasm. *Cancer Cell* **30**, 764-778, doi:10.1016/j.ccell.2016.10.002 (2016).
- 218 Zuber, J. *et al.* RNAi screen identifies Brd4 as a therapeutic target in acute myeloid leukaemia. *Nature* **478**, 524-528, doi:10.1038/nature10334 (2011).
- 219 Dawson, M. A. *et al.* Inhibition of BET recruitment to chromatin as an effective treatment for MLL-fusion leukaemia. *Nature* **478**, 529-533, doi:10.1038/nature10509 (2011).
- 220 Bandukwala, H. S. *et al.* Selective inhibition of CD4+ T-cell cytokine production and autoimmunity by BET protein and c-Myc inhibitors. *Proc Natl Acad Sci U S A* **109**, 14532-14537, doi:10.1073/pnas.1212264109 (2012).
- 221 Lu, P. *et al.* The BET inhibitor OTX015 reactivates latent HIV-1 through P-TEFb. *Sci Rep* **6**, 24100, doi:10.1038/srep24100 (2016).
- 222 Romero, F. A. *et al.* Disrupting Acetyl-Lysine Recognition: Progress in the Development of Bromodomain Inhibitors. *J Med Chem* **59**, 1271-1298, doi:10.1021/acs.jmedchem.5b01514 (2016).
- 223 Brand, M. *et al.* Small molecule inhibitors of bromodomain-acetyl-lysine interactions. *ACS Chem Biol* **10**, 22-39, doi:10.1021/cb500996u (2015).
- 224 Hartwig, J. F., Kawatsura, M., Hauck, S. I., Shaughnessy, K. H. & Alcazar-Roman, L. M. Room-Temperature Palladium-Catalyzed Amination of Aryl Bromides and Chlorides and Extended Scope of Aromatic C-N Bond Formation with a Commercial Ligand. *The Journal of Organic Chemistry* **64**, 5575-5580, doi:10.1021/jo990408i (1999).
- 225 Ma, D. & Cai, Q. N,N-Dimethyl Glycine-Promoted Ullmann Coupling Reaction of Phenols and Aryl Halides. *Organic Letters* **5**, 3799-3802, doi:10.1021/ol0350947 (2003).
- 226 Mispelaere-Canivet, C., Spindler, J.-F., Perrio, S. & Beslin, P. Pd2(dba)3/Xantphos-catalyzed cross-coupling of thiols and aryl bromides/triflates. *Tetrahedron* **61**, 5253-5259, doi:10.1016/j.tet.2005.03.078 (2005).

- 227 Sanden, E., Eberstal, S., Visse, E., Siesjo, P. & Darabi, A. A standardized and
reproducible protocol for serum-free monolayer culturing of primary paediatric brain
tumours to be utilized for therapeutic assays. *Sci Rep* **5**, 12218, doi:10.1038/srep12218
(2015).
- 228 Seidel, S., Garvalov, B. K. & Acker, T. in *Stem Cell Protocols* Vol. 1235 *Methods in
Molecular Biology* 263-275.
- 229 Veselska, R. *et al.* Nestin expression in the cell lines derived from glioblastoma
multiforme. *BMC Cancer* **6**, 32, doi:10.1186/1471-2407-6-32 (2006).
- 230 Mohammad, F. *et al.* EZH2 is a potential therapeutic target for H3K27M-mutant
pediatric gliomas. *Nat Med* **23**, 483-492, doi:10.1038/nm.4293 (2017).
- 231 Yin, Y., Qiu, S. & Peng, Y. Functional roles of enhancer of zeste homolog 2 in gliomas.
Gene **576**, 189-194, doi:10.1016/j.gene.2015.09.080 (2016).
- 232 Pang, B. *et al.* EZH2 promotes metabolic reprogramming in glioblastomas through
epigenetic repression of EAF2-HIF1alpha signaling. *Oncotarget* **7**, 45134-45143,
doi:10.18632/oncotarget.9761 (2016).
- 233 Rizq, O. *et al.* Dual Inhibition of EZH2 and EZH1 Sensitizes PRC2-Dependent Tumors
to Proteasome Inhibition. *Clin Cancer Res* **23**, 4817-4830, doi:10.1158/1078-
0432.CCR-16-2735 (2017).
- 234 Honma, D. *et al.* Novel orally bioavailable EZH1/2 dual inhibitors with greater
antitumor efficacy than an EZH2 selective inhibitor. *Cancer Sci*, doi:10.1111/cas.13326
(2017).
- 235 Murugesan, D. *et al.* Discovery and structure-activity relationships of pyrrolone
antimalarials. *J Med Chem* **56**, 2975-2990, doi:10.1021/jm400009c (2013).
- 236 Ernst, J. B., Ruhling, A., Wibbeling, B. & Glorius, F. Trichloromethylthiolation of N-
Heterocycles: Practical and Completely Regioselective. *Chemistry* **22**, 4400-4404,
doi:10.1002/chem.201600377 (2016).
- 237 Bourgeois-Cury, A. & Gore, J. Diels-Alder reaction of 2,5-dimethylpyrrole derivatives
in the aqueous phase. *Bull. Soc. Chim. Fr.* **129**, 490-495 (1992).
- 238 Skaddan, M. B. Novel synthesis of [13C4,15N]1H-pyrrole-2,3,5-tricarboxylic acid: an
important biomarker for melatonin metabolism. *Journal of Labelled Compounds and
Radiopharmaceuticals* **53**, 73-77, doi:10.1002/jlcr.1704 (2010).
- 239 Loy, N. S., Choi, S., Kim, S. & Park, C. M. The synthesis of pyrroles and oxazoles
based on gold alpha-imino carbene complexes. *Chem Commun (Camb)* **52**, 7336-7339,
doi:10.1039/c6cc01742h (2016).
- 240 Zhang, Z. *et al.* Synthesis of multisubstituted pyrroles from doubly activated
cyclopropanes using an iron-mediated oxidation domino reaction. *J Org Chem* **79**,
11226-11233, doi:10.1021/jo5018487 (2014).
- 241 Fabis, F., Dallemagne, P., Rault, S. & Robba, M. A NEW EFFICIENT SYNTHESIS
OF 3-AMINO-1-PHENYLPYRROLE. *Organic Preparations and Procedures
International* **27**, 236-239, doi:10.1080/00304949509458461 (1995).
- 242 Mital, A., Murugesan, D., Kaiser, M., Yeates, C. & Gilbert, I. H. Discovery and
optimisation studies of antimalarial phenotypic hits. *Eur J Med Chem* **103**, 530-538,
doi:10.1016/j.ejmech.2015.08.044 (2015).
- 243 Chen, X., Yang, M. & Zhou, M. Efficient synthesis of substituted pyrroles through
Pd(OCOCF3)2-catalyzed reaction of 5-hexen-2-one with primary amines. *Tetrahedron
Letters* **57**, 5215-5218, doi:<https://doi.org/10.1016/j.tetlet.2016.10.029> (2016).
- 244 Kobeissi, M., Yazbeck, O. & Chreim, Y. A convenient one-pot synthesis of
polysubstituted pyrroles from N-protected succinimides. *Tetrahedron Letters* **55**, 2523-
2526, doi:<https://doi.org/10.1016/j.tetlet.2014.03.021> (2014).
- 245 Meng, G. & Szostak, M. General Olefin Synthesis by the Palladium-Catalyzed Heck
Reaction of Amides: Sterically Controlled Chemoselective N-C Activation. *Angew
Chem Int Ed Engl* **54**, 14518-14522, doi:10.1002/anie.201507776 (2015).
- 246 Meng, G., Szostak, R. & Szostak, M. Suzuki-Miyaura Cross-Coupling of N-
Acylpyrroles and Pyrazoles: Planar, Electronically Activated Amides in Catalytic N-C
Cleavage. *Org Lett* **19**, 3596-3599, doi:10.1021/acs.orglett.7b01575 (2017).

- 247 Overberger, C. G., Palmer, L. C., Marks, B. S. & Byrd, N. R. Azo Compounds.1
Biradical Sources. The Synthesis of Some 1,1-Disubstituted Hydrazines. *Journal of the*
248 *American Chemical Society* **77**, 4100-4104, doi:10.1021/ja01620a040 (1955).
- 248 De, S. K. Cobalt(II) chloride as a novel and efficient catalyst for the synthesis of 1,2,5-
trisubstituted pyrroles under solvent-free conditions. *Heteroatom Chemistry* **19**, 592-
595, doi:10.1002/hc.20482 (2008).
- 249 De, S. K. Simple Synthesis of Pyrroles Under Solvent-Free Conditions. *Synthetic*
Communications **38**, 2768-2774, doi:10.1080/00397910701833791 (2008).
- 250 Pittet, A. O., Pascale, J. V. & Hruza, D. E. Neue heterocyclische aromamittel und ihre
herstellung. DE2312996A1 (1973).
- 251 Kim, B. H. *et al.* Synthesis of two distinct pyrrole moiety-containing arenes from
nitroanilines using Paal-Knorr followed by an indium-mediated reaction. *Org Biomol*
Chem **14**, 265-276, doi:10.1039/c5ob02101d (2016).
- 252 Lee, H. & Kim, B. H. Indium-mediated one-pot pyrrole synthesis from nitrobenzenes
and 1,4-diketones. *Tetrahedron* **69**, 6698-6708, doi:10.1016/j.tet.2013.05.113 (2013).
- 253 Walia, A., Kang, S. & Silverman, R. B. Microwave-assisted protection of primary
amines as 2,5-dimethylpyrroles and their orthogonal deprotection. *J Org Chem* **78**,
10931-10937, doi:10.1021/jo401778e (2013).
- 254 Royal Society of New South, W. *Journal and proceedings of the Royal Society of New*
South Wales. Vol. v.70 (1937) (Royal Society of New South Wales., 1937).
- 255 Li, D., Zang, H., Wu, C. & Yu, N. 1-Methylimidazolium hydrogen sulfate catalyzed
convenient synthesis of 2,5-dimethyl-N-substituted pyrroles under ultrasonic
irradiation. *Ultrason Sonochem* **20**, 1144-1148, doi:10.1016/j.ultsonch.2013.01.019
(2013).
- 256 Joshi, S. D., Kumar, D., More, U. A., Yang, K. S. & Aminabhavi, T. M. Design and
development of pyrrole carbaldehyde: an effective pharmacophore for enoyl-ACP
reductase. *Medicinal Chemistry Research* **25**, 672-689, doi:10.1007/s00044-016-1517-y
(2016).
- 257 Yonekura, K., Oki, K. & Tsuchimoto, T. Indium-Catalyzed Formal N-Arylation and N-
Alkylation of Pyrroles with Amines. *Advanced Synthesis & Catalysis* **358**, 2895-2902,
doi:10.1002/adsc.201600656 (2016).
- 258 Ilyin, P. V., Pankova, A. S. & Kuznetsov, M. A. Direct and Efficient Synthesis of
Pyrrole-3-carbaldehydes by Vilsmeier–Haack Formylation of Pyrroles with Sterically
Crowded Amides. *Synthesis* **44**, 1353-1358, doi:10.1055/s-0031-1290763 (2012).
- 259 Deng, S. *et al.* Pyrrolo- and thiazolo-pyridine compounds, and methods of use thereof.
US7696223B2 (2008).
- 260 Osman, N. A. *et al.* Discovery of novel Tetrahydrobenzo[b]thiophene and pyrrole based
scaffolds as potent and selective CB2 receptor ligands: The structural elements
controlling binding affinity, selectivity and functionality. *Eur J Med Chem* **122**, 619-
634, doi:10.1016/j.ejmech.2016.07.012 (2016).
- 261 Mironov, A. F., Kharitonova, O. V., Efimkin, A. G. & Solomentseva, T. A. New Iodo-
and Nitro-substituted Pyrroles. *Russian Journal of Organic Chemistry* **41**, 1654-1656,
doi:10.1007/s11178-006-0013-0 (2005).
- 262 Reisch, J. Die Bildung von Pyrrolen aus γ -Acetylenketonen. *Archiv der Pharmazie* **298**,
591-598, doi:10.1002/ardp.19652980907 (1965).
- 263 Mellini P., M. B., Borovika D, Polletta L, Carnevale I, Saladini S, Stazi G, Zwergel C,
Trapencieris P, Ferretti E, Tafani M, Valente S, and Mai A. Pyrazole-based inhibitors of
Enhancer of Zeste Homolog 2 induce apoptosis and autophagy in cancer cells. .
Philosophical Transactions Royal Society B (Accepted September 2017, now in
press), doi:10.1098/rstb.2017.0150 (2017).
- 264 Miele, E. *et al.* The histone methyltransferase EZH2 as a druggable target in SHH
medulloblastoma cancer stem cells. *Oncotarget* **8**, 68557-68570,
doi:10.18632/oncotarget.19782 (2017).

- 265 Xia, Y. *et al.* Synthesis and evaluation of polycyclic pyrazolo[3,4-d]pyrimidines as PDE1 and PDE5 cGMP phosphodiesterase inhibitors. *J Med Chem* **40**, 4372-4377, doi:10.1021/jm970495b (1997).
- 266 Boldron, C. *et al.* N-[6-(4-butanoyl-5-methyl-1H-pyrazol-1-yl)pyridazin-3-yl]-5-chloro-1-[2-(4-methyl piperazin-1-yl)-2-oxoethyl]-1H-indole-3-carboxamide (SAR216471), a novel intravenous and oral, reversible, and directly acting P2Y₁₂ antagonist. *J Med Chem* **57**, 7293-7316, doi:10.1021/jm500588w (2014).
- 267 Kurihara, T., Uno, T. & Sakamoto, Y. Reaction of ethyl 3-ethoxymethylene-2,4-dioxovalerate with monosubstituted hydrazines. *Journal of Heterocyclic Chemistry* **17**, 231-233, doi:10.1002/jhet.5570170205 (1980).
- 268 Wei, F. Z. *et al.* Epigenetic regulation of autophagy by the methyltransferase EZH2 through an MTOR-dependent pathway. *Autophagy* **11**, 2309-2322, doi:10.1080/15548627.2015.1117734 (2015).
- 269 Liu, T. P., Lo, H. L., Wei, L. S., Hsiao, H. H. & Yang, P. M. S-Adenosyl-L-methionine-competitive inhibitors of the histone methyltransferase EZH2 induce autophagy and enhance drug sensitivity in cancer cells. *Anticancer Drugs* **26**, 139-147, doi:10.1097/CAD.000000000000166 (2015).
- 270 Alimova, I. *et al.* Targeting the enhancer of zeste homologue 2 in medulloblastoma. *Int J Cancer* **131**, 1800-1809, doi:10.1002/ijc.27455 (2012).
- 271 Smits, M. *et al.* EZH2-regulated DAB2IP is a medulloblastoma tumor suppressor and a positive marker for survival. *Clin Cancer Res* **18**, 4048-4058, doi:10.1158/1078-0432.CCR-12-0399 (2012).
- 272 Po, A. *et al.* Hedgehog controls neural stem cells through p53-independent regulation of Nanog. *EMBO J* **29**, 2646-2658, doi:10.1038/emboj.2010.131 (2010).
- 273 Zhang, P. *et al.* ABCB1 and ABCG2 restrict the brain penetration of a panel of novel EZH2-Inhibitors. *Int J Cancer* **137**, 2007-2018, doi:10.1002/ijc.29566 (2015).
- 274 Kumar, A. *et al.* EZH2 Inhibitor GSK126: Metabolism, drug transporter and rat pharmacokinetic studies. *Medical Research Archives; No 3 (2015)* (2015).
- 275 Albrecht, B. K. *et al.* Modulators of methyl modifying enzymes, compositions and uses thereof. WO2013120104A2 (2013).
- 276 Blackledge, J. R. C. W. *et al.* Enhancer of zeste homolog 2 inhibitors. WO2014177982A1 (2014).
- 277 Svete, J., Aljaž-Rožič, M. & Stanovnik, B. 2-Benzoyl-2-ethoxycarbonylvinyl-1 and 2-benzoylamino-2-methoxy-carbonylvinyl-1 as N-protecting groups in peptide synthesis. Their application in the synthesis of dehydropeptide derivatives containing N-terminal 3-heteroaryl-amino-2,3-dehydroalanine. *Journal of Heterocyclic Chemistry* **34**, 177-193, doi:10.1002/jhet.5570340128 (1997).
- 278 Cumming, J. G. *et al.* Discovery and characterization of MAPK-activated protein kinase-2 prevention of activation inhibitors. *J Med Chem* **58**, 278-293, doi:10.1021/jm501038s (2015).
- 279 Kim, C. K., Krasavage, B. A. & Maggiulli, C. A. A new synthesis of 5,7-dicarboxy-2,1-benzisoxazolin-3-one. *Journal of Heterocyclic Chemistry* **22**, 127-128, doi:10.1002/jhet.5570220131 (1985).
- 280 Ohki, H. *et al.* Studies on 3'-quaternary ammonium cephalosporins--IV. Synthesis and antibacterial activity of 3'-(2-alkyl-3-aminopyrazolium) cephalosporins related to FK037. *Bioorg Med Chem* **5**, 1685-1694 (1997).
- 281 Anderson, K. W. *et al.* Pyrazoles as 11-beta-hsd-1. WO2007107470A2 (2007).
- 282 Li, J.-F., Zhu, Y.-Q., Wang, X. & Yang, H.-Z. Synthesis and herbicidal activities of a series of di(aminopyrazoly) ketone derivatives. *Journal of Heterocyclic Chemistry* **44**, 749-755, doi:10.1002/jhet.5570440401 (2007).
- 283 Stefancich, G., Corelli, F., Massa, S., Silvestri, R. & Di Santo, R. Heterocyclic systems. VII Synthesis of 1H-pyrazolo[3,4-e]indolizine derivatives. *Journal of Heterocyclic Chemistry* **24**, 1199-1202, doi:10.1002/jhet.5570240451 (1987).
- 284 Menozzi, G., Schenone, P., Mosti, L. & Mattioli, F. Synthesis of 5-substituted 1-aryl-1H-pyrazole-4-acetonitriles, 4-methyl-1-phenyl-1H-pyrazole-3-carbonitriles and

- pharmacologically active 1-aryl-1H-pyrazole-4-acetic acids. *Journal of Heterocyclic Chemistry* **30**, 997-1002, doi:10.1002/jhet.5570300427 (1993).
- 285 Momose, Y., Maekawa, T., Odaka, H. & Kimura, H. 5-membered n-heterocyclic compounds with hypoglycemic and hypolipidemic activity. WO2001038325A1 (2001).
- 286 Deshayes, C., Chabannet, M. & Gelin, S. Synthesis of some 1H, or 2H,4H-benzo[4,5]cyclohepta[1,2-c]pyrazol-4-one derivatives. *Heterocycles* **20**, 1581-1585 (1983).
- 287 Deshayes, C., Chabannet, M. & Gelin, S. Synthesis of some 5-aryl-4,5-dihydropyrazolo[1,5-a]quinolines and 5-aryl-4,5-dihydro-10H-pyrazolo[1,5-b][2]benzazepines from 1-phenyl- or 1-benzyl-5-styrylpyrazoles. *Synthesis*, 1088-1089, doi:10.1055/s-1982-30081 (1982).
- 288 Strah, S., Golobič, A., Golič, L. & Stanovnik, B. Alkyl (E,Z)-2-(2-benzoyl-2-ethoxycarbonyl-1-ethenyl)amino-3-dimethylaminopropenoates in the synthesis of fused pyrimidinones. A facile route to 3-aminoazino-4H-pyrimidin-4-ones. *Journal of Heterocyclic Chemistry* **34**, 1511-1517, doi:10.1002/jhet.5570340521 (1997).
- 289 Flynn, D. L., Petillo, P. A. & Kaufman, M. D. Methods and Compositions for the Treatment of Myeloproliferative Diseases and other Proliferative Diseases. US20120225057A1 (2011).
- 290 Menozzi, G., Mosti, L. & Schenone, P. Reaction of 2-dimethylaminomethylene-1,3-diones with dinucleophiles. VI. Synthesis of ethyl or methyl 1,5-disubstituted 1H-pyrazole-4-carboxylates. *Journal of Heterocyclic Chemistry* **24**, 1669-1675, doi:10.1002/jhet.5570240634 (1987).
- 291 Massa, S., Mai, A., Artico, M. & Corelli, F. Heterocyclic system. XI. Synthesis of 1H,4H-pyrazolo[4,3-b]pyrrolizine and 2H,4H-pyrazolo[4,3-b]pyrrolizine derivatives. *Journal of Heterocyclic Chemistry* **27**, 1805-1808, doi:10.1002/jhet.5570270653 (1990).
- 292 Miura, S. *et al.* Heterocyclic amide compound and use thereof. WO2007052843A1 (2007).
- 293 Hohwy, M. *et al.* Novel prostaglandin D synthase inhibitors generated by fragment-based drug design. *J Med Chem* **51**, 2178-2186, doi:10.1021/jm701509k (2008).
- 294 Ronci, M. *et al.* Proteomic analysis of human Sonic Hedgehog (SHH) medulloblastoma stem-like cells. *Mol Biosyst* **11**, 1603-1611, doi:10.1039/c5mb00034c (2015).
- 295 Infante, P. *et al.* Gli1/DNA interaction is a druggable target for Hedgehog-dependent tumors. *EMBO J* **34**, 200-217, doi:10.15252/embj.201489213 (2015).
- 296 Luo, Y., Xiao, F., Qian, S., Lu, W. & Yang, B. Synthesis and in vitro cytotoxic evaluation of some thiazolylbenzimidazole derivatives. *Eur J Med Chem* **46**, 417-422, doi:10.1016/j.ejmech.2010.11.014 (2011).
- 297 Mochona, B., Jackson, T., McCauley, D., Mazzio, E. & Redda, K. K. Synthesis and Cytotoxic Evaluation of Pyrrole Hetarylazoles Containing Benzimidazole/Pyrazolone/1,3,4-Oxadiazole Motifs. *J Heterocycl Chem* **53**, 1871-1877, doi:10.1002/jhet.2501 (2016).
- 298 deParrodi, C. A., Quintero-Cortés, L. & Sandoval-Ramírez, J. A Short Synthesis of Astemizole. *Synthetic Communications* **26**, 3323-3329, doi:10.1080/00397919608004642 (1996).
- 299 Nguyen, T., Yang, T. & Go, M. L. Functionalized acridin-9-yl phenylamines protected neuronal HT22 cells from glutamate-induced cell death by reducing intracellular levels of free radical species. *Bioorg Med Chem Lett* **24**, 1830-1838, doi:10.1016/j.bmcl.2014.02.006 (2014).
- 300 Minami, N. *et al.* Preparation of N-[(aralkylamino)alkyl]-4-aryl-3-butenamides as antiischemic agents. EP399358A2 (1990).
- 301 Griffioen, G. *et al.* Piperazine thiazole derivatives useful in the treatment of tauopathies such as alzheimer's disease. EP2744798B1 (2013).
- 302 Kane, J. M. *et al.* Substituted 4-(1h-benzimidazol-2-yl-amino)piperidines useful for the treatment of allergic diseases. WO1997019074A1 (1997).

- 303 Janssens, F., Stokbroekx, R., Torremans, J. & Luyckx, M. N-Heterocycl-4-
piperidinamines. US4219559A (1980).
- 304 Wagner, E., Wittmann, H. J., Elz, S. & Strasser, A. Pharmacological profile of
astemizole-derived compounds at the histamine H1 and H4 receptor--H1/H4 receptor
selectivity. *Naunyn Schmiedebergs Arch Pharmacol* **387**, 235-250, doi:10.1007/s00210-
013-0926-4 (2014).
- 305 Janssens, F. E., Sommen, F. M., Surleraux, D. L. N. G. & Van, R. Y. E. M. 1-(1,2-
disubstituted piperidinyl)-4-substituted piperidine derivatives as tachykinin receptor
antagonists. WO1997024324A1 (1997).
- 306 Ostrowski, K. & Barnard, E. A. Application of isotopically labelled specific inhibitors
as a method in enzyme cytochemistry. *Exp Cell Res* **25**, 465-468 (1961).
- 307 Willems, L. I., Overkleeft, H. S. & van Kasteren, S. I. Current developments in activity-
based protein profiling. *Bioconjug Chem* **25**, 1181-1191, doi:10.1021/bc500208y
(2014).
- 308 Cravatt, B. F., Wright, A. T. & Kozarich, J. W. Activity-based protein profiling: from
enzyme chemistry to proteomic chemistry. *Annu Rev Biochem* **77**, 383-414,
doi:10.1146/annurev.biochem.75.101304.124125 (2008).
- 309 Murale, D. P., Hong, S. C., Haque, M. M. & Lee, J. S. Photo-affinity labeling (PAL) in
chemical proteomics: a handy tool to investigate protein-protein interactions (PPIs).
Proteome Sci **15**, 14, doi:10.1186/s12953-017-0123-3 (2016).
- 310 Hashimoto, M. & Hatanaka, Y. Recent Progress in Diazirine-Based Photoaffinity
Labeling. *European Journal of Organic Chemistry* **2008**, 2513-2523,
doi:10.1002/ejoc.200701069 (2008).
- 311 Lapinsky, D. J. Tandem photoaffinity labeling-bioorthogonal conjugation in medicinal
chemistry. *Bioorg Med Chem* **20**, 6237-6247, doi:10.1016/j.bmc.2012.09.010 (2012).
- 312 Sadakane, Y. & Hatanaka, Y. Photochemical fishing approaches for identifying target
proteins and elucidating the structure of a ligand-binding region using carbene-
generating photoreactive probes. *Anal Sci* **22**, 209-218 (2006).
- 313 Smith, E. & Collins, I. Photoaffinity labeling in target- and binding-site identification.
Future Med Chem **7**, 159-183, doi:10.4155/fmc.14.152 (2015).
- 314 Sakurai, K., Ozawa, S., Yamada, R., Yasui, T. & Mizuno, S. Comparison of the
reactivity of carbohydrate photoaffinity probes with different photoreactive groups.
Chembiochem **15**, 1399-1403, doi:10.1002/cbic.201402051 (2014).
- 315 A. Fleming, S. Chemical reagents in photoaffinity labeling. *Tetrahedron* **51**, 12479-
12520, doi:[https://doi.org/10.1016/0040-4020\(95\)00598-3](https://doi.org/10.1016/0040-4020(95)00598-3) (1995).
- 316 Dubinsky, L., Krom, B. P. & Meijler, M. M. Diazirine based photoaffinity labeling.
Bioorg Med Chem **20**, 554-570, doi:10.1016/j.bmc.2011.06.066 (2012).
- 317 Geurink, P. P., Prely, L. M., van der Marel, G. A., Bischoff, R. & Overkleeft, H. S.
Photoaffinity labeling in activity-based protein profiling. *Top Curr Chem* **324**, 85-113,
doi:10.1007/128_2011_286 (2012).
- 318 Terstappen, G. C., Schlupen, C., Raggiaschi, R. & Gaviraghi, G. Target deconvolution
strategies in drug discovery. *Nat Rev Drug Discov* **6**, 891-903, doi:10.1038/nrd2410
(2007).
- 319 Lang, K. & Chin, J. W. Bioorthogonal reactions for labeling proteins. *ACS Chem Biol* **9**,
16-20, doi:10.1021/cb4009292 (2014).
- 320 Kolb, H. C., Finn, M. G. & Sharpless, K. B. Click Chemistry: Diverse Chemical
Function from a Few Good Reactions. *Angew Chem Int Ed Engl* **40**, 2004-2021 (2001).
- 321 Kennedy, D. C. *et al.* Cellular consequences of copper complexes used to catalyze
bioorthogonal click reactions. *J Am Chem Soc* **133**, 17993-18001,
doi:10.1021/ja2083027 (2011).
- 322 Debets, M. F., van der Doelen, C. W., Rutjes, F. P. & van Delft, F. L. Azide: a unique
dipole for metal-free bioorthogonal ligations. *Chembiochem* **11**, 1168-1184,
doi:10.1002/cbic.201000064 (2010).
- 323 Baskin, J. M. *et al.* Copper-free click chemistry for dynamic in vivo imaging. *Proc Natl
Acad Sci U S A* **104**, 16793-16797, doi:10.1073/pnas.0707090104 (2007).

- 324 Laughlin, S. T., Baskin, J. M., Amacher, S. L. & Bertozzi, C. R. In vivo imaging of
membrane-associated glycans in developing zebrafish. *Science* **320**, 664-667,
doi:10.1126/science.1155106 (2008).
- 325 McKay, C. S., Blake, J. A., Cheng, J., Danielson, D. C. & Pezacki, J. P. Strain-
promoted cycloadditions of cyclic nitrones with cyclooctynes for labeling human cancer
cells. *Chem Commun (Camb)* **47**, 10040-10042, doi:10.1039/c1cc13808a (2011).
- 326 Ning, X. *et al.* Protein modification by strain-promoted alkyne-nitrone cycloaddition.
Angew Chem Int Ed Engl **49**, 3065-3068, doi:10.1002/anie.201000408 (2010).
- 327 Yu, Z., Pan, Y., Wang, Z., Wang, J. & Lin, Q. Genetically encoded cyclopropene
directs rapid, photoclick-chemistry-mediated protein labeling in mammalian cells.
Angew Chem Int Ed Engl **51**, 10600-10604, doi:10.1002/anie.201205352 (2012).
- 328 Song, W., Wang, Y., Qu, J., Madden, M. M. & Lin, Q. A photoinducible 1,3-dipolar
cycloaddition reaction for rapid, selective modification of tetrazole-containing proteins.
Angew Chem Int Ed Engl **47**, 2832-2835, doi:10.1002/anie.200705805 (2008).
- 329 Song, W., Wang, Y., Qu, J. & Lin, Q. Selective functionalization of a genetically
encoded alkene-containing protein via "photoclick chemistry" in bacterial cells. *J Am
Chem Soc* **130**, 9654-9655, doi:10.1021/ja803598e (2008).
- 330 Hewings, D. S. *et al.* 3,5-dimethylisoxazoles act as acetyl-lysine-mimetic bromodomain
ligands. *J Med Chem* **54**, 6761-6770, doi:10.1021/jm200640v (2011).
- 331 Hewings, D. S. *et al.* Optimization of 3,5-dimethylisoxazole derivatives as potent
bromodomain ligands. *J Med Chem* **56**, 3217-3227, doi:10.1021/jm301588r (2013).
- 332 Brand, M. *Developing small molecule ligands for the study of Bromodomain-Histone
interactions. PhD Thesis (Supervisor Prof. SJ Conway)*, Oxford University, (2016).
- 333 Lennox, A. J. & Lloyd-Jones, G. C. Preparation of organotrifluoroborate salts:
precipitation-driven equilibrium under non-etching conditions. *Angew Chem Int Ed
Engl* **51**, 9385-9388, doi:10.1002/anie.201203930 (2012).
- 334 Li, Z. *et al.* Design and synthesis of minimalist terminal alkyne-containing diazirine
photo-crosslinkers and their incorporation into kinase inhibitors for cell- and tissue-
based proteome profiling. *Angew Chem Int Ed Engl* **52**, 8551-8556,
doi:10.1002/anie.201300683 (2013).
- 335 Kambe, T., Correia, B. E., Niphakis, M. J. & Cravatt, B. F. Mapping the protein
interaction landscape for fully functionalized small-molecule probes in human cells. *J
Am Chem Soc* **136**, 10777-10782, doi:10.1021/ja505517t (2014).
- 336 Bianchi, A. & Bernardi, A. Traceless Staudinger ligation of glycosyl azides with triaryl
phosphines: stereoselective synthesis of glycosyl amides. *J Org Chem* **71**, 4565-4577,
doi:10.1021/jo060409s (2006).
- 337 Ikeda, Y. & Behrman, E. J. Improved Synthesis of Photo-leucine. *Synthetic
Communications* **38**, 2276-2284, doi:10.1080/00397910802138454 (2008).
- 338 Wang, Q. *et al.* Bioconjugation by copper(I)-catalyzed azide-alkyne [3 + 2]
cycloaddition. *J Am Chem Soc* **125**, 3192-3193, doi:10.1021/ja021381e (2003).
- 339 Li, Z. *et al.* "Minimalist" cyclopropene-containing photo-cross-linkers suitable for live-
cell imaging and affinity-based protein labeling. *J Am Chem Soc* **136**, 9990-9998,
doi:10.1021/ja502780z (2014).
- 340 Hayakawa, K., Yodo, M., Ohsuki, S. & Kanematsu, K. Novel bicycloannulation via
tandem vinylation and intramolecular Diels-Alder reaction of five-membered
heterocycles: a new approach to construction of psoralen and azapsoralen. *Journal of
the American Chemical Society* **106**, 6735-6740, doi:10.1021/ja00334a044 (1984).
- 341 Warburg, O. The Metabolism of Carcinoma Cells. *The Journal of Cancer Research* **9**,
148 (1925).
- 342 Vander Heiden, M. G., Cantley, L. C. & Thompson, C. B. Understanding the Warburg
effect: the metabolic requirements of cell proliferation. *Science* **324**, 1029-1033,
doi:10.1126/science.1160809 (2009).
- 343 Baenke, F., Peck, B., Miess, H. & Schulze, A. Hooked on fat: the role of lipid synthesis
in cancer metabolism and tumour development. *Dis Model Mech* **6**, 1353-1363,
doi:10.1242/dmm.011338 (2013).

- 344 Beloribi-Djefalia, S., Vasseur, S. & Guillaumond, F. Lipid metabolic reprogramming
in cancer cells. *Oncogenesis* **5**, e189, doi:10.1038/oncsis.2015.49 (2016).
- 345 Luo, X. *et al.* Emerging roles of lipid metabolism in cancer metastasis. *Mol Cancer* **16**,
76, doi:10.1186/s12943-017-0646-3 (2017).
- 346 Nomura, D. K. & Cravatt, B. F. Lipid metabolism in cancer. *Biochim Biophys Acta*
1831, 1497-1498, doi:10.1016/j.bbalip.2013.08.001 (2013).
- 347 Engelman, J. A., Luo, J. & Cantley, L. C. The evolution of phosphatidylinositol 3-
kinases as regulators of growth and metabolism. *Nat Rev Genet* **7**, 606-619,
doi:10.1038/nrg1879 (2006).
- 348 Rancoule, C. *et al.* Lysophosphatidic acid (LPA) as a pro-fibrotic and pro-oncogenic
factor: a pivotal target to improve the radiotherapy therapeutic index. *Oncotarget* **8**,
43543-43554, doi:10.18632/oncotarget.16672 (2017).
- 349 Mills, G. B. & Moolenaar, W. H. The emerging role of lysophosphatidic acid in cancer.
Nat Rev Cancer **3**, 582-591, doi:10.1038/nrc1143 (2003).
- 350 Pyne, N. J. & Pyne, S. Sphingosine 1-phosphate and cancer. *Nat Rev Cancer* **10**, 489-
503, doi:10.1038/nrc2875 (2010).
- 351 Patmanathan, S. N., Wang, W., Yap, L. F., Herr, D. R. & Paterson, I. C. Mechanisms of
sphingosine 1-phosphate receptor signalling in cancer. *Cell Signal* **34**, 66-75,
doi:10.1016/j.cellsig.2017.03.002 (2017).
- 352 Wang, D. & Dubois, R. N. Eicosanoids and cancer. *Nat Rev Cancer* **10**, 181-193,
doi:10.1038/nrc2809 (2010).
- 353 Moore, G. Y. & Pidgeon, G. P. Cross-Talk between Cancer Cells and the Tumour
Microenvironment: The Role of the 5-Lipoxygenase Pathway. *Int J Mol Sci* **18**,
doi:10.3390/ijms18020236 (2017).
- 354 Kuhajda, F. P. *et al.* Fatty acid synthesis: a potential selective target for antineoplastic
therapy. *Proc Natl Acad Sci U S A* **91**, 6379-6383 (1994).
- 355 Menendez, J. A. & Lupu, R. Fatty acid synthase and the lipogenic phenotype in cancer
pathogenesis. *Nat Rev Cancer* **7**, 763-777, doi:10.1038/nrc2222 (2007).
- 356 Angeles, T. S. & Hudkins, R. L. Recent advances in targeting the fatty acid biosynthetic
pathway using fatty acid synthase inhibitors. *Expert Opin Drug Discov* **11**, 1187-1199,
doi:10.1080/17460441.2016.1245286 (2016).
- 357 Maier, T., Leibundgut, M. & Ban, N. The crystal structure of a mammalian fatty acid
synthase. *Science* **321**, 1315-1322, doi:10.1126/science.1161269 (2008).
- 358 Jones, S. F. & Infante, J. R. Molecular Pathways: Fatty Acid Synthase. *Clin Cancer Res*
21, 5434-5438, doi:10.1158/1078-0432.CCR-15-0126 (2015).
- 359 Currie, E., Schulze, A., Zechner, R., Walther, T. C. & Farese, R. V. Cellular Fatty Acid
Metabolism and Cancer. *Cell metabolism* **18**, 153-161, doi:10.1016/j.cmet.2013.05.017
(2013).
- 360 Kuemmerle, N. B. *et al.* Lipoprotein lipase links dietary fat to solid tumor cell
proliferation. *Mol Cancer Ther* **10**, 427-436, doi:10.1158/1535-7163.MCT-10-0802
(2011).
- 361 Nieman, K. M. *et al.* Adipocytes promote ovarian cancer metastasis and provide energy
for rapid tumor growth. *Nat Med* **17**, 1498-1503, doi:10.1038/nm.2492 (2011).
- 362 Nomura, D. K. *et al.* Monoacylglycerol lipase regulates a fatty acid network that
promotes cancer pathogenesis. *Cell* **140**, 49-61, doi:10.1016/j.cell.2009.11.027 (2010).
- 363 da Silva, T. F., Sousa, V. F., Malheiro, A. R. & Brites, P. The importance of ether-
phospholipids: a view from the perspective of mouse models. *Biochim Biophys Acta*
1822, 1501-1508, doi:10.1016/j.bbadis.2012.05.014 (2012).
- 364 Brites, P., Waterham, H. R. & Wanders, R. J. Functions and biosynthesis of
plasmalogens in health and disease. *Biochim Biophys Acta* **1636**, 219-231,
doi:10.1016/j.bbalip.2003.12.010 (2004).
- 365 Wallner, S. & Schmitz, G. Plasmalogens the neglected regulatory and scavenging lipid
species. *Chem Phys Lipids* **164**, 573-589, doi:10.1016/j.chemphyslip.2011.06.008
(2011).

- 366 Tsukahara, T., Haniu, H. & Matsuda, Y. Effect of alkyl glycerophosphate on the
activation of peroxisome proliferator-activated receptor gamma and glucose uptake in
C2C12 cells. *Biochem Biophys Res Commun* **433**, 281-285,
doi:10.1016/j.bbrc.2013.02.101 (2013).
- 367 Xu, Y., Tanaka, M., Arai, H., Aoki, J. & Prestwich, G. D. Alkyl lysophosphatidic acid
and fluoromethylene phosphonate analogs as metabolically-stabilized agonists for LPA
receptors. *Bioorg Med Chem Lett* **14**, 5323-5328, doi:10.1016/j.bmcl.2004.08.019
(2004).
- 368 Melnikova, V. & Bar-Eli, M. Inflammation and melanoma growth and metastasis: the
role of platelet-activating factor (PAF) and its receptor. *Cancer Metastasis Rev* **26**, 359-
371, doi:10.1007/s10555-007-9092-9 (2007).
- 369 Chiang, K. P., Niessen, S., Saghatelian, A. & Cravatt, B. F. An enzyme that regulates
ether lipid signaling pathways in cancer annotated by multidimensional profiling. *Chem
Biol* **13**, 1041-1050, doi:10.1016/j.chembiol.2006.08.008 (2006).
- 370 Wood, R. & Snyder, F. Characterization and identification of glyceryl ether diesters
present in tumor cells. *J Lipid Res* **8**, 494-500 (1967).
- 371 Snyder, F. & Wood, R. Alkyl and alk-1-enyl ethers of glycerol in lipids from normal
and neoplastic human tissues. *Cancer Res* **29**, 251-257 (1969).
- 372 Jessani, N. *et al.* A streamlined platform for high-content functional proteomics of
primary human specimens. *Nat Methods* **2**, 691-697, doi:10.1038/nmeth778 (2005).
- 373 Chang, J. W., Nomura, D. K. & Cravatt, B. F. A potent and selective inhibitor of
KIAA1363/AADACL1 that impairs prostate cancer pathogenesis. *Chem Biol* **18**, 476-
484, doi:10.1016/j.chembiol.2011.02.008 (2011).
- 374 Lodhi, I. J. & Semenkovich, C. F. Peroxisomes: a nexus for lipid metabolism and
cellular signaling. *Cell Metab* **19**, 380-392, doi:10.1016/j.cmet.2014.01.002 (2014).
- 375 Davis, P. A. & Hajra, A. K. Stereochemical specificity of the biosynthesis of the alkyl
ether bond in alkyl ether lipids. *J Biol Chem* **254**, 4760-4763 (1979).
- 376 de Vet, E. C., Hilkes, Y. H., Fraaije, M. W. & van den Bosch, H. Alkyl-
dihydroxyacetonephosphate synthase. Presence and role of flavin adenine dinucleotide.
J Biol Chem **275**, 6276-6283 (2000).
- 377 Nenci, S. *et al.* Precursor of ether phospholipids is synthesized by a flavoenzyme
through covalent catalysis. *Proc Natl Acad Sci U S A* **109**, 18791-18796,
doi:10.1073/pnas.1215128109 (2012).
- 378 de Vet, E. C., Ijlst, L., Oostheim, W., Wanders, R. J. & van den Bosch, H. Alkyl-
dihydroxyacetonephosphate synthase. Fate in peroxisome biogenesis disorders and
identification of the point mutation underlying a single enzyme deficiency. *J Biol Chem*
273, 10296-10301 (1998).
- 379 Thai, T. P. *et al.* Impaired membrane traffic in defective ether lipid biosynthesis. *Hum
Mol Genet* **10**, 127-136 (2001).
- 380 Benjamin, D. I. *et al.* Ether lipid generating enzyme AGPS alters the balance of
structural and signaling lipids to fuel cancer pathogenicity. *Proc Natl Acad Sci U S A*
110, 14912-14917, doi:10.1073/pnas.1310894110 (2013).
- 381 Wang, D. & Dubois, R. N. Epoxyeicosatrienoic acids: a double-edged sword in
cardiovascular diseases and cancer. *J Clin Invest* **122**, 19-22, doi:10.1172/JCI61453
(2012).
- 382 Kendall, A. C. & Nicolaou, A. Bioactive lipid mediators in skin inflammation and
immunity. *Prog Lipid Res* **52**, 141-164, doi:10.1016/j.plipres.2012.10.003 (2013).
- 383 Zhu, Y. *et al.* Role and mechanism of the alkylglycerone phosphate synthase in
suppressing the invasion potential of human glioma and hepatic carcinoma cells in
vitro. *Oncol Rep* **32**, 431-436, doi:10.3892/or.2014.3189 (2014).
- 384 Forneris, F., Orru, R., Bonivento, D., Chiarelli, L. R. & Mattevi, A. ThermoFAD, a
Thermofluor-adapted flavin ad hoc detection system for protein folding and ligand
binding. *FEBS J* **276**, 2833-2840, doi:10.1111/j.1742-4658.2009.07006.x (2009).

- 385 Piano, V. *et al.* Discovery of Inhibitors for the Ether Lipid-Generating Enzyme AGPS
as Anti-Cancer Agents. *ACS Chem Biol* **10**, 2589-2597,
doi:10.1021/acscchembio.5b00466 (2015).
- 386 Irwin, J. J., Sterling, T., Mysinger, M. M., Bolstad, E. S. & Coleman, R. G. ZINC: a
free tool to discover chemistry for biology. *J Chem Inf Model* **52**, 1757-1768,
doi:10.1021/ci3001277 (2012).
- 387 Slater, E. C. The mechanism of action of the respiratory inhibitor, antimycin. *Biochim
Biophys Acta* **301**, 129-154 (1973).
- 388 Matulis, D., Kranz, J. K., Salemme, F. R. & Todd, M. J. Thermodynamic stability of
carbonic anhydrase: measurements of binding affinity and stoichiometry using
ThermoFluor. *Biochemistry* **44**, 5258-5266, doi:10.1021/bi048135v (2005).
- 389 Huang, L. S., Cobessi, D., Tung, E. Y. & Berry, E. A. Binding of the respiratory chain
inhibitor antimycin to the mitochondrial bc1 complex: a new crystal structure reveals an
altered intramolecular hydrogen-bonding pattern. *J Mol Biol* **351**, 573-597,
doi:10.1016/j.jmb.2005.05.053 (2005).
- 390 Bartolini, S. *et al.* 6-[1-(2,6-difluorophenyl)ethyl]pyrimidinones antagonize cell
proliferation and induce cell differentiation by inhibiting (a nontelomeric) endogenous
reverse transcriptase. *J Med Chem* **48**, 6776-6778, doi:10.1021/jm0507330 (2005).
- 391 Chen, S. *et al.* The involvement of RhoA and Wnt-5a in the tumorigenesis and
progression of ovarian epithelial carcinoma. *Int J Mol Sci* **14**, 24187-24199,
doi:10.3390/ijms141224187 (2013).
- 392 Turunen, S. P., Tatti-Bugaeva, O. & Lehti, K. Membrane-type matrix metalloproteases
as diverse effectors of cancer progression. *Biochim Biophys Acta* **1864**, 1974-1988,
doi:10.1016/j.bbamcr.2017.04.002 (2017).
- 393 Chen, T., You, Y., Jiang, H. & Wang, Z. Z. Epithelial-mesenchymal transition (EMT):
A biological process in the development, stem cell differentiation, and tumorigenesis. *J
Cell Physiol* **232**, 3261-3272, doi:10.1002/jcp.25797 (2017).
- 394 La Monica, S. *et al.* Gefitinib inhibits invasive phenotype and epithelial-mesenchymal
transition in drug-resistant NSCLC cells with MET amplification. *PLoS One* **8**, e78656,
doi:10.1371/journal.pone.0078656 (2013).
- 395 Koay, M. H., Crook, M. & Stewart, C. J. Cyclin D1, E-cadherin and beta-catenin
expression in FIGO Stage IA cervical squamous carcinoma: diagnostic value and
evidence for epithelial-mesenchymal transition. *Histopathology* **61**, 1125-1133,
doi:10.1111/j.1365-2559.2012.04326.x (2012).
- 396 Gregerson, C. E. *et al.* Oxidative coupling of Michael acceptors with aryl nucleophiles
produced through rhodium-catalyzed C-C bond activation. *Org Biomol Chem* **15**, 5944-
5948, doi:10.1039/c7ob01212h (2017).
- 397 Suryavanshi, G. M., Sudalai, A. & Kamble, R. B. Diphenyloxiranes, process for
preparation thereof, and its use in an enantioselective synthesis of (+)-sertraline.
WO2016088138 (2016).
- 398 Wen, J., Jiang, J. & Zhang, X. Rhodium-Catalyzed Asymmetric Hydrogenation of
alpha,beta-Unsaturated Carbonyl Compounds via Thiourea Hydrogen Bonding. *Org
Lett* **18**, 4451-4453, doi:10.1021/acs.orglett.6b01812 (2016).
- 399 Nakatsuji, H., Ueno, K., Misaki, T. & Tanabe, Y. General, robust, and
stereocomplementary preparation of beta-ketoester enol tosylates as cross-coupling
partners utilizing TsCl-N-methylimidazole agents. *Org Lett* **10**, 2131-2134,
doi:10.1021/ol800480d (2008).
- 400 Duan, Z. C., Hu, X. P., Zhang, C. & Zheng, Z. Enantioselective Rh-catalyzed
hydrogenation of 3-aryl-4-phosphonobutenoates with a P-stereogenic BoPhoz-type
ligand. *J Org Chem* **75**, 8319-8321, doi:10.1021/jo101849b (2010).
- 401 Remiszewski, S., Koyuncu, E., Sun, Q. & Chiang, L. Anti-hcmv compositions and
methods. WO2016077240A2 (2016).
- 402 Shipps, J. G. W. *et al.* Inhibitors of fatty acid binding protein (fabp). WO2010056631
(A1) (2010).

- 403 Renaudat, A. *et al.* Palladium-catalyzed beta arylation of carboxylic esters. *Angew Chem Int Ed Engl* **49**, 7261-7265, doi:10.1002/anie.201003544 (2010).
- 404 Pesyan, A. & Balandrin, M. F. Novel compounds advantageous in the treatment of central nervous system diseases and disorders. US20160137592A1 (2016).
- 405 Marcantoni, E. *et al.* Crucial role of elusive isomeric eta-complexes in gas-phase electrophilic aromatic alkylations. *J Org Chem* **70**, 4133-4141, doi:10.1021/jo050019q (2005).
- 406 Yates, C. M., Shaver, S. R. & Hoekstra, W. J. Metalloenzyme inhibitor compounds. WO2017117393 (2017).
- 407 Ognyanov, V. I. *et al.* Design of potent, orally available antagonists of the transient receptor potential vanilloid 1. Structure-activity relationships of 2-piperazin-1-yl-1H-benzimidazoles. *J Med Chem* **49**, 3719-3742, doi:10.1021/jm060065y (2006).
- 408 Palmer, W. *et al.* Bromodomain inhibitors for treating disease. US20160060260A1 (2016).
- 409 Kimura, T., Kamata, K. & Mizuno, N. A bifunctional tungstate catalyst for chemical fixation of CO₂ at atmospheric pressure. *Angew Chem Int Ed Engl* **51**, 6700-6703, doi:10.1002/anie.201203189 (2012).
- 410 Nale, D. B. & Bhanage, B. M. Copper-catalyzed efficient synthesis of a 2-benzimidazolone scaffold from 2-nitroaniline and dimethyl carbonate via a hydrosilylation reaction. *Green Chemistry* **17**, 2480-2486, doi:10.1039/C4GC02408G (2015).
- 411 Cai, S. X. *et al.* Structure-activity relationships of alkyl- and alkoxy-substituted 1,4-dihydroquinoxaline-2,3-diones: potent and systemically active antagonists for the glycine site of the NMDA receptor. *J Med Chem* **40**, 730-738, doi:10.1021/jm960654b (1997).
- 412 Montalvao, S. *et al.* Synthesis and Biological Evaluation of 2-Aminobenzothiazole and Benzimidazole Analogs Based on the Clathrocin Structure. *Arch Pharm (Weinheim)* **349**, 137-149, doi:10.1002/ardp.201500365 (2016).
- 413 Beckett, R. P. *et al.* Substituted imidazoheterocycles. WO2008157751A2 (2008).
- 414 Gege, C. *et al.* Metalloprotease inhibitors containing a heterocyclic moiety. WO2008109181A2 (2008).
- 415 Heemskerk, J. E., McCall, J. M. & Barnes, K. D. Isoindoline compounds for the treatment of spinal muscular atrophy and other uses. WO2009042907A1 (2009).
- 416 Razeto, A. *et al.* The crucial step in ether phospholipid biosynthesis: structural basis of a noncanonical reaction associated with a peroxisomal disorder. *Structure* **15**, 683-692, doi:10.1016/j.str.2007.04.009 (2007).
- 417 Zomer, A. W., de Weerd, W. F., Langeveld, J. & van den Bosch, H. Ether lipid synthesis: purification and identification of alkyl dihydroxyacetone phosphate synthase from guinea-pig liver. *Biochim Biophys Acta* **1170**, 189-196 (1993).

Acknowledgments

At the end of these three years PhD, I have to express my gratefulness for all the help and support that I received from different people. It has been a long and hard way, and if I was able to arrive to the end, it is also thank to each one of you.

First of all I want to thank my supervisor and mentor, Prof. Antonello Mai. He initiated me to the fantastic world of Epigenetics and Medicinal Chemistry, also known as Neverlab. His teachings and advices have been always precious to me, and contributed to grow a deep passion for science and research. Even more, I feel so grateful for the trust he always had in me, and for all the opportunities he gave me to improve my scientific knowledge and expertise. Any time I had a presentation or a speech, knowing that he was in the audience has been always a great thing to me, he accompanied and supported me in these moments like no one ever did. He has been kind and professional, but also gentle, as a father would be. He always had the “power” to push me to never give up and do my best, to see forward, to look for the next goal. I want to remember one funny episode with him. One day happened that after a steppy and not easy synthesis, me and Annalisa finally made the desired final compound. We were so happy that we were jumping and hugging each other, but suddenly the Prof. came into the lab. He looked at us quite amazed and asked what happened. When we told him he just said: “Well done! Now go for the next final!”. This is the right spirit!

The last four years would have not been the same without the supervision, the help and advices of Sergio. I could have not asked for some better lab manager. He was feeding my passion for chemistry and science every day with new challenges, reinforcing that “thirst for knowledge” that should be typical of a real scientist, reinforcing that feeling to do better and improve every day even in the details. I want to thank him for trusting me, and accepting my mistakes and my limits, but also for helping me to find a way to overcome these barriers. With him being in the lab has been like being at home. There have been hard times for me, but I knew that I could speak with him as a friend or a brother. I will never forget what he said once, it was something like: “Chemistry is like to climb a mountain: the way up can be terribly hard, but you can reach the top. Later on, on the way down, you just think how much more beautiful was the way up”.

A special thank is due to all my lab-mates in the last three years: Clem, Bia (my first and lovely lab-mate), Diana (a super chemist and super girl with whom we had great time in the lab and not only), Roberta, Annalisa, Maria Antonietta, Alessia Lenoci, Alessia Lucidi, Solomon and Daniela. As the lab has been like home, they have been like my second family. Working long hours in the lab is not always easy, but with good mates, passion for your job and a lot of patience, you can make it extraordinary. I would like to spend few words to thank Clem, who has been constantly present during these three years, always ready to help me and give me good

advices. We have been spending together long time, discussing and often arguing about several topics, but I can say I have found not a good lab-mate, but also a good friend. My last year has been special also thank to the “electric” Annalisa: we can not count the hours that we spent together in the lab, but we can be sure that all what we did has been driven by a common passion for science and chemistry. She has been really a nice surprise at the end of my PhD, a friend that I hope to keep with me forever.

Thanks are due to Prof. Roberto Pellicciari, with whom I had the pleasure and the honor to work as a visiting PhD student in his company TES Pharma during my second year. The time spent working in TES Pharma was really fruitful, there I had the chance to compare myself with a great team of senior scientists, and to learn how each step of the drug discovery process works. I want to thank Prof. Pellicciari to give me the opportunity to work in TES and discover a different and parallel way to make science than what I was used to in University. Specially, I am very grateful to have met a team of motivated, brilliant and restless scientists as my colleagues in TES Pharma: Daniela, Francesca, Tiziana, Lara, Gianmario, Andrea, Nicola, Marco, and Emiliano. I have been learning a lot from each of them, and I am very grateful for their patience and dedication, teaching me all what I know about molecular biology, protein production and purification, set up of a biological assay and analysis of chemical-physical properties of drug candidates.

I want to thank Prof. Stuart Conway, who hosted me in his group for five months during my last year PhD. I have been more than half an hour late at my first appointment with him: it was my first day in Oxford and I could not find the correct building. Finally, I managed to find his office and he did not even need an explanation, he was already smiling at me. Working with Prof. Conway has been one of the most productive, interesting and fruitful experiences I have ever had. At the beginning I was afraid of all the extra activities he proposed, and I was afraid not to be good enough, but then I realized that each of these activities helped me to grow in science and learn something new. I can remember that before each report I felt nervous, because I felt like I did not do enough or I did not reach my goal, but each time he was able to see something good and positive in what I did and give me new energy and motivation to go on and do better. So, I want to thank him for all the opportunities he gave me and for trusting in me and in my abilities till the end, even when my chemistry seemed not to work. His support was crucial to get to the point.

Here I want to thank all the Conway group: Anthony, Amy, James, Larissa, Holly, Jess, Amelie, Loane, Catherine, Maze, Coco, Mus, Ewen, Charles and Joe. For every one of them I have at least a funny story to tell, and a lot of good memories. They have been my every day for five unforgettable months. Thanks are due to Matthias Schiedel (Maze), he was a great tutor and he

gave me the chance to grow a lot in science. As he told me during my last day in Oxford, he was not the kind of tutor one would expect, he was not the one who solved my problems, but he was always present and always ready to support me. In this way he did much more than one would expect, he let me hate my chemistry, he let me make my mistakes, he let me try all what I could, he let me be wrong, and in this way he let me grow as a scientist and as a chemist like I never did. I am so grateful for this. I also want to thank Mus, my best lab-mate ever! I want to thank him for all the times he has been patient and nice with me, for all the times I was exhausted with my chemistry and he tried to cheer me up. I want to thank him for making me laugh an infinite number of times with funny stories and jokes, or for surprising me with magic tricks. I want to thank him for all the time he spent listening to me (even that day so late in the night, while we were still working). I will never forget all of this. Thanks are due to Ludo and Lucy for all the nice chats about science, and life in general and for their advices and support during my time in Oxford. In particular, want to thank Ludo for his patience and availability, for all the times he was my week-end lab-mate, allowing me to work when no one of my group was present. I want to thank him for all the time spent together speaking about chemistry, for teaching me a lot about that, for being with me in a difficult moment of my life and making it less hard to stand, for making jokes and, even more, making me trust in myself.

I want to spend some words to thank also Dr. Paola B. Arimondo. I have been working with her during my Master thesis preparation, but she has been constantly present during the years of my PhD. I learnt from her the importance of multidisciplinary approach in science. Specially, I am grateful for the precious advices she gave me at the end of my PhD, helping me not to give up and taking the good decision in front of a difficult choice.

Thanks are due to Prof. Tripodi, Prof. Cutruzzolà, Prof. Vittorioso and all the advisory board of the PhD School in Life Science, first of all for giving me the chance to do a PhD within this prestigious and multidisciplinary school, but also for organizing interesting and productive activities like Journal Club and seminars, and for all the support and advices during these three years.

I am really convinced that the support, trust, and love of my family played an important role during these years. My parents have been always an example to follow and a secure reference. My sisters are the biggest gift I have received from life, they are my sun and my strength. Here I want to thank all of them, that walked all the way with me during the last three years, even when I have been far away. You have been, and are still, one of my biggest strength and motivation to go on. I feel a bit like a tree, without roots it will never grow and produce fruits, so my family is like the roots to me, giving strength and bringing nutrition.

Together with my family, also my friends walked this way with me: Maria Elisa, Manu, Monica, Alexandra, Leda, Giorgia, Giulia, Ornella. In particular, I want to thank my best friend Maria Elisa: she was always present and pushed me through, even though she may have not realized that. As I told her some days ago: “Time passes by and things change, the frame changes, the players change, but you are still the one that is dancing with me”.

One last special thank is due to that man which accompanied and supported me during the last months, making my life more colorful and happy.

It has been hard to get to the end, a PhD requires a lot of energy, and it might be exhausting, but I think that the hardest part is to believe in what you are doing. As everyone in life, also during my PhD I have been living good and bad moments...there have been times in which I felt no trust in myself and I was afraid to go on, however those have been few. Do you want to know the reason why I went on and I got to the point? The reason is called faith, the reason is called passion, the reason is the same why when you fall in love you can not avoid to sing all the time. And after these three years I can say that, what first scared me, is now the reason why I like this job. At the beginning I was afraid because I didn't know all, so I felt inadequate. Now this feeling is what is pushing me to do better every day, what is making me feel like a scientist and researcher: the humility to say I don't know.

"Siamo chimici, cioè cacciatori: nostre sono "le due esperienze della vita adulta" di cui parlava Pavese, il successo e l'insuccesso, uccidere la balena bianca o sfasciare la nave; non ci si deve arrendere alla materia incomprensibile, non ci si deve sedere. Siamo qui per questo, per sbagliare e correggerci, per incassare colpi e renderli."

Primo Levi, da "Il sistema periodico", "Nichel"